

UNIVERSITY OF SOUTHAMPTON

Faculty of Engineering and the Environment

Effect of Sleeper and Ballast Interventions on Rail
Track Performance

by

Taufan Abadi

Thesis for the degree of Doctor of Philosophy

January 2015

For my daughter LaaLaa

UNIVERSITY OF SOUTHAMPTON

ABSTRACT

FACULTY OF ENGINEERING AND THE ENVIRONMENT

School of Civil Engineering and the Environment

Doctor of Philosophy

EFFECT OF SLEEPER AND BALLAST INTERVENTIONS ON RAIL TRACK

PERFORMANCE

by Taufan Candra Abadi

During its life cycle ballast may undergo up to 10 maintenance tamps until it eventually becomes life expired and requires replacement, typically after approximately 30 years. Such maintenance and the eventual renewal forms a significant annual cost to a ballasted rail network. Railway ballast has several functions, including the transfer of wheel loads to the subgrade as stresses of acceptable magnitude. The sleeper/ballast boundary is the first stage in this load transfer process. Railway ballast is usually graded in the size range 20 to 65 mm, so the number of particles in contact with a sleeper may be relatively small. The discrete and non-uniform nature of these contacts may cause localised stress concentrations leading to ballast breakage and wear. In particular, the use of modern concrete sleepers and hard igneous ballast particles leads to high localised contact stresses that can damage both sleepers and ballast in a way that wooden sleepers may not have in the past. It is therefore of importance to understand better the load transfer mechanisms, the inherent variability in magnitude, the spatial distribution and area of contact positions between sleeper and ballast. There are also advantages if more sustainable arrangements of track standard design could be found through selecting better performing sleeper types and ballast gradations, sleeper to ballast surface interface modifications and changing the profile of the ballast shoulder. The insights gained can lead to an improved performance of this interface, hence longer in-service lifetimes and reduced maintenance requirements and cost.

This research presents results from a laboratory parametric study exploring the performance of different sleeper and ballast designs. Cyclic loading tests were carried out using the Southampton Railway Testing Facility (SRTF) which represents a slice of one sleeper bay of track 650 mm wide confined by rigid sides that enforce plane strain conditions. The subgrade was represented by a 12 mm thick rubber mat. The sleeper is placed on 300 mm thick ballast layer and subjected to an equivalent 20 tonne axle load applied at 3Hz for at least 3 million loading cycles. Measurements were made of the vertical permanent settlement, resilient deflection and ballast pressure. In addition to these, pressure paper was used to give reliable stress and contact area information at the sleeper/ballast, ballast/wall and ballast/subgrade interfaces.

The results show that certain interventions result in slower rates of permanent ballast settlement and those resilient ranges of movement vary with sleeper type and presence of under sleeper pads (USPs). Little or no correlation was found between settlement and resilient movements. The susceptibility of a ballast/sleeper combination to permanent settlement is considered an indicator of the propensity of a length of track to generate differential settlement which would eventually require maintenance. The development of ballast pressure in longitudinal direction depends on the sleeper type being used on the track. The results obtained from the analysis of the pressure paper show several key findings. (1) The sleeper is supported by relatively few contact points numbering in the low hundreds with very high localised stresses developing within an actual contact area of less than 1% of the total. (2) The inclusion of USPs, a finer grading and changes to the sleeper material increase the number and area of contacts and reduce maximum stresses at the sleeper/ballast interface, although these benefits are less clear at the subgrade. (3) Changing a uniformly graded ballast grading to a more broadly graded ballast reduces the magnitude of contact pressure to the subgrade. (4) Ballast migrates from beneath the railseats towards the sleeper ends. The research concludes that the use of USPs, twin block sleepers, finer ballast gradations and shallower shoulder slope all have the potential to reduce maintenance requirements.

Contents

ABSTRACT	I
CONTENTS	III
LIST OF TABLES	VII
LIST OF FIGURES	XIII
LIST OF SYMBOLS	XXIII
LIST OF ABBREVIATIONS	XXV
DECLARATION OF AUTHORSHIP	XXVII
ACKNOWLEDGEMENTS	XXIX
CHAPTER 1: INTRODUCTION	1
1.1	Background of the study	1
1.2	Knowledge gaps	3
1.3	Aim and objectives	5
1.4	Outline of the thesis	6
CHAPTER 2: BACKGROUND	9
2.1	Introduction	9
2.2	Rail track structures	9
2.2.1	Slab track	9
2.2.2	Ballasted track	10
2.3	Components of ballasted track	10
2.3.1	Subgrade	11
2.3.2	Sub-ballast	11
2.3.3	Ballast	12
2.3.4	USPs	19
2.3.5	Sleeper	19
2.3.6	Fastening and pad	20
2.3.7	Rail	21
2.4	Track requirements	22
2.5	Summary	23
CHAPTER 3: REVIEW OF TRACK CATEGORIES AND LOADING	25
3.1	Introduction	25
3.2	Rolling stock in the UK	25
3.3	Categorisation of track	26
3.4	Track design	27
3.5	Track forces	28
3.5.1	Vertical forces	29
3.5.2	Lateral forces	29
3.5.3	Longitudinal forces	29
3.5.4	Impact forces	29
3.6	Vertical load distribution mechanisms: a review of theoretical models	30
3.6.1	Vertical load distribution to the sleepers	30
3.6.2	Vertical load distribution mechanism through the trackbed layers	35
3.7	Summary	40
CHAPTER 4: REVIEW OF CURRENT BALLAST ASSESSMENT TECHNIQUES AND GRADINGS	43
4.1	Introduction	43
4.2	Current ballast assessment techniques	43

4.2.1	Load resistant characterisation	44
4.2.2	Assessment of stability	45
4.2.3	Assessment of weathering	46
4.2.4	Cementing characteristics of ballast	47
4.2.5	Identification of ballast composition	47
4.3	Ballast gradings	47
4.3.1	British ballast specification	48
4.3.2	American ballast specification	50
4.3.3	Canadian ballast specification	52
4.3.4	Australian ballast specification	53
4.4	Tests on ballast gradings	55
4.4.1	Investigation using laboratory testing	55
4.4.2	Investigation using DEM tests	58
4.5	General observations into ballast gradings	61
4.6	Summary	63
CHAPTER 5:	BALLAST BEHAVIOUR CHARACTERISTICS, EXISTING BALLAST SETTLEMENT MODELS AND PRESSURE DISTRIBUTION BENEATH THE SLEEPER	65
5.1	Introduction	65
5.2	Ballast behaviour characteristics	65
5.2.1	Ballast box test	65
5.2.2	Triaxial test	67
5.2.3	Real track observation data and tests	68
5.3	Existing ballast settlement models	69
5.3.1	Okabe's model	71
5.3.2	The Office for Research and Experiments model	71
5.3.3	Shenton's model	72
5.3.4	Jeffs and Marich's model	73
5.3.5	Hettler's model	75
5.3.6	Alva-Hurtado and Selig's model	76
5.3.7	Stewart and Selig's model	76
5.3.8	Selig and Waters's model	79
5.3.9	Sato's model	79
5.3.10	Henn's model	80
5.3.11	Thom and Oakley's model	80
5.3.12	CEDEX's track box model	81
5.3.13	Varandas et al's model	81
5.3.14	Indraratna et al's model	82
5.3.15	General observation on ballast settlement models	82
5.4	Pressure distribution beneath the sleeper	83
5.5	Summary	85
CHAPTER 6:	APPARATUS AND TEST PREPARATION	87
6.1	Introduction	87
6.2	The SRTF apparatus	87
6.2.1	Loading system	89
6.2.2	Specimen preparation	89
6.2.3	Cyclic loading test procedure	91

6.2.4	Summary of test procedure	92
6.3	Justification of rubber mat and thickness used within the modified SRTF apparatus ·	93
6.3.1	Tests on rubber mat	94
6.4	Instrumentation	104
6.4.1	Pressure plates	104
6.4.2	Pressure paper	105
6.4.3	LVDI's	109
6.5	Definition of comparative measures	110
6.5.1	Permanent settlement	111
6.5.2	Sleeper deflection	111
6.5.3	Spring stiffness	112
6.5.4	Ballast pressure	112
6.5.5	Mobilised earth pressure ratio	113
6.5.6	Pressure paper	114
6.5.7	Particle breakage/degradation	116
6.5.8	Lateral movement of ballast on shoulder slope	117
6.6	Testing variables evaluated	118
6.6.1	Sleepers	118
6.6.2	Ballast gradings	119
6.6.3	Sleeper/ballast interface modifications	123
6.6.4	Other investigations	126
6.7	Summary of tests carried out	133
6.7.1	Parametric study	133
6.7.2	Test Details	134
CHAPTER 7:	EXPERIMENTAL RESULTS AND INTERPRETATION	137
7.1	Introduction	137
7.2	Main parameters of comparison	137
7.2.1	Permanent settlement	137
7.2.2	Sleeper deflection	142
7.2.3	Spring stiffness	146
7.2.4	Ballast pressure	153
7.2.5	Mobilised earth pressure ratio	158
7.2.6	Pressure paper	160
7.2.7	Particle breakage	179
7.3	Lateral movement of ballast on shoulder slope	184
7.4	In the case of steel and plastic sleepers	185
7.4.1	Permanent settlement	186
7.4.2	Sleeper deflection	187
7.4.3	Spring stiffness	190
7.5	Sand ingress test	192
7.5.1	Permanent settlement	193
7.5.2	Sleeper deflection	194
7.5.3	Spring stiffness	196
7.5.4	Ballast pressure	198
7.5.5	Mobilised earth pressure ratio	200

7.5.6	Pressure paper	201
7.5.7	Particle breakage	205
7.6	A trial test on combined variables	210
7.6.1	Permanent settlement	210
7.6.2	Spring stiffness	211
7.7	A comparison of results of permanent settlement and spring stiffness	212
7.8	A proposed ballast permanent settlement model	214
7.8.1	Comparing the modified SRTF apparatus data to the existing settlement models	214
7.8.2	A proposed ballast settlement model	216
CHAPTER 8:	CONCLUSIONS AND FURTHER RESEARCH	225
8.1	Conclusions	225
8.2	Relevance for practice	231
8.3	Recommendation for further research	232
APPENDICES	235
REFERENCES	255

List of tables

Table 1.1: Potential for a fully loaded freight train to remove lorries (after Network Rail, 2010).....	1
Table 1.2: Freight marginal cost (after McCullough, 2007)	2
Table 2.1: Sources of fouling in UK (after Selig and Waters, 1994).....	14
Table 2.2: Fouling category based on FI and k_h (Selig et al., 1993).....	15
Table 2.3: FI comparison of two methods (after Aursudkij, 2007).....	16
Table 2.4: PSD of stoneblowing aggregate (after Network Rail, 2009)	18
Table 3.1: The class number and name, maximum speed and approximate axle load of some passenger trains (after Network Rail, 2011)	25
Table 3.2: Line categorisation based on daily traffic load (after UIC, 2009a).....	26
Table 3.3: Required DSSS (k) (maximum axle load 25 tonnes) (after Network Rail, 2005)	28
Table 3.4: Data used to create the graphs of percentage of wheel load exerted on the sleepers.....	32
Table 3.5: Influence factor A (top line) and B (bottom line) for vertical stresses due to a uniformly loaded circular area at any distance (a) from the circular centre (after Whitlow, 2001)	36
Table 3.6: Influence factors due to strip load (after Das, 2008).....	37
Table 3.7: Summary of analysis results of the stress under the ballast by presented methods.....	39
Table 3.8: Material properties used in finite element analyses (after Powrie et al., 2007)	40
Table 4.1: The Original (2000) ballast specification (after Network Rail, 2000)	48
Table 4.2: Ballast grading accordance with EN13450 (after British Standards Institution, 2002, British Standards Institution, 2013).....	49
Table 4.3: The New (2005) specification for ballast particles (after Network Rail, 2000)	49
Table 4.4: Recommended AREMA ballast gradings (after AREMA, 2000).....	51
Table 4.5: Modified AREMA No.3 grading (after Norfolk Southern Corporation, 2011)	51
Table 4.6: CNR ballast grading (after Canadian National Railway, 2007)	52
Table 4.7: CP Rail ballast gradings (after Canadian Pacific Rail, 1984).....	52
Table 4.8: SAA Ballast specification (after Indraratna and Salim, 2005)	53
Table 4.9: Queensland rail ballast specification (after Indraratna and Salim, 2005)	53
Table 4.10: ARTC ballast specification (after Australian Rail Track Corporation Ltd, 2007).....	53
Table 4.11: RailCorp ballast specification (after RailCorp Engineering Specification Track, 2009)	54
Table 4.12: Comparison of Australian standard and recommended ballast gradings (after Indraratna and Salim, 2005)	56
Table 5.1: Properties of ballast in Shenton's test.....	67
Table 5.2: Ballast constant, C (after Stewart and Selig, 1982b)	77
Table 6.1: Results of rubber mat test using penetrometer.....	95
Table 6.2: The procedure of loading and unloading load in rubber mat test.....	96
Table 6.3: Results of rubber mat test using the Instron machine.....	97
Table 6.4: Results of rubber mat test using ballast sandwich on the 15 mm thickness.....	99
Table 6.5: Results of rubber mat test using ballast sandwich on 6 mm thickness	99
Table 6.6: Results of ballast sandwich test without rubber mat.....	100
Table 6.7: The max and min RI values recorded on the ranges of pressure paper.....	108
Table 6.8: The detail of number and location of pressure papers instrumentation.....	109
Table 6.9: Calibration values of LVDTs used.....	110

Table 6.10: Dimension of the sleepers used in the tests.....	119
Table 6.11: Comparison of ballast properties from Cliffe Hill quarry to the current standard NR ballast product specification (after Network Rail, 2000)	119
Table 6.12: UK aggregate size designations (after British Standards Institution, 2009c).....	119
Table 6.13: The average of PSD test results of Cliffe Hill quarry ballast	120
Table 6.14: The percentage of proportion each grading in each variant grading	121
Table 6.15: Key detail of variant ballast gradings	122
Table 6.16: Permeability coefficients (k_p) of tested ballast gradings.....	123
Table 6.17: Properties of USPs used in the tests (after Tiflex, 2013).....	124
Table 6.18: Stiffness categorisation of USPs (after Auer et al., 2013).....	124
Table 6.19: The material properties of sand used as a fouling material	128
Table 6.20: A comparison of material properties of gabbro and granite (after Marinos and Hoek, 2001, SBD Crushers, 2010).....	129
Table 6.21: The dimensions of a grid, ballast and sand parameters, and the calculated mass of sand.....	130
Table 6.22: The current standard NR, 1/3 rd and 1/5 th scales ballast gradings (after Ajayi, 2014).....	132
Table 6.23: The properties of polypropylene and polyethylene fibres used in the tests (after Ajayi, 2014)	132
Table 6.24: Parameter space investigated.....	134
Table 6.25: Detail of sleeper intervention tests carried out	134
Table 6.26: Detail of ballast intervention tests carried out.....	135
Table 6.27: Detail of sand ingress tests carried out.....	135
Table 7.1: Permanent settlement and percentage reduction of permanent settlement into baseline test at number of loading cycles of each sleeper intervention test.....	139
Table 7.2: Permanent settlement and percentage reduction of permanent settlement in twin-block sleeper tests with number of loading cycles with USP inclusion	140
Table 7.3: Permanent settlement and percentage reduction of permanent settlement into baseline test at number of loading cycles of each ballast intervention test	141
Table 7.4: The most to the least of permanent settlement reduction and percentage of improvement at 2 million (M) to 3M loading cycles	142
Table 7.5: The behaviour of deflection at ends and middle section of sleeper and the results into the sleeper in each sleeper intervention test.....	144
Table 7.6: The behaviour of deflection at ends and middle section of sleeper and the results into the sleeper in each sleeper intervention test.....	146
Table 7.7: Average four corner spring stiffness and percentage change of the spring stiffness compared to the baseline test at number of loading cycles of each sleeper intervention test.....	149
Table 7.8: Average four corner spring stiffness and percentage reduction of spring stiffness into twin-block sleeper test at number of loading cycles of each test with USPs inclusion.....	150
Table 7.9: Area weighted spring stiffness and percentage reduction of spring stiffness into baseline test at number of loading cycles of each sleeper intervention test.....	150
Table 7.10: Area weighted spring stiffness and percentage reduction of spring stiffness into twin-block sleeper test at number of loading cycles of each test with USPs inclusion.....	150
Table 7.11: Average four corner spring stiffness and percentage reduction of spring stiffness into baseline test at number of loading cycles of each ballast intervention test	152
Table 7.12: Area weighted spring stiffness and percentage increase of spring stiffness into baseline test at number of loading cycles of each ballast intervention test.....	153
Table 7.13: Key earth pressure ratios	158

Table 7.14: Summary of the highest and lowest of measured earth pressures in data recorded by all plates for all loading cycles in sleeper intervention tests.....	159
Table 7.15: Summary of the highest and the lowest of measured earth pressures in data recorded by all plates for all loading cycles in ballast intervention tests.....	159
Table 7.16: The number of particle contact at sleeper/ballast interface in sleeper intervention tests	164
Table 7.17: The number of particle contact at sleeper/ballast interface in ballast intervention tests.	164
Table 7.18: The percentage of particle contact area at sleeper/ballast interface in sleeper intervention tests.....	164
Table 7.19: The percentage of particle contact area at sleeper/ballast interface in ballast intervention tests.....	165
Table 7.20: The number and area of particle contacts at the ballast/sleeper interface in each test, and the implied average contact pressure.....	165
Table 7.21: The number and area of particle contacts at the ballast/sleeper interface in each test, and the implied average contact pressure.....	165
Table 7.22: Proportions of the ballast/subgrade interface area over which the contact pressure is at least 0.5MPa in sleeper intervention tests.....	168
Table 7.23: Proportions of the ballast/subgrade interface area over which the contact pressure is at least 0.5MPa in ballast intervention tests.....	169
Table 7.24: Proportions of the ballast/subgrade interface area over which the contact pressure is at least 2.5MPa in sleeper intervention tests.....	169
Table 7.25: Proportions of the ballast/subgrade interface area over which the contact pressure is at least 2.5MPa in ballast intervention tests.....	169
Table 7.26: The magnitude of particle pressure at ballast/subgrade interface in sleeper intervention tests.....	170
Table 7.27: The magnitude of particle pressure at ballast/subgrade interface in ballast intervention tests.....	170
Table 7.28: The range of load per m ² subgrade area on sleeper intervention tests.....	170
Table 7.29: The range of load per m ² subgrade area on ballast intervention tests.....	171
Table 7.30: Magnitude of vertical pressure on subgrade determined by both pressure paper and 2:1 load spread methods and its comparison factor in sleeper intervention tests.....	171
Table 7.31: Magnitude of vertical pressure on subgrade determined by both pressure paper and 2:1 load spread methods and its comparison factor in sleeper intervention tests.....	171
Table 7.32: Proportions of the ballast/wall interface area over which the contact pressure is at least 0.5MPa in sleeper intervention tests.....	172
Table 7.33: Proportions of the ballast/wall interface area over which the contact pressure is at least 0.5MPa in ballast intervention tests.....	172
Table 7.34: Proportions of the ballast/wall interface area over which the contact pressure is at least 2.5MPa in sleeper intervention tests.....	172
Table 7.35: Proportions of the ballast/wall interface area over which the contact pressure is at least 2.5MPa in ballast intervention tests.....	173
Table 7.36: The magnitude of particle pressure at ballast/wall interface in sleeper intervention tests.....	173
Table 7.37: The magnitude of particle pressure at ballast/wall interface in ballast intervention tests	173
Table 7.38: The range of load per m ² ballast area on sleeper intervention tests.....	173
Table 7.39: The range of load per m ² ballast area on ballast intervention tests.....	174
Table 7.40: Magnitude of ballast pressure determined by both pressure paper and pressure plate methods and its comparison factors in sleeper intervention tests.....	174

Table 7.41: Magnitude of ballast pressure determined by both pressure paper and pressure plate methods and its comparison factors in ballast intervention tests	174
Table 7.42: Measured and potential contacts	178
Table 7.43: The rank of number of ballast particle breakages (found by visual observation) on sleeper and ballast interventions	179
Table 7.44: The percentage of total loss of mass of ballast particles on sleeper and ballast intervention tests	183
Table 7.45: Permanent settlement and percentage reduction of permanent settlement into baseline test at number of loading cycles (percentage of sand ingress introduced) in sand ingress test.....	194
Table 7.46: Four corner spring stiffness and percentage increase of spring stiffness into baseline test at number of loading cycles (percentage of sand ingress introduced) in sand ingress test	197
Table 7.47: Area weighted spring stiffnesses and percentage increase of spring stiffness into baseline test at number of loading cycles (percentage of sand ingress introduced) in sand ingress test.....	198
Table 7.48: Summary of the highest and the lowest of measured earth pressure among the data recorded by all plates for entire loading cycles in the baseline and sand ingress tests.....	200
Table 7.49: The number of particle contact at sleeper/ballast interface in baseline and sand ingress tests	201
Table 7.50: The percentage of particle contact area at ballast/subgrade interface in baseline and sand ingress tests rated by 2.5-10MPa pressure paper	202
Table 7.51: The percentage of particle contact area at ballast/subgrade interface in baseline and sand ingress tests rated by 10-50MPa pressure paper	202
Table 7.52: The magnitude of particle pressure at ballast/subgrade interface in baseline and sand ingress tests.....	203
Table 7.53: The range of load per m ² subgrade area in baseline and sand ingress tests.....	203
Table 7.54: Magnitude of vertical pressure on subgrade analysed by both pressure paper and 2:1 load spread methods and its comparison factor for baseline and sand ingress tests.....	203
Table 7.55: Proportions of the ballast/wall interface area over which the contact pressure is at least 2.5MPa in baseline and sand ingress tests.....	203
Table 7.56: The magnitude of particle pressure at ballast/wall interface in baseline and sand ingress tests	204
Table 7.57: The range of load per m ² ballast area in baseline and sand ingress tests.....	204
Table 7.58: Magnitude of ballast pressure analysed from pressure paper and measured by pressure plate and its comparison factor in baseline and sand ingress tests	204
Table 7.59: The number of ballast particle breakages found in baseline and sand ingress test based on visual observation	207
Table 7.60: Percentage of total loss of mass of randomly picked ballast used in baseline and sand ingress tests.....	209
Table 7.61: Detail of the combination of sleeper and ballast interventions carried out.....	210
Table 7.62: Detail of settlement models for comparison	214
Table 7.63: The exponent numbers obtained by curve fitting for each test.....	218
Table 7.64: Ballast property and the corresponding permanent settlement at the first loading cycle for each test using the same sleeper type (G44 sleeper) and load magnitude (98.1kN).....	220
Table 7.65: Load efficiency, sleeper material, shape, interface, shoulder slope and reinforcement factors for the proposed ballast settlement model.....	221
Table 8.1: Italian State railways specification for ballast (after Geological Society, 2001)	235
Table 8.2: Spanish railways specification for ballast (after Geological Society, 2001)	235
Table 8.3: French railways ballast PSD (after Indraratna and Salim, 2005).....	235

Table 8.4: Swedish ballast specification (after Tolppanen et al., 2002).....	236
Table 8.5: Ballast specification in Turkey (after Kaya, 2004).....	236
Table 8.6: Diameter railway ballast particle based on type of sleepers (after Ministry of Science and Technology Department of Technical and Vocational Education, 2007).....	236
Table 8.7: Ballast specification in India (after East Central Railway, 2005)	236
Table 8.8: Loading and unloading data of the test on rubber mats using the Instron machine	238
Table 8.9: Ballast sandwich test results on the 15 mm rubber mat thickness.....	239
Table 8.10: Ballast sandwich test results on the 6 mm rubber mat thickness.....	240
Table 8.11: Ballast sandwich test results without rubber mat	240
Table 8.12: Calibration results of pressure paper ranged 0.5-2.5MPa for various applied loads and holding times.....	242
Table 8.13: Calibration results of pressure paper ranged 2.5-10MPa for various applied loads and holding times.....	242
Table 8.14: Calibration results of pressure paper ranged 10-50MPa for various applied loads and holding times.....	242

List of figures

Figure 1.1: Cross sections of track structure (after Esveld, 2001)	2
Figure 1.2: Substructure contributions to settlement (after Selig and Waters, 1994).	3
Figure 2.1: Cross section of slab track (after Esveld, 2001).....	9
Figure 2.2: Slab track running lines (PORR TECHNOBAU UND UMWELT AG, 2014).....	9
Figure 2.3: Truck structure components (after Selig and Waters, 1994)	11
Figure 2.4: Vertical displacement of various ballast thicknesses on soft and stiff clay subgrade respectively under 10 tonnes axle load analysed by finite element approach (Allan, 2012).....	12
Figure 2.5: Cross section railway track structure (Selig and Waters, 1994)	13
Figure 2.6: Fouled railway track (Kaewunruen, 2011).....	13
Figure 2.7: Ballast fouling phases (after Huang and Tutumluer, 2011).....	14
Figure 2.8: Sources of ballast fouling in North America (Selig and Waters, 1994) and Australia (Indraratna et al., 2011).....	15
Figure 2.9: Effect of particle rearrangement on particle breakage (Selig and Waters, 1994).....	18
Figure 2.10: Rail cross section	21
Figure 2.11: Fishplate connection system (De Bold, 2011)	21
Figure 2.12: CWR (De Bold, 2011)	22
Figure 3.1: Track category based on EMGTPA and speed (Railway Group Standard, 1999)	27
Figure 3.2: Required trackbed thickness (Network Rail, 2005).....	28
Figure 3.3: An illustration of uplift force occurrences (after Selig and Waters, 1994).....	29
Figure 3.4: Sources of impact force on the track (after Indraratna et al., 2011).....	30
Figure 3.5: Vertical wheel load distribution (Esveld, 2001)	30
Figure 3.6: BOEF diagram (after Esveld, 2001).....	31
Figure 3.7: Percentage of wheel load carried by sleepers for various k values, $a = 650 \text{ mm}$ and $I = 30383000 \text{ mm}^4$	32
Figure 3.8: Percentage of wheel load carried by centre sleeper for various rail dimensions.....	33
Figure 3.9: Percentage of wheel load carried by centre sleeper for various a and $I = 30383000 \text{ mm}^4$	33
Figure 3.10: Percentage of load carried by sleeper on various substructure stiffnesses (after INNOTRACK, 2008)	34
Figure 3.11: Axle load distribution factor (DF) (after Standards Australia, 2003)	34
Figure 3.12: Axle load DF for the sleeper (after Remennikov and Kaewunruen, 2007).....	35
Figure 3.13: Vertical load distribution onto the trackbed (Selig and Waters, 1994)	35
Figure 3.14: Stress due to strip load (after Das, 2008).....	37
Figure 3.15: Fadum's chart influence factor for uniformly loaded rectangular area (Fadum, 1948) (after Das, 2008, Powrie, 2004, Powrie, 2014b, Whitlow, 2001)	38
Figure 3.16: Diagram of 2:1 load spread method (after Doyle, 1980, after Esveld, 2001, Radampola, 2006).....	38
Figure 3.17: Comparison of vertical stress distribution under a uniformly loaded circular area by load spread and Boussinesq's methods (after Doyle, 1980, Radampola, 2006)	39
Figure 3.18: Variation of vertical stress with depth below the sleeper end for different mesh densities (Powrie et al., 2007).....	40
Figure 4.1: Flakiness index gauge.....	46
Figure 4.2: Elongation index gauge	46

Figure 4.3: Comparison of NR's ballast original 2000 into new 2005 specification	50
Figure 4.4: PSD of modified AREMA No 3 used by NSC	51
Figure 4.5: Comparison of CP2 and CNR ballast gradings	52
Figure 4.6: Comparison of EN13450 category A to Australian railway ballast gradings	54
Figure 4.7: PSD of ballast for cyclic triaxial tests (Indraratna and Salim, 2005)	55
Figure 4.8: Axial and volumetric strain of different PSD tested (Indraratna and Salim, 2005).....	55
Figure 4.9: Effect of PSD on particle breakage (Indraratna and Salim, 2005).....	56
Figure 4.10: Comparison of PSD of Australian standard and the recommended grading	57
Figure 4.11: Norwegian railway ballast compared to AREMA No 4 gradings	57
Figure 4.12: Average of permanent vertical deformation against number of loads (Nalsund, 2010)...	58
Figure 4.13: Permanent axial deformation compared with amount of ballast particle breakage smaller than D_{Min} in test specimen (Nalsund, 2010).....	58
Figure 4.14: Normalized 0.45 power grading chart (Tutumluer et al., 2009)	59
Figure 4.15: PSD of observed ballast gradings (Tutumluer et al., 2009).....	60
Figure 4.16: PSD of observed ballast plotted on normalized 0.45 power (Tutumluer et al., 2009)	60
Figure 4.17: Comparison of limit of ballast gradings (Australia, U.S, Canada and UK)	62
Figure 4.18: Comparison of median ballast gradings (Australia, U.S, Canada and UK)	62
Figure 5.1: Ballast box apparatus (Stewart et al., 1985).....	65
Figure 5.2: Cross section of box test apparatus (after Stewart and Selig, 1984)	66
Figure 5.3: Horizontal stresses on side panels and on end panels respectively (Stewart et al., 1985) ..	66
Figure 5.4: PSD of ballast used in Shenton's test.....	67
Figure 5.5: Shenton's triaxial test (Shenton, 1978)	68
Figure 5.6: Permanent axial strain of triaxial sample (Shenton, 1978)	68
Figure 5.7: Track settlement (after Shenton, 1978).....	69
Figure 5.8: Close up figures of track settlement (after Shenton, 1978).....	69
Figure 5.9: Settlement of sleeper under repeated load (Okabe, 1961).....	71
Figure 5.10: Relationship between permanent strains at first and tenth load (after Shenton, 1978)....	72
Figure 5.11: Track settlement at different parts of the world (after Shenton, 1984)	72
Figure 5.12: Cross section of Jeffs and Marich's apparatus (after Jeffs and Marich, 1987)	73
Figure 5.13: Settlement curves obtained by Jeffs and Marich (after Jeffs and Marich, 1987).....	74
Figure 5.14: Settlement data obtained with first cycle shifted (after Jeffs and Marich, 1987)	74
Figure 5.15: Settlement data obtained with 50,000 cycles shifted (after Jeffs and Marich, 1987).....	74
Figure 5.16: Adjusting the coefficient ϵ_1 for varying load (after Ford, 1995).....	78
Figure 5.17: Permanent strain after first cycle for low confining stress (after Alva-Hurtado and Selig, 1981, after Ford, 1995, Selig and Alva-Hurtado, 1982).....	78
Figure 5.18: Typical idealised pressure distribution along the sleeper (AREMA, 2003a, Lees, 2009)..	83
Figure 5.19: Sleeper base contact pressure distribution (after Shenton, 1978)	84
Figure 5.20: Variation of pressure in ballast with depth (Shenton, 1978).....	84
Figure 6.1: Current SRTF apparatus.....	87
Figure 6.2: Elevation C-C.....	87
Figure 6.3: A plan view of modified SRTF apparatus.....	88
Figure 6.4: Elevation A-A of modified SRTF apparatus (after Le Pen, 2008).....	88

Figure 6.5: Elevation B-B (vertical scale exaggerated).....	88
Figure 6.6: The arrangement of loading system	89
Figure 6.7: Sample preparation for the modified SRTF apparatus test	89
Figure 6.8: Placing sleeper on the top of ballast.....	90
Figure 6.9: The arrangement of the sleeper on the ballast and instrumentation of LVDTs	90
Figure 6.10: The plan view of LVDT locations.....	90
Figure 6.11: Loading beam and load controller connection.....	90
Figure 6.12: The SRTF (a) empty and (b) ready for a test	91
Figure 6.13: A typical graph of applied static load against displacement at first loading cycle	91
Figure 6.14: Characteristic of cyclic loading applied during the tests.....	92
Figure 6.15: Sleepers deflection for section of Channel Tunnel Rail Link (CTRL) (Bowness et al., 2005).....	93
Figure 6.16: The physical appearance of (a) 15 mm and (b) 6 mm rubber mats thickness	94
Figure 6.17: Penetrometer.....	94
Figure 6.18: Applied pressure against displacement graphs of rubber mat test using penetrometer....	95
Figure 6.19: Instron machine.....	96
Figure 6.20: Rubber mat test arrangement.....	96
Figure 6.21: Applied pressure against displacement graphs of rubber mat test using the Instron machine.....	97
Figure 6.22: The steel square tube used in ballast sandwich test	98
Figure 6.23: Sample preparation for ballast sandwich tests	98
Figure 6.24: The arrangement of ballast sandwich test	98
Figure 6.25: Applied pressure against displacement graphs of rubber mat test using ballast sandwich on 15 mm thickness.....	99
Figure 6.26: Applied pressure against displacement graphs of rubber mat test using ballast sandwich on 6 mm thickness	100
Figure 6.27: Applied pressure against displacement graphs of ballast sandwich test without rubber mat	100
Figure 6.28: Comparison of the mean displacement value of ballast sandwich tests	101
Figure 6.29: The Tiflex Ltd MSH machine and Geometric Ballast Plate (GBP)	101
Figure 6.30: The results of rubber mat test on static load of MSH through flat plate and GBP.....	102
Figure 6.31: The results of rubber mat tests on dynamic load of MSH through flat plate and GBP.	102
Figure 6.32: Comparison of rubber mat test results carried out by different methods.....	103
Figure 6.33: Location of instrumented plates and dummy panels.....	104
Figure 6.34: Front face view of pressure plates, dummy panel and load cells.....	104
Figure 6.35: The types and range level of pressure papers (AJP Automotive Ltd, 2014).....	105
Figure 6.36: Two-sheet pressure paper (A J P Automotive Ltd, 2011, AJP Automotive Ltd, 2014)..	105
Figure 6.37: Mono-sheet pressure paper (A J P Automotive Ltd, 2011, AJP Automotive Ltd, 2014)	106
Figure 6.38: Standard continuous pressure chart (A J P Automotive Ltd, 2011, AJP Automotive Ltd, 2014).....	106
Figure 6.39: The pressure papers used for calibration.....	107
Figure 6.40: The set of known loads and metal rods used for calibration test.....	107

Figure 6.41: Red patches recorded on the pressure papers in calibration process.....	107
Figure 6.42: Pressures against RI for various ranges of pressure paper.....	108
Figure 6.43: The locations of pressure papers (a) on rubber mat, (b) on the wall of modified SRTF and (c) at the sleeper soffit.....	109
Figure 6.44: LVDT's instrumentation on the sleeper.....	110
Figure 6.45: An illustration of the LVDT locations on the sleeper to analyse permanent settlement by weighted area method.....	111
Figure 6.46: The arrangement of labelled pressure plates used in each test.....	113
Figure 6.47: (a) Idealised PSD, (b) visualisation of sleeper/particle contact with discrete sizes in log distribution for two particle sizes.....	115
Figure 6.48: Sieves and shaker for PSD test.....	117
Figure 6.49: PSD graphs of Cliffe Hill quarry ballast and other gradings used for the tests.....	120
Figure 6.50: PSD of variant gradings compared to NR grading.....	121
Figure 6.51: PSD of variant gradings compared to the RailCorp grading.....	122
Figure 6.52: PSD graphs for NR and 10/20 gradings used for TLB system.....	126
Figure 6.53: The TLB system under construction: (a) the upper surface of the 10/20 mm material, level with the sleeper soffit, and (b) following placement of the final covering of standard ballast ..	126
Figure 6.54: Cross section profile of TLB system test.....	126
Figure 6.55: High ballast shoulders at Haltwhistle on the railway line between Carlisle and Newcastle upon Tyne (courtesy of Prof. William Powrie).....	127
Figure 6.56: Cross section profile of standard tests.....	127
Figure 6.57: Cross section profile of RPS slope test.....	127
Figure 6.58: PSD graphs of sand used as a fouling material.....	128
Figure 6.59: PSD graphs of gabbro ballast compared to the current standard NR ballast grading....	129
Figure 6.60: PSD graphs of sand compared to PSD graphs of gabbro ballast.....	129
Figure 6.61: Notional grid pattern for quantifying mass of sand.....	130
Figure 6.62: The view of ballast after the first introduction of sand (15%) and before any loading cycles applied at (a) left shoulder slope, (b) right shoulder slope and (c) crib and ballast shoulder ..	131
Figure 6.63: The view of ballast surface (a) after 5.25 million loading cycles (assumed 100% void filled), (b) filling ballast cribs before loading, (c) ballast surface after 10 million loading cycles, and (d) ballast surface was saturated by sand at the end of test.....	131
Figure 6.64: PSD graphs of LB sand, 1/5th, and 1/3rd scaled, and NR standard ballast (Ajayi, 2014, Ajayi et al., 2014a, Ajayi et al., 2014b).....	132
Figure 6.65: The Fibres used in the tests (a) polypropylene and, (b) polyethylene (Ajayi, 2014).....	132
Figure 6.66: Fibre reinforced ballast test under construction: (a) the mixture of Polyethylene fibre with the ballast before compaction, (b) the arrangement prior to loading beam placement.....	133
Figure 7.1: Typical graph of applied static load against deformation in first load cycle.....	138
Figure 7.2: Permanent settlement graph of each sleeper intervention test.....	138
Figure 7.3: Permanent settlement graph of each sleeper intervention test after it was zeroed at 10 loading cycles.....	139
Figure 7.4: Permanent settlement graph of each ballast intervention test.....	140
Figure 7.5: Permanent settlement graph of each ballast intervention test after it was zeroed at 10 loading cycles.....	141
Figure 7.6: The average of four corner sleeper deflection of each sleeper intervention test.....	143
Figure 7.7: The average of sleeper middle section deflection of each sleeper intervention test.....	143

Figure 7.8: The average of four corner sleeper deflection of each ballast intervention test.....	145
Figure 7.9: The average of sleeper middle section deflection of each sleeper intervention test.....	145
Figure 7.10: The average four corners spring stiffness of each sleeper intervention test.....	147
Figure 7.11: The average spring stiffness obtained by area weighted method for each sleeper intervention test.....	147
Figure 7.12: Deflection graphs of USP 1 and 2, mono-block and mono-block with USP inclusions	148
Figure 7.13: Deflection graphs of USP 1 and 2, twin-block and twin-block with USP inclusions	148
Figure 7.14: Spring stiffness graphs of USP 1 and 2, mono-block and mono-block with USP inclusion	148
Figure 7.15: Spring stiffness graphs of USP 1 and 2, twin-block and twin-block with USP inclusion	149
Figure 7.16: The average of four corners spring stiffness for each ballast intervention test.....	151
Figure 7.17: The average of spring stiffness obtained by area weighted method for each ballast intervention test.....	152
Figure 7.18: The behaviour of pressure at longitudinal direction of each plate in G44 sleeper test...	154
Figure 7.19: The behaviour of pressure at longitudinal direction of each plate in twin-block sleeper test.....	154
Figure 7.20: Variation of maximum longitudinal pressure of plate 1 with the number of loading cycles for mono-block sleeper	155
Figure 7.21: Variation of minimum longitudinal pressure of plate 1 with the number of loading cycles for mono-block sleeper	155
Figure 7.22: Variation of maximum longitudinal pressure of plate 4 with the number of loading cycles for mono-block sleeper	156
Figure 7.23: Variation of minimum longitudinal pressure of plate 4 with the number of loading cycles for mono-block sleeper	156
Figure 7.24: Variation of maximum longitudinal pressure of plate 3 with the number of loading cycles for twin-block sleeper	157
Figure 7.25: Variation of minimum longitudinal pressure of plate 3 with the number of loading cycles for twin-block sleeper	158
Figure 7.26: Particle contact histories at the sleeper/ballast interface under the railseat (a, c) and the centre of the sleeper (b): mono-block sleeper, effect of sleeper material.....	161
Figure 7.27: Particle contact histories at the sleeper/ballast interface: G44 sleeper, effect of increasing the proportion of fine material in the ballast	162
Figure 7.28: Particle contact histories at the sleeper/ballast interface: G44 sleeper, effect of a modified TLB system	162
Figure 7.29: Particle contact histories at the sleeper/ballast interface: G44 sleeper, effect of a RPS slope	162
Figure 7.30: Particle contact histories at the sleeper/ballast interface: G44 sleeper, effect of fibre reinforced ballast	163
Figure 7.31: Particle contact histories at the sleeper/ballast interface: G44 sleeper, effect of USPs..	163
Figure 7.32 Particle contact histories at the sleeper/ballast interface: twin-block concrete sleeper, effect of USPs	163
Figure 7.33. Contact areas recorded at the ballast/subgrade interface with mono-block sleepers made of different materials.....	166
Figure 7.34: Contact areas recorded at the ballast/subgrade interface with G44 sleepers and effect of increasing the proportion of fine material in the ballast	166

Figure 7.35. Contact areas recorded at the ballast/subgrade interface with G44 sleepers and TLB system.....	167
Figure 7.36: Contact areas recorded at the ballast/subgrade interface with G44 sleepers and RPS slopes	167
Figure 7.37: Contact areas recorded at the ballast/subgrade interface with G44 sleepers and fibre reinforced.....	167
Figure 7.38: Contact areas recorded at the ballast/subgrade interface with G44 sleeper and USPs..	167
Figure 7.39. Contact areas recorded at the ballast/subgrade interface with a twin-block concrete sleeper and USPs	168
Figure 7.40. Number of contacts versus D50: measurements and estimates (dashed lines)	177
Figure 7.41. Number of contacts versus D50: measurements and estimates (dashed lines)	178
Figure 7.42: Typical ballast particle breakage identified by visual observation.....	179
Figure 7.43: PSD graphs of ballast in baseline test, before and after the test.....	180
Figure 7.44: PSD graphs of ballast in twin-block test, before and after the test	181
Figure 7.45: PSD graphs of ballast in variant 3 test, before and after the test.....	181
Figure 7.46: PSD graphs of randomly selected particles on variant 1 before and after test	182
Figure 7.47: PSD graphs of randomly selected particles on twin-block before and after test.....	182
Figure 7.48: PSD graphs of randomly selected particles on variant 2 before and after test	182
Figure 7.49: PSD graphs of randomly selected particles on variant 3 before and after test	183
Figure 7.50: Ballast particle movements on the shoulder slope at (a) prior to testing, (b) during harvesting the data at 0.25 million loading cycles and (c) the end of twin-block sleeper test	184
Figure 7.51: Ballast particle movements on the shoulder slope at (a) prior to testing, (b) during harvesting the data at 0.25 million loading cycles and (c) the end of variant 3 test	185
Figure 7.52: Ballast particle movements on the shoulder slope at (a) prior to testing, (b) during harvesting the data at 0.25 million loading cycles and (c) the end of RPS slope test.....	185
Figure 7.53: Permanent settlement of steel and plastic tests compared with other sleeper and ballast intervention tests after zeroed at 10 loading cycles.....	186
Figure 7.54: A sleeper chair for a proper rail arrangement on plastic and timber sleepers.....	187
Figure 7.55: Average sleeper ends deflection of the tests on steel and plastic sleepers compared with the baseline test.....	187
Figure 7.56: Average middle section of sleeper deflection of the tests on steel and plastic sleepers compared with the baseline test	188
Figure 7.57: Average sleeper deflection near the railseat of the tests on steel and plastic sleepers	188
Figure 7.58: Deflected shape of steel sleeper (hogging) at 3 million loading cycles.....	189
Figure 7.59: Deflected shape of plastic sleeper at 3 million loading cycles	189
Figure 7.60: The average spring stiffness of the tests using steel and plastic sleepers compared with spring stiffness of other sleeper and ballast intervention tests	190
Figure 7.61: The average of spring stiffness at the location of near railseat in the tests using steel and plastic sleepers compared to spring stiffness of other tests	191
Figure 7.62: The average of spring stiffness at each section of steel sleeper.....	191
Figure 7.63: The average of spring stiffness at each section of plastic sleeper	192
Figure 7.64: Permanent settlement graphs of baseline and sand ingress tests	193
Figure 7.65: Permanent settlement graphs of baseline and sand ingress tests zeroed after 10 loading cycles.....	193
Figure 7.66: The average four corner sleeper deflection for baseline and sand ingress tests	195

Figure 7.67: The average of sleeper middle section deflection of baseline and sand ingress test.....	195
Figure 7.68: Average four corner spring stiffness of baseline and sand ingress tests.....	196
Figure 7.69: Spring stiffness averaged by area weighted method of baseline and sand ingress tests ..	197
Figure 7.70: Variation of maximum and minimum longitudinal ballast pressure of plate 1 with number of loading cycles for baseline and sand ingress tests.....	199
Figure 7.71: Variation of maximum and minimum longitudinal ballast pressure of plate 4 with number of loading cycles for baseline and sand ingress tests.....	199
Figure 7.72: The contact areas recorded at the ballast/sleeper interface in baseline and sand ingress tests.....	201
Figure 7.73: Contact areas recorded on the pressure paper rated 2.5-10MPa at the ballast/subgrade interface in baseline and sand ingress tests.....	202
Figure 7.74: Contact areas recorded on the pressure paper rated 10-50MPa at the ballast/subgrade interface in baseline and sand ingress tests.....	202
Figure 7.75: Ballast and sand in the modified SRTF apparatus, a) immediately after loading stage, b) with ballast and sand were removed.....	206
Figure 7.76: Appearance of ballast surface underneath the sleeper after sleeper removal viewed from opposite ends	206
Figure 7.77: Flour-like fines arising from sand crushing brought to the ballast and sleeper surface because of cyclic movement of the sleeper	206
Figure 7.78: Close up of ballast and sand under the sleeper shows the ballast/sleeper interface area for right railseats (a) progressing through to left railseat (f).....	207
Figure 7.79: PSD graphs of ballast after testing taken from different locations compared to prior to the baseline test.....	208
Figure 7.80: PSD graphs of ballast after testing taken from different locations compared to prior to the sand ingress test	208
Figure 7.81: PSD graphs of randomly selected particles on variant 3 before and after test.....	209
Figure 7.82: PSD graphs of randomly selected particles on variant 3 before and after test.....	209
Figure 7.83: Area weighted average of permanent settlement of combination 1 and other tests which had a parameter included on the combination1 test.....	211
Figure 7.84: Area weighted spring stiffness for combination 1 and other related tests	212
Figure 7.85: The spring stiffness and corresponding ballast permanent settlement (without zeroing) at 1 million loading cycles from sleeper and ballast intervention test	213
Figure 7.86: The spring stiffness and corresponding ballast permanent settlement (without zeroing) at 3 million loading cycles from sleeper and ballast intervention test	213
Figure 7.87: The spring stiffness and corresponding ballast permanent settlement (re-zeroed at 10 loading cycles) at 1 million loading cycles from sleeper and ballast intervention test	213
Figure 7.88: The spring stiffness and corresponding ballast permanent settlement (re-zeroed at 10 loading cycles) at 3 million loading cycles from sleeper and ballast intervention test	214
Figure 7.89: Comparison of permanent settlement graphs based on previous models compared to the modified SRTF apparatus data.....	215
Figure 7.90: A close up view of ballast settlement graphs based on previous models and the modified SRTF data.....	215
Figure 7.91: Ballast permanent settlement graphs of baseline test for sleeper and ballast interventions (20 tonnes axle load) and baseline test for sand ingress test (32 tonnes axle load).....	216
Figure 7.92: Curve fitting of two baseline data tests using logarithmic curve	217
Figure 7.93: Curve fitting of two baseline data tests using power curve	217
Figure 7.94: Linear curve fitting for the influence of higher load to the exponent number	219

Figure 7.95: Curve fitting to determine a relationship between porosity (n) and permanent settlement at the first loading cycle	220
Figure 7.96: Comparison of ballast permanent settlement graphs of some tests obtained by the modified SRTF apparatus and the results of the proposed ballast settlement model	222
Figure 7.97: Comparison of ballast permanent settlement graphs obtained by the proposed settlement model and the modified SRTF apparatus test.....	223
Figure 8.1: Applied pressure against deflection graphs of rubber mat tests using Instron machine..	238
Figure 8.2: Applied pressure against deflection graphs of ballast sandwich test on 15 mm rubber mat thickness.....	239
Figure 8.3: Applied pressure against deflection graphs of ballast sandwich test on 6 mm rubber mat thickness.....	240
Figure 8.4: Applied pressure against deflection graphs of ballast sandwich test without rubber mat	241
Figure 8.5: PSD graphs of ballast in different locations on plastic sleeper test, before and after testing	243
Figure 8.6: PSD graphs of ballast in different locations on timber sleeper test, before and after testing	243
Figure 8.7: PSD graphs of ballast in different locations on steel sleeper test, before and after testing	243
Figure 8.8: PSD graphs of ballast in different locations on mono-block sleeper with USP 1 test, before and after testing.....	244
Figure 8.9: PSD graphs of ballast in different locations on mono-block sleeper with USP 2 test, before and after testing.....	244
Figure 8.10: PSD graphs of ballast in different locations on twin-block sleeper with USP 1 test, before and after testing.....	244
Figure 8.11: PSD graphs of ballast in different locations on twin-block sleeper with USP 2 test, before and after testing.....	245
Figure 8.12: PSD graphs of ballast in different locations on variant 1 test, before and after testing.	245
Figure 8.13: PSD graphs of ballast in different locations on variant 2 test, before and after testing.	245
Figure 8.14: PSD graphs of ballast in different locations on RPS slope test, before and after testing	246
Figure 8.15: PSD graphs of ballast in different locations on fibre test, before and after testing.....	246
Figure 8.16: PSD graphs of randomly selected particles on plastic sleeper before and after test.....	247
Figure 8.17: PSD graphs of randomly selected particles on timber sleeper before and after test	247
Figure 8.18: PSD graphs of randomly selected particles on steel sleeper before and after test	247
Figure 8.19: PSD graphs of randomly selected particles on mono-block + USP 1 before and after test	248
Figure 8.20: PSD graphs of randomly selected particles on mono-block + USP 2 before and after test	248
Figure 8.21: PSD graphs of randomly selected particles on twin-block + USP 1 before and after test	248
Figure 8.22: PSD graphs of randomly selected particles on twin-block + USP 2 before and after test	249
Figure 8.23: PSD graphs of randomly selected particles on TLB before and after test	249
Figure 8.24: PSD graphs of randomly selected particles on RPS slope before and after test.....	249
Figure 8.25: PSD graphs of randomly selected particles on RPS slope before and after test.....	250

Figure 8.26: Ballast particle movements on the shoulder slope at (a) prior to testing, (b) during harvesting the data at 0.25 million loading cycles and (c) the end of mono-block sleeper with USP 1 test.....	251
Figure 8.27: Ballast particle movements on the shoulder slope at (a) prior to testing, (b) during harvesting the data at 0.25 million loading cycles and (c) the end of mono-block sleeper with USP 2 test.....	251
Figure 8.28: Ballast particle movements on the shoulder slope at (a) prior to testing, (b) during harvesting the data at 0.25 million loading cycles and (c) the end of twin-block sleeper with USP 1 test	251
Figure 8.29: Ballast particle movements on the shoulder slope at (a) prior to testing, (b) during harvesting the data at 0.25 million loading cycles and (c) the end of twin-block sleeper with USP 2 test	252
Figure 8.30: Ballast particle movements on the shoulder slope at (a) prior to testing, (b) during harvesting the data at 0.25 million loading cycles and (c) the end of steel sleeper.....	252
Figure 8.31: Ballast particle movements on the shoulder slope at (a) prior to testing, (b) during harvesting the data at 0.25 million loading cycles and (c) the end of plastic sleeper test.....	252
Figure 8.32: Ballast particle movements on the shoulder slope at (a) prior to testing, (b) during harvesting the data at 0.25 million loading cycles and (c) the end of timber sleeper test	253
Figure 8.33: Ballast particle movements on the shoulder slope at (a) prior to testing, (b) during harvesting the data at 0.25 million loading cycles and (c) the end of TLB system test.....	253
Figure 8.34: Ballast particle movements on the shoulder slope at (a) prior to testing, (b) during harvesting the data at 0.25 million loading cycles and (c) the end of fibre reinforced ballast test.....	253
Figure 8.35: Ballast particle movements on the shoulder slope at (a) prior to testing, (b) during harvesting the data at 0.25 million loading cycles and (c) the end of combination 1 test.....	254

List of symbols

a	Sleeper spacing
a_1	Empirical coefficient
A, B	Influence factors
A_e	An equivalent axle load
b	A pressure threshold that settlement does not occur or sleeper width
b_1	Empirical coefficient
B_{ic}	Initial degree of ballast compaction
c_1, c_2, c_3	Constants produced by regressions
C	Ballast settlement constant
C_1, C_2, C_3, C_4, C_5	Constants produced by regressions
C_b	Ballast settlement constant for box test
C_p	Permeability constant
C_{Stat}	Static stiffness of USP
C_u	Uniformity coefficient
C_z	Concavity coefficient
D_{90}, D_{60}, D_{10}	Particle size 90%, 60% and 10% of the sample will be finer than
d	Aggregate size being considered
d_1	Permanent vertical settlement after 1 st cycle
d_N	Permanent vertical settlement after N th cycles
d_{max}, d_{min}	Maximum, minimum particle sizes
D	Maximum aggregate size
$D(x)$	Shearing force
E	Void ratio
e_b, e_f	Void ratio of clean ballast and fouling material
f	Angularity factor for rounded grains
F	Equivalent load amplitude using the linear mean value
g	Parameter which adjusts curve for fineness or coarseness
G_c	Aggregate grading
G_{sb}, G_{sf}	Specific gravity of clean ballast and fouling material
H	Granular layer thickness (m)
I_{fsl}	Influence factors for strip load
I_R	Influence factor for rectangular area
K_1, K_2	Constant values
K_{min}	Minimum mobilised lateral earth pressure ratio
k	Vertical track modulus per unit length
k_d	Vertical track modulus per sleeper spacing
k_i	Spring stiffness (kN/mm)
k_h	Hydraulic conductivity
k_p	Permeability coefficient
K_{max}	Maximum mobilised lateral earth pressure ratio
K_s	A factor as a function of sleeper type and size
k_s	Modulus of subgrade reaction
L	The lift given by the tamping machine or sleeper length
L_{ef}	Higher load correction factor

$M(x)$	Moment
M_b, M_f	Dry mass of clean ballast and fouling material
M_{sf}	Sleeper material factor
n	Initial porosity of ballast
N	Number of repeated loading cycles
P	A concentrated wheel load
$P_{4.75}, P_{0.075}, P_{13.2}$	Percentage passing sieve size 4.75 mm, 0.075 mm and 13.2 mm
P_c	Allowable subgrade pressure recommended by AREA (138kPa)
P_m	Vertical stress applied on the ballast surface
P_p	Percentage finer than an aggregate size
p	Sleeper/ballast contact pressure
$p(x)$	The continuous contact pressure between the longitudinal sleeper and base
$q(x)$	Vertical wheel load
q	Average uniform pressure over the loaded area (kPa)
Q	Axle load
r	The scaling factor
R	Radius of the loaded area (m)
R_f	Reinforcement factor
R_s	The logarithmic settlement rate
S_1	Settlement at first loading cycle
S	Settlement (mm)
S_a	Second period of settlements
S_i	Initial settlement due to the initial loading cycles
S_N	Settlement after N loading cycles
S_{fr}	Coefficient related to the running speed of ordinary freight trains
S_{if}	Sleeper/ballast interface factor
SL_f	Shoulder slope profile factor
S_s	Specific surface
S_{sf}	Sleeper shape factor
S_{WN}	Permanent settlement weighted area method
V_1, V_2	Void volume of re-compacted ballast particle fouling material
V_{pf}	Magnitude of vertical pressure at sleeper soffit
$w(x)$	Deflection
z	Vertical depth to any points beneath the sleeper
ϵ_1	Permanent strain at first loading cycles
ϵ_N	Permanent strain after N^{th} loading cycles
$\theta(x)$	Angular deflection
ϕ_{mob}	Mobilised angle of effective shearing resistance
φ	Friction angle
δ	Range of movement (deflection) read by the LVDT
δ_{Se}	Average sleeper end deflection
δ_{Sm}	Average sleeper middle deflection
σ	Stress under the sleeper
σ_1, σ_3	The major and minor principal stresses
σ_z	Vertical stress at any point z

List of abbreviations

AC	Alternating current
AREA	American Railway Engineering Association
AREMA	American railway engineering and maintenance-of-way association
ARTC	Australian Rail Track Corporation
ASTM	American standard testing for material
BOEF	Beam on elastic foundation
BS	British Standard
CNR	Canadian National Railway
CP	Canadian Pacific
CTRL	Channel Tunnel Rail Link
CWR	Continuously welded rail
DB	Deutsche Bahn
DC	Direct current
DEM	Discrete element modelling
DMU	Diesel multiple unit
DF	Distribution factor
DSSS	Dynamic sleeper support stiffness
EMGTPA	Equivalent Million Gross Tonnes per Annum
EMU	Electric multiple unit
EN	Euro Norm
FI	Fouling index
FWD	Falling weight deflectometer
GBP	Geometric ballast plate
HGV	Heavy goods vehicles
HS 1	High speed 1
ICFEP	Imperial College's finite element program
IM	Infrastructure managers
LB	Leighton Buzzard
Ltd	Limited
LVDTF	Linear variable differential transformer
MSH	Mayes servo hydraulic
NR	Network rail
NSC	Norfolk Southern Corporation
ORE	Office for research and experiments
PBI	Pneumatic ballast injection
PSD	Particle size distribution
PVC	Percentage void contamination
RI	Red intensity
RIC	Rail Infrastructure Corporation
RGS	Railway group standard
RPS	Re-profile shoulder
RTF	Railway test facility
SRTF	Southampton railway testing facility
STBSA	Standard track ballast and stone blower aggregate

TGV	Train a grande vitesse
TLB	Two layered ballast
UIC	Union Internationale des Chemins de Fer
UK	The United Kingdom
US	The United States
USP	Under sleeper pad
VCI	Void contaminant index

Declaration of authorship

I, Taufan Abadi

declare that the thesis entitled

Effect of Sleeper and Ballast Interventions on Rail Track Performance

and the work presented in the thesis are both my own, and have been generated by me as the result of my own original research. I confirm that:

- This work was done wholly or mainly while in candidature for a research degree at this University;
- Where any part of this thesis has previously been submitted for a degree or any other qualification at this University or any other institution, this has been clearly stated;
- Where I have consulted the published work of others, this is always clearly attributed;
- Where I have quoted from the work of others, the source is always given. With the exception of such quotations, this thesis is entirely my own work;
- I have acknowledged all main sources of help;
- Where the thesis is based on work done by myself jointly with others, I have made clear exactly what was done by others and what I have contributed myself;
- Parts of this work are in review for publication as:
Abadi, T., Le Pen, L., Zervos, A., Priest, J. and Powrie, W (2014).“Measuring the number and area of ballast particle contacts by pressure paper”. *ASCE Geotechnical Special Publication* (In Press).
Abadi, T., Le Pen, L., Zervos, A., Priest, J. and Powrie, W (2014).“Measuring the area and number of ballast particle contacts at sleeper/ballast and ballast/subgrade interfaces”. *The International Journal of Railway Technology (IJRT)* (In Press).

Signed:

Date:.....

Acknowledgements

In the name of Allah, the beneficent and the merciful. Praise is to Allah, the almighty, on whom ultimately I depend for sustenance and guidance.

This thesis is the last stage of my research journey in obtaining a PhD with the support and encouragement of numerous people hence I would like to thank all those people who made this research possible.

First of all, I would like to express my deepest gratitude to my supervisory team consisting of Prof. William Powrie, Dr. Antonis Zervos and Dr. Jeffrey Priest (former academic supervisor at the University of Southampton) for the opportunity given to carry out this research and for allowing me to grow as a researcher. Your advice on my research has been invaluable. I am extremely indebted to my guide Dr. Louis Le Pen, who is also a member of my supervisory team for guiding me at the critical stage on early year of my PhD, his understanding, encouragement, personal attention, valuable advice, constructive criticism and extensive discussions around my research which have provided good and smooth basis for my PhD. I also gratefully acknowledge Dr. Anthony Lock for his help in providing a solution to a problem in processing huge data tests which made my work much easier.

I owe a great deal of appreciation and gratitude to Jacqui Holmes, Carole Walker, Rod Anderson, Steven Alexander, Geoff Watson, Dave Lynock, Earl Peters, Roger Newton, Harvey Skinner and Karl Scammell who were always available for me to sort out all administration issues and to provide technical and labour supports during my research. My special acknowledgment goes to Jacquy Newton, Amy Parker, Victoria McOuat and Kate Robinson for proof reading my English in this thesis.

My warm appreciation is due to Sam Rushworth, William Nock, Sinthuja Aingaran, Aingaran Sellaiya, Letisha Rorke, Sujeevan Vinayagamoorthy, Edgar Ferro and my entire fellow PhD student as well as my fellow lab mates who provided covers for the works carried out during the weekend and/or university closure periods. A very best appreciation goes to Femi Ajayi with whom not only this PhD journey but also the story of happiness and sadness are always shared.

I would like to thank my parents and family in Indonesia who support me continuously. Words are not enough to express how grateful I am for your prayer and spiritual support through my life in the UK. I'm also very much thankful to my fellow Indonesians in Southampton who are always willing to help in any circumstances.

Finally, thanks to Tiflex Ltd who provided under sleeper pads for testing and last but not least, for financial support I would like to thank EPSRC (Engineering and Physical Sciences Research Council) where the funding formed part of TRACK21 project (grant: EP/H044949).

Chapter 1: Introduction

1.1 Background of the study

There are many transportation modes to carry passenger and freight services. However, a changed attitude towards environmental issues and traffic congestion on the roads has led to rail routes being used more intensively than ever before.

Train travel is far safer than air and road (www.foe.co.uk, 2001). Rail passenger services also offer other advantages such as; a generally more relaxing journey, the ability to enjoy the scenery, a less tiring journey on long distance travel, and for business travellers the ability to work whilst on the train.

Although travelling by road offers door to door delivery which rail cannot match, most train services are much faster and more reliable than road travel especially as road routes are often delayed by congestion. Reliability in delivering goods and materials is crucial to businesses and rail is able to transport high volumes by joining several carriages into trains. In the last decade freight train demand has increased by market share in a number of bulk sectors such as construction materials, coal, and waste. Freight volume from the Far East shipped into ports like Southampton and Felixstowe has increased by over 25% for freight containers transported onwards by rail (Network Rail, 2010).

Travelling by train has environmental advantages compared with other modes of transport. However, trains still have an environmental impact. In average freight train is equivalent to 50 heavy goods vehicles (HGV) that would otherwise have to use the roads. At the port of Felixstowe, there are 250,000 containers a year carried by freight trains; this is equivalent to 1,000 fewer lorries a day having to use the congested A14 (www.freightonrail.org.uk, 2001-2011). Network Rail (NR) claims that each freight train can typically replace around 60 lorry journeys or 1.6 million lorry journeys per year and the equivalent of 55,000 lorry movements of domestic rubbish (Network Rail, 2010). Table 1.1 shows the equivalent HGVs that a train can replace by commodity type.

Table 1.1: Potential for a fully loaded freight train to remove lorries (after Network Rail, 2010)

Commodity	Fully loaded train potential (tonnes)	Equivalent number of HGV
Coal	1,500	52
Metal and ore	1,000 to 2,500	60
Construction materials	1,500 to 3,000	77
Oil and petroleum	2,000	69
Consumer goods	600 to 1,100	43
Other traffic	1,000 to 1,500	43

In comparison with road, freight rail produces less than approximately 10% nitrogen oxide and fine particulates. There is also a 76% reduction in CO₂ emissions over road freight per tonne carried and 85% less air pollution than a jet aircraft. Haulage by rail only consumes 33% as much energy as by road (Profillidis, 2006). On average, a gallon of fuel will move a tonne of goods 246 miles on a railway, but only 88 miles by road meaning that overall trains use up to 70% less energy (Network

Rail, 2010) (Train Chartering Company Ltd, 2011). Therefore, travelling by train will not only reduce CO₂ emissions that contribute to climate change but also use less energy and space.

In the United States (U.S), Gerard J. McCullough summarized in the Transportation Research Board (TRB) special report 246 P. 90 (Transportation Research Board, 1996), a comparison of the full marginal cost of freight transportation from Minnesota to Mississippi River Port by trucks and rail in representative corridors with \$/truckload as the measuring unit. Table 1.2 presents the comparison results on each category listed and shows that rail is cheaper than truck in each category.

Table 1.2: Freight marginal cost (after McCullough, 2007)

Category	Truck	Rail
Congestion	6.25	0.00
Accident	26.11	9.19
Pollution	6.75	1.43
Energy security	3.63	0.39
Noise	0.00	0.78
Public infrastructure	61.02	0.00
Carrier cost	427.94	113.0
Total	531.70	124.87

Trains can take passengers and freight anywhere and over any distance as long as there are rail tracks connecting origin to destination. Rail track consists of rails, rail fastenings, rail pads, sleepers, ballast, with or without sub-ballast on top of subgrade (Figure 1.1).

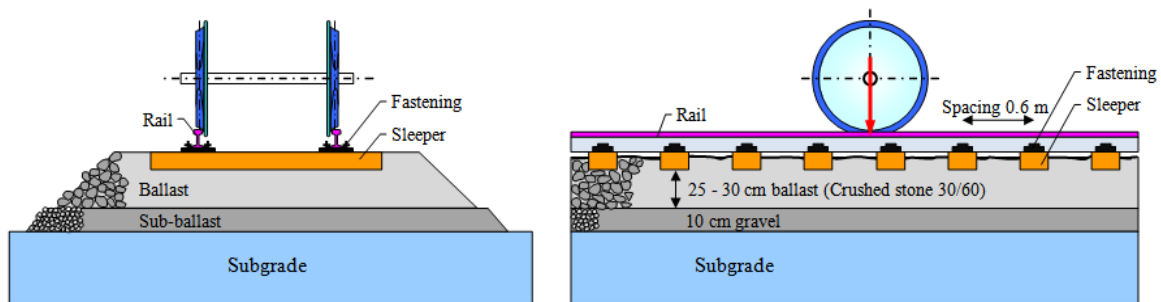


Figure 1.1: Cross sections of track structure (after Esveld, 2001)

The layer between the sleeper and the subgrade is termed the trackbed. The main functions of the trackbed are to provide stability and to reduce the pressure caused by train passage to an acceptable level without causing excessive settlement or failure of the natural ground. It may also function as a drain. Normally trackbed consists of two layers; sub-ballast and ballast. Generally sub-ballast is composed of sand while ballast is a uniformly graded, crushed, angular rock and has particle size much bigger than the sub-ballast.

Ballast is the main source of rail track deterioration. Figure 1.2 shows a typical profile of the relative contribution of substructure layers on track settlement with a good subgrade soil foundation as a comparator (Selig and Waters, 1994). Ballast generally contributes much more to the track settlement than either the sub-ballast or subgrade.

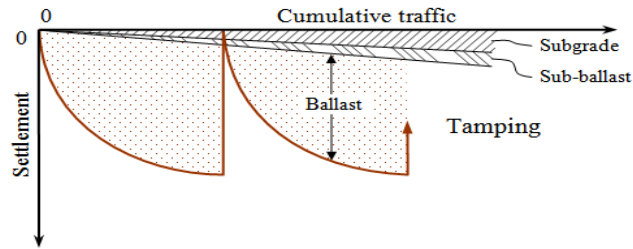


Figure 1.2: Substructure contributions to settlement (after Selig and Waters, 1994).

To return the track to its design line and level, ballast needs to be maintained and this is traditionally done by tamping. Tamping is a process that consists of lifting the track and squeezing laterally the ballast under the sleeper to fill the space generated. However, tamping causes ballast particle breakage and decreases ballast performance with time. More importantly, tamping messes up the structure of the ballast that has become established over tens or hundreds of thousands of loading cycles. Ballast performance also decreases as the proportion of voids that are fouled increases and this worsens as ballast degrades. Particle breakage and degradation, due to load applied by the train and dirt from fouling sources (such as fines material from subgrade and /or dirt from coal wagons) will fill ballast voids and this process will continue until the ballast requires cleaning or renewal. Therefore, it is very important to choose and to use good quality ballast having a grading optimized for best performance. Best performance is defined in terms of reduced vertical settlement while maintaining the capability to drain water.

1.2 Knowledge gaps

Sleepers and ballast are two of the ballasted track components that can potentially be altered or optimised. Sleepers in use around the world are available in different materials and shapes. However, owing to the lack of performance data of each sleeper type, there is confusion over which performs optimally on the track.

A relatively recent development to increase the service life of ballast is the use of under sleeper pads (USP), which are attached to the sleeper soffit. USPs are made in various thicknesses to fit the required design. Mechanical properties relating to the USPs are usually obtained through standard tests. However, on actual track, a USP may not always perform as it should. Primarily, this is due to the nature of the ballast contact not being accurately modelled in standard tests.

Ballast specifications generally favour uniform grading to fulfil drainage requirements. On the other hand, ballast must provide high shear strength to provide stability with minimal track deformation and this is normally best achieved with a well graded ballast. Over the years, concrete and highway aggregates have become more broadly graded. Despite this, railway ballast particles tend to be uniformly graded worldwide, with the uniformity coefficient (C_u) ranging between 1 and less than 3. C_u is defined as:

$$C_u = \frac{D_{60}}{D_{10}} \quad \text{Equation 1.1}$$

where D_{60} and D_{10} are the particle size that 60% and 10% respectively of the sample will be finer than.

Current ballast grading specifications have come about at least in part due to the historical need to provide large fouling reservoirs that allow the ballast to continue to provide drainage even when significantly fouled. However, the need to provide fouling reservoirs has reduced because the sources of fouling have reduced:

- Coal wagons spilling dust onto the track are rare.
- Ballast pumping causing fouling is well understood.
- Modern passenger trains no longer put waste onto the track.

Tests to optimise ballast grading through modification of its particle size distribution (PSD), whilst still ensuring stability of railway track structure and drainage requirements are met, have not been carried out systematically. Optimisation will also need to consider the longevity and maintenance of the ballast as well as responsible usage of ballast natural resources. Optimised ballast is also the cheapest ballast. Recent research projects on ballast grading have been conducted in Australia (Indraratna and Salim, 2005), Norway (Nalsund, 2010) and the U.S (Tutumluer et al., 2009). In Australia and Norway research into ballast grading was carried out using triaxial tests while in the U.S to investigate the American Railway Engineering and Maintenance-of-Way Association (AREMA) gradings Discrete Element Modelling (DEM) approaches have been preferred. However, railway ballast behaviour under cyclic loading was investigated using triaxial or box tests with rigid cell walls, which have a major shortcoming in terms of representing the actual lateral confinement of ballast on track.

Railway ballast could form two layers, which were normally created as the result of track maintenance using stoneblowing method. Stoneblowing involves lifting and packing below the sleeper with smaller grade ballast, which is blown under the sleepers to level the track. The performance and behaviour of two layered ballast was earlier investigated by Anderson and Key (2000). Further research was carried out by Claisse et al (2003) and Claisse and Calla (2006) to investigate the optimum particle size, for particles placed in the crib to act as a reservoir to fill the under-sleeper voids created due to loading cycles. However, the tests were carried out using a relatively small triaxial apparatus which had boundary conditions different to those of real track.

Ballast shoulders provide lateral confinement which has an important role in preventing lateral strain of ballast and hence track settlement. It appears that there is no international consensus regarding the ballast shoulder slope profiles. Railway authorities in each country have their own standard of ballast shoulder profile to be employed, which may be different from one to another. A literature review on railway track profile guidance employed in the United Kingdom (UK) showed that there is no standard to be followed in profiling the shoulder slopes; it is believed that ballast shoulders generally stand as close to their natural angle. Therefore, the role of the ballast shoulder slope in confining track deformation was also investigated.

Fouled ballast has been a subject of debate and discussion. The behaviour of fouled ballast was previously investigated through intensive research by Huang and Tutumluer (2011), Huang et al (2009), Indraratna et. al (2014) and Tutumluer et al (2008). The results seemed to be in agreement that the presence of fouling materials in ballast decreases ballast drainage capacity. Since this has become a general consensus among railway authorities around the world, the advantages which might be obtained due to the presence of fouling material in the ballast have been ignored. To investigate

the possible advantages of the presence of a fouling material (i.e. sand) in the ballast, full scale tests were carried out. These tests were also used to model track behaviour in a desert area.

The most recent development employed to improve the strength the ballast on the track is the application of geosynthetics. Geosynthetics in the form of geogrids were placed within the ballast layer beyond the depth of tamping. Previous research involving geosynthetics has been carried out by Bathurst and Raymond (1987), Indraratna and Salim (2003), Indraratna et al (2006b), and McDowell et al (2006). A geotextile can also be placed between the ballast and sub-ballast to provide filtration and/or increased strength and to acts as a barrier against the migration of fine particles from the sub-ballast/subgrade into the ballast while still permitting drainage (Chrismer and Richardson, 1986). Geosynthetics have also been used as a local barrier to prevent groundwater from infiltrating the trackbed to maintain drainage (Lacy and Panne, 1987). The most recent research carried out was on ballast with random fibre reinforcement. This research was carried out by Ajayi (2014) using Leighton Buzzard (LB) sand (Fraction A) as the starting point. The investigation was continued on scaled ballast and has shown promising results. However, all the tests carried out in the research were employing triaxial apparatus which has issues regarding boundary conditions and it was important to validate the results through a full scale test. Full scale tests on random fibre reinforced ballast were intended not only to validate the results obtained by previous tests using triaxial apparatus, but also to become trial tests prior to the application on the actual track.

In trackbed design, load distribution is assumed to occur either uniformly or with an idealised shape beneath the sleeper. However load transfer behaviour at the sleeper/ballast interface is highly variable both within and between individual sleepers. This is a result of the relatively large particle sizes of ballast in relation to a typical sleeper footprint. Railway ballast is usually graded so that the number of particles in contact with a sleeper may be relatively small and the discrete and non-uniform nature of these contacts may cause breakage and wear due to very high localised stresses. Therefore, the idealisations underestimate the load distribution at sleeper/ballast interface and to investigate the actual number and the area of contact at sleeper/ballast and ballast/subgrade interfaces, pressure paper was utilised.

All the research identified in literature used either numerical modelling or laboratory element tests that do not fully represent field conditions. For the purposes of this research, a full scale laboratory representation of the track was used to simulate field conditions and investigate the potential benefits. This thesis describes a series of observations and measurements made on full scale apparatus, purpose-built to investigate the performance of ballast due to the influence of sleeper and ballast interventions and other modifications. The observations sought to establish qualitative and quantitative data on the effects of different parameters on the track performance, which may provide a longer service life with less maintenance.

1.3 Aim and objectives

The aim of the research is to develop an improved understanding of how modifications to the sleeper and ballast may influence the performance of track, specifically:

1. Effect of sleeper types and type of sleeper/ballast interface.
2. Effect of ballast grading, geometry, fouling by fine sand and reinforcement.

To meet the aim of this research, testing objectives were set for a series of full scale tests in the Southampton Railway Testing Facility (SRTF) to investigate the effect of:

- ✚ Sleeper type, by testing mono-block concrete (G44), twin-block concrete, steel, plastic, and timber sleepers on the current standard NR ballast grading.
- ✚ Ballast grading, through tests where the current standard NR ballast grading was modified by adding finer particles.
- ✚ USPs, by testing two different types of USP both employing G44 and twin-block concrete sleepers.
- ✚ A two layered ballast (TLB) system constructed from two different gradings; the current standard NR ballast grading at the base and 10/20 grading on top.
- ✚ Re-profiling the trackbed geometry, by testing with a shallower shoulder slope than current practice in the UK.
- ✚ Fibre reinforcement in the ballast.
- ✚ The presence of fine sand as a fouling material within the ballast.

In addition to these objectives, full scale tests were also used to estimate the number and area of contact at sleeper/ballast interfaces along with the particle contact area and pressures at ballast/subgrade interface using pressure paper.

For all the tests carried out, the main comparison was made on the basis of:

- Permanent settlement, sleeper deflection and spring stiffness
- Ballast pressure
- Lateral earth pressure coefficients
- Number of particle contacts at sleeper soffit and corresponding pressure.
- Particle breakage/degradation

Some of tests that are for different reason considered unsuitable for comparison are presented separately.

1.4 Outline of the thesis

Following this introduction, the thesis is organised into seven further chapters and consists of two distinguishable parts. The first part, Chapters 2 to 5, concerns the review of literature and previous work. The second part, Chapters 6 to 8, assembles the new information obtained from the research carried out in this thesis.

Chapter 2 describes the background to the research. It contains a general review of railway track structures including both slab track and traditional ballasted track. The advantages and disadvantages of these track structures are highlighted and compared. The components of ballasted track are described.

Chapter 3 describes rolling stock in the UK and gives a basic description of the different forms of track categorisation based on loading and speed for general baseline track design. The track forces and the vertical loads likely to reach the sleeper and subgrade are also explored in this chapter, thus justifying later testing parameters.

In Chapter 4, current ballast assessment techniques are reviewed. The characteristics of ballast, ballast behaviour and ballast properties desirable for railway track use are summarized. This chapter also reviews the existing ballast specifications of rail authorities around the world. A subset of the specification used by major rail authorities worldwide is compared with consideration given to the PSD used. Previous research that has investigated the effect of ballast grading is also discussed and critically appraised.

Within Chapter 5, the characteristics of ballast behaviour in terms of vertical settlement and horizontal stresses are discussed. Existing ballast settlement models are presented. Existing settlement models are used for later comparison with the permanent settlement data obtained from the tests carried out for this research. The assumed pressure distribution between the sleeper and the ballast is also described for later comparison with the test results using pressure paper.

Chapter 6 contains a short description of the SRTF apparatus. The modifications were made to the original SRTF apparatus are highlighted and the main materials used in this research and methods of validation or calibration are introduced. The results from materials testing are also discussed. Ballast sample preparation, the instrumentation used and the loading system in the apparatus are also described. Testing variables are evaluated and parametric studies as well as test details are also presented.

Chapter 7 presents experimental results and interpretation. The processed test results that quantify permanent settlement, spring stiffness, ballast pressure in the longitudinal direction, number of contacts and the contact area/pressure of the ballast at the sleeper soffit are compared. Results of mobilised earth pressure ratio and particle breakage are presented, as well as results of lateral movement of ballast on the shoulder slope which was monitored optically. Some tests which were considered to have either had issues during the sample preparation (i.e. tests on steel and plastic sleepers) or were carried out for different purposes (i.e. sand ingress and a trial combined variables test) are discussed separately. Results of permanent settlement and spring stiffness, and a comparison produced using the existing ballast settlement models and a proposed ballast settlement model based on the properties and data obtained from the modified SRTF apparatus are also presented.

Chapter 8 presents the conclusions based on the completed test results, discusses their relevance for practice and gives recommendations for further research.

Chapter 2: Background

2.1 Introduction

As the demand for railway journeys has been increasing worldwide, an increased volume of rail traffic, heavier axle loads, and higher speeds on rail routes has been the result (Office for National Statistics, 2014) (Department for Transport, 2013) (Powrie, 2014a). To support this demand through improved design of the track system it is necessary to understand the behaviour of the track foundation under dynamic traffic loading by knowing the role of each track component. In this chapter, the types of track structure and the role of each track component are described.

2.2 Rail track structures

A good track structure provides a stable, safe and efficient method to guide train wheels running at various speeds and axle loads. There are two types of rail track structures commonly used worldwide. These are slab and ballasted tracks.

2.2.1 Slab track

The term slab track is used to describe a non-ballasted track structure that may comprise combinations of concrete slab, sleepers and road pavement. Figures 2.1 and 2.2 show a cross section and a view of slab track running lines.

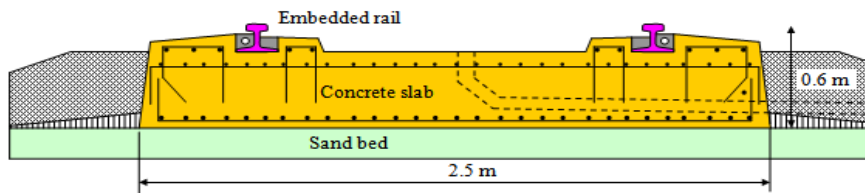


Figure 2.1: Cross section of slab track (after Esveld, 2001)



Figure 2.2: Slab track running lines (Porr Technobau und Umwelt Ag, 2014)

The main reasons for slab track application are the increased scarcity of good ballast and the desire to provide the stronger and durable structure required to carry increasing loading of heavy haul freight as well as the increased traffic of passenger trains where lengthy routine maintenance and repairs are more difficult to carry out (Bilow and Randich, 2000, Indraratna and Salim, 2005). Slab track use has

increased greatly since 1899 when the Southern Railroad built a concrete slab under existing track to stabilize a section of track on poor soil (Bilow and Randich, 2000).

The major advantages of slab track over ballasted track are low maintenance, a relatively low structure height and weight, higher stability and releasing less dust to the environment at least at the point of use (Esveld, 2001). However, slab track is significantly more expensive to construct and after a derailment it takes much more time and effort to recover the track (Esveld, 2001).

2.2.2 Ballasted track

Ballasted track is a traditional type of rail track structure widely used in almost every country. This type of rail track structure consists of rails, supported by sleepers on a ballast bed. The ballast bed rests on a layer called either sub-ballast or subgrade which forms the transition layer to the rail track structure formation (Esveld, 2001). The main advantages of ballasted track are its relatively low construction cost, the ease of maintenance of track components and geometry and its good drainage properties (Esveld, 2001). However, ballasted track has some disadvantages (Esveld, 2001, Indraratna and Salim, 2005):

- a. The track has the tendency to move both laterally and vertically after a period of time. The phenomenon of movement in the vertical direction is known as ‘track deterioration’, where the rail level gradually becomes irregular due to the uneven subsidence of railway ballast being compacted by train loads.
- b. The permeability (hydraulic conductivity) is reduced due to contamination (voids being filled by “fines” particles).
- c. Wheels and rails can be damaged through ballast aggregates being thrown onto the rails and run over.
- d. The relatively heavy and high track structure requires stronger construction for bridges and via-ducts.
- e. Frequent track maintenance and track condition reviews are required due to the increasing rate of ballast deterioration with train passage.

The decision to select a particular rail track structure will depend not only on the train speed and the expected axle load but also on the length of service life, local conditions, availability of basic materials and maintenance costs. Since the first railway system was introduced, the ballasted rail track structure has not changed significantly. This classic ballasted rail track structure with a satisfactory maintenance regime can still satisfy high performance demands, as demonstrated by the Train a Grande Vitesse (TGV) tracks in France (Esveld, 2001).

2.3 Components of ballasted track

On ballasted track, vertical and lateral alignment must be maintained and each track component must perform its required functions under any circumstances (Indraratna and Salim, 2005). Figure 2.3 shows the configuration of ballasted track divided into two major components; substructure and superstructure. Substructure describes all the material below the sleeper, which consists of subgrade, sub-ballast and ballast. Superstructure describes the upper section of the ballasted track, which consists of sleepers, fastening systems and rails. Substructure and superstructure are separated by the ballast to sleeper interface (Selig and Waters, 1994).

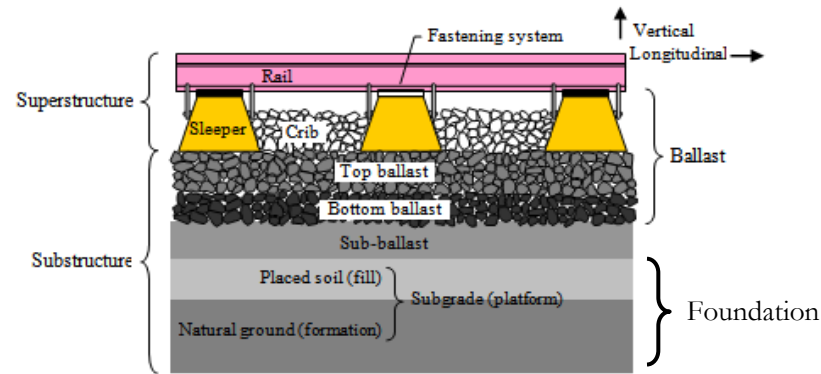


Figure 2.3: Truck structure components (after Selig and Waters, 1994)

2.3.1 Subgrade

The foundation of the railway track structure is made up of subgrade which contains placed soil that can be the natural ground or a combination of fill material and natural ground at depth. The subgrade must provide a stable and suitable base for construction of the sub-ballast and ballast layers. On main line railways where high-speed trains run, subgrade has been made of sand and gravel together with the natural ground (De Bold, 2011). The purpose of the subgrade is to support the track structure while limiting deflections. Every subgrade type undergoes some deflection (strain) as loads (stresses) are applied. The total displacement experienced by the subgrade will be transmitted to other components in the railway structure. Deflection on subgrade will be low if the subgrade has a higher elastic modulus (is stiffer).

Subgrade is expected to carry a lower stress than the ballast layer. However subgrade is still one of the sources of rail track differential settlement. To design a good subgrade, it is essential that adequate data regarding subgrade stiffness and strength is available on a year round basis, particularly during a spring thaw and following heavy precipitation events (AREMA, 2003b).

2.3.2 Sub-ballast

Railway track can be built with or without a sub-ballast layer; sub-ballast is generally composed of sand or fine materials (smallest sizes of angular particle) similar to that used in the construction of highways. The sub-ballast layer prevents overstressing of subgrade, increases or reduces the stiffness of the track system and forms a transition zone between the ballast and subgrade which avoids migration of soil into the ballast. Theoretically, the grading of sub-ballast should form a filter zone. However, this function is not adequately performed because historically, insufficient attention has been placed to sub-ballast grading (AREMA, 2003b). Sub-ballast offers the cheapest option to otherwise thicker ballast (Lim, 2004) and has some other important functions that cannot be fulfilled by ballast alone. These functions are (Selig and Waters, 1994):

1. Prevention of subgrade attrition by ballast. The presence of water leads to slurry formation and sub-ballast prevents this pumping source.
2. Shedding water and permitting drainage. Sub-ballast will intercept water coming from the top and bottom layers and direct it away from the subgrade to ditches at the side of the railway track.

The absence of a sub-ballast layer in railway track where the subgrade is not a naturally suitable material will lead to higher maintenance costs. Suitable sub-ballast materials are broadly graded

naturally occurring or processed sand-gravel mixtures, crushed natural aggregates or slag (Selig and Waters, 1994).

2.3.3 Ballast

Ballast has long been used by railways to provide support for the rail-sleeper system and a free draining medium. Ballast is ideally composed of coarse aggregates sourced from blasted igneous rock, although if this is not available metamorphic or well-cemented sedimentary rock quarries may also perform well (Clifton et al., 1987). The origin of ballast varies from country to country depending on the quality and availability of rock, environmental regulations and cost (Indraratna and Salim, 2005). There are many examples of material being used as ballast throughout the world including limestone, granite, basalt, rhyolite, gneiss, dolomite, quartzite, gravel, and slag. Angular stones are preferable as interlock with each other and thus reduce track movement. Weaker materials such as limestone are not particularly suitable as they can degrade under load. Granite is one of the better materials although more expensive (Bonnett, 2005). There is no a universal consensus concerning the proper specification for the ballast material to provide the best track performance: *“the choice of ballast type, grading, and the thickness of the layer is usually governed by tradition, availability, or oversimplified guidelines that do not integrate all of the important factors”* (Selig, 1985).

The main role of the ballast is to attenuate the relatively high stress immediately beneath the sleeper to a level that can be withstood on a long term basis by the subgrade. The standard depth of ballast is 300 mm; however it is packed up to 500 mm around the sleeper ends to create lateral confinement. Ideally the thickness of the ballast is dependent on the quality of the subgrade; the stronger the subgrade, the thinner the ballast layer required and vice versa. However, if the ballast layer is too thin, repeated loading can lead to localized ballast penetration into subgrade. A thicker ballast layer should spread the loads better resulting in lower displacement at the rail.

Alan (2012) conducted a finite element study to investigate the influence of ballast thickness to the vertical displacement on the top of the sleeper under a 10 ton axle load and for two subgrade conditions represented by Young’s modulus values of 20MPa and 78MPa corresponding to soft and stiff clay subgrade, respectively. The results of the study (Figure 2.4) show that a thicker ballast layer prevents higher stress reaching the sub-ballast and/or subgrade layer and hence reduces vertical displacement.

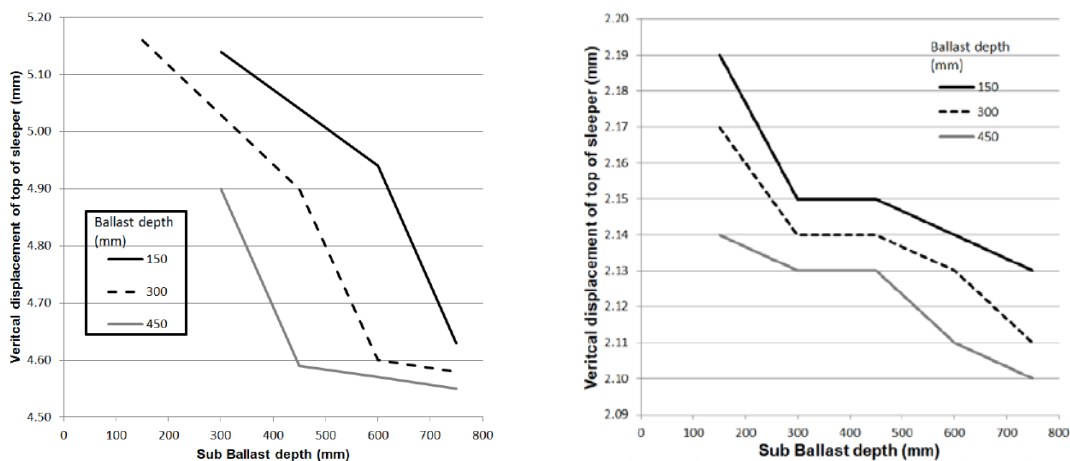


Figure 2.4: Vertical displacement of various ballast thicknesses on soft and stiff clay subgrade respectively under 10 tonnes axle load analysed by finite element approach (Allan, 2012)

Apart from attenuating the high pressure at the sleeper/ballast interface, providing a free draining medium and supporting the rail sleeper system, ballast also (Selig and Waters, 1994) and (Hay, 1982):

1. Provides track resilience and absorbs airborne noise.
2. Facilitates maintenance surfacing and lining operations to adjust track geometry through rearranging ballast particles by tamping.
3. Inhibits vegetation growth.
4. Provides a dry supporting medium for the service life of sleeper.

Ballast zone

Railway ballast in the track may be subdivided into four zones (Figure 2.5). These zone are (Selig and Waters, 1994):

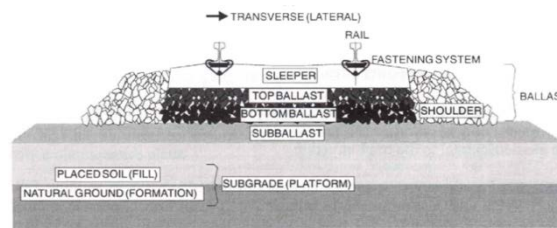


Figure 2.5: Cross section railway track structure (Selig and Waters, 1994)

1. Crib ballast. Crib ballast is the ballast located between the sleepers. The crib ballast provides pressure on the ballast below the sleepers, increasing the stability of the track and preventing longitudinal movement of the sleepers.
2. Shoulder ballast. Shoulder ballast is located beyond the sleeper ends down to the bottom of the ballast layer. The main function of shoulder ballast is to protect the track from buckling due to temperature induced rail stresses, with or without trains present.
3. Top ballast. Top ballast is located below the sleepers, and is disturbed by tamping.
4. Bottom ballast. Bottom ballast is located under the sleepers, and is not disturbed by the maintenance process and commonly the more fouled portion.

Ballast fouling

Ballast fouling (Figure 2.6) refers to the condition of the railway ballast when the voids in between aggregate particles are filled with fines material. During its life under traffic loading, ballast particles under the sleepers can move extensively with respect to one another. The contact area between ballast particles is relatively very small resulting in very high contact stresses between the ballast particles. For the limestone ballast these high stresses cause fracture and abrasion and producing fines materials that reduce ballast voids and foul the ballast layer.



Figure 2.6: Fouled railway track (Kaewunruen, 2011)

The addition of fouling material from other sources makes the degradation rate increase and the ballast voids become smaller (Figure 2.7a). Fully fouled ballast (Figure 2.10b) has the voids in between contacting aggregates filled with fines particles. As the ballast layer becomes heavily fouled (Figure 2.10c), aggregate to aggregate contact may be eliminated leading to reduction in effective shear strength.

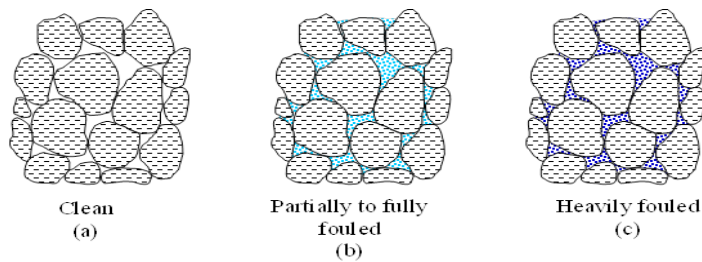


Figure 2.7: Ballast fouling phases (after Huang and Tutumluer, 2011)

Selig and Water (1994) concluded and agreed with the study result on North America freight lines carried out by Kerr (2003) that there are five sources of ballast fouling:

- a. Ballast breakage. This cannot be avoided. Even new ballast may already have some particle breakage due to the transportation process, dumping of the material at the sites and compaction. This initial condition is the starting point for the ballast; further breakages in the ballast may occur in service through weathering, traffic loading, and ballast tamping.
- b. Infiltration of fines from the ballast surface.
- c. Wear and weathering of the sleeper.
- d. Infiltration from the underlying granular layers.
- e. Subgrade infiltration.

Selig and Water (1994) investigated ballast fouling in the UK and North America. In the cases studied, ballast fouling in the UK was generally caused by external sources. After removing the fouling material, ballast particles were still in good quality after 15 years of service. However, findings from North American sites provided contradictory result that the main source of ballast fouling was ballast breakage and this may be due to different mineral types. The sources of ballast fouling parameters in UK, North American and Australian sites are presented in Table 2.1 and Figure 2.8.

Table 2.1: Sources of fouling in UK (after Selig and Waters, 1994)

No	Source	Degrading	
		kg/sleeper	% of total
1.	Ballast delivery	29	7
2.	Tamping (7 insertions during renewal and 1 tamp/year for 15 years at 4 kg/tamp).	88	20
3.	Attrition from concrete sleeper wear and traffic loading of 0.2 kg/sleeper/million tons of traffic	90	21
4.	External input at 15 kg/year (wagon spillage of 4.0 kg/m ² /year and air bone dirt of 0.8 kg/m ² /year)	225	52
	Total	432	100

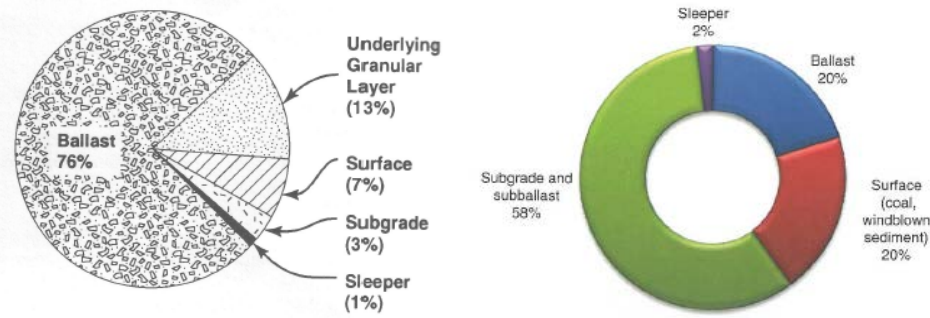


Figure 2.8: Sources of ballast fouling in North America (Selig and Waters, 1994) and Australia (Indraratna et al., 2011)

The effect of ballast fouling or the severity of ballast problems depends on the type, size, water content of fouling materials and the quantity (degree) of ballast fouling found within the ballast. Fines sourced from silt alone and clay combined with fine from ballast abrasion will form an abrasive slurry and an increasing proportion of clay and silt-sized fouling particles (smaller than 0.075 mm) impedes and reduces drainage as well as particle interlocking resulting in differential settlement of the track (Raymond and Diyaljee, 1979b).

However, the presence of the fine gravel and sand-size fouling particles usually will increase the shear strength and stiffness of the ballast as long as the ballast particle still form the ballast structural skeleton i.e. the ballast particles remain in contact with each other (Han and Selig, 1997). As the mass of sand and fine-gravel-sized fouling particles (0.075-19 mm) increases, the resiliency to vertical deformation of the ballast and void space decreases and the ballast becomes denser but its capability to drain water decreases. In some cases fouled or dirty ballast creates wet spots in the presence of water, leading to a reduction in stiffness of track support and hence loss of track geometry. As an example, coal dust as one of fouling materials was suspected as the main factor of two derailments occurred in 2005 at the joint coal line of Burlington Northern Santa Fe (BSNF) and Union Pacific in Powder River Basin (PRB) in Wyoming, the largest source of incremental low sulphur coal supplies in the U.S, which interrupted the supply of coal to power plants (Dombrow et al., 2009) (Huang et al., 2009).

Selig et.al (1993) carried out research into the effect of the degree of fouling on hydraulic conductivity (k_h). The results from this work are presented in Table 2.2. The degree of fouling is represented by Fouling Index (FI) parameter, which is defined by:

$$FI = P_{4.75} + P_{0.075} \quad \text{Equation 2.1}$$

where: $P_{4.75}$ and $P_{0.075}$ are percentage passing sieve sizes of 4.75 mm and 0.075 mm respectively.

Table 2.2: Fouling category based on FI and k_h (Selig et al., 1993)

Fouling category	FI	k_h (mm/sec)
Clean	< 1	25-50
Moderately clean	1-9	2.5-25
Moderately fouled	10-19	1.5-2.5
Fouled	20-39	0.005-1.5
Highly fouled	>39	< 0.005

Within the UK, Selig and Waters (1994) assumed that ballast would become completely fouled when a 30% proportion of the weight of the particles were smaller than 14 mm.

Equation 2.1 was used to quantify the degree of ballast fouling at North American sites while Ionescu (2004) investigated and proposed an equation to determine the degree of FI based on the ballast grading used in Australia. The equation proposed by Ionescu (2004) is a modification of Equation 2.1 based upon the percentage of passing particular sieve sizes and PSD that:

$$FI_P = P_{13.2} + P_{0.075} \quad \text{Equation 2.2}$$

$$FI_D = \frac{D_{90}}{D_{10}} \quad \text{Equation 2.3}$$

where: $P_{13.2}$ is a percentage passing sieve size 13.2 mm and D_{90} and D_{10} are the largest particle sizes in the smallest 90% and 10% of particles respectively.

Aursudkij (2007) summarised ballast FI criteria introduced by Selig and Waters (1994) for North American sites and Ionescu (2004) for Australian ballast grading (Table 2.3).

Table 2.3: FI comparison of two methods (after Aursudkij, 2007)

FI			Classification
$FI = P_{0.075} + P_{4.75}$ (Selig and Waters, 1994)	$FI_P = P_{0.075} + P_{13.2}$ (Ionescu, 2004)	$FI_D = D_{90}/D_{10}$ (Ionescu, 2004)	
< 1	< 2	< 2.1 and $P_{13.2} \leq 1.5\%$	Clean
1 to < 10	2 to < 10	2.1 to < 4	Moderately clean
10 to < 20	10 to < 20	4 to < 9.5	Moderately fouled
20 to < 40	20 to < 40	9.5 to < 40	Fouled
≥ 40	≥ 45	≥ 40 , $P_{13.2} \geq 40\%$, $P_{0.075} > 5\%$	Highly fouled
$P_X =$ Percentage passing at X mm / 100 and $D_Y =$ Particle size at Y percentage passing (mm)			

The fouling indices mass based on Equations 2.1 to 2.3 provide false information in volumetric terms if the fouling material has a different specific gravity (Indraratna et al., 2010). Feldman and Nissen (2002) introduced the percentage void contamination (PVC) equation to investigate the decreasing of voids in ballast as:

$$PVC = \frac{V_2}{V_1} \times 100\% \quad \text{Equation 2.4}$$

In Equation 2.4, V_1 is the void volume of re-compacted ballast particles and V_2 is the volume of re-compacted fouling material (particles passing a 9.5 mm sieve), respectively. However, measuring the PVC parameter is time consuming and does not consider the effect of the in situ void ratio, the grading of the ballast and the fouling material or the specific gravity of fouling materials. Indraratna et al., (2010) introduced a new parameter known as the Void Contaminant Index (VCI) which takes into consideration these omissions:

$$VCI = \frac{(1+e_f)}{e_b} \times \frac{G_{sb}}{G_{sf}} \times \frac{M_f}{M_b} \times 100\% \quad \text{Equation 2.5}$$

where G_{sb} , e_b and M_b are specific gravity, void ratio and dry mass of clean ballast respectively, and G_{sf} , e_f , and M_f are specific gravity, void ratio and dry mass of fouling material, respectively.

Ballast maintenance

Railway track is expensive and a long term investment. As the traffic history accumulates, the settlement of ballast and subgrade continues to increase until the track has deteriorated to a state at which it can no longer support the desired level of service. Track deterioration is the gradual

worsening of track geometry and is caused by three major factors: random settlement of the ballast, lack of straightness of rails and dynamic forces caused by vehicles. This leads to track maintenance being required to keep the track geometry level, maintain riding quality, and satisfy safety constraints. Track maintenance is the overall process of maintenance and renewal required to ensure that the track meets all safety and quality standards at minimum cost (Esveld, 2001).

A large part of the budget is spent on the maintenance of the track and this is a major factor in the economics of competition of a successful railway business. In the UK for every £100 spent in providing the end product, £25 is spent on infrastructure (e.g. track, structures and signalling) and £13 of this is for track alone (Campbell, 1984) while U.S railroads spend tens of millions of dollars each year on ballast and ballast-related maintenance (Chrismer and Read, 1994). Most of the maintenance budget goes on ballast maintenance interventions. Increasing ballast maintenance costs due to heavier loading and challenging track conditions is a major concern facing the railway authorities. BNSF railway spend 200 million US dollars annually or approximately 17% of the capital budget for ballast maintenance and surfacing (Lees, 2009) while in 2012/13, Network Rail spent £3.8 billion or 42% out of a total expenditure of £9 billion on maintenance and renewals (Network Rail, 2013). Therefore, there has always been a challenge to minimise maintenance costs since the last 30 years.

The most common methods of ballast maintenance are tamping, stoneblowing and cleaning/renewal.

Ballast tamping

Until 1945, UK railway track maintenance was carried out through manual labour. However in 1933, a Swiss contractor succeeded in designing a purely mechanical track tamping device (Esveld, 2001). A tamping machine corrects the track level by packing existing ballast from between to under the sleeper by means of vibrating tines, leaving a ridge of ballast beneath each sleeper and looser ballast between the sleepers (Gaskin et al., 1978). The lifting sequence of the tamping process disturbs and dilates the ballast layer to a depth of 150 to 200 mm under the sleeper. The tamping process thus loosens the ballast leading to a higher rate of settlement after tamping. This maintenance operation decreases the relative compaction of the ballast under the sleeper by 10-12% when a large rise of 38 to 50 mm is applied (Stewart and Selig, 1984). Ballast particles pushed to fill the space under sleeper remain in a relatively loose condition. These particles create new contact points between particles that may fracture under stress. These sequences become the normal life-cycle of ballast in railway tracks and involve cost. The presence of higher proportions of clay and silt-sized particles in the ballast will render the maintenance process difficult to complete because the tamping machine cannot penetrate and rearrange the ballast (Aursudkij, 2007).

Selig and Waters (1994) performed a ballast particle breakage test consisting of 1) 500,000 loading cycles without maintenance (without being disturbed) and 2) five repeats of 100,000 loading cycles with maintenance or particle rearrangement. The test results show that the maintenance process produced more than twice the particle breakage than when maintenance was omitted (see Figure 2.9).

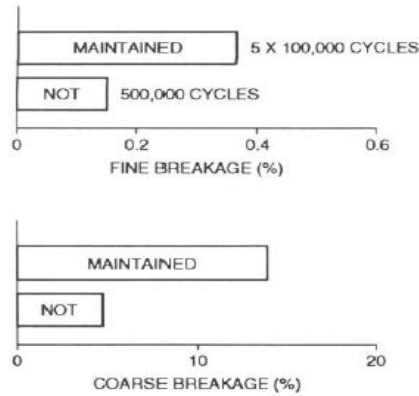


Figure 2.9: Effect of particle rearrangement on particle breakage (Selig and Waters, 1994)

Lim (2004) summarised the research conducted by Wright (1983) who investigated the effect of tamping in the track laboratory at British Rail (BR) and came to the conclusion that approximately 2 to 4 kg of fine particles less than 14 mm were generated per tamp for a single sleeper.

Stoneblowing

In the 1970s the BR Research Division started to investigate an alternative maintenance practice to tamping. Prior to the introduction of mechanised tamping, the maintenance of the railway track level was achieved by measured shovel packing. The mechanised form of this measured shovel packing is known as Pneumatic Ballast Injection (PBI) or stoneblowing (Anderson and Key, 2000, Fair and Anderson, 2003).

Although it is usually used only after tamping has become ineffective and is not widely used outside the UK, the stoneblowing process lifts a short section of the rails and attached sleepers with minimum disturbance to the existing ballast. Smaller single sized stones of approximately 20 mm diameter are blown using compressed air into the void under each railseat of the sleeper. This single size has been adopted as the preferred size based on experience from hand shovel packing (Anderson and Key, 2000). The sleeper is then re- set on top of the injected stone pads. This process creates two layers of granular foundations for each sleeper. As there has been very minimal disturbance to the existing well compacted ballast during the process, no increase in the rate of settlement would be expected under subsequent traffic loading. The stone blowing process is thought to create less damage to the ballast than mechanised tamping processes.

The single size of stoneblowing aggregates must have a consistent mixture of sizes mainly between 14 to 20 mm to conform to the limits given in Table 2.4 (Network Rail, 2009):

Table 2.4: PSD of stoneblowing aggregate (after Network Rail, 2009)

Sieve size(mm)	Percentage passing by mass (%)
20	100
14	20-0
10	2-0
2	0.5-0
0.063	0.2-0

Ballast cleaning and renewal

Eventually the ballast layer will reach its life expectancy in terms of performance and will need to be cleaned or renewed when there is 40% pollution and/or there are more than 30% of fines of less than 22 mm size (Esveld, 2001).

Cleaning fouled ballast is normally carried out using a ballast cleaning machine that holds and lifts the track grid to a certain level to provide a gap. The top ballast layer and uppermost ballast bed material are excavated using a chain with excavating teeth attached and transported to vibrating screens. These screens separate large stones, fines, and dirt. The clean ballast is returned to the track while fines and dirt are disposed of.

2.3.4 USPs

Railway track may have USPs as one of its components. USPs are a relatively recent development and are often termed performance pads (as USPs improve mechanical performance rather than mitigate noise). USPs are specially made pads attached at the sleeper soffit to be in contact with the ballast. The thickness of USP is variable and USPs mainly have been used in newly built high speed railway tracks in central Europe in recent years (Johansson et al., 2006, Schneider et al., 2011, Witt, 2008). USPs are formed either in single or multiple layers whereby an outer material protects an inner material from abrasive wear. The materials must be chosen in order to obtain suitable damping and stiffness. The requirements for USPs are resistance against abrasive wear by the stones, especially against the sharp corners of the stones and the ability to withstand the loading from passing trains without losing their elastic properties.

The main reasons for USPs application are to reduce the damage to the ballast by increasing the contact area thereby reducing contact stresses (Johansson et al., 2006, Lakusic et al., 2010, Witt, 2008) and to minimise some discontinuities of track stiffness which typically present in transition zones (Insa et al., 2013). USPs have been shown to modify elastic deflection and permanent settlements (Auer et al., 2013). USPs are generally considered to improve the track quality (e.g. track geometry quality, ballast protection, reduction of ballast and sleeper wear and rail corrugation) (UIC, 2008b, UIC, 2009b).

2.3.5 Sleeper

Sleepers are to be laid between the rails and ballast to tie the rails at the correct gauge, and distribute the load transmitted through the rails over a larger area of ballast underneath (Esveld, 2001). Sleepers were probably first used en masse on the Liverpool and Manchester Railway; although opened in 1830, sleepers were not used on the route until 1837 replacing the unconnected stone supports first tried (Morgan, 1971).

Sleepers are typically formed as rectangular blocks with most lengths between 2500 to 2600 mm for standard gauge and between 2000 to 2200 mm for narrow gauge track (Round, 1993). Millions of them are manufactured, transported, and distributed to satisfy the demand of new lines or line upgrades. There are a variety of sleeper materials and shapes in use worldwide; however since the earliest stages of railway track development and until relatively recently, timber has been the

dominant material used. The majority of timber sleeper require treatment by chemical substances to extend the service life. However these chemical substances might have environmental negative impacts and incur additional evaluation disposal costs. Durability may also be an issue. To overcome these limitations and to accommodate greater train speeds and higher axle load trains, new materials have emerged, of these, reinforced concrete is today the sleeper material of choice. Despite this, wooden sleepers continue to be specified in certain conditions depending on engineering judgement. For example hard track support conditions such as ballasted over bridges can be softened by specifying wooden sleepers as is the case in at least some UK railway maintenance/renewal regions.

Concrete sleepers are generally pre-cast concrete beams which are reinforced internally with pre-stressed steel (British Standards Institution, 2009a, Taylor, 1993). The advantages of concrete over wooden sleepers are that they have a longer service life and superior load capacity. Such sleepers are also heavier than their wooden predecessors and this greater weight contributes to greater positional inertia (e.g. reduces the risk of rail buckles). However, whereas wood on ballast was able to spread contact forces over larger areas by allowing ballast to indent into the more compliant wood, concrete sleepers do not allow this so their use has perhaps inadvertently introduced higher contact stresses between the ballast and sleeper. Pre-stressed concrete sleepers also require heavy machinery and special equipment to install.

Another recent development to fill the gap between cheapest and expensive options is the use of steel sleepers. Steel sleepers (British Standards Institution, 2000) are often seen as sturdier than timber and less expensive than pre-stressed concrete. Although steel sleepers require less ballast, they have not been widely used, mainly because installation by standard means for which most machinery is designed is problematic, so that it is difficult to create a homogeneous contact with the ballast within their “n” shaped profiles. Perhaps due to these installation difficulties, one case study showed that steel sleepers settle more than timber sleepers (Manalo et al., 2010). Steel sleepers may also be susceptible to corrosion particularly at the railseats where they can be at risk of fatigue. For these reasons steel sleepers have been viewed by practising engineers as a novelty and only applied as a last resort for lines on sand ballast (Office of Transport Safety Investigation, 2005) where they can be easily installed by pushing into the ballast.

Probably the most recent sleeper material tried to fulfil the requirement without any drawback is plastic or plastic composite. Plastic or plastic composite sleepers can be made of various combinations of raw materials (e.g. plastic, rubber and waste fibreglass) to create a sleeper with the compliance of a wood and the durability of concrete. Where recycled materials are used there is an added advantage in sustainability terms. However, they have not gained widespread use, at least in the UK.

2.3.6 Fastening and pad

The fastening system is the structural connection between the rail and sleeper. Fastenings are classified into two types, rigid and elastic. Rigid fastenings connect the rails to sleepers with nails or bolts while elastic fastenings connect rails to the sleepers with clips. The primary components of the fastening systems are the mechanical fastener and the rail pad (Remennikov and Kaewunruen, 2007).

There are many varieties of fastening; the choice of fastening greatly depends on the properties and structure of the sleeper (Esveld, 2001). The fastening system acts to resist vertical, longitudinal, lateral and overturning forces on the rails, and to damp vibration and impact (Esveld, 2001, Selig and Waters, 1994). Continuously Welded Rail (CWR) track is very popular nowadays and requires a fastening system with greater elasticity; therefore is an absolute necessity in the case of concrete sleepers which are susceptible to impact.

Other components of the fastening system are rail pads, which transfer the rail load to the sleeper while filtering out the high frequency force components.

2.3.7 Rail

Rails are longitudinal steel members (with a cross section shown in Figure 2.10), which guide and support the train wheels. Rails are laid longitudinally and act as a beam to transfer highly concentrated wheel loads to the sleepers, which are placed evenly along the rail length.



Figure 2.10: Rail cross section

The stiffness of the rails needs to be sufficient to carry out its function without excessive deflection between sleepers. The smoothness of the vertical and lateral rails and train wheel profiles influences the guidance of the rolling vehicle. Consequently, any surface defects on the wheel surface or on the rails can cause large dynamic loads on the rail track structure when trains are running on high speed. This is highly detrimental to the track structure.

To connect rail sections, bolted and welded joints may be used. Bolted joints (connected with drilled plates/fishplates) (Figure 2.11) however cause vibration and extra dynamic load, which lower passenger comfort and accelerate failure around the joints due to the discontinuity of the rails. At the joint area, the combination of impact load and stiffness is reduced producing high stresses on ballast and subgrade. This increases the rate of ballast degradation, fouling and settlement which leads to uneven track. Consequently, frequent maintenance is required in this area.



Figure 2.11: Fishplate connection system (De Bold, 2011)



Figure 2.12: CWR (De Bold, 2011)

Due to problems caused by bolted joints, CWR (Figure 2.12) has been chosen to replace bolted joints on the most important and heavily used passenger and freight lines and to reduce the maintenance cost, wear and tear on rolling stock, damage to the substructure, extend rail life, and improve riding quality.

However, CWR causes large longitudinal forces in the rails leading potentially to track lateral movement, and increases the risk of rail breakage or track buckling from temperature induced changes. Additionally, CWR attaches higher costs associated with welding, transporting and laying longer rails. Additional expense will also be incurred in changing worn and defective rails and in sleeper replacement.

2.4 Track requirements

Load distribution on the railway structure is a function of stiffness and flexibility. A good railway track structure needs to meet the following requirements (Hay, 1982):

a. Stiffness

The single best indicator of a railway track structure's strength, life and quality is the vertical deflection under load. Excessive deflection causes differential movement and wear between track components. It also leads to the deterioration of ballast through abrasion of the particles, muddy and pumping track and permanent settlement. Pressure transmitted to the subgrade must be within the allowable capability of that subgrade. Therefore the stiffness needs to be enough, for the pressure pulses from different axles to be merged into one pulse, thereby permitting some increase in speed.

b. Resilience

Resilience is important and needed within the design limit to provide a smooth ride for the trains to not only to prevent the breakage of train and track components, and coach contents but also to absorb shock, impact, vertical oscillation, and vibration. However, resilience is the opposite of stiffness.

c. Resistance to permanent settlement

Permanent settlement is the accumulated irrecoverable settlement that occurs through the track service life. Permanent settlement occurs in the ballast, sub-ballast and subgrade. One of the problems causing permanent settlement is deflection. Excessive deflection leads to permanent settlement and the greater the deflection the more rapidly the permanent settlement will occur. Although permanent settlement is relatively simple to measure, the prediction of permanent settlement is comparatively complex. The final result of permanent settlement is rough railway track.

d. Stability

Stability is the ultimate test of a good railway track structure and is defined as a degree of permanence or ability to remain in the desired vertical and lateral position (is not having too much permanent settlement or lateral movement).

2.5 Summary

Railway track consists of different components which for ballasted track can be categorised into a superstructure and a substructure. Superstructure and substructure components are combined and built to facilitate transportation of passengers and freight from one location to another with a smooth ride, in an efficient and safe manner. However, each component has its own characteristics that may lead to either a positive or negative impact.

Railway tracks need to be maintained, which is costly. Maintenance is still required in a durable railway track, however the maintenance costs may not be too much. A durable or good track consists of combined components that provide sufficient stiffness, resilience and stability to support train loads with minimal permanent settlement.

Chapter 3: Review of track categories and loading

3.1 Introduction

Train and track interactions generate substantial forces on railway tracks. Analysis and design of railway track structures have to take into account both static and dynamic loads.

This chapter describes rolling stock in the UK (section 3.2), and the different forms of track categorisation based on loading and speed according to both Union Internationale des Chemins de Fer (UIC) and UK Railway Group Standards (RGS) (sections 3.3 and 3.4). The various mechanisms of vertical load transfer to the sleeper and through the ballast are reviewed in sections 3.5 and 3.6. Analytical results of the load magnitude reaching the sleeper and the pressure reaching the subgrade are used as guidance for the applied load and for comparison with the instrumentation data in the laboratory tests respectively.

3.2 Rolling stock in the UK

In the UK, most passenger rolling stock falls into three broad types. These are locomotive hauled vehicles, electric multiple units (EMUs) and diesel multiple units (DMUs) (Network Rail, 2011). Each type of rolling stock is identified by a specific name and class number. The class number and name, maximum speed and approximate axle load of some passenger trains are presented in Table 3.1. The first digit has same significance e.g.1 = diesel mechanical and diesel hydraulic, 2 = diesel electric, 3 = alternating current (AC) electric and 4 = direct current (DC) electric (Network Rail, 2011).

Table 3.1: The class number and name, maximum speed and approximate axle load of some passenger trains (after Network Rail, 2011)

Class number	Class name	Maximum speed (mph)	Approximate axle load (tonnes)
334	Juniper	90	10
350, 350/2	Desiro UK	100	11
365	Networker Express	100	9.5
375/6	Electrostar	100	11
378/2	Capitalstar	75	10
390	Pendolino	125	13
395	Javelin	140	11
170/3	Turbostar	100	11.5
175/0	Coradia 1000	100	12.6
180	Adelante	125	12.6
220	Voyager	125	11.6
221	Super Voyager	125	13.7
222	Meridian	125	12.5
444	Desiro UK	100	11

These passenger train types were chosen to include those with the highest speed and the heaviest axle load. Other train types have lower speed and weight than in Table 3.1. However, passenger trains in the UK typically have an average axle load less than 20 tonnes.

3.3 Categorisation of track

The requirements for track quality and track bearing strength depend to a large extent on the load characteristics, while requirements relating to design, maintenance, renewal and inspection of the track vary according to usage and speed. Traffic load is one of the keys factors having a direct bearing on track maintenance (UIC, 2009a). Depending on the type of the traffic and the load being carried, lines are classified into several groups (categories) to facilitate economic assessment and to compare the different Infrastructure Managers (IM). These intended categories of track can be used to design railway track, primarily by adjusting the thickness of the trackbed layers. This section describes the track categorisation based on UIC and UK RGS. The NR design standard for track sleeper support stiffness in relation to line speed is also presented.

Line categorisation is determined on the basis of a theoretical traffic load. Traffic load represents the amount of load from the train passing along the rail track and results from the conversion of various train loadings into equivalent passenger train loads in which speed and wear effects by axle load have been taken into account.

UIC classifies train traffic load into six groups based on the daily traffic (Table 3.2), as described in more details in the UIC code 714R (UIC, 2009a).

Table 3.2: Line categorisation based on daily traffic load (after UIC, 2009a)

UIC group	Daily traffic (T_L) (Gross tonnes)
1	$T_L > 130,000$ tonnes/day
2	$80,000$ tonnes/day $< T_L < 130,000$ tonnes/day
3	$40,000$ tonnes/day $< T_L < 80,000$ tonnes/day
4	$20,000$ tonnes/day $< T_L < 40,000$ tonnes/day
5	$5,000$ tonnes/day $< T_L < 20,000$ tonnes/day
6	$T_L < 5,000$ tonnes/day

In the UK, RGS uses the Equivalent Million Gross Tonnes per Annum (EMGTPA) as a measure of the annual tonnage/traffic load carried by a section of track, taking into account the variation in track damage caused by normal traffic. This EMGTPA calculation is broadly adopted from UIC leaflet 714R for “Theoretical Traffic Load” (Railway Group Standard, 1999), with a fully seated loading condition assumed for passenger vehicles. UK RGS categorises the track based on the combination of EMGTPA and line speed (Figure 3.1). The speed used to determine the track category should be the maximum permissible or enhanced permissible speed, which is the speed permitted over a section of line that applies to a specific type of train operating at cant deficiencies in excess of those permitted at the permissible speed (Railway Group Standard, 2001).

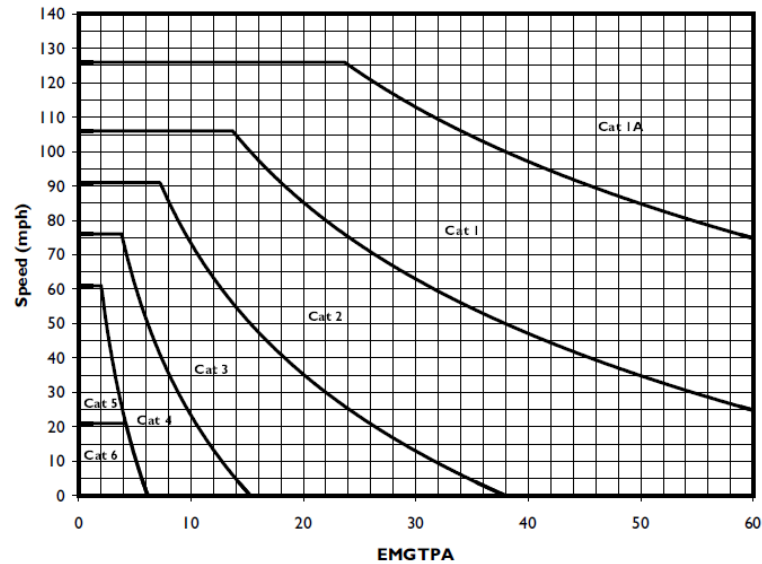


Figure 3.1: Track category based on EMGTPA and speed (Railway Group Standard, 1999)

The curved portion of the track category boundary (Figure 3.1) up to 25 EMGTPA is based on current and past experience. Above 25 EMGTPA the curve has been extrapolated to reflect the anticipated rate of track deterioration and associated risks on very heavily used lines (Railway Group Standard, 1999).

3.4 Track design

Historically, track design methods are based on the provision of a thickness of ballast sufficient to reduce the stresses to an acceptable magnitude on a long term cyclic basis for the sub-ballast and subgrade. The load used in track design is essentially based on static axle load. However the passage of a train causes a complex load to be imposed on the railway structure. The complexity is due to the load on multi train wheel spacing, the varying track support conditions and the dynamic behaviour of the vehicles. To simplify the inclusion of dynamic load in design, the pseudo static load due to the weight and an idealised vehicle motion are multiplied by a factor called the dynamic amplification factor (DAF). However the accuracy of DAF is questionable (Priest and Powrie, 2009) and there is some concern that dynamic loading may cause instability problems in granular materials resulting in reduced track strength and the potential for horizontal shear failure (Lees, 2009). Excessive elastic settlement caused by rapid application and removal of the wheel loads and the accumulation of large permanent settlement resulting from many repetitions of individual wheel loads are two of the problems related to the performance of ballast materials (Knutson, 1976).

To design railway tracks, the initial steps are to set the designated EMGTPA (for maintenance planning) and the intended track category. Using Figure 3.1, a speed line corresponding to these two parameters then can be defined. To achieve a defined speed line, a trackbed layer must provide a support which is defined using the Dynamic Sleeper Support Stiffness (DSSS). NR standard (NR/SP/TRK/9039: 2005) (Network Rail, 2005) recommends the required DSSS (Table 3.3) and the corresponding trackbed thickness (Figure 3.2) for use in designing new tracks and the existing lines.

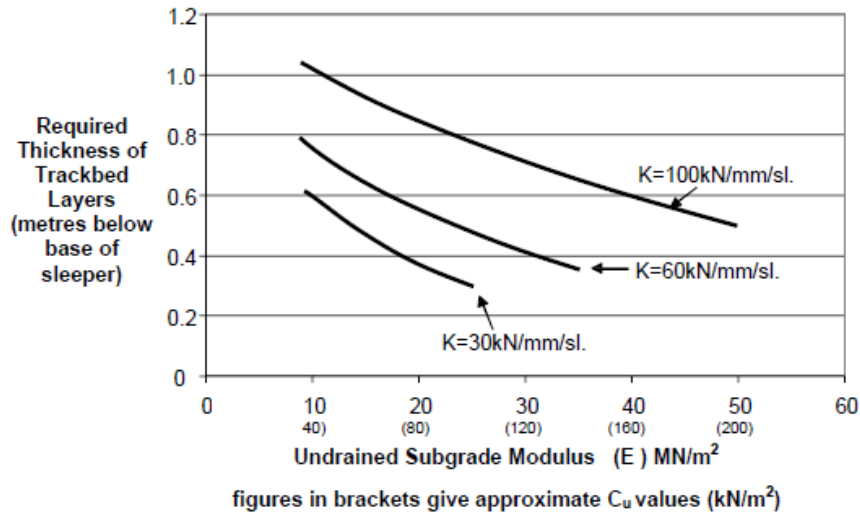


Figure 3.2: Required trackbed thickness (Network Rail, 2005)

Table 3.3: Required DSSS (k) (maximum axle load 25 tonnes) (after Network Rail, 2005)

		Minimum (k) kN/mm/sleeper end
Absolute value		30
Existing main lines	With geogrid reinforcement	30
	Without reinforcement	60
New track	Up to 100 mph	60
	Above 100 mph	100

In current track design to determine the required total depth of trackbed layer, this recommendation has considered static and dynamic load and been derived using a combination of empirical data and multilayer elastic theory. Further theoretical models for load transfer also exist and are explored in this chapter.

3.5 Track forces

To design track substructure, a basic understanding of the type and magnitude of forces that the track substructure must support is needed. Types of forces imposed on track structure are classified as mechanical (dynamic and static) and thermal. The track structure needs to restrain repeated vertical, longitudinal, and lateral forces as well as moment loading resulting from traffic, and changing temperature.

Maximum stresses and strains in the track system occur under dynamic loading conditions. The dynamic interaction between the train wheel and the rail is a function of the track, vehicle and train characteristics, operating and environmental conditions. Forces applied to the track by moving rail vehicles are a combination of a static load and superimposed dynamic components. The difference between the dynamic and static load is known as the dynamic increment. The magnitude of dynamic load can be up to 2.4 times the static load (Selig and Waters, 1994).

Temperature change induces thermal stresses in the rail which cause expansion or contraction of the steel. In a continuous welded rail, thermally induced forces acting in the longitudinal direction may tend to compress the rails potentially leading to buckling in the vertical or lateral direction, or tend to tension the rail potentially leading to breakage if the resistance is not sufficient (Selig and Waters, 1994) or if there is flaw in the rail.

3.5.1 Vertical forces

Vertical forces act perpendicular to the plane of the track and are due to the vertical wheel and uplift forces (Selig and Waters, 1994):

Vertical wheel force

The vertical wheel force is often simplified as a static component equal to the vehicle weight divided by the number of wheels. On moving trains, combining this vertical wheel force with track geometry, vehicle dynamics and/or rail and wheel conditions can produce variety of dynamic forces.

Uplift force

Figure 3.3 illustrates the reaction to the vertical load on a rail at the wheel contact points; the rail tends to lift up, moving away from the wheel. If this uplift force is not countered by the weight of the sleeper and rail together with ballast confinement (frictional forces), the sleeper will lift momentarily. This movement causes a pumping action on the trackbed which, if it sits on cohesive soil or fully fouled ballast, can cause track components to deteriorate.

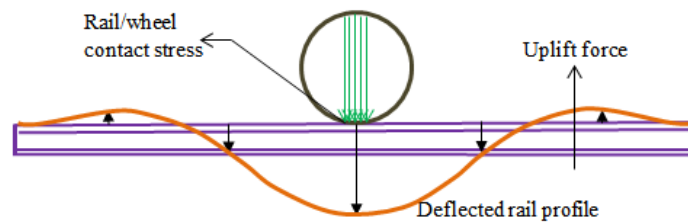


Figure 3.3: An illustration of uplift force occurrences (after Selig and Waters, 1994)

3.5.2 Lateral forces

Lateral forces act perpendicularly to the longitudinal direction (centreline) of the track. On canted tracks the lateral force may be resolved into vertical and horizontal components. Selig and Waters (1994) described two principal sources of lateral force: 1) lateral wheel force and 2) buckling reaction force. Lateral wheel forces occur due to the friction between the wheel and rail surfaces as well as forces caused by the wheel flanges on the rails. These are due to the movement of the train as the reaction to the track geometry. The development of compressive stress in rails as a result of high temperatures may result in buckling reaction forces occurring in the lateral direction.

3.5.3 Longitudinal forces

Longitudinal forces act on the rail head and parallel to the longitudinal direction of the track. Selig and Waters (1994) described longitudinal forces due to braking and accelerating by trains and thermal expansion and contraction of the rails.

3.5.4 Impact forces

The running rail is not always perfectly smooth. Construction imperfections or transitions and damaged rails and wheels generate impact forces causing track deterioration, noise and vibration. The main sources of impact forces are dipped rails, turnouts, crossings, insulated joints, an expansion

gap between two rail segments, imperfect rail welds, rail corrugations, wheel-flats, wheel-shells and worn wheels (Indraratna et al., 2011); some of these are illustrated in Figure 3.4.

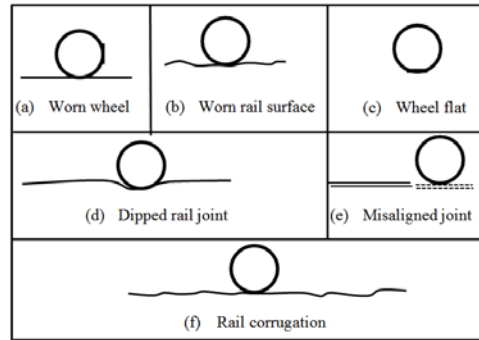


Figure 3.4: Sources of impact force on the track (after Indraratna et al., 2011)

The effect of train speed on impact force was studied by Leong and Murray (2008), which led to a conclusion that doubling the speed of a train would increase impact forces by approximately 140%. This agrees with the conclusion of Priest and Powrie (2009) that for constant sleeper support stiffness, the apparent dynamic loads increase with train speed.

3.6 Vertical load distribution mechanisms: a review of theoretical models

Vertical load from train wheels is transferred through the rails and distributed to each component of the trackbed beneath the rails. Figure 3.5 illustrates the mechanism and provides an approximate magnitude of pressure for each track component due to the application of train vertical wheel load. In this section the mechanisms of train vertical load distribution to the sleeper and the subgrade are discussed. These are intended to give not only the appropriate applied load magnitude for full scale tests in the laboratory but also the pressure range experienced by subgrade.

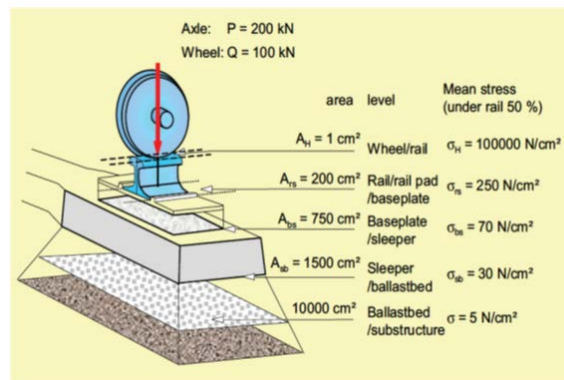


Figure 3.5: Vertical wheel load distribution (Esveld, 2001)

3.6.1 Vertical load distribution to the sleepers

To give a good estimate of load magnitude for the sleeper in full scale laboratory tests, the well-known Beam on an Elastic Foundation (BOEF) theory was used (Esveld, 2001, Hetenyi, 1946, Raymond, 1985a, Timoshenko, 1927).

In this section, the results by the BOEF analyses are compared with the results in previous published works (e.g. Remennikov and Kaewunruen (2007), Kaewunruen and Remennikov (2008), INNOTRACK (2008), Sadeghi and Barati (2010), and Sadeghi and Shoja (2013)) and also with the

recommendation of railway authorities (e.g. Standard Australia (2003) and Network Rail (2005)) to determine the load to be applied to the sleeper in full scale laboratory tests.

BOEF model

Figure 3.6 illustrates the BOEF model. Within the track structure, rails are assumed to act as long beams supported along their entire length by equally spaced sleepers to sustain the large wheel loads applied on it. The investigation of how this type of construction behaves and reacts to the applied load led to a theory of interaction between a beam of moderate bending stiffness and an elastic foundation. This imposes reaction forces on the beam proportional to the deflection of the foundation. This fundamental theory applied to track structure is able to calculate the pressure under the rail, rail deflections and the load magnitude on the sleepers.

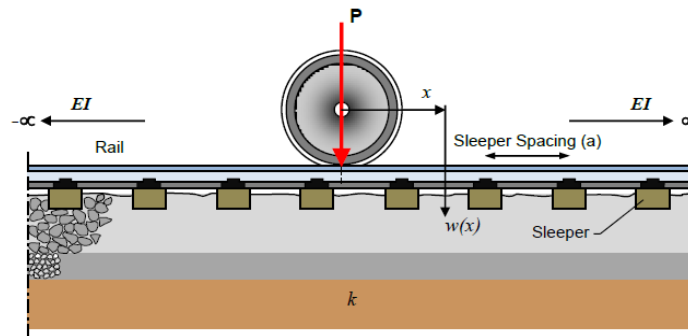


Figure 3.6: BOEF diagram (after Esveld, 2001)

The behaviour of the foundation in the BOEF analysis is often modelled using Winkler's theory (Timoshenko, 1927); further investigation was carried out by Hetenyi (1946). This theory provides calculated bending moments close to those measured in a test on freshly tamped track (Raymond, 1985a). The governing equation of a uniform beam on a Winkler foundation is:

$$EI \frac{d^4 w}{dx^4} + p(x) = q(x) \quad \text{Equation 3.1}$$

where: $q(x)$ = vertical wheel load

$p(x)$ = the continuous contact pressure between the longitudinal sleeper and base

$$p(x) = k w(x) \quad \text{Equation 3.2}$$

$$EI \frac{d^4 w}{dx^4} + k w(x) = q(x) \quad \text{Equation 3.3}$$

When a very long rail-sleeper beam is subjected to a concentrated wheel load P at $x = 0$, Hetenyi (1946) derived the solution for Equation 3.1 as:

$$w(x) = \frac{P\lambda}{2k} e^{-\lambda x} [\cos \lambda x + \sin \lambda x] \quad \text{Equation 3.4}$$

$$M(x) = \frac{P}{4\lambda} e^{-\lambda x} [\cos \lambda x - \sin \lambda x] \quad \text{Equation 3.5}$$

$$D(x) = -\frac{P}{2} e^{-\lambda x} \cos \lambda x \quad \text{Equation 3.6}$$

$$\theta(x) = -\frac{P\lambda^2}{k} e^{-\lambda x} \sin \lambda x \quad \text{Equation 3.7}$$

$$\lambda = \sqrt[4]{\frac{k}{4EI}} \quad \text{Equation 3.8}$$

where $w(x)$, $M(x)$, $D(x)$ and $\theta(x)$ are deflection, moment, shearing force and angular deflection at position x respectively.

Stewart and Selig (1982a) stated that two of the most influential variables on overall track response were ballast depth and sleeper spacing. The equations above (Equations 3.1 to 3.8) do not explicitly include the sleeper spacing. To investigate the influence of sleeper spacing (a), it is sensible to substitute the vertical track modulus per unit length, (k), by vertical track modulus per sleeper (k_d) as shown in Equation 3.9 (Raymond, 1985a).

$$k = \frac{k_d}{a} \tag{Equation 3.9}$$

Therefore Equation 3.4 will become:

$$k_d w(x) = \frac{P a \lambda}{2} e^{-\lambda x} [\cos \lambda x + \sin \lambda x] \tag{Equation 3.10}$$

Table 3.4: Data used to create the graphs of percentage of wheel load exerted on the sleepers

Variable	Value	Description	Notes
E (N/mm ²)	205,000	Rail elasticity.	Typical value for steel elasticity.
I (mm ⁴)	16,411,000 18,160,000 19,878,000 20,178,000 23,379,000 30,383,000	Moment of inertia for rails 46EI, 49EI, 50EI, 50E6, 54EI, and 60EI respectively.	(British Standards Institution, 2011).
k (N/mm/mm)	Varied	Vertical track modulus.	Adopted from literature e.g. (Le Pen, 2008).

Based on the calculation using the BOEF Equations 3.4 to 3.10 and taking realistic rail dimensions as in Table 3.4, the percentages of the wheel load carried by the sleepers for various vertical track moduli, rail dimensions and sleeper spacing are presented in Figures 3.7 to 3.9.

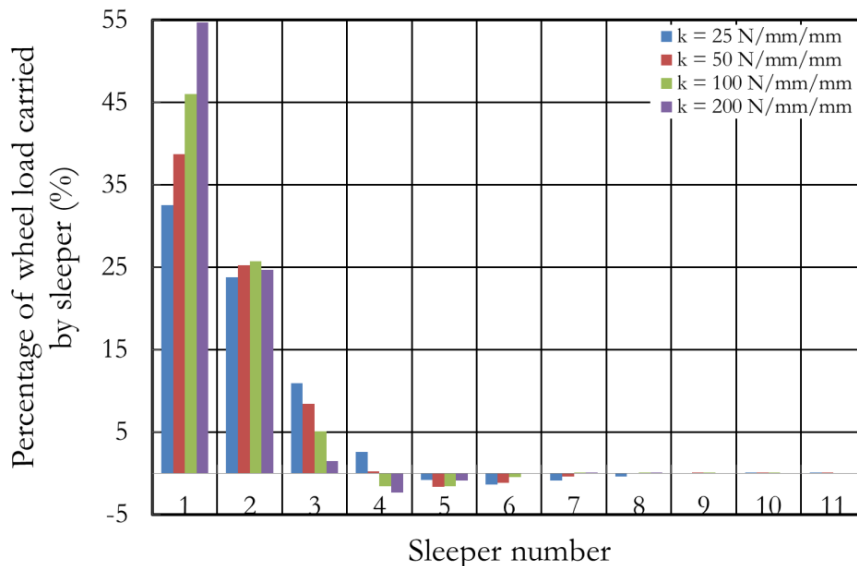


Figure 3.7: Percentage of wheel load carried by sleepers for various k values, $a = 650$ mm and $I = 30383000$ mm⁴

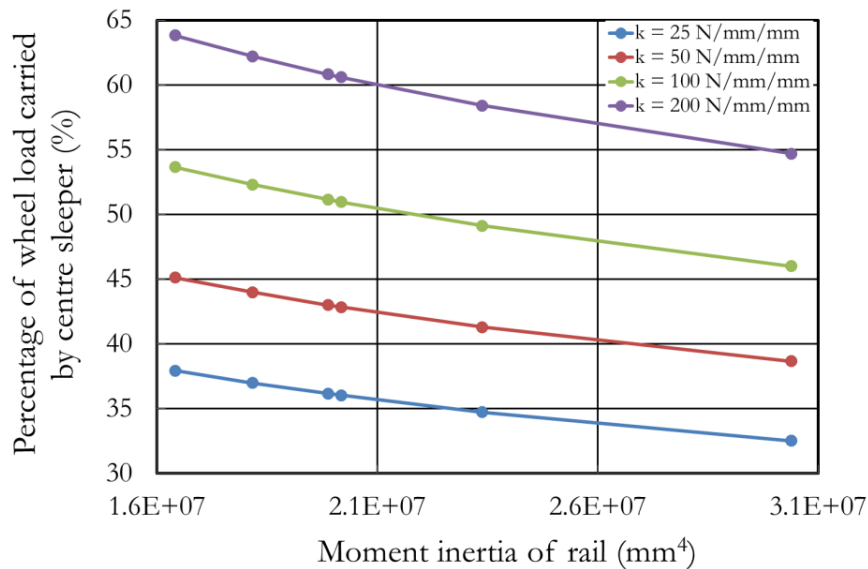


Figure 3.8: Percentage of wheel load carried by centre sleeper for various rail dimensions

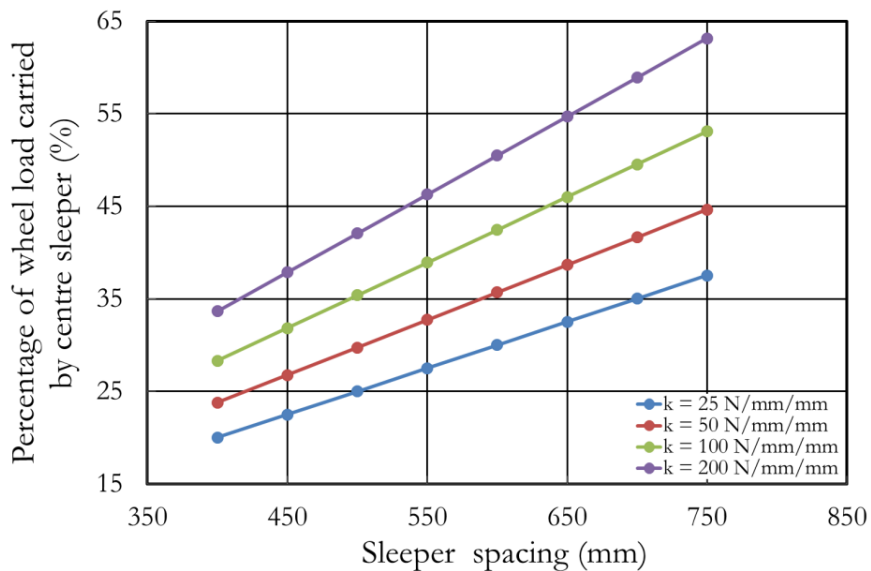


Figure 3.9: Percentage of wheel load carried by centre sleeper for various a and I = 30383000 mm⁴

Figures 3.7 to 3.9 show that a rail in a low global stiffness track will experience large displacement and as a result more sleepers will be involved in sharing the load, leading to lower forces on the sleepers. A high global stiffness rail will lead to a contrary result.

Recommendations from previous researchers

The estimation of percentage of train axle load carried by the sleepers has been investigated and the results have been published by previous researchers e.g. Remennikov and Kaewunruen (2007), Kaewunruen and Remennikov (2008), INNOTRACK (2008), Sadeghi and Barati (2010), and Sadeghi and Shoja (2013). However among those who previously conducted research, INNOTRACK (2008) has provided the parameters used in most detail and is comparable to the results obtained by BOEF model analysis.

INNOTRACK (2008) conducted analysis to estimate the percentage of train axle load carried by the sleeper using the theory of a beam resting on resilient support according to Zimmermann. This theory is a simplification of BOEF theory at $x = 0$ (Equation 3.10).

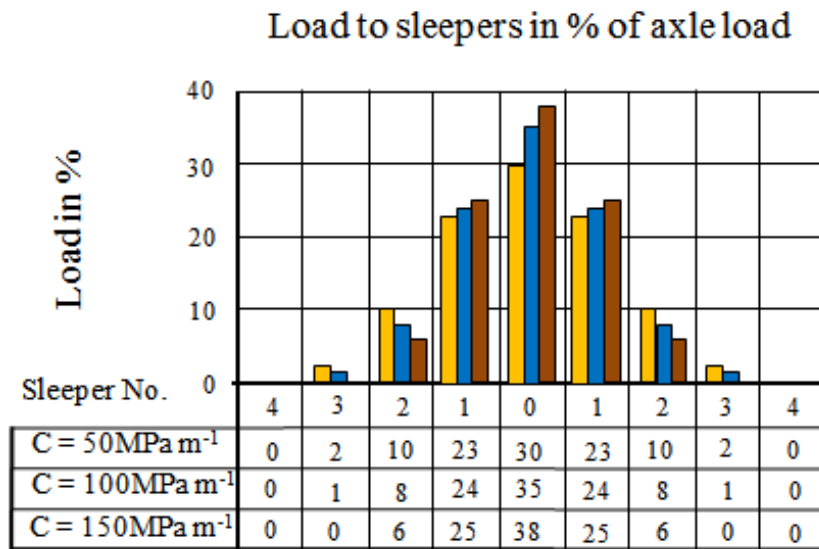


Figure 3.10: Percentage of load carried by sleeper on various substructure stiffnesses (after INNOTRACK, 2008)

The final calculation of the percentage train axle load acting on the sleepers for various trackbed qualities (Figure 3.10) was produced using parameters of UIC60 rail, B91 S/1 sleepers and a sleeper spacing of 600 mm. The substructure stiffness was characterised by the coefficient of loading capacity (C).

Standards of railway authorities

Different railway authorities may use different estimates of the percentage of an axle load carried by sleepers. In this section, the estimates adopted by the standard in Australian and the UK are presented.

Australian standard

In the Australian standard (Standards Australia, 2003), for a given sleeper spacing the proportion of vertical axle load carried by an individual sleeper should be obtained using Figure 3.11. The distribution factors (DF) in Figure 3.11 are based on rails equal to or heavier than 47 kg/m. However, the Australian standard recommends using Equation 3.4 to determine the proportion for a better estimation. This recommendation was followed the study conducted by Remennikov and Kaewunruen (2007); the results of which are presented in Figure 3.12.

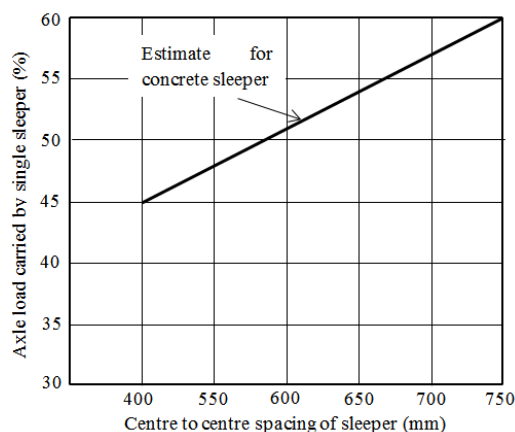


Figure 3.11: Axle load distribution factor (DF) (after Standards Australia, 2003)

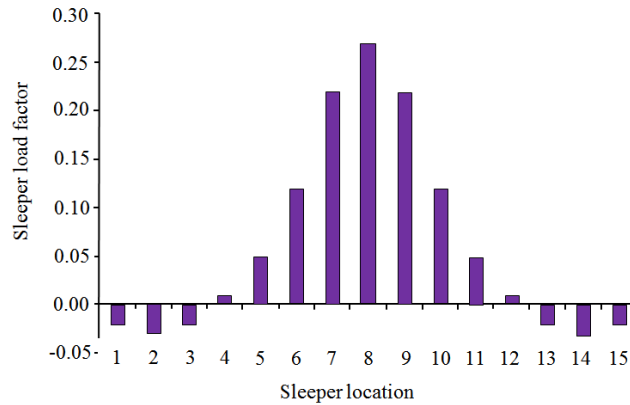


Figure 3.12: Axle load DF for the sleeper (after Remennikov and Kaewunruen, 2007)

Network Rail (NR) standard

The Network Rail standard does not state the percentage of the axle load carried by sleepers explicitly. However, it is stated in the Network Rail manual of formation and treatment, NR/SP/TRK/9039 at section 7.6.2 of Falling Weight Deflectometer (FWD) that “Each test sleeper is disconnected from the rail in turn and a pulse of load, having a peak value of 12.5 tonnes (typically the maximum load seen by a sleeper under a passing 25 tonnes axle load), is applied three times” (Network Rail, 2005). Therefore, based on this statement NR has assumed that the percentage of axle load carried by the sleeper is 50%.

3.6.2 Vertical load distribution mechanism through the trackbed layers

The fundamental engineering of the vertical load distribution mechanism through the trackbed is reasonably well understood. It involves the distribution of vertical load from the sleeper soffit onto the surface area of packed ballast and its transfer through to the subgrade (Geological Society, 2001). The behaviour of a granular material under repeated loading has generally been recognised as being a nonlinear and stress-dependent (Stewart and Selig, 1984). To estimate the vertical pressure on the ballast layer resulting from sleeper loading, the mechanism needs to be assumed or known. Selig and Waters (1994) provided a simple illustration (Figure 3.13) of how the wheel load is distributed onto track structure.

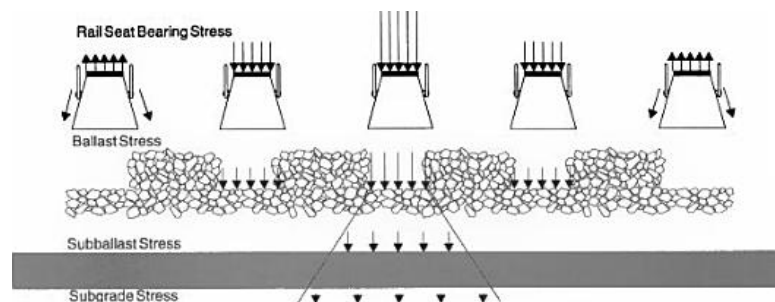


Figure 3.13: Vertical load distribution onto the trackbed (Selig and Waters, 1994)

There are comprehensive theories available to determine the load distribution on the substructure layer. In this Section, load distribution using Boussinesq’s elastic theory, the load spread method and the Talbot’s equation are described. To estimate the magnitude of pressure on the subgrade layer, the analysis using each method with the parameters applicable to the laboratory tests is presented. The results of each analysis are compared.

Boussinesq's elastic theory

This theory assumes that ballast and the subgrade layers form a half space that is semi-infinite, elastic, and homogeneous. The railseat load can be assumed uniformly distributed over a circular, strip, or rectangular area equivalent to the assumed contact area between the sleeper and the ballast. The vertical pressure at any point beneath the sleeper, due to a uniformly distributed vertical load over a circular area is defined by:

$$q \left[1 - \frac{z^3}{(R^2 + z^2)^{1.5}} \right] \quad \text{Equation 3.11}$$

where: q = Average uniform pressure over the loaded area (sleeper base) (kPa).

R = Radius of the loaded area (m).

z = Vertical depth to any point beneath the sleeper.

For the same condition, numerical method can also be used an alternative approach and demonstrated a reasonable accuracy by applying partial influence factors A and B. This is presented in Table 3.5 to the equation:

$$\sigma_z = q (A + B) \quad \text{Equation 3.12}$$

Table 3.5: Influence factor A (top line) and B (bottom line) for vertical stresses due to a uniformly loaded circular area at any distance (r) from the circular centre (after Whitlow, 2001); a is a radius

z/a	r/a	0	0.2	0.4	0.6	0.8	1.0	1.2	1.5	2.0	3.0
0		1.0	1.0	1.0	1.0	1.0	0.5	0.0	0.0	0.0	0.0
		0.0	0.0	0.0	0.0	0.0	0.0	0.0	0.0	0.0	0.0
0.2		0.804	0.798	0.779	0.735	0.630	0.383	0.154	0.053	0.017	0.004
		0.188	0.193	0.208	0.235	0.260	0.085	-0.078	-0.044	-0.016	-0.004
0.4		0.629	0.620	0.592	0.538	0.443	0.310	0.187	0.086	0.031	0.008
		0.320	0.323	0.327	0.323	0.269	0.124	-0.008	-0.045	-0.025	-0.008
0.6		0.486	0.477	0.451	0.404	0.337	0.256	0.180	0.100	0.041	0.011
		0.378	0.375	0.363	0.382	0.254	0.144	0.045	-0.021	-0.025	-0.010
0.8		0.375	0.368	0.347	0.312	0.266	0.213	0.162	0.102	0.048	0.014
		0.381	0.374	0.351	0.307	0.238	0.153	0.075	0.006	-0.018	-0.010
1.0		0.293	0.288	0.270	0.247	0.215	0.179	0.143	0.098	0.052	0.017
		0.353	0.346	0.321	0.278	0.220	0.154	0.092	0.028	-0.010	-0.011
1.2		0.232	0.228	0.217	0.199	0.176	0.151	0.126	0.092	0.053	0.019
		0.315	0.307	0.285	0.248	0.201	0.149	0.100	0.044	0.000	-0.010
1.5		0.168	0.166	0.159	0.148	0.134	0.119	0.103	0.080	0.051	0.021
		0.256	0.250	0.233	0.207	0.174	0.137	0.102	0.057	0.014	-0.007
2.0		0.106	0.104	0.101	0.096	0.090	0.083	0.075	0.063	0.045	0.022
		0.179	0.181	0.166	0.152	0.134	0.113	0.093	0.064	0.028	0.000
3.0		0.051	0.051	0.050	0.049	0.047	0.045	0.042	0.038	0.032	0.020
		0.095	0.094	0.091	0.086	0.080	0.073	0.066	0.054	0.035	0.011
4.0		0.030	0.030	0.029	0.028	0.028	0.027	0.026	0.025	0.022	0.016
		0.057	0.057	0.056	0.054	0.051	0.048	0.045	0.040	0.031	0.015
5.0		0.019	0.019	0.019	0.019	0.019	0.018	0.018	0.018	0.016	0.012
		0.038	0.038	0.037	0.036	0.035	0.034	0.031	0.028	0.025	0.015
10.0		0.005	0.005	0.005	0.005	0.005	0.005	0.005	0.005	0.004	0.004
		0.010	0.009	0.009	0.009	0.009	0.009	0.009	0.009	0.008	0.008

A uniform load over a circular area can be substituted by the strip load method to obtain the pressure produced beneath the sleeper. The vertical pressure at any location (x, z) loaded by an evenly distributed strip load (Figure 3.14) can be determined as:

$$\sigma_{zi} = \frac{q}{\pi} [\beta + \sin \beta \cos (\beta + 2\delta)] \quad \text{Equation 3.13}$$

where: q = average uniform contact pressure between the sleeper and the ballast (kPa).
 σ_{zi} = pressure at depth z and location i .
 B = width of the sleeper
 β, δ = shown on Figure 3.14

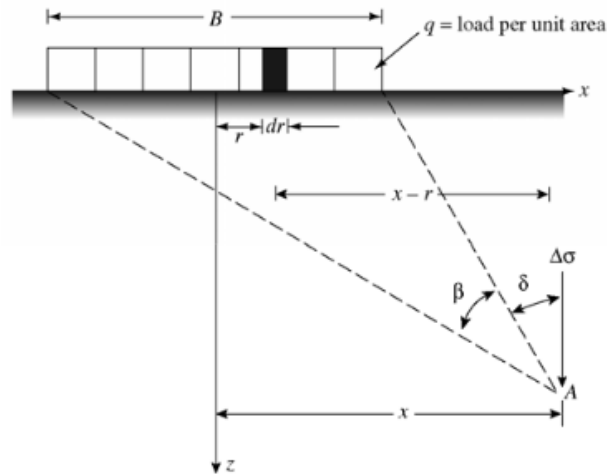


Figure 3.14: Stress due to strip load (after Das, 2008)

Equation 3.13 can be simplified by introducing the influence factors for a strip load (I_{fsl}) (Table 3.6) to become:

$$\sigma_{zi} = q I_{fsl} \quad \text{Equation 3.14}$$

Table 3.6: Influence factors due to strip load (after Das, 2008)

$2z/B$	$2x/B$				
	0	0.5	1.0	1.5	2.0
0	1.000	1.000	0.500	—	—
0.5	0.959	0.903	0.497	0.089	0.019
1.0	0.818	0.735	0.480	0.249	0.078
1.5	0.668	0.607	0.448	0.270	0.146
2.0	0.550	0.510	0.409	0.288	0.185
2.5	0.462	0.437	0.370	0.285	0.205
3.0	0.396	0.379	0.334	0.273	0.211
3.5	0.345	0.334	0.302	0.258	0.216
4.0	0.306	0.298	0.275	0.242	0.205
4.5	0.274	0.268	0.251	0.226	0.197
5.0	0.248	0.244	0.231	0.212	0.188

Apart from these two methods, the most widely used method in soil engineering design is the method of pressure due to a uniformly loaded rectangular area. The increase in vertical pressure beneath one corner of a rectangular area carrying a uniform load (q) is expressed by:

$$\sigma_z = q I_R \quad \text{Equation 3.15}$$

I_R (Figure 3.15) is an influence factor dependent on the length (L) and breadth (B) of the loaded area, and the depth (z) of the point at which pressure is required. The parameter n (B/z) and m (L/z) are combined to express the value of I_R .

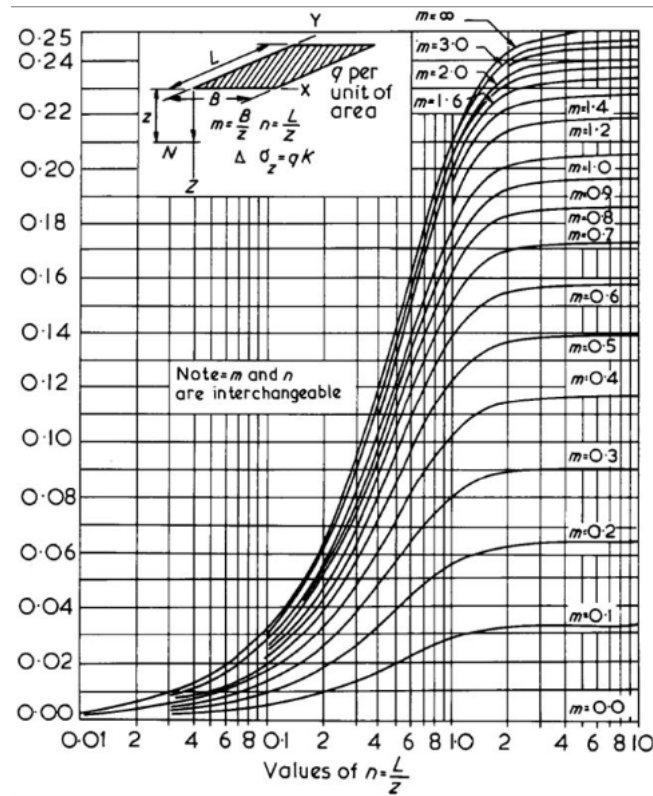


Figure 3.15: Fadum's chart influence factor for uniformly loaded rectangular area (Fadum, 1948) (after Das, 2008, Powrie, 2004, Powrie, 2014b, Whitlow, 2001)

Load spread method

The main assumption of the load spread method (Figure 3.16) is that vertical load is distributed vertically with the spread slope or an angle of 1:1 or 2 (vertical) : 1 (horizontal) (Sadeghi, 2012). This is the most commonly used to simplify the method in practice. The average pressure ($\sigma_{Average}$) of 2:1 load spread method is obtained by:

$$\sigma_{Average} = \frac{P}{[(B + z)(L + z)]} \tag{Equation 3.16}$$

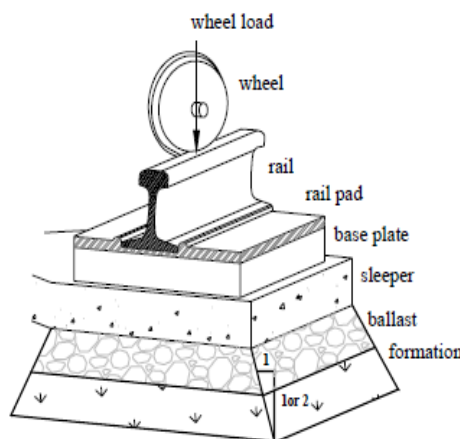


Figure 3.16: Diagram of 2:1 load spread method (after Doyle, 1980, after Esveld, 2001, Radampola, 2006)

A comparison of Boussinesq's and the load spread methods detailed above was carried out in 1991 by the Department of Industrial Research UK, specifically examining a load spread over a circular area. Figure 3.17 shows that load spread of 2: 1 provides a closer result to Boussinesq's than 1:1 load spread methods.

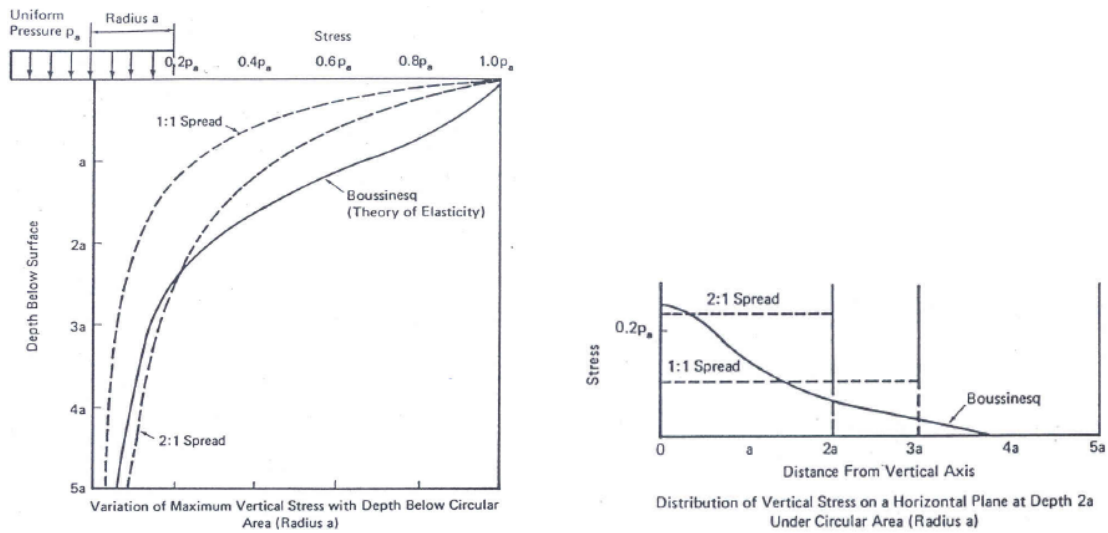


Figure 3.17: Comparison of vertical stress distribution under a uniformly loaded circular area by load spread and Boussinesq's methods (after Doyle, 1980, Radampola, 2006)

Talbot's equation

The American Railway Engineering Association (AREA) recommended the Talbot's equation as an empirical equation developed based on field tests conducted during the 1910s and 1920s. Li and Selig (1998a), stated the Talbot equation as:

$$H = 0.24 \left(\frac{P_m}{P_c} \right)^{0.8} \quad \text{Equation 3.17}$$

where: H = Granular layer thickness (m)

P_c = Allowable subgrade pressure recommended by AREA (138kPa)

P_m = Vertical stress applied on the ballast surface

However Li and Selig (1998a) showed that the Talbot equation applies only to a universal subgrade soil condition. A universal allowable subgrade pressure of 138kPa will lead to difficulty in soft soil conditions and be too conservative in strong soil conditions.

To provide a comparison, the previously described methods and equations are used to calculate the magnitude of pressure for the subgrade layer. The analysis results are presented and compared in Table 3.7. The trackbed parameters used for calculation are:

- 300 mm thickness of ballast
- 250 cm length by 28.5 wide (7125 cm²) of G44 sleeper
- 10 tonnes of vertical load giving a uniform pressure of 140.35kPa at the sleeper soffit

Table 3.7: Summary of analysis results of the stress under the ballast by presented methods

Method	Applied equation, table and figure	Calculated stress to subgrade (kPa)
Analytical circular load	Equation 3.11	138.57
Strip load	Equation 3.14 and Table 3.6	74.60
Rectangular load	Equation 3.15 and Figure 3.15	77.47
Numerical circular load	Equation 3.12 and Table 3.5	138.02
1:1 spread load	Equation 3.16 and Figure 3.16	36.45
2:1 spread load	Equation 3.16 and Figure 3.16	61.05
Talbot equation	Equation 3.17	106.19

In addition to these methods, the application of finite element has been used to investigate the stresses in the ground below ballasted railway track. Powrie et al.(2007), investigated the changes in stress of the ground underneath ballasted trackbed when trains travel over the rails using the finite element software of ABAQUS/STANDARD in two and three dimensional analyses.

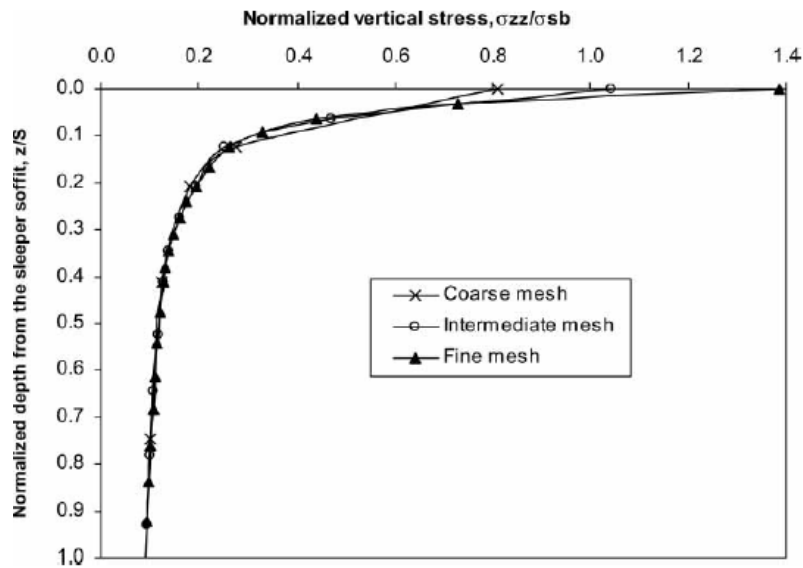


Figure 3.18: Variation of vertical stress with depth below the sleeper end for different mesh densities (Powrie et al., 2007)

Table 3.8: Material properties used in finite element analyses (after Powrie et al., 2007)

Component description	Young's modulus (MPa)	Poisson's ratio	Unit weight (kN/m ³)	Remarks
Rail	210,000	0.3	76.93	Cross-section 78 mm wide x 153 mm deep
Sleeper	34,000	0.3	23.52	Cross-section 242 mm wide x 200 mm deep
Ballast	310	0.3	16.66	
Sub-ballast	130	0.49	22.54	
Prepared subgrade	100	0.49	19.6	
Natural ground	30	0.49	19.6	Gibson soil, $E = 30 + mz$, $m = 4.5$

Figure 3.18 shows the analysis result of finite element method in two dimensions for various types of mesh densities using the material properties presented in Table 3.8. Plotting the parameter of G44 sleeper length and the uniform pressure of 140.35kPa into Figure 3.18, the magnitude of vertical pressure inserted to the subgrade layer is 49.12kPa. This result is closer to the result for a 2:1 spread load and Boussinesq's elastic theory using strip load methods in Table 3.7.

3.7 Summary

The design of a track substructure needs to take into account both static and dynamic loading. Static and dynamic loads are converted into traffic load and combined with the train speed to define the track categorisation. Traffic load is the general baseline of load that represents the cumulative load from the different types of train passing. This baseline is used to design rail track by adjusting the thickness of trackbed layer.

The applied load used for the full scale tests in the laboratory within this research thesis was based on methods of analysis which have been well established and used in previous works. There is an agreement that the magnitude percentage of axle load being transferred to the sleeper is dependent to the dimensions of the rail, sleeper spacing, and sleeper support stiffness. Based on the comparison of results of analyses using BOEF theory, beam resting on resilient support theory and the recommendations in railway authority standards, the percentage of the axle load transferred to the centre sleeper was approximated to 50%. This percentage may be higher on railway track with a high sleeper support stiffness and wider spacing between sleepers. However, since typically railway tracks within the UK have a sleeper spacing of 650 mm and the recommended value of sleeper support stiffness for the track rack using the DSSS method is normally less than 100kN/mm/sleeper end, the magnitude of 50% of axle load transferred to the centre sleeper is sufficient. Consequently the applied vertical load for the full scale laboratory tests is defined as 10 tonnes or 98.1kN, which corresponds to a train having a 20 ton axle load (a typical axle load for passenger trains in the UK).

The vertical load applied onto a sleeper produces pressure on top of the ballast surface through the sleeper base. The pressure on the ballast surface is transferred through the ballast thickness and finally reaches the subgrade layer. Analytical, numerical, and finite element methods can be used to estimate the magnitude of pressure exerted to the subgrade layer due to the application of a vertical load. Based on the analytical and numerical methods presented in this chapter and the research using two dimensional finite element analysis conducted by Powrie et al. (2007), the magnitude of pressure inserted to subgrade layer due to the application of 98.1kN vertical load through a G44 sleeper may have the pressure values shown in Table 3.7.

The spread load method with a load spread of 2:1 provides the closest value to the other analytical and numerical methods. Therefore, analysis using a spread load of 2:1 is sufficient to estimate the pressure exerted on the subgrade layer. In addition to this, it is clearly seen that the vertical pressure at a certain depth caused by a uniformly distributed vertical load over circular area is always greater than that beneath a rectangular area, including the special case of a square. Therefore, applying the assumption of a circular surface load is conservative.

Chapter 4: Review of current ballast assessment techniques and gradings

4.1 Introduction

This Chapter describes the current global assessment technique used to specify the aggregate materials for use as railway ballast which are applied by most railway authorities. The tests used to obtain the parameters based on engineering assessments that are typically required to determine the suitability of quarried materials to be used as ballast are also described. The parameters from the tests on ballast sourced from Cliffe Hill quarry used for the laboratory tests in this research are also presented.

This Chapter pays particular attention to current ballast gradings applied in both the UK and other countries around the world. Some comparisons of ballast PSD between particular railway authorities are presented and previous research into ballast gradings is critically appraised.

4.2 Current ballast assessment techniques

The industrial specification for railway ballast has criteria related to shape, angularity, particle size and PSD (Selig and Roner, 1987), as well as the type of parent rock that is acceptable. The parent rock material is required to be strong enough to resist surface attrition and degradation caused by the hammering action of rail traffic (Geological Society, 2001). The parent rock of Cliffe Hill quarry ballast used in this research is Granodiorite, an intrusive igneous rock and classified as granite.

The increasing cost of railway track substructure maintenance has made the selection of appropriate aggregate for ballast applications a matter of considerable financial importance. It is considered to be more cost effective to use first class ballast in high intensity high speed and/or heavy freight routes than in little used branch lines. It is important to assess any prospective ballast material relative to other available materials and to evaluate the associated costs and benefits. Coarse angular material is preferred as railway ballast, because these particles have a natural tendency to form a stable isotropically homogeneous layer with no planes of weakness.

A good ballast material is expected to cope under short and long term loading in terms of elastic response, permanent deformation and degradation. Elastic response governs the ability of the ballast to return to its original shape or position after an applied load has been removed. AREA recommends that railway track structure deflection including ballast and subgrade, should not exceed 6.35 mm (Kerr, 2003). This deflection value seems high and is presumably a worst case scenario. Permanent settlement and degradation occur due to repeated loading, which leads to particle re-arrangement breakage. To be able to provide the elastic response and withstand repeated loading, ballast must have the following characteristics (modified from (Kerr, 2003)):

- a. Strength to resist the crushing action of superimposed track and dynamic traffic loading.
- b. Hardness to resist abrasion at particle contacts and to withstand wear.
- c. Toughness to resist breakdown by fracturing under impact loads.
- d. Durability to resist abrasion and weathering.
- e. Stability, to achieve this, ballast needs to be suitably graded and appropriate shape.

A number of tests are available to assess the potential of rock to become railway ballast particles (Selig, 1985). However, there appear to be two key reasons why ballast may be unsatisfactory. The first is because of the excessive breakdown of ballast particles and the second is due to instability of the ballast bed as the result of unsuitable of ballast shape (Gaskin and Raymond, 1976). Engineering tests for ballast employed around the world are detailed below:

4.2.1 Load resistant characterisation

Commonly available load resistance tests into an assemblage of grains are as follows (Selig and Waters, 1994):

- a. Impact test. The impact value gives relative measure of resistance to sudden shock loading or impact. In this test the prepared specimen is placed in a steel mould and is subjected to 15 blows of a 14 kg weight falling freely from a height of 380 mm. The impact values expressed in percentage is the ratio of the weight of the fines produced to the total sample weight.
- b. Crushing value test. The crushing test provides relative measure of the resistance of an aggregate to crushing under gradually applied load. A specimen is prepared and placed in a steel mould 154 mm diameter and 134 mm deep. A load is applied to the top of this specimen and is gradually increased to 390kN in 10 minutes. The crushing value expressed in percentage is the ratio of the weight of the fines produced compared to the total sample weight.
- c. Los Angeles abrasion test. This test is a dry test to measure ballast particle toughness or tendency for breakage. It consists of revolving 10 kg of ballast with 12 steel balls weighing a total of 5 kg in a large steel drum for 1000 revolutions. The impact of the steel balls on the ballast particles causes crushing. The ballast is removed and washed on a 4.25 mm sieve. The Los Angeles abrasion value is the quantity of material finer than 4.25 mm sieve generated by the test compared to the original sample weight. This measurement is more significant to the ballast for used in the track for trains with a heavier axle load. Based on this test Cliffe Hill quarry ballast has Los Angeles abrasion value of 16 (Midland Quarry, 2011).
- d. Deval abrasion test. This test was originally used in England for evaluating highway materials and was adopted for use in the railway industry. This test is considered by BR to be the best indicator of ballast performance in service. It can be used to define the minimum durability required to achieve the desired ballast life in the British climate with concrete sleepers. A specimen mass of 5 kg is rotated in a cylinder mounted on a shaft with the axis inclined 30 degree to the axis of rotation of the shaft. The cylinder is rotated 10,000 times at a rate of 30-33 rotation per minute (RPM). The attrition value is the mass of particles generated that are finer than a 2.36 mm size sieve, expressed as a percentage of the initial specimen mass. This test may be conducted with dry ballast particles or by adding an equal mass of clean water to the dry specimen. Cliffe Hill quarry ballast has Deval abrasion test value of 6.5% (Midland Quarry, 2011).
- e. Mill abrasion test. This test is a wet abrasion test which involves revolving 3 kg of ballast together with water in a 229 mm external diameter porcelain jar for 10,000 revolutions at approximately 33 RPM. This type of rolling causes ballast wear without crushing. The Mill abrasion value is the mass of material finer than a 0.075 mm sieve generated by the test compared to the original sample weight. The Mill abrasion test measures aggregate mineral hardness, which was found to be the most significant variable influencing the rate of accumulation of permanent vertical deformation by Raymond and Diyaljee (1979b).

- f. Clay lumps and friable particle test. This test defines clay lumps and friable particles as particles that can be broken by fingers after the aggregate has been soaked in water for 24 ± 4 hours. This test can also be an additional test to PSD test of ballast to determine the fines content, which potentially can fill the ballast voids.

These tests measure mainly the toughness of an aggregate and are only slightly affected by the hardness of its minerals (Raymond, 1985b).

4.2.2 Assessment of stability

Properties of ballast that relate to its ability to provide a stable support are (Raymond, 1985b):

The bulk density

The bulk density of the ballast largely governs the performance of the track in terms of both vertical and lateral resistance to movement (holding capacity) of the track. The track holding capacity will increase as the track mass increases. Other material properties that are related to or influence the bulk density are (Selig and Waters, 1994):

- a. Particle specific gravity. This is an important factor influencing ballast bulk density (unit weight) which can be determined by a water displacement method.
- b. Absorption. Water absorption is an indication of the rock porosity which relates to its strength. Absorption is also part of the specific gravity test.
- c. Rodded unit weight. This test is used to determine the dry density of ballast by compacting the ballast into a rigid cylindrical container through the use of tamping with steel rod. The container size is depends upon the aggregate particle size and normally has container volume of 0.028 m^3 , with a height and diameter of 33 cm. Ballast is placed in three equal height layers and twenty five vigorous tamps with steel rod are applied to each layer.

Particle shape and texture

A shape factor for railway ballast was developed by Raymond in conjunction with research for the Canadian railroads. The shape and texture of particles is theoretically the result of ballast production. A good ballast particle interlock requires a minimum of elongated or flaky particles e.g. rejection of rock sources with a slate-like structure. Particle shape and texture have been recognised as having a major effect on railway track structure stability. The tests for particle shape and texture are outlined below (Selig and Waters, 1994):

- a. Flatness or flakiness. Flatness and flakiness are different names for the same shape characteristic. The British Standard (BS), BS EN933-3:1997 defines a flaky particle as one in which the ratio of thickness to width is less than 0.6. The flakiness index is the percentage by weight of flaky particles (passing the gauge shown in Figure 4.1) in a sample.

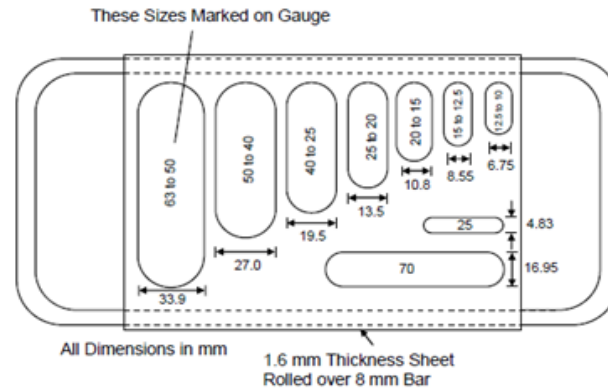


Figure 4.1: Flakiness index gauge

In the U.S, the U.S Army Corps of Engineers defines a flat particle as one with a thickness to width ratio less than 1/3. Flatness is the percentage by weight of flat particles in a sample. Cliffe Hill quarry has flakiness index test of 15% based on the BS.

- b. Elongation. The BS 812-105.2:1990 defines an elongated particle as one with length to width ratio of more than 1.8.

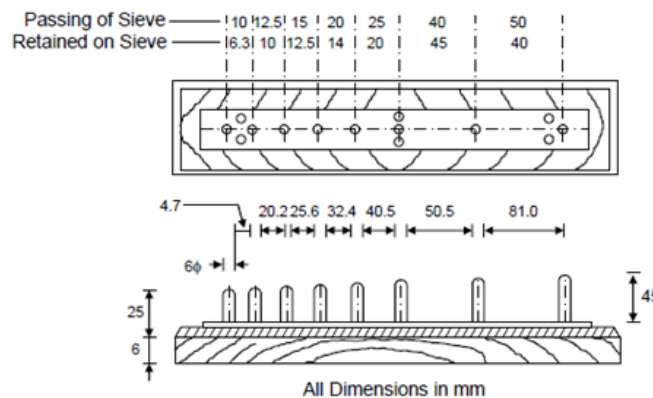


Figure 4.2: Elongation index gauge

The U.S Army Corps of Engineers defines an elongated particle as one with a length to width ratio greater than 3. In both cases the elongation index is the percentage by weight of elongated particles (smaller than the slot on the gauge shown in Figure 4.2) in a sample.

- c. Sphericity. This test is a measure of how much the shape of a particle deviates from a sphere. The perfect sphere has a sphericity of one.
- d. Angularity or roundness. This is a measure of the sharpness of the edges and corners of an individual particle.
- e. Fracture particles. This test has been defined by the Canadian Pacific (CP) railroad. A fractured face is a freshly exposed rock surface with minimum dimension of at least 1/3 the maximum particle dimension. A particle is considered fractured if it has 3 or more fractured faces.
- f. Surface texture. Surface texture has an important influence on ballast performance and it relates to the frictional characteristics of the fractured surface. However, there is no widely accepted test to measure this characteristic.

4.2.3 Assessment of weathering

The two tests commonly specified to assess the potential of aggregates to degrade or weaken due to weathering are:

1. Soundness test. This test simulates the weathering characteristics of an aggregate or more precisely its ability to resist the weathering process. The real test of soundness is where ballast particles are alternatively immersed and then dried using a salt solution. The salt solution that has been recommended by ASEA is Sodium Sulphate, although Magnesium Sulphate was suggested as a more appropriate solution to use in this test by Raymond (1985b). The importance of the soundness test will be more significant in regions where both atmospheric pollution and freeze-thaw are greatest.
2. Freeze-thaw breakdown. This test is to check the resistance of ballast to frost action, swelling and softening and uses oven dry ballast particles which are immersed either partially or completely in water or a water-alcohol solution. The test indicates the ability of the ballast particles to retain water which could freeze and cause degradation during daily freeze-thaw cycles or could react chemically with minerals. This absorption test is carried out in relation to the rainfall during the time of year freeze-thaw cycles occur and the impurities of the local rainwater where material is to be used (Raymond, 1985b). Particles with fractured surfaces may offer more opportunity for penetration of water and hence for freeze-thaw degrading. Elongated, angular particles offer more surface area than smooth, spherical particles (Selig and Waters, 1994).

4.2.4 Cementing characteristics of ballast

The term cemented ballast is used to describe a variety of conditions ranging from moist to dry, heavily fouled ballast to ballast conditions in which the coarse particles are bound together in a matrix formation. The bonding types of cementing in ballast can be created through chemical reactions, cohesion from capillarity attraction (due to fouling materials) or a secondary bonding mechanism. The type of cementing occurring in the ballast can be determined by soaking the ballast in water. Chemical bonding will remain strong whereas the other types of bonds will weaken and be lost once placed in water (Selig and Waters, 1994).

4.2.5 Identification of ballast composition

Boucher and Selig (1987) stated that the performance of ballast in track is not only a function of field conditions, particle shape and grading but also factors identified by petrographic analysis. Petrographic analysis uses a hand lens or low powered of microscope to examine samples of freshly broken rock to determine mineralogical characteristics in the selection of a suitable quarry (Clifton et al., 1987, Raymond, 1979, Raymond, 1985b, Watters et al., 1987). The value of the petrographic analysis depends to a large extent on the ability of the petrographer to correlate data provided on the source and proposed use of the material with findings of the petrographic examination. To support petrographic analysis, chemical analysis also needs to be conducted to determine the type and proportion of constituent elements in a material and to identify and estimate the potential for chemical breakdown. This analysis normally uses standard analytical chemistry techniques and X-ray diffraction and will be most useful for the fines in ballast since petrographic analysis will generally be adequate for visible rock particles.

4.3 Ballast gradings

Size and grading are important parameters for railway ballast. The size of ballast was selected based on trial and error with different sizes over the years. The selection based on size would allow efficient

and easy maintenance of the track with a tamping machine (Claisse and Calla, 2006). This opinion agrees with the ballast categorisation based on the maintenance process introduced by Raymond (1979) that due to the operation of high speed and high density traffic, little time is allowed for track maintenance and requires predominantly mechanical maintenance procedures. Raymond (1979) categorised the maintenance process based on the nominal maximum of ballast particle size that maintenance by predominantly machine, mixed machine and labour and predominantly labour is suitable for the particle size of 65 mm, 40 mm and 25mm respectively. This provides the reason that ballast used by railway authorities around the world tends to be uniformly graded (Raymond and Diyaljee, 1979c) and the selected ballast grading for railway track use is independent of the aggregate source with field production based on the use of two or three sieves (Raymond, 1985b).

A balanced compromise has evolved in North America by reducing a common top size to 38 mm in order to achieve a better grading. The optimum grading of ballast should ideally be in between uniformly and broadly graded aggregates that provide higher strength and less settlement. The optimum grading should still give sufficient hydraulic conductivity (permeability) along with sufficient initial density, shear strength, resilient modulus and be easy to be maintained. However, broadly graded ballast may segregate during handling and transportation (Klassen et al., 1987, Raymond, 1985b).

This Section describes current ballast grading in the UK and other countries around the world. Particular attention is paid to standard ballast grading employed in Australia, the U.S and Canada for comparison while the rest are provided in Appendix A.

4.3.1 British ballast specification

Ballast in the UK must comply with the Railway Track Line Specification, RT/CE/S/006 (Network Rail, 2000) in terms of its grading, properties and shape. There are two ballast specifications in the UK; the original 2000 specification and the new 2005 specification. The original (2000) specification requires the ballast grading to comply with a certain size distribution; 28 to 50 mm for Standard Track Ballast and Stone Blower Aggregate (STBSA) (British Standards Institution, 2004). Table 4.1 presents the PSD for the original (2000) specification.

Table 4.1: The Original (2000) ballast specification (after Network Rail, 2000)

Sieve size (mm)	Percentage passing sieve (%)
63	100
50	100-97
37.5	65-35
28	20-0
14	2-0
1.18	0.8-0

Table 4.2: Ballast grading accordance with EN13450 (after British Standards Institution, 2002, British Standards Institution, 2013)

Sieve size (mm)	Ballast size of 31.5-50 mm			Ballast size of 31.5-63 mm		
	Percentage passing by mass					
	Grading category					
	A	B	C	D	E	F
80	100	100	100	100	100	100
63	100	100-97	100-95	99-97	99-95	99-93
50	99-70	99-70	99-70	99-65	99-55	70-45
40	65-30	70-30	75-25	65-30	75-25	40-15
31.5	25-1	25-1	25-1	25-1	25-1	7-0
22.4	3-0	3-0	3-0	3-0	3-0	7-0
31.5 to 50	≥ 50	≥ 50	≥ 50	-	-	-
31.5 to 63	-	-	-	≥ 50	≥ 50	≥ 85

NOTE 1: The requirement for passing through a 22.4 mm sieve applies to railway ballast sampled at the place of production.
NOTE2: In certain circumstances a 25 mm sieve may be used as an alternative to the 22.4 mm sieve when tolerance of 0-5 would apply (0-7 for category F)

European countries have a standard produced by all interested parties through a transparent, open and consensus based process. The European Standard or Euro Norm (EN) provides rules and guidelines around products, services and systems to increase product safety and quality as a key component of the single European market. The EN standard specifies railway ballast grading as shown in Table 4.2. The purpose of the different grading categories shown in Table 4.2 is to define the value of fine particle content (passing through the 0.5 mm sieve), fines particles (passing through the 0.063 mm sieve), particle length, degradation of railway ballast during transport, maximum percentage passing through the 22.4 mm sieve and environmental conditions.

The new (2005) UK specification recommends EN13450 grading category A as an equivalent of the STBA grading requirement and thus EN13450 has been established as the railway ballast standard in the UK (British Standard, 2002). This standard recommends a consistent mixture of ballast particles sizes in the range 31.5 to 50 mm to conform to Table 4.3.

Table 4.3: The New (2005) specification for ballast particles (after Network Rail, 2000)

Sieve size (mm)	Percentage passing sieve (%)
63	100
50	100-70
40	65-30
31.5	25-0
22.4	3-0
32-50	≥50

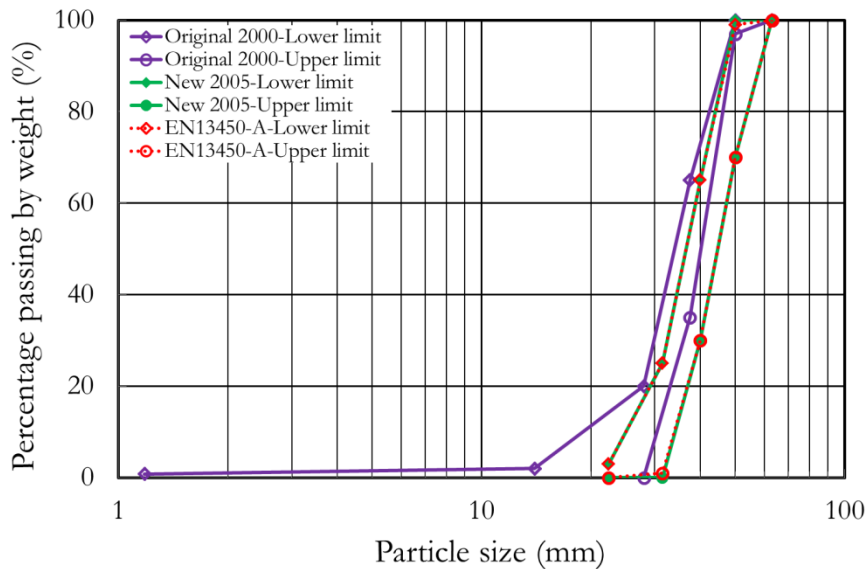


Figure 4.3: Comparison of NR's ballast original 2000 into new 2005 specification

Figure 4.3 shows that the recommendation to follow envelope grading of EN13450 category A implies the use of larger ballast particles. However, the main reason for the recommendation is unclear and perhaps it is just to accommodate a mechanical maintenance process.

Apart from the UK, some other countries have also employed EN13450 as standard ballast grading. These countries are:

1. Germany. Ballast for use on the Deutsche Bahn (DB) in Germany is required to consist of a quarried rock that is judged on the basis of the appropriate DIN standard and must have a compressive strength of at least 180 N/mm². The ballast grading needs to comply with EN13450 category D (Deutsche Bahn, 2004).
2. Finland. Railway tracks in Finland employ a ballast grading envelope of EN13450 in different categories for specific lines. The main lines in Finland employ category F of EN13450 as the ballast grading envelope whilst categories C and E are used for low trafficked track (Kuula-Vaisanen and Kaivola, 2002).
3. Norway. In Norway the railway network is divided into 5 categories according to the number of passengers and freight tonnage. However, this division is not reflected in the ballast requirement in Norway or other countries. Ballast used in Norway employs grading envelope category E of EN13450 for every category of track (Nalsund, 2010).

4.3.2 American ballast specification

In the early days of the U.S. railroad industry, a various materials were used for railway ballast to support the track superstructure. Almost any ballast material which could be procured at low cost was used and considered satisfactory under traffic loading. Common rock materials considered suitable in the U.S for ballast were granite, trap rocks, quartzite, dolomites and hard limestone. As limestone degrades, it tends to produce fine particles that cement together and thus is not the best ballast choice if other hard rock material is economically available (Unified Facilities Criteria, 2004). Table 4.4 shows ballast gradings recommended by AREMA (AREMA, 2000).

Table 4.4: Recommended AREMA ballast gradings (after AREMA, 2000)

AREMA No	Nominal size (mm)	Percentage passing (%)									
		75 mm	63 mm	50 mm	37.5 mm	25 mm	19 mm	12.5 mm	9.5 mm	4.75 mm	2.36 mm
24	63-19	100	100-90		60-25		10-0	5-0	-	-	-
25	63-9.5	100	100-80	85-60	70-50	50-25	-	20-5	10-0	3-0	-
3	50-25	-	100	100-95	70-35	15-0	-	5-0	-	-	-
4A	50-19	-	100	100-90	90-60	35-10	10-0	-	3-0	-	-
4	37.5-19	-	-	100	100-90	55-20	15-0	-	5-0	-	-
5	25-9.5	-	-	-	100	100-90	75-40	35-15	15-0	5-0	-
57	25-4.75	-	-	-	100	100-90	-	60-25	-	10-0	5-0

Note 1: Grading number 24, 25, 3, 4A, and 4 are main line ballast materials. Grading number 5 and 57 are yard ballast materials.

Table 4.5: Modified AREMA No.3 grading (after Norfolk Southern Corporation, 2011)

Sieve size (mm)	Percentage passing (%)	
	AREMA 3	Modified 3
63.0	100	100
50.0	100-95	100-95
37.50	70-35	65-30
25.0	15-0	15-0
12.5	5-0	5-0

AREMA No. 4 grading is identical to American Standard Testing for Material (ASTM) C33 grading 4. Additionally, ASTM C33 grading 56 is very similar to AREMA grading No. 5. Most railway companies in the U.S. implement AREMA gradings; only Norfolk Southern Corporation (NSC) has modified AREMA grading No. 3 for heavy tonnage tracks and uses AREMA grading No. 5 for the yard (Norfolk Southern Corporation, 2011). The modification carried out by NSC to the AREMA No 3 grading is presented in Table 4.5 and Figure 4.4.

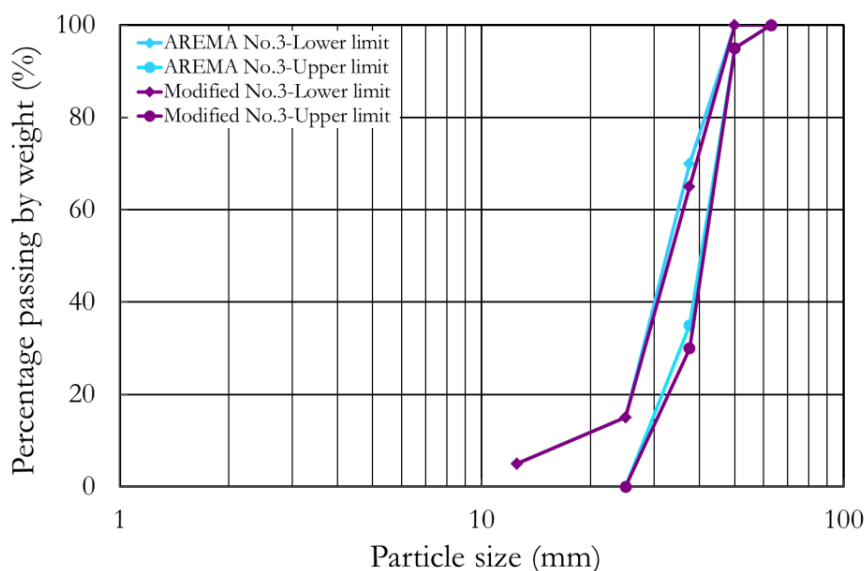


Figure 4.4: PSD of modified AREMA No 3 used by NSC

The results presented in Figure 4.4 show that NSC has increased the proportion of bigger size ballast particle. The scientific reasons of choosing this slightly bigger grading than AREMA No 3 by NSC are not clear.

4.3.3 Canadian ballast specification

Canadian National Railway (CNR) adopted AREMA No.5 grading (Table 4.6). This type of grading has ballast particles ranging from 9.5 to 25 mm, the PSD is still categorised as a uniform grading in the smaller size.

Table 4.6: CNR ballast grading (after Canadian National Railway, 2007)

Nominal size (mm)	Percentage passing (%)
37.5	100
25	100-90
19	75-40
12.5	35-15
9.5	15-0
4.75	5-0

Conversely in the U.S, AREMA grading No.5 is used for yard ballast material. The main purpose of applying finer ballast grading to the yard is to provide improved walking conditions along the track. This finer grading does not impinge track on drainage as the construction practice for yard facilities ensures quick run off for ground water through the under track and yard drainage systems. Tables 4.7 shows the ballast gradings used in Canada by Canadian Pacific Rail (CP).

Table 4.7: CP Rail ballast gradings (after Canadian Pacific Rail, 1984)

Grading	Nominal size (mm)	Percentage passing (%) of size (mm)								
		63	50	37.5	25	19	12.5	9.5	4.75	0.075
CP5	50–25	100	100-90	70-35	5-0				3-0	2-0
CP4	37.5-19		100	100-90	55-20	5-0			3-0	2-0
CP3	37.5–12.5		100	100-90	90-70	50-30	20-0	5-0	3-0	2-0
CP2	37.5-9.5		100	100-90	90-70	70-50	45-25	25-10	3-0	2-0

Note: Ballast grading 2 and 3 are for crushed gravel, 4 is for crushed gravel, crushed rock or slag and 5 is for crushed rock or slag.

Comparing CNR’s ballast grading with the smallest CP’s ballast grading available (i.e. CP2) shows that in general, CNR’s grading has a larger particle smaller than CP2’s grading and has a higher quantity of middle size particles. The PSD is for both gradings is presented in Figure 4.5.

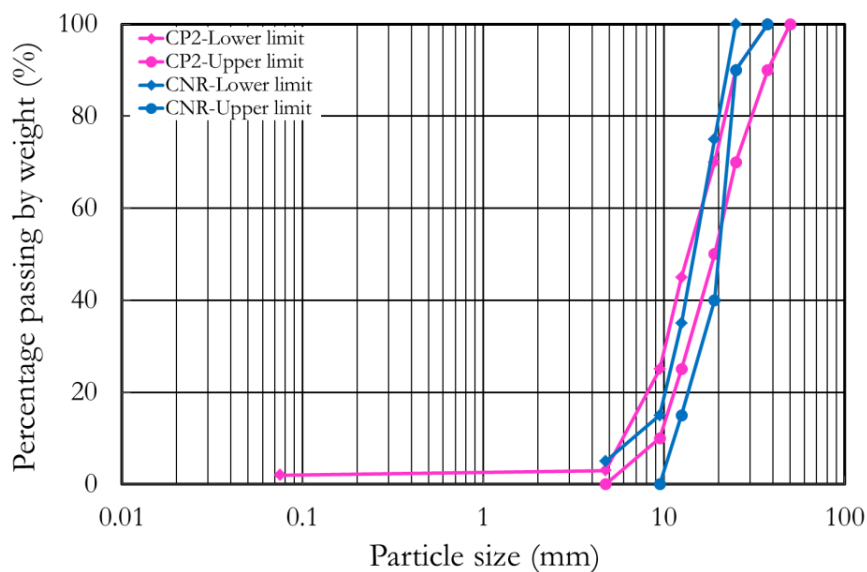


Figure 4.5: Comparison of CP2 and CNR ballast gradings

The application of uniformly graded ballast in a smaller size by CNR was due to a review of the research on uniform grading conducted by Raymond and Diyaljee (1979c). This led to a conclusion that uniformly graded ballast in smaller sizes deforms less.

4.3.4 Australian ballast specification

Table 4.8 shows the railway ballast grading recommended by the Standard Association of Australia (SAA), which is composed of medium to coarse size aggregate ranging from 20 to 60 mm. These recommended grading envelopes are used and altered slightly by different rail authorities e.g. Queensland Rail and Australian Rail Track Corporation (ARTC) in New South Wales without considering the sleeper type. The ballast grading envelopes used by specific railway authorities in Australia are presented in Tables 4.9 and 4.10.

Table 4.8: SAA Ballast specification (after Indraratna and Salim, 2005)

Sieve size (mm)	Percentage passing (%)			
	Nominal size (mm)			
	60	60 (steel sleeper)	50	50 (Graded aggregate)
63.0	100	100	-	-
53.0	100-85	100-95	100	100
37.5	65-20	70-35	100-90	100-70
26.5	20-0	30-15	55-20	-
19.0	5-0	15-5	15-0	60-40
13.2	2-0	10-0	-	-
9.5	-	1-0	5-0	30-10
4.75	1-0	-	1-0	20-0
1.18	-	-	-	10-0
0.075	1-0	1-0	1-0	1-0

Table 4.9: Queensland rail ballast specification (after Indraratna and Salim, 2005)

Sieve size (mm)	Percentage passing (%)
63.0	100
53.0	100-95
37.5	64-42
26.5	10-4
19.0	5-2
13.2	4-1
9.5	3-0
4.75	0

Table 4.10: ARTC ballast specification (after Australian Rail Track Corporation Ltd, 2007)

Sieve size (mm)	Nominal size 60 mm
	Percentage passing (%)
63.0	100
53.0	100-85
37.5	65-20
26.5	20-0
19.0	5-0
13.2	2-0
4.75	1-0
0.075	1-0

RailCorp engineering standard ballast specification uses a slightly smaller grading envelope than the Queensland and ARTC rail authorities. RailCorp ballast specification is based on the recommendation of research results from Wollongong University, Australia which are discussed in next section. The grading used by RailCorp is shown in Table 4.11.

Table 4.11: RailCorp ballast specification (after RailCorp Engineering Specification Track, 2009)

Sieve size (mm)	Ballast graded	
	Standard	Fine
	Nominal size (mm)	
	60 (Graded ballast)	50 (Graded aggregate)
	Percentage passing (%)	
63.0	100	-
53.0	100-85	100
37.5	70-50	100-70
26.5	35-20	-
19.0	20-10	60-40
13.2	10-2	-
9.5	5-0	30-20
4.75	2-0	20-10
2.36	-	5-10

Note: Standard ballast grade is used for any area on new or existing track line and Fine ballast grade is used only on the existing siding with the radius more than 800 meters.(after Railcorp Engineering Standard Track, 2009a)

Figure 4.6 compares Australian railway authorities' ballast gradings with EN13450 standard category A. In general, the lower limit of ballast grading used by Australian railway authorities is smaller than the lower limit of ballast grading of EN13450 standard category A. This encourages the thought that the ballast grading in the UK could be optimised to be more broadly graded or could employ a smaller grading envelope than the standard currently in use.

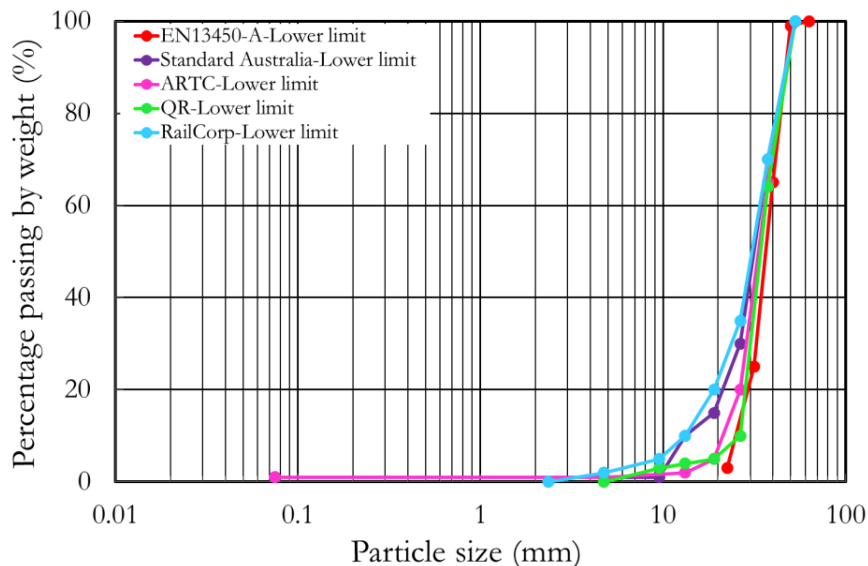


Figure 4.6: Comparison of EN13450 category A to Australian railway ballast gradings

Apart from the ballast grading previously discussed, in other countries e.g. Italy, Spain, France, Sweden, Turkey, India, and Japan, ballast for railway substructure is employed based on the policy of railway authority and also considers the sleeper type. The grading envelopes and the recommended ballast materials employed by these countries are presented in Appendix A.

4.4 Tests on ballast gradings

There is no extensive research regarding the performance of different ballast gradings. The tests that have been carried out use two principal methods of investigation:

1. Experiments in the laboratory.
2. Modelling using DEM.

4.4.1 Investigation using laboratory testing

Figure 4.7 shows four different ballast gradings tested by Indraratna et.al (2005) using cyclic triaxial apparatus to evaluate the effects of PSD on the behaviour of ballast settlement and degradation. In this research, specimens were subjected to an effective confining pressure of 45kPa and to simulate the train axle loads running at high speed, cyclic loading with a maximum deviator stress (q_{max}) of 300kPa was applied at a frequency of 20Hz.

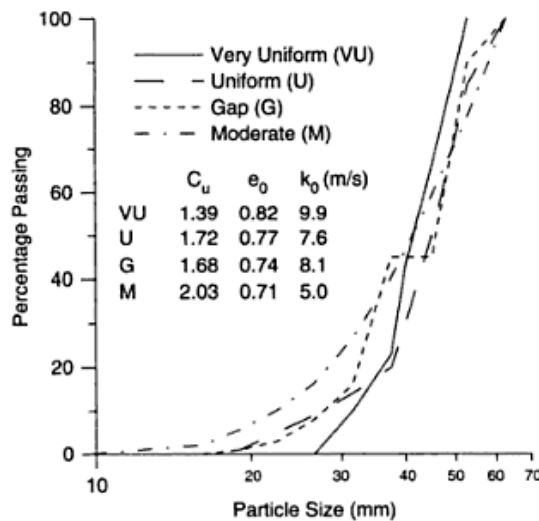


Figure 4.7: PSD of ballast for cyclic triaxial tests (Indraratna and Salim, 2005)

The tests conducted by Indraratna et.al have also shown the effect of PSD on the axial and volumetric strain and particle breakage of the ballast under cyclic loading. The test results are shown in Figures 4.8 and 4.9.

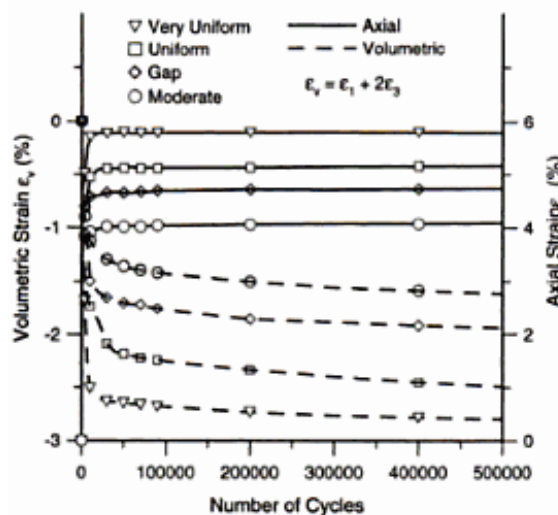


Figure 4.8: Axial and volumetric strain of different PSD tested (Indraratna and Salim, 2005)

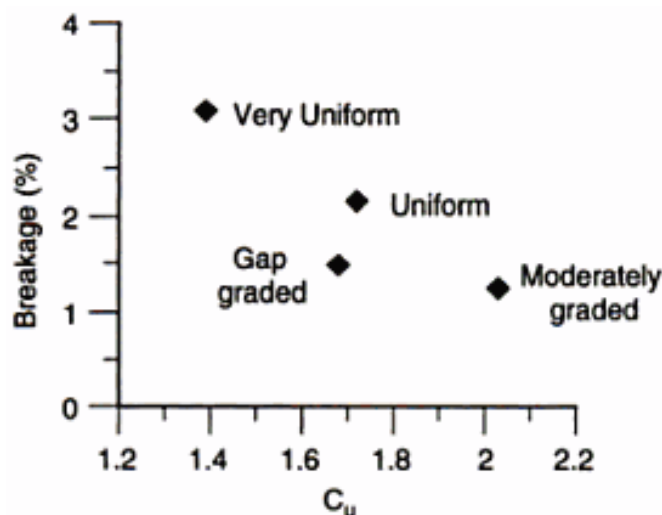


Figure 4.9: Effect of PSD on particle breakage (Indraratna and Salim, 2005)

The test results reveal that ‘very uniform’ to ‘uniform’ samples provided higher axial and volumetric strains. In contrast, ‘gap-graded’ and ‘moderately graded’ distributions provided denser packing thus decreased the settlement. The tests also showed a relationship between the C_u value and particle breakage; ballast breakage decreases as the value of C_u increases, with the exception of the gap graded specimen. Based on these test findings, Indraratna and Salim (2005) recommended a grading that has a distribution similar to the moderate grading shown in Figure 4.7 and has a C_u value exceeding 2.2 but not more than 2.6. The recommended ballast grading is relatively more well-graded than current Australian Standards presented in Table 4.8. Table 4.12 compares the percentage of particles at the same sieve size in the Australian Standard and the ballast grading recommended by Indraratna and Salim (2005).

Table 4.12: Comparison of Australian standard and recommended ballast gradings (after Indraratna and Salim, 2005)

Sieve size (mm)	Australian standard (AS2758)	Recommended ballast (Indraratna and Salim, 2005)
63.0	100	100
53.0	100-85	100-85
37.5	65-20	70-50
26.5	20-0	35-20
19.0	5-0	20-10
13.2	2-0	10-2
9.5	-	5-0
4.75	1-0	2-0
2.36	-	0.0
0.075	1-0	

The recommended ballast grading has a reduced quantity of 37.5 mm sized particles and an increased quantity of particles smaller than 26 mm.

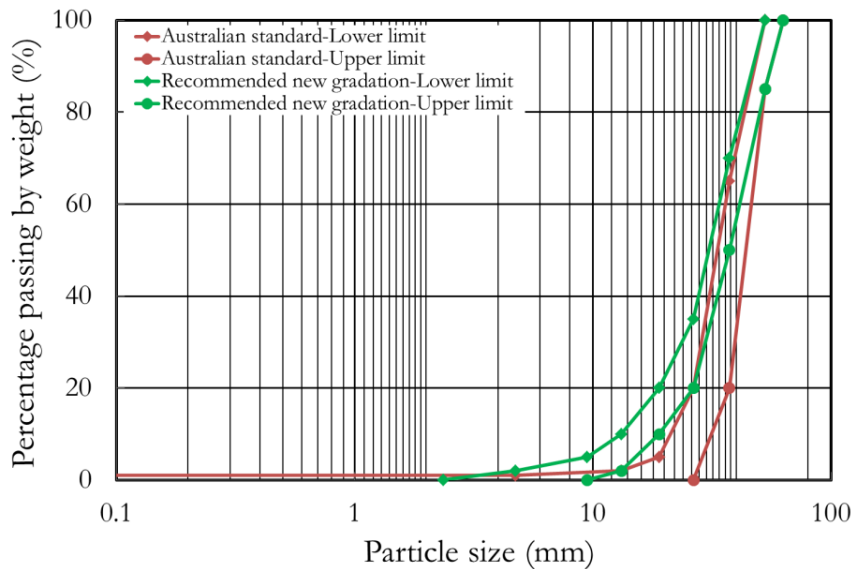


Figure 4.10: Comparison of PSD of Australian standard and the recommended grading

The recommended ballast grading also has an extra sieve size and limits the smallest particle able to pass through to 2.36 mm. Introducing an extra sieve size to limit the particle size as discussed above accommodates the drainage requirement with this grading. As a result, the new composition of ballast particles in the recommended ballast grading shifts the original Australian Standard ballast PSD toward its lower limit as shown in Figure 4.10. This recommended ballast grading has been employed by RailCorp Engineering as its ballast grading specification and is claimed to provide a stronger and more resilient track without causing any significant delay in drainage from the substructure (Indraratna and Salim, 2005).

Laboratory tests to investigate the behaviour of ballast grading have also been carried out in Norway using triaxial tests. The main goal of this research was to compare ballast grading applied by Norwegian railway with AREMA No.4 grading. Norwegian railway ballast follows EN13450 standard category E (Nalsund, 2010) and in this research the Norwegian ballast gradings have been represented by two different grading types known as E-fine and E-coarse. Figure 4.11 shows the PSDs for the ballasts used in the tests.

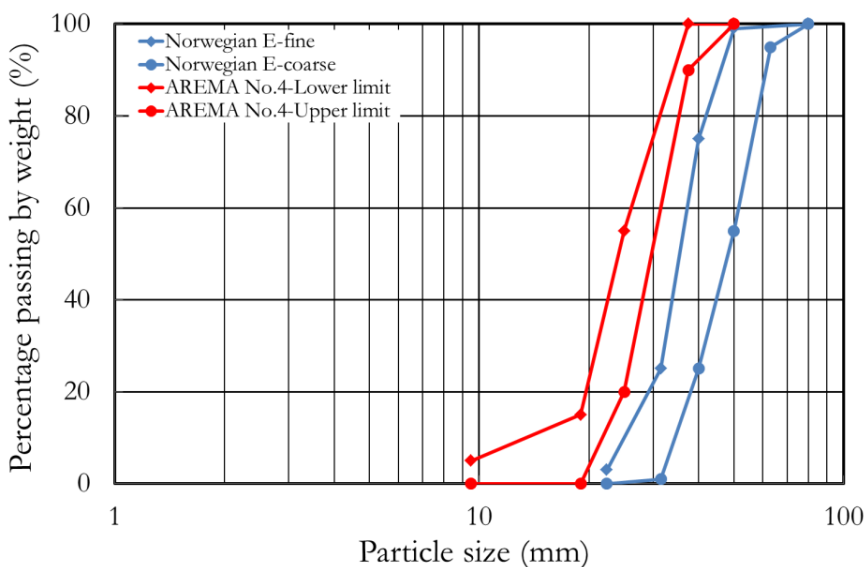


Figure 4.11: Norwegian railway ballast compared to AREMA No 4 gradings

The specimen used for triaxial testing in this research was 300 mm in diameter and 600 mm in height. The parent rock of ballast used in the tests was Meta Sandstone, which is claimed to be harder than granite. A static confining air pressure of 60kPa and a dynamic axial stress of 250kPa were applied. These triaxial tests were carried out using a 5Hz cycle rate as long term cyclic loading to simulate railway traffic corresponding to a 250kN axle load. In a total of 4 million cycles, 110 million gross tons was achieved in 4 steps with 1 million cycles for each step. This research simulated the ballast condition with and without tamping processes. The tamping process was simulated by dismantling the specimen after each million cycles. Particle breakage was investigated by sieving the ballast particles at each dismantling. The sample was then re-compacted prior to applying the next 1 million cycles. Particle breakage material was accumulated from each 1 million cycle step and sieved after the total 4 million load application to give the total amount of particle breakage. This research concluded that a change to a denser PSD has advantages in reducing permanent strain and minimising ballast particle breakage as shown in Figures 4.12 and 4.13. To conclude, the grading of AREMA No.4 performed better than Norwegian railway ballast.

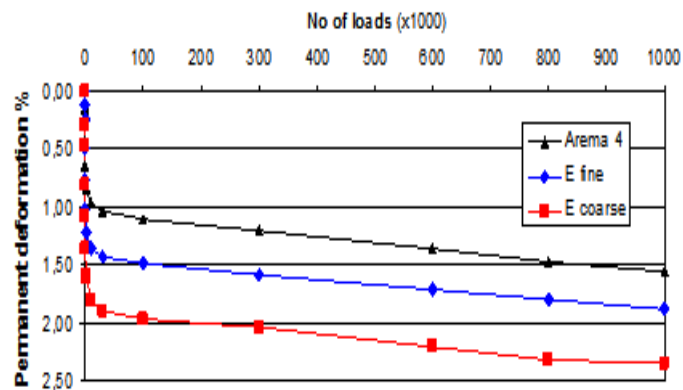


Figure 4.12: Average of permanent vertical deformation against number of loads (Nalsund, 2010)

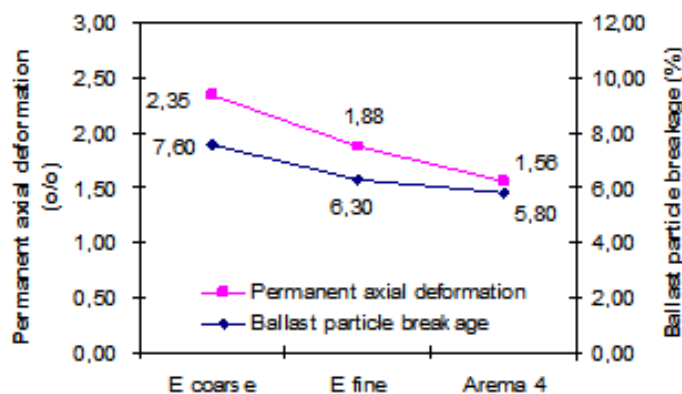


Figure 4.13: Permanent axial deformation compared with amount of ballast particle breakage smaller than D_{Min} in test specimen (Nalsund, 2010)

4.4.2 Investigation using DEM tests

Tutumluer et al (2009) investigated the effect of grading on ballast settlement using an image-aided DEM approach. The mechanical behaviour of ballast layers with different aggregate gradings, including those of the AREMA grading currently in use, was simulated using a full scale track DEM model. The research used the concept of 0.45-power maximum density charts. Concept 0.45-power density chart was originally developed by Fuller and Thompson (1907) using Equation 4.1.

$$P_p = \left(\frac{d}{D}\right)^g \times 100\% \quad \text{Equation 4.1}$$

where: P_p = Percentage finer than an aggregate size.

d = Aggregate size being considered.

D = Maximum aggregate size.

g = Parameter which adjusts curve for fineness or coarseness.

The values of g are considered to be 0.5 for maximum packing of smooth spheres and 0.45 for the maximum packing for aggregate to determine the maximum density line. The maximum density line, i.e. the grading that produces the maximum density appears as a straight line from zero to the maximum aggregate size in the mixture. Using this line, the weight percentage corresponding to any particle size can be calculated. However, the suggested g values were less than the g values recommended by Gaskin et al (1978) which was in the range of 0.7 to 1.0.

A maximum aggregate size of 76 mm was used in Equation 4.1 to determine the maximum density line. The P values are plotted along the y axis. The particle sizes are raised to the power of 0.45, normalised by the maximum value obtained and plotted along the x axis. It was stated in this study that if a sieve size has been set to the minimum size of which ballast particles cannot pass through, the grading curve for the rest of the particles still remains a straight line and the characteristic grading graphs can be generated for different minimum aggregate sizes. However, depending on the minimum size chosen, the grading line will have different slope as shown in Figure 4.14.

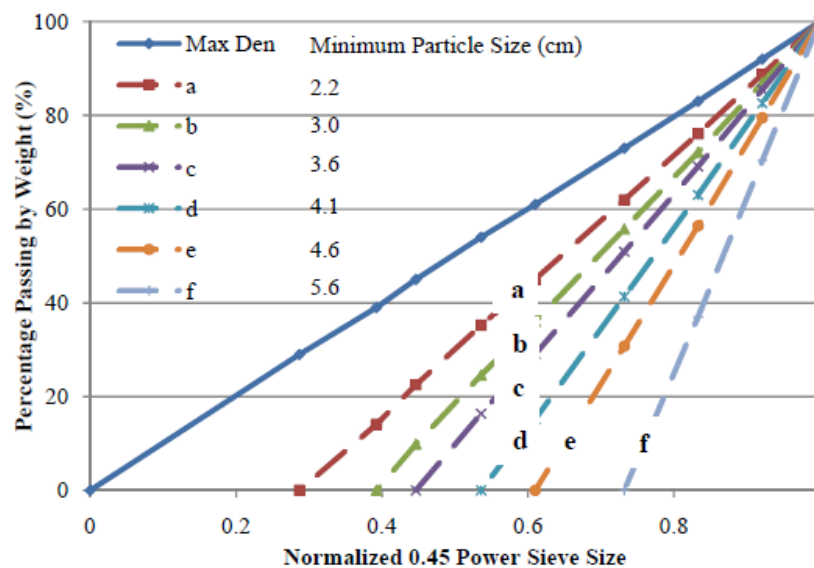


Figure 4.14: Normalized 0.45 power grading chart (Tutumluur et al., 2009)

In this study, typical ballast grading used in Australia (The Rail Infrastructure Corporation (RIC) and Queensland), France and the current standard gradings of AREMA No. 24, No. 3 and No. 4 were considered. Figure 4.15 shows the PSD of the ballasts used in the study. The ballast gradings of RIC, AREMA No.3 and France were represented by the Queensland ballast grading since their PSDs were similar. The grading of AREMA No. 4 falls on the left hand side to represent a smaller parallel PSD. AREMA No. 24 grading is very different from the others since it not only has a different size distribution but also a different maximum particle size.

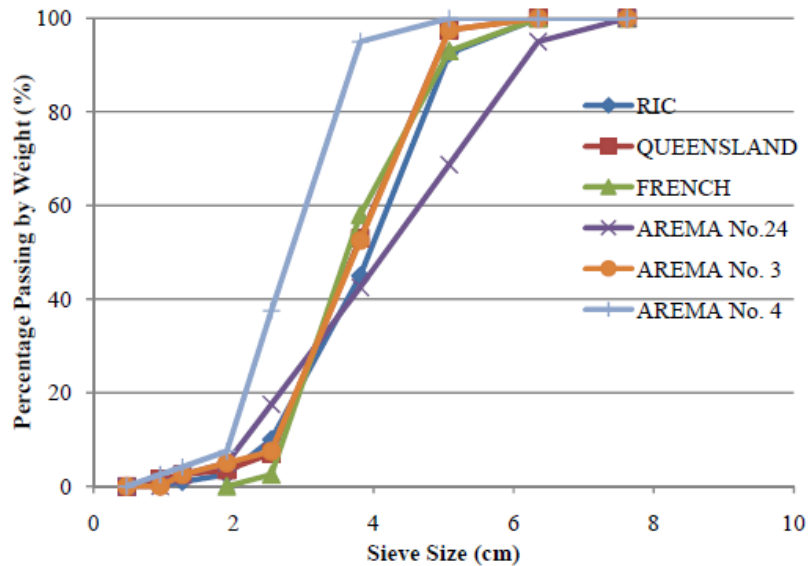


Figure 4.15: PSD of observed ballast gradings (Tutumluer et al., 2009)

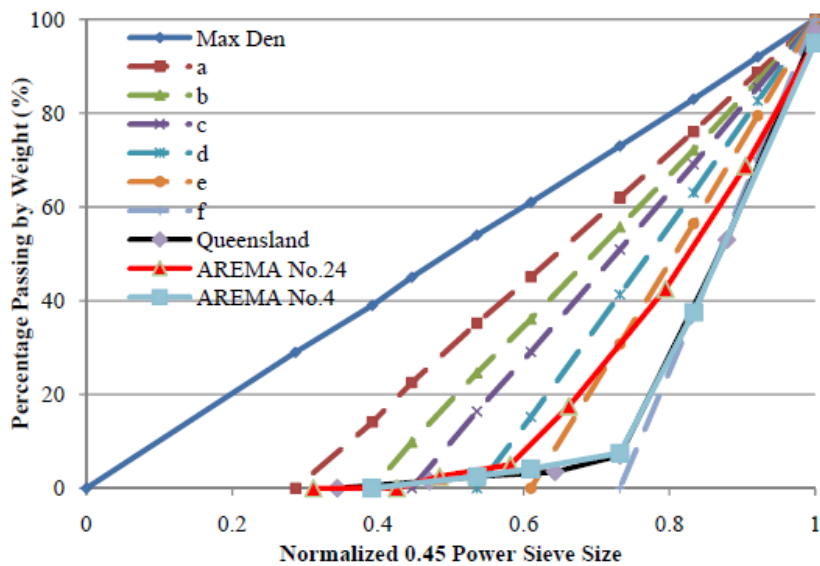


Figure 4.16: PSD of observed ballast plotted on normalized 0.45 power (Tutumluer et al., 2009)

Each percentage of passing particles for each size was plotted along the y axis with the corresponding 0.45 powered sieve sizes along the x axis. Figure 4.16 presents the results of this analysis, showing the Queensland, AREMA No. 4 and No. 24 gradings fall very close to the characteristic grading curve f while the grading of AREMA No.24 has fallen closer to curve e. This implies that the grading of AREMA No. 24 is more densely graded than the other grading types.

The main goal of the DEM study by Tutumluer et al. (2009) was to observe the effect of grading on ballast volumetric properties and settlement performance by an investigation into the air void content of the characteristic ballast grading curve. The results revealed that more uniformly graded aggregate assemblies generally had larger air voids but a higher tendency to produce permanent settlement under repeated train loading. Although larger voids are desirable for better drainage, when particles finer than 36 mm exist in the grading, the stability of void structures and the resistance to permanent settlement is better. The research concluded that the AREMA No.24 grading would result in less settlement than other existing grading. Moreover, according to the DEM methodology employed in the research, there is also room to further engineer current specifications, including AREMA No. 24

grading, by optimising the grading for a minimum allowable particle size of 36 mm, which still accommodates large enough air voids for drainage and minimises the overall settlement potential in the ballast.

All the research results agree that broadly graded ballast performs better than uniformly graded ballast. The initial results provided one change in standard for in service railways. This was at RailCorp, Australia which now uses broadly graded ballast. Based on these results and the evidence provided, there is the potential for NR to optimise the current ballast grading in use. This could be achieved by changing the uniformly graded ballast for more broadly graded ballast in order to increase its stability performance. This optimisation should also include some possible modifications and improvements to current practice and on railway tracks that are currently in use. The availability of large apparatus to perform full scale tests in the laboratory will improve the test methodology when using small sample models. The tests using large apparatus are expected to provide similar results as will be experienced in the field as the field boundary conditions can be simulated.

4.5 General observations into ballast gradings

Based on observations carried out on ballast gradings used worldwide, it seems there is an agreed particle size, particle material or parent rock of coarse aggregate that can be used as railway ballast. However, different opinions among railway authorities as to the appropriate portion of ballast particle retained on a certain size of sieve and the current available ballast grading are followed. Although international standards for grading are often very similar, there is no universal consensus concerning the proper specification for the ballast material to provide the best track performance. In any case, ballast choice may also depend on what is locally available (Selig, 1985) and the selected ballast grading for railway track use is largely independent of the aggregate source provided it meets the applicable abrasion and fracture resistance standards (if they exist: in developing countries there may be no such requirements).

In most countries, ballast design is based on a few sizes and the difference from the smallest to the largest in a given ballast ranges between 1.5 to 8 times. A smaller number reflects ballast that is uniform whereas a higher number represents a broadly graded ballast. In terms of the grading employed in the countries considered, some key differences can be identified:

- Ballast grading in some European countries is different in terms of the percentage of particles passing through identical sieve sizes, even though there is an EN13450 standard as guidance. Although EN13450 has 6 grading options; very few European countries (e.g. U.K, Germany, Norway, and Finland) follow the EN13450 standard exactly for ballast.
- The recommendation of NR to follow EN13450 standard category A and the modification of AREMA No. 3 grading by NSC show a tendency to change the original particle size towards a larger size. There is no clear scientific reason behind this. However, a contradictory decision has been made by RailCorp in Australia to modify the original standard in Australia towards a smaller size, based on intensive research at the University of Wollongong.
- Smaller sizes of ballast grading have become the preferred choice for CNR even though this grading is directed at yard ballast material in the U.S. The PSD is still categorised as a uniformly graded and is based on the results of the research on uniform gradings conducted by Raymond and Diyaljee (1979c).

- Ballast grading with a C_u value higher than 2 following the PSD recommended by the University of Wollongong (Indraratna and Salim, 2005) has become the choice for RailCorp and is incorporated into the engineering standard in this region of Australia. This grading is still categorised as uniformly graded since the value of C_u is less than 3.
- Comparing the grading most predominantly specified in the UK, the U.S, Canada (CNR) and Australia (RailCorp), Figures 4.17 and 4.18 show that CNR uses the finest grading and RailCorp has the broadest grading.

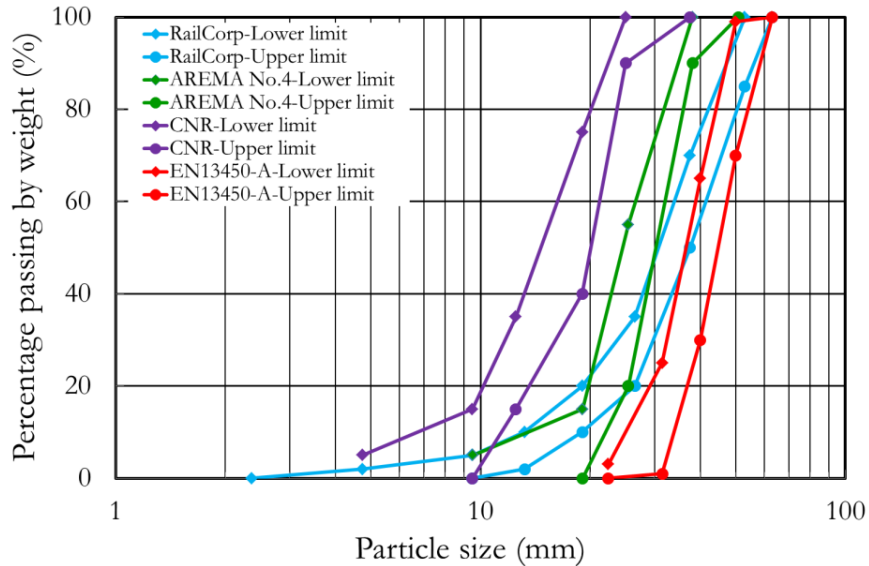


Figure 4.17: Comparison of limit of ballast gradings (Australia, U.S, Canada and UK)

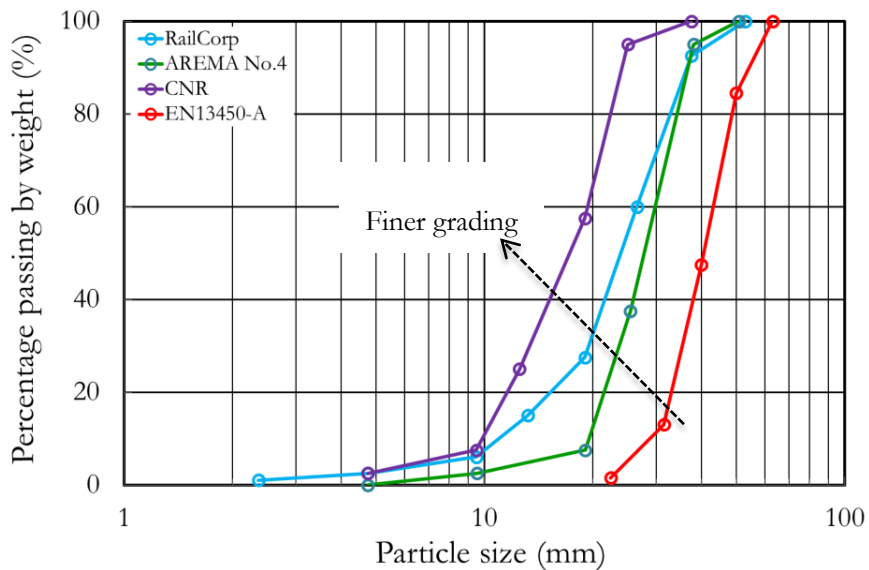


Figure 4.18: Comparison of median ballast gradings (Australia, U.S, Canada and UK)

Railway ballast worldwide tends to be formed of particles between 20 mm and 65 mm with a C_u value of less than 3. Moreover, for European countries, ballast with a C_u value of less than 2 is recommended by EN13450 standard. This clearly shows that ballast gradings used by railway authorities around the world have favoured uniform gradings since at least 35 years ago (Raymond and Diyaljee, 1979a) (AREMA, 2000, British Standards Institution, 2013, Canadian Pacific Rail, 1984). The specification of uniform gradings has come about at least partly due to the historical need to provide a large reservoir for fines that allows the ballast to continue function as a drain even after a

substantial amount of fouling material has occupied the initial void space (which is generally considered to reduce the performance). On the other hand, ballast must provide a high shear strength for stability with minimal trackbed settlement and resilient movement, and these are normally best achieved by well graded aggregates (e.g. Raymond (1985b)). Therefore the optimum grading of ballast should ideally be in between uniformly and broadly graded aggregates to satisfy these opposing needs.

Currently in developed countries there is scope to optimise the historical ballast grading because there is a reduced need to provide fouling reservoirs since the two principal sources of ballast fouling (environmental and from the trackbed) have reduced. For example coal wagons spilling dust onto the track are now rarer in the UK and mechanisms of trackbed fouling such as ballast pumping from soft clay subgrades are better understood and can be controlled by providing sufficient trackbed drainage and the appropriate use of geotextiles and sand blankets in problem locations.

Although railway authorities are inherently conservative when it comes to changing long standing ballast gradings there have been three recent research projects that have recommended more broadly graded ballasts: (1) Australia (Indraratna and Salim, 2005), (2) Norway (Nalsund, 2010) and (3) the U.S (Tutumluer et al., 2009). Only the first of these has resulted in changes to standards for in service railways (RailCorp Engineering Specification Track, 2009) (RailCorp Engineering Standard Track, 2009b). The variant grading adopted by Railcorp in Australia met a criterion that the C_u should lie between 2.2 and 2.6 (Indraratna and Salim, 2005), which was considered to be acceptable to retain sufficient drainage capability.

4.6 Summary

Understanding of the best materials to be used for ballast has increased significantly over the years. Every ballast specification attempts to assess, at least implicitly, the performance of ballast under loading. The best quality ballast will have a low risk of breakdown and high permeability over its lifecycle. It is generally accepted that granite sourced from igneous angular rock is the preferred option for railway ballast.

In terms of ballast grading, worldwide railway authorities still view uniformly graded ballast as the best option. Every railway authority has applied its own ballast specification and it is very difficult to identify the original scientific reasons behind these. Consequently, it is not clear whether the applied specification is the result of intensive research or is just a historical inheritance.

European countries have a standard for ballast grading, EN13450, that advises 6 categories of ballast grading specifications. However only the UK (category A), Germany (category D), Finland (categories F, C and E) and Norway (category E) railway authorities follow this suggested specification, while other European countries opt to use their own ballast grading.

It seems that most railway authorities hesitate to modify the historic ballast grading, probably due to an inherently conservative predisposition. The necessity for railway ballast to be a free draining material is still kept firmly in mind, although research on ballast grading has been conducted in Norway and the U.S using laboratory triaxial tests and DEM method respectively. These two methods of research were used to investigate the behaviour of particular ballast gradings and concluded that a broad grading with a variety of particle sizes will perform better than uniformly

graded material, without reducing the drainage capability. Research has also been conducted in Australia to modify the Australian ballast standard specification. The findings resulted in the RailCorp railway authority changing their ballast standard specification from uniformly graded to more broadly graded. However, all the research identified in the literature into varying ballast grading was only conducted using either numerical modelling methods or laboratory element tests with relatively small specimens that do not fully represent field conditions. Some of the laboratory tests carried out using scaled and simplified samples were not representative of the actual size and formation structurally. Jeffs and Marich (1987) stated that the test results concluded on ballast settlement conducted by Okabe (1961) using triaxial tests did not appear to be evident of second settlement phase, often being formulated as a linear cyclic component. Therefore, in optimising the current standard NR grading by modifying it to be more broadly graded, larger scale laboratory tests and field trials are still needed to investigate the potential benefits.

Chapter 5: Ballast behaviour characteristics, existing ballast settlement models and pressure distribution beneath the sleeper

5.1 Introduction

The understanding of how ballast performs its function has grown steadily through laboratory and field tests. It is now universally accepted that track settlement is caused by repeated and complex traffic loading with the severity of the settlement depending on the quality and the behaviour of the ballast, sub-ballast and subgrade (Dahlberg, 2001, Dahlberg, 2004). In this Chapter ballast behaviour characteristics are discussed based on ballast box tests, triaxial tests and real track observation data (section 5.2). Following this, some existing ballast settlement models are described and discussed in section 5.3 together with the assumed pressure distribution beneath the sleeper (section 5.4).

5.2 Ballast behaviour characteristics

Two key characteristics of ballast behaviour, namely the build-up of horizontal stresses and the rate of settlement, have been intensively investigated. Some of these investigations were carried out using ballast box tests, triaxial tests and the data from real track observation.

5.2.1 Ballast box test

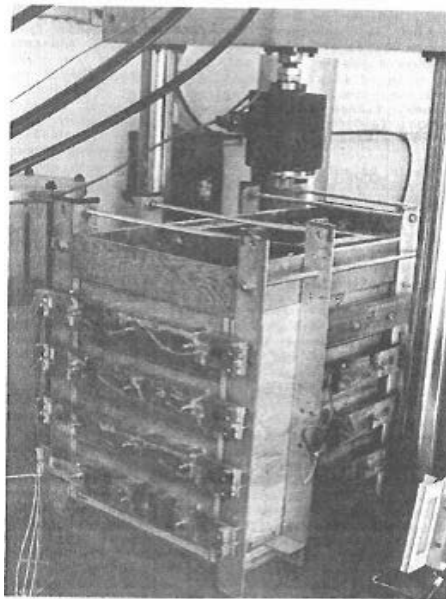


Figure 5.1: Ballast box apparatus (Stewart et al., 1985)

Figure 5.1 shows a ballast testing box (Stewart and Selig, 1984). This test examines the nature and extent of horizontal ballast stresses and simulates conditions in the track near the rail seat and the adjacent crib area. To do this, the ballast box was constructed with instrumented side and end panels to measure horizontal stresses. A flexible bottom was incorporated to represent subgrade layer as shown in Figure 5.2.

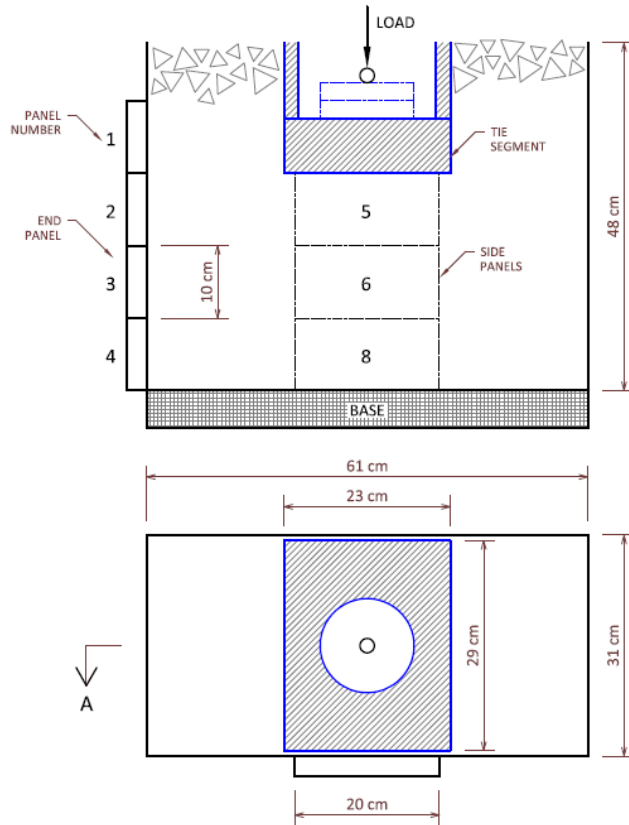


Figure 5.2: Cross section of box test apparatus (after Stewart and Selig, 1984)

In Stewart and Selig's experiments, the ballast box was loaded through a section of sleeper approximately 290 mm by 230 mm located directly below a rail. The box itself was 610 mm long by 310 mm wide. The length was intended to represent half of the crib width on either side of the sleeper segment. The ballast layer was 300 mm deep. The maximum cyclic load applied in this test was approximately 2 tonnes and this load was expected to produce stresses of 300kPa at the base of sleeper segment. These stresses were equal to the stresses at the base of the sleeper beneath the rail seat due to a 15 ton wheel load. Trap rock to AREA No.4 grading was chosen as the ballast material. The physical state of the ballast prior to cyclic loading was intended to be representative of the conditions found under the sleeper rail seat after a maintenance tamping operation (loose). Typical results of horizontal stresses at the side panels and end panels are shown in Figure 5.3.

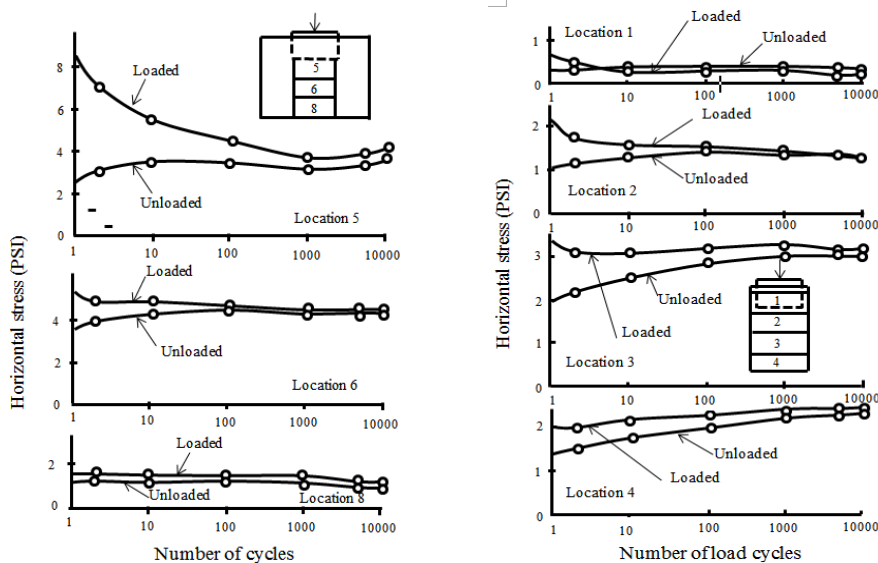


Figure 5.3: Horizontal stresses on side panels and on end panels respectively (Stewart et al., 1985)

The results showed a rapid build-up of horizontal stresses during the first application of load and high residual stresses developed after the first unloading. Furthermore, the horizontal stresses in the loaded state decreased and the residual stresses increased up to about 100 cycles. The horizontal stresses then tended to stabilize and the unloaded value was similar to the loaded value after 100 cycles.

5.2.2 Triaxial test

Research conducted by Shenton (1978) using triaxial tests on ballast suggested a minimum sample diameter of 230 mm is required when the maximum particle size is 38 mm.

Table 5.1: Properties of ballast in Shenton's test

Sieve size (mm)	Percentage of passing by weight
38	100%
32	87%
25	45%
19	7%
13	0%
Wet attrition value	12.5%
Dry attrition value	4.6%
Crushing strength 27%	27%
Impact strength 19%	19%
Flakiness index 17%	17%
Elongation index 17%	17%

Table 5.1 shows the Limestone ballast properties used in the Shenton's tests and its PSD is presented in Figure 5.4.

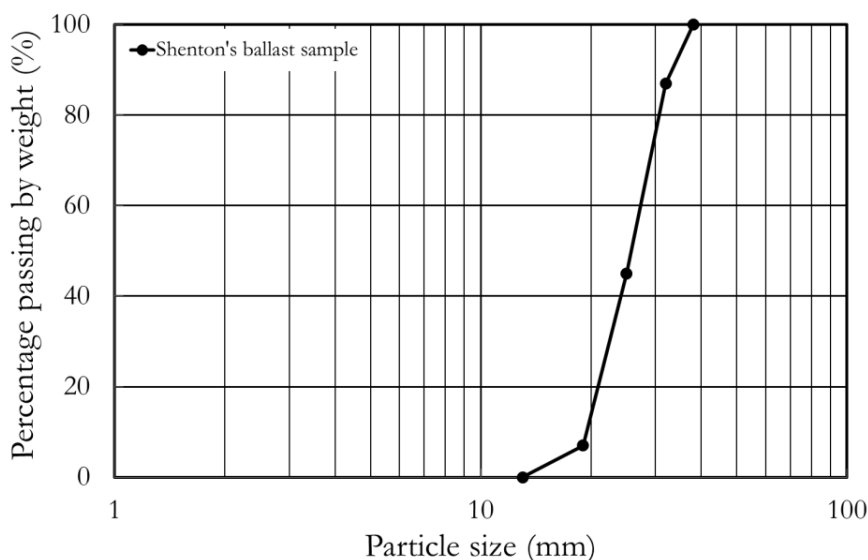


Figure 5.4: PSD of ballast used in Shenton's test

The triaxial sample was produced by placing dry ballast into four layers in a split cylindrical mould lined with a rubber triaxial membrane. Each of these layers was given 3, 12 or 18 blows with a standard tamping ram to produce the porosity required.

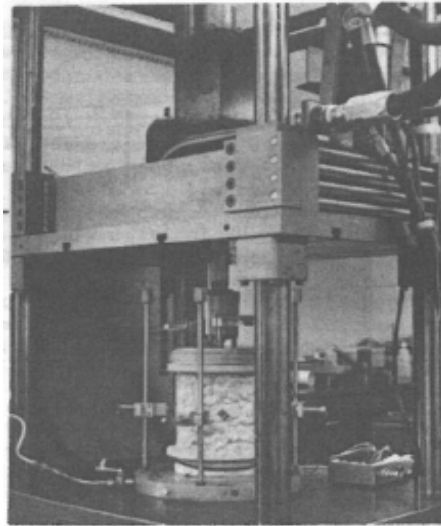


Figure 5.5: Shenton's triaxial test (Shenton, 1978)

The samples were tested using the load frame apparatus as shown in Figure 5.5. Measurements were made of the applied axial load and the permanent and elastic axial strain. The permanent lateral strains were measured by four displacement gauges at sample mid-height. Throughout the tests the maximum axial pressure applied for cyclic loading was 333kPa and the confining pressure maintained at 39kPa by applying suction to the sample interior (the sample was surrounded by a membrane).

The key outcomes from this research were the rapid development of permanent axial strain (Figure 5.6) at the beginning of the test and rapid reduction of in-cycle settlement with increasing number of loading cycles applied.

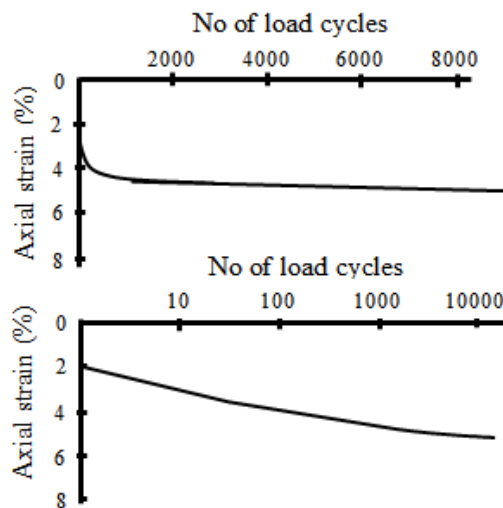


Figure 5.6: Permanent axial strain of triaxial sample (Shenton, 1978)

5.2.3 Real track observation data and tests

Shenton (1978) presented Figure 5.7 showing the vertical profile along one rail of a typical section of track. Each of the lines on the figure represents the profile after a certain period of time. The top line shows the settlement of ballast immediately after fresh ballast has been laid or post maintenance and the two lower lines show ballast settlement after 3 and 8 weeks of traffic. It can be seen that large movements of the track take place in the period soon after maintenance.

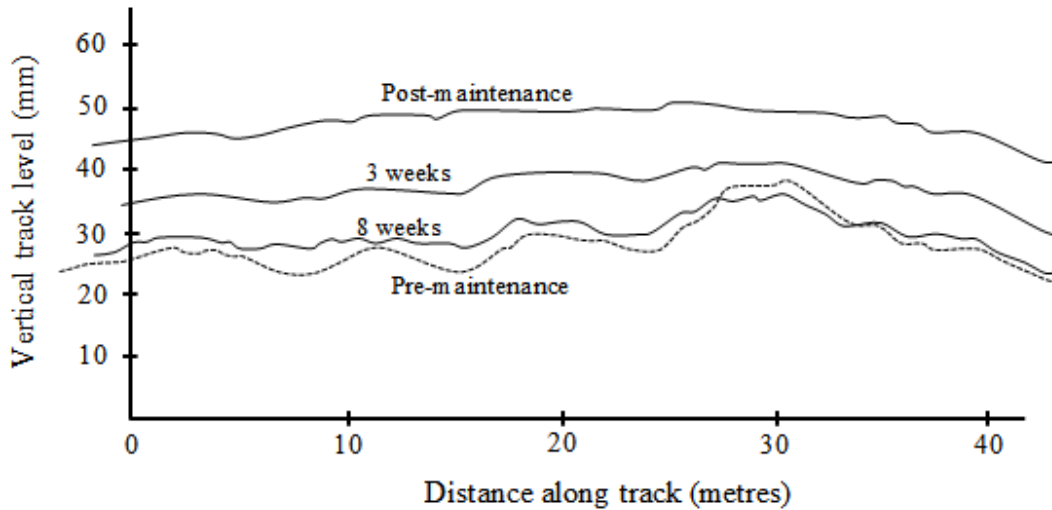


Figure 5.7: Track settlement (after Shenton, 1978)

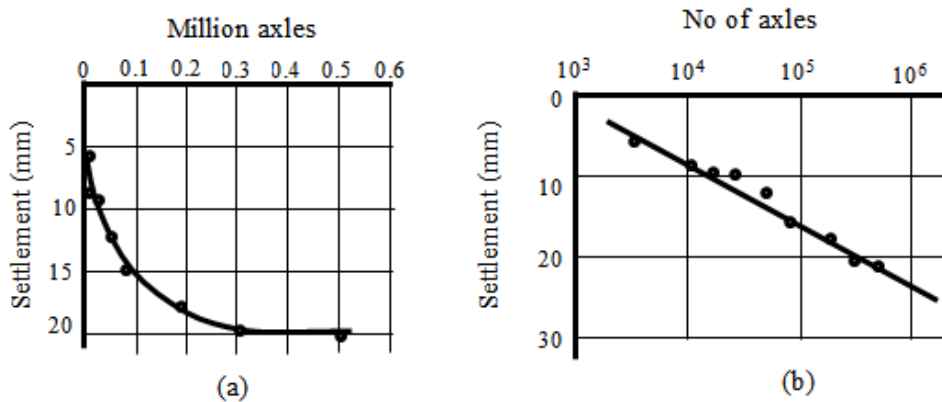


Figure 5.8: Close up figures of track settlement (after Shenton, 1978)

The settlement - time relationship in Figure 5.7 is more clearly seen in Figure 5.8 where graph (a) shows the extremely rapid settlement on following a maintenance process. Graph (b) shows an approximation for the settlement law; the settlement is proportional to the logarithm of the cumulative numbers of axles (Shenton, 1978). Shenton (1984) also concluded that the maximum load has a dominant effect on ballast settlement and loads below 50% of the maximum are not significant contributors. This agrees with Raymond and Bathurst's conclusion (1987) that a certain ballast support has a critical load level that, if exceeded, will cause a dramatic increase in ballast settlement when previously lighter loads were applied.

5.3 Existing ballast settlement models

Differential settlement of railway ballast and foundations can result from different sleepers experiencing different loads or differential settlement of sleepers under identical loads leading to the deterioration of vertical railway track geometry.

Shenton (1984) concluded that there can only be six mechanisms of deterioration. These six mechanisms which can all take place simultaneously and interactively are:

- a. Dynamic forces. The irregularities of rail running surfaces and vertical geometry will lead to variation in the vertical load from a wheel reaching sleepers. The sleepers which consistently experience the highest loads will settle the most, causing track fault. These dynamic loads are the main driver of track deterioration.

- b. Rail shape. A lack of straightness due to the manufacturing process or misalignments produced at welds can create defects in the longitudinal shape of the rail. This defect results in some sleepers carrying different loads from others even when axle loads are constant.
- c. Sleeper spacing. The sleeper spacing governs the load carried by an individual sleeper. A narrow spacing will transfer lesser load onto the sleeper than a wider spacing hence causing less settlement and differential settlement if the sleeper spacing varies along the track.
- d. Sleeper support. The individual sleeper elastic support governs the load carried by an individual sleeper. A sleeper having a stiff support will carry more load than the adjacent sleepers with softer supports and will have a tendency to settle more.
- e. Ballast settlement. The intrinsic lack of homogeneity and random arrangement of ballast particles causes a random settlement of ballast under a given load. This contributes to differential settlement of the track.
- f. Substructure. The final contribution to the differential settlement comes from the deeper ballast and subgrade as a substructure layer. However, the movement arising from settlement in this layer is neglected since most of the track foundations have been designed adequately.

Permanent settlement in ballast results from two basic mechanisms; compaction and particle rearrangement. The first load cycles create large settlement due to a ballast compaction process and particle rearrangement causes minor permanent deformation which develops with increasing number of loading cycles applied. Holtendorff (2001) described parameters influencing permanent settlement of ballast as:

Deviatoric stress: At a certain level of the deviatoric stress, the friction resistance at the point of contact between ballast particles will be exceeded. As a consequence the particles start to move and rotate around each other. This causes a tendency to horizontal spreading.

Vibrations: Passing trains induce vibration of the ballast. These vibrations reduce the confining pressure in the crib and ballast shoulder causing ballast particles to start spreading laterally.

Degradation: Particle slip and tamping processes cause abrasion and breakage in ballast in the form of fine materials. These fine materials and external sources occupy the ballast voids and progressively foul the ballast which leads to an increase of the damping degree of material which in turn increases the normal and tangential forces upon the contact surface. Budiono et al (2004) explained that particles will break if the normal force becomes larger than the bearing resistance and if the tangential force at a contact surface becomes larger than the shear resistance at the constant surface, the particles will slide relative to each other and start to spread horizontally.

Subgrade stiffness: The stiffness of the subgrade has a significant influence on the ballast settlement. The more the subgrade deforms the more the ballast particles are able to move in different directions.

Previous sections have reported some laboratory and field tests which evidence rapid settlement of ballast when freshly laid or after the tamping process. The rate of settlement then decreases with increasing traffic. It is often assumed that the settlement of the track is proportional to the logarithm of the number of axles or tonnage; however the first thing to consider is the general form of the law governing the settlement of the ballast. This section will review some the better-known ballast settlement models.

5.3.1 Okabe's model

Figure 5.9 presents the relationship of ballast settlement with the number of loading cycles proposed by Okabe (1961). The initial settlement is more significant with gradually decreasing increments of settlement with later cycles so that the settlement continues in proportion to the logarithmic of the number of loading cycles (Equation 5.1).

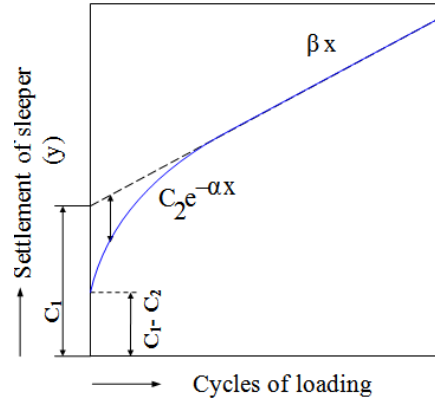


Figure 5.9: Settlement of sleeper under repeated load (Okabe, 1961)

$$y = C_1 - C_2 e^{-\alpha x} + \beta x \quad \text{Equation 5.1}$$

where y represents permanent settlement, C_1 is a total amount of permanent settlement due to the compaction of the ballast, $C_2 e^{-\alpha x}$ is the residual amount of settlement after x loading cycles, β is the coefficient of lateral ballast spreading and α is the coefficient of ballast compaction. $C_1 - C_2$ is the amount of the gap and play between ballast particles. All the parameters were obtained by curve fitting on the real data.

5.3.2 The Office for Research and Experiments model

The Office for Research and Experiments (ORE) of the International Union of Railway (1970) conducted measurements to ascertain the stress induced in the ballast, blanket and formation layers beneath a railway track. The studies were undertaken both in the field and laboratory to determine the behaviour of the ballast layer in the track foundation under the action of repetitive loads. The main conclusion of the measurements on the ballast was that the permanent settlement per load cycle reduces considerably as the number of loading cycles increases. The first load application produces a very large permanent settlement which is extremely dependent upon the initial ballast bulk density.

ORE had also conducted research using BR triaxial tests under controlled stress conditions on Derbyshire limestone and Meldon stone ballast with two different densities. This led to a conclusion that permanent settlement of ballast is predictable by the approximate model:

$$\epsilon_N = 0.082 (100n - 38.2) (\sigma_1 - \sigma_3)^2 (1 + 0.2 \log N) \quad \text{Equation 5.2}$$

where: ϵ_N = Permanent strain after N^{th} loading cycles.

n = Initial porosity of sample.

$(\sigma_1 - \sigma_3)$ = Deviator stress (0.1377MPa).

σ_1, σ_3 = The major and minor principal stresses.

N = Number of repeated loading cycles.

5.3.3 Shenton's model

Shenton (1978) continued the laboratory testing undertaken by ORE using triaxial tests as described in section 5.2.2. Shenton's results were consistent with those of ORE and he further examined the log curves for many more samples and concluded that the slope of the line was proportional to the strain produced by the first load cycles. The settlement at the 10th cycle as a proportion of the first cycles is shown in Figure 5.10.

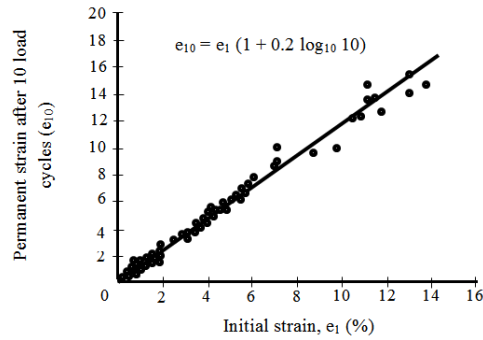


Figure 5.10: Relationship between permanent strains at first and tenth load (after Shenton, 1978)

Shenton proposed a relationship to predict ongoing settlement based on this link of:

$$\epsilon_N = \epsilon_1 (1 + 0.2 \log_{10} N) \quad \text{Equation 5.3}$$

where ϵ_1 and ϵ_N are the permanent strain at first and Nth loading cycles respectively.

This relationship permits settlement rates to be predicted based on the permanent settlement after the first load cycle only. The influence of the first cycle demonstrates the importance of compaction; that greater initial density has the effect of reducing subsequent settlement. Shenton (1984) also examined worldwide data (Figure 5.11) to investigate the effect of heavier axle loads which was underestimated in the earlier relationship.

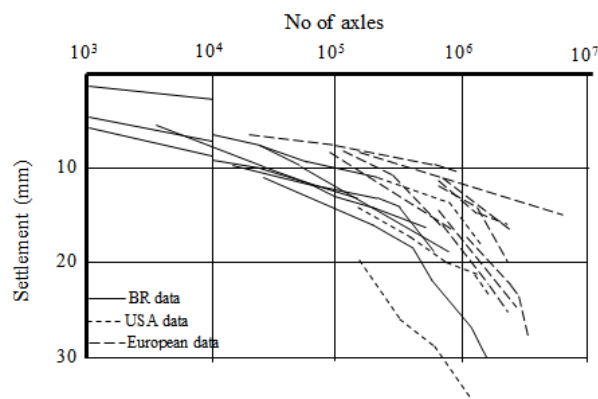


Figure 5.11: Track settlement at different parts of the world (after Shenton, 1984)

Comparing the laboratory and field experiments led to an approximation that the settlement is considered to be proportional to the fifth root of the number of loading cycles combined with a constant value and modelled by:

$$S = K_1 N^{0.2} + K_2 N \quad \text{Equation 5.4}$$

$K_1 N^{0.2}$ predominates up to 1 million cycles and $K_2 N$ only becomes relatively significant above this value. In addition to the number of loading cycles, the influence of axle load, sleeper spacing and the

lift given by the tamping machine were taken into account after being investigated using triaxial tests. This leads to re-arrangement of Equation 5.4 as:

$$S = K_s \frac{A_e}{20} \left((0.69 + 0.028L) N^{0.2} + (2.7 \times 10^{-6})N \right) \quad \text{Equation 5.5}$$

where: S = Settlement (mm).

K_s = a factor as a function of sleeper type and size, ballast and subgrade that for normal U.K track is 1.1.

L = the lift given by the tamping machine.

A_e = an equivalent axle load which is described as:

$$A_e = \left(\frac{A_1^5 N_1 + A_2^5 N_2 + A_3^5 N_3 + \dots}{N_1 + N_2 + N_3 + \dots} \right)^{0.2} \quad \text{Equation 5.6}$$

where: N_1 is number cycles having a load of A_1 etc.

5.3.4 Jeffs and Marich's model

Jeffs and Marich (1987) proposed a settlement model based on the results of laboratory ballast settlement tests. The detail of their apparatus is presented in Figure 5.12 and it was claimed that a circular tub containing up to 250 kg ballast with the ratio of dimensions shown gave the most repeatable results. The tests considered degradation, the elastic response of the ballast, grading, ballast particle shapes, bed depth, lateral ballast spreading and settlement characteristics, in response to a variety of controlled vertical load conditions. The parameters influencing the settlement e.g. maximum and minimum load, ballast type, ballast grading, sleeper type and ballast compaction were included as part of the investigation.

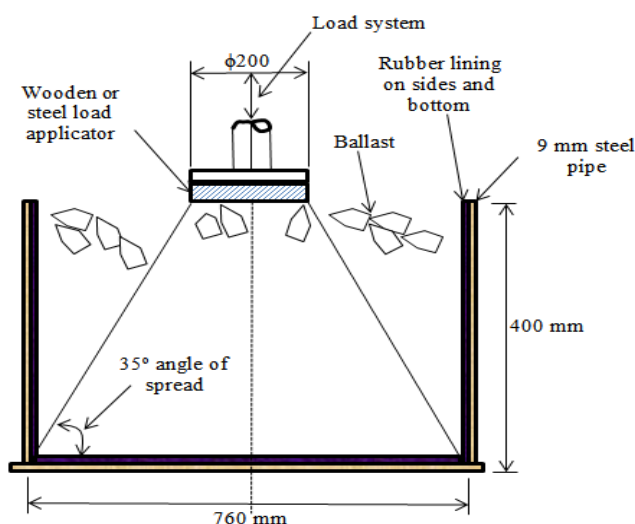


Figure 5.12: Cross section of Jeffs and Marich's apparatus (after Jeffs and Marich, 1987)

Figure 5.13 shows two curves representing typical settlement results to show that a rapid period of settlement occurs initially followed by a relatively linear period. This linear period does not agree with equation 5.3, but suggests that cyclic settlement approaches a linear relationship with the number of loading cycles. This period is not only affected by ballast lateral spread but also by the re-arrangement of ballast particle due to the failure of a contact point within the ballast bed, which then causes a sustained shift in the load path in the surrounding ballast.

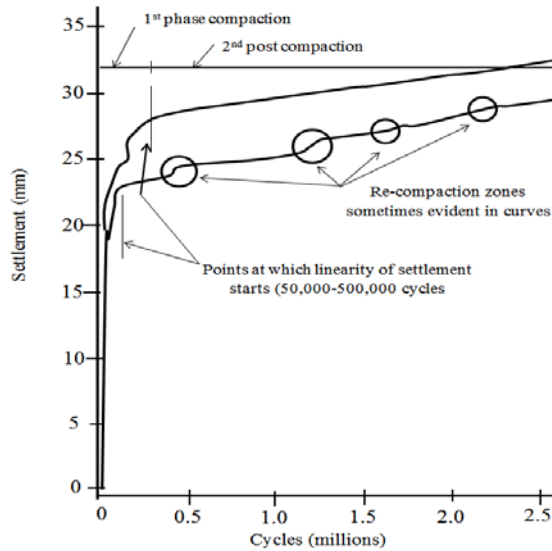


Figure 5.13: Settlement curves obtained by Jeffs and Marich (after Jeffs and Marich, 1987)

The results obtained by Jeffs and Marich (1987) (Figure 5.13) are however consistent with ORE results which suggest that the initial settlement curve is controlled directly by the initial level of compaction. To minimise the influence of initial ballast conditions, the settlement obtained due to the application of first load cycle was removed. Figure 5.14 shows the settlement curves after the first cycle data has been removed.

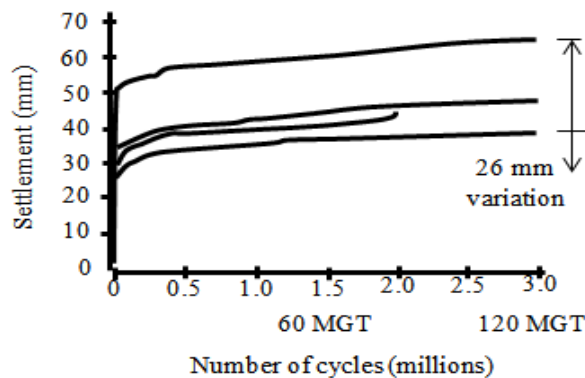


Figure 5.14: Settlement data obtained with first cycle shifted (after Jeffs and Marich, 1987)

To achieve a high level of repeatability, Jeffs and Marich (1987) suggested removing more initial cycles, up to 50,000 cycles. Figure 5.15 shows the settlement curves starting at 50,000 cycles. The post 50,000 cycles region represents the second settlement phase which is independent of the initial conditions.

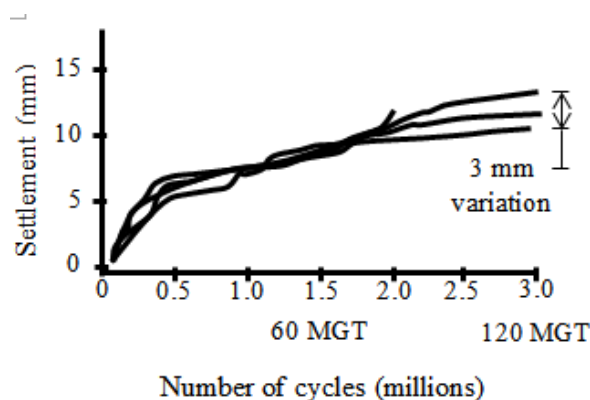


Figure 5.15: Settlement data obtained with 50,000 cycles shifted (after Jeffs and Marich, 1987)

Based on these analyses Jeffs and Marich (1987) proposed a settlement model and used post 200,000 cycles as a cut off to eliminate the variation due to the initial conditions.

$$S_N = C_1 + C_2 \log N + C_3 N ; N \leq 200,000 \text{ as } 1^{\text{st}} \text{ phase} \quad \text{Equation 5.7}$$

$$S_N = C_4 + C_5 N ; N > 200,000 \text{ as } 2^{\text{nd}} \text{ phase} \quad \text{Equation 5.8}$$

where C_1, C_2, C_3, C_4, C_5 are constants produced by regression and N is the number of loading cycles.

5.3.5 Hettler's model

Mauer (1995) described Hettler's settlement model. Hettler (1984) carried out tests with cyclic loads on single sleepers which were a third of the real scale and on 8 sleeper track models using four hydraulic power cylinders for load simulation. The single sleeper was centrally loaded and the 8 sleeper track segment was simultaneously loaded at two sleepers to simulate two axle loadings. Hettler's results indicated that the permanent track settlement, (S_N) after N loading cycles was a function of both initial track settlement (S_1) after the first load cycle and the total number of loading cycles (N) and was modelled as:

$$S_N = S_1 f(N) \quad \text{Equation 5.9}$$

Hettler devised a logarithmic approach for the settlement as a function of loading cycles as follows:

$$f(N) = 1 + C \ln (N) \quad \text{Equation 5.10}$$

Values between 0.25 and 0.55 were suggested for the settlement constant C . However, the mean value of 0.43 was preferred based on the results of repeated constant axle load tests on both track models. To model the relationship based on the ORE data using Hettler's model, the appropriate value of C would be 0.46.

To take different load amplitudes (F_i) into account, Hettler interpreted F as equivalent load amplitude using the linear mean values which was defined as:

$$F = \frac{1}{N} \sum_{i=1}^N F_i \quad \text{Equation 5.11}$$

As an addition to Equation 5.9, Hettler developed an assumption that the initial settlement (S_1) may be a non-linear function of the loading amplitude (F) as shown by:

$$S_1 = S_1(F) \quad \text{Equation 5.12}$$

To derive this relationship, Hettler carried out tests with different axle load amplitudes (Q) and scaled the results back to the size of a regular track. Hettler noted an amplitude ratio of the axle load (Q) to the sleeper forces F of 1.62 derived a relationship from a graphical representation as:

$$S_1 = r (F)^{1.6} \quad \text{Equation 5.13}$$

where r is the scaling factor, $r = 0.00095 \text{ (mm/kN}^{1.6}\text{)}$.

Substituting the parameters into Equation 5.9 from Equations 5.10 and 5.13, the settlement model can be re-written as:

$$S_N = r (F)^{1.6} (1 + C \ln (N)) \quad \text{Equation 5.14}$$

Mauer (1995) also mentioned a suggestion by Holzlohner (1978) that the settlement law be divided into two loading periods: an initial loading period comprising the first N_i cycles and a second period comprising the following cycles (N_a). The settlement model is defined as:

$$S_N = S_i + S_a \quad \text{Equation 5.15}$$

where S_i and S_a are the settlements due to the initial N_i and the following N_a loading cycles respectively. S_a in the second period is given by:

$$S_a = R_s \ln \left(\frac{N_a}{N_i} + 1 \right) \quad \text{Equation 5.16}$$

or

$$S_a = R_s \ln \left(\frac{N_{\text{total}}}{N_i} \right) \quad \text{Equation 5.17}$$

where: R_s is the logarithmic settlement rate.

5.3.6 Alva-Hurtado and Selig's model

Alva-Hurtado and Selig (1981) investigated permanent strain behaviour of railway ballast through laboratory triaxial tests. In this research, the railway ballast used was granite with angular particles ranging in size from 5 to 30 mm, with D_{50} size of 20 mm. The ballast uniformity (C_u) and concavity (C_z) coefficients were 2 and 1 respectively. C_z is defined as:

$$C_z = \frac{(D_{30})^2}{(D_{10} \times D_{60})} \quad \text{Equation 5.18}$$

where D_{60} , D_{30} and D_{10} are the particle size that 60%, 30% and 10% respectively of the sample will be finer than.

Two different ballast physical states; uncompacted (1.53 kg/m^3) and compacted (1.62 kg/m^3) were used to represent the range of ballast density that was measured at sites. Uncompacted ballast was prepared by hand placing ballast particles in a compaction mold. Compacted ballast was prepared by applying 20 blows to three equal layers. Triaxial sample tests were 152 mm in diameter and 381 mm high, saturated under back pressure and isotropically consolidated at a constant effective confining pressure selected in the range of 35 to 138kPa.

Alva-Hurtado and Selig (1981) proposed the relationship between the permanent strain after the first cycle, ϵ_N and the number of loading cycles (N) based on the test results using two approaches of curve fitting; linear and nonlinear regression. In linear regression, the relationship was in excellent agreement with Equation 5.3 proposed by Shenton (1978). The relationship obtained using nonlinear regression is:

$$\epsilon_N = (0.85 + 0.38 \log N) \epsilon_1 + (\epsilon_1)^2 (0.05 - 0.09 \log N) \quad \text{Equation 5.19}$$

where ϵ_1 is the permanent strain at first loading cycle.

5.3.7 Stewart and Selig's model

To investigate the amount of permanent settlement that occurs due to stress levels and the number of constant-amplitude loads, cyclic triaxial tests were conducted on compacted ballast by Stewart and

Selig (1984). This investigation led to a conclusion that the settlement of ballast with given material properties and density strongly depends on the loading amplitude and history. This means that when the loading amplitude increases above any previously applied value, the permanent deformation increases immediately, following a new asymptotic path and the final deformation does not depend on the sequence of loading. The linear relationship proposed by Shenton (1978) was adopted and stated in general terms to account for initial compaction as:

$$\varepsilon_N = \varepsilon_1 (1 + C \log_{10} N) \quad \text{Equation 5.20}$$

where: ε_1 and ε_N are the permanent strain at the first and N^{th} loading cycles respectively.

N is the number of loading cycles and C is a ballast constant.

Stewart and Selig (1982b) stated that C was not the same for all the ballast tested and proposed values for each site and ballast type (Table 5.2) based on triaxial tests.

Table 5.2: Ballast constant, C (after Stewart and Selig, 1982b)

Site and ballast type	Value of C
Leeds slag (wood section)	0.34
Leeds Granite (concrete section)	0.26
Lorraine Limestone	0.40
Aberdeen and FAST trap-rock	0.25
FAST Wyoming Granite	0.29

This is in contrast to Shenton (1978), Equation 5.3, in which C was always 0.2. Stewart and Selig (1982b) recommended the use of 0.29 for the ballast constant in Equation 5.20.

In addition to the triaxial tests, experiments were conducted using the box test apparatus as described in section 5.2.1 which also aimed to simulate the settlement properties of ballast due to repeated vertical loading. Permanent settlement trends based on the results of ballast box tests were similar to those observed in the repeated load triaxial tests in that the settlement was linearly related to the log of the number of loading cycles and could be expressed by Equation 5.3, except that d_1 and d_N replace ε_1 and ε_N . The relationship is expressed as:

$$d_N = d_1 (1 + C_b \log N) \quad \text{Equation 5.21}$$

where: d_1 = Permanent vertical deflections of the sleeper after 1st cycles.

d_N = Permanent vertical deflections of the sleeper after N^{th} cycles.

C_b = Settlement constant for the box tests which are 0.35 and 0.63 for compacted and un-compacted sample respectively.

Based on Equation 5.20, if the initial load produced curve A is increased after certain number of loading cycles, the curve would immediately join the upper line at B and continue just as if the load had always been higher. Ford (1995) considered this to be unreasonable and proposed a way of shifting the abscissa of the new curve so that it intersects the previous curve at the current operating point as shown in Figure 5.16.

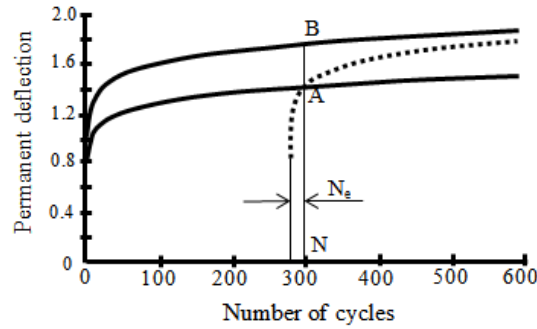


Figure 5.16: Adjusting the coefficient ϵ_1 for varying load (after Ford, 1995)

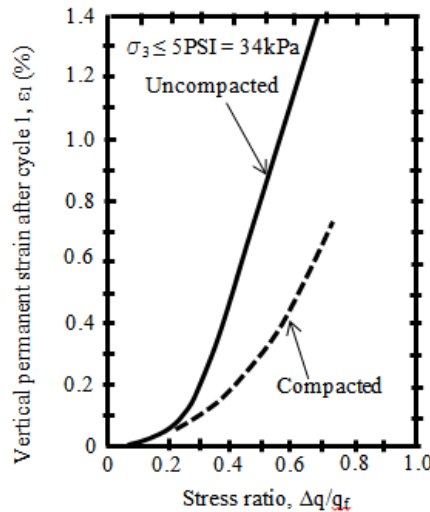


Figure 5.17: Permanent strain after first cycle for low confining stress (after Alva-Hurtado and Selig, 1981, after Ford, 1995, Selig and Alva-Hurtado, 1982)

This shifted curve is used to calculate subsequent deformations. To calculate the new curve, a new value for ϵ_1 must be determined to represent the new load. To find the new value for ϵ_1 is straightforward using Figure 5.17 if the magnitude of the next load is known (Δq and q_f are the amplitude of applied stress and the failure stress respectively).

A new value for the number of loading cycles (N_e) also needs to be determined to represent the shift of the origin by inverting Equation 5.20 to make number of cycles the subject.

$$N_e = 10^{\left[\frac{(\epsilon_N - \epsilon_1)}{C} \right]} \quad \text{Equation 5.22}$$

where ϵ_N and ϵ_1 are the current value of permanent strain and the initial permanent strain corresponding to the new load respectively and C is ballast constant and assumed not to be affected by load.

It can be noted that if the new load is heavier than in previous cycles, N_e will be smaller than the actual number of previous cycles; if the new load is lighter, N_e will be larger.

The strain after next cycle can now be calculated by incrementing this calculated value of N_e by one and substituting Equation 5.20 together with the new value of ϵ_1 to become:

$$\epsilon_N = \epsilon_1 \left(1 + C \log_{10} (N_e + 1) \right) \quad \text{Equation 5.23}$$

To estimate the permanent settlement caused by the application of different magnitudes of load, this process needs to be repeated for each load and the total of number cycles is obtained by counting the number of times this procedure is carried out.

5.3.8 Selig and Waters's model

Selig and Waters (1994) considered further the relationship proposed by Stewart and Selig (1984), Equation 5.20, relating the permanent strain after N cycles, ϵ_N to the permanent strain after one cycle, ϵ_1 :

$$\epsilon_N = \epsilon_1(1 + C \log N) \quad \text{Equation 5.24}$$

Based on data from their triaxial and the ORE tests, the suitable C values for this equation were 0.2 and 0.41 for perhaps, compacted and uncompacted ballast respectively.

The trends obtained from box tests were analysed by Selig and Waters (1994) and compared to semi log, hyperbolic, parabolic and power law mathematical relationships to produce an expression of permanent settlement after N cycles, S_N (mm). The best fit equation is:

$$S_N = 4.318 N^{0.17} \quad \text{Equation 5.25}$$

Track settlement measurements carried out at the Facility for Accelerated Service Testing (FAST) in Colorado were also summarised by Selig and Waters (1994). The summary showed that for the ballast strain at N cycles, ϵ_N the best fit equation for the FAST track data is:

$$\epsilon_N = 0.0035 N^{0.21} \quad \text{Equation 5.26}$$

5.3.9 Sato's model

In Japan, ballast settlement has been investigated since 1950 which led to the ballast settlement model proposed by Okabe (1961) (Equation 5.1). Sato (1995) used this model to investigate the coefficient of track deterioration which was used in the design of the Tokaido Shinkansen. Sato (1995) used constants C_1 , C_2 , α and β to represent the short-term and long-term settlement behaviour. The first part of Equation 5.1 describes the short-term settlement of the track. The factors C_1 and C_2 represent the magnitude of the initial stage settlement and the factor α indicates how quickly the initial settlement attenuates. This first phase shows the initial rapid settlement corresponds to the process densification of the ballast.

The second part of the equation describes the long-term settlement in which the track settles in proportion to the number of loading cycles. This is a result of the lateral movement of ballast particles under the sleeper, depending on the characteristics of the load and track structure. In this model there is no distinction made between loadings of different magnitudes. The severity of this phase is represented by the parameter β , which should be small to keep the track settlement small. Sato(1995) stated that the parameter β is influenced by the following factors:

- a. The β value of crushed stone is 1/6 to 1/7 that of gravel.
- b. β is proportional to the square of the velocity of the repeated loading.
- c. β of ballast contaminated with soil is smaller than clean ballast in a dry state and worse if it is wet.
- d. β is proportional to sleeper pressure.

- e. β is proportional to ballast vibration. Ballast vibration will cause slip between the particle and thereby rearrangement of ballast particles. This can lead to ballast densification or a movement of particles away from under the sleeper.

Sato (1997a) presented another model for growth of track settlements (S_i, S_j) involving sleeper-ballast contact pressure p as the key parameter. These two formulations are:

$$S_i = a (p - b)^2 \quad \text{for } p > b \quad \text{Equation 5.27}$$

$$S_j = A p^n \quad \text{Equation 5.28}$$

In Equation 5.27 ballast settlement is described by two parameters a , and b . The b parameter is a threshold value of pressure below which settlement does not occur. In Equation 5.28 A is a coefficient and n is a power index. Based on these two equations, Sato (1997b) introduced the equation for accumulated settlement (S_N) for the number of loading cycles (N) as:

$$S_N = S_j N \quad \text{Equation 5.29}$$

5.3.10 Henn's model

Dahlberg (2001) described a German model, emanating from Henn (1978) and investigated by Demharter (1982) in which settlement (S) depends on the sleeper-ballast pressure (p) and on the number of loading cycles (N). In this model, settlement was divided into three terms:

$$S = c_1 + c_2 p + c_3 p^{1.21} \ln N \quad \text{Equation 5.30}$$

The initial phase (densification/compaction) in this model is limited to less than 10^4 cycles, while a secondary phase (ballast wear and lateral spread) is valid for 10^4 cycles onward. c_1 , c_2 , and c_3 are constants and it is noted that the power of 1.21 on p is not very high compared with Sato's model due to the better ballast quality used in the tests in which this model is based, which was better able to resist high loads.

5.3.11 Thom and Oakley's model

Thom and Oakley (2006) investigated ballast settlement using data from tests using the University of Nottingham full scale Railway Test Facility (RTF). The data set was limited and the tests all had the same subgrade soil categorised as soft silt and the same ballast thickness of 300 mm beneath the sleepers. The tests conducted represented well controlled and repeatable conditions, under the application of a load equivalent to a 250kN axle load. The suggested relationship between settlement (S (mm)) and loading cycles (N) is:

$$S = [\log_{10} (N) - 2.4]^2 \quad \text{Equation 5.31}$$

No data have yet been collected from the RTF at different load levels and with different subgrades, therefore to predict the behaviour of ballast settlement with different axle loads and subgrade variation it has been decided to follow Sato's model and to assume a linear relationship with axle load and also with stress under the sleeper σ which can be described as:

$$S = [\log_{10} (N) - 2.4]^2 \left(\frac{\sigma}{160} \right) \left(\frac{47}{k_s} \right) \quad \text{Equation 5.32}$$

where: σ and k_s are stress under the sleeper and modulus of subgrade reaction respectively.

160 and 47 are constant factors of normalised load (kPa) and subgrade modulus (MN/m) applied on the tests respectively.

Thom and Oakley (2006) also reviewed several permanent deformation equations and concluded that all models were approximate and represent a best fit to the data for a particular type of railway, subgrade, ballast type in a particular country and a particular type of test.

5.3.12 CEDEX's track box model

The rail track accelerated testing facility at CEDEX has dimensions of 21 m long, 5 m wide and 4 m deep to accommodate full scale tests. This CEDEX box test was used by Cuellar et al (2011) to simulate the passage of a Eurostar train with a 165kN axle load. The best fit equation of permanent settlement to the experimental data in the tests was:

$$S_N = 0.07 N^{0.1625} \quad \text{Equation 5.33}$$

where S_N is the permanent settlement after N 165kN axle load applications.

5.3.13 Varandas et al's model

Varandas et al. (2013) proposed a settlement model to determine the ballast settlement subjected to an arbitrary loading sequence and accounting for the loading history. The proposed model reflects observations or assumptions which that:

- The settlement of the ballast is proportional to the amplitude of the applied load.
- The loading history plays a decisive role on the settlement response.
- The densification of ballast decreases with an increasing number of load cycles if the loading amplitude remains constant.

The proposed settlement model determines the settlement at the surface of the ballast caused by the application of successive cycles according to:

$$u_{p,n} = \frac{\gamma}{M_\theta} \int_0^{F_n} F^\alpha \left(\frac{1}{h(F)+1} \right)^\beta F \quad \text{Equation 5.34}$$

$$S_N = \sum_{n=1}^N u_{p,n} \quad \text{Equation 5.35}$$

$$M_\theta = \frac{F_0^{(\alpha+1)}}{\alpha+1} \sum_{n=1}^{N_0} \left(\frac{1}{n} \right)^\beta \quad \text{Equation 5.36}$$

where $u_{p,n}$ is the permanent deformation produced during load cycle n , S_N is the total settlement after N load cycles, F_n is the loading amplitude of the force passing through this sleeper to the ballast at load cycle n , M_θ is a normalizing parameter, F_0 is a reference loading amplitude, N_0 is a reference number of cycles, $h(F)$ represents the loading history and α, β , and γ are positive parameters.

If F_n is a constant loading amplitude, then the function $h(F)$ can be replaced by the number of cycles passed and Equation 5.33 can be simplified to:

$$u_{p,n} = \frac{\gamma}{M_\theta} \frac{F_n^{\alpha+1}}{(\alpha+1)} \left(\frac{1}{n} \right)^\beta \quad \text{Equation 5.37}$$

Therefore the corresponding accumulated settlement will be given by:

$$S_N = \frac{\gamma}{M_0} \frac{F_n^{\alpha+1}}{(\alpha+1)} \sum_{n=1}^N \left(\frac{1}{n}\right)^\beta \quad \text{Equation 5.38}$$

It shows that the parameter α expresses the dependence of the settlement on the loading amplitude and the parameter β controls the progression of the settlement rate with the number of load cycles. Comparing Equations 5.34 and 5.36, it can be seen that M_θ was derived so that parameter γ represents the total settlement after N_0 loading cycles with constant loading amplitude F_0 . Therefore γ has a clear physical meaning: it is the accumulated settlement in the reference test with loading amplitude F_0 and number of loading cycles N_0 .

5.3.14 Indraratna et al's model

Indraratna et al (1997) conducted tests on railway ballast using a large-scale oedometer which could accommodate a test sample of 450 mm in diameter with repeated loading. The ballast sample used was latite ballast with tests on both uncompacted and compacted samples with void ratios of 0.95 and 0.74 respectively. The corresponding initial densities of uncompacted and compacted ballast were 1.41 t/m³ and 1.59 t/m³ and the applied axial pressures varied from 50kPa to 560kPa to model the train with 30 ton axle loads. Initially Indraratna et al (1997) adopted Stewart and Selig's Model as expressed on Equation 5.20 and rearranged the expression as:

$$S_N = S_1(a \log N + 1) \quad \text{Equation 5.39}$$

Based on the properties of ballast and the axial pressure applied on the tests, the data obtained suggested that the parameter of (a) was 0.345 and S_1 were 9.68 mm and 2.31 mm for uncompacted and compacted conditions respectively. After investigation, Indraratna et al (2013) proposed an empirical equation to predict track settlement (S_N) with the degree of fouling being considered and defined by:

$$S_N = a_1 + \frac{b_1}{1 - VCI} \log_{10} N \quad \text{Equation 5.40}$$

where VCI is Void Contamination Index, $0 \leq VCI < 1$, a_1 and b_1 are empirical coefficients, and N is number of loading cycles.

Equation 5.38 is just a modification of the previous equation i.e. Equation 5.3 introduced by Shenton (1978) on fresh ballast that confirms the settlement data obtained by Indraratna and Salim (2003).

5.3.15 General observation on ballast settlement models

Comparing all introduced ballast settlement models leads to the finding that in fact, most settlement models have similar pattern in describing the behaviour of ballast settlement under cyclic loading. Most models present two phases of settlement which are initial rapid settlement due to densification/compaction and secondary settlement due to ballast wear and lateral spread with the application of load. The secondary settlement is typically caused by several basic mechanisms of ballast and subgrade behaviour (Dahlberg, 2001, Dahlberg, 2006, Holtendorff, 2001, Tzanakakis, 2013):

- Densification of ballast and subgrade caused by particle rearrangement produced by repeated train loading.

- Volume reduction caused by particle breakdown from train loading or environmental factors and abrasive wear.
- Inelastic recovery on unloading due to micro-slip between ballast particles at loading.
- Movement of ballast and subgrade particles away from under the sleepers.
- Lateral and possibly longitudinal movement of sleepers causing the ballast beneath the sleepers to be pushed away.
- The effect of parcel slip can occur during whole time operation. The range of slip strongly depends on the horizontal confinement that had been built up earlier and gradually diminished during vibration impact. The lower confinement pressure the more likely it is that the particles will slip against each other.
- Subgrade penetration into ballast voids.
- Subgrade stiffness influences the quantity of ballast settlement. The more the subgrade deforms elastically the more the ballast particle are able to move into different directions.

5.4 Pressure distribution beneath the sleeper

Zakeria and Sadeghi (2007) summarised earlier research recommendations that in trackbed design, the pressure distribution beneath the sleeper is commonly idealised as either uniform or “w” shaped. Most railway authorities also work on an assumption that the pressure beneath the sleeper is of a uniform distribution or is concentrated toward the end of the sleeper. Lees (2009) also presented a figure of contact pressure distribution beneath the sleeper based on the investigation conducted by AREMA (Figure 5.18) which also shows “w” shaped distribution. BR agrees with this finding that the largest pressure is directly under the rail wheel while the middle of sleeper does not or should not rest on the ballast (Round, 1993).

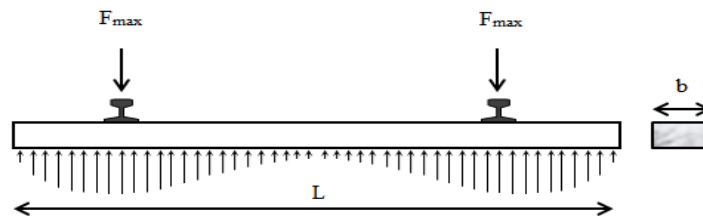


Figure 5.18: Typical idealised pressure distribution along the sleeper (AREMA, 2003a, Lees, 2009)

BR developed a method to determine the required ballast depth for a given subgrade strength based on the assumption that the weaker the subgrade, the greater the depth of ballast needed. However, the method assumes that the ballast layer acts as a continuum with uniform load transfer properties. In reality, the load transfer behaviour of ballast is highly dependent on its structure due to the large particle sizes in relation to typical sleeper footprint and ballast layer depth (Aingaran, 2014). For the purposes of evaluating the maximum contact pressure transferred to the ballast, the “w” shaped pressure distribution may then be transformed to two equivalent area rectangles (as described by Esveld (2001)) beneath each railseat using an approximation such as Equation 5.41 (AREMA, 2003a).

$$\sigma_{\max} = \frac{3 F_{\max}}{b L} \quad \text{Equation 5.41}$$

where F_{\max} is the maximum railseat load per rail including any dynamic factor if appropriate and b and L are the sleeper length and width respectively assuming a single rectangular based sleeper (mono-block). The multiplier 3 comes from assuming that 2/3 of the sleeper length (1/3 of the

sleeper length per rail) is loaded by the equivalent rectangular pressure distributions. For a 5 tonne railseat load this implies a maximum contact pressure of 210kPa for a G44 sleeper of dimensions 2.5 m (L) \times 0.285 m (b) (British Standards Institution, 2009a).

While this idealisation can be useful, the load transfer behaviour at the sleeper/ballast interface is highly variable both within and between individual sleepers and may also vary with cycles of loading. This is a result of the relatively large particle sizes of ballast in relation to a typical sleeper footprint and varying rates of permanent settlement of the ballast with loading cycles. The number of ballast particles involved in directly supporting the sleeper can be small. Shenton (1978) also estimated that a sleeper which has been in track for some time may only have 100 to 200 particles in contact with it. This condition made the measurement of accurate pressures in the ballast extremely difficult (Shenton, 1978). The nearest approach which BR research had done in the 1970s was to define the boundary stresses condition by means of pressure cells mounted along the base of sleeper and cells buried just below the bottom of the ballast layer for a range of different ballast depths (Shenton, 1978). Figure 5.19 shows that for the same railseat load, when the pressure is averaged over a smaller local area equivalent to the size of the measuring pressure plate, the maximum contact pressure is slightly higher than the idealisation of Equation 5.41 at nearly 300kPa. The size of the pressure plates used to produce Figure 5.19 was not reported, although it may be inferred from the changes in direction of the line of best fit.

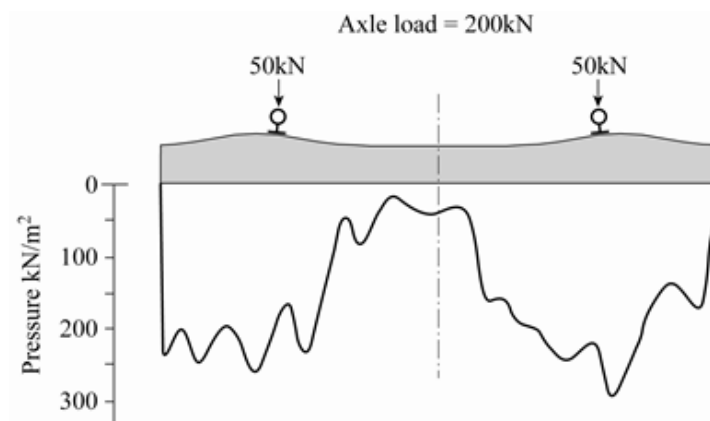


Figure 5.19: Sleeper base contact pressure distribution (after Shenton, 1978)

Shenton (1978) also carried out pressure measurement within the ballast and concluded that the measurement result closely follows the Boussinesq pressure distribution curve (Figure 5.20), which provides a reasonable approximation of vertical pressure within the ballast layer.

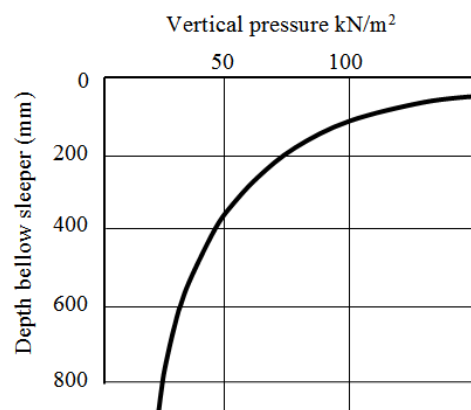


Figure 5.20: Variation of pressure in ballast with depth (Shenton, 1978)

The approximation of Equation 5.41 and the measurements by BR assume that the variations in pressures can be characterised by averaging over contact areas that are large in relation to individual particle contact areas. This is an assumption that increasingly breaks down as the area of interest approaches the area of interaction between individual particle/sleeper contacts. In this research, pressure paper was used to obtain an accurate data set at sleeper/ballast and ballast/subgrade as well as ballast/wall interfaces.

5.5 Summary

The ballast can be considered as a stabilised material after the particles have been interlocked with each other. Considerable effort has been devoted to predicting the behaviour and permanent settlement of ballast due to cyclic loading through different approaches based on the results of either laboratory, field tests or model simulation.

There is a general consensus that:

1. There is always a rapid change of horizontal pressure during initial loading cycles when the ballast is prevented from lateral spread or strain. The change is due to the loading and unloading of ballast which causes the horizontal pressure to either increase or decrease. Further loading cycles lead to stabilisation of the horizontal pressure and the unloaded value tends to converge to the loaded value. This means that there are only slight differences between the loaded and unloaded horizontal pressures and that the horizontal pressures tend to become constant over each loading cycle.
2. The conclusions of previous research on the ballast (e.g. Shenton (1978)) stated that the accumulation of permanent axial strain or settlement after a number of loading cycles can be related to the first load cycle. Most ballast settlement models agree that ballast settlement can be divided into two phases. The rate of strain or settlement produced in the first phase is fast, after ballast is laid or after tamping. The magnitude of this settlement is dependent on the initial ballast compaction and the applied load. The second phase is relatively slow and has a linear relationship between settlement and the log of the number of loading cycles. This second phase is described by settlement models using different parameters. However all models are approximations and representing a best fit to data obtained in particular tests for a particular type of railway, subgrade and ballast in a particular country using mostly relatively smaller or scaled tests which the test field conditions might not be represented. Although there were available data taken through direct field measurements from some sites, the difficulties of obtaining an initial condition prior to comparison leads to inconsistencies in the models produced. Therefore, it is important to model ballast settlement using data from full scale tests in the laboratory, in which the conditions in field can be approached as closely as possible.
3. It is challenging to measure accurately the vertical pressure applied by the sleeper onto the ballast surface beneath the sleeper. This leads to idealisations having been made to simplify the analyses in estimating the magnitude of the pressure transferred to the ballast surface. Some field tests have been carried out by attaching instrumentation directly to the sleeper soffit and/or on top of layers underneath of the sleeper. This instrumentation has produced average pressures which are also the result of a simplification process. The pressures recorded by the instrumentation were averaged over the area of the instrument used in the tests which are normally fixed without taking into consideration the number of particles actually in contact. Therefore, in this research, pressure

paper has been used to investigate ballast particle contact pressures and the number as well as the area of contacts.

Chapter 6: Apparatus and test preparation

6.1 Introduction

This chapter describes the set-up of the modified SRTF apparatus used in this research and goes on to describe the loading system, specimen preparation and cyclic loading test procedure (6.2). Modifications made to the earlier version of the SRTF apparatus are described and a justification for the use of a rubber mat to represent a slightly compressible subgrade is provided (6.3). In section 6.4, the instrumentation used in the tests is described together with processing method for evaluating combined measurements (6.5). Finally, the details of the tests carried out in this research and the testing variables evaluated (6.6) are described and tabulated (6.7).

6.2 The modified SRTF apparatus

The modified SRTF is a full scale testing apparatus representing a section of track and has been further developed from the earlier apparatus as described in Le Pen (2008). Figure 6.1 shows a photograph of the current version of the SRTF apparatus.



Figure 6.1: Current SRTF apparatus

Modifications were made so that the apparatus would be more suited to the application of many millions of loading cycles (e.g. use of rubber mat) because previously the apparatus had not been used for this. Figures 6.2 to 6.5 show the modified SRTF apparatus construction details.

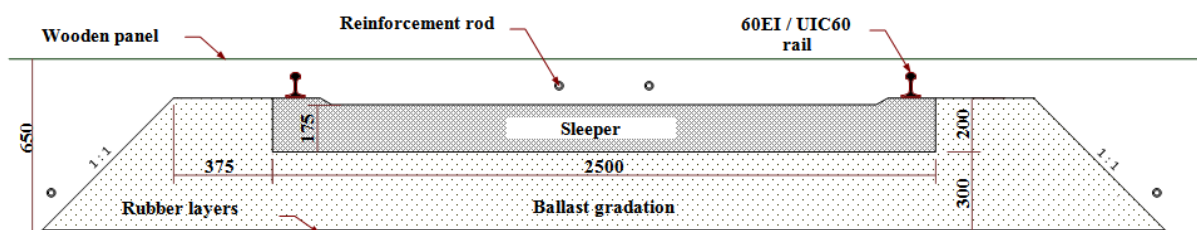


Figure 6.2: Elevation C-C

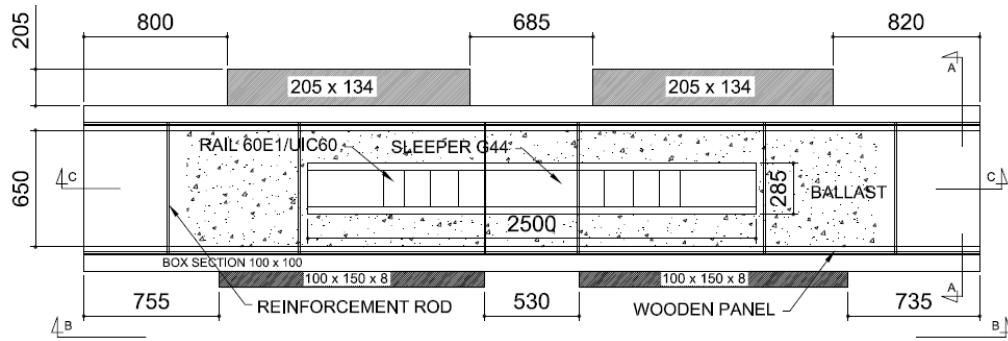


Figure 6.3: A plan view of modified SRTF apparatus

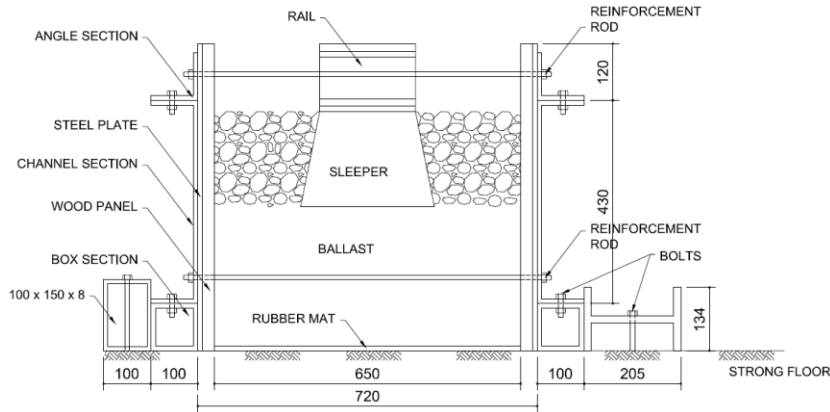


Figure 6.4: Elevation A-A of modified SRTF apparatus (after Le Pen, 2008)

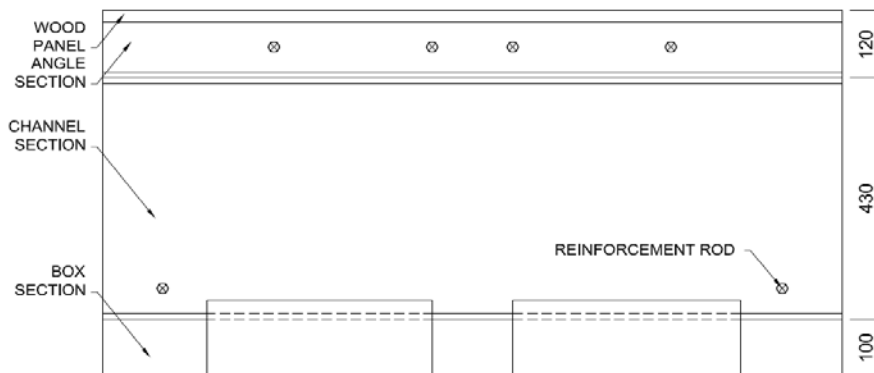


Figure 6.5: Elevation B-B (vertical scale exaggerated)

The sides of the modified apparatus are constructed of heavy steel sections to prevent any significant flexure of the walls during testing and maintain as near as practicable a plane strain condition. Wooden and steel panels of dimensions 500 mm x 650 mm are attached firmly to the inside walls of the modified SRTF apparatus using countersunk bolts. The wooden panels on the front are removable to allow easy placement of pressure plates to measure confining pressure. The inner face of each wall of the modified SRTF apparatus was covered by a double layer of plastic sheet to minimise friction at the contact with the ballast.

A 12 mm rubber layer was placed at the base to represent a compressible subgrade compliant with the minimum Dynamic Sleeper Support Stiffness (DSSS) recommended by NR (Table 3.3) for new 100 mph track. This means that an equivalent spring stiffness of 60kN/mm/sleeper end is achieved. As will be shown later, for the loading applied this means that the whole substructure system deflected less than 1 mm for an equivalent 20 tonne axle load (described in section 3.4).

6.2.1 Loading system

The Instron hydraulic loading actuator used was capable of loading up to 250kN either in tension or in compression and had a stroke length of ± 125 mm controlled by a type 8400 Instron controller. This controller also provided continuous output for the load and deflection to the data logger and automatically tuned so that loading signals were compatible with the response of the sample. The accuracy of this vertical hydraulic loading cell is 1% of stroke length and 1% of actual load (Le Pen, 2008).

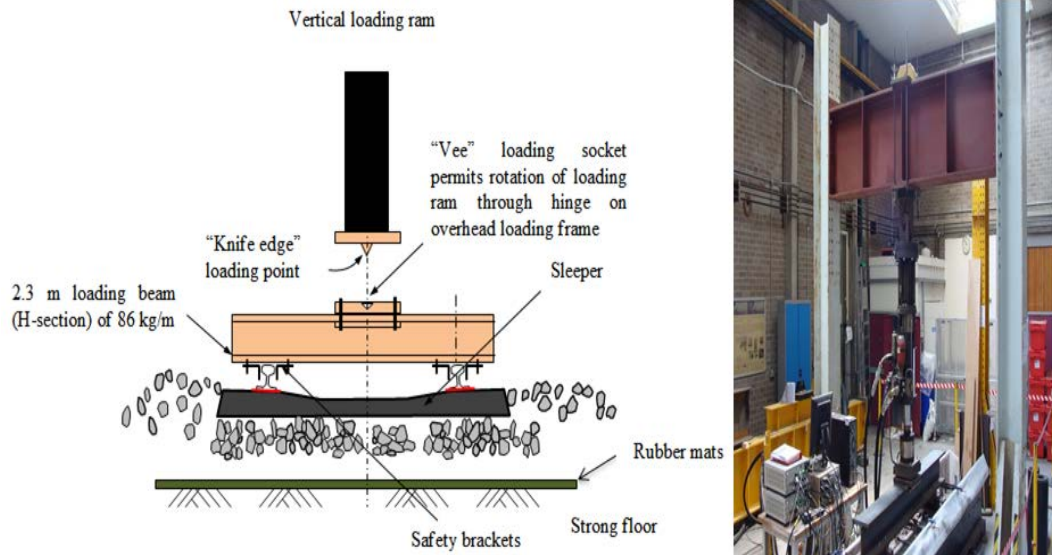


Figure 6.6: The arrangement of loading system

The hydraulic loading actuator (Figure 6.6) was attached to a portal frame by a hinge at a certain height above the loading point to give enough space for putting the sleeper and loading beam in place. This also allowed the vertical ram to follow the v-notch loading point to the centre of the sleeper without any eccentricity.

6.2.2 Specimen preparation

Figure 6.7 shows ballast filling and other test preparation procedures. Prior to ballast placement, pressure paper was fixed to various locations (described in more detail in section 6.4.2). Instrumented panels containing load cells (described in section 6.4.1) were also placed on the sidewalls to measure the confining pressure.

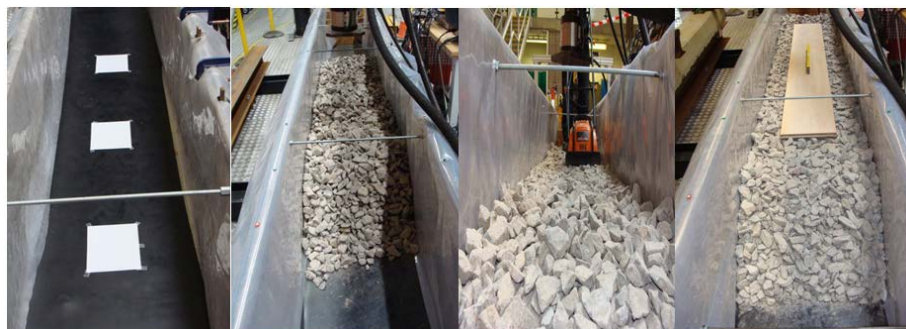


Figure 6.7: Sample preparation for the modified SRTF apparatus test

Figure 6.7 shows ballast being further levelled with the aid of a wooden board. A sleeper with 0.4 m long part-lengths of rails was then placed on top of the ballast (Figure 6.8).



Figure 6.8: Placing sleeper on the top of ballast

The crib and shoulder ballast were placed up to the top sleeper surface and the intended shoulder width was constructed at the same time (Figure 6.9). After placing the sleeper and ballast, LVDT's (described in section 6.4.3) were attached at the designated locations (Figures 6.9 and 6.10).



Figure 6.9: The arrangement of the sleeper on the ballast and instrumentation of LVDTs

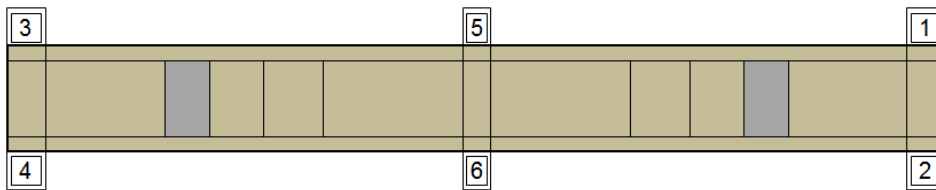


Figure 6.10: The plan view of LVDT locations

Finally, a loading beam was lowered and placed across the railheads and the hydraulic loading cell knife edge was placed in the v-notch loading socket attached on the loading beam (Figure 6.11). Prior to placing the loading beam, measurements were recorded continuously from all instruments and the specimen was left in place for a minimum of 24 hours to give the ballast time to stabilise under its self-weight. Figure 6.12 shows the modified SRTF (a) empty and (b) ready for a test.

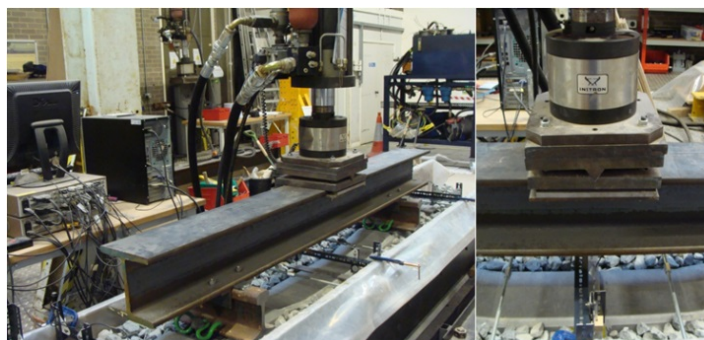


Figure 6.11: Loading beam and load controller connection

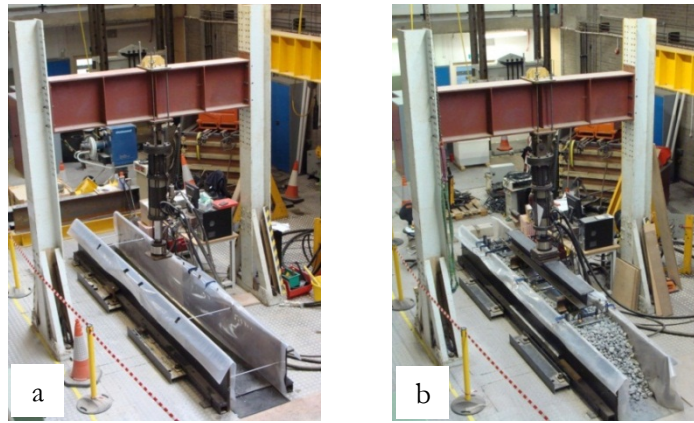


Figure 6.12: The SRTF (a) empty and (b) ready for a test

6.2.3 Cyclic loading test procedure

Prior to the cyclic loading, a single static load was applied to precondition the ballast. This static load was ramped from 5kN up to 98.1kN and was held for a short duration then subsequently reduced to a minimum load of 5kN. Prior to increasing back to the midpoint, the load was also held at 5kN for a short duration. The application of static load was counted as the first loading cycle. Figure 6.13 shows a typical graph of applied load against displacement for the first loading cycle.

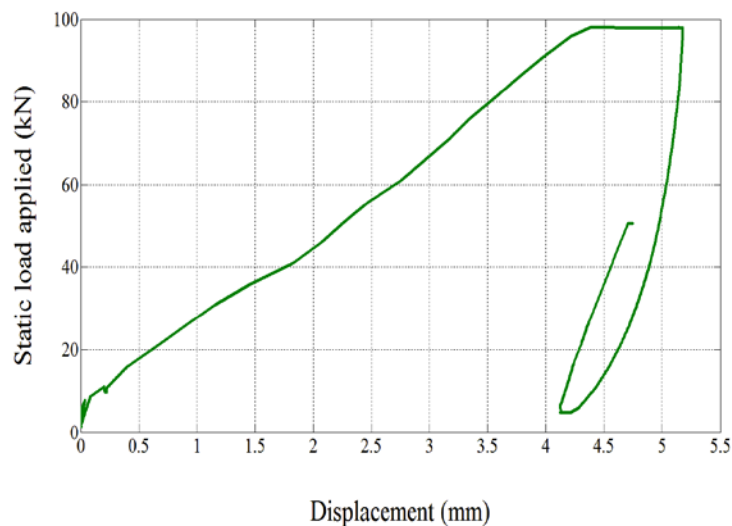


Figure 6.13: A typical graph of applied static load against displacement at first loading cycle

Cyclic loading was applied using a sinusoidal load form at 3Hz between 5kN and 98.1kN. The load values represent a net additional load present after allowing for the dead weight of the sleeper and rails on a 0.65 m length of real track and adjusting for the weight of the loading beam. The loading range was chosen to be equivalent to a pseudo static application of a 20 tonne axle load, which was discussed in chapter 3. The frequency of cyclic loading applied was chosen to be 3Hz based on consideration of the pressure and flow capacity of the hydraulic pump in the laboratory and also that it is known that other types of cyclic test within industry (i.e. to define dynamic stiffness or bedding modulus of USPs) use a minimum of 3Hz loading frequency (British Standards Institution, 2014). Therefore it did not relate directly to a particular train speed, although if averaged over a typical train length for the bogie passing frequency this might correspond to approximately 54 m/s or 120 mph. The characteristics of the sinusoidal load form applied after the first cycle are shown in Figure 6.14.

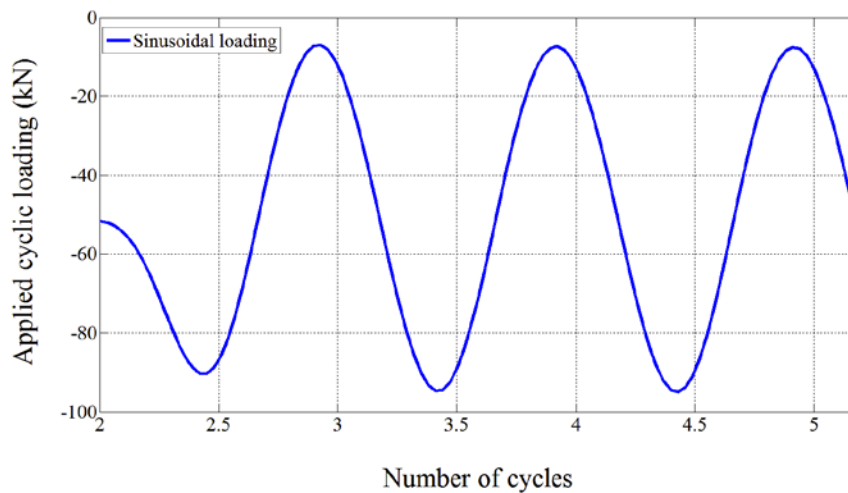


Figure 6.14: Characteristic of cyclic loading applied during the tests

6.2.4 Summary of test procedure

All the tests were designed to represent a condition of freshly laid ballast so after each test the sleeper was removed and the entirety of the ballast was emptied and replaced by fresh ballast. PSD tests on the ballast were always carried out before and after each the test. The common test procedures are summarised as follows:

- a. A rubber mat was placed on the strong floor at the base of the ballast layer using a combination of 1×6 mm and 2×3 mm thicknesses to give a total thickness of 12 mm. For each test, the top 3 mm was replaced as this top layer showed signs of wear (particle indentations) whereas the lower layers appeared unaffected.
- b. Dry ballast was placed to a 300 mm depth up to the level of the sleeper soffit and compacted with a total of 22 passes using a 22 kg plate vibrator of $400 \text{ mm} \times 320 \text{ mm}$ with a 5kN compaction force and the surface was levelled at the same time. Careful levelling of the ballast surface was achieved by use of a wooden board of similar dimensions to the sleeper footprint, a level and careful hand adjustment of any low/high spots.
- c. The sleeper was placed. The crib and shoulder ballast were added. Shoulder ballast was placed to form a 375 mm width and a natural 1V:1H slope (except where this was varied and stated as part of the test plan). The crib and shoulder ballast surfaces were placed to the same level as the sleeper top.
- d. The loading beam was placed across the 60E1 (UIC60) railheads and lined up with the connection for the hydraulic actuator.
- e. A single pseudo static bedding load was applied from 5kN to 98.1kN at a slow loading rate (5kN/s) to remove the major permanent bedding settlement from the virgin loading line and to ensure a stable connection for subsequent cyclic loading. This load was held for a short duration then subsequently reduced to a minimum load of 5kN. The application of this static load was counted as the first loading cycle.
- f. At least 3 million loading cycles were applied at frequency of 3Hz with a sinusoidal wave form. The load was calculated as an equivalent net load for real track (allowing for the dead weight of the loading arrangement) to be between 5kN to 98.1kN. The maximum load represents trains with a 20 tonne axle load and assumes a 50% load transfer to a sleeper immediately beneath an axle (see Chapter 3 for a description of the loading calculations).

- g. Instrument readings were recorded at a frequency of 100Hz.
- h. In all tests, the same amount of time between set up and the start of loading was maintained to avoid pauses of different length during which pause the ballast could have the opportunity to creep.
- i. At the end of each test, everything was removed from the modified SRTF apparatus including the ballast, and replaced afresh for the subsequent test to ensure repeatability of initial conditions.

More detailed description of other unique stages particular to certain tests are described in section 6.6.4.

6.3 Justification of rubber mat and thickness used within the modified SRTF apparatus

One of the modifications introduced to the SRTF apparatus was the use of a rubber mat, placed at the bottom of the apparatus in the place of the wooden soft board used by Le Pen (2008). The role of the rubber mat was to model a uniform subgrade condition for the entire series of tests and to mimic the subgrade behaviour in terms of resilient deflection as well as ensuring that the global cyclic deflection including the ballast movement is comparable to that seen on real in-service tracks. Figure 6.15 shows previous measurements of track movement by Bowness et al (2005), indicating that the deflection of a sleeper is commonly less than 1 mm for high quality track on High Speed 1 (HS1) that is well maintained. Elsewhere deflections of over 5 mm on poor quality track with hanging sleepers may occur (Le Pen et al., 2014b).

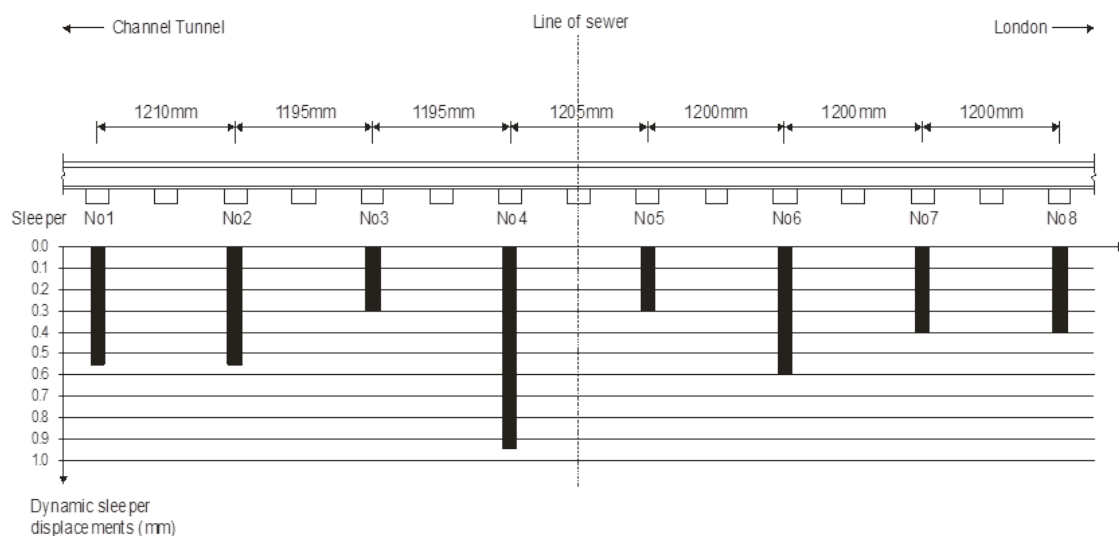


Figure 6.15: Sleepers deflection for section of Channel Tunnel Rail Link (CTRL) (Bowness et al., 2005)

In this research, the tests consider settlement due to sleeper/ballast interaction only as there is no subgrade to settle. The susceptibility of a ballast/sleeper combination to permanent settlement is considered an indicator of the propensity of a length of track to generate differential settlement, which would eventually require maintenance.

The rubber mat used for the tests in this research was supplied by Technix Rubber & Plastic Limited (Ltd) and is available in varying thicknesses. Based on the information provided by the company, the rubber mat has the following material properties:

- a) Minimum tensile strength: 3.0MPa.
- b) Minimum elongation at break: 250%.

c) Specific gravity: 1.5 gram/cm³.

6.3.1 Tests on rubber mat

Tests on the rubber mat were carried out using different methods. Penetrometer, Instron machine and Tiflex's testing facility were used to investigate the deflection behaviour of rubber mat when loaded through an even surface and when loaded through ballast. The thicknesses of rubber mat used in the tests were 15 mm and 6 mm. However, both thicknesses were tested only by the Instron and ballast sandwich methods. Figure 6.16 shows the physical appearance of the rubber mats tested.

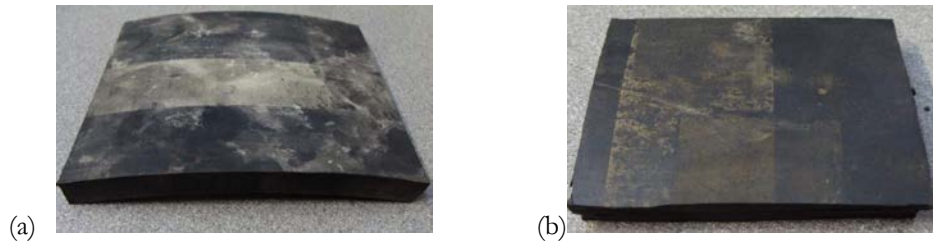


Figure 6.16: The physical appearance of (a) 15 mm and (b) 6 mm rubber mats thickness

The results from all the test methods are presented and compared, together with the results obtained when the same test method was applied to the different thickness of rubber mats.

Rubber mat test using penetrometer

Method

The penetrometer used for rubber mat test (Figure 6.17) was a Farnell product and has a capacity up to 6 kg/cm² or 600kPa. To measure the deflection at the same time as this penetrometer being pushed to the rubber mat, a dial gauge, which was calibrated to the nearest 0.01 mm, was used as an additional instrument.



Figure 6.17: Penetrometer

The rubber mat used for this test was a 160 mm sided square in plan view of 15 mm thickness. It was laid on a strong flat surface for evenly support. The penetrometer dial reading was zeroed before the test was carried out. The dial gauge used to measure deflection corresponding to the penetrated pressures was also zeroed prior to the test. The penetrometer dial tip and dial gauge were located adjacent to each other to obtain readings for the same location. The penetrometer dial tip was pushed into the rubber mat by a constant pressure shown on the penetrometer reading. The pressure reading and the resulting deflection were recorded simultaneously. This test was repeated several times under different applied pressures.

Results

The results of rubber mat test using penetrometer are presented in Table 6.1 and Figure 6.18.

Table 6.1: Results of rubber mat test using penetrometer

Pressure (kPa)	Displacement (mm)
0	0
325	0.5
490	1.0
490	1.0
510	1.5
520	1.5
525	1.5

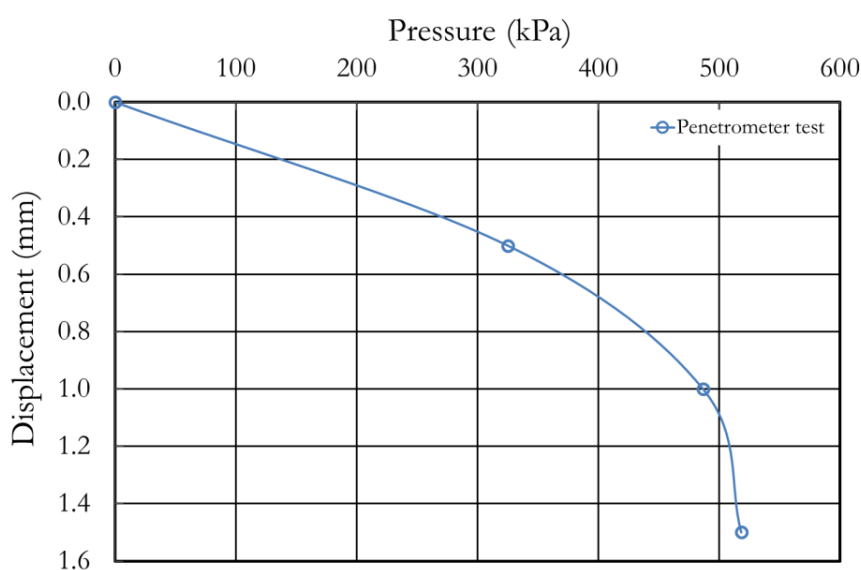


Figure 6.18: Applied pressure against displacement graphs of rubber mat test using penetrometer

The test results (Figure 6.18) are used to estimate the average deflection of the rubber mat using the 2:1 load spread method of chapter 3. However, it is important to note that 2:1 load spread method assumes a continuous or uniform load while in reality the contact point will be small. Based on this calculation (Table 3.7), a pressure of magnitude 0.6105 kg/cm² or 61.05kPa may be applied to the rubber mat. Plotting the pressure value of 61.05kPa into Figure 6.18 gives an average displacement of 0.09 mm. The important point however, is that this displacement is small.

Rubber mat test using Instron machine

Method

Two different rubber mats, 100 mm square and of thicknesses 15 mm and 6 mm, were tested. The machine used was an Instron XL2000 (Figure 6.19) with a load capacity up to 100kN, though the maximum load applied was 5kN. This was sufficient to cover the potential pressure applied by ballast to rubber mat, based on the 2:1 load spread method.



Figure 6.19: Instron machine

The rubber mat specimen was placed between steel plates having the same plan area as the specimen and positioned centrally below the loading ram. The loading cap was lowered so that it just touched the surface of the top plate. A digital dial gauge was attached and set to zero (Figure 6.20).



Figure 6.20: Rubber mat test arrangement

The load on these tests was applied in increments with a 10 minute holding time for each step (Table 6.2). The load was applied and kept constant for 10 minutes before it was reduced to 100N and then again kept constant for 10 minutes prior to the application of a higher load. This sequence was repeated until the maximum designated load was applied as shown in Table 6.2.

Table 6.2: The procedure of loading and unloading load in rubber mat test

Step	Starting load (N)	Ending load (N)	Holding time (minutes)	Cumulative time (minutes)
1	0	100	10	10
2	100	200	10	20
3	200	500	10	30
4	500	100	10	40
5	100	1000	10	50
6	1000	100	10	60
7	100	2000	10	70
8	2000	100	10	80
9	100	3000	10	90
10	3000	100	10	100
11	100	4000	10	110
12	4000	100	10	120
13	100	5000	10	130
14	5000	100	10	140

The Instron machine was used in load control mode and operator skill was required to match the load at the appropriate stages of the test to within $\pm 5\%$. Loads were always maintained constant

during the holding time. In practice this meant that the load had to be increased manually as there was a tendency for the load to drop off due to creep in displacement control mode.

Results

Table 6.3 and Figure 6.21 show the results of rubber mat test using the Instron machine at the peak displacement of applied loading while the loading and unloading data and graphs are provided in Appendix B.

Table 6.3: Results of rubber mat test using the Instron machine

Pressure (kPa)	Rubber mat thickness	
	15 mm	6 mm
	Displacement (mm)	
0	0	0
10	0.05	0.05
20	0.09	0.07
50	0.13	0.1
100	0.18	0.12
200	0.25	0.14
300	0.33	0.17
400	0.4	0.2
500	0.48	0.22

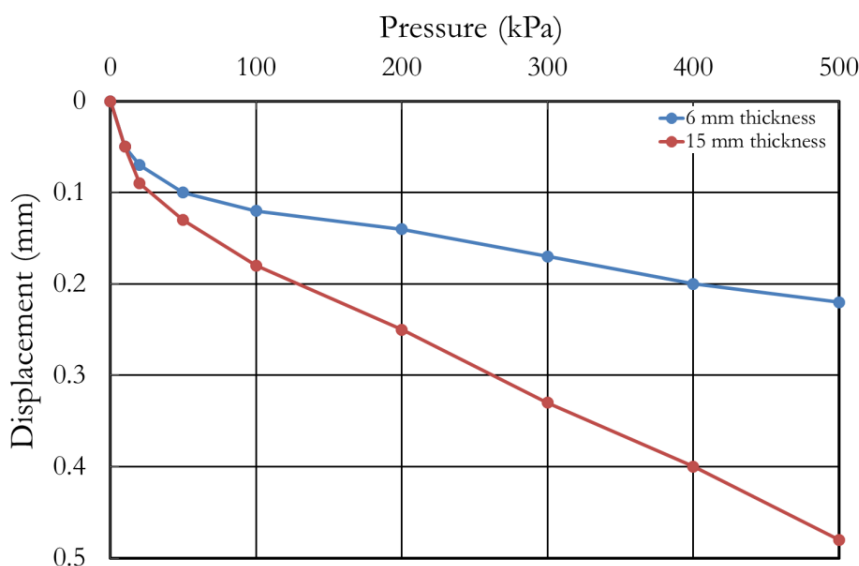


Figure 6.21: Applied pressure against displacement graphs of rubber mat test using the Instron machine

Figure 6.21 compares the test results for 6 mm and 15 mm rubber mat thicknesses. According to Figure 6.21 a pressure of 61.05kPa (from the 2:1 spread load method in Table 3.7) will give corresponding displacements of 0.1 mm and 0.13 mm for the 6 mm and 15 mm rubber mat thicknesses respectively. The loading and unloading data in Appendix B also show that the rubber mat is not a purely elastic material since creep occurs after unloading.

Ballast sandwich tests

The purpose of these tests was to measure the resilience of the rubber mat when loaded through ballast as the closest approach to model the actual ballast/rubber mat contact that will occur in reality.

Method

The rubber mat used in the ballast sandwich test was a 160 mm square in plan view and of 15 mm thickness, and placed on a rigid base. To confine the ballast layer laterally, a square steel tube was fabricated. The tube has external dimensions of 190 mm wide \times 190 mm long \times 295 mm high and internal dimensions of 170 mm wide \times 170 mm long \times 295 mm high (Figure 6.22).



Figure 6.22: The steel square tube used in ballast sandwich test

The rubber mat specimen was placed on top of a rigid steel plate located inside and at the bottom of the square tube. Ballast was placed inside the square tube and on top of the rubber mat specimen. The square tube was gently shaken to help compact the ballast. The ballast was topped up while continuing shaking until the desired height was reached, with an even surface that was checked using a spirit-level (Figure 6.23).



Figure 6.23: Sample preparation for ballast sandwich tests

Figure 6.24 shows a rigid metal plate that was placed on top of the ballast surface and fitted within the square tube. A preload of 100 N was applied to ensure a positive contact between all parts of the arrangement. Dial gauges were placed at each corner of the top loading plate to measure displacement. This preload was left for at least 24 hours to allow the ballast to stabilise and ensure the deflection was not changing. Prior to the commencement of the test, the preload was unloaded and all the equipment was re-set. The dial gauges were also zeroed. The loading procedure previously presented in Table 6.2 was used.



Figure 6.24: The arrangement of ballast sandwich test

Results

The results of the ballast sandwich test in terms of interim peak loads and corresponding displacements are shown in Table 6.4 and Figure 6.25. The original load and displacements data are available in Appendix C.

Table 6.4: Results of rubber mat test using ballast sandwich on the 15 mm thickness

Pressure (kPa)	Displacement corner 1 (mm)	Displacement corner 2 (mm)	Displacement corner 3 (mm)	Displacement corner 4 (mm)
0	0	0	0	0
3.54	0.02	0	0.05	0.04
7.09	0.1	0	0.12	0.08
17.72	0.33	0.11	0.32	0.17
35.43	0.68	0.16	0.81	0.4
70.86	1.18	0.46	1.34	0.77
106.29	1.71	0.93	1.19	1.27
141.72	2.18	1.35	2.4	1.72
177.15	2.61	1.75	2.89	2.16

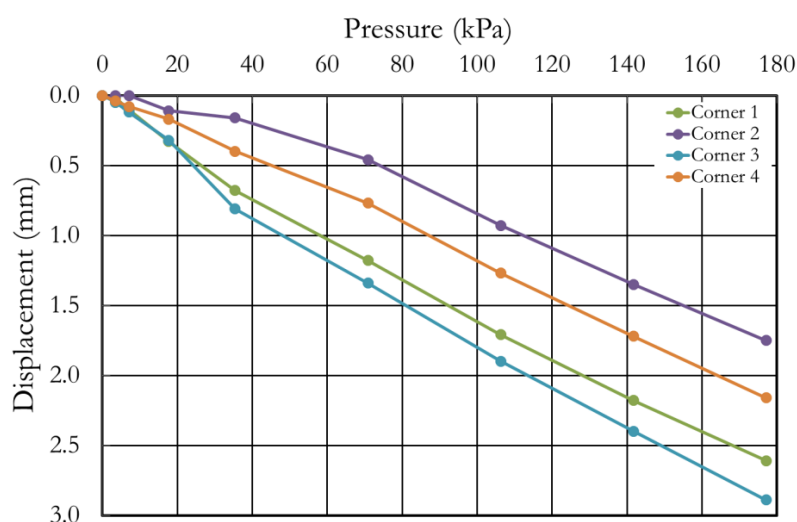


Figure 6.25: Applied pressure against displacement graphs of rubber mat test using ballast sandwich on 15 mm thickness

Similar tests were conducted using a rubber mat of 6 mm thickness and also without a rubber mat. The results of these tests in terms of interim peak loads and the corresponding displacements are presented in Tables 6.5 and 6.6 and Figures 6.26 and 6.27 respectively. The original data for these tests are available in Appendix D.

Table 6.5: Results of rubber mat test using ballast sandwich on 6 mm thickness

Pressure (kPa)	Displacement corner 1 (mm)	Displacement corner 2 (mm)	Displacement corner 3 (mm)	Displacement corner 4 (mm)
0	0	0	0	0
3.54	0.01	0	0	0
7.09	0.07	0.06	0	0.05
17.72	0.33	0.29	0.14	0.24
35.43	0.83	0.63	0.37	0.59
70.86	1.48	1.11	0.74	1.09
106.29	2.17	1.66	1.17	1.65
141.72	2.69	2.23	1.68	2.17
177.15	3.07	2.71	1.99	2.53

Table 6.6: Results of ballast sandwich test without rubber mat

Pressure (kPa)	Displacement corner 1 (mm)	Displacement corner 2 (mm)	Displacement corner 3 (mm)	Displacement corner 4 (mm)
0	0.00	0.00	0.00	0.00
3.54	0.00	0.00	0.00	0.00
7.09	0.00	0.01	0.00	0.00
17.72	0.03	0.09	0.05	0.01
35.43	0.08	0.13	0.11	0.08
70.86	0.19	0.26	0.21	0.17
106.29	0.28	0.35	0.31	0.28
141.72	0.42	0.52	0.48	0.43
177.15	0.63	0.73	0.69	0.71

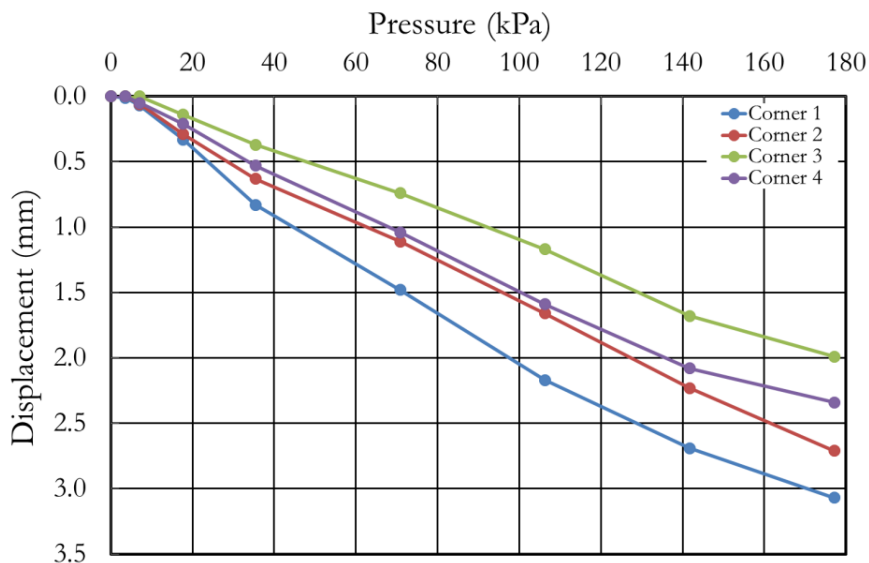


Figure 6.26: Applied pressure against displacement graphs of rubber mat test using ballast sandwich on 6 mm thickness

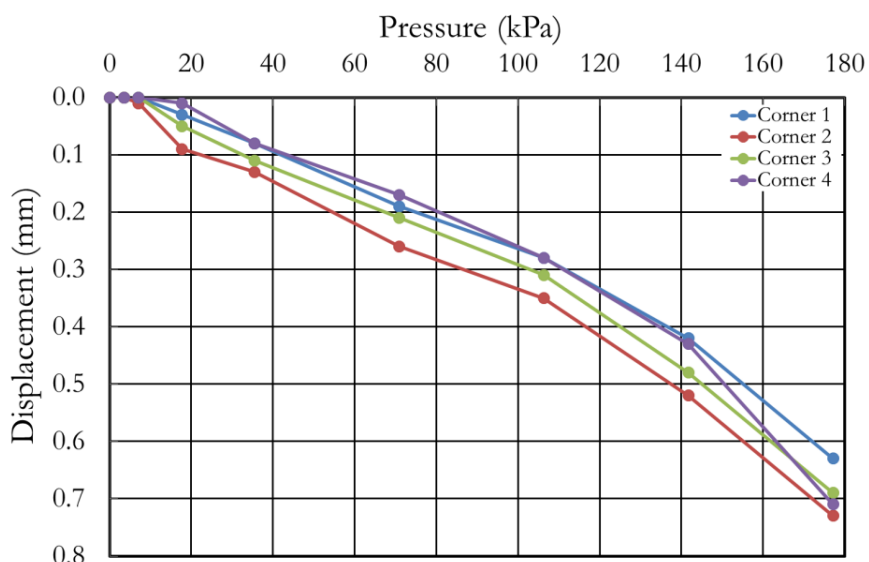


Figure 6.27: Applied pressure against displacement graphs of ballast sandwich test without rubber mat

To compare the results of the ballast sandwich test method, the displacement of four corners of the loading steel plate of each test was averaged to obtain a mean value to represent each test. Figure 6.28 shows the comparison of the mean displacement value obtained by each test at peak load.

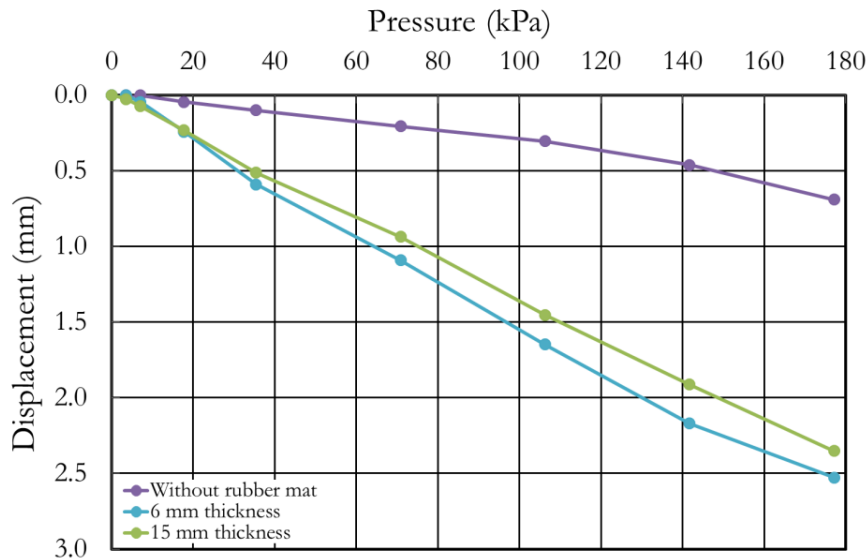


Figure 6.28: Comparison of the mean displacement value of ballast sandwich tests

Figure 6.28 shows that when the rubber mat is loaded through a ballast medium the thickness of the rubber mat is of less importance as the penetration of the particles into the rubber is the main influence on the total displacement. According to the ballast sandwich test, a pressure of 61.05kPa without a rubber mat and then with 15 mm and 6 mm rubber mat thicknesses will give average displacements of 0.18 mm, 0.82 mm, and 0.95 mm respectively. The displacement in the ballast is in the range of 19% to 22% of the total displacement and was mostly caused by rearrangement of ballast particles as the confinement of the steel box would prevent any lateral movement during the tests.

Rubber test by Tiflex Ltd

Method

As an additional and comparative test, the rubber mat was also tested by Tiflex Ltd using the Mayes Servo Hydraulic (MSH) rig in their laboratory. Figure 6.29a illustrates the machine, which was fitted with a 1000kN load cell. This machine has the ability to carry out static and dynamic tests. The displacement was measured over 4 points using 25 mm range displacement transducers located at the corners of the platen. Two additional transducers of 5 mm range also were used and were located at opposite corners. The procedures of static and dynamic tests by Tiflex Ltd were not provided, however they were carried out according to BN 918 145-1 and DIN 45673-1.

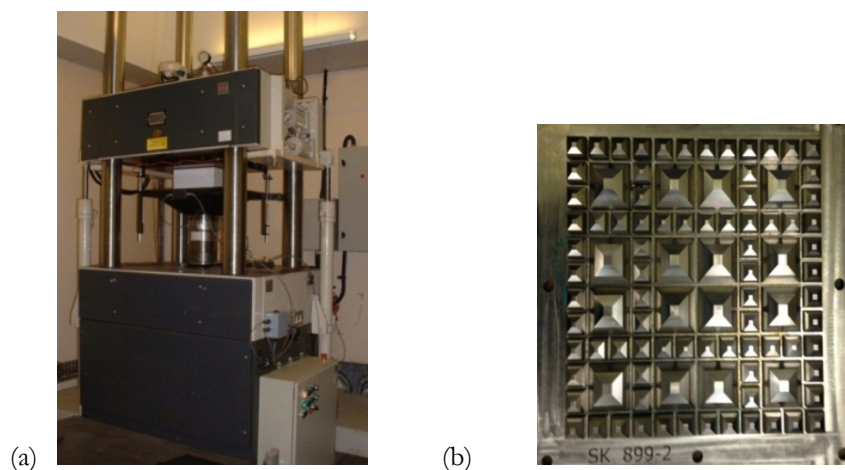


Figure 6.29: The Tiflex Ltd MSH machine and Geometric Ballast Plate (GBP)

Tests on the rubber mat were conducted with static and dynamic applied loading. In static tests the rubber mat was subjected to three loading cycles between 6kPa and 250kPa. The results recorded were from the third cycle. The dynamic test was carried out using loads of between 20 and 100kPa. The entire data set was captured and recorded using a software programme developed by Excel Control Systems. These static and dynamic loads were applied not only through a flat surface plate but also through a geometric ballast plate (GBP; Figure 6.18b), designed to model ballast particle contact during the test.

Results

The results of the test on different thicknesses of rubber mat using the MSH machine with the application of static and dynamic loading applied through the flat plate and the GBP are shown on Figures 6.30 and 6.31 respectively.

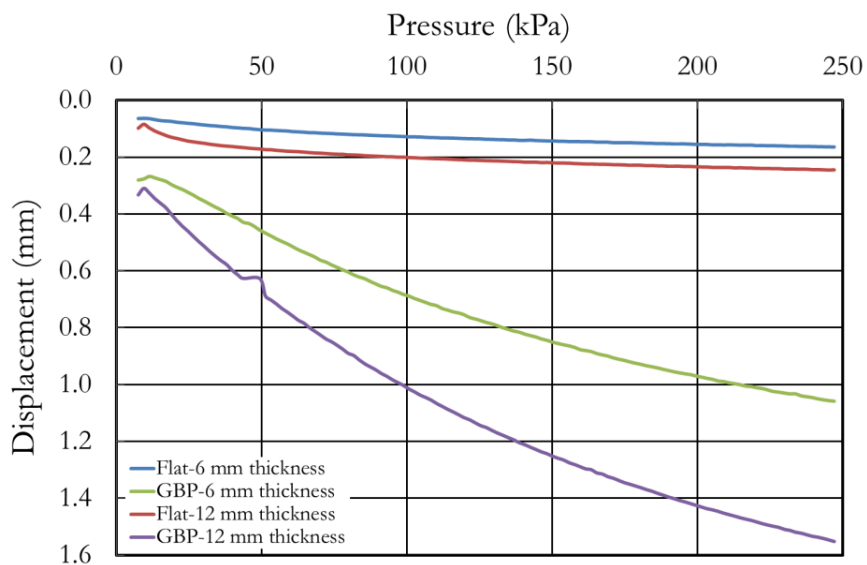


Figure 6.30: The results of rubber mat test on static load of MSH through flat plate and GBP

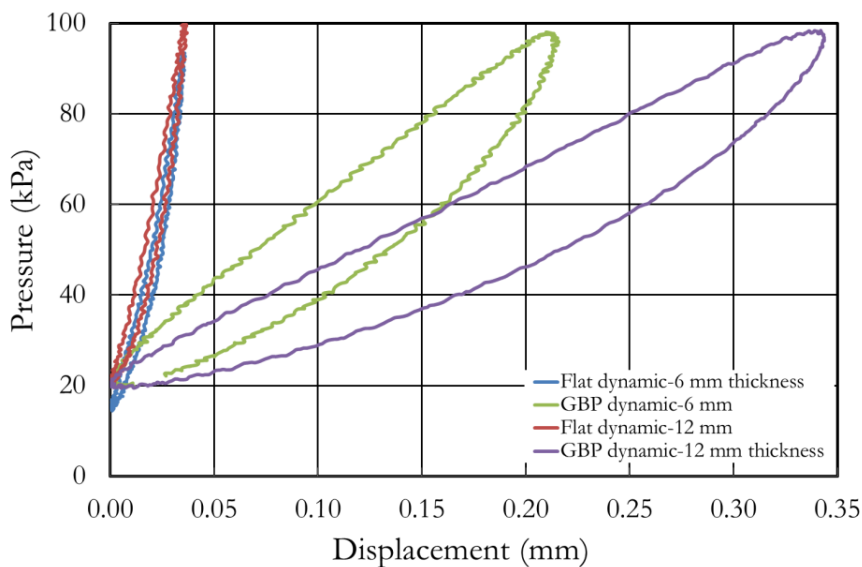


Figure 6.31: The results of rubber mat tests on dynamic load of MSH through flat plate and GBP

The test results (Figures 6.30 and 6.31) using the MSH machine through a flat plate surface on the rubber mat produced a lower displacement than the test results through GBP in both static and

dynamic tests. The dynamic load test produced less deflection than the corresponding static load test. A loading pressure of 61.05kPa gives displacements of 0.110 mm and 0.180 mm for flat plate surface and 0.517 mm and 0.761 for GBP for rubber mat thickness of 6 mm and 12 mm respectively, according to Figure 6.30.

Comparison of all rubber mat test results

Figure 6.32 shows a comparison of all test results of rubber mat using all the applied methods described at various thicknesses.

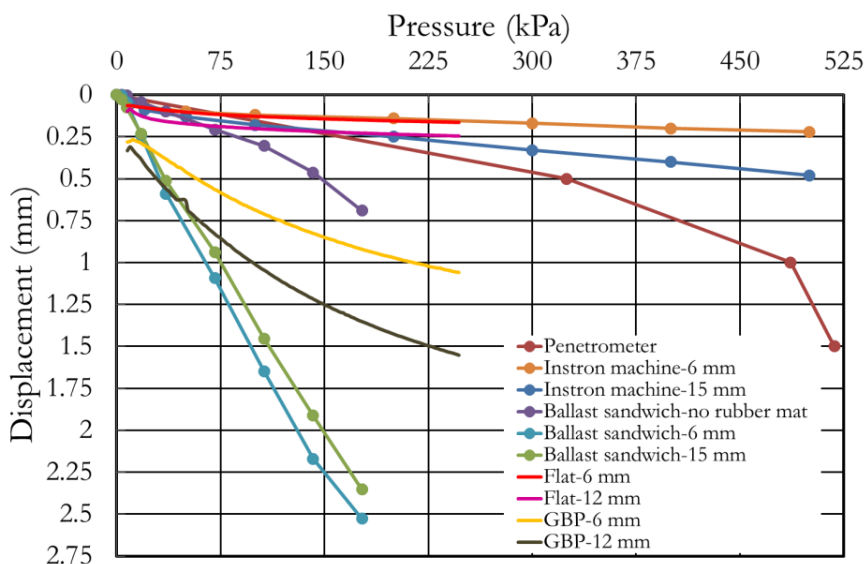


Figure 6.32: Comparison of rubber mat test results carried out by different methods

In general, for the same magnitude of pressure applied (61.05kPa), the same results of displacement (0.13 mm) were obtained by the tests using penetrometer and Instron machine on the rubber mat of 15 mm thickness. However, for the same thickness of rubber mat (15 mm), the results of ballast sandwich tests are higher than both penetrometer and Instron tests. The results from the tests carried out at Southampton agree with the results obtained from rubber mat tests using Tiflex Ltd.'s MSH machine. Comparing the test results using flat surface on rubber mat with 6 mm thickness shows that both Instron test and MSH machine provided the same result of displacement (0.1 mm). However, the same results on the same rubber mat thickness of 6 mm were not achieved using ballast sandwich and GBP tests. The ballast sandwich test produced a higher displacement than the GBP test. This is due to the different contact conditions which show that the particle contact areas on the rubber mat of the ballast sandwich test being less than in the test using GBP (the GBP does not give few enough loading points). The results also show that when the rubber is loaded through ballast medium, higher displacements are seen compared to when the same pressure is applied uniformly or using a penetrometer. Repeat tests on the rubber mat gave consistent results and showed that the sample thickness governed the final displacement of the sample being tested. However, when loaded through a real ballast medium in which the contact area is not a constant parameter, the thickness of the rubber mat is of less importance than the penetration of the particles into the rubber mat, which has greater influence on the total displacement produced. This is shown in the result of ballast sandwich tests (Figure 6.32), although there might be an error during the test, that the results from rubber mat thickness of 6 mm are higher than from rubber mat thickness of 15 mm.

Based on the ballast sandwich test a pressure of 61.05kPa on the rubber mat thickness of 6 mm produced an average deflection of 0.95 mm. This is approximately 10 times greater than the displacement obtained using the Instron machine to load a rubber mat of the same thickness through a flat plate surface. Comparing the test results obtained using Tiflex Ltd.'s MSH machine shows that the tests through GBP give displacement approximately 4 to 5 times higher than tests through a flat plate surface. Regardless of the discrepancies, all tests give a deflection of the rubber mat of less than 1 mm, which is comparable to the results of the field investigation carried out by Bowness et al (2005). It is also comparable to the resilience a resilient of good track and ensures the minimum required of DSSS recommended by NR (Table 3.3) is achieved since for 20 tonnes axle load (the assigned load for the tests, described in section 3.2) the whole substructure system should deflect less than 1 mm.

6.4 Instrumentation

For all tests carried out in this research, instrumentation consisting of pressure plates, pressure paper and LVDTs was used. This section describes their set up and where relevant the calibration tests carried out.

6.4.1 Pressure plates

To measure pressures developed in the ballast under the simulated track loading, the wall of the modified SRTF apparatus was instrumented using 4 pressure plates at designated locations (Figure 6.33). Each plate bore onto 4 load cells, whose output at zero load and calibration factor (lbs/mV) were determined before and after each test.

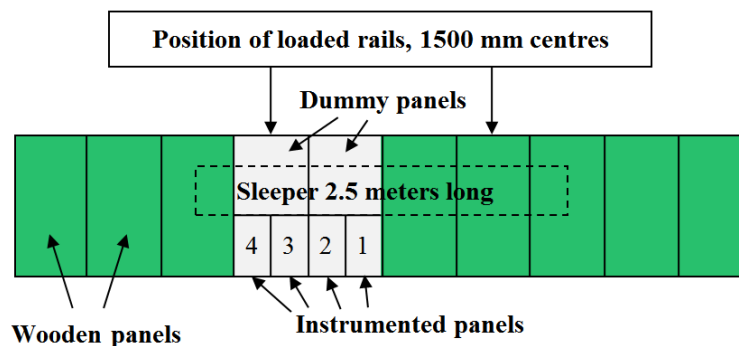


Figure 6.33: Location of instrumented plates and dummy panels

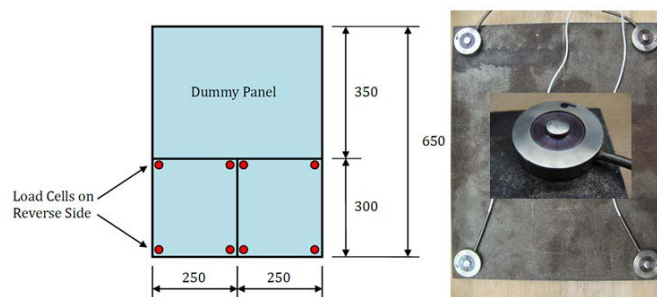


Figure 6.34: Front face view of pressure plates, dummy panel and load cells

The pressure plates (Figure 6.34) consisted of 10 mm thick load cells attached to 12 mm thick steel plates giving a total thickness nearly the same as for the 25 mm thick wooden panels elsewhere on the side walls of the modified SRTF apparatus. The plates were placed only to the level of the sleeper

soffit (300 mm high) above the base so dummy steel panels were placed above them (Figure 6.34) to ensure no gap was left. It is recognized that the instrumented and dummy steel panels have stiffness greater than the wooden panel, but in view of the relatively small thickness this is not significant.

6.4.2 Pressure paper

To investigate the sleeper to ballast and ballast to subgrade contacts, as well as contacts between the ballast and the wall of the modified SRTF apparatus, pressure paper was used to record the number and the area of contacts and to assess the magnitude of ballast particle contact pressures. Prior to its use in the tests, the pressure paper was calibrated. The application of pressure paper in this research is novel. Therefore in this section, the principle of operation and the calibration of the pressure paper are described. The results of the pressure paper calibration process are presented, followed by a description of the locations of pressure paper used in the tests.

An overview of pressure paper

Pressure paper consists of a thin film made of micro-encapsulated colour forming and colour developing materials (A J P Automotive Ltd, 2011, AJP Automotive Ltd, 2014). Its properties are described in detail by Fuji Film (2013) and it can be purchased for different pressure sensitivity ranges. There are seven types of pressure paper available covering the pressure range 0.05 to 300MPa (Figure 6.35).

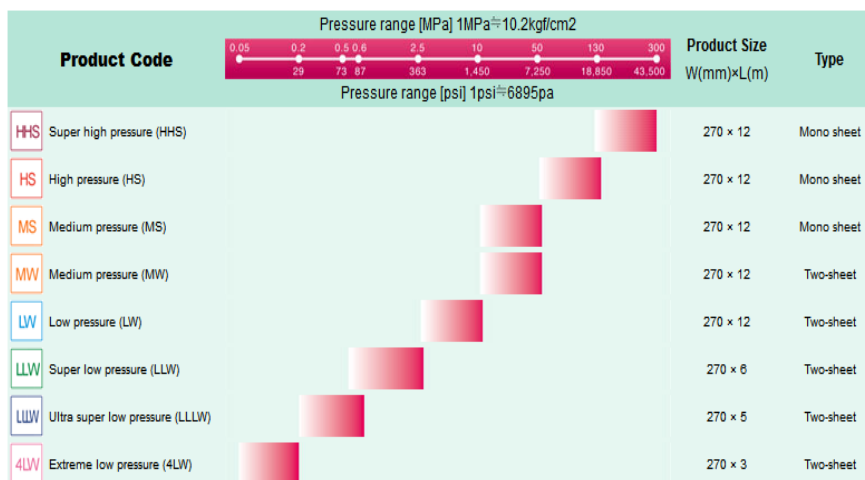


Figure 6.35: The types and range level of pressure papers (AJP Automotive Ltd, 2014)

Pressure papers are also available in two different forms as:

1. Two-sheet pressure paper. This is composed of an A-film, which is coated with a micro-encapsulated colour-forming material, and a C-film, which is coated with a colour developing material. The A-film and C-film must be positioned with the coated sides facing each other (Figure 6.36) in the application.

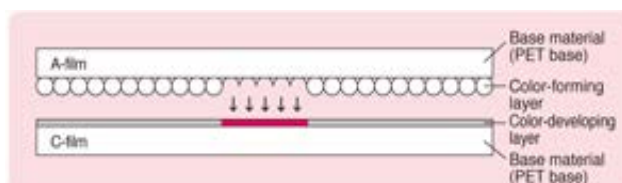


Figure 6.36: Two-sheet pressure paper (A J P Automotive Ltd, 2011, AJP Automotive Ltd, 2014)

2. Mono-sheet pressure paper. Within this form (Figure 6.37), the colour developing material is coated on a polyester (PET) base, with the micro-encapsulated colour forming material layered on top.

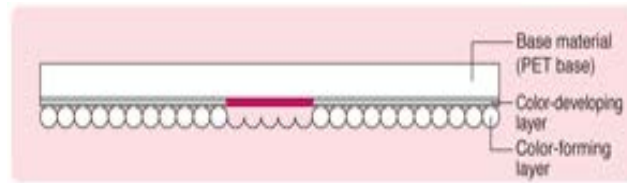


Figure 6.37: Mono-sheet pressure paper (A J P Automotive Ltd, 2011, AJP Automotive Ltd, 2014)

The application of pressure onto pressure paper will break the micro-encapsulated colour-forming material, transferring to the colour developing material and generating a red colour. A red colour (patch) impression of varying intensity is formed proportional to the magnitude of pressure and pressure distribution. AJP Automotive Ltd (2011, AJP Automotive Ltd, 2014) provides charts showing the relation between pressure and colour density (Figure 6.38).

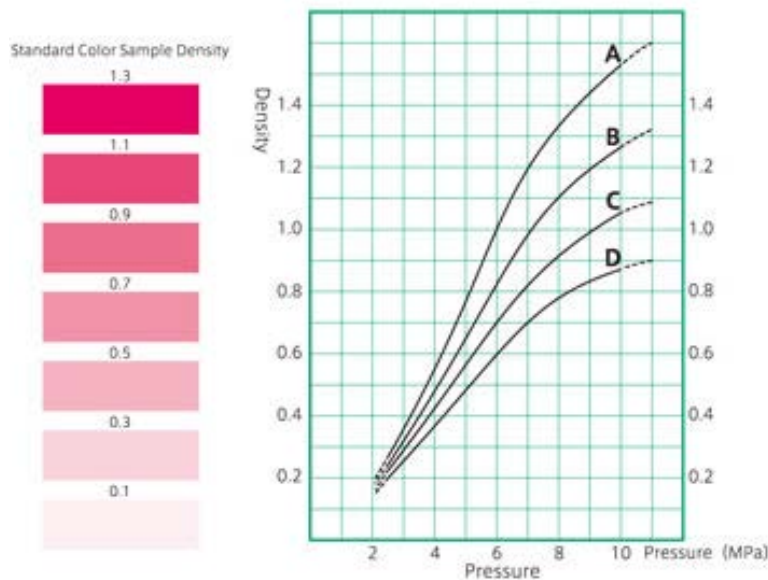


Figure 6.38: Standard continuous pressure chart (A J P Automotive Ltd, 2011, AJP Automotive Ltd, 2014)

When a pressure is applied to the pressure paper, it creates a uniform colour pattern in a similar shape to the media of the pressure. However, the red colour intensity will increase within a certain time before beginning to fade. Therefore colour analysis through the scanning process needs to be done within an hour to give representative results (Andussies, 2011).

Calibration of pressure paper

To verify the relationship between red intensity (RI) and pressure, calibration checks were carried out. Two-sheet pressure paper type for the range of pressures of 0.5-2.5MPa, 2.5-10MPa and 10-50MPa were tested. These two-sheet pressure papers were cut to desired dimensions and the rough surface of each sheet was placed against a steel backing and rigidly supported (Figure 6.39).

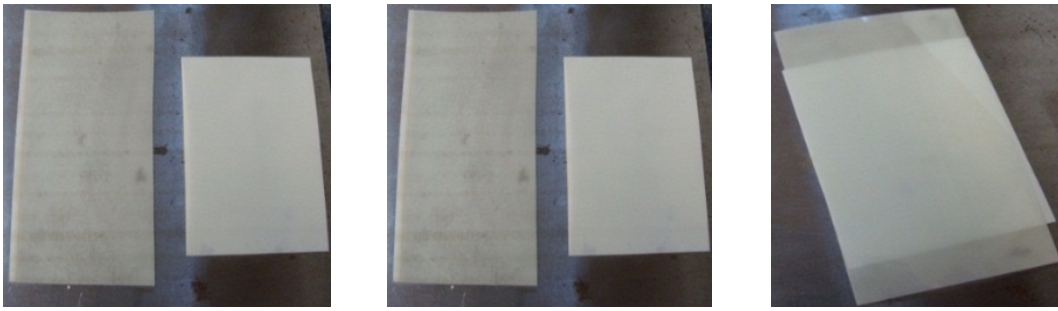


Figure 6.39: The pressure papers used for calibration

To apply pressure, a set of known weights was placed onto steel shapes of known contact areas (Figure 6.40). A metal rod of 5 mm square cross sectional dimensions was used for pressure paper in range of 0.5-2.5MPa and a metal rod with cross sectional dimensions of 20 mm square was used for 2.5-10MPa and 10-50MPa.



Figure 6.40: The set of known loads and metal rods used for calibration test

The metal rods were placed onto the pressure paper to apply uniform pressure with known loads in 2 minute durations. This produced a red patch (Figure 6.41). The red patches produced were scanned.

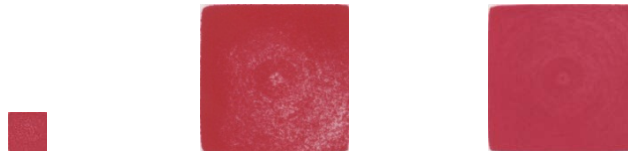


Figure 6.41: Red patches recorded on the pressure papers in calibration process

An Epson Perfection V33 was recommended by the pressure paper manufacturer (A J P Automotive Ltd, 2011) to scan the pressure paper, with controls in place to ensure the lighting condition remained the same. The red patch on the pressure paper was scanned following loading. The images were analysed to determine the RI using a bespoke script implemented in Matlab (MathWorks, 2014). To evaluate the influence of time on the RI, the scanning process was repeated after a range of elapsed times (holding times) up to three months. After three months the RI associated with a given pressure may be lower than immediately after loading. The same script was used to determine this reduction so that this could be allowed for.

Results of pressure paper calibration

It is known that RI of red patches produced at any range of pressure paper will increase for a certain time before beginning to fade (Andussies, 2011). Therefore, to accommodate the fluctuation of the RI values, the RI is presented in terms of maximum (max) and minimum (min) values. Table 6.7

shows the results of pressure paper calibration while Figure 6.42 shows the relationship between applied pressure and the RI values, indicating the maximum (initial, represented by top lines) and minimum (represented by the bottom lines, after a delay of three months) values of RI recorded with the ranges of pressure paper under the application of known loads. The data obtained in the pressure paper calibration process are given in detail in Appendix E.

Table 6.7: The max and min RI values recorded on the ranges of pressure paper

Range of pressure paper (MPa)								
0.5-2.5			2.5-10.0			10.0-50.0		
Applied pressure (MPa)	RI		Applied pressure (MPa)	RI		Applied pressure (MPa)	RI	
	Max	Min		Max	Min		Max	Min
0	0	0	0	0	0	0	0	0
0.1	11.95	10.33	0.5	5.98	4.61	2.5	5.28	4.52
0.2	23.29	20.81	1.0	9.27	8.19	5.0	8.60	7.65
0.3	26.43	23.14	1.5	11.66	10.40	7.5	12.28	10.84
0.4	34.65	31.51	2.0	15.96	14.42	10.0	18.02	16.59
0.5	36.20	32.56	2.5	20.65	18.67	20.0	38.38	35.16
1.0	56.30	53.08	5.0	40.98	37.70	30.0	48.98	44.49
1.5	62.07	58.55	7.5	54.06	49.26	40.0	53.55	48.81
2.0	66.27	60.96	10.0	61.91	56.35	50.0	58.67	53.28
2.5	68.08	62.7						

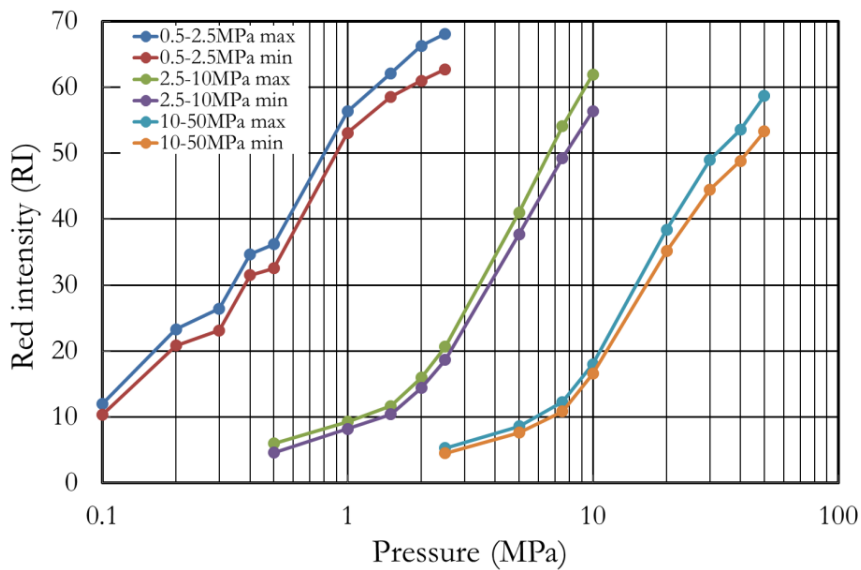


Figure 6.42: Pressures against RI for various ranges of pressure paper

Figure 6.42 shows that the RI will decrease from the maximum by an average of 9.2% to 11.31 % during a three month holding time. Therefore, the pressure paper will give up to $\approx 10\%$ error if it is not scanned within 1 hour of a load being applied and this conforms to the pressure paper manufacturer advice.

Designated locations of pressure paper in the test

Pressure paper was used to investigate sleeper to ballast and ballast to sub-grade contact areas and pressure at the scale of individual particles. In this research, pressure paper with stated sensitivities in the ranges 2.5 to 10MPa, and 10 to 50MPa was found to be suitable. Sheets of the pressure paper measuring 200 mm \times 250 mm were placed at key locations on the rubber mat, on the side wall of

modified SRTF apparatus and at the sleeper soffit (Figure 6.43 and Table 6.8) in each test to measure the interfaces between sleeper/ballast and ballast/subgrade respectively.



Figure 6.43: The locations of pressure papers (a) on rubber mat, (b) on the wall of modified SRTF and (c) at the sleeper soffit

Table 6.8: The detail of number and location of pressure papers instrumentation

Interface	Number of sheet of pressure paper	Location details	The purpose of the test	Sensitivity of paper used
At the sleeper soffit (sleeper/ballast)	3	One is put in the middle and the other two are for each side of the sleeper directly under the railseat.	To investigate the number and area of contact and the magnitude of pressures at sleeper/ballast interface.	10 to 50MPa
On the rubber mat (ballast/subgrade)	3	Directly below the pressure paper attached at sleeper soffit	To investigate the magnitude of pressures inserted by ballast particles to subgrade.	2.5 to 50MPa
On the wall of modified SRTF (ballast/wall)	2	One is put on the position of the middle of sleeper and slightly away toward railseat.	To investigate ballast pressure experienced by ballast crib in longitudinal direction of the track.	2.5 to 50MPa

6.4.3 LVDTs

LVDTs were used to measure the vertical and horizontal movements of the sleeper. In the case of mono-block sleepers, vertical LVDTs were placed on both sides of the sleeper at each corner and in the middle. A horizontal LVDT was also placed at the sleeper end to check whether the sleeper was moving laterally, in all cases no significant lateral movement occurred. These LVDTs were fixed to brackets, firmly clamped to the sides of the modified SRTF apparatus and positioned so as to measure the vertical deflection of a level plate glued to the sleeper (Figure 6.44). Therefore all measured movement of the sleeper was relative to the modified SRTF apparatus walls. Two additional LVDTs were used in the tests on twin-block concrete sleepers, so that the four corners of each block were monitored using a total of 8 LVDTs.

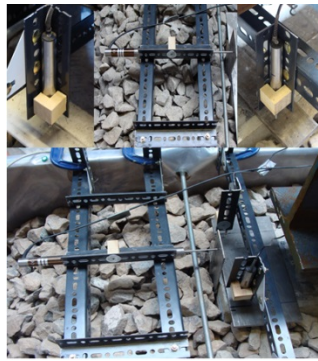


Figure 6.44: LVDTs instrumentation on the sleeper

All LVDTs were connected to a Vishay type 5100B data logging system (Vishay Intertechnology Inc, 2006). Data was logged at frequencies of 1Hz for the first slowly applied cycle and 100Hz for the later cycles during which the load was applied at 3Hz, thus providing 33 data points per loading cycle. The accuracy of the data logger was to the nearest tenth of a millivolt and the channels were filtered using an inbuilt 5Hz Butterworth filter to remove any higher frequency noise, leaving the relevant data for the major experimental behaviour (mainly at 3Hz as this was the frequency of loading applied). The calibration constants of the LVDTs used are given in Table 6.9.

Table 6.9: Calibration values of LVDTs used

LVDT range (mm)	Calibration used mV per mm	Deflection per mV (mm)	Position measured
± 15	152.1	0.006574	Vertical
± 15	152.8	0.006545	Vertical
± 15	144.2	0.006937	Vertical
± 15	145.6	0.006866	Vertical
± 15	154.9	0.006455	Vertical
± 25	45.5	0.021970	Horizontal
± 15	142.6	0.007013	Vertical
± 15	310.1	0.003225	Vertical
± 15	308.8	0.003238	Vertical

6.5 Definition of comparative measures

In Chapter 1, it was stated that for all the tests carried out the main comparisons were made on the basis of:

- Permanent settlement (LVDTs)
- Sleeper deflection (range of movement during a cycle) (LVDTs)
- Spring stiffness (LVDTs)
- Ballast pressure (pressure plates)
- Lateral earth pressure ratios (pressure plates)
- Contacts pressure (pressure paper) and potential contact comparison
- Particle breakage/degradation (visual observation, PSD and measurement of random ballast particles)
- Lateral movement of ballast on shoulder slope (photos)

In this section, the methods used to analyse the experimental results to calculate the above quantities are presented.

6.5.1 Permanent settlement

Under cyclic loading, railway ballast undergoes permanent vertical settlement due mainly to densification, lateral spread and degradation of ballast particles beneath the sleeper (Raymond and Bathurst, 1987). However, of greater relevance to an operational railway is the development of differential settlement along the length of the track. Limiting the potential for individual sleepers to settle should also reduce the potential differential settlement along a length of track. It is therefore of interest to evaluate the potential for changes in the sleeper/ballast specification to reduce the settlement of individual sleepers. It is also known that settlement forms an approximately log/linear relationship with the number of loading cycles so that the initial cycles of loading (as the ballast beds in) have a much greater contribution per cycle to the total settlement. Due to the large contribution to permanent settlement of the first cycle, applying the load at 3Hz from the outset is potentially beyond the ability of the hydraulic controller to attain the target load. Therefore the initial cycle of load was applied as a gradual loading and unloading of static load (described in Section 6.2.3).

There are different methods for combining and presenting the data from the different measurement locations to characterise the sleeper settlement. In this research, an area weighted method is proposed as a means to provide a characteristic measure of settlement that takes into account the whole sleeper. In the area weighted method, each LVDT (Figure 6.45) is weighted in proportion to the area of sleeper soffit nearest to it. For mono-block sleeper the two middle LVDTs are given twice the weighting of the as LVDTs at sleeper ends. The two middle LVDTs are weighted for the middle area nearest to each of them ($2 \times (2 \times \frac{1}{8}) = \frac{1}{2}$) and the four corner LVDTs are weighted for the corner area nearest to each of them ($4 \times (\frac{1}{8}) = \frac{1}{2}$). For the twin-block sleeper each of the eight LVDTs placed on the corners of the two blocks is weighted equally.

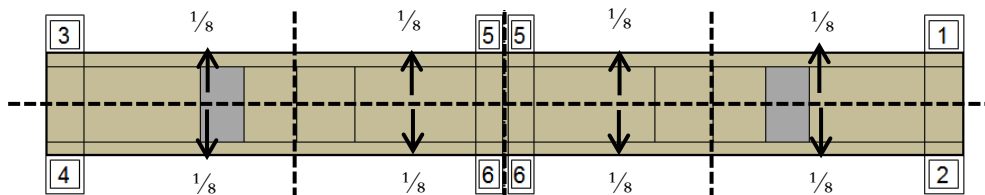


Figure 6.45: An illustration of the LVDT locations on the sleeper to analyse permanent settlement by area weighted method

6.5.2 Sleeper deflection

To investigate the deflection of each sleeper used in each test, the analysis is carried out by grouping of data. The range of LVDT movement, $(\delta_{iMax} - \delta_{iMin})$, δ_i at the four corners and the middle section of sleeper are averaged separately as follows:

$$\delta_{Sc} = \frac{\delta_1 + \delta_2 + \delta_3 + \delta_4}{4} \quad \text{Equation 6.1}$$

$$\delta_{Sm} = \frac{\delta_5 + \delta_6}{2} \quad \text{Equation 6.2}$$

where δ_1 , δ_2 , δ_3 , δ_4 , δ_5 and δ_6 , are range of movement (deflection) read by each corresponding numbered LVDT.

Equations 6.1 and 6.2 are used to compare the deflection behaviour of end and middle of sleeper with the application of cyclic loading.

6.5.3 Spring stiffness

There is no uniform consensus on the definition of sleeper support stiffness. However, the most general understanding seems to reflect the elastic rail deflection that takes place under a wheel load. In real track, several methods are required since the relationship between vertical load and vertical deflection is nonlinear and the variation of sleeper support stiffness may be more difficult to deal with. Therefore measurements at several load levels are generally required (Selig and Li, 1994). It is probably due to its relative simplicity, it is usual to represent sleeper support stiffness as a linear spring stiffness per sleeper end (i.e. per wheel load). In this research, two methods for analysing spring stiffness are used. These two methods are the average of the four corner and the area weighted method and are defined as follows:

In relation to a measured load and deflection, a spring stiffness can be defined as:

$$k = \frac{F}{2 \times \delta} \quad \text{Equation 6.3}$$

where: k = Spring stiffness (kN/mm)
 F = Applied load (kN)
 δ = Deflection read by the LVDT

Since the load for the tests on the modified SRTF apparatus is a cyclic loading which has a maximum and a minimum applied load, Equation 6.3 is modified for the cyclic range of applied load and range of vertical movement:

$$k = \frac{\text{Range of applied load}}{\text{Range of the LVDT's movement}} = \frac{F_{\text{Max}} - F_{\text{Min}}}{2 (\delta_{\text{Max}} - \delta_{\text{Min}})} \quad \text{Equation 6.4}$$

where: $F_{\text{Max}}, F_{\text{Min}}$ are maximum and minimum applied load in cyclic loading
 $\delta_{\text{Max}}, \delta_{\text{Min}}$ are maximum and minimum reading of LVDT appropriate to applied load

Calculating a spring stiffness requires only that the vertical deflection be defined. This is done either as:

1. The average of the LVDTs at the four corners
2. The area weighted average of all the LVDTs used

6.5.4 Ballast pressure

In each test, four pressure plates were placed along the inside wall of one side of the modified SRTF apparatus as described in Section 6.4.1. Each load cell in each pressure plate was connected to a data logger to provide a direct measurement of pressure in the longitudinal direction that develops under the simulated track loading condition. This data logger had the same specification and setting as the data logger used for recording the data of LVDTs and loading system used in the tests.

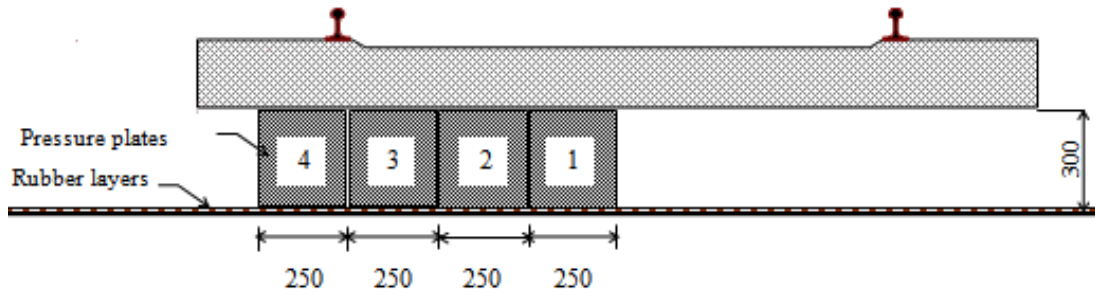


Figure 6.46: The arrangement of labelled pressure plates used in each test

In this research, two types of sleeper (mono-block and twin-block) were used and it is important to compare one test to others with the same boundary conditions. For analysis, each plate within the arrangement was labelled (Figure 6.46) and since there was an inherent variability between tests, a comparison was carried out using the plates which showed the clearest trends. For the tests using mono-block sleepers, the behaviour of ballast pressure recorded by pressure plates 1 and 4 in each test carried out was compared. This was chosen due to plates 1 and 4 have being in different locations so that they and hence boundary conditions may behave differently. Plate 1 was located in the middle section of the sleeper (centre of the track) and confined not only by the ballast in all directions but also by the sleeper on the top. The ballast at plate 4, being closer to the shoulder, would be expected to have a lesser degree of lateral confinement.

The twin-block sleeper has a symmetric shape without any portion in the middle section. Pressure plates 2 and 4 are thus arguably symmetrical and it was decided to use data recorded by pressure plate 3 for comparison.

6.5.5 Mobilised earth pressure ratio

The mobilised earth pressure ratio is analysed using the data of horizontal pressure from pressure plates which are then compared with the vertical pressure, which was simplified to be the same as the pressure applied to the ballast surface at the sleeper soffit. The maximum and minimum pressures recorded by the pressure plates correspond to the maximum and minimum vertical pressures applied on the test. As the ballast was clean dry and free-draining, there was no effect of pore water pressure. The ratio of earth pressure, K_i is defined as:

$$K_i = \frac{\sigma'_h}{\sigma'_v} \quad \text{Equation 6.5}$$

where σ'_h and σ'_v are horizontal and vertical effective pressures respectively.

Vertical load was assumed to be distributed uniformly to the ballast bed surface; the maximum and minimum vertical pressures in each test therefore depend on the sleeper soffit area in use. In each test, only the vertical pressure applied by sleeper soffit was increased or reduced due to cyclic loading procedure. If the vertical effective pressure is increased while the horizontal effective pressure remains approximately constant or increases less quickly; or where the horizontal pressure is reduced while the vertical pressure remains constant, K_i becomes the minimum mobilised earth pressure ratio, K_{min} . On the other hand, if the horizontal effective pressure is increased while the vertical effective pressure remains constant or is reduced or where the vertical pressure is reduced while the horizontal stress remains approximately constant, K_i becomes the maximum mobilised earth pressure ratio,

K_{max} . To analyse the mobilised earth pressure ratio, Equation 6.5 is used for both the maximum and the minimum.

The data used for analysing the mobilised earth pressure ratios can also be used to estimate the mobilised angle of effective shearing resistance (ϕ'_{mob}) for the maximum vertical pressure:

$$\sin \phi'_{mob \max} = \frac{[(\sigma'_V - \sigma'_h)]}{[(\sigma'_V + \sigma'_h)]} \quad \text{Equation 6.6}$$

and for the minimum vertical pressure

$$\sin \phi'_{mob \min} = \frac{[(\sigma'_h - \sigma'_V)]}{[(\sigma'_V + \sigma'_h)]} \quad \text{Equation 6.7}$$

If the friction angle (ϕ) of ballast is known, the limiting active (K_a) and passive (K_p) earth pressure ratios and the normal consolidation value (K_o) (Jaky, 1948) can also be determined using:

$$K_a = \frac{[(1 - \sin \phi)]}{[(1 + \sin \phi)]} \quad \text{Equation 6.8}$$

$$K_p = \frac{[(1 + \sin \phi)]}{[(1 - \sin \phi)]} \quad \text{Equation 6.9}$$

$$K_o = 1 - \sin \phi \quad \text{Equation 6.10}$$

6.5.6 Pressure paper

The pressure paper was recovered at the end of each test and the contact regions analysed in terms of number, area and where possible level of pressure present. The pressure paper was left in place for the entire test. It therefore provided a cumulative record of the contact positions and the maximum local pressures over the whole of the loading history, and this must be borne in mind when interpreting the results. To analyse the data recorded on pressure paper, the number of contact points was counted manually, by the same person in each case, while the total contact area was determined by thresholding and segmenting the images at the same cut-off values using bespoke Adobe Photoshop CS2 software. It is also worth noting that:

- The paper stated by the manufacturer to be sensitive between 10 to 50MPa can provide data to as low as 2.5MPa.
- The paper with a stated sensitivity range of 2.5 to 10MPa provides data to as low as 0.5MPa.
- Where pressures exceed the maximum sensitivity of the paper, the paper remained red to its maximum RI and still provides a record of contact at the location.

In relation to one of the results provided by pressure paper (number of contacts), a further intention in designing the variant ballast gradings was to maintain as closely as possible a linear particle size distribution on the log scale while fixing the maximum size of D_{90} close to the existing value for the current standard NR ballast grading of about 49 mm. By making some simplifying assumptions, it is possible to gain some insights into how having a distribution that is linear on a log PSD plot influences the density of the packing achievable and to estimate the number of potential contacts available at a bounding surface. To estimate the number of contacts potentially available, a method was developed as follows:

Assume that the PSD distribution is linear on a log scale between D_{10} and D_{90} e.g.as shown in Figure 6.47 (a).

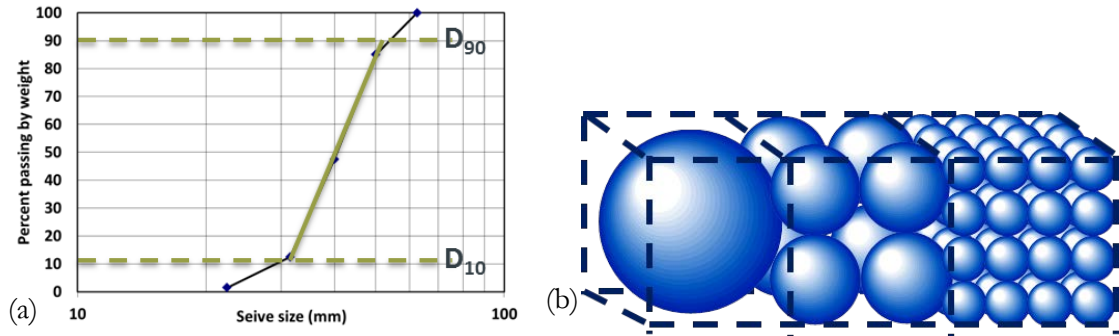


Figure 6.47: (a) Idealised PSD, (b) visualisation of sleeper/particle contact with discrete sizes in log distribution for two particle sizes

Therefore:

$$\% \text{ passing} = m \cdot \ln (D_n) + C \quad \text{Equation 6.11}$$

It can then be shown that the ratio of particles of size D_A to D_B (where there are equivalent mass fractions of each particle size) potentially in contact with a flat surface assuming square packing is found from:

$$\sqrt[2]{\frac{1}{D_A^3}} : \sqrt[2]{\frac{1}{D_B^3}} \quad \text{Equation 6.12}$$

This is shown visually in Figure 6.47 (b) for three particle sizes and can be described thus; one large particle providing one contact is equivalent in mass to 8 particles of half the diameter size (though these only provide 4 contacts) and 64 particles of one quarter of the size (though these only provide 16 contacts). Hence each side of Equation 6.12 is built up from the need to:

1. invert the cube of the particle size to obtain the number of particles per unit volume [the 1, 8 or 64 in Figure 6.47 (b)],
2. take the cube root of the resulting value to obtain the number of particles per unit length [1, 2 or 4 in Figure 6.47 (b)]
3. square this result to obtain the number of particles per unit area (the 1, 4 or 16 in Figure 6.47 (b))

The ratio expressed in Equation 6.12 can be used to develop an equation to estimate the number of contacts against a flat surface provided the overall PSD is linear on a log scale and can be characterized by a *discrete* number of particle sizes. If these criteria are met then the “potential” number in contact with a flat bounding surface can be determined using the formula:

$$\text{Number of contacts} = \left(\frac{A_{\text{sleeper}}}{N \times D_A^2} \right) \times \left(\frac{\sqrt[2]{\frac{1}{D_A^3}} + \sqrt[2]{\frac{1}{D_B^3}} + \dots + \sqrt[2]{\frac{1}{D_N^3}}}{\sqrt[2]{\frac{1}{D_A^3}}} \right) \quad \text{Equation (6.13)}$$

Where N is the number of discrete particle sizes evaluated (where the mass of particles in each size fraction is equivalent), D_A to D_N are the particle diameters for each size fraction and A_{sleeper} is the contact area of the sleeper soffit. The first bracketed term on the right hand side of Equation 6.13 determines the number of the largest size fraction particles (D_A) in contact with the $1/N$ proportion of the sleeper soffit area, the second bracketed term sums the ratio of D_A sized particles to the remaining size fractions D_B to D_N , by multiplying these two terms together the total number of contacts is obtained. Equation 6.13 can be applied to any log linear PSD distribution where m and C

are known and D_A to D_N can be determined by manipulation of Equation 6.11. However, it is perhaps simpler to read the particle sizes from a PSD graph such as Figure 6.47 (a). This simplified method to estimate the potentially available ballast to sleeper contacts will be used later as a control for those measured using the pressure paper.

6.5.7 Particle breakage/degradation

Ballast particles experience very little contact with adjacent particles resulting in high stress concentrations. This high stress causes the sharp edges and corners of ballast particle break, which reduces angularity and decreases the angle of internal friction and contributes to increase settlement allegedly. The increase in particle breakage causes the strength of material to decrease (Marsal, 1967). After completion of the cyclic loading stage, the degree of ballast particle breakage was investigated by visual observation, PSD test and weighing of selected ballast particles.

Visual observation

After each test was completed, the crib and shoulder ballast were manually removed to the depth of the sleeper soffit. This was undertaken to ensure the ballast particles beneath the sleeper were undisturbed and kept separated from the crib ballast. When this process was completed, the sleeper was lifted and removed from the ballast bed surface, leaving an even surface to make visual observation easier. The visual observation involved counting the number of particle breakages after the test was completed. This investigation compares the initial condition of the particle at the ballast bed surface after compaction and prior to placing the sleeper. Visual observation only detects obvious breakages of the ballast that can clearly be seen by eye. Therefore, any breakages on a very small scale that might occur at the ballast corners and edges and cannot be visualised by eye were not taken into account.

PSD test

Particle breakage can be investigated by PSD tests comparing the PSD of the ballast before and after testing. Ballast samples for measurement after testing were taken from beneath the railseats and the middle section of sleeper. The railseat areas were assumed to be the most critical for ballast breakage owing to the position of the applied loading. Each PSD test was carried out on a ballast sample of approximately 120 kg. This is more than suggested by BS 812-102: 1989 (British Standards Institution, 1989), which indicates a minimum mass of sample required for PSD tests to BS 1377-2: 1990 (British Standards Institution, 1990) as about 60 kg.

PSD tests were carried out to broadly in accordance with BS 1377-2: 1990 (British Standards Institution, 1990). Sieve analysis was carried out by dry sieving method in accordance with BS 812: Part 103.1: 1985, using a mechanical sieve shaker machine (Figure 6.48) run at a frequency of 50Hz and an amplitude of 3.4 mm for ten minutes duration.



Figure 6.48: Sieves and shaker for PSD test

Twelve sieve sizes were used, 63 mm, 50 mm, 40 mm, 37.5 mm, 31.5 mm, 25 mm, 22.4 mm, 16 mm, 13.2 mm, 11.2 mm, 9.5 mm and 4.75 mm, which consistent with the recommendations of BS 1377-2: 1990 (British Standards Institution, 1990).

Measurement of selected ballast particles

Fifty numbered, randomly selected ballast particles retained on a 31.5 mm sieve were spread directly underneath of sleeper soffit during preparation for each test. The decision to use a larger size than 31.5 mm of ballast particle were to avoid the possibility of losing particles when emptying the ballast from the modified SRTF apparatus and the bigger particles are more likely to break. The analyses carried out into these fifty ballast particle were PSD test and total loss of mass (by weighing each ballast particle used on this method before and after loading applied to investigate any changing of weight occurs).

6.5.8 Lateral movement of ballast on shoulder slope

Lateral movement of the ballast on shoulder slope was also investigated. The intention was to look at the lateral movement of the ballast shoulder, which was monitored by means of a camera fixed to a tripod taking sequential pictures at intervals from the beginning of the test throughout the entire sequence loading cycles, to investigate lateral spread as a potential cause of ballast settlement. The analysis was carried out by comparing the initial picture prior to testing with pictures taken during the loading cycles and at the end of the tests. Any planned change in camera position was accounted for in the image analysis; otherwise subsequent pictures were discarded. Visually comparing the sequence of pictures to show the ballast movements is difficult to present in this thesis, as moving media are required to show this effectively. Therefore, the pictures were analysed using embedded MATLAB (MathWorks, 2014) code. The difference between sequential grayscale images has been assessed to highlight movements of ballast particles on the shoulder slope; in the figures these are shown in white. The results of this analysis indicate where the greatest differences between pictures were detected, and hence the locations of the greatest movement of ballast particles.

6.6 Testing variables evaluated

The tests carried out in this research were planned to explore permanent settlement, sleeper deflection, spring stiffness, ballast pressure and the number and area of ballast particle contacts while the following were varied:

- sleeper and/or ballast type
- the sleeper/ballast interface
- the profile of the ballast bed

The main variables investigated are described in the following sections;

6.6.1 Sleepers

There are a variety of materials available to construct sleepers in the form of a mono-block, or in the case of concrete sleepers in the form of a mono or twin-block. However despite this potential variety of materials available, in the field, sleepers are most commonly made of concrete, although some historical stock of wooden sleepers remains, generally in slower speed categories of track. Plastic and steel sleepers are novel alternatives that are currently only deployed in rare circumstances. Wooden sleepers are also specified for new track in some niche applications. Changing material costs may also be expected to influence the choice for future sleeper deployment, particularly if legislation is used to favour more sustainable options.

Combining the cost and the performance on the track, there is uncertainty over which material is optimal. In France, pre-stressed twin-block concrete sleeper is preferred however these are not used on the UK classic network. While accepted practice is to specify concrete sleepers, the possibility of these two forms which are widely used implies that there is some doubt as to which is the optimal shape. In France, twin-block concrete sleepers have been widely used for both high speed and slower branch lines. In the UK, mono-block concrete sleepers are used although twin-block sleepers have also been used on HS1 to follow French high speed practice.

To investigate the influence of sleeper material and geometry on track performance, several types of sleeper were tested. The types of sleeper used in the tests were in the form of mono-block and twin-block sleepers. Mono-block sleepers were represented by reinforced concrete (British Standards Institution, 2009a), steel (British Standards Institution, 2000), plastic, and timber while twin-block sleepers (British Standards Institution, 2009b) were represented by reinforced concrete. Two different types of mono-block concrete sleeper were used for different test purposes. The mono-block concrete sleepers were produced by Tarmac (G44) and PCM Strescon Overseas Ventures Ltd (PCM). The G44 sleeper was used in the tests to investigate the influence of sleeper and ballast interventions while the PCM sleeper was used to investigate the presence of a fouling material. Therefore, there was no intention to compare these types of mono-block concrete sleeper. Table 6.10 presents the measured dimensions of the sleepers used in the tests.

Table 6.10: Dimension of the sleepers used in the tests

Type of sleeper		Dimension of sleeper (mm)			Soffit area (cm ²)
		Width	Height	Length	
Mono-block:					
Concrete:	Tarmac G44	285	200	2500	7,125
	PCM	295	171	2600	7,670
Steel		265	100	2160	5,724
Plastic		250	150	2600	6,500
Timber		250	130	2600	6,500
Twin-block:					
Concrete B450		295	245	2415	4,956

6.6.2 Ballast gradings

In preparation for the main testing phase of this research, the granite ballast aggregate was sourced from Cliffe Hill quarry, Leicestershire, LE67 1FA, U.K. Prior to use in the test, railway ballast properties provided by the quarry were compared with the current standard NR ballast specification. Table 6.11 shows that the properties of the ballast used for the tests complied with the current standard NR ballast specification and so the ballast is suitable for use in the UK. In addition to these, tests carried out to determine the specific gravity (Gs) indicate of 2.78.

Table 6.11: Comparison of ballast properties from Cliffe Hill quarry to the current standard NR ballast product specification (after Network Rail, 2000)

Type of test	Aggregate maximum test value	
	NR's specification	Cliffe Hill
Sieve size 0.5 mm	0.6% (percentage passing by mass)	0.19% (sieve test)
Flakiness index	35%	15%
Los Angeles abrasion	20	16
Micro deval abrasion	7%	6.5%
Gs	-	2.78 (laboratory test)

Specifically for ballast grading tests, other gradings (Table 6.12) were also sourced from the same quarry. Cliffe Hill quarry also provides aggregates that meet not only NR ballast requirements (Network Rail, 2000) but also industry standard aggregate grading specifications (British Standards Institution, 2009c).

Table 6.12: UK aggregate size designations (after British Standards Institution, 2009c)

Aggregate size d/D (mm)	Aggregate grading category
20/40	G _c 85/20
20/31.5	G _c 85/35
10/20	G _c 85/20
6.3/14	G _c 85/20
4/10	G _c 85/20

All gradings obtained comply with the relevant aggregate grading category (Table 6.12), which is described in BS EN13403 in millimetres with the designation of d/D, where d and D are the lower and upper limiting sieve sizes respectively. The majority of particles in the aggregate should lie between these two values. For example, aggregate grading category G_c85/20 describes as an aggregate grading with a minimum of 85% passing the upper sieve size D and a maximum of 20% passing the lower sieve size d. PSD tests on the ballast sourced were carried out on three different samples and consistently provided the same results. The average of the three PSD test results for railway ballast is

presented in Table 6.13. PSD tests were also carried out on the other gradings sourced and the results are presented in Figure 6.49.

Table 6.13: The average of PSD test results of Cliffe Hill quarry ballast

Sieve size (mm)	Weight retained (kg)	Percentage of retained (%)	Total percentage retained (%)	Total percentage passing (%)
63	0.0	0.0	0.0	100
50	6.22	5.19	5.19	94.81
40	42.77	35.69	40.88	59.12
31.5	50.67	42.28	83.17	16.83
22.4	18.82	15.71	98.87	1.13
0	1.35	1.13	100.00	0.00
Total	132.0			

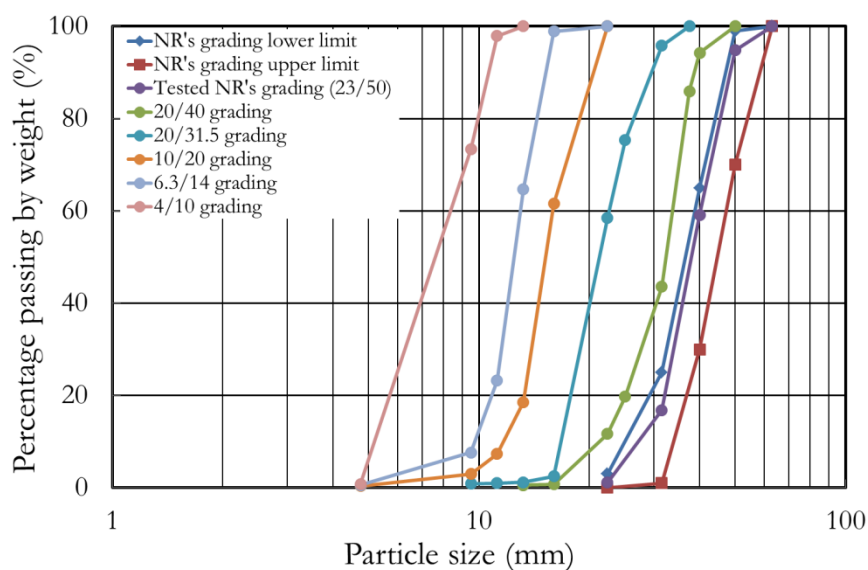


Figure 6.49: PSD graphs of Cliffe Hill quarry ballast and other gradings used for the tests

Figure 6.49 confirms that ballast from Cliffe Hill quarry is within the current standard for NR ballast grading.

The current standard NR ballast grading was tested and used as a baseline test (not only for ballast intervention tests but also for sleeper intervention tests). To investigate ballast interventions, some variant ballast gradings were tested using the same G44 sleeper. To design the variant ballast gradings for testing, the current standard NR ballast grading was modified by adding intermediate and/or smaller particles (aggregate size in Table 6.12) to obtain more broadly graded ballast. It is hypothesized that more broadly graded ballast exhibits a potentially denser packing with greater coordination number, increases the capability to transfer stresses through from the sleeper to the subgrade, and gives a larger and more stable interface number of contacts that cover a larger area of the sleeper. It is thus expected to develop less settlement and a higher peak shear strength, potentially extending the life of ballast and sleeper.

The design of variant gradings was controlled to maintain an acceptable minimum hydraulic conductivity to fulfil drainage requirements. There are several methods to create a densely packing grading including Fuller and Thompson's method (Fuller and Thompson, 1907) and the Haystack method (Richardson, 2005). However, those methods only work to create dense grading for highway

mixture asphalt and concrete while railway ballast has a limit on the proportion of small particles to fulfil drainage requirements and limit the possibility of ballast flight at higher train speeds.

Since there are some practical restrictions on the type of grading that can be employed in the track, the variant gradings were designed to be able to provide a minimum hydraulic conductivity in the presence of fouling material (Ionescu, 2004, Selig et al., 1993). The recommendation made by Indraratna and Salim, (2005), who suggested that ballast grading needs to have a C_u exceeding 2.2, but not more than 2.6 was also considered. The small particles employed in new variants were restricted to have a size limitation (i.e. grading 10/20) to avoid ballast flight caused by high speed train (Quinn et al., 2010). In addition to those criteria, visual observation was always conducted to avoid creating a grading which has the potential for segregation.

In creating variant gradings, the percentage portion of intermediate and small particle added to NR grading was quantified by total weight. Table 6.14 shows the percentage of each constituent material in each variant grading. To investigate the influence of varying the grading, four variant ballast gradings were prepared.

Table 6.14: The percentage of proportion each grading in each variant grading

Grading	The percentage portion of			
	NR (23/50)	20/40	20/31.5	10/20
NR	100%			
Variant 1	70%		30%	
Variant 2	75%			25%
Variant 3	25%	25%	25%	25%

Figures 6.50 and 6.51 compare the PSD of variant gradings with the tested NR's grading and the recommended grading applied by RailCorp in Australia respectively.

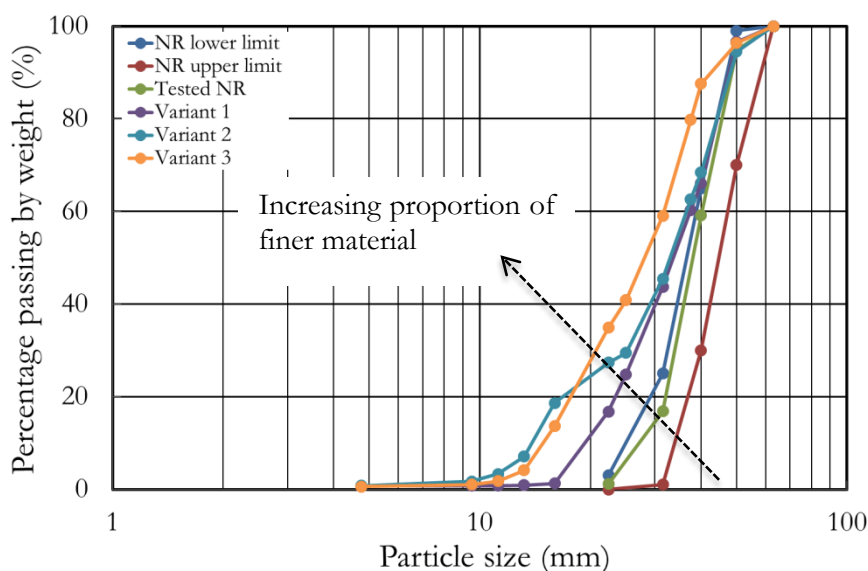


Figure 6.50: PSD of variant gradings compared to NR grading

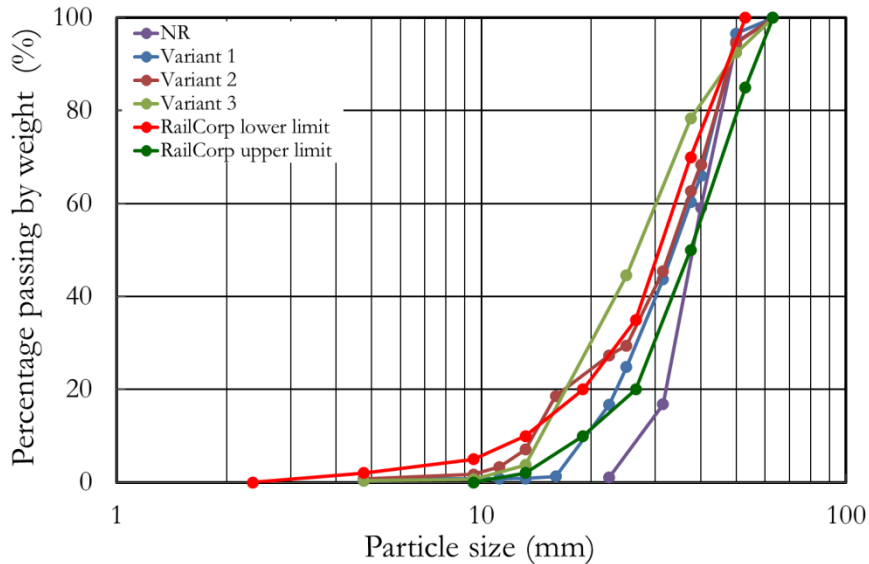


Figure 6.51: PSD of variant gradings compared to the RailCorp grading

These variant gradings were chosen from several design gradings based on simplicity having increased density and still being categorised as clean or moderate clean ballast according to Table 2.2. The following preliminary checks were carried out on the variant gradings:

Checking the increased density

The density of each variant ballast grading was measured using a box test method. The measurement was carried out by filling up a box of dimensions of 300 mm wide × 300 mm length × 300 mm deep using methods designed to create (1) a loose and (2) a dense sample. The volume and weight were used to determine the dry bulk densities. The loose sample was obtained by shovelling ballast into the box but not letting the ballast fall through any height. To obtain the dense condition vibration/shaking was used and the box was filled in layers. Vibration/shaking was applied to each layer by the sieve shaker which was set uniformly for all the tests to achieve the maximum density possible. At the end of the vibration process, ballast was manually added to obtain a level surface at the box top. However with this testing method it was difficult to create an even surface at the ballast top. Therefore, the dense condition achieved in this test on the variant gradings might not be the densest possible one. The uniformity coefficient, selected D values and the maximum and minimum densities of each variant and the current standard NR ballast gradings are presented in Table 6.15.

Table 6.15: Key detail of variant ballast gradings

Grading	The value of (mm)									Density value of condition (kg/m ³)	
	D ₀	D ₁₀	D ₃₀	D ₅₀	D ₆₀	D ₇₀	D ₉₀	D ₁₀₀	C _u	Loose	Dense
NR	0	27.56	34.33	38.00	40.00	43.18	49.09	63.0	1.45	1,418	1,625
Variant 1	0	19.52	26.94	33.85	37.69	41.50	47.50	63.0	1.93	1,453	1,672
Variant 2	0	14.67	28.08	33.08	36.92	41.00	48.50	63.0	2.52	1,517	1,681
Variant 3	0	15.48	20.00	27.22	30.00	34.23	47.50	63.0	1.94	1,512	1,744
10/20	0	12.14	14.71	16.00	16.71	17.86	20.71	22.86	1.38	1,432	1,608

Checking hydraulic conductivity

Hydraulic conductivity is an important parameter for predicting water flow through the soil. Generally, hydraulic conductivity is measured on soil samples in the laboratory or carrying out field tests. An approximate estimate of permeability of a granular aggregate can also be obtained from the PSD graph and this method has long been used. The most commonly used and straight forward of all available formulas are those of Hazen and Kozeny-Carman.

Hazen's formula

$$k_p = C_p(D_{10})^2 \quad \text{Equation 6.14}$$

where k_p is permeability coefficient (m/sec), D_{10} is particle size (mm) for which 10% of the sample will be finer and C_p is a factor that usually taken as 0.01-0.015.

Kozeny-Carman's formula

$$k_p = \frac{2}{f S_s^2} \left(\frac{e^3}{1+e} \right) \quad \text{Equation 6.15}$$

where k_p is permeability coefficient (m/sec) and S_s is specific surface defined as

$$S_s = \frac{6}{\sqrt{\frac{d_{\max}}{d_{\min}}}} \quad \text{Equation 6.16}$$

d_{\max} and d_{\min} are maximum (50 mm) and minimum (4.75 mm) particle sizes respectively, e is the void ratio and f is an angularity factor (1.25 for sub rounded grains and 1.4 for angular grains).

The formulae described in this section were used to analyse the value of permeability coefficient of tested ballast gradings. Values of 0.01, 1.4, and 1.85 were used for C_p , f and S respectively. The values of void ratio, D_{10} of each tested gradings and the calculated permeabilities are presented in Table 6.16.

Table 6.16: Permeability coefficients (k_p) of tested ballast gradings

Grading	Grading properties		k_p value (m/sec)	
	D_{10} (mm)	e	Hazen's formula	Kozeny-Carman's formula
NR	27.56	0.711	7.5955	0.08768
Variant 1	19.52	0.636	3.8103	0.06564
Variant 2	14.67	0.634	2.1521	0.06510
Variant 3	15.48	0.578	2.3963	0.05108

Table 6.16 shows that Kozeny-Carman's formula provides the smallest value of k_p . These k_p values represent a more critical (conservative) condition than the k_p values obtained by Hazen's formula. Based on the criteria listed in Table 2.2, the k_p values of the current standard NR ballast and all variant gradings analysed by Kozeny-Carman's formula are still in the region of those for clean ballast.

6.6.3 Sleeper/ballast interface modifications

Railway ballast typically consists of 25 to 50 mm diameter particles and this mass of ballast which may be 300 mm deep supports the sleeper which is only 285 mm wide. Therefore, the load transfer

behaviour of ballast is highly dependent on its structure owing to the large particle size in relation to typical sleeper footprint and ballast depth (Aingaran, 2014), so that in many cases the behaviour of the ballast is more that of a structure rather than a continuum.

To explore the potential solutions which can be applied to increase the life-cycle of ballast and lead to longer intervals between maintenance, modification of the sleeper/ballast interface by the introduction of USPs and two layered ballast (TLB) system was investigated. These modifications have the same intention, which is to increase the load distributing area by increasing either the contact area or the number of contacts.

USPs

To explore how a “performance” USP alters the sleeper/ballast interface, two types of USP provided by Tiflex Ltd. were tested. These types of USP are representative of a number of products currently available, supplied by a variety of companies. The two types tested were FC500 and FC208GF (Tiflex, 2013) with the mechanical properties shown in Table 6.17. Henceforth these USPs will be described as either USP 1 or 2.

Table 6.17: Properties of USPs used in the tests (after Tiflex, 2013)

Identifications	Type of USPs in the tests	
	1	2
Technical ID	FC500	FC208GF
Thickness	4 mm	9 mm
Weight	6 kg/m ²	5.6 kg/m ²
Bending modulus	0.352 N/mm ³	0.126-0.207 N/mm ³
Stiffness (C _{Stat})	0.228-0.311 N/mm ³	0.079-0.105 N/mm ³
Core material	Trackelast FC500	Bonded cork

Auer et al.(2013) conducted tests on different USP materials and proposed a classification (Table 6.18) based on stiffness.

Table 6.18: Stiffness categorisation of USPs (after Auer et al., 2013)

Categorised USPs	C _{Stat} (N/mm ³)
Stiff	$0.25 \leq C_{Stat} \leq 0.35$
Medium	$0.15 \leq C_{Stat} < 0.25$
Soft	$0.10 \leq C_{Stat} < 0.15$
Very soft	$C_{Stat} < 0.10$

USP 1 was made of a blend of thermoplastic materials and elastomeric inclusions as the core, while USP 2 was made of a high quality cellular rubber bonded cork. According to the stiffness values, USP 1 and USP 2 are categorised as stiff and soft USP respectively. These USPs were tested attached to both G44 (British Standards Institution, 2009a) and twin-block concrete (B450) type sleepers (British Standards Institution, 2009b). It is possible to cast these USPs onto to the sleepers at manufacture; however for these tests the USPs were fixed to sleeper soffits using epoxy glue.

Two layered ballast (TLB) system

Another possible modification to the ballast could be to provide graded layers of ballast. Anderson and Key (2000) carried out model tests on a TLB system to explore its performance when smaller

aggregates were placed as a layer immediately beneath the sleeper. This was intended to investigate the behaviour after a stone blowing maintenance process (Fair, 2003, Fair and Anderson, 2003) in which smaller sized particle (10 to 20 mm) are “blown” beneath the railseats to restore track level and smooth out short wavelength faults.

Anderson and Key's (2000) test was conducted in an apparatus that consisted of a plate steel box, approximately 1,000 mm long \times 800 mm wide \times 600 mm deep. A rubber mat 10 mm thick was glued into the bottom of this box to simulate the action of subgrade. Field-size materials were used for the main ballast bed and the test bed was loaded by means of a model reinforced concrete sleeper of dimensions 600 mm long \times 100 mm wide \times 100 mm deep. After each test, it was assumed that the majority of the bed remained undisturbed, therefore only the top 100 mm was rearranged and the broken particles were removed and replaced by new material. The load applied on most of the tests was cycled from 2.1 to 18.2kN to model sleeper stresses on the ballast of 35 to 303kPa. However, it is stated in the conclusion that the tests do not replicate exactly the situation in real track which in the model sleeper was much smaller than the real sleeper. Therefore there were loading effects on the ballast beds from neighbouring sleepers and the materials as well as the stress levels needed to be scaled down.

Tests on a TLB system were also conducted by Claisse et al (2003) and Claisse and Calla (2006) to investigate whether placing smaller sized aggregate in the crib could provide a reservoir of material that would fill any ballast voids under sleepers that may occur due to cyclic loading and prevent any voiding (hanging sleeper). Tests were conducted using a tenth of scale model of ten-sleeper assembly of sleepers made of wood. The ballast particles were also reduced by a factor of 10 in their linear dimension. In these tests, the base was constructed of steel plate with sandpaper attached to model subgrade roughness. Two sleeper sizes were used 28 mm to model a standard British railway sleeper at 280 mm and 15 mm as an alternative size to the standard British railway sleeper. Sleeper spacings of 55 mm and 70 mm were used and the standard railway ballast was modelled as 5 mm stone and stone blowing particle size was model by 2 mm sand. Both 5 mm and 2 mm particle sizes were used for crib ballast in the tests. Cyclic loading for these tests was from 1 to 8kN. The results of these tests were validated by box tests and a full scale single sleeper test.

However, the idea of replacing crib ballast with smaller size aggregate is not suitable for the current need for high speed trains since the presence of smaller aggregate near the surface can cause the phenomenon of ballast flight (Quinn et al., 2010) due to train induced air turbulence (Jing et al., 2012, Kwon and Park, 2006, Lazaro et al., 2011, Quinn et al., 2010, Saussine, 2013).

In this research a type of two layered ballast system was simulated with finer particles beneath the sleeper but protected from ballast flight by a covering of regular ballast within the crib and shoulder. This system has the same overall geometry as other tests and was constructed of a 250 mm depth of NR ballast grading and 50 mm of 10/20 aggregate (i.e. particles used for stone blowing) to create a 300 mm two layered ballast/aggregate depth below the sleeper soffit. Positioning the smaller aggregate on top was expected to increase the number and overall area of contact points with the sleeper.

Figures 6.52, 6.53 and 6.54 show the PSDs of the current standard NR ballast and 10/20 gradings used, views of the TLB system at different stages of construction and the cross section profile details.

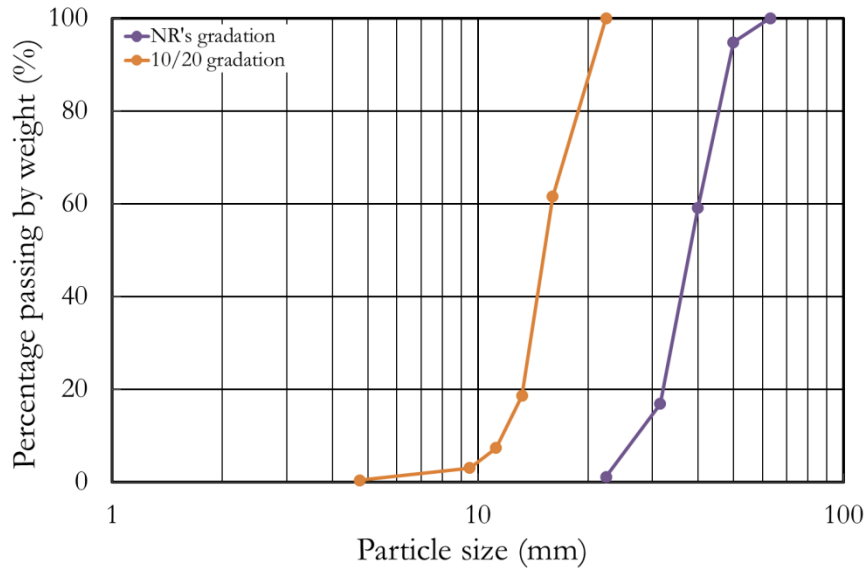


Figure 6.52: PSD graphs for NR and 10/20 gradings used for TLB system

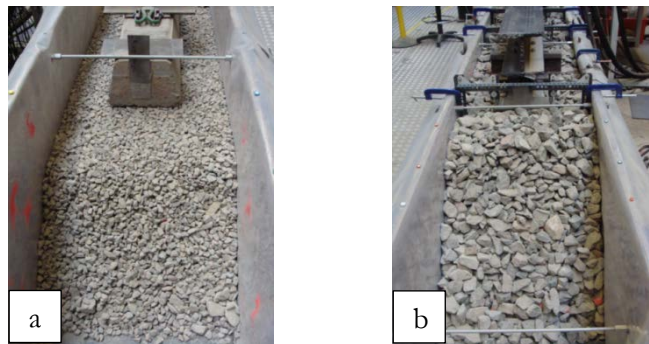


Figure 6.53: The TLB system under construction: (a) the upper surface of the 10/20 mm material, level with the sleeper soffit, and (b) following placement of the final covering of standard ballast

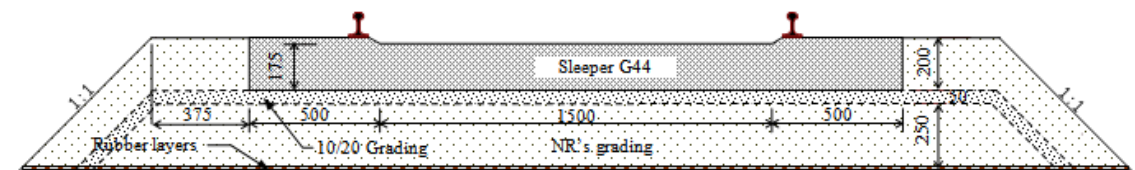


Figure 6.54: Cross section profile of TLB system test

6.6.4 Other investigations

In addition to the main tests of sleeper/ballast interventions, the effect of re-profiling the shoulder slope, introducing a fouling material (sand) and introducing random fibre reinforcements were also investigated.

Re-profiled shoulder (RPS) slope

There is limited research to investigate the influence of ballast profile, thus a lack of published and freely available data. The influence of ballast shoulder profile was initially investigated by Selig (1980). Further observations were conducted by Le Pen (2008) using the SRTF in the laboratory and Kabo

(2006) using a numerical method looking at lateral resistance offered by the ballast shoulder. The results were in agreement that an increased width of the ballast shoulder increases the lateral resistance. However, the data on the influence of the ballast shoulder slope on ballast settlement due to lateral spread are unavailable.

The ballast adjacent to the track plays an important role in preventing lateral strain of ballast (Le Pen and Powrie, 2011) and hence track settlement. It appears that there is no international consensus regarding the shoulder slope. In Germany a 1V:1.25H slope of shoulder has been recommended ((Marx and Mobmann, 2012)). In Australia, a shallower slope of 1V:1.5H has been applied by most railway authorities (e.g. (Country Regional Network, 2013)). In the U.S, a slope of 1V:2H has become a recommendation (AREMA, 2012, Raymond, 1987). Lastly the UIC standards (UIC, 2008a) also recommend a 1V:2H slope. In the UK however, there is no standard to be followed in profiling the shoulder slope and it is believed that the ballast often stands at its natural angle of repose with a slope of approximately 1V:1H, making it potentially susceptible to lateral strain and leaving the track poorly supported at the sleeper ends. This can be seen in Figure 6.55 showing pictures taken by Prof. William Powrie of a high ballast shoulder (deep slope) at Haltwhistle on the railway line between Carlisle and Newcastle upon Tyne.



Figure 6.55: High ballast shoulders at Haltwhistle on the railway line between Carlisle and Newcastle upon Tyne (courtesy of Prof. William Powrie)

To investigate the influence of shoulder slope on the ballast settlement behaviour, a test with re-profiled shoulders, set to a slope of 1:2 instead of 1:1, was carried out. The test used G44 sleeper and the current standard NR ballast grading. Figures 6.56 and 6.57 compare the standard and modified shoulder slope's profiles.

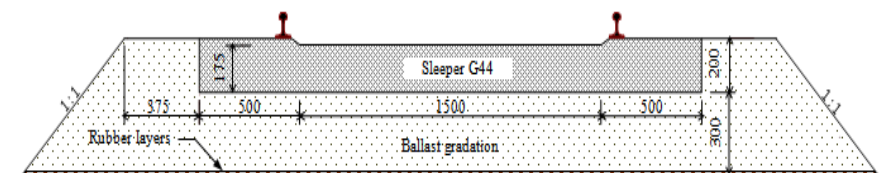


Figure 6.56: Cross section profile of standard tests

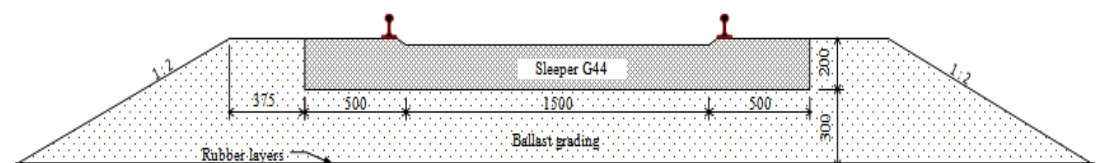


Figure 6.57: Cross section profile of RPS slope test

The presence of fouling material (sand ingress)

Fouling materials in ballast have been traditionally an enemy of the performance of railway tracks. Railway tracks in desert areas are the most exposed to sand problems. Driven by wind, sand enters, contaminates and fills the voids between ballast particles. The end product is that the ballast voids become completely filled by sand.

To model railway tracks in desert area, the effect of the presence of dry sand as a fouling material in the ballast on the track performance was investigated. Two tests were carried out using the modified SRTF apparatus to represent field conditions. These two tests are denoted as a baseline test (without sand) and a sand ingress test (gradual sand ingress into the ballast). The sand used in sand ingress test had particle size range of 0-5 mm with the percentage of fines (0-0.075 mm) less than 3%. The PSD and material properties of the sand used in the test are presented in Figure 6.58 and Table 6.19.

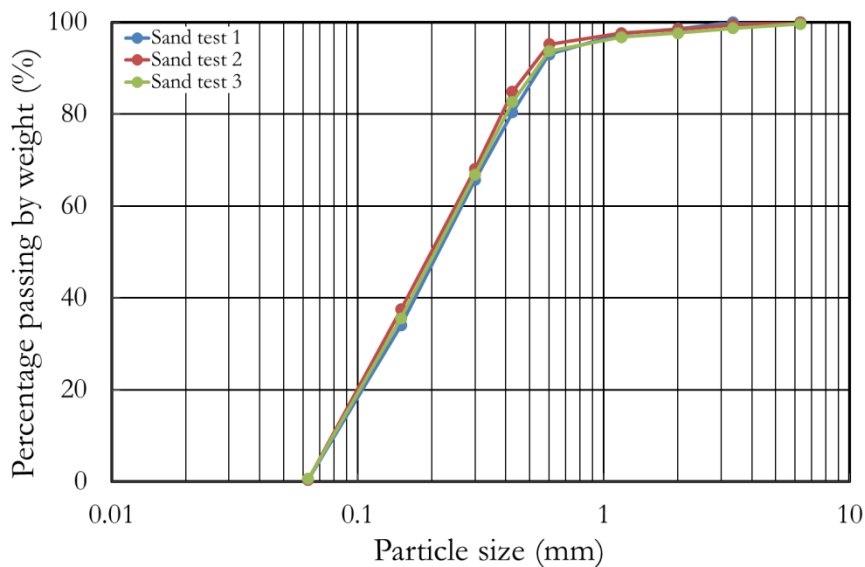


Figure 6.58: PSD graphs of sand used as a fouling material

Table 6.19: The material properties of sand used as a fouling material

Type of test	Maximum test value
Specific gravity	2.74
Loose density (kg/m ³)	1472.35
Dense density (kg/m ³)	1788.10

In these tests, the ballast type used was gabbro rather than granite. Gabbro is a type of intrusive igneous rock similar to granite. However gabbro is a mafic rock (high in magnesium and iron mineral) while granite is felsic rock (high in silica); therefore gabbro is denser and darker in colour than granite. The material properties and PSD graphs of the gabbro ballast used in these tests are presented in Figures 6.59 to 6.60 and Table 6.20.

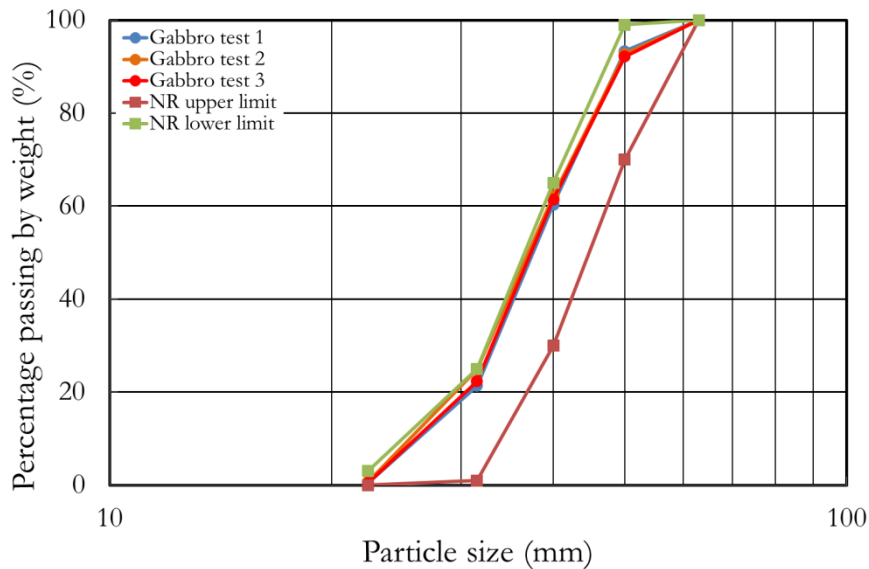


Figure 6.59: PSD graphs of gabbro ballast compared to the current standard NR ballast grading

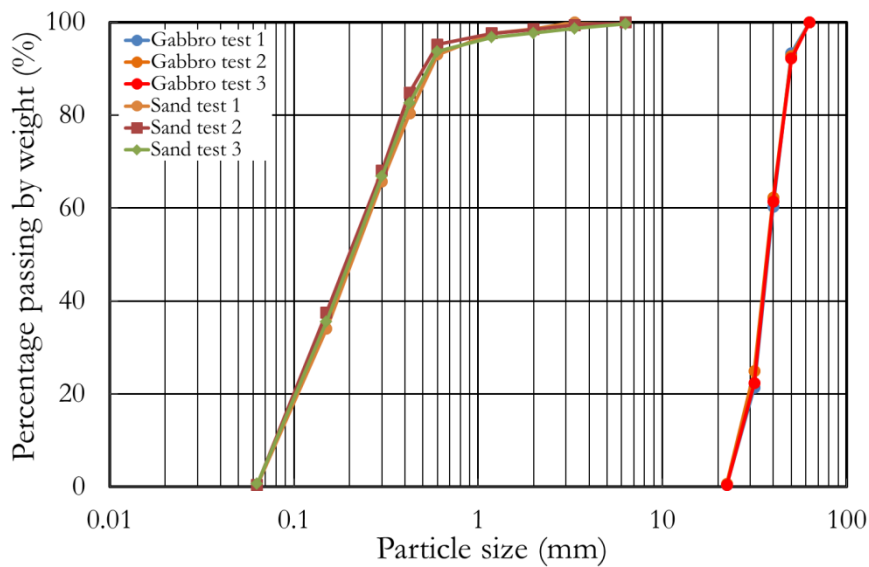


Figure 6.60: PSD graphs of sand compared to PSD graphs of gabbro ballast

Table 6.20: A comparison of material properties of gabbro and granite (after Marinis and Hoek, 2001, SBD Crushers, 2010)

Type of test	Maximum test value	
	Gabbro	Granite
Passing sieve size 0.5 mm	0.07%	0.19% (actual sieve test)
Flakiness index	16%	15%
Los Angeles abrasion	12%	16
Micro deval abrasion	1%	6.5%
Specific gravity	2.96	2.78
Water absorption	0.10%	0.312%
Uniaxial compression strength (MPa)	250	>250
Moh's hardness scale	5-7	6-7

In these two tests, a maximum load of 156.96kN was applied for cyclic loading to represent an equivalent axle load of 32 ton and the sleeper spacing for the tests was 600 mm. Otherwise, the test preparation and procedure remained the same as for the sleeper and ballast intervention tests.

However, in the sand ingress test, some steps were carried out in addition to the baseline test procedure. These involved the introduction of controlled amounts of sand into the ballast after defined number of loading cycles. A known volume of sand was introduced to the ballast surface and allowed to enter the ballast voids below the sleeper soffit. The sand was introduced at predetermined steps i.e. every 0.5 million loading cycles, with the aim of filling 15%, 30%, 45%, 60%, 80%, and 100% of the ballast void space. A further sand ingress stage was carried out to fill ballast voids in the crib above the sleeper soffit and to achieve complete saturation of ballast by sand.

To ensure a uniform distribution of sand in the ballast, a grid pattern (Figure 6.61) was used in placing the sand. The mass of sand introduced into each grid cell/section was quantified based on the density tests carried out on the sand using a vibrating sieve shaker and the porosity of the ballast in the modified SRTF apparatus. Table 6.21 shows the dimensions of the grid and the parameters of the ballast and sand used for calculating the mass of sand added in each grid cell for each percentage increment.

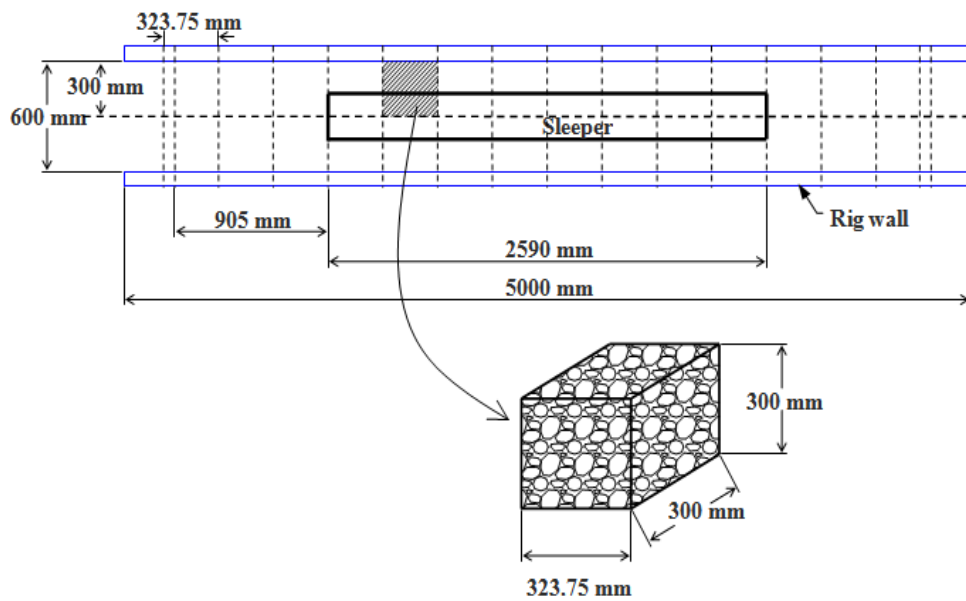


Figure 6.61: Notional grid pattern for quantifying mass of sand

Table 6.21: The dimensions of a grid, ballast and sand parameters, and the calculated mass of sand

Dimensions of the grid:	
Length (mm)	323.75
Width (mm)	300
Depth (mm)	300
Volume of a grid for sand ingress(m ³)	0.0291375
Grain specific gravity of ballast	2.96
Porosity of ballast	0.427
Sand density(kg/m ³)	1788.10
Mass of sand for a grid of 15% void (kg)	3.34
Mass of sand for a grid of 20% void (kg)	4.45

Once the sand had been introduced into the ballast (Figure 6.62), a further 0.5 million loading cycles, at the same load and frequency previously used were applied. This step was repeated for the next sand ingress increment until 100% of the voids were filled.

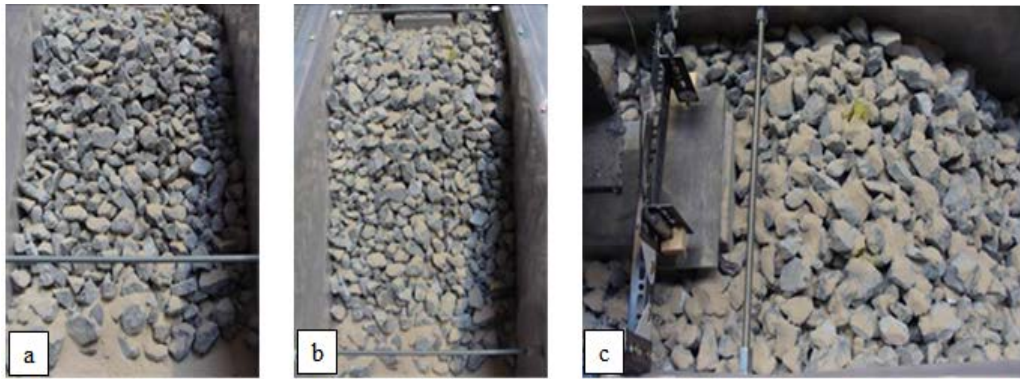


Figure 6.62: The view of ballast after the first introduction of sand (15%) and before any loading cycles applied at (a) left shoulder slope, (b) right shoulder slope and (c) crib and ballast shoulder

After the voids were 100% filled with sand, a further 2.25 million loading cycles were applied to ensure the entire ballast void below the sleeper soffit was saturated (Figure 6.63a). The sand ingress process was continued after the loading cycles reached 5.25 million by introducing more sand to each grid cell until the sand entirely covered the ballast surface at ballast crib and ballast shoulder areas (Figure 6.63b). Additional sand was gradually introduced during loading cycles to maintain and ensure that at the ballast surface there was always enough sand to replace the quantities of sand which may be lost due to sand densification in the voids and/or degradation (Figure 6.63c) until 10.25 million loading cycles were reached when the test was completed (Figure 6.63d). It can also be seen in Figure 6.63 (c) that cribs remained filled with sand and it was assumed that the voids in the ballast below sleeper soffit were also completely filled.

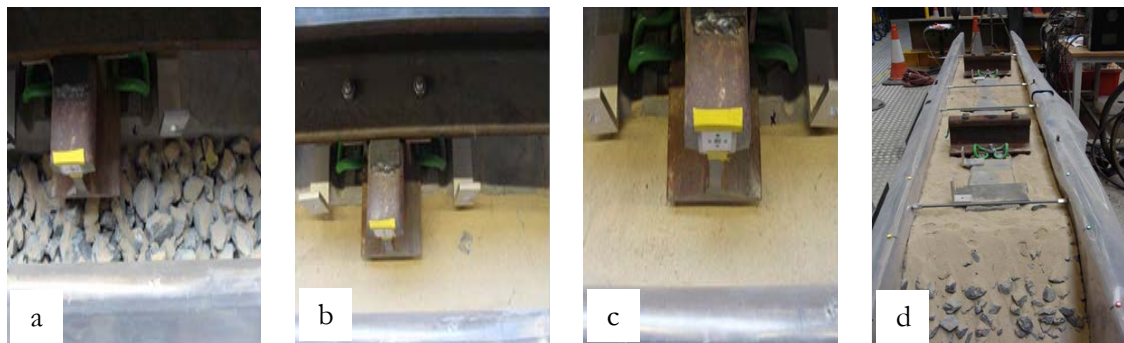


Figure 6.63: The view of ballast surface (a) after 5.25 million loading cycles (assumed 100% void filled), (b) filling ballast cribs before loading, (c) ballast surface after 10 million loading cycles, and (d) ballast surface was saturated by sand at the end of test

Fibre reinforced ballast

Ajayi (2014), Ajayi et al (2014a) and Ajayi et al (2014b) carried out triaxial tests to investigate how the introduction of fibre reinforcement affects the performance of railway ballast. Initial tests were carried out on LB sand (Fraction A) and then on two levels of scaled railway ballast which were parallel grading of 1/5 and 1/3 of the current standard NR ballast grading. The grading envelope of the two levels of scaled ballast used in the tests is presented in Table 6.22 and the PSD graphs of LB sand, the current standard NR, 1/3rd and 1/5th ballast gradings in Figure 6.64.

Table 6.22: The current standard NR, 1/3rd and 1/5th scales ballast gradings (after Ajayi, 2014)

Percentage of passing by weight (median of NR range)	Sieve size (mm)	1/3 rd scale (mm)	1/5 th scale (mm)
100	62.5	20.83	12.5
85	50	16.67	10.0
47.5	40	13.33	8
12.5	31.5	10.50	6.3
1.5	22.4	7.47	4.5

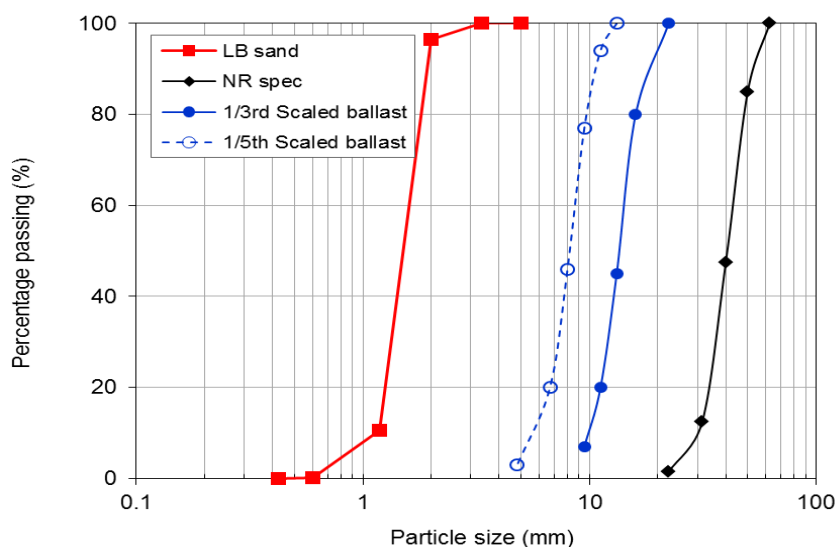


Figure 6.64: PSD graphs of LB sand, 1/5th, and 1/3rd scaled, and NR standard ballast (Ajayi, 2014, Ajayi et al., 2014a, Ajayi et al., 2014b)

Ajayi (2014), Ajayi et al (2014a) and Ajayi et al (2014b) used polypropylene fibre to reinforce LB sand and polyethylene fibre to reinforce both scaled ballasts. The physical appearance of these two types of fibre is shown in Figure 6.65.

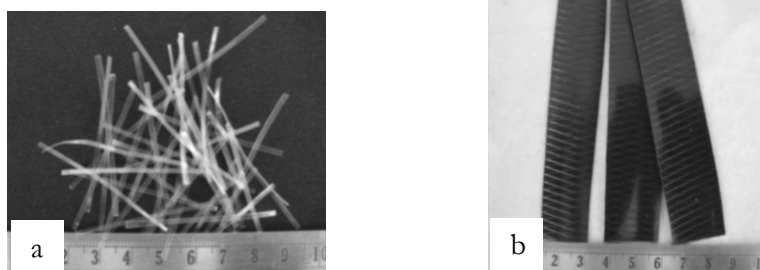


Figure 6.65: The Fibres used in the tests (a) polypropylene and, (b) polyethylene (Ajayi, 2014)

These two types of fibre have good chemical and heat resistance, very low water absorption, and were used in form of strips (tape). Their mechanical properties are summarised in Table 6.23.

Table 6.23: The properties of polypropylene and polyethylene fibres used in the tests (after Ajayi, 2014)

	Polypropylene	Polyethylene
Specific gravity	0.905	0.920
Tensile strength	~ 42MPa	20.3MPa ¹ , 11.2MPa ²
Softening temperature	135°C	85°C
Moisture absorption	< 0.1%	< 0.1%
Note: 1 and 2 are in longitudinal and transverse respectively		

The research carried out by Ajayi (2014) has shown promising results. Therefore, to demonstrate the feasibility of polyethylene fibre in a real application, a test was carried out in the modified SRTF apparatus using the current standard NR ballast grading in conditions representative of these in the field.

The dimensions of polyethylene fibre used for full scaled ballast were 300 mm long, 100 mm wide, and 0.5 mm thick with its bulk density of 910 kg/m³. The test preparation, procedure, setting-up and instrument was the same as for other tests with the exception of blending the polyethylene fibres with the ballast prior to placing it into the modified SRTF apparatus. To ensure a uniform blend of ballast and polyethylene fibres, mixing was carried out in small batches of a known mass of polyethylene fibres and ballast.

The trial mixture used consisted of 0.2% polyethylene fibre content by weight and blending involved placing ballast and fibres into plastic containers in consecutive layers and then carefully pouring the mixture into the modified SRTF apparatus. Placing of the mixture into the modified SRTF apparatus was carried out with great care to avoid segregation occurring and to produce a uniform distribution of polyethylene fibres within the ballast (Figure 6.66).

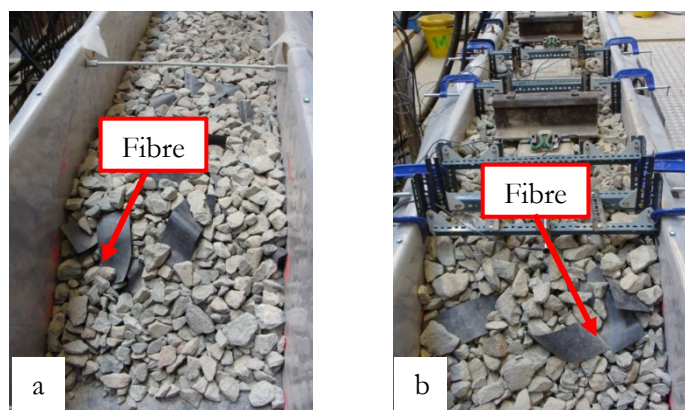


Figure 6.66: Fibre reinforced ballast test under construction: (a) the mixture of Polyethylene fibre with the ballast before compaction, (b) the arrangement prior to loading beam placement

6.7 Summary of tests carried out

6.7.1 Parametric study

Table 6.24 summarises the tests carried out in this research, indicating the parameters varied in each case. The different modifications made were categorised as interventions relating to the sleeper, the ballast or both.

The variables considered include two different types of USP and four variant ballast gradings. To fully investigate this parameter space would require a very large number of tests, but many of these combinations are expected to give relatively similar results. Therefore tests were limited to investigating combinations (indicated by ticks) considered most likely to either demonstrate better performance and/or to provide data for comparison.

Table 6.24: Parameter space investigated

	Sleeper interventions (with and without USP)								
	G44			Twin-block			Timber	Steel	Plastic
	None	USP1	USP2	None	USP1	USP2	None	None	None
NR ballast- Granite	✓	✓	✓	✓	✓	✓	✓	✓	✓
Bespoke gradings with increasing higher proportion of finer material	✓								
	✓								
	✓			✓					
Shallower shoulder (NR ballast)	✓								
Two layered ballast	✓								
Shallower shoulder (smaller grading)					✓				
Fibre reinforced ballast	✓								
	Ballast interventions (with and without sand)								
	PCM								
	None					Sand			
NR ballast-Gabbro	✓					✓			

6.7.2 Test Details

In total, twenty two tests were carried out, usually to 3 million loading cycles, although some tests were continued up to 10.25 million loading cycles and three tests were curtailed after 0.25 million loading cycles owing to a fault with the apparatus. The details of all the tests carried out are presented in Tables 6.25 to 6.27.

In Tables 6.25 to 6.27, the porosity (n) of ballast grading in each test is also presented. The degree of porosity was determined based on the mechanical properties and the weight of ballast used for each test in the modified SRTF apparatus.

Table 6.25: Detail of sleeper intervention tests carried out

Test label (for graphs)	Sleeper type	Ballast grading	Ballast porosity (%) (n)	USP	Shoulder slope	Total load cycles applied (millions)	
Baseline	G44	NR	41.75	No	1:1	3.0	
			40.16				
Twin-block	Twin-block		41.99			4.5	
Plastic	Plastic		40.39			4.0	
Timber	Timber		40.20			3.5	
Steel	Steel		42.24			3.5	
Mono-block+ USP 1	G44		40.88			1	3.0
Mono-block+ USP 2			43.05			2	4.0
Twin-block+ USP 1	Twin-block		44.01			1	4.5
Twin-block+ USP 2			43.93			2	6.0

Table 6.26: Detail of ballast intervention tests carried out

Test label (for graphs)	Sleeper type	Ballast grading	Ballast porosity (%)(n)	USP	Shoulder slope	Total load cycles applied (millions)
Baseline	G44	NR	41.75	No	1:1	3.0
			40.16			
Variant 1		Variant 1	38.89		3.0	
Variant 2		Variant 2	38.80			
Variant 3		Variant 3	36.64		5.0	
TLB		TLB	37.41		4.0	
RPS		RPS	41.09		1:2	3.5
Fibre		NR + fibre	41.37		1:1	5.0

Table 6.27: Detail of sand ingress tests carried out

Test label (for graphs)	Sleeper type	Ballast grading	Ballast porosity (%)(n)	Sand	Shoulder slope	Total load cycles applied (millions)
Baseline	PCM	NR-gabbro	43.24	No	1:1	4.0
Sand ingress		NR-gabbro	42.72	Yes		10.25

Chapter 7: Experimental results and interpretation

7.1 Introduction

In this Chapter the experimental results are presented and discussed. The Chapter is divided into 6 main sections (7.2 to 7.7). Section 7.2 presents a comparison of the main measured/calculated parameters subdivided by the category of intervention (sleeper or ballast). Section 7.3 presents photos taken to observe any ballast movement on the ballast shoulder slope to show further evidence of the mechanisms at work. Steel and plastic sleepers are presented as special cases for reasons that will become clear in Section 7.4. The test on ballast fouling by sand ingress is described in Section 7.5. Based on a review of the test results, a trial test of a combination of the most promising interventions for both ballast and sleepers is presented in Section 7.6. The experimental results of permanent settlement and spring stiffness are correlated in Section 7.7. They are compared with ballast settlement models from the literature and a new ballast settlement model is proposed and evaluated in Section 7.8.

7.2 Main parameters of comparison

In Chapters 1 and 6, the main parameters of comparison were described and can be categorised as follows:

- Permanent settlement
- Sleeper deflection
- Spring stiffness
- Ballast horizontal (longitudinal) pressure
- Mobilised earth pressure ratio
- Particle contacts - number, area and pressure
- Particle breakage/degradation
- Lateral movement of ballast on the shoulder slope

Section 7.2 goes through each category of measurement and interprets the data to assess the influence of each test variables.

7.2.1 Permanent settlement

Figure 7.1 shows a typical graph of load against deflection for the first loading cycle. This is typical of all the tests. There was significant variation between each of the eight measurement locations. This can be explained by the difficulty in preparing a level surface such that on first loading, particles initially supporting the sleeper slightly proud of the local ballast were pushed into the ballast and the sleeper was forced into contact with a greater number of supporting ballast particles.

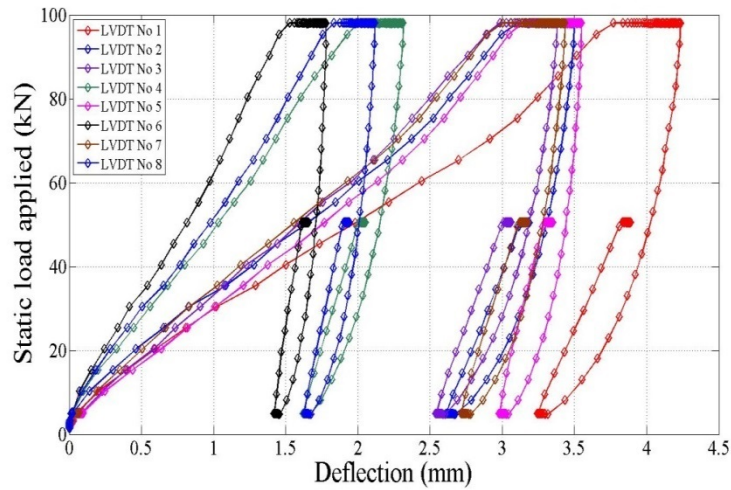


Figure 7.1: Typical graph of applied static load against deformation in first load cycle

It can be seen that as the load increases to the maximum, the vertical settlement increases correspondingly. On unloading there was small elastic recovery leaving a large permanent settlement.

Results from sleeper intervention tests

As summarised in Table 6.25, nine tests were carried out on the current standard NR ballast grading with different sleeper types and materials as well as modifications made at the sleeper soffit of G44 and twin-block sleepers. Plastic and steel sleeper are a special case for reasons that will become clear and are presented in a later section of this chapter.

Figure 7.2 shows the results of permanent settlement (area weighted method) against the number of loading cycles on a log scale with the results were zeroed before the first load cycle.

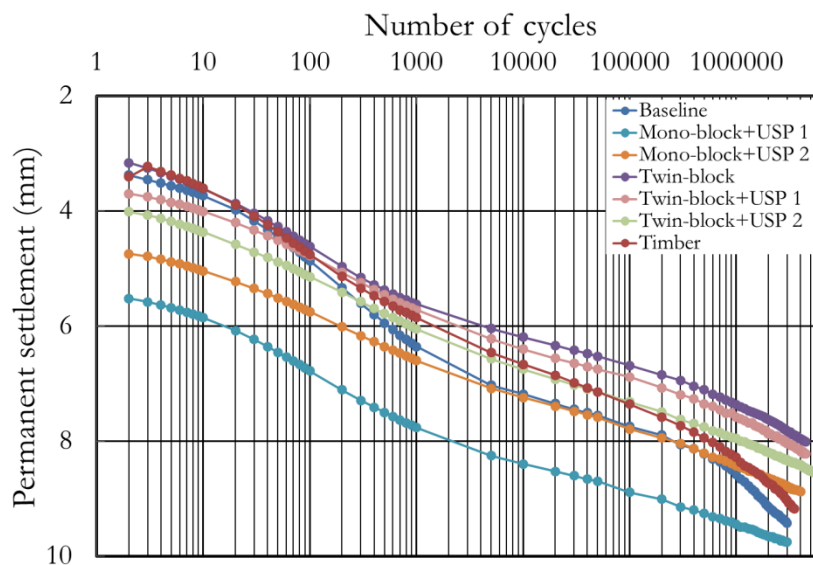


Figure 7.2: Permanent settlement graph of each sleeper intervention test

From Figure 7.2 as the number of loading cycle increases the rate of vertical settlement is in many cases approximately linear on a log scale (i.e. reduces with loading cycles). There is also significant variation in the magnitude of settlement over the first loading cycle (as shown by the differing starting points of each line at cycle 2). These variations can be explained as a result of the particulate nature of

ballast and the small number of ballast particles initially in contact with the sleeper soffit. To eliminate or minimise the uncertainty from the initial loading cycles of the ballast and make comparisons clearer, the permanent settlements are zeroed after 10 loading cycles (Figure 7.3).

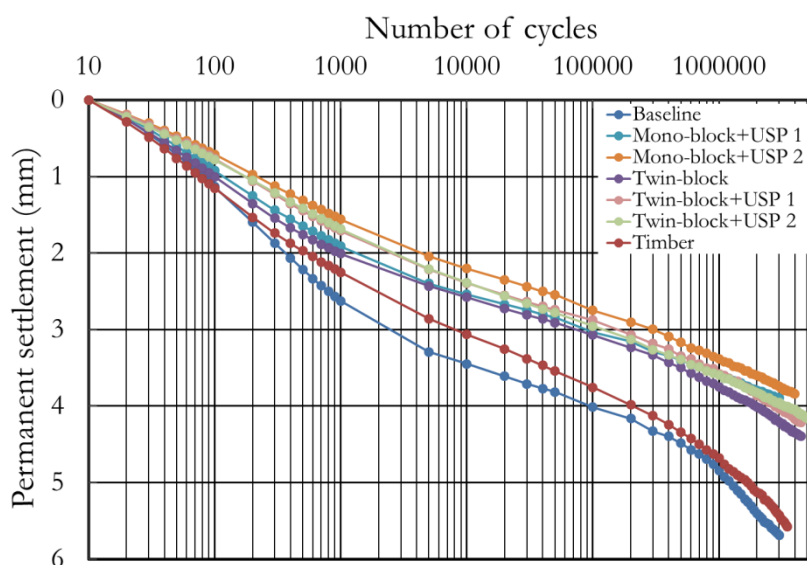


Figure 7.3: Permanent settlement graph of each sleeper intervention test after it was zeroed at 10 loading cycles

Discussion of settlement results for sleeper intervention tests

Each test involving a sleeper intervention showed a similar trend of vertical permanent settlement, with a rapid rate of settlement occurring at the beginning of the test and gradually reducing with the number of loading cycles. The difference in the initial settlements on the first cycle also shows that the application of the same amount of compaction energy on the same ballast grading does not guarantee creating the same initial condition, although following the first loading cycle different behavioural trends become apparent. The initial vertical permanent settlement of the ballast is consistent with ORE (1970) results which suggest that the initial vertical permanent settlement is controlled directly by the initial degree of compaction. Based on the graph of permanent settlement zeroed after 10 loading cycles (Figure 7.3), the improvements of permanent settlement produced by each sleeper intervention into baseline test are presented in Tables 7.1 and 7.2.

Table 7.1: Permanent settlement and percentage reduction of permanent settlement into baseline test at number of loading cycles of each sleeper intervention test

Test label	Total loading cycles applied (millions)	Permanent settlement (mm) at			Percentage reduction of permanent settlement (%) at		
		Loading cycles (millions)			Loading cycles (millions)		
		1	2	3	1	2	3
Baseline	3.0	4.85	5.40	5.69	-	-	-
Twin-block	4.5	3.75	4.01	4.21	22.5	25.8	26.1
Timber	3.5	4.68	5.12	5.42	3.5	5.2	4.7
Mono-block+ USP 1	3.0	3.58	3.80	3.89	26.0	29.8	31.6
Mono-block+ USP 2	4.0	3.39	3.60	3.74	30.1	33.4	34.2
Twin-block+ USP 1	4.5	3.58	3.86	4.03	26.2	28.5	29.1
Twin-block+ USP 2	6.0	3.59	3.82	3.96	25.9	29.2	30.5

Table 7.2: Permanent settlement and percentage reduction of permanent settlement in twin-block sleeper tests with number of loading cycles with USP inclusion

Test label	Total loading cycles applied (millions)	Permanent settlement (mm) at			Percentage reduction of permanent settlement (%) at		
		Loading cycles (millions)			Loading cycles (millions)		
		1.5	3.0	4.5	1.5	3.0	4.5
Twin-block	4.5	3.91	4.21	4.40	-	-	-
Twin-block+ USP 1	4.5	3.72	4.03	4.21	4.7	4.1	4.2
Twin-block+ USP 2	6.0	3.72	3.96	4.10	4.7	5.9	6.7

Table 7.1 and 7.2 show some important trends. Key amongst these is that at 3 million loading cycles, all sleeper interventions tested performed better than the baseline test. For the different sleeper types, the permanent settlement of the timber sleeper was 5% less than that of baseline test, and the twin-block sleeper settled 26% less than the baseline test. The attachment of USPs 1 and 2 onto G44 concrete sleepers reduced the permanent settlement by 32% and 34% compared with the baseline test and the use of USPs with twin-block sleepers performed similarly reducing of 29% and 31%. However, there was relatively little improvement gained when comparing the permanent settlement for the twin-block sleeper (26%) with the twin-block sleepers with USPs (29% and 31%). Overall, the application of USP 2 on the G44 sleeper produced the most benefit compared with the baseline case (34%).

Comparing the test results for the concrete and timber mono-block sleeper types, the sleeper made from the softer material has settled less. This is attributed to the indentation of the ballast particles into the softer sleeper material providing a more stable contact and load distribution system.

Results from ballast intervention tests

Seven tests were carried out with different interventions (Table 6.26) and a G44 sleeper. Figure 7.4 shows the permanent settlement with number of loading cycles from the beginning of each test and Figure 7.5 shows the permanent settlement zeroed after 10 loading cycles.

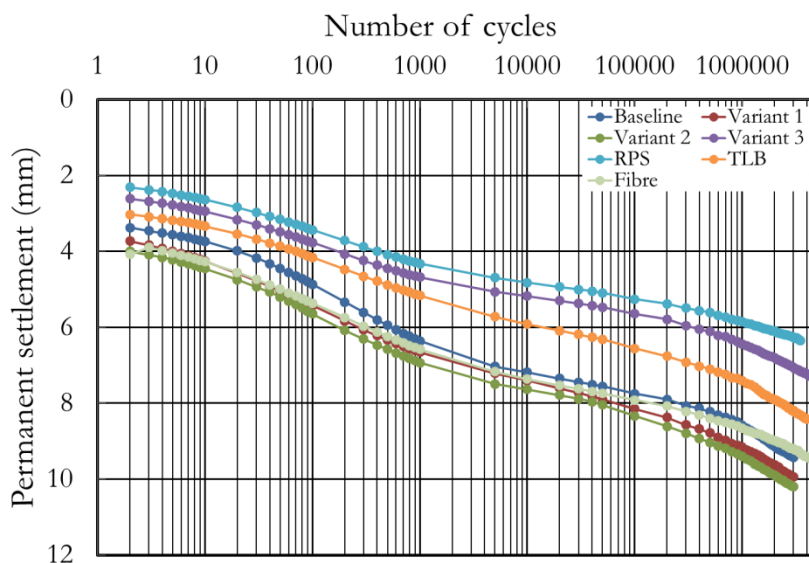


Figure 7.4: Permanent settlement graph of each ballast intervention test

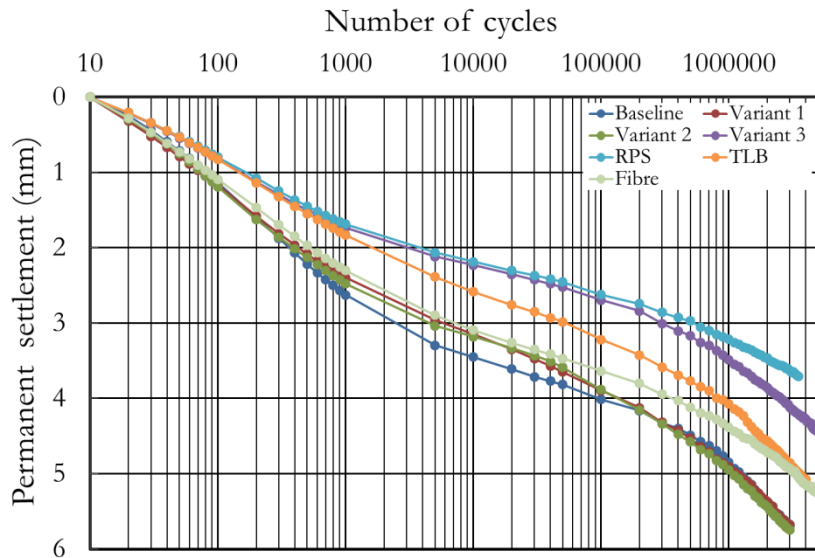


Figure 7.5: Permanent settlement graph of each ballast intervention test after it was zeroed at 10 loading cycles

With the ballast interventions, the same general trend as for the sleeper intervention tests is apparent: a reducing rate of permanent settlement appearing approximately linear on a log scale as the number of loading cycles increase.

Discussion of settlement results for ballast intervention tests

Figure 7.5 shows that each ballast intervention produced less permanent settlement than the baseline test. Key values from Figure 7.5 are tabulated in Table 7.3.

Table 7.3: Permanent settlement and percentage reduction of permanent settlement into baseline test at number of loading cycles of each ballast intervention test

Test label	Total loading cycles applied (millions)	Permanent settlement (mm) at			Percentage reduction of permanent settlement (%) at		
		Loading cycles (millions)			Loading cycles (millions)		
		1	2	3	1	2	3
Baseline	3.0	4.85	5.40	5.69	-	-	-
Variant 1	3.0	4.91	5.37	5.68	-1.3	0.6	0.2
Variant 2	3.0	4.95	5.44	5.74	-2.1	-0.6	-0.9
Variant 3	5.0	3.49	3.86	4.12	28.0	28.6	27.6
TLB	4.0	4.07	4.56	4.85	16.0	15.6	14.7
RPS	3.5	3.21	3.46	3.63	33.7	35.9	36.2
Fibre	5.0	4.38	4.72	4.93	9.5	12.7	13.3

Figure 7.5 and Table 7.3 show that variant 1 and 2 produced less permanent settlement than the baseline test for the first 0.25 million loading cycles. However, although variants 1 and 2 showed less permanent settlement, at points in the tests from 0.25 to 3 million loading cycles the permanent settlement was very similar to the baseline test. It is thought that for variant 1 and 2 the finer proportions of material introduced were not sufficient to significantly alter the behaviour. Subsequently variant 3 was designed to introduce greater proportions of finer material. This last variant tested demonstrated the potential for changes to the grading to significantly reduce permanent settlement; in this last case; variant 3 produced ~28% less permanent settlement than the baseline test at 3 million loading cycles.

At 3 million loading cycles, the TLB system and fibre reinforced ballast also produced 15% and 13% respectively less permanent settlement than that of baseline test. However, the greatest reduction in permanent settlement was produced by RPS slope test, 36% less than that of baseline test. Previous works by Lackenby et al (2007) concluded that ballast confinement has a significant influence on decreasing ballast settlement thus increasing track stability. Apart from shallower shoulder slopes, confining pressure in the ballast could also be increased by sleeper shapes (to preventing lateral ballast movement) and by increasing the shoulder height (Lackenby et al., 2007) for the same slope (no sharpening the slope).

Summary of permanent settlement results

The intervention results in order of the percentage reduction in permanent settlement from 10 to 3 million loading cycles compared with the baseline test are presented in Table 7.4 (column 2). The less effective ballast variants (1 and 2) are omitted as they showed little difference to the baseline test. Table 7.4 shows that the RPS slope is the most effective at reducing permanent settlement; the second most effective intervention is the application of USP 2 on a mono-block concrete G44 sleeper.

Table 7.4: The most to the least of permanent settlement reduction and percentage of improvement at 2 million (M) to 3M loading cycles

Test label	Overall reduction of permanent settlement at 3 million loading cycles (%)	Settlement 2M to 3M loading cycles (mm)	Percentage of improvement for long term basis (2M to 3M loading cycles)
RPS	36.2	0.1664	41.7
Mono-block+ USP 2	34.2	0.1410	50.6
Mono-block+ USP 1	31.6	0.0982	65.6
Twin-block+ USP 2	30.5	0.1316	53.9
Twin-block+ USP 1	29.1	0.1709	40.1
Variant 3	27.6	0.2555	10.5
Twin-block	26.1	0.1954	31.5
TLB	14.7	0.2896	-1.5
Fibre	13.3	0.2162	24.2
Timber	4.7	0.2993	-4.9

To investigate the potential for reducing the rate of settlement after greater numbers of loading cycles, the settlement between 2 million to 3 million loading cycles is presented in column 3 of Table 7.4. Column 4 shows the percentage difference to the baseline test for the settlement between 2 million to 3 million loading cycles. At this later stage in the cyclic loading, the introduction of USPs is the most effective intervention (40 - 66%) for reducing settlement.

7.2.2 Sleeper deflection

For sleepers on freshly laid or just tamped ballast the contact area is often idealised as being mainly bellow the railseats (Raymond, 1978). This is justified because track laying methods are intended to pack ballast beneath the railseats and provide the greatest support immediately beneath the rails. However, this pressure distribution can vary with loading cycles. For example where ballast is not maintained a gap can develop below the sleeper ends of mono-block sleepers giving rise to a condition known as centre binding (Raymond, 1978); (Turcke and Raymond, 1979). In this case, a

significant portion of the rail loads would be carried by the ballast contacting the central portion of sleeper. The tendency towards centre binding is also influenced by the sleeper bending stiffness, for example the bending stiffness of a concrete sleeper is about 4.5 to 6 times greater than that of a timber sleeper (Stewart, 1985). This leads the timber sleeper conform more to the ballast surface and a to more uniformly distributed surface load than with a mono-block concrete sleeper. To investigate the tendency towards centre binding in key tests (sleeper and ballast interventions), the deflection data are plotted for LVDTs at the sleeper ends and those at the middle and then compared.

Results from sleeper intervention tests

Figures 7.6 and 7.7 show the average deflection for (1) the four corner and (2) the middle sections of each sleeper against the number of loading cycles for sleeper intervention tests (linear scale).

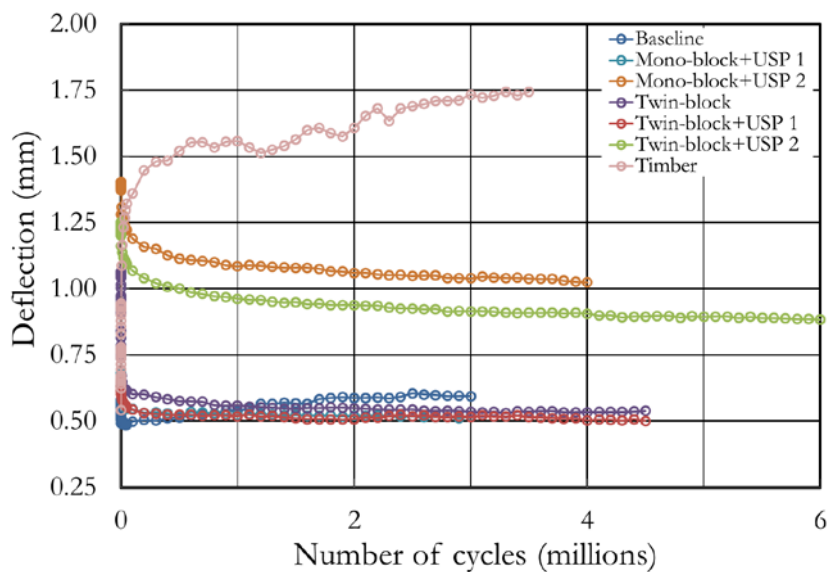


Figure 7.6: The average of four corner sleeper deflection of each sleeper intervention test

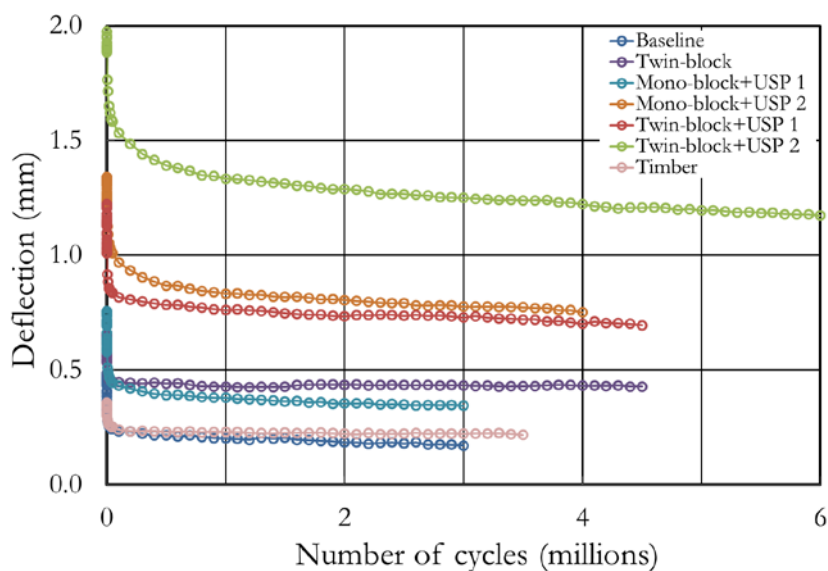


Figure 7.7: The average of sleeper middle section deflection of each sleeper intervention test

Discussion of sleeper deflection results for sleeper intervention tests

Initially, deflection at the sleeper ends and in the middle is reasonably uniform. However with loading cycles, the ongoing sleeper deflection at the ends (corners) or middle can be characterised as either reducing or increasing with the number of loading cycles. Comparing deflection behaviour at the sleeper ends and the middle shows whether the sleeper is deflecting uniformly or whether there is a trend for hogging or sagging with increased number of loading cycles. Based on Figures 7.6 and 7.7 trends for deflection and bending trends are summarised in Table 7.5.

Table 7.5: The behaviour of deflection at ends and middle section of sleeper and the results into the sleeper in each sleeper intervention test

Test label	Total loading cycles applied (millions)	Trend with loading cycles for sleeper:		Deflected sleeper shape tended to (uniform, sagging or hogging)
		Ends	Middle	
Baseline	3.0	Increasing	Reducing	Hogging
Twin-block	4.5	Reducing		Uniform
Timber	3.5	Increasing		Hogging
Mono-block+ USP 1	3.0	Reducing		Uniform
Mono-block+ USP 2	4.0			
Twin-block+ USP 1	4.5			
Twin-block+ USP 2	6.0			

Table 7.5 shows that the mono-block sleepers (G44 and timber) tend to hog over the course of loading cycles (centre binding). Figures 7.6 and 7.7 show that the timber sleeper hogs/centre binds the most, which may be explained as a result of its lower bending stiffness than the concrete sleepers. Hogging by the timber sleeper shows a disagreement with the conclusion of Stewart (1985) that sleeper bending stiffness influences the tendency toward centre binding. Based on the results in Table 7.5, centre binding arises due to the shape of the sleeper in use. In the field, centre binding on mono-block sleepers may cause sleeper failure and instability of the track. However the sleepers used in these laboratory tests were carefully inspected for any signs of distress, which confirmed that the occurrence of hogging in these tests was well within the capacity of the sleepers. Table 7.5 also shows that for track that is not maintained e.g. by tamping, twin-block sleepers perform the best.

The introduction of USPs onto G44 sleeper maintained uniform deflections and prevented the development of hogging. Uniform deflections were also maintained throughout the tests using twin-block sleepers with or without the inclusion of USPs. This can be explained as a result of the nature of the loading from the twin-block sleeper, with its twin footprints localised to each railseat and the negligible bending stiffness of the metal attachment between the two blocks so that the two blocks of the sleeper were able to act more independently.

Results from ballast intervention tests

The deflection of the four corner and middle section of each sleeper with number of loading cycles is presented in Figures 7.8 and 7.9 respectively.

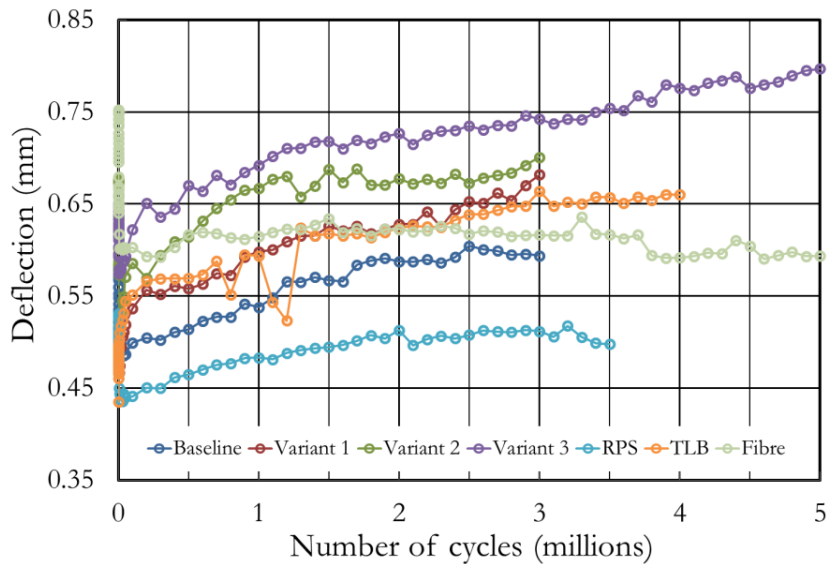


Figure 7.8: The average of four corner sleeper deflection of each ballast intervention test

Figure 7.8 shows that the four corner deflection of variant 3 is the highest amongst the ballast intervention tests. This may be because variant 3 is the finest grading tested in this research (followed by variant 2 and 1) and consequently had the greatest initial density. This higher initial density had a lesser ability to compact and it settled less overall leading to a more pronounced hard spot beneath the middle sleeper and hence more bending. The smallest average four corners deflection was produced by the RPS slope test which can be explained by the additional confining pressure provided to the ballast beneath the sleeper ends. For the middle section of the sleeper, the deflection (Figure 7.9) of each ballast intervention test is similar apart from the test on fibre reinforced ballast. The introduction of fibre to reinforce the ballast perhaps introduces more elasticity into the ballast matrix. In the case of TLB system test, the deflection graph shifted at approximately 1.2 million loading cycles. This was because a hydraulic fault with the loading system caused an interruption to the test. It is perhaps worth noting that in all tests (described in Section 6.2.4) it was important to allow the same amount of elapsed time between set up and the start of loading. This is because any pause can allow the ballast the opportunity to creep, and on continuing with the test discontinuities in the data can then be observed.

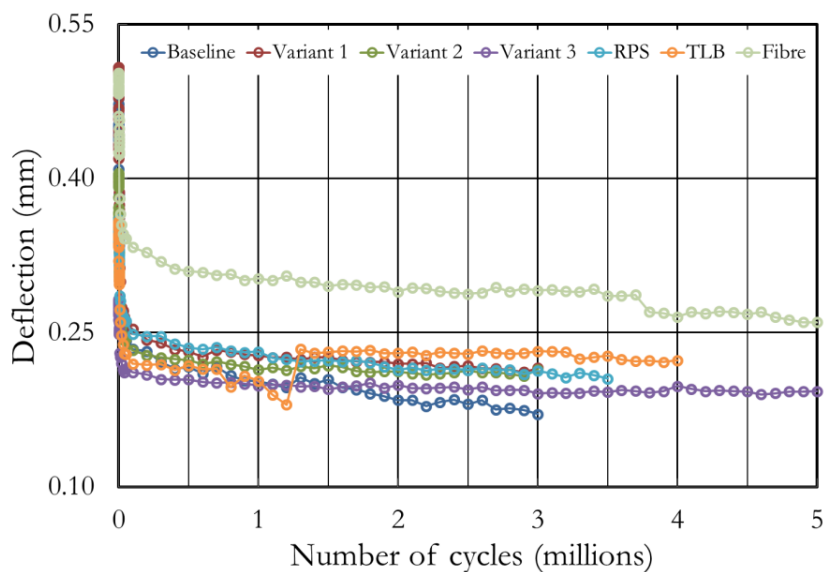


Figure 7.9: The average of sleeper middle section deflection of each sleeper intervention test

Discussion of sleeper deflection results for ballast interventions

For the ballast intervention tests, the deflections of the four corners and the middle sections of each sleeper are presented in Table 7.6.

Table 7.6: The behaviour of deflection at ends and middle section of sleeper and the results into the sleeper in each sleeper intervention test

Test label	Total loading cycles applied (millions)	The behaviour of deflection with number of loading cycles		Deflected sleeper shape
		Sleeper ends	Middle section	
Baseline	3.0	Increasing	Reducing	Hogging
Variant 1	3.0			
Variant 2	3.0			
Variant 3	5.0			
RPS	4.0			
TLB	3.5			
Fibre	5.0			

The results in Table 7.6 agree with the earlier findings of the tests using mono-block sleepers without USPs, that during cyclic loading the deflected sleeper tended towards a hogging shape.

7.2.3 Spring stiffness

For an applied load, the equivalent spring stiffness can be calculated/inferred from the deflection of the sleeper at the point of application of the load or at the sleeper end. This means spring stiffness can be for the sleeper ends and the middle section of the sleeper. In the earlier results of deflection, it was shown that mono-block sleepers showed greater corner deflections and the middle reduced over the loading cycles whereas twin-block sleepers were more consistent. This leads to a suitable method is required for comparing the results which is valid for any sleeper types. Therefore, in this section, spring stiffness is determined as either the average of the four corner deflections measured or using the area weighted method to take advantage of all deflection measurement locations on the sleeper (see Section 6.5.3). The results for both methods are presented in this section.

Results from sleeper intervention tests

Figure 7.10 shows a graph of the average four corner spring stiffness for each sleeper intervention. The spring stiffness for the mono-block sleeper increases up to a certain number loading cycles before it gradually decreases, perhaps tending to a constant value. However, tests on twin-block and G44 sleepers with USPs showed a pattern of increasing spring stiffness with the number of loading cycles. The introduction of USPs to G44 and twin-block sleepers acted to reduce the absolute value at any given number of loading cycle, render more consistent and gradually increase the spring stiffness with number of loading cycles perhaps tending to a limiting value.

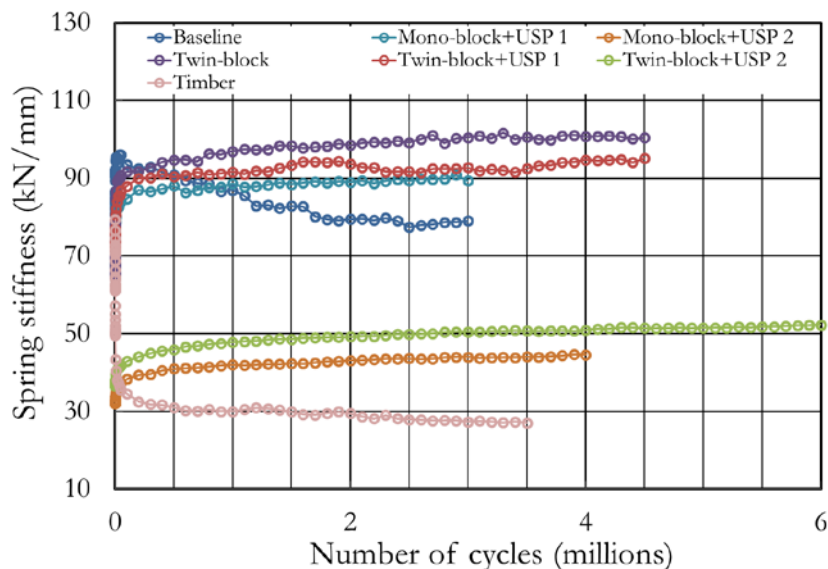


Figure 7.10: The average four corners spring stiffness of each sleeper intervention test

Figure 7.11 shows a graph of the area weighted spring stiffness for each sleeper intervention.

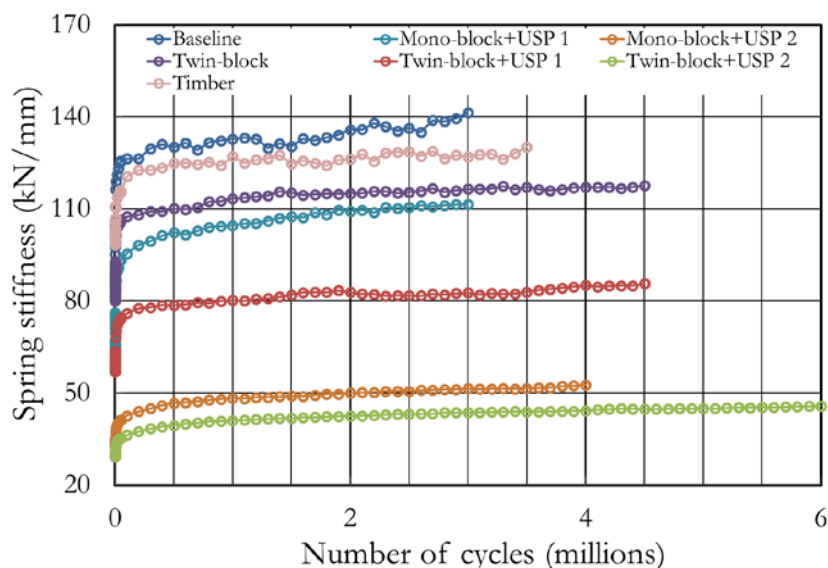


Figure 7.11: The average spring stiffness obtained by area weighted method for each sleeper intervention test

Figure 7.11 shows a trend of increasing area weighted spring stiffness with number of loading cycles regardless of sleeper types or modifications at sleeper soffit. The results from the tests with the inclusion of USPs are lower and more consistent.

The spring stiffness results with and without USPs can be used to analyse the contribution to the deflection and spring stiffness of each USP using the equations:

$$\delta_{\text{sleeper} + \text{USP}} = \delta_{\text{sleeper}} + \delta_{\text{USP}} \quad \text{Equation 7.1}$$

$$\frac{1}{k_{\text{sleeper} + \text{USP}}} = \frac{1}{k_{\text{sleeper}}} + \frac{1}{k_{\text{USP}}} \quad \text{Equation 7.2}$$

where δ_i and k_i are deflection and spring stiffness of component i .

In the following figures the area weighted method for each parameter calculation is used (as this is considered the most robust parameters making use of all the available deflection measurements). Figures 7.12 and 7.13 present a comparison of deflection graphs and Figures 7.14 and 7.15 a

comparison of spring stiffnesses of USP 1 and 2 determined using Equations 7.1 and 7.2 from the graphs for the tests using mono-block (G44) and twin-block sleepers with and without USPs inclusion.

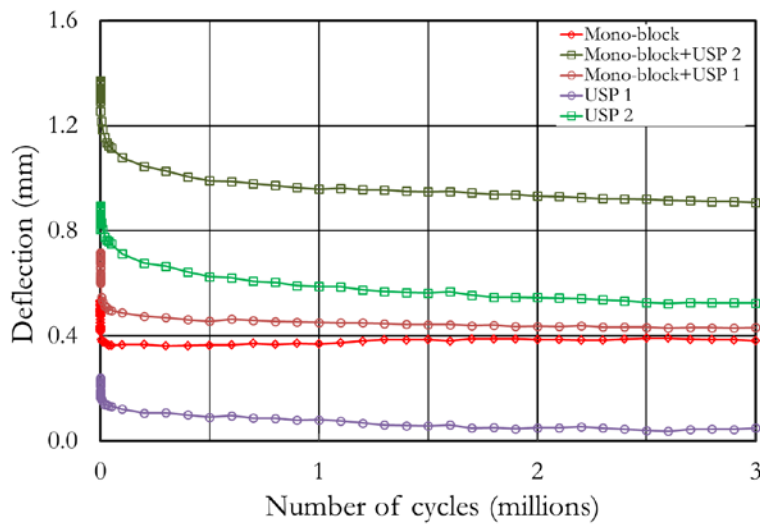


Figure 7.12: Deflection graphs of USP 1 and 2, mono-block and mono-block with USP inclusions

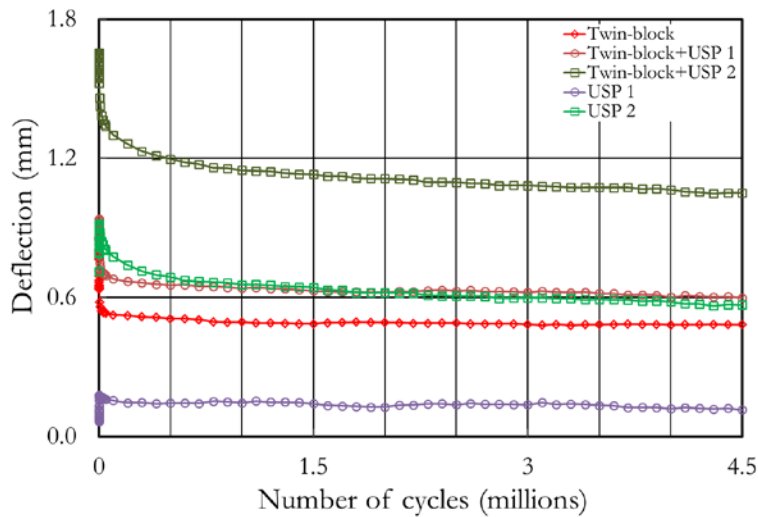


Figure 7.13: Deflection graphs of USP 1 and 2, twin-block and twin-block with USP inclusions

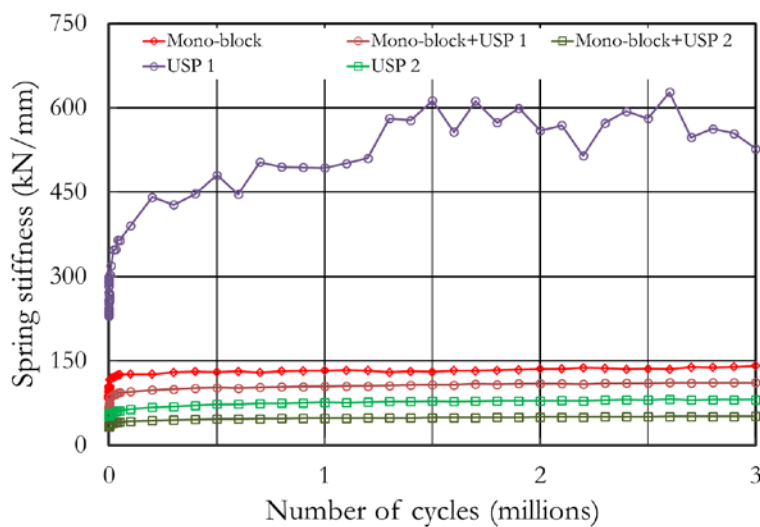


Figure 7.14: Spring stiffness graphs of USP 1 and 2, mono-block and mono-block with USP inclusion

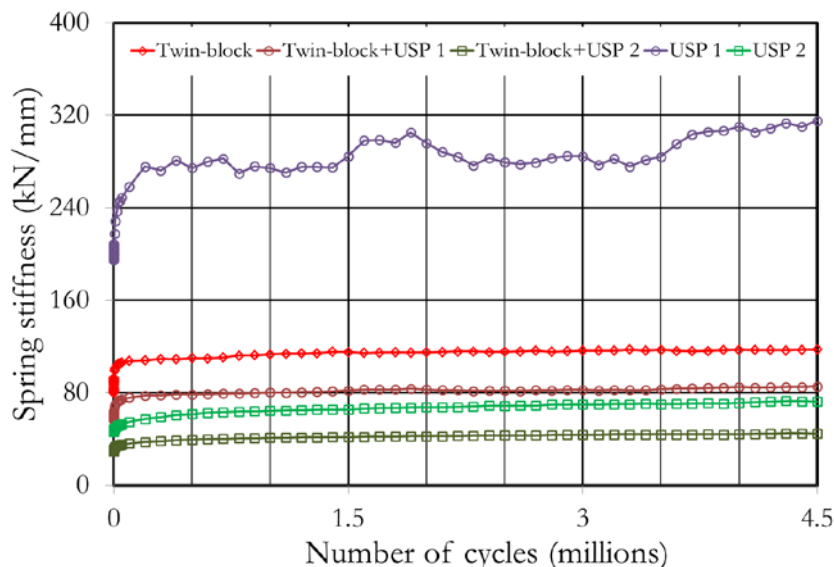


Figure 7.15: Spring stiffness graphs of USP 1 and 2, twin-block and twin-block with USP inclusion

Discussion of spring stiffness results for sleeper intervention tests

Based on the average four corner spring stiffness (Figure 7.10), the percentage change in the spring stiffness for each sleeper intervention compared with the baseline test is presented in Table 7.7.

Table 7.7: Average four corner spring stiffness and percentage change of the spring stiffness compared to the baseline test at number of loading cycles of each sleeper intervention test

Test label	Total loading cycles applied (millions)	Spring stiffness (kN/mm) at			Percentage reduction or increase of spring stiffness (%) at		
		Loading cycles (millions)			Loading cycles (millions)		
		1	2	3	1	2	3
Baseline	3.0	86.95	79.48	79.03	-	-	-
Twin-block	4.5	96.96	98.46	100.50	-11.5	-23.9	-27.2
Timber	3.5	29.97	29.43	27.31	65.5	63.0	65.4
Mono-block+ USP 1	3.0	88.60	88.98	89.35	-1.9	-12.0	-13.1
Mono-block+ USP 2	4.0	42.03	43.13	44.01	51.7	45.7	44.3
Twin-block+ USP 1	4.5	91.66	93.71	92.76	-5.4	-17.9	-17.4
Twin-block+ USP 2	6.0	47.83	49.22	50.47	45.0	38.1	36.1

It can be seen that at 3 million loading cycles, the spring stiffness of timber sleeper is 65% lower than that of baseline test. This is the lowest spring stiffness in any of the sleeper intervention tests. At the other extreme, the test on a concrete twin-block sleeper produced the highest spring stiffness (27% higher than that of baseline test). The attachment of USP 1 to mono-block and twin-block sleepers strangely produced higher spring stiffnesses (13% and 17% respectively) than that of baseline test, this is probably because the four corner method did not adequately capture the overall sleeper behaviour and the stiffest USP was perhaps able to mitigate against ballast migration from below the sleeper ends thus retaining more support at the corners with minimal additional compliance. The attachment of USP 2 to mono-block and twin-block sleepers produced the lowest spring stiffnesses on concrete sleepers (44% and 36% respectively) compared with the baseline test.

The twin-block tests were carried out over more loading cycles than the mono-block tests. Table 7.8 shows additional data for these tests considering the full number of loading cycles.

Table 7.8: Average four corner spring stiffness and percentage reduction of spring stiffness into twin-block sleeper test at number of loading cycles of each test with USPs inclusion

Test label	Total loading cycles applied (millions)	Spring stiffness (kN/mm) at			Percentage reduction of spring stiffness (%) at		
		Loading cycles (millions)			Loading cycles (millions)		
		1.5	3.0	4.5	1.5	3.0	4.5
Twin-block	4.5	98.35	100.50	100.38	-	-	-
Twin-block+ USP 1	4.5	93.34	92.76	95.06	5.1	7.7	5.3
Twin-block+ USP 2	6.0	48.54	50.47	51.46	50.6	49.8	48.7

Comparing the four corner spring stiffnesses for the twin-block sleeper with and without the inclusion of UPSs, Table 7.8 shows that at 4.5 million loading cycles the inclusion of USP 1 and 2 produced lower spring stiffnesses (5% and 49% respectively).

The spring stiffnesses from the area weighted method (Figure 7.11) are presented in Table 7.9.

Table 7.9: Area weighted spring stiffness and percentage reduction of spring stiffness into baseline test at number of loading cycles of each sleeper intervention test

Test label	Total loading cycles applied (millions)	Spring stiffness (kN/mm) at			Percentage reduction or increase of spring stiffness (%) at		
		Loading cycles (millions)			Loading cycles (millions)		
		1	2	3	1	2	3
Baseline	3.0	132.82	135.82	141.44	-	-	-
Twin-block	4.5	113.39	115.09	116.49	14.6	15.3	17.6
Timber	3.5	127.10	126.22	126.93	4.3	7.1	10.3
Mono-block+ USP 1	3.0	104.63	109.29	111.53	21.2	19.5	21.1
Mono-block+ USP 2	4.0	48.41	49.94	51.44	63.6	63.2	63.6
Twin-block+ USP 1	4.5	80.23	82.87	82.66	39.6	39.0	41.6
Twin-block+ USP 2	6.0	41.14	42.49	43.66	69.0	68.7	69.1

The area weighted method showed a trend of increasing spring stiffness with loading cycles in all tests. This method of comparison is considered more representative than the four corner spring stiffness because it uses all measurement locations on the sleeper. Table 7.9 shows that at 3 million loading cycles, the spring stiffness of the baseline test is the highest of all the sleeper intervention tests. The spring stiffnesses produced by twin-block and timber sleepers were 18% and 10% lower respectively than that of baseline test. The attachment of USP 1 and 2 to a mono-block G44 sleeper also produced spring stiffnesses 21% and 64% lower respectively than the baseline test. Tests on twin-block sleepers with the inclusion of USPs 1 and 2 produced spring stiffnesses 42% and 69% lower respectively than that of baseline test. Table 7.10 shows data to further loading cycles for the twin-block tests.

Table 7.10: Area weighted spring stiffness and percentage reduction of spring stiffness into twin-block sleeper test at number of loading cycles of each test with USPs inclusion

Test label	Total loading cycles applied (millions)	Spring stiffness (kN/mm) at			Percentage reduction of spring stiffness (%) at		
		Loading cycles (millions)			Loading cycles (millions)		
		1.5	3.0	4.5	1.5	3.0	4.5
Twin-block	4.5	115.61	116.49	117.55	-	-	-
Twin-block+ USP 1	4.5	82.01	82.66	85.63	29.1	29.0	27.2
Twin-block+ USP 2	6.0	41.79	43.66	44.78	63.9	62.5	61.9

Table 7.10 shows that at 4.5 million loading cycles, the introduction of USP 1 and 2 to twin-block sleeper produced spring stiffness 27% and 62% lower respectively than that of the twin-block sleeper test.

While the inclusion of USPs produced lower spring stiffnesses, the spring stiffness graphs also show smoother behaviour through the loading cycles compared to the tests without USPs (Figure 7.11). It may be hypothesised that the attachment of USPs maintains a more uniform spring stiffness with loading cycles through creating a more homogenous interface with the ballast, thus minimising the potential for settlement.

A further observation regarding USPs is that the area weighted deflection and spring stiffnesses for the same type of USP using mono-block G44 and twin-block sleepers are different (Figures 7.12 to 7.15). This may be explained by the different sleeper shapes and bending stiffness. Overall, the order of area weighted spring stiffness correlates to the sleeper soffit areas. Thus the twin-block sleeper with its smaller soffit area has a lower spring stiffness than the G44 sleeper. The spring stiffnesses of USPs found using Equations 7.1 and 7.2 and plotted on Figures 7.14 and 7.15 provide more reliable data than the mechanical properties supplied by the manufacturer. This is because the manufacturer's data were obtained through standardised tests (European standards e.g. BN 918 145-1 and DIN 45673-1) that do not represent the track on loading condition.

Results from ballast intervention tests

Figure 7.16 presents graphs of the average four corner spring stiffness for each ballast intervention test. This shows that the spring stiffnesses increase up to a certain number of loading cycles and then gradually decrease with further loading. The spring stiffnesses produced by the area weighted method are plotted in Figure 7.17. These show that the spring stiffness increases with the number of loading cycles throughout each test. These general trends are the same as for the sleeper intervention tests.

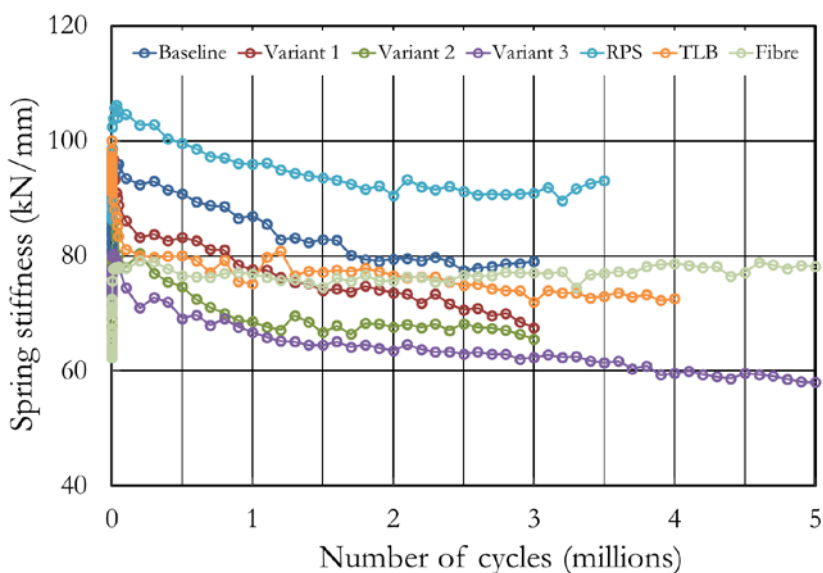


Figure 7.16: The average of four corners spring stiffness for each ballast intervention test

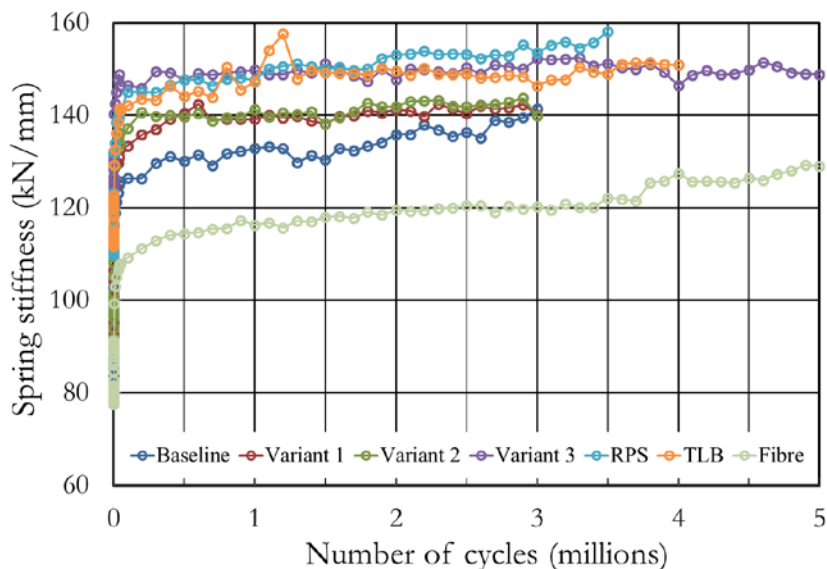


Figure 7.17: The average of spring stiffness obtained by area weighted method for each ballast intervention test

Discussion of spring stiffness results for ballast intervention tests

In Figure 7.16, the test on fibre reinforced ballast showed a markedly different behaviour from the other tests. In this test after reaching a value of about 75kN/mm early on, the four corner spring stiffness remained consistently at this value and did not show the reduction with increasing loading cycles apparent in the other ballast intervention tests. It is hypothesised that this may be explained by the mobilisation of tensile strength in the fibres with ongoing settlement with loading cycles, thus restricting lateral movement or in effect providing confining stress to the ballast below the sleeper ends and in the shoulders.

Table 7.11 presents a comparison for the four corner spring stiffness values from the ballast intervention tests.

Table 7.11: Average four corner spring stiffness and percentage reduction of spring stiffness into baseline test at number of loading cycles of each ballast intervention test

Test label	Total loading cycles applied (millions)	Spring stiffness (kN/mm) at			Percentage reduction or increase of spring stiffness (%) at		
		Loading cycles (millions)			Loading cycles (millions)		
		1	2	3	1	2	3
Baseline	3.0	86.95	79.48	79.03	-	-	-
Variant 1	3.0	77.63	73.61	67.53	10.7	7.4	14.6
Variant 2	3.0	68.59	67.61	65.54	21.1	14.9	17.1
Variant 3	5.0	66.76	63.55	62.36	23.2	20.0	21.1
RPS	4.0	95.96	90.54	90.93	-10.4	-13.9	-15.1
TLB	3.5	75.17	76.60	71.98	13.5	3.6	8.9
Fibre	5.0	76.84	75.68	77.06	11.6	4.8	2.5

Table 7.11 shows that at 3 million loading cycles, the RPS test produced the highest average four corner spring stiffness (15% higher than the baseline test). This agrees with the finding of Selig (1980) that confinement from the ballast shoulder increases the support stiffness. However, the spring stiffnesses produced by other ballast intervention tests were lower than the baseline test. The ballast grading variants 1, 2, and 3 produced spring stiffnesses 15%, 17% and 21% lower respectively than the baseline test. The TLB and fibre reinforced tests also produced spring stiffness 9% and 2.5% lower respectively than the baseline test.

The spring stiffness obtained by the area weighted method (Figure 7.17) shows that apart from the fibre reinforced ballast test, all other tests produced higher spring stiffness than the baseline test. A comparison of area weighted spring stiffnesses is presented in Table 7.12.

Table 7.12: Area weighted spring stiffness and percentage increase of spring stiffness into baseline test at number of loading cycles of each ballast intervention test

Test label	Total loading cycles applied (millions)	Spring stiffness (kN/mm) at			Percentage reduction or increase of spring stiffness (%) at		
		Loading cycles (millions)			Loading cycles (millions)		
		1	2	3	1	2	3
Baseline	3.0	132.82	135.82	141.44	-	-	-
Variant 1	3.0	139.12	141.15	140.07	4.7	3.9	-1.0
Variant 2	3.0	141.25	141.83	139.86	6.3	4.4	-1.1
Variant 3	5.0	149.80	147.71	152.24	12.8	8.8	7.6
RPS	4.0	147.59	153.08	153.51	11.1	12.7	8.5
TLB	3.5	147.17	149.59	146.34	10.8	10.1	3.5
Fibre	5.0	116.32	119.48	120.27	-12.4	-12.0	-15.0

In Figure 7.17, ballast grading variants 1 and 2 produced spring stiffnesses higher than the baseline test almost throughout the entire number of loading cycles applied. However, at 3 million loading cycles, their spring stiffness was almost the same as the baseline test. Tests on ballast grading variant 3 and TLB produced spring stiffness 8% and ~4% higher respectively than the baseline test. However, the test on the RPS slope produced the highest spring stiffness, 9% higher than that of baseline test. The test on fibre reinforced ballast produced a spring stiffness 15% lower than the baseline test.

Comparing Figures 7.16 and 7.17 shows that the four corner and the area weighted spring stiffnesses are different. This is because the four corner spring stiffness was analysed using the data from measurements at the location of sleeper ends only where these locations have less ballast confinement than the middle section on the mono-block sleeper, while the area weighted spring stiffness was determined using all the measurement data available on the sleeper. The area weighted spring stiffnesses produced in all ballast intervention tests (Figure 7.17) also showed a trend of increasing spring stiffness with number of loading cycles. This agrees with the trend of spring stiffness in the sleeper intervention tests. This means that the trend of area weighted spring stiffness is consistent and suitable for comparison as well as being more reliable than the four corner spring stiffness.

7.2.4 Ballast pressure

As described in Section 6.5.4, data from pressure plates 1 and 4 are used to compare the results from tests using mono-block sleepers while pressure plate 3 is used to compare results from tests using twin-block sleepers. To assess if this is a reasonable basis for comparison, in the tests on G44 and twin-block sleepers on the current standard NR ballast grading, the maximum and minimum pressures recorded from each plate are plotted against number of loading cycles (Figures 7.18 and 7.19 respectively).

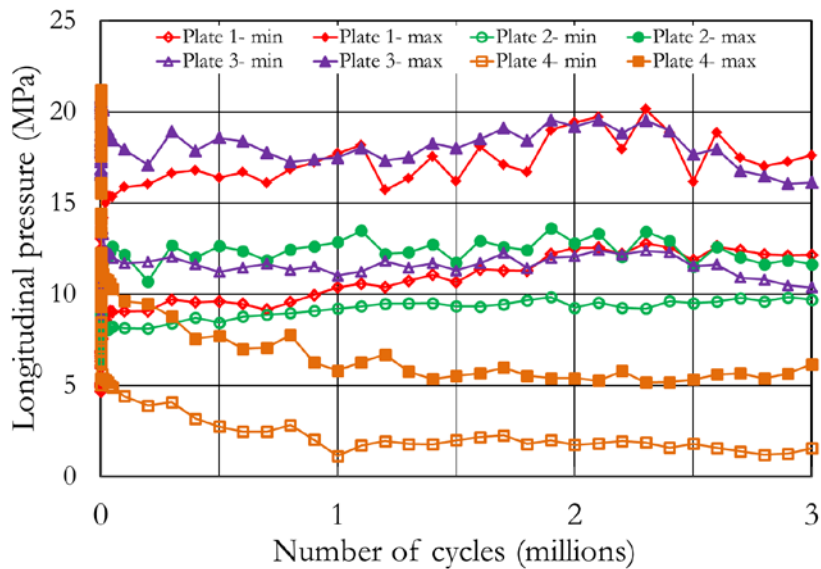


Figure 7.18: The behaviour of pressure at longitudinal direction of each plate in G44 sleeper test

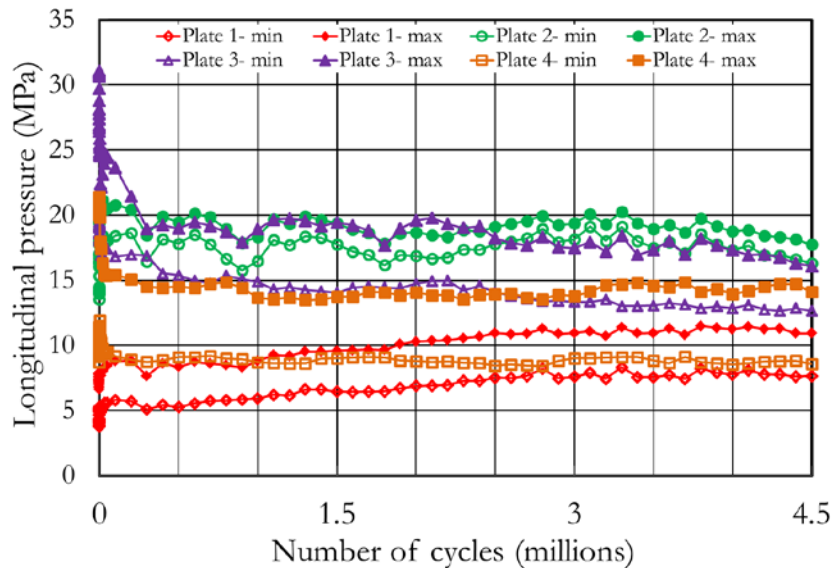


Figure 7.19: The behaviour of pressure at longitudinal direction of each plate in twin-block sleeper test

In the tests using mono-block sleepers (Figure 7.18), the pressure at plate 1 tends to increase with the number of loading cycles while at plate 4, the pressure tends to reduce with the number of loading cycles. This may be because the ballast in the middle section of the apparatus was more constrained by both vertical pressures from the sleeper and the greater distance to the ballast shoulder. At the shoulder areas near plate 4, the confinement was from a relatively small volume of adjacent ballast. Therefore it is considered that comparison of these two plates under opposing conditions (maximum and minimum ability of ballast to strain) will provide the most consistent insight into the behaviour of the ballast over the duration of the tests. For the pressure plate used in the twin-block sleeper tests, the pressure of each plate tends to move toward a steady magnitude with increasing number of loading cycles (Figure 7.19). This behaviour may be a result of the shape of the twin-block sleeper, which gives a symmetric loading condition into the locations of pressure plate 3 (described in Section 6.5.4). Therefore it was a correct decision to compare the pressure in the ballast based on plate 3.

There were only two types of sleeper shape used in this research, therefore to compare the results within the same boundary conditions, ballast pressure is compared based on the sleeper shape; mono-block and twin-block sleepers.

Results from the mono-block sleeper tests

There were twelve tests (Section 6.7.2) carried out using mono-block sleepers. For these tests the behaviour of ballast pressure of plate 1 and 4 under the maximum and minimum loads for mono-block sleepers are presented in Figures 7.20 to 7.23.

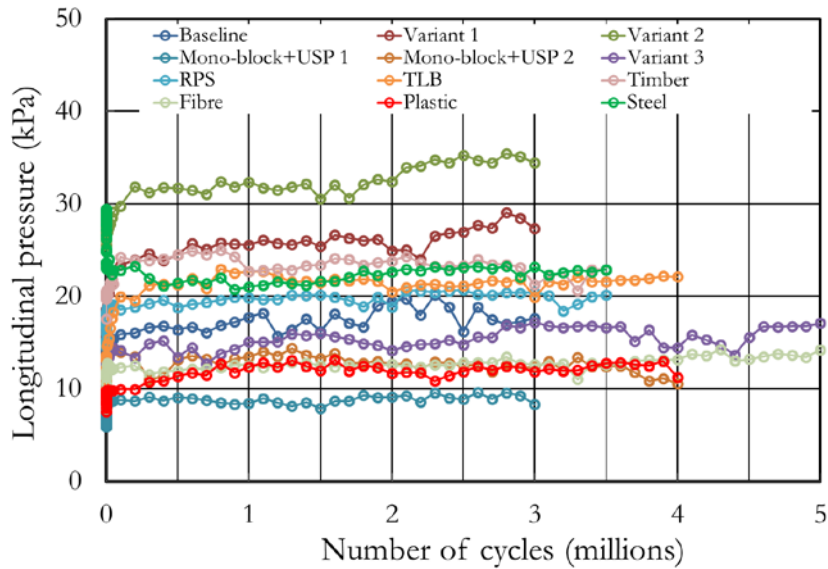


Figure 7.20: Variation of maximum longitudinal pressure of plate 1 with the number of loading cycles for mono-block sleeper

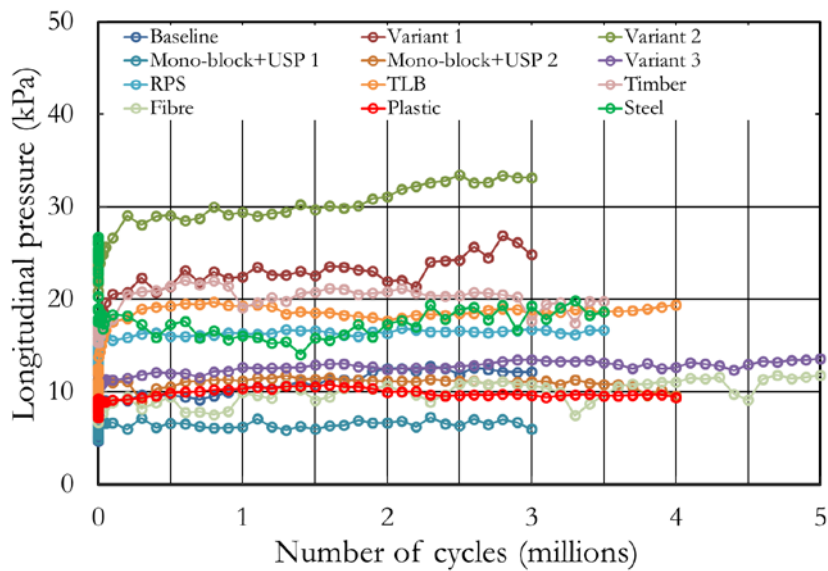


Figure 7.21: Variation of minimum longitudinal pressure of plate 1 with the number of loading cycles for mono-block sleeper

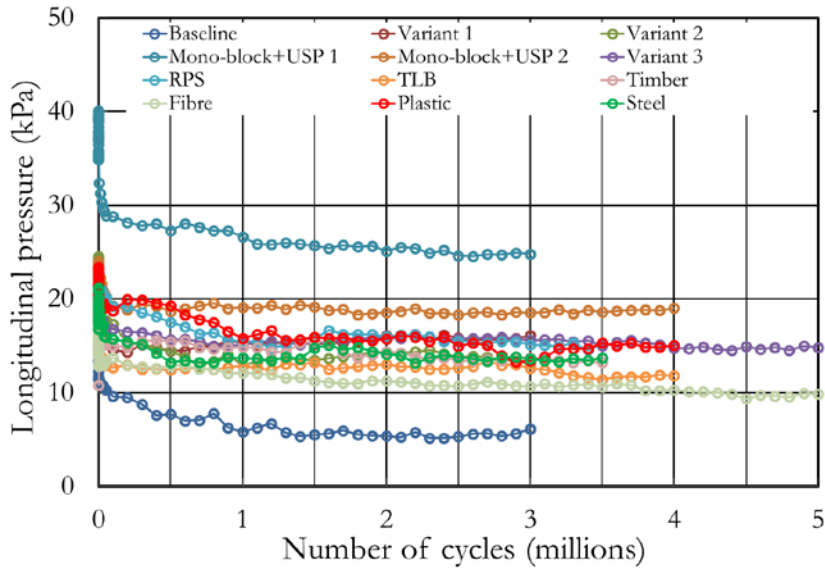


Figure 7.22: Variation of maximum longitudinal pressure of plate 4 with the number of loading cycles for mono-block sleeper

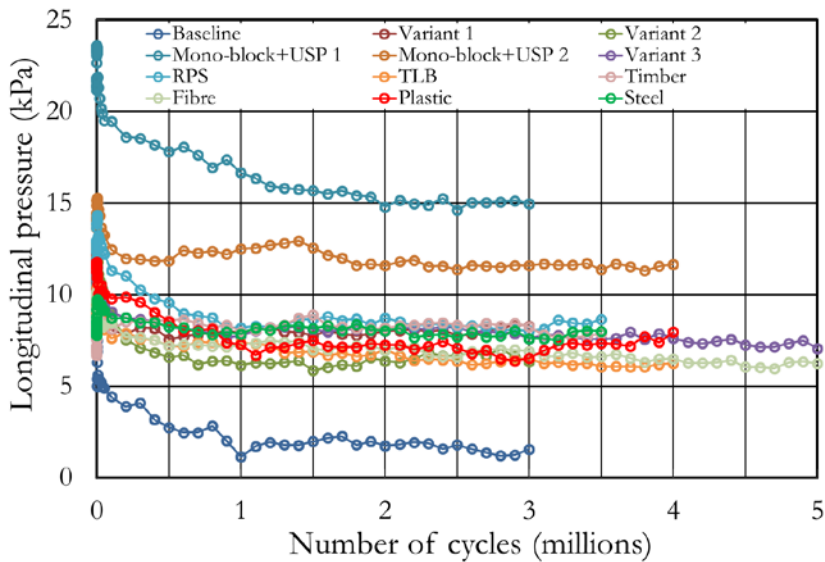


Figure 7.23: Variation of minimum longitudinal pressure of plate 4 with the number of loading cycles for mono-block sleeper

Discussion of ballast pressure results for mono-block sleeper tests

Both the maximum and minimum ballast pressures (Figures 7.20 to 7.23) show various initial magnitudes. These relate to the initial condition of ballast (as placed) and on the number of ballast particles in contact with the plates. This leads to a difficulty in normalising and comparing the magnitude of pressure to the same initial state. However, the behaviour of pressure under cyclic loading can still be observed and compared.

In each test, the ballast pressure at plate 1 (at the middle section of sleeper/centre of the track) showed a similar trend of an increase with the number of loading cycles (Figure 7.20 and 7.21). An increase in longitudinal pressure at the middle section of sleeper also indicates the densification of ballast at the central line of track. However, there is no clear pattern to the development of ballast pressure in the middle section of the track caused by the modification introduced either to ballast or sleeper.

A uniform trend was also shown by pressure plate 4 in each test. However, an opposite behaviour to that of pressure plate 1 was noted. The ballast pressure at pressure plate 4 decreased rapidly during the initial loading cycles (Figures 7.22 and 7.23), and a gradual reduction continued with further loading cycles until it reached a constant value. A reduction in ballast pressure implies a reduction in ballast confinement in this zone. This behaviour was consistent and supported the earlier findings of the average four corner spring stiffness and deflections in the tests without the inclusion of USPs, which showed a reduction of spring stiffness and an increase in deflection with number of loading cycles. This behaviour also agrees with previous work by Lackenby et al (2007), who stated that ballast confinement (confining pressure) has a significant influence on ballast surface stiffness.

Although the initial magnitudes of ballast pressure at plate 4 in each test were different, it seems that the introduction of USPs was the most effective way to keep the longitudinal pressure in the shoulder areas relatively high.

Result from twin-block sleeper tests

Three tests were carried out using twin-block sleepers (Section 6.7.2). As stated in section 6.5.4, for comparison the results from pressure plate 3 were used. This was not only because the location of plate 3 (Figure 6.46) was at the most critical location (near the load applied point), but also because the ballast boundary condition was approximately the same at both ends. The ballast pressure at plate 3 under the maximum and minimum vertical loads for twin-block sleepers is presented in Figures 7.24 and 7.25.

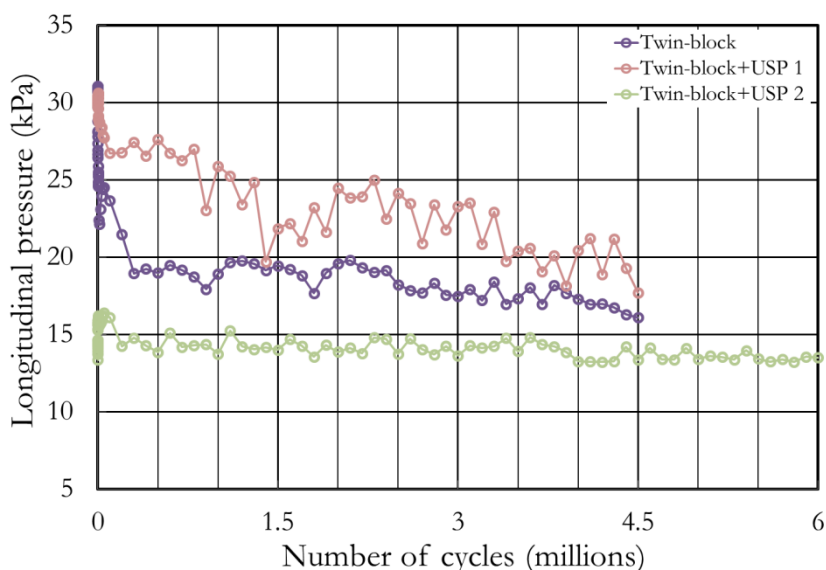


Figure 7.24: Variation of maximum longitudinal pressure of plate 3 with the number of loading cycles for twin-block sleeper

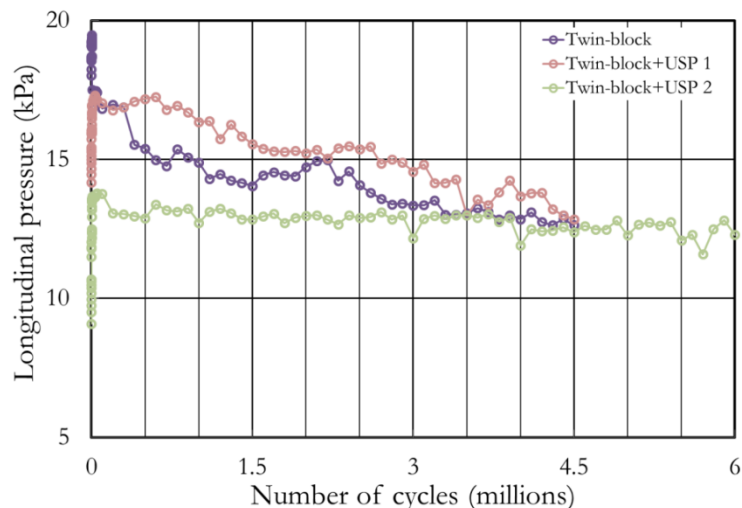


Figure 7.25: Variation of minimum longitudinal pressure of plate 3 with the number of loading cycles for twin-block sleeper

Discussion of ballast pressure results for twin-block sleeper tests

A consistent behaviour of ballast pressure is shown at pressure plate 3 in each test, in that the longitudinal pressure decreases with the number of loading cycles toward a certain magnitude. Tests carried out on twin-block sleepers also show variations of initial pressure which depended on ballast preparation. However, the behaviour always showed a movement of pressure towards a certain magnitude, regardless of the ballast pressure at the beginning of the test. The attachment of USPs to twin-block sleeper soffits seems to make no significant change to either the behaviour or the magnitude of ballast pressure at the end of the test.

7.2.5 Mobilised earth pressure ratio

In sleeper and ballast intervention tests, the maximum and minimum cyclic vertical loads (98.1kN and 5kN respectively) were converted to equivalent average pressures for the soffit area of the sleeper being tested (Table 6.10). These two average pressures, together with the pressure plate data, are used to determine the mobilised earth pressure ratio and mobilised angle of effective shearing resistance using the equations given in Section 6.5.5 for all sleeper and ballast intervention tests.

Sleeper and ballast interventions

Triaxial tests by Indraratna and Salim (2002) suggested that the apparent friction angle of latite basalt ballast was in the range 45 to 55 degrees. Using Equations 6.8 to 6.10 (in Section 6.5.5) the corresponding values of K_a , K_p and K_o for those friction angles are presented in Table 7.13.

Table 7.13: Key earth pressure ratios

Friction angle(°)	K_a	K_p	K_o
45	0.172	5.829	0.293
55	0.099	10.059	0.181

Tables 7.14 and 7.15 show the maximum and minimum vertical pressures and the corresponding mobilised earth pressure ratio based on the measured pressures, as well as the mobilised angle of effective shearing resistance (ϕ'_{mob}) implied on each test. The maximum and minimum horizontal

pressures used in the calculation were the highest and lowest measured horizontal pressures recorded by all plates for all of the loading cycles applied.

Table 7.14: Summary of the highest and lowest of measured earth pressures in data recorded by all plates for all loading cycles in sleeper intervention tests

Test ID	Average vertical pressure (kPa)		Measured Horizontal pressure (kPa)		Mobilised earth pressure ratios		ϕ'_{mob} implied by ($^{\circ}$)	
	Max	Min	Max	Min	K_{min}	K_{max}	K_{min}	K_{max}
Baseline (G44)	137.68	7.02	21.22	13.59	0.154	1.936	47.15	18.59
Plastic	150.92	7.69	23.39	15.01	0.155	1.952	47.02	18.81
Timber			24.98	22.04	0.166	2.866	45.66	28.86
Steel	171.38	8.74	29.44	26.70	0.172	3.055	44.95	30.45
Twin-block	197.94	10.09	31.07	19.47	0.157	1.930	46.77	18.51
Mono-block + USP 1	137.68	7.02	40.05	23.59	0.291	3.360	33.31	32.77
Mono-block + USP 2			23.96	15.28	0.174	2.177	44.71	21.74
Twin-block + USP 1	197.94	10.09	31.33	22.41	0.158	2.221	46.65	22.28
Twin-block + USP 2			26.56	16.99	0.134	1.684	49.79	14.76

Table 7.15: Summary of the highest and the lowest of measured earth pressures in data recorded by all plates for all loading cycles in ballast intervention tests

Test ID	Average vertical pressure (kPa)		Measured Horizontal pressure (kPa)		Mobilised earth pressure ratios		ϕ'_{mob} implied by ($^{\circ}$)	
	Max	Min	Max	Min	K_{min}	K_{max}	K_{min}	K_{max}
Baseline	137.68	7.02	21.22	13.59	0.154	1.936	47.15	18.59
Variant 1			29.03	26.87	0.211	3.828	40.66	35.86
Variant 2			35.43	33.44	0.257	4.764	36.23	40.77
Variant 3			20.73	15.69	0.151	2.235	47.53	22.44
TLB			22.96	19.69	0.167	2.805	45.54	28.32
RPS			25.02	19.97	0.182	2.845	43.79	28.68
Fibre			24.41	18.32	0.177	2.610	44.37	26.49

Although there are also data available from pressure paper instrumentation at the ballast/wall and ballast/subgrade interfaces, these data are not suitable for use to determine the mobilised earth pressure ratio. This is because the pressure paper recorded a cumulative contact area and the highest particle pressure within the entire loading testing applied, which may provide higher results. The data from the pressure paper may be valid for analysing the mobilised earth pressure ratio only if the true contact is known, whereas the area recorded on the pressure paper developed with number of loading cycles applied (described in a later section).

Discussion of mobilised earth pressure ratio

The pressures measured on the plates tended to increase, reduce or stay at the same with loading cycles depending on their position. The final pressure distributions are reflected in the mobilised earth pressure ratios based on an average vertical pressure on the sleeper soffit. At the maximum and minimum vertical pressures, the mobilised earth pressure ratio moves towards the active and passive conditions respectively. This can be seen by comparing K_{max} and K_{min} in Tables 7.14 and 7.15 to Table 7.13. The mobilised earth pressure ratios at the minimum vertical load are between 1.5 and 5. These are significantly above the estimated normal consolidation earth pressure ratio obtained using the method of Jaky (1948)(Table 7.13). This is because ballast at the minimum load is effectively overconsolidated (Brooker and Ireland, 1965).

The mobilised angle of effective shearing resistance in sleeper and ballast intervention tests at the maximum and minimum vertical pressures was found to be in the range of 14 to 50 degrees (Tables 7.14 and 7.15) based on a simplified methodology. This range agrees with conclusion of Shenton (1978) that the mobilised earth pressure ratio varies indicating that the ballast was acting more as a structure than as an elastic continuum. In Table 7.15, it is also shown that the introduction of proportion of finer particles into the current standard of NR ballast grading to be variant gradings is able to reduce structural behaviour of ballast toward continuum where the mobilised angle of effective shearing resistance (ϕ'_{mob}) implied by K_{max} increases significantly. The peak of this range perhaps indicates the maximum shearing resistance of the ballast. A 50 degrees is in close agreement with the data collected by Aingaran (2014). It also appears in Le Pen et al (2014a) and the results of previous research carried out by for example: Shenton (1978), Stewart et al (1985), Indraratna and Salim (2002), Indraratna et al (2006a), Rujikiatkamjorn et al (2012), Aingaran (2014) and Ajayi (2014), although the work carried out by the last two were on scaled ballast. Shenton (1978) investigated limestone ballast using four different sizes using triaxial tests. The confining pressures used for the tests were 20kN/m², 40kN/m² and 60kN/m² to represent the range expected to be encountered by ballast on a normal railway. The mobilised angle of effective shearing resistance obtained in these tests was 56 degrees, which is slightly higher than the range inferred from the tests using the modified SRTF apparatus. Stewart et al (1985) carried out ballast box tests (Chapter 5) and considered that for ballast, a higher mobilised angle of effective shearing resistance was possible at a low vertical pressure. The results from ballast box tests also suggested that the mobilised angle of effective shearing resistance was in the range 45.5 to 56.5 degrees. Research by Indraratna and Salim (2002) and Indraratna et al (2006a) showed an angle of effective shearing resistance of 55.5 degrees at a lower confining pressure of 10kPa.

7.2.6 Pressure paper

Pressure paper was placed at selected locations in all tests (for details see Section 6.5.6). In this Section, results from the pressure paper present in sleeper and ballast intervention tests are presented and compared. Parts of the work reported in this section have been written up in collaboration with the project supervisors and are currently being reviewed for publication (Abadi et al., 2013, Abadi et al., 2014, Abadi et al., "in review").

Results from sleeper and ballast intervention tests

To investigate the influence of sleeper and ballast interventions, fifteen tests are reported in this thesis. All tests were carried out to at least 3 million loading cycles with some tests continued to up to 6 million loading cycles (Tables 6.25 and 6.26). The grade of pressure paper used in what was intended to be the baseline test on a G44 sleeper with the current standard NR ballast grading was subsequently found to have an unsuitable pressure range. Thus for comparative purposes the test on a G44 sleeper with ballast grading variant 1 is used as the baseline. This is considered acceptable because the performance of this ballast grading was found to be almost identical to the current standard NR ballast grading in terms of overall permanent settlement (section 7.2.1) and spring stiffness (section 7.2.3). Also, the relatively small quantity of finer material used in variant 1 meant that the grading remained close to the current standard NR ballast grading (Table 6.14 and Figure

6.50) and should provide approximately the same number of potential contacts estimated by Equation 6.13 (values given later).

The results allow an evaluation of the relative merits of the sleeper type, ballast grading, and modification to the sleeper/ballast interface through the provision of USPs. Furthermore, in addition to the comparison with other tests, the number of contacts for each arrangement is also compared with the number of contacts potentially available for a given grading based on a simplified method of analysis.

The results are presented and categorised for each interface where pressure paper was present at: 1) sleeper/ballast; 2) ballast/subgrade and 3) ballast/wall.

Sleeper/ballast interface

At the sleeper/ballast interface, pressure paper recorded the number and area of contacts between ballast and sleeper soffit as well as the magnitude of pressure. For the pressure paper placed at this location, it was found that the contacts could reliably be recorded using pressure paper rated 10 to 50MPa (as described in Section 6.4.2). Over the course of the cyclic loading, the pressure paper was abraded and wore through at a small number of less stable particle/sleeper contacts, which moved about from cycle to cycle. This had implications for the measurements taken. Where the pressure paper wore through, a surrounding area of red meant that contacts could still be counted and their area reconstructed using a hole filling function as described in Section 6.5.6. However, due to the abraded locations, it was difficult to obtain representative image for MATLAB code for reliably analysing the highest magnitude of particle pressure present.

In the test with the steel sleeper, no pressure paper could be placed at the sleeper/ballast interface owing to the hollowed out sleeper shape.

Figures 7.26 to 7.32 show a comparison with variant 1 (baseline) of the contacts recorded by pressure paper located at the sleeper soffit for mono-block sleepers made of different materials (Figure 7.26); an increase in the amount of finer material in the ballast (Figure 7.27), the modified two layer ballast system (Figure 7.28), a re-profiled ballast shoulder slope (Figure 7.29), fibre reinforced ballast (Figure 7.30) and the presence of USPs on G44 (Figure 7.31) and twin-block (Figure 7.32) sleepers.

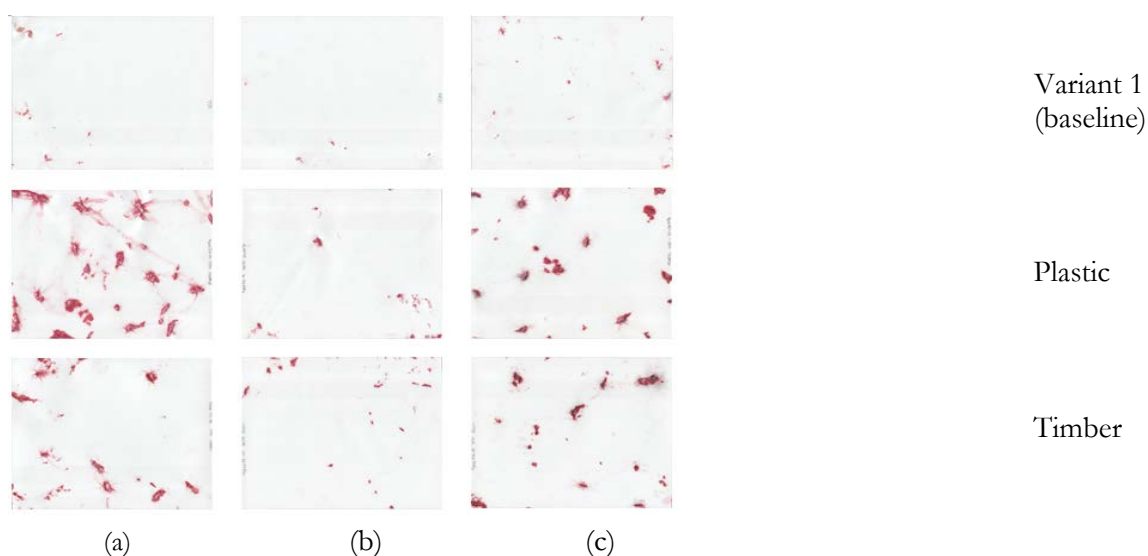


Figure 7.26: Particle contact histories at the sleeper/ballast interface under the railseat (a, c) and the centre of the sleeper (b): mono-block sleeper, effect of sleeper material

In Figure 7.26, it can be seen that the contacts beneath the railseats are more pronounced. This can be explained as a result of particles nearer the sleeper ends being more easily displaced towards the sleeper ends owing to the relatively lower confinement compared with the sleeper middle. The larger red marks therefore represent a merging of all the contact locations of individual particles that have moved around. It is also worth noting that in general these larger marks are later counted as individual contact locations. Figure 7.27 shows that as the proportion of finer particles increases, the number of contacts increases.

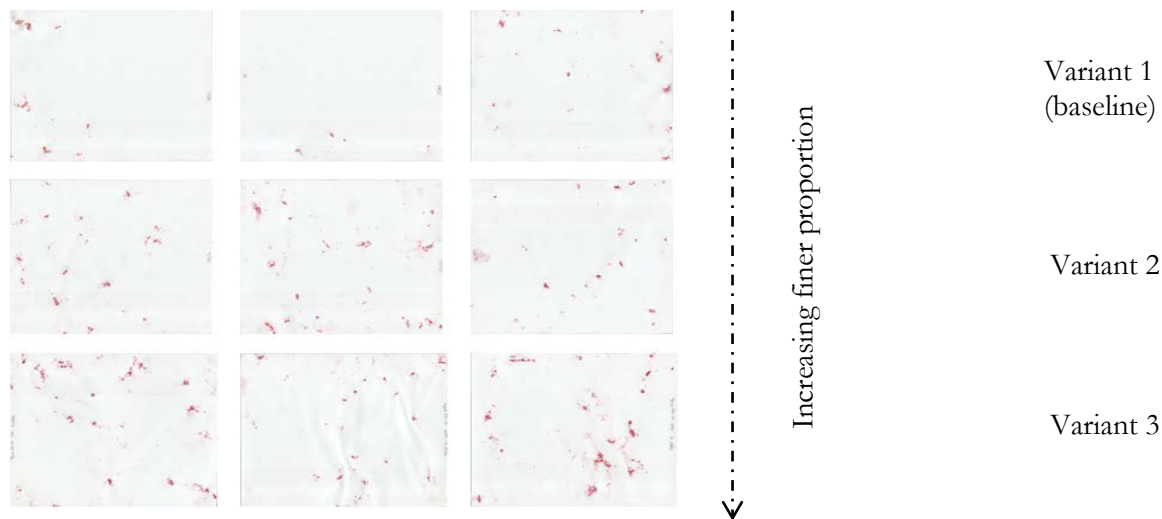


Figure 7.27: Particle contact histories at the sleeper/ballast interface: G44 sleeper, effect of increasing the proportion of fine material in the ballast

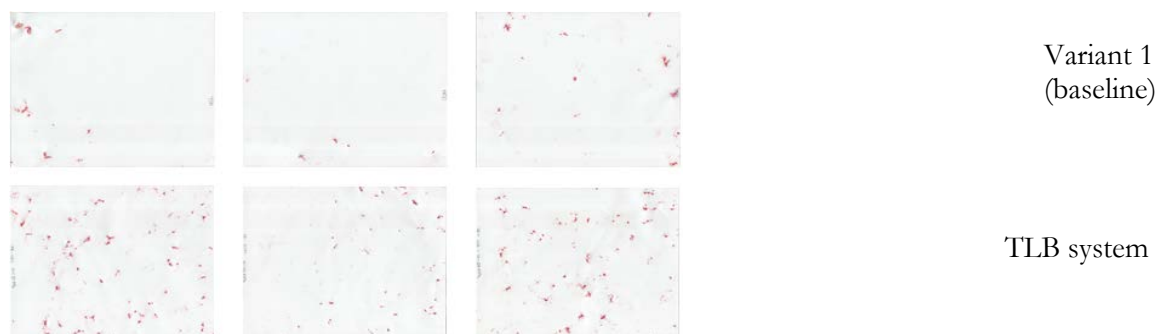


Figure 7.28: Particle contact histories at the sleeper/ballast interface: G44 sleeper, effect of a modified TLB system

In Figure 7.28 the contacts appear more uniformly distributed for the two layered ballast test which had the finest grading. More contacts are also present in the RPS slopes and fibre reinforced ballast (Figures 7.29 and 7.30), although many of these are small and difficult to distinguish.

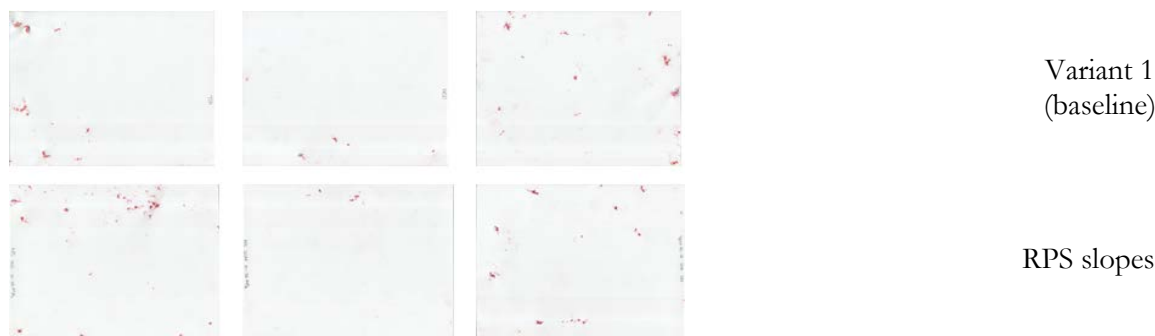


Figure 7.29: Particle contact histories at the sleeper/ballast interface: G44 sleeper, effect of a RPS slope

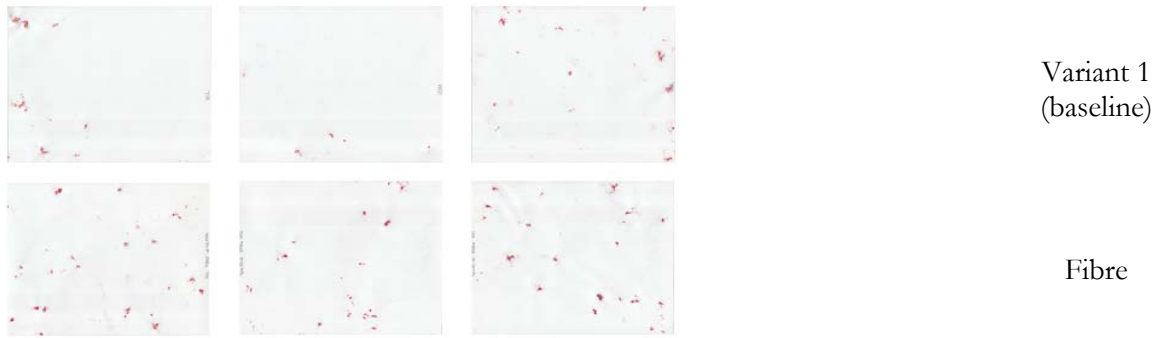


Figure 7.30: Particle contact histories at the sleeper/ballast interface: G44 sleeper, effect of fibre reinforced ballast

For the bottom left image in Figure 7.31, some blue colour distortion is apparent around the edge of this piece of paper caused by moisture from the ballast which was not completely dry when it was placed into the modified SRTF apparatus. However this blue distortion did not interfere with the red intensity data. For the tests in which USPs were fitted to both G44 and twin-block concrete sleepers, individual particle contacts were clearly present over larger areas than for the same sleeper without the USP (Figures 7.31 and 7.32).

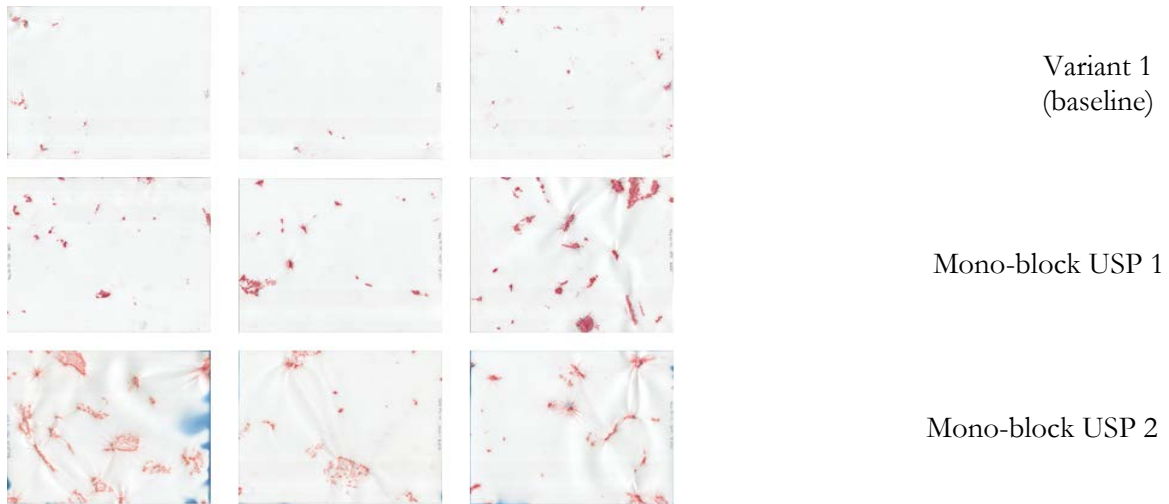


Figure 7.31: Particle contact histories at the sleeper/ballast interface: G44 sleeper, effect of USPs

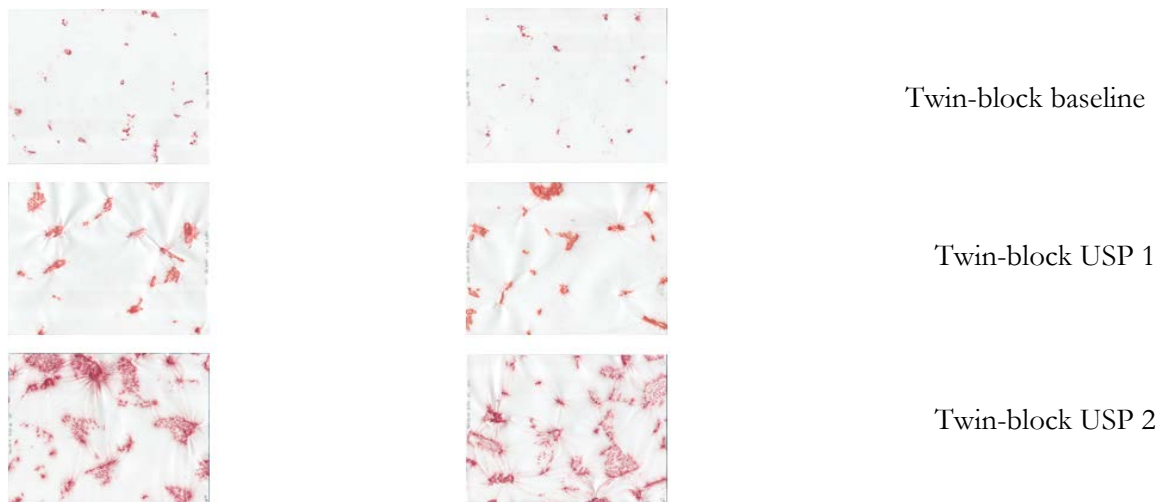


Figure 7.32 Particle contact histories at the sleeper/ballast interface: twin-block concrete sleeper, effect of USPs

Tables 7.16 and 7.17 present the numbers of contact recorded by pressure paper at each location at each sleeper/ballast interface and normalised for the full area of the sleeper/ballast interface present

in each test (i.e. the number of contacts for all pressure paper present in that test was multiplied by the ratio of the area of pressure paper present to the area of the sleeper soffit).

Table 7.16: The number of particle contact at sleeper/ballast interface in sleeper intervention tests

Test ID	Sleeper	Number of contact on the pressure paper at			Contact per sleeper, 10-50MPa pressure paper
		Left railseat	Middle	Right railseat	
Variant 1	G44	11	4	16	147
Plastic	Plastic	40	18	25	360
Timber	Timber	37	32	28	420
Twin-block	Twin-block	7	N/A	26	164
		18		31	243
Mono-block + USP 1	G44	21	17	28	314
Mono-block + USP 2		37	26	31	447
Twin-block + USP 1	Twin-block	28	N/A	26	268
Twin-block + USP 2	Twin-block	Sleeper soffit area was covered by pressure paper			329

Table 7.17: The number of particle contact at sleeper/ballast interface in ballast intervention tests

G44 sleeper		Number of contact on the pressure paper at			Contact per sleeper, 10-50MPa pressure paper
Test ID	Ballast grading	Left railseat	Middle	Right railseat	
Variant 1	Increasing finer proportion	11	4	16	147
Variant 2		23	24	26	347
Variant 3		65	52	59	836
TLB	Two layered	94	69	113	1,311
RPS	NR	43	21	31	451
Fibre		29	25	28	390

Tables 7.18 and 7.19 present the percentage contact area recorded on pressure paper at each location and the average contact area per sleeper. This is the percentage of red area over the pressure paper. Given that the areas of red were not necessarily all under pressure at the same time, this is likely to be an overestimate of the actual area of contact at any given time.

Table 7.18: The percentage of particle contact area at sleeper/ballast interface in sleeper intervention tests

Test ID	Sleeper	Percentage of contact area recorded on the pressure paper at			Percentage of contact area per sleeper, 10-50MPa pressure paper
		Left railseat	Middle	Right railseat	
Variant 1	G44	0.21	0.05	0.29	0.18
Plastic	Plastic	5.98	0.53	2.72	3.08
Timber	Timber	2.35	0.65	1.69	1.56
Twin-block	Twin-block	0.08	N/A	0.23	0.16
		0.69		0.37	0.53
Mono-block + USP 1	G44	0.74	0.93	3.25	1.64
Mono-block + USP 2		1.54	0.60	1.02	1.05
Twin-block + USP 1	Twin-block	2.50	N/A	3.31	2.91
Twin-block + USP 2	Twin-block	Sleeper soffit area was covered by pressure paper			4.75

Table 7.19: The percentage of particle contact area at sleeper/ballast interface in ballast intervention tests

G44 sleeper		Percentage of contact area recorded on the pressure paper at			Percentage of contact area per sleeper, 10-50MPa pressure paper
Test ID	Ballast grading	Left railseat	Middle	Right railseat	
Variant 1	Increasing finer proportion	0.21	0.05	0.29	0.18
Variant 2		0.35	0.50	0.28	0.38
Variant 3		0.68	0.34	0.86	0.63
TLB	Two layered	0.69	0.25	0.62	0.52
RPS	NR	0.32	0.04	0.24	0.20
Fibre		0.42	0.30	0.47	0.40

A further approximation was introduced by the assumption that the proportions of contact area are the same over the pressure paper and over the sleeper as a whole. Although the pressure determined by RI analysis of the pressure paper is not considered reliable and so discarded from the data presented in this Section, an estimate of the apparent average contact pressure may be made by dividing the maximum applied load by the contact area.

The results of the analysis are presented in Tables 7.20 and 7.21.

Table 7.20: The number and area of particle contacts at the ballast/sleeper interface in each test, and the implied average contact pressure

Test ID	Notes	Number of contacts per sleeper, 10-50MPa pressure paper	Percentage contact area per sleeper, 10-50MPa pressure paper	Average contact pressure (MPa)
Variant 1		147	0.18	76.5
Plastic	NR	360	3.08	4.9
Timber		420	1.56	9.7
Twin-block		243	0.53	37.3
Mono-block + USP 1	Stiff	314	1.64	8.4
Mono-block + USP 2	Soft	447	1.05	13.1
Twin-block + USP 1	Stiff	268	2.91	6.8
Twin-block + USP 2	Soft	329	4.75	4.2

Table 7.21: The number and area of particle contacts at the ballast/sleeper interface in each test, and the implied average contact pressure

Test ID	Notes	Number of contacts per sleeper, 10-50MPa pressure paper	Percentage contact area per sleeper, 10-50MPa pressure paper	Average contact pressure (MPa)
Variant 1	Increasing finer proportion	147	0.18	76.5
Variant 2		347	0.38	36.2
Variant 3		836	0.63	21.9
TLB	Two layered	1311	0.52	26.5
RPS	NR	451	0.20	68.8
Fibre		390	0.40	34.4

Although the analysis of pressure paper is not determined as the same way as AREMA's approach, where pressure paper provides the actual contact area while AREMA uses a larger averaged sleeper contact, it can be seen that these average contact pressures based on the measured area of sleeper/ballast contacts are many times greater than those estimated using the AREMA approximation of Equation 5.41, which gives 210kPa for a G44 sleeper.

At the base of the ballast layer

It was difficult to count the contact points at the ballast to rubber mat interface owing to the overlapping of red patches. However, the presence of the rubber mat meant there was less abrasion and lower maximum stresses at the contacts so that no wear holes appeared.

Figures 7.33 to 7.39 show the pressure paper sheets with a range of 2.5-10MPa placed at the base of the ballast layer, after each test.

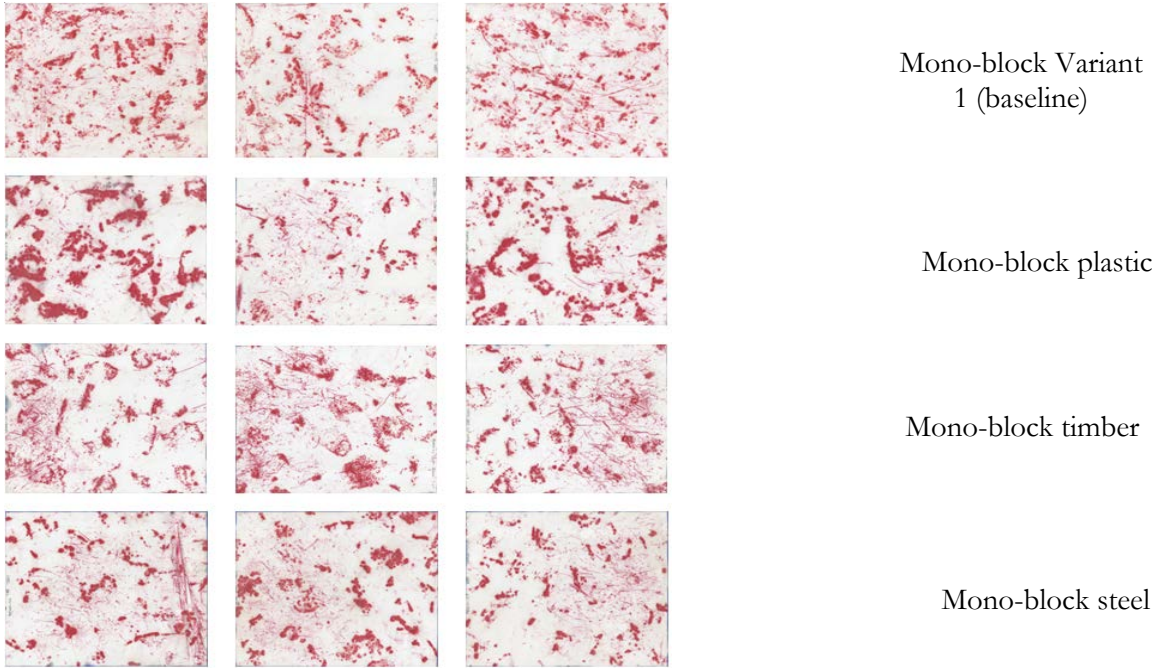


Figure 7.33. Contact areas recorded at the ballast/subgrade interface with mono-block sleepers made of different materials

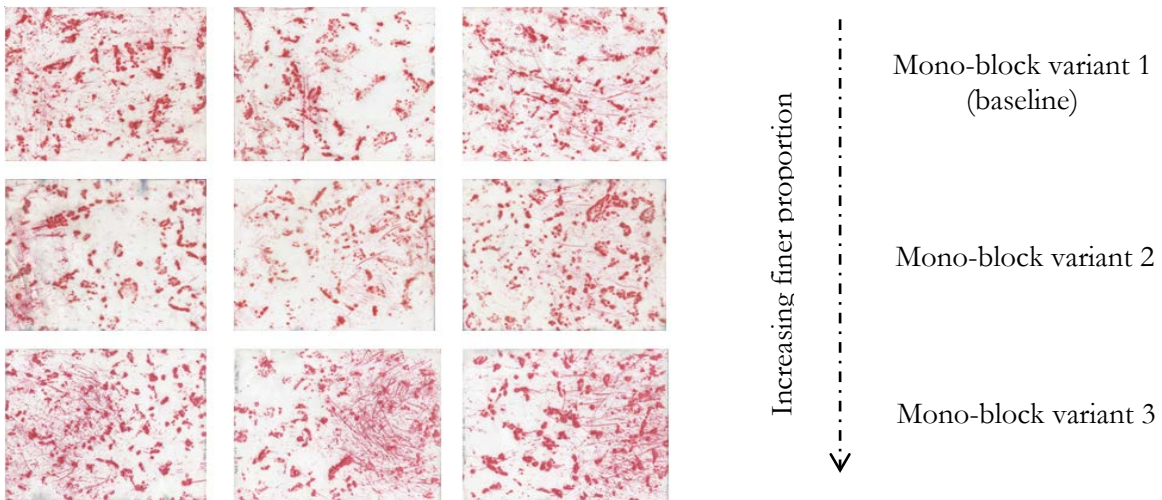


Figure 7.34: Contact areas recorded at the ballast/subgrade interface with G44 sleepers and effect of increasing the proportion of fine material in the ballast

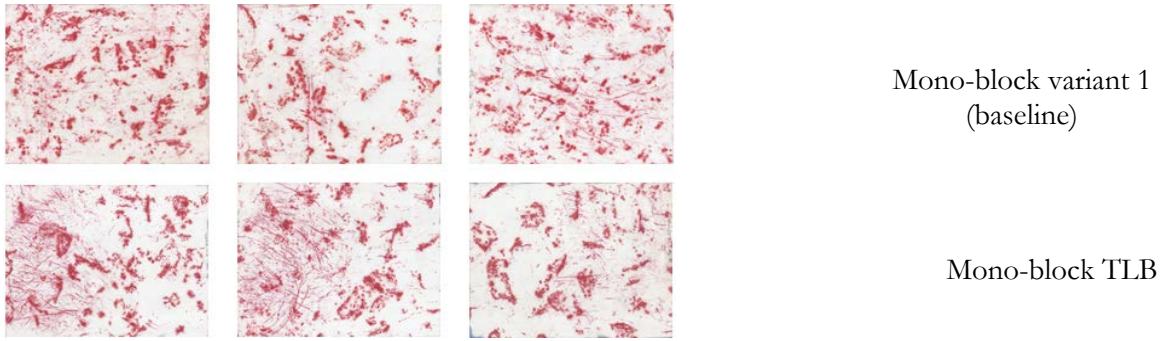


Figure 7.35. Contact areas recorded at the ballast/subgrade interface with G44 sleepers and TLB system

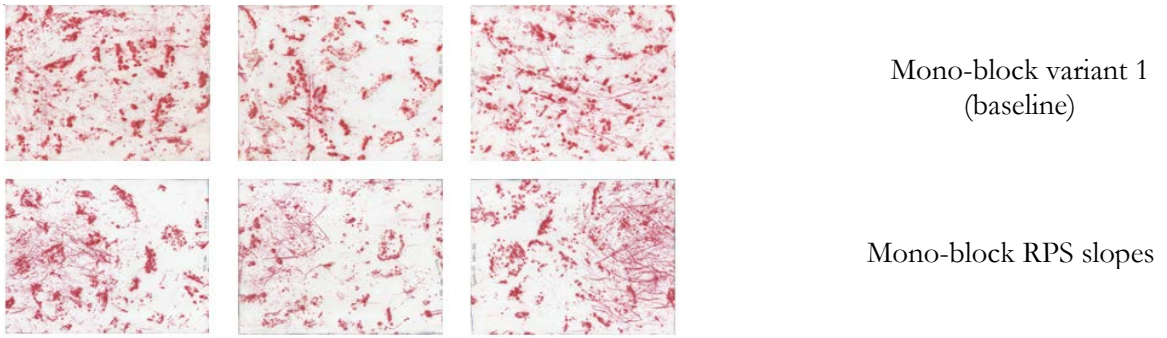


Figure 7.36: Contact areas recorded at the ballast/subgrade interface with G44 sleepers and RPS slopes

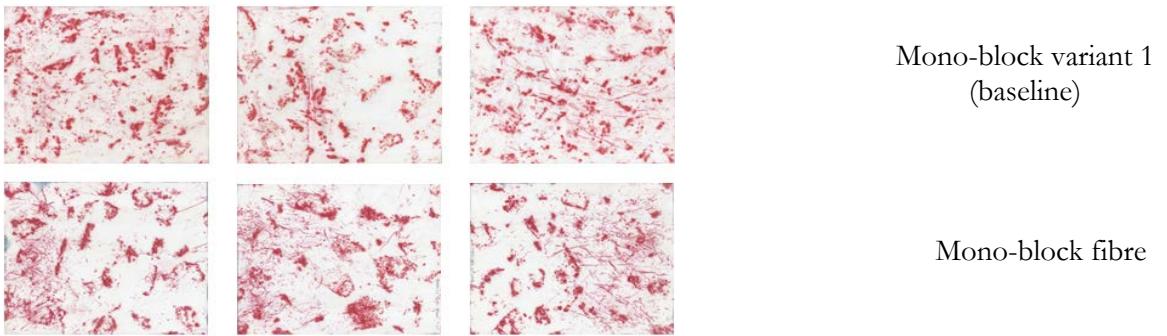


Figure 7.37: Contact areas recorded at the ballast/subgrade interface with G44 sleepers and fibre reinforced

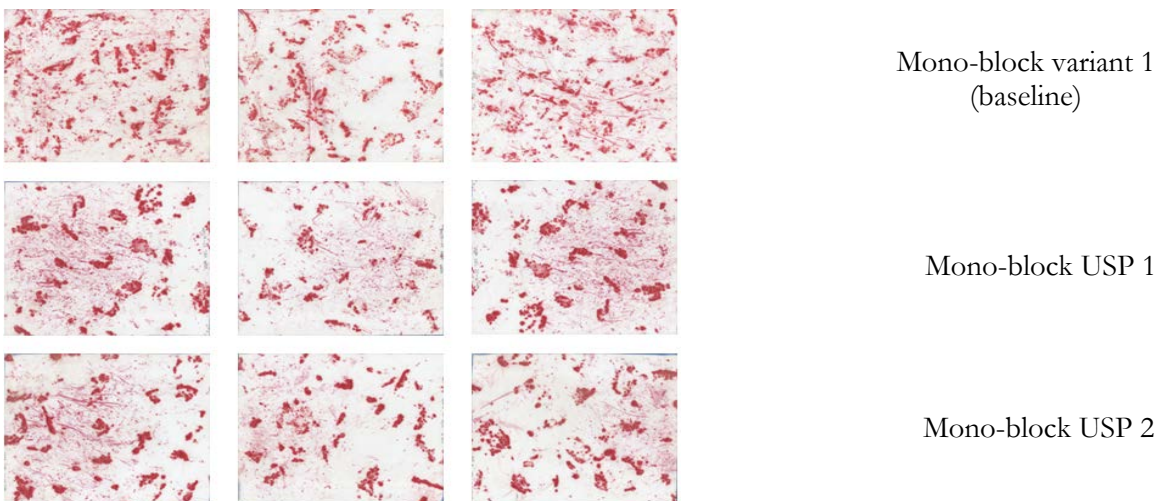


Figure 7.38: Contact areas recorded at the ballast/subgrade interface with G44 sleeper and USPs

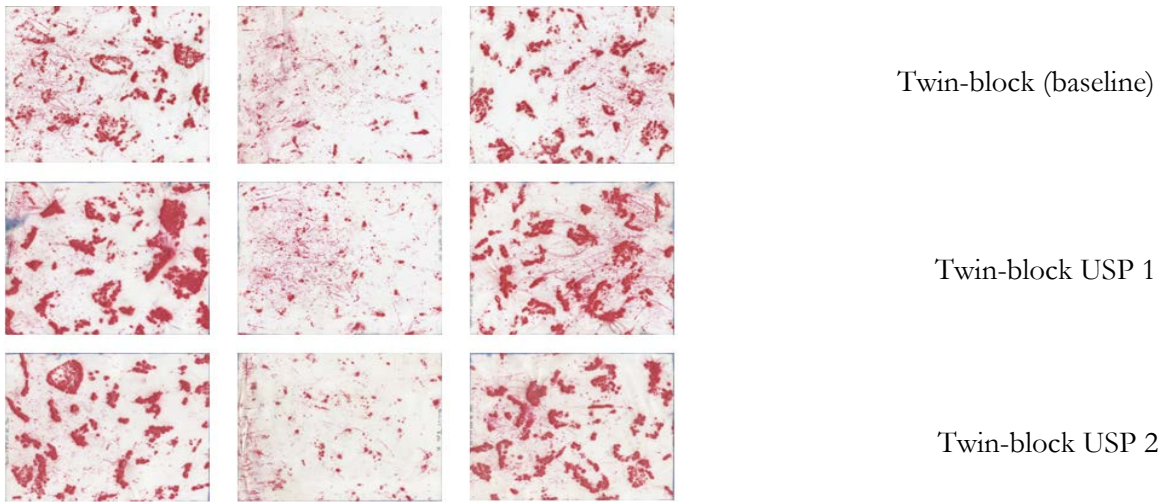


Figure 7.39. Contact areas recorded at the ballast/subgrade interface with a twin-block concrete sleeper and USPs

In general (Figures 7.33 to 7.39), the pressure paper below the railseats shows more red and evidence of individual contacts migrating sideways from under the sleeper. It is also apparent that the central pressure paper below the twin-block sleeper has a much reduced contact area, which may be explained by the shape of the sleeper.

Tables 7.22 to 7.25 present the percentage of contact area at ballast/subgrade interface recorded on the pressure paper with the pressure range of 2.5-10MPa and 10-50MPa which show that the contact areas at the ballast/subgrade interface are substantially greater than the contact areas at the sleeper/ballast interface (Tables 7.18 and 7.19). This is attributed to the particles pushing into the rubber mat to different degrees, giving a larger area of contact and a wider range of pressures with lower maximum values.

Table 7.22: Proportions of the ballast/subgrade interface area over which the contact pressure is at least 0.5MPa in sleeper intervention tests

Test ID	Sleeper	Percentage of contact area recorded on the pressure paper at the location of			Average % contact area on the subgrade, by 2.5-10MPa rated paper (> 0.5MPa)
		Left railseat	Middle	Right railseat	
Variant 1	G44	14.42	9.80	12.25	12.16
Plastic	Plastic	20.91	7.02	17.21	15.05
Timber	Timber	12.59	13.56	12.18	12.78
Steel	Steel	11.23	13.75	8.62	11.20
Twin-block	Twin-block	10.74	3.13	7.48	7.12
		13.19	4.25	13.52	10.32
Mono-block + USP 1	G44	12.81	6.89	17.52	12.41
Mono-block + USP 2		12.76	9.04	10.4	10.73
Twin-block + USP 1	Twin-block	22.70	5.12	21.05	16.29
Twin-block + USP 2	Twin-block	16.95	3.35	18.35	12.88

Table 7.23: Proportions of the ballast/subgrade interface area over which the contact pressure is at least 0.5MPa in ballast intervention tests

G44 sleeper		Percentage of contact area recorded on the pressure paper at the location of			Average % contact area on the subgrade, by 2.5-10MPa rated paper (> 0.5MPa)
Test ID	Ballast grading	Left railseat	Middle	Right railseat	
Variant 1	Increasing finer proportion	14.42	9.80	12.25	12.16
Variant 2		10.72	7.43	12.15	10.10
Variant 3		16.41	15.42	18.80	16.88
TLB	Two layered	14.14	13.16	10.19	12.50
RPS	NR	12.26	7.63	12.99	10.96
Fibre		18.60	8.10	18.65	15.12

Table 7.24: Proportions of the ballast/subgrade interface area over which the contact pressure is at least 2.5MPa in sleeper intervention tests

Test ID	Sleeper	Percentage of contact area recorded on the pressure paper at the location of			Average % contact area on the subgrade, by 10-50MPa rated paper (> 2.5MPa)
		Left railseat	Middle	Right railseat	
Variant 1	G44	4.68	2.33	5.31	4.11
Plastic	Plastic	12.59	3.59	10.35	8.84
Timber	Timber	4.77	2.37	4.76	3.97
Steel	Steel	6.45	5.32	6.70	6.16
Twin-block	Twin-block	8.19	2.52	5.41	5.37
Mono-block + USP 1	G44	9.29	4.86	9.45	7.87
Mono-block + USP 2		8.24	4.46	3.93	5.54
Twin-block + USP 1	Twin-block	8.13	4.76	12.10	8.33
Twin-block + USP 2	Twin-block	7.27	2.83	7.00	5.70

Table 7.25: Proportions of the ballast/subgrade interface area over which the contact pressure is at least 2.5MPa in ballast intervention tests

G44 sleeper		Percentage of contact area recorded on the pressure paper at the location of			Average % contact area on the subgrade, by 10-50MPa rated paper (> 2.5MPa)
Test ID	Ballast grading	Left railseat	Middle	Right railseat	
Variant 1	Increasing finer proportion	4.68	2.33	5.31	4.11
Variant 2		2.58	1.93	2.76	2.42
Variant 3		4.86	3.12	6.20	4.73
TLB	Two layered	5.09	2.64	4.93	4.22
RPS	NR	4.31	1.54	4.23	3.36
Fibre		8.07	2.03	9.31	6.47

The magnitudes of pressure from the ballast particles onto subgrade were analysed based on the RI recorded on the pressure paper with the range of 10-50MPa together with the pressure paper calibration graph (Figure 6.42). The lower range of pressure paper is not reported because it was found that the RI recorded always reached the highest calibration value (i.e. the actual pressures were always beyond the range of the pressure paper). Table 7.26 and 7.27 present the magnitudes of particle pressure onto the subgrade layer. Ranges of values are given taking into account the upper and lower bounds of the pressure paper calibration curve in Figure 6.42.

Table 7.26: The magnitude of particle pressure at ballast/subgrade interface in sleeper intervention tests

Test ID	Magnitude of particle pressure (MPa) at the location of			Average of particle pressure on the subgrade, by 10-50MPa rated paper (> 2.5MPa)
	Left railseat	Middle	Right railseat	
Variant 1 (G44)	13.38-14.41	21.50-25.00	10.00-10.89	14.96-16.77
Plastic	47.72-50.00			47.72-50.00
Timber	33.93-44.55	37.50-48.18	36.43-47.73	35.95-46.82
Steel	42.38-50.00	30.00-40.00	36.07-46.82	36.15-45.61
Twin-block	27.69-36.67	45.71-50.00	28.85-37.78	34.08-41.48
Mono-block + USP 1	50.00-50.00	41.43-50.00	36.67-45.71	42.70-48.57
Mono-block + USP 2	36.42-46.67	36.42-46.67	50.00-50.00	40.95-47.78
Twin-block + USP 1	27.50-35.00	28.50-36.43	24.50-28.50	26.83-33.31
Twin-block + USP 2	38.57-49.09	40.00-50.00	33.57-43.64	37.38-47.58

Table 7.27: The magnitude of particle pressure at ballast/subgrade interface in ballast intervention tests

G44 sleeper		Magnitude of particle pressure (MPa) at the location of			Average of particle pressure on the subgrade, by 10-50MPa rated paper (> 2.5MPa)
Test ID	Ballast grading	Left railseat	Middle	Right railseat	
Variant 1	Increasing finer proportion	13.38-14.41	21.50-25.00	10.00-10.89	14.96-16.77
Variant 2		13.97-16.76	11.76-12.79	12.21-13.24	12.65-14.26
Variant 3		31.79-42.27	36.79-47.27	27.50-34.64	32.03-41.39
TLB	Two layered	32.14-42.73	29.75-39.64	30.0-40.0	30.63-40.79
RPS	NR	37.50-48.18	29.25-38.57	29.50-40.00	32.08-42.25
Fibre		43.18-50.0	39.29-50.0	41.82-50.0	41.43-50.00

The average contact area and average magnitude of particle pressure (Tables 7.26 to 7.27) are used to analyse the range of load on a defined subgrade area. Tables 7.28 and 7.29 present the results of the analysis of the range of load on the subgrade per unit area.

Table 7.28: The range of load per m² subgrade area on sleeper intervention tests

Test ID	Notes	Proportions area of contacts on subgrade, 10-50MPa pressure paper	Average range of particle pressure on subgrade (MPa), 10-50MPa pressure paper	Range of load per m ² subgrade area (MN)
Variant 1		4.11	14.96-16.77	0.61-0.69
Plastic	NR	8.84	47.72-50.00	4.22-4.42
Timber		3.97	35.95-46.82	1.43-1.86
Steel		6.16	36.15-45.61	2.23-2.81
Twin-block		5.37	34.08-41.48	1.83-2.23
Mono-block + USP 1	Stiff	7.87	42.70-48.57	3.36-3.82
Mono-block + USP 2	Soft	5.54	40.95-47.78	2.27-2.65
Twin-block + USP 1	Stiff	8.33	26.83-33.31	2.23-2.77
Twin-block + USP 2	Soft	5.70	37.38-47.58	2.13-2.71

Table 7.29: The range of load per m² subgrade area on ballast intervention tests

Test ID	Notes	Proportions area of contacts on subgrade, 10-50MPa pressure paper	Average range of particle pressure on subgrade (MPa), 10-50MPa pressure paper	Range of load per m ² subgrade area (MN)
Variant 1	Increasing finer proportion	4.11	14.96-16.77	0.61-0.69
Variant 2		2.42	12.65-14.26	0.31-0.35
Variant 3		4.73	32.03-41.39	1.52-1.96
TLB	Two layered	4.22	30.63-40.79	1.29-1.72
RPS	NR	3.36	32.08-42.25	1.08-1.42
Fibre		6.47	41.43-50.00	2.68-3.24

The range of load per m² subgrade area (Tables 7.28 and 7.29) is then compared to the average of vertical pressure on subgrade based on 2:1 load spread method with the inclusion of ballast self-weight to obtain comparison factors. The average vertical pressure on the subgrade in each test is dependent on the sleeper dimensions and the bulk density of the ballast in use. Therefore, for each test the average of vertical pressure on subgrade may be different although the test used an identical sleeper. Tables 7.30 and 7.31 present the magnitudes of pressure analysed by both the 2:1 spread method and the pressure paper and the comparison factor which is calculated by pressure measured by pressure paper over the pressure analysed by 2:1 spread method.

Table 7.30: Magnitude of vertical pressure on subgrade determined by both pressure paper and 2:1 load spread methods and its comparison factor in sleeper intervention tests

Test ID	Notes	Range of load per m ² subgrade area (MN)	Average vertical pressure (2:1 spread method with the inclusion of self-weight of ballast) (kPa)	Comparison factor
Variant 1	NR	0.61-0.69	65.99	9.2-10.5
Plastic		4.22-4.42	67.70	62.3-65.3
Timber		1.43-1.86	67.70	21.1-27.47
Steel		2.23-2.81	76.75	29.1-36.6
Twin-block		1.83-2.23	78.45	23.3-28.4
Mono-block + USP 1	Stiff	3.36-3.82	65.93	51-57.9
Mono-block + USP 2	Soft	2.27-2.65	66.11	34.3-40.1
Twin-block + USP 1	Stiff	2.23-2.77	78.39	28.4-35.3
Twin-block + USP 2	Soft	2.13-2.71	78.40	27.2-34.6

Table 7.31: Magnitude of vertical pressure on subgrade determined by both pressure paper and 2:1 load spread methods and its comparison factor in sleeper intervention tests

Test ID	Notes	Range of load per m ² subgrade area (MN)	Average vertical pressure (2:1 spread method with the inclusion of self-weight of ballast) (MPa)	Comparison factor
Variant 1	Increasing finer proportion	0.61-0.69	65.99	9.2-10.5
Variant 2		0.31-0.35	66.16	4.7-5.3
Variant 3		1.52-1.96	66.35	22.9-29.5
TLB	Two layered	1.29-1.72	66.69	19.3-25.8
RPS	NR	1.08-1.42	65.99	16.4-21.5
Fibre		2.68-3.24	65.94	40.6-49.1

On the wall of modified SRTF apparatus

Pressure paper was placed at two locations on the opposite internal face of the apparatus from the pressure plates. Thus data obtained could be compared with the pressure plate results. The same analysis as for ballast/sleeper and ballast/subgrade interfaces was applied. Tables 7.32 to 7.35, 7.36 to 7.37 and 7.38 to 7.39 present the proportion of contact area, the magnitude of particle pressure and the range of load per m² ballast area at ballast/wall interface respectively.

Table 7.32: Proportions of the ballast/wall interface area over which the contact pressure is at least 0.5MPa in sleeper intervention tests

Test ID	Sleeper	Percentage of contact area recorded on the pressure paper at the location of		Average % contact area on the wall by 2.5-10MPa rated paper (> 0.5MPa)
		Left railseat	Middle	
Variant 1	G44	4.19	4.20	4.20
Plastic	Plastic	3.07	3.43	3.25
Timber	Timber	4.02	2.51	3.27
Steel	Steel	3.47	2.66	3.07
Twin-block	Twin-block	3.06	2.69	2.88
Mono-block + USP 1	G44	3.19	5.3	4.25
Mono-block + USP 2		2.55	4.56	3.56
Twin-block + USP 1	Twin-block	2.71	2.84	2.78
Twin-block + USP 2	Twin-block	2.56	2.24	2.40

Table 7.33: Proportions of the ballast/wall interface area over which the contact pressure is at least 0.5MPa in ballast intervention tests

G44 sleeper		Percentage of contact area recorded on the pressure paper at the location of		Average % contact area on the wall, by 2.5-10MPa rated paper (> 0.5MPa)
Test ID	Ballast grading	Left railseat	Middle	
Variant 1	Increasing finer proportion	4.19	4.20	4.20
Variant 2		2.47	3.44	2.96
Variant 3		3.54	3.60	3.57
TLB	Two layered	2.29	2.16	2.23
RPS	NR	2.33	3.51	2.92
Fibre		1.90	2.17	2.04

Table 7.34: Proportions of the ballast/wall interface area over which the contact pressure is at least 2.5MPa in sleeper intervention tests

Test ID	Sleeper	Percentage of contact area recorded on the pressure paper at the location of		Average % contact area on the wall, by 10-50MPa rated paper (> 2.5MPa)
		Left railseat	Middle	
Variant 1	G44	1.53	1.70	1.62
Plastic	Plastic	1.39	1.85	1.62
Timber	Timber	1.49	0.78	1.14
Steel	Steel	0.87	1.04	0.96
Twin-block	Twin-block	1.46	1.22	1.34
Mono-block + USP 1	G44	1.50	2.84	2.17
Mono-block + USP 2		1.14	2.80	1.97
Twin-block + USP 1	Twin-block	1.02	1.29	1.16
Twin-block + USP 2	Twin-block	1.03	0.98	1.01

Table 7.35: Proportions of the ballast/wall interface area over which the contact pressure is at least 2.5MPa in ballast intervention tests

G44 sleeper		Percentage of contact area recorded on the pressure paper at the location of		Average % contact area on the wall, by 10-50MPa rated paper (> 2.5MPa)
Test ID	Ballast grading	Left railseat	Middle	
Variant 1	Increasing finer proportion	1.53	1.70	1.62
Variant 2		0.85	1.11	0.98
Variant 3		0.94	0.89	0.92
TLB	Two layered	1.01	0.93	0.97
RPS	NR	0.66	1.01	0.84
Fibre		0.76	0.95	0.86

Table 7.36: The magnitude of particle pressure at ballast/wall interface in sleeper intervention tests

Test ID	Magnitude of particle pressure (MPa) at the location of		Average of particle pressure on the wall, by 10-50MPa rated paper (> 2.5MPa)
	Left railseat	Middle	
Variant 1 (G44)	23.00-27.00	24.75-28.75	23.88-27.88
Plastic	42.73-50.00	45.91-50.00	44.32-50.00
Timber	37.50-48.18	43.64-50.00	40.57-49.09
Steel	24.10-28.21	24.10-28.21	24.10-28.21
Twin-block	33.33-43.57	28.85-37.78	31.09-40.68
Mono-block + USP 1	30.00-40.00	41.43-50.00	35.72-45.00
Mono-block + USP 2	32.86-43.81	43.81-50.00	38.34-46.91
Twin-block + USP1	31.43-41.36	40.00-50.00	35.72-45.68
Twin-block + USP 2	30.00-40.00	26.50-31.38	28.25-35.69

Table 7.37: The magnitude of particle pressure at ballast/wall interface in ballast intervention tests

G44 sleeper		Magnitude of particle pressure (MPa) at the location of		Average of particle pressure on the wall, by 10-50MPa rated paper (> 2.5MPa)
Test ID	Ballast grading	Left railseat	Middle	
Variant 1	Increasing finer proportion	23.00-27.00	24.75-28.75	23.88-27.88
Variant 2		20.76-23.85	26.54-32.22	23.65-28.04
Variant 3		28.25-36.43	33.57-44.09	30.91-40.26
TLB	Two layered	35.00-45.45	25.25-29.50	30.13-37.48
RPS	NR	39.64-50.00	38.57-49.09	39.11-49.55
Fibre		43.21-50.00	36.79-47.73	40.00-48.87

Table 7.38: The range of load per m2 ballast area on sleeper intervention tests

Test ID	Notes	Proportions area of contacts on the wall, 10-50MPa pressure paper	Average range of particle pressure on the wall (MPa), 10-50MPa pressure paper	Range of load per m ² ballast area (MN)
Variant 1	NR	1.62	23.88-27.88	0.39-0.45
Plastic		1.62	44.32-50.00	0.72-0.81
Timber		1.14	40.57-49.09	0.46-0.56
Steel		0.96	24.10-28.21	0.23-0.27
Twin-block		1.34	31.09-40.68	0.42-0.55
Mono-block + USP 1	Stiff	2.17	35.72-45.00	0.78-0.98
Mono-block + USP 2	Soft	1.97	38.34-46.91	0.76-0.92
Twin-block + USP 1	Stiff	1.16	35.72-45.68	0.41-0.53
Twin-block + USP 2	Soft	1.01	28.25-35.69	0.29-0.36

Table 7.39: The range of load per m² ballast area on ballast intervention tests

Test ID	Notes	Proportions area of contacts on the wall, 10-50MPa pressure paper	Average range of particle pressure on the wall (MPa), 10-50MPa pressure paper	Range of load per m ² ballast area (MN)
Variant 1	Increasing finer proportion	1.62	23.88-27.88	0.39-0.45
Variant 2		0.98	23.65-28.04	0.23-0.27
Variant 3		0.92	30.91-40.26	0.28-0.37
TLB	Two layered	0.97	30.13-37.48	0.29-0.36
RPS	NR	0.84	39.11-49.55	0.33-0.42
Fibre		0.86	40.00-48.87	0.34-0.42

The range of load per m² ballast area (Tables 7.38 and 7.39) is compared to the ballast pressure measured by pressure plates. Tables 7.40 and 7.41 present the magnitude of ballast pressures analysed by both pressure paper and pressure plate methods and the comparison factor which is calculated by dividing the pressure measured by the pressure paper by the pressure measured by the pressure plate.

Table 7.40: Magnitude of ballast pressure determined by both pressure paper and pressure plate methods and its comparison factors in sleeper intervention tests

Test ID	Notes	Range of load per m ² ballast area (MN), 10-50MPa rated pressure paper	Maximum ballast pressure measured by plates (kPa)	Comparison factor
Variant 1	NR	0.39-0.45	29.04	13.4-15.5
Plastic		0.72-0.81	23.39	30.8-34.6
Timber		0.46-0.56	24.98	18.4-22.4
Steel		0.23-0.27	29.44	7.8-9.2
Twin-block		0.42-0.55	31.07	13.5-17.7
Mono-block + USP 1	Stiff	0.78-0.98	40.05	19.5-24.5
Mono-block + USP 2	Soft	0.76-0.92	23.96	31.8-38.4
Twin-block + USP 1	Stiff	0.41-0.53	31.32	13.1-16.9
Twin-block + USP 2	Soft	0.29-0.36	26.56	10.9-13.6

Table 7.41: Magnitude of ballast pressure determined by both pressure paper and pressure plate methods and its comparison factors in ballast intervention tests

Test ID	Notes	Range of load per m ² ballast area (MN), 10-50MPa rated pressure paper	Maximum ballast pressure measured by plates (kPa)	Comparison factor
Variant 1	Increasing finer proportion	0.39-0.45	29.04	13.4-15.5
Variant 2		0.23-0.27	35.43	6.5-7.6
Variant 3		0.28-0.37	20.73	13.5-17.8
TLB	Two layered	0.29-0.36	22.96	12.6-15.7
RPS	NR	0.33-0.42	25.02	13.2-16.8
Fibre		0.34-0.42	24.41	13.9-17.2

Discussion of pressure paper results and further analysis of number of contact

The data for the sleeper/ballast interface (Tables 7.16 to 7.19), show considerable variability in terms of contacts and areas. The particles in contact were perhaps predominantly the larger ballast particles as the surface preparation using the vibratory compaction plate tended to cause the finer particles to travel to the bottom. That downward migration of finer particles occurs during vibration is well known, see e.g. Gaskin et al (1978). The variability may also arise partly because the pressure paper was not placed over the full sleeper soffit area, so that extrapolating to the full area will introduce

some uncertainty. There will also be some differences between repeat experiments due to the inherent variability of the distribution and number of contact locations achieved. Nonetheless, some important trends can be observed.

At the sleeper/ballast interface, the number of contacts for a G44 sleeper on the ballast with a grading similar to the current standard NR ballast grading (variant 1) was 147. This is within the range suggested by Shenton (1978) of 100 to 200. For a twin-block sleeper, the value obtained was 243. The twin block sleeper has a smaller base area so the increase compared to the G44 sleeper is perhaps unexpected; however this higher number of contacts could be because the twin-block sleeper was tested to 4.5 million loading cycles (while the G44 sleeper was to 3 million loading cycles). The results might also be explained by the twin-block sleeper having a smaller footprint area, different sleeper shape and lower bending stiffness, which could give rise to a different pattern of loading and be more effective in mobilising and retaining particle contacts over the loading history (twin-block gives a better seating on the ballast).

The material from which the sleeper is made also influences the number of contacts and the overall contact area. Plastic and timber mono-block sleepers showed 2 and 3 times greater numbers of contacts and 17 and 9 times larger percentage contact areas respectively than the G44 sleeper. This is thought to be primarily a result of the softer sleeper material allowing the ballast to indent into it and bring into play a larger number of contacts by pressing past the first contacting particles before then contacting others sitting lower down. Visually, more ballast particle indentations were observed at the end of testing in the plastic than in the timber sleeper soffit; this was reflected in the percentage area of contact, which was about double that of the wooden sleeper. The plastic and timber sleepers show reverse trends for the number of contacts and the overall contact areas. While the wooden sleeper had a greater number of contacts, the plastic sleeper had fewer contacts but spread over a greater area. This might have been because the plastic and wooden sleepers have differing bending stiffnesses hence different patterns of loading. This possibility is supported by the observation during testing that the plastic sleeper showed much greater bending beneath the railseats.

Changing the ballast grading by introducing finer materials was highly successful in increasing the number of contacts and the percent contact area. Ballast variant 3 increased the number of contacts by a factor of 5 (to 836) and the contact area by up to 3.5 times, while the modified TLB ballast system with its finer layer of 10/20 material below the sleeper increased the number of contacts nearly tenfold (to 1311) and the area of actual contact by a factor of ~ 3 .

Re-profiling the shoulder slope to 1V:2H increased the number of contacts by slightly more than 3 times, although the total contact area was only increased by 11% compared with the baseline test. It is thought that this is a result of the RPS slope being more effective in providing lateral restraint, hence preventing the sleeper/ballast contacts from moving as much thus additional stable contacts were developed as a result of the gradual vertical settlement of the sleeper. The less effective lateral restraint provided by shoulders with 1V:1H slopes meant that instead of new contacts being created, cyclic loading caused ballast particles to move laterally with the result that the fewer contacts present moved significantly over the course of the test. A similar effect was also apparent for the test with fibre reinforced ballast, in which the number of contacts increased by slightly more than 2.5 times and the contact area by a factor of 2.

The attachment of USPs 1 and 2 to the G44 sleeper soffit increased the number of contacts by between 2 and 3 times and the contact area by a factor of 9 and 6 respectively. As USP 2 was the softer, it was expected to show an increased number of contacts and overall contact area over USP 1; however while the number of contacts increased the contact area reduced. Again perhaps this reflects natural variation and experimental uncertainty from extrapolating the paper areas to the full sleeper. It is possible that mobility of contact also plays apart.

The attachment of USPs to the twin-block concrete sleeper soffits increased the number of contacts by between 10% and 35% and the area of contact by a factor of 5.5 to 9. Again as for the G44 sleeper this may be explained as a result of the more compliant material with the softer USPs giving the larger number and area of contacts. In this case, as expected, USP 2 showed both greater numbers of contacts and the greater area percent contact.

Comparison of apparent contact pressure at the sleeper/ballast interface using a simplistic method of estimation (Tables 7.20 and 7.21) illustrates that the average contact pressure can be drastically reduced by the use of plastic, timber, USPs and finer gradings in comparison to the basic configurations of either G44 or twin-block concrete sleepers on the current standard NR ballast grading. In all cases, however, the average estimated contact pressures are much greater than that obtained from a simple averaging based on an effective railseat area using for example Equation 5.41. As an illustration the average contact stress based on Equation 5.41 is less than 0.3% of that found based on the actual contact area for a G44 sleeper with ballast variant 1 after 3 million loading cycles.

At the bottom of the ballast layer at the interface with the subgrade, the percentage areas of contact were much larger beneath the railseats than in the middle of the mono-block sleeper (Figures 7.33 to 7.39 and Tables 7.24 and 7.25). This may be a result of the ballast beneath the railseats migrating sideways from underneath the track. The contact area is then overestimated, being in effect the sum of all contact areas during the test. Overall the range of contact areas was between 7% and 17% for contact pressures greater than 0.5MPa but there is considerable noise in the data. It appears that by the time the pressures have transferred through the ballast layer, there is much less variation at the ballast/subgrade interface, almost regardless of the type of ballast or sleeper used. However, while trends are less clear, it is perhaps worth noting that the finest ballast grading (variant 3) showed the highest contact area at the subgrade while the lowest contact area at the subgrade was given by the twin-block sleeper on the current standard NR ballast grading. At the ballast subgrade interface, in general, ballast particle pressure was still very high (Tables 7.26 and 7.27). Combining the contact area and the magnitude of the inter particle pressure into the analysis (Tables 7.25 and 7.26) also shows no clear pattern; however changing the ballast grading was the most effective way of reducing the particle contact pressure to the subgrade.

Comparison factors, i.e. the ratios of the average pressure on the subgrades determined by the pressure paper and using the 2:1 load spread method (Tables 7.30 and 7.31), show no clear trend. However, comparison factors ranging between 4 and 66 times might be an indication that ballast particles on the subgrade moved during cyclic loading. A large factor suggests small area and high contact pressure.

Tables 7.34 and 7.35 show that in the longitudinal direction, contact areas in the middle section of a mono-block sleeper are larger than in the railseat area with the exception of the tests on variant 3, TLB system, timber and twin-block sleepers. These exceptions may be due to the initial condition of ballast (as prepared) and the shape of the sleeper (i.e. twin-block sleeper). Longitudinal pressures in the middle section were also higher than in the railseat area. These results agree with those from the pressure plates, which also showed a higher ballast pressure developing in the middle section of the sleeper.

Comparing the magnitudes of the pressures obtained from the pressure paper and the pressure plate shows that the contact area recorded on the pressure paper increased between 6 to 35 times. This indicates that the ballast particles in this location also moved during the cyclic loading.

To estimate the number of contacts potentially available in each of the ballast gradings tested in this research, the ballast particle data presented in Table 6.15 are used. It shows that the D_{90} of all ballast gradings (Table 6.15) is generally close to 49 mm and each D_{50} of them is also known. These two values are used in Equation 6.11 to determine the coefficients m and C . When m and C are already determined, any desired value of D_A , D_B to D_N can also be estimated. If a range of D_{50} values is chosen, the theoretical number of contacts can be estimated using Equation 6.13 and plotted against the variation in D_{50} . The calculated potentially available number of contacts can then be compared with those measured (Tables 7.16 and 7.17) as shown in Figure 7.40.

In Figure 7.40, five particle sizes corresponding to D_{90} , D_{70} , D_{50} , D_{30} , and D_{10} have been evaluated to produce estimate curves of potentially available contacts.

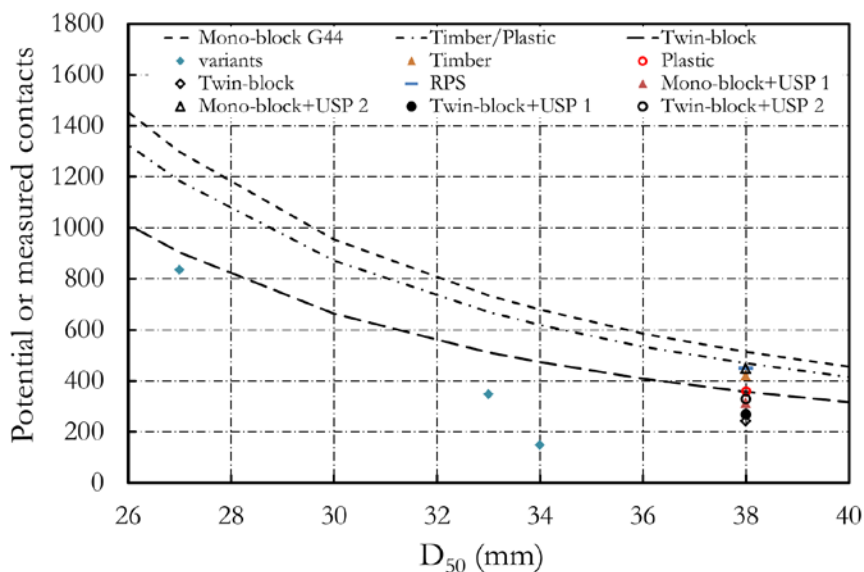


Figure 7.40. Number of contacts versus D_{50} where D_{90} is kept constant of 49 mm: measurements and estimates (dashed lines)

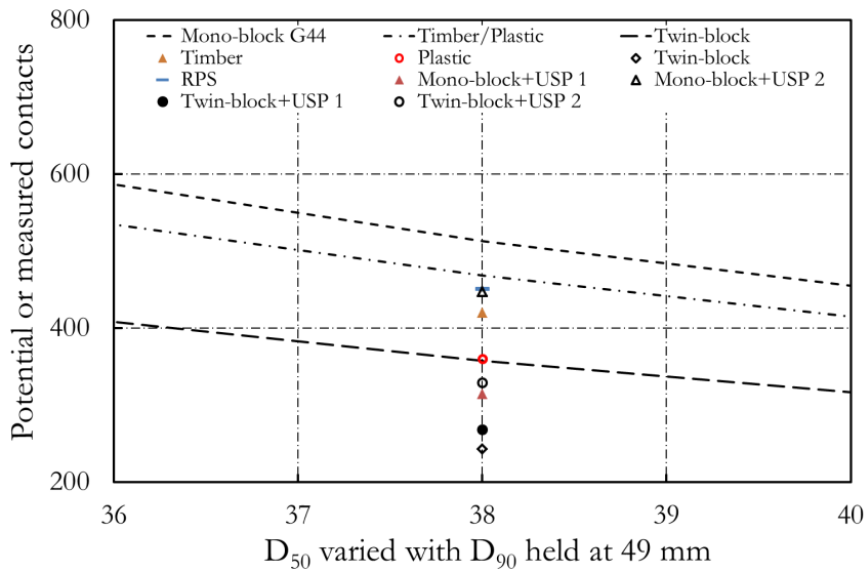


Figure 7.41. Number of contacts versus D50: measurements and estimates (dashed lines)

Most of the combinations tested used the current standard NR ballast grading and hence the majority of data points plot along a vertical line where $D_{50} = 38$ mm. Figure 7.41 shows a close up of this region. Figures 7.40 and 7.41 show that the gradings tested have a lower number of contacts than the estimated potential number of contacts available. The difference between the measured and the potential number of contacts can be viewed as an indication of the quality of the surface preparation achieved and/or the benefit from USPs, wood, plastic compared with concrete. It is also worth noting that the real particles are not spherical.

Table 7.42 compares the measured and calculated potential contacts and shows a parameter termed the “contact efficiency” which is defined as the measured number of contacts divided by the theoretically calculated potentially available contacts. For completeness the potential number of contacts estimated for a mono-block sleeper on the current standard NR ballast grading is included, although no comparable measurements are available for this. It can be observed that the number of potential contacts for the test using mono-block G44 sleeper on the current standard NR ballast grading is about 25% less than estimated for variant 1.

Table 7.42: Measured and potential contacts

Sleeper type	Test ID	Measured contacts	Potential contacts	Contact efficiency (%)
Mono-block	Baseline	N/A	513	N/A
	Variant 1	147	679	21.6%
	Variant 2	347	735	47.2%
	Variant 3	836	1297	64.5%
	Plastic	360	468	76.9%
	Timber	420	468	89.7%
	RPS	451	513	87.9%
	+ USP 1	314	513	61.2%
	+ USP 2	447	513	87.1%
Twin-block	Baseline	243	357	68.1%
	+ USP 1	268	357	75.1%
	+ USP 2	329	357	92.2%
Mono-block	TLB	1311	2917	44.9%

Table 7.42 also includes the test on 10/20 aggregate (the modified TLB test) although this test was not plotted on the graphs owing to the much different D_{90} value. Comparing the contact efficiencies

(Table 7.42) and the measured contacts shows that while the use of finer gradings can increase the absolute number of contacts mobilised, there are more effective ways to mobilise greater proportions of the potentially available contacts. The use of timber sleepers, a shallower ballast shoulder, and the use of USP 2 all mobilise more than 80% of the potentially available contacts.

7.2.7 Particle breakage

Section 6.5.7 described how ballast particle breakage was investigated by visual observation, PSD and using measurement of random randomly selected ballast particles methods.

Visual observation

In visual observation, the results are subjective/user dependent. There is also a limit to the amount of breakage visually detectable such that small breakage of asperities may be neglected. Figure 7.42 shows a typical example of ballast breakage that would be identified by visual assessment.



Figure 7.42: Typical ballast particle breakage identified by visual observation

Results from sleeper and ballast intervention tests

Visual observation of ballast breakage was only carried out at the sleeper/ballast interface, directly under the sleeper soffit. Ballast breakages from visual observation are ordered from the highest to the lowest and the corresponding permanent settlements are also presented in Tables 7.43.

Table 7.43: The rank of number of ballast particle breakages (found by visual observation) on sleeper and ballast interventions

Test ID	Ballast grading	Total load cycles applied (millions)	Number of broken particle	Settlement at 3M loading cycles after zeroed at 10 cycles (mm)
Baseline	NR	3.0	11	5.69
Variant 2	Variant 2	3.0	8	5.74
Steel	NR	3.5	6	9.81
Twin-block+ USP 2	NR	6.0	4	3.96
Plastic	NR	4.0	3	3.54
Timber	NR	3.5	3	5.42
Variant 1	Variant 1	3.0	2	5.68
Variant 3	Variant 3	5.0	2	4.12
Mono-block+ USP 2	NR	4.0	2	3.74
Twin-block	NR	4.5	2	4.21
Mono-block+ USP 1	NR	3.0	1	3.89
TLB	TLB	4.0	None	4.85
RPS	RPS	3.5	None	3.63
Fibre	NR + fibre	5.0	None	4.93
Twin-block+ USP 1		4.5	None	4.03

Discussion of the results

Based on the visual observation findings (Table 7.43), broken particles occurred in most tests. However, in all cases the number remained relatively small (a maximum of 11 in the baseline test) and there is no clear pattern of relationship between the number of broken particles and the corresponding accumulative permanent settlement (the order of number broken particles is not followed by the order of accumulative of permanent settlement of the ballast).

Breakage mostly occurred in large particles at the edges of sleeper soffit. Hardin (1985) observed that the potential for breakage of a soil particle increases with its size due to the greater probability of defects being present. It is also hypothesised that the breakage could be explained by the ballast particles at the edges of sleeper soffit experiencing more severe combined compression and shear forces compared with particles within the sleeper foot print.

PSD method

Sieving was carried out to compare the PSD graphs prior to and after each test. For this, ballast samples were taken from below the railseats and the middle section of the sleeper after each test.

Results from sleeper and ballast intervention tests

Most before and after PSD tests showed minor changes which could have been attributed to natural variation between samples rather than breakage during the experiments. Thus only data where the changes were more significant are presented in this section, these include results from baseline, twin-block sleeper and variant 3 tests (Figures 7.43 to 7.45). Other results are presented in Appendix F. Also, while initially sieving was carried out using the same sieve size as that used to specify railway ballast (Figure 7.43) later tests incorporated more sieve sizes so as to capture more reliably any trends that may have been present (Figures 7.44 and 7.45).

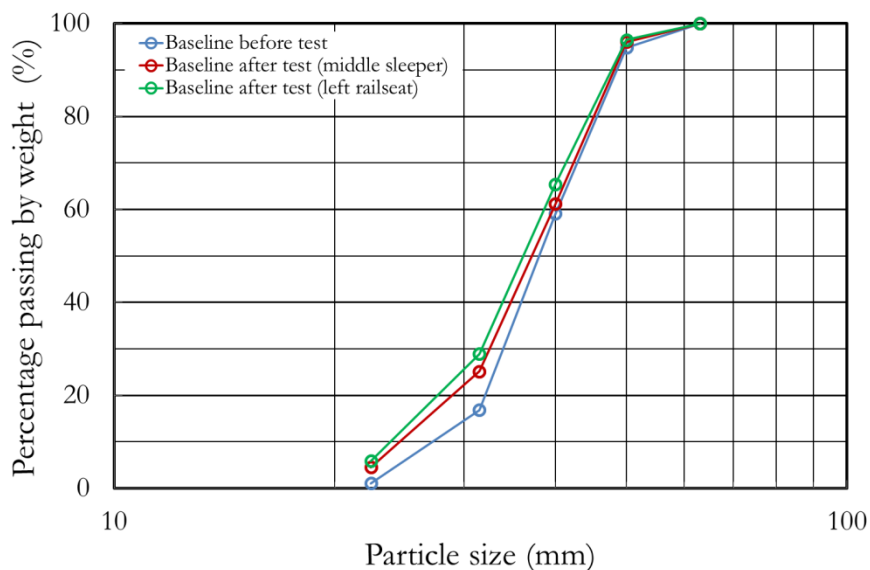


Figure 7.43: PSD graphs of ballast in baseline test, before and after the test

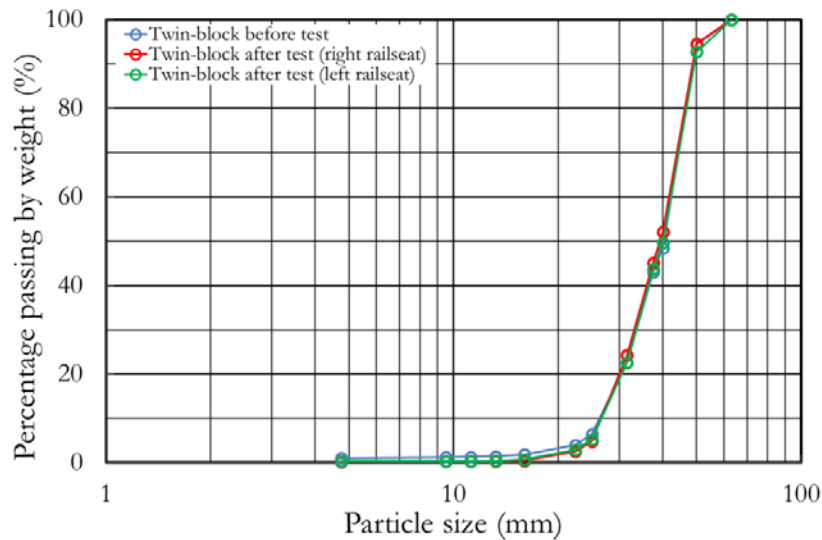


Figure 7.44: PSD graphs of ballast in twin-block test, before and after the test

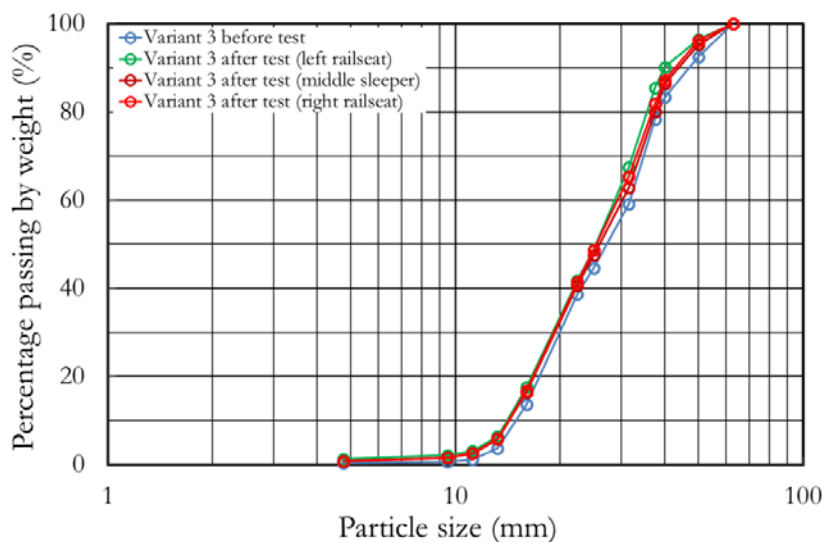


Figure 7.45: PSD graphs of ballast in variant 3 test, before and after the test

Discussion of the results

The results of particle breakage analysis using PSD method (Figures 7.43 to 7.45) show a very minor change of PSD graph of each test before and after cyclic loading. However, difficulties in selecting exactly the same ballast sample for use before and after each test mean that the small changes detected could be attributed to natural variation.

Measurement of selected ballast particles

For some of the tests 50 particles were randomly selected and each marked with a unique identification prior to cyclic loading, so that they could be recovered at the end of testing. These selected particles were placed at the sleeper/ballast interface.

Results from sleeper and ballast intervention tests

Figures 7.46 to 7.49 show the before and after PSD test of 50 randomly selected particles present in the variant 1, twin-block, variant 2 and variant 3 tests while the results from other tests are available in Appendix G. In the test on variant 2 (Figure 7.48), no difference can be detected.

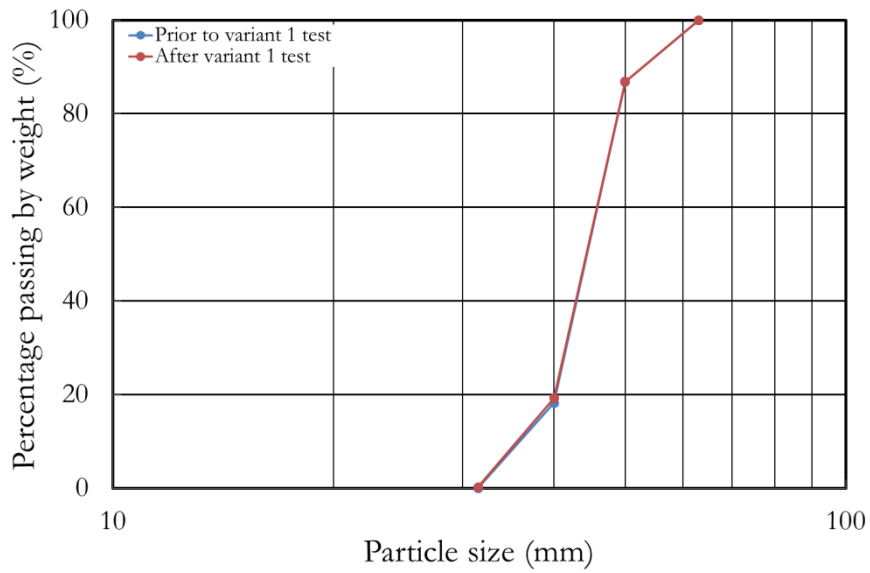


Figure 7.46: PSD graphs of randomly selected particles on variant 1 before and after test

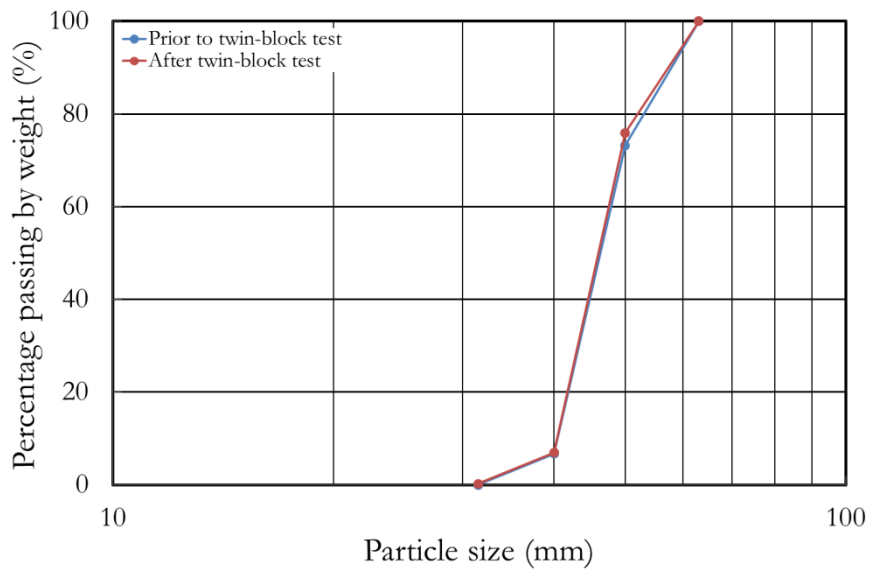


Figure 7.47: PSD graphs of randomly selected particles on twin-block before and after test

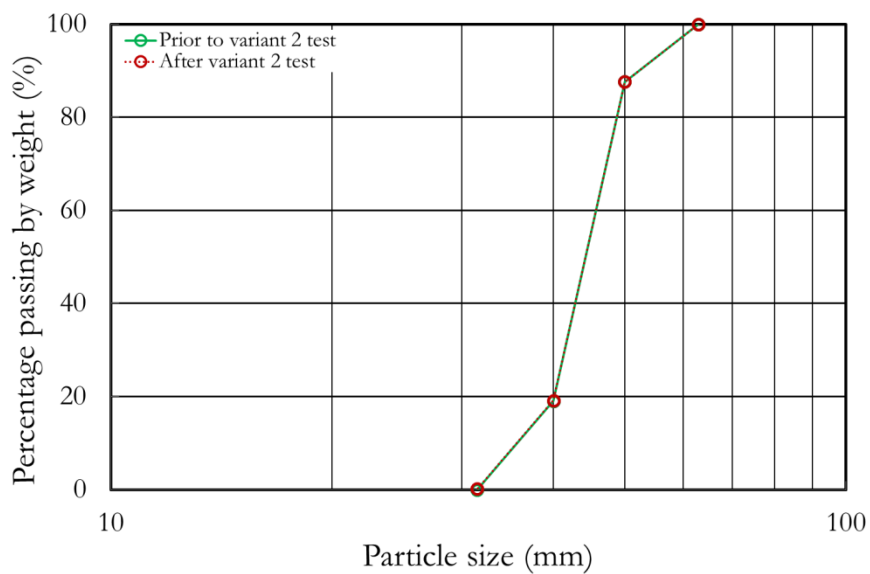


Figure 7.48: PSD graphs of randomly selected particles on variant 2 before and after test

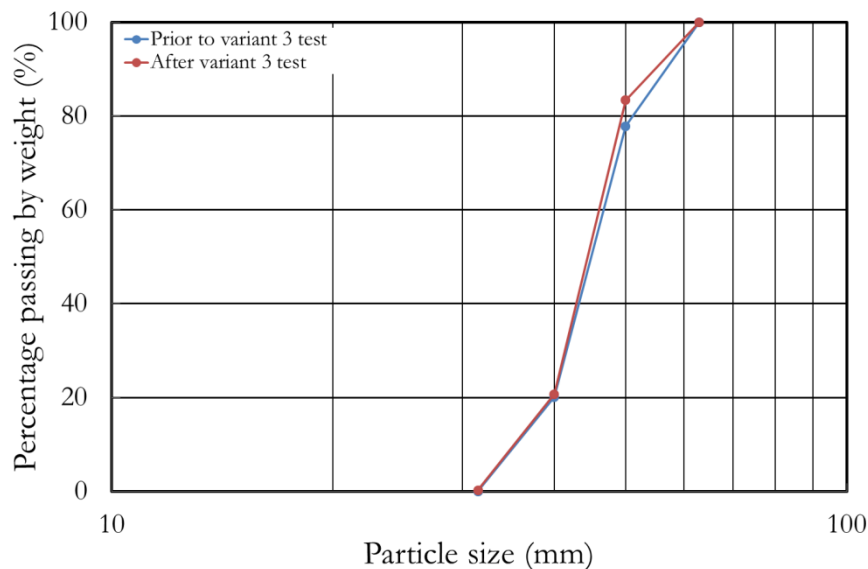


Figure 7.49: PSD graphs of randomly selected particles on variant 3 before and after test

To avoid such a case in variant 2 test (Figure 7.48) where a change cannot be detected, the 50 randomly selected particles were also individually weighed prior to and after each test. The maximum and the minimum loss of mass of each ballast particle in use as well as the average of loss for the 50 randomly selected particles in each test were recorded. The results from this method are presented in Table 7.44.

Table 7.44: The percentage of total loss of mass of ballast particles on sleeper and ballast intervention tests

Test ID	Ballast grading	Total load cycles applied (millions)	Range of min to max loss of mass of individual particle (%)	The average loss of mass for 50 particles (%)
Baseline	NR	3.0	N/A	N/A
Twin-block		4.5	0.07-1.44	0.25
Plastic		4.0	0.03-0.39	0.13
Timber		3.5	0-0.49	0.09
Steel		3.5	0.01-1.67	0.15
Mono-block+ USP 1		3.0	0.05-0.54	0.17
Mono-block+ USP 2		4.0	0.05-0.37	0.14
Twin-block+ USP 1		4.5	0.07-0.68	0.19
Twin-block+ USP 2		6.0	0-8.05	0.47
Variant 1		Increasing finer proportion	3.0	N/A
Variant 2	3.0			0.18
Variant 3	5.0		0.05-5.19	0.29
TLB	TLB	4.0	0-0.14	0.06
RPS	RPS	3.5	0.01-0.41	0.10
Fibre	NR + fibre	5.0	0.02-0.59	0.12

Discussion of the results

The PSD tests confirm that only minor breakage occurred in any of the tests. There was also a small reduction in weight of the 50 randomly selected particles occurs in each test. The maximum reduction in the weight of a single particle in all tests was 8.05% (test on twin-block + USP 2) but the average reduction in mass for 50 randomly selected particles was less than 0.5% in all tests. This shows that the reduction of mass may be attributed to surface abrasion rather than breakage. It is also worth noting that breakage will depend on sleeper type, magnitude of vertical load applied and quality of

ballast material. Furthermore Lackenby et al (2007) carried out triaxial tests on a latite basalt ballast and concluded that certain ranges of confining pressure existed such that breakage could be minimised. The stress paths present in the modified SRTF apparatus tests appear to be well within the capacity of the ballast used to resist significant breakage.

In the total of 50 randomly selected ballast particles used in the tests on different sleeper materials, less breakage occurred in the tests using plastic and timber sleeper with only 0.13% and 0.09% loss of total mass respectively. This may be because the softer material of these sleepers allows the ballast to embed rather than break. These results demonstrate that the ballast particles are not undergoing significant breakage and agree with the results of previous work carried out by Jeffs and Marich (1987) that little change in gradation or particle degradation occurred.

7.3 Lateral movement of ballast on shoulder slope

Photographs were taken of the ballast shoulder slopes at key numbers of loading cycles during the tests to obtain a record of any changes as they developed. This method was applied to 12 out of 15 tests.

Results from Sleeper and Ballast Intervention Tests

Figures 7.50 to 7.52 show the movement of ballast particles on shoulder slope in the tests of twin-block sleeper, variant 3 and the RPS slope respectively. The figures analysed from other tests are available in Appendix H. These figures were produced by subtracting the contrast from images at different numbers of loading cycles from the initial image: if the images are exactly identical, subtraction leads to a black image. Where particles have moved about, the subtraction is not zero and shows as a shade of grey/white.

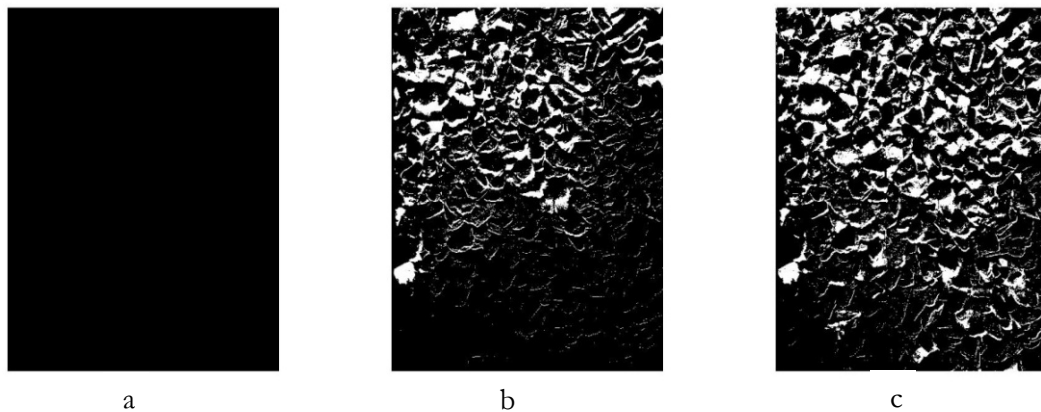


Figure 7.50: Ballast particle movements on the shoulder slope at (a) prior to testing, (b) during harvesting the data at 0.25 million loading cycles and (c) the end of twin-block sleeper test

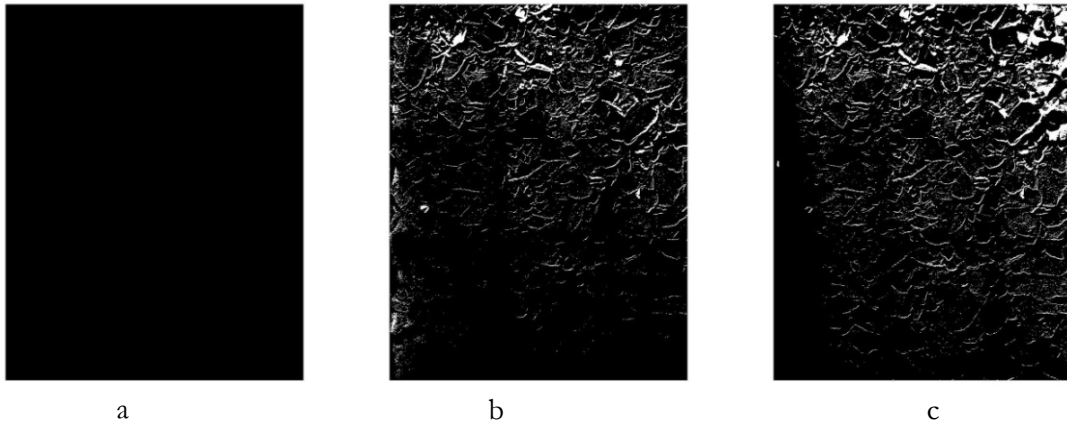


Figure 7.51: Ballast particle movements on the shoulder slope at (a) prior to testing, (b) during harvesting the data at 0.25 million loading cycles and (c) the end of variant 3 test

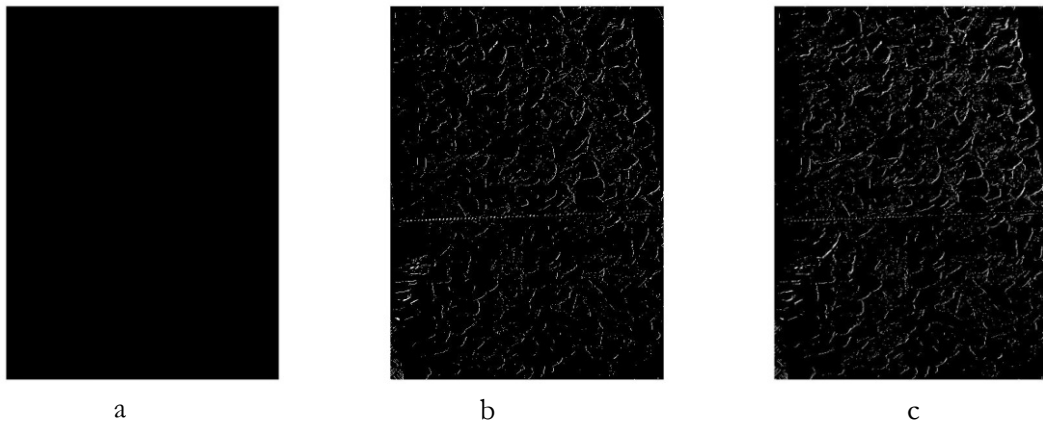


Figure 7.52: Ballast particle movements on the shoulder slope at (a) prior to testing, (b) during harvesting the data at 0.25 million loading cycles and (c) the end of RPS slope test

Discussion of the results

The analysis shows that there were movements of ballast particle on the shoulder slope due to cyclic loading in every test. Comparing the development of ballast movements on the shoulder slope (white indicates more movement in Figures 7.50 to 7.52) shows that the RPS slope test has by a considerable margin the least white colour, representing the least movement of ballast particles on the shoulder slope. This confirms that the RPS slope was able to resist more effectively ballast particles moving laterally during cyclic loading. This observation supports the many earlier favourable findings from this test that the RPS slope provides: more lateral confinement, the least ballast particle abrasion, low permanent settlement and a high spring stiffness.

7.4 In the case of steel and plastic sleepers

The results of the tests using steel and plastic sleepers are separated from those presented in the earlier section on sleeper intervention tests because of specific issues with each test. These are that (1) it proved problematic to place the steel sleeper uniformly onto the prepared ballast bed due to its hollowed out section (2) the plastic sleeper was supplied without the chairs needed to make a robust connection between the loading rails and the sleeper. Each issue appeared to dominate the results. In the case of the steel sleeper, problems with bedding the sleeper uniformly onto the ballast are also present in the field. However, mechanical methods of installation may be able to achieve more uniform placement. For the plastic sleeper, the test is unrepresentative of how this sleeper is intended

to be used but gives some insight into the influence of the effect of using a much lower stiffness material on sleeper behaviour.

7.4.1 Permanent settlement

Figure 7.53 shows permanent settlement graphs (averaged by area weighted method) for the tests using steel and plastic sleepers compared with other selected sleeper and ballast intervention tests.

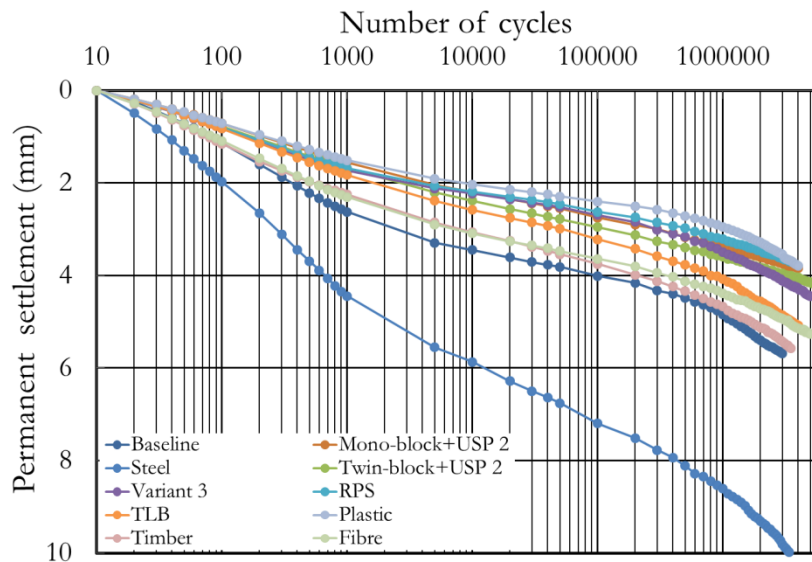


Figure 7.53: Permanent settlement of steel and plastic tests compared with other sleeper and ballast intervention tests after zeroed at 10 loading cycles

Discussion of the results

Based on Figure 7.53, the steel sleeper performs the worst of all sleeper intervention tests. This was probably due to a poor installation of the steel sleeper onto the ballast bed. Difficulties in steel sleeper installation also occur in the field, an Office of Transport Safety Investigation (2005) into steel sleeper use was carried out prior to allowing steel sleeper application for the main line in the state of New South Wales (NSW), Australia. The investigation led to recommendations for the correct installation of steel sleepers by insertion and tamping using a specially developed and standardised procedure. Incorrect steel sleeper installation was found to lead to instability. It was also noted that tamping of steel sleepers was problematic. For optimum performance, tamping is required to fill the steel sleeper’s hollowed out section or “pod” adequately and evenly with ballast. However, directly observing the quality of pod filling from tamping is difficult; it could appear that the tamping was successful in providing a uniform lift to the track, while visual observation through holes in the sleeper tops may give false impression that the pod was completely filled whereas there was still a ballast deficiency at other sections of steel sleeper. If the filling of steel sleeper pods is not consistently achieved or if there is an inadequate compaction of ballast in the pod then the level of the ballast in the pod may settle down over time. Loose ballast within the sleeper pods can lead to the development of track misalignments, hanging sleepers and perhaps the occurrence of mud pumping (Office of Transport Safety Investigation, 2005). Regardless of the issues of steel sleeper installation for the laboratory test, the permanent settlement is consistent with the observation of Manalo et al (2010) that steel sleepers settle more than timber sleepers.

The plastic sleeper may have appeared to perform well in having the least permanent settlement among all the tests carried out (Figure 7.53). However, this is misleading. The low rate of permanent settlement accumulation of the plastic sleeper became apparent after the first 0.25 million loading cycles. Because of this unexpected behaviour, additional visual observations were carried out and it was seen that during cyclic loading, the sleeper deflection at the railseats was larger than the sleeper ends with the sleeper deflecting in a pronounced “ω” shape. This led to a bias in the recorded permanent settlement results due to the placement of the LVDTs, which were not able to capture the base of “ω” shaped deflection. The pronounced bending shape of the plastic sleeper was later realised to be because the sleeper had been supplied without the fixing chairs (Figure 7.54). These chairs, which are also used on timber sleepers, are substantial blocks of metal and provide a load spreading connection to pass the load from the rail foot over a larger area onto the sleeper. In the test reported here the chairs were omitted and the concentrated load going into the sleeper directly from the rail foot is probably responsible for the pronounced deflected shape. In contrast, concrete sleepers have a much greater bending stiffness and do not require such chairs for load transfer.



Figure 7.54: A sleeper chair for a proper rail arrangement on plastic and timber sleepers

The result of permanent settlement from the test using plastic sleeper (Figure 7.53) is therefore not representative. However, the test shows that a proper arrangement of the railseat is crucial for both testing in the laboratory and installation on the track.

7.4.2 Sleeper deflection

Figures 7.55 to 7.57 show the average of sleeper deflection for both steel and plastic sleepers for the sleeper ends, the middle section of the sleeper and the railseat respectively, with the previous two locations compared with the baseline test.

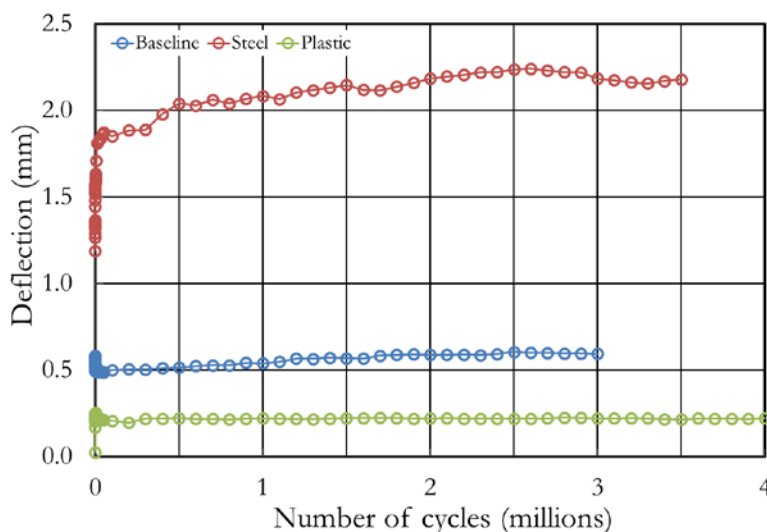


Figure 7.55: Average sleeper ends deflection of the tests on steel and plastic sleepers compared with the baseline test

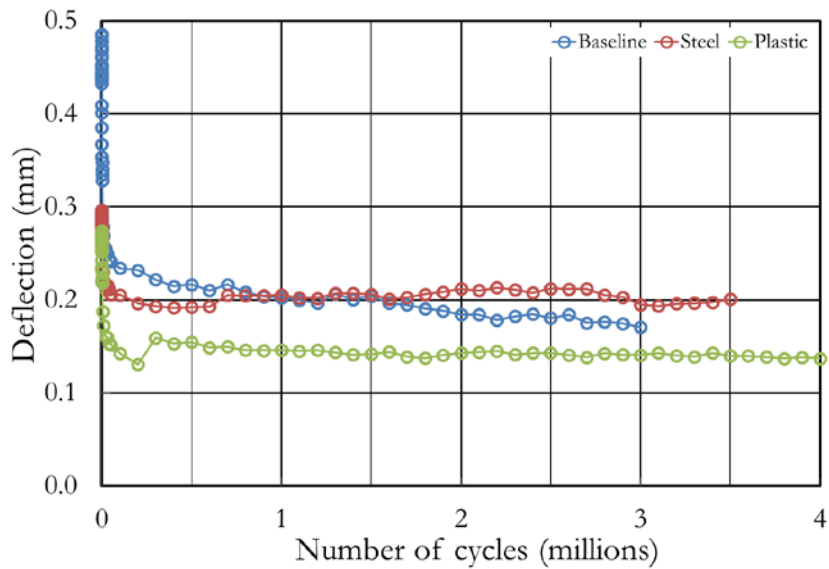


Figure 7.56: Average middle section of sleeper deflection of the tests on steel and plastic sleepers compared with the baseline test

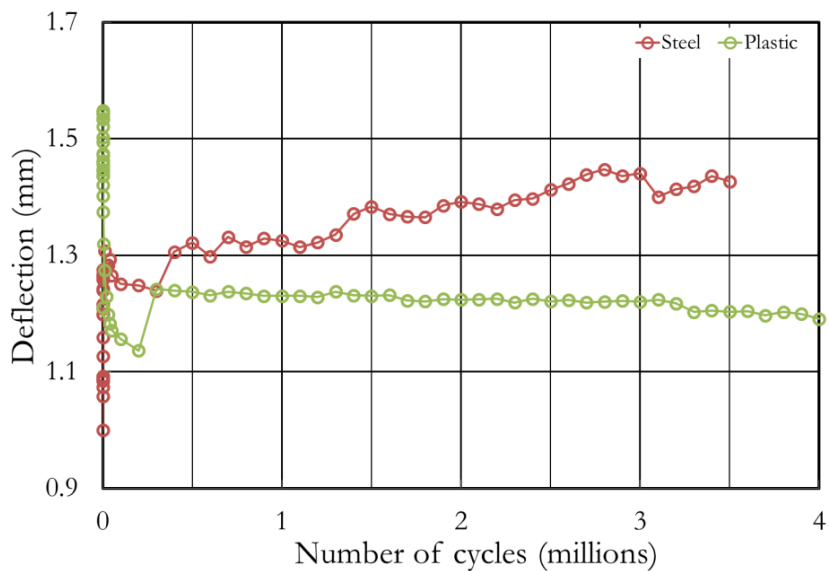


Figure 7.57: Average sleeper deflection near the railseat of the tests on steel and plastic sleepers

Discussion of the results

The deflection data from the tests using steel and plastic sleepers (Figures 7.55 to 7.57) show that during cyclic loading the steel sleeper was hogging. This is apparent from the increase in deflection at the sleeper ends and the reduction in deflection in the middle section of the steel sleeper. The magnitude of the deflection near the railseat for the steel sleeper was within these two extremes. Figure 7.58 shows the deflected shape of steel sleeper at 3 million loading cycles, which confirms that steel sleeper was hogging during cyclic loading.

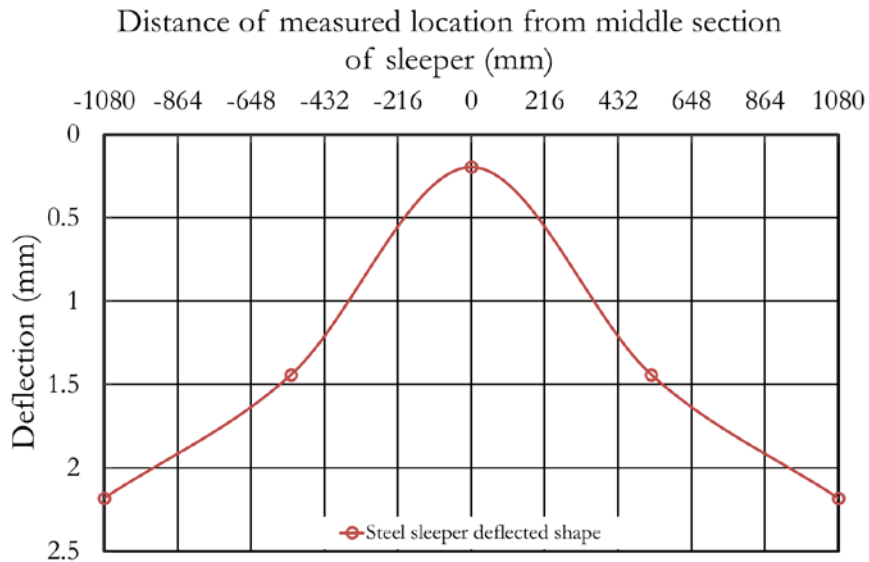


Figure 7.58: Deflected shape of steel sleeper (hogging) at 3 million loading cycles

Non uniform sleeper support from a poor installation leads to instability and can lead to train derailment. Manalo et al (2010) and the investigation undertaken by Office of Transport Safety Investigation (2005) concluded that railseats of steel sleepers can experience fatigue which may be more likely if combined with poor installation and vibration induced from the train. These can loosen the sleeper/rail fastenings and lead to instability of the track.

In the case of plastic sleeper, the deflection at the ends, middle section and near the railseat of plastic sleeper (Figures 7.55 to 7.57) confirms that during cyclic loading, the plastic sleeper formed a “ω” shape with a larger deflection near the railseat than at both the middle section and at the ends. The results show the importance of a proper load transfer arrangement on the sleeper in both laboratory tests and in track applications.

Figures 7.59 illustrates the findings from the test on plastic sleeper without the rail chairs, showing the loaded plastic sleeper deflected shape at 3 million loading cycles.

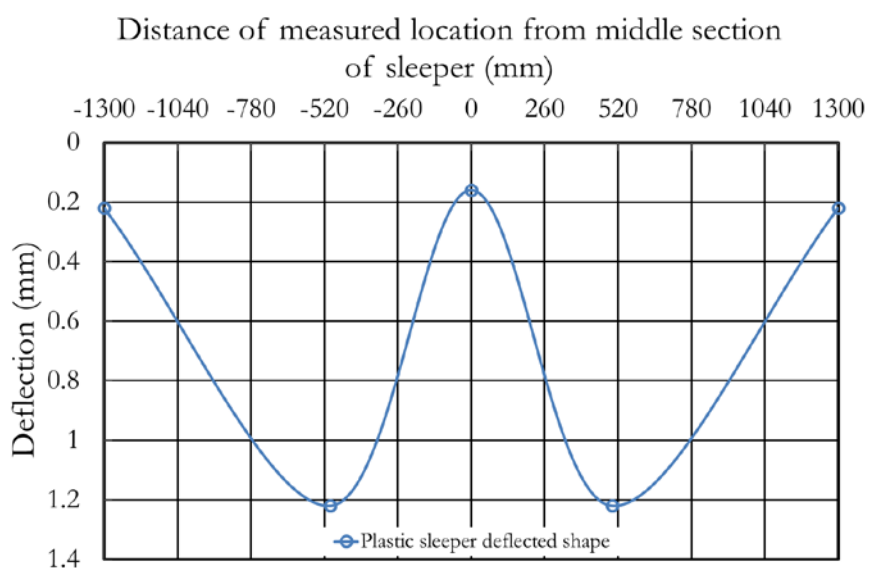


Figure 7.59: Deflected shape of plastic sleeper at 3 million loading cycles

7.4.3 Spring stiffness

Figure 7.60 shows the spring stiffness (averaged by area weighted method) from tests using steel and plastic sleepers with by other tests shown for comparison.

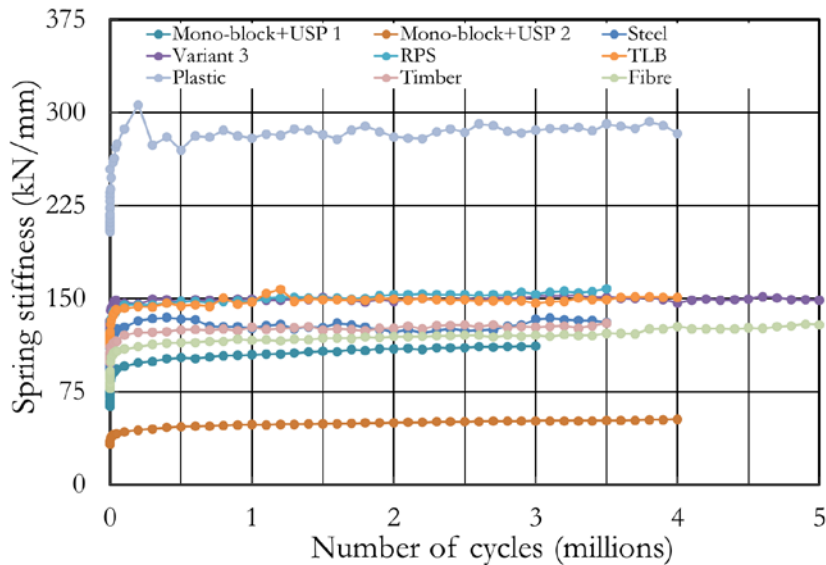


Figure 7.60: The average spring stiffness of the tests using steel and plastic sleepers compared with spring stiffness of other sleeper and ballast intervention tests

Discussion of the results

The calculated spring stiffness (Figure 7.60) shows that the spring stiffness for steel sleeper is within the range of spring stiffnesses from the other tests carried out. However, the test using the plastic sleeper produced the highest spring stiffness, which was almost double the spring stiffness of the RPS slope test which was the highest among the other ballast and sleeper intervention tests. This is because the pronounced “ ω ” shape of the plastic sleeper during cyclic loading was not captured with the location of LVDTs used, resulting in an artificially high spring stiffness.

In some of the tests including those on the steel and plastic sleepers, two LVDTs were located near the railseat. Using these LVDTs, the spring stiffness at this location can be determined. However, these LVDTs were excluded from the area weighted method in analysing both permanent settlement and spring stiffness elsewhere because of a wish to compare all tests consistently (regardless sleeper type) and also because in most tests the sleeper end movement and railseat movement were close.

Figure 7.61 shows a comparison of the average spring stiffness near the railseat in the tests using steel and plastic sleepers, with the spring stiffness at the same location in other tests where these data were available. It is worth noting that the spring stiffness in this location is not comparable with the area weighted method. This is because the railseat is closer to the sleeper end than to the middle section of sleeper. Therefore, the spring stiffness at this location is always lower than the area weighted spring stiffness regardless of whether a rail chair was present or absent.

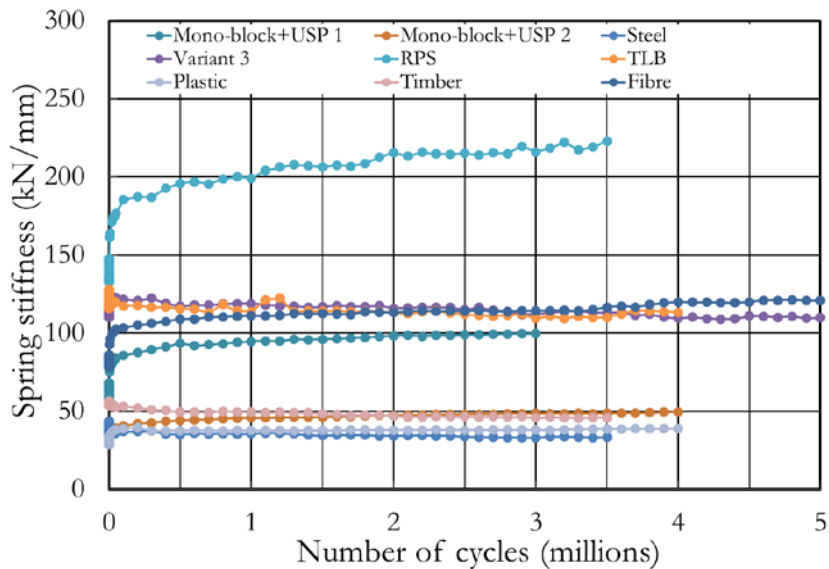


Figure 7.61: The average of spring stiffness at the location of near railseat in the tests using steel and plastic sleepers compared to spring stiffness of other tests

It can be seen that the spring stiffness produced by the tests using the steel and plastic sleepers near the railseat is lower than that of other tests. This then led to an investigation into spring stiffness at each section of both steel and plastic sleepers.

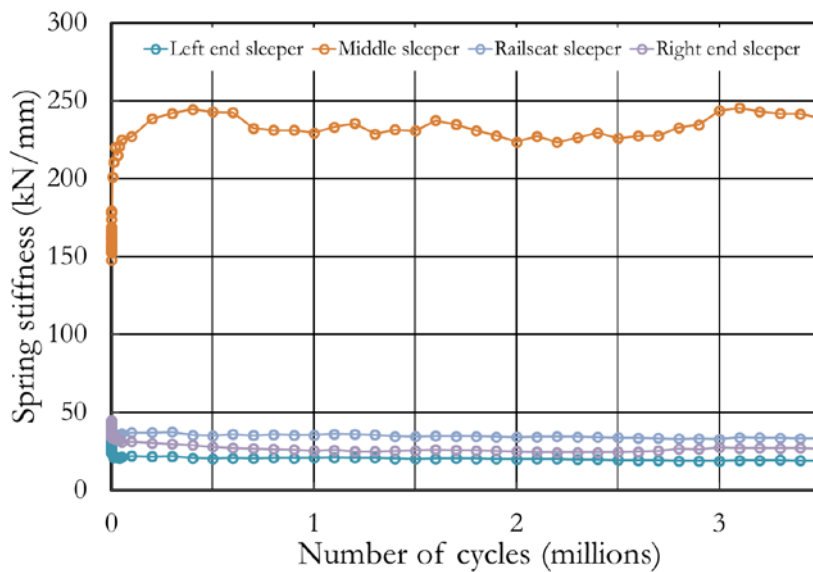


Figure 7.62: The average of spring stiffness at each section of steel sleeper

Figure 7.62 shows that at the railseat and sleeper ends the spring stiffness was relatively low and consistent (30 to 40kN/mm). However at the middle section of the sleeper it was much higher (~250kN/mm). The steel sleeper therefore formed a loaded hogged shape right from the first cycle, and become only slightly more pronounced with loading cycles. This was probably due either to the difficulty of installation and/or was an effect from the hollowed out shape of the steel sleeper.

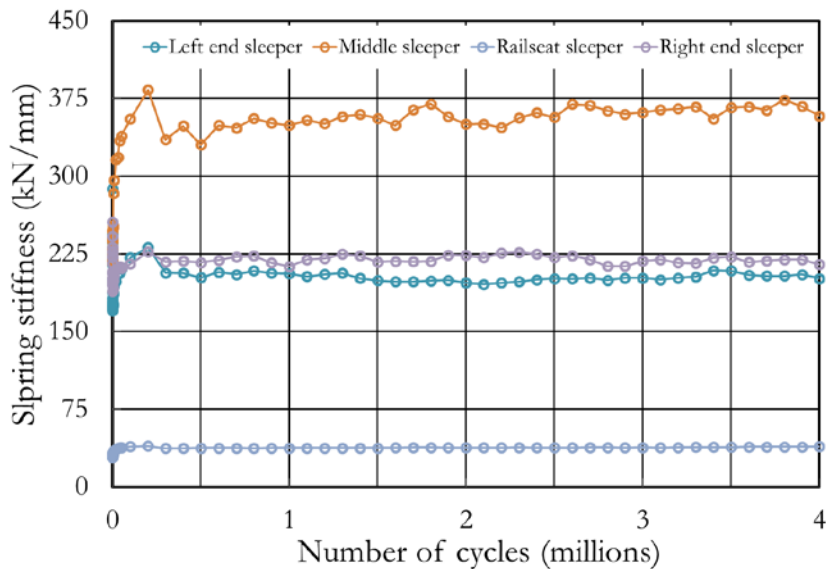


Figure 7.63: The average of spring stiffness at each section of plastic sleeper

Figure 7.63 shows that for the plastic sleeper, the spring stiffness at both ends was similar ($\sim 225\text{kN/mm}$). However at the railseat it was much lower ($\sim 40\text{kN/mm}$) and at the sleeper middle it was much higher ($\sim 360\text{kN/mm}$) consistent with the pronounced “ ω ” shape observed. Again this loaded shape was present from the first cycle and became only slightly more pronounced with loading cycles mainly due to a stiffening of the support beneath the sleeper middle.

7.5 Sand ingress test

To investigate the effect of the presence of sand as a fouling material in the ballast, two tests were carried out (summarised in Table 6.27). One of these two tests represented a baseline test, which was carried out on the current standard NR ballast grading using a mono-block PCM concrete sleeper (PCM Strescon Overseas Ventures Limited, 2014). Although the ballast followed the same grading as the current standard NR ballast, the parent rock was gabbro (described in Section 6.6.4). The testing was carried out using the same procedure as all other tests (described in Section 6.2.4) except that the PCM sleeper was subjected to a maximum static vertical load of 156.96kN . Thus the cyclic loading was a sinusoidal load at 3Hz between 5kN and 156.96kN . The instruments used and analyses carried out are similar to the sleeper and ballast intervention tests.

This work was carried out as part of a study to assess the impact of sand ingress on a ballasted railway to be located in the United Arab Emirates (UAE) where sand ingress from desert wind is a common occurrence. However, the findings may also be generalised to all ballasted railway in arid/desert landscapes.

Parts of the work written up in this thesis were also included in a report prepared for Eni-Saipem S.p.A. (Priest et al., 2013). Therefore the author would like to thank Eni-Saipem S.p.A. for allowing inclusion of this work within this thesis and to thank those who were closely involved with these tests for their contributions and support including Giovanni Cesaretti and Stefano Martinati (although many others were also involved).

7.5.1 Permanent settlement

Figure 7.64 presents the permanent settlement graphs of baseline and sand ingress tests as it occurred from the beginning of each test whilst Figure 7.65 shows the permanent settlement of baseline and sand ingress tests zeroed after 10 loading cycles.

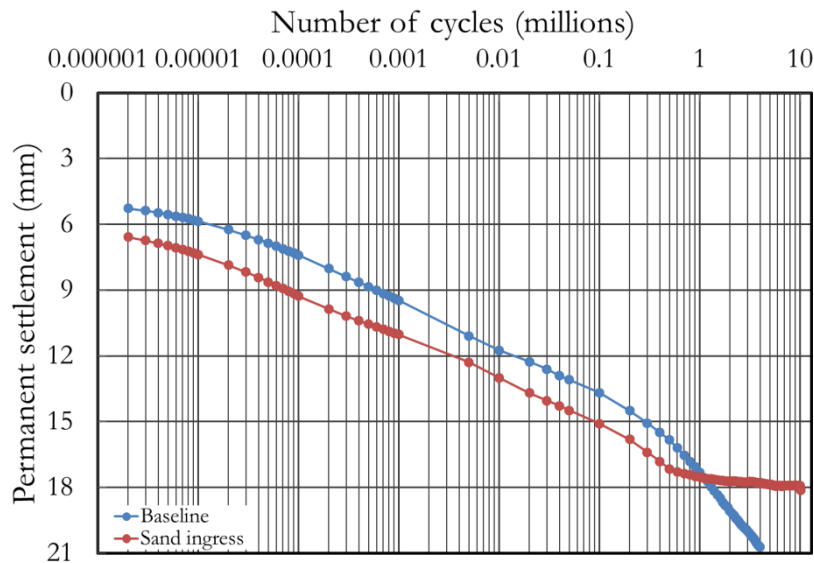


Figure 7.64: Permanent settlement graphs of baseline and sand ingress tests

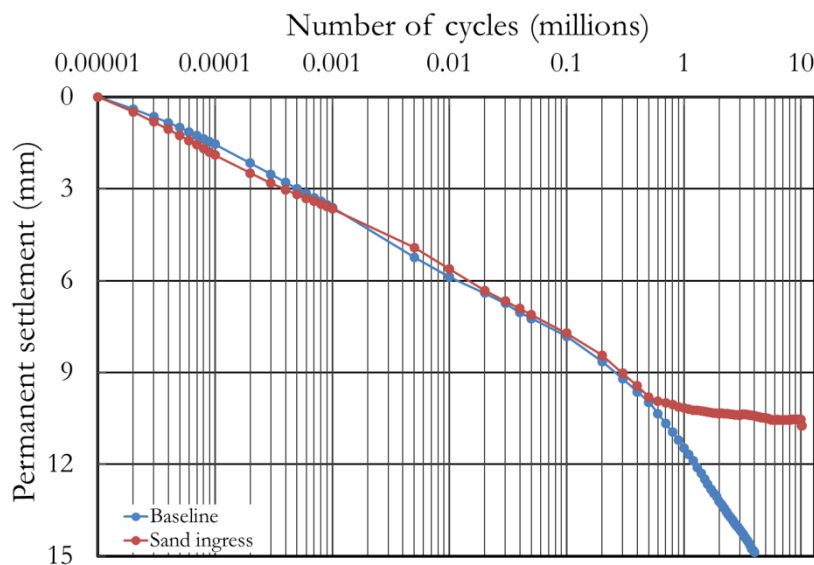


Figure 7.65: Permanent settlement graphs of baseline and sand ingress tests zeroed after 10 loading cycles

Discussion of the results

The permanent settlements in the baseline and sand ingress tests (Figure 7.64) show that both sleepers follow similar patterns of settlement with the rate reducing with later cycles so that it appears almost linear on a log scale of the number of loading cycles. Although the magnitudes of the initial settlements were different, after 10 loading cycles (Figure 7.65) the permanent settlement behaviour is consistent throughout the entire 0.5 million loading cycles prior to the first introduction of sand. This confirms that tests using the modified SRTF apparatus with the same arrangement of specimen and loading would produce a repeatable result after the initial variability of the first loading cycles is removed.

In the sand ingress test after 0.5 million loading cycles, a volume of sand sufficient to occupy 15% of the ballast voids under sleeper soffit was added. The sand was placed by raining it down onto the exposed crib and shoulder surface following a grid pattern. The placed sand then quickly migrated through the ballast voids and settled at the bottom of ballast layer. The introduction of sand immediately altered the rate of permanent settlement, drastically reducing it (Figure 7.65) compared with the baseline test. It may be hypothesised that as the sand worked its way down through the ballast, sand particles became lodged around the ballast contacts, thereby restricting rotation or inter-particle slippage which in turn led to a reduction in the rate of permanent settlement. In addition to this mechanism, it is also hypothesised that once the sand reached the base of the modified SRTF apparatus, the sand infilled around the ballast particles providing additional support to the base of each ballast particle, thereby reducing the peak contact stresses carried to the subgrade represented by the rubber mat. A summary of permanent settlement at key numbers of loading cycles for both tests is presented in Table 7.45, which also shows the percentage reduction of permanent settlement of sand ingress test compared with the baseline test. Key numbers of loading cycles are those immediately prior to an introduction of sand.

Table 7.45: Permanent settlement and percentage reduction of permanent settlement into baseline test at number of loading cycles (percentage of sand ingress introduced) in sand ingress test

Test label	Total loading cycles applied (millions)	Permanent settlement (mm) at						
		Loading cycles (millions)						
		0.5	1.0	1.5	2.0	2.5	3.0	4.0
		Percentage of ballast void (%) occupied by sand at the corresponding loading cycle						
		0	15	30	45	60	80	100
Baseline	4.0	9.97	11.47	12.48	13.20	13.73	14.14	14.87
Sand ingress	10.25	9.80	10.17	10.28	10.35	10.36	10.40	10.42
Percentage reduction of permanent settlement		1.73	11.39	17.66	21.60	24.54	26.45	29.93

In the sand ingress test at 4 million loading cycles, the ballast voids were at 100% filled by sand. Further sand was introduced at 5.25 million loading cycles to fill the ballast shoulders and cribs and ensure the ballast voids below the sleeper soffit remained 100% filled with sand. At 3 million loading cycles the permanent settlement was ~26% less than that in the baseline test (Table 7.45). After this, the ongoing settlement for the sand ingress test had been virtually halted, this can be seen in Figure 7.65 where from 3 to 10 million loading cycles the sand ingress test settlement line is almost parallel to the number of loading cycles axis. At 10 million loading cycles, the magnitude of load was increased to 242kN (the maximum load capacity of hydraulic actuator used) to investigate the behaviour of ballast support in relation to permanent settlement of ballast. This led to a small increase in settlement right at the end of the test (Figure 7.65).

7.5.2 Sleeper deflection

In the sand ingress tests, the average four corner deflection was compared (Figure 7.66) and similar investigations were also carried out for the middle section of the sleeper (Figure 7.67).

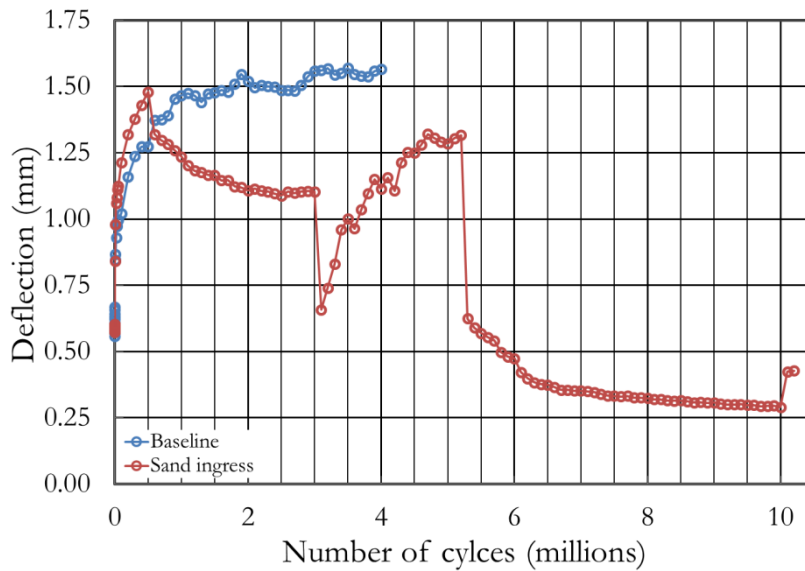


Figure 7.66: The average four corner sleeper deflection for baseline and sand ingress tests

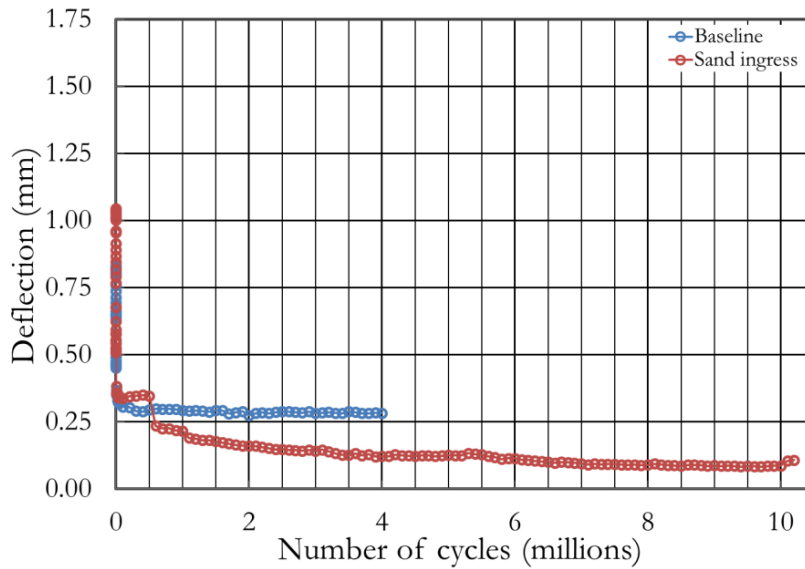


Figure 7.67: The average of sleeper middle section deflection of baseline and sand ingress test

Discussion of the results

Figure 7.66 shows that the average four corner sleeper deflection in the baseline test increased with the number of loading cycles throughout the test. This same behaviour occurred for the sand ingress test prior to sand introduction at 0.5 million loading cycles. After the first introduction of sand, the four corner deflection started to reduce (relative to the baseline test) and this trend of reducing deflection with number of loading cycles continued through all stages of sand introduction below the sleeper up until 100% filling at 3 million loading cycles. When 100% of the ballast voids below the sleeper had been filled with sand (i.e. at 3 million loading cycles), the four corner deflection reduced significantly. After this abrupt change, the four corner deflection then gradually increases until it attains approximately the same magnitude as just after the first introduction of sand (to fill 15% of the ballast voids below the sleeper). It is hypothesised that at 3 million cycles sand initially filled up to the level of the sleeper soffit, completely filling any gaps between the ballast and the sleeper creating a shorter distance of interface with a more uniform pressure distribution. However, with cycles of load the sand immediately beneath the sleeper became compacted or crushed so that the distance of

interface gradually increased. Thus the trend for increasing deflection after 3 million loading cycles is an indication of the compaction of the sand into the ballast voids below the sleeper soffit. Filling the crib and shoulder ballast voids at 5.25 million loading cycles created a reservoir of sand able to fall into and fill any gap between the sleeper and ballast, resulting in the ongoing reduction of in-cycle deflection to 10 million loading cycles.

In the sand ingress tests, the load was intended to be equivalent to a 32 tonne axle load, the maximum permitted on the railway to be built. As a consequence of the higher load the sleepers showed more extremely hogged loaded shapes that became apparent from early on in each test. To better illustrate the severe hogging that developed in these tests, the deflection at the sleeper middle is plotted separately (Figure 7.67) so that a comparison can be made with the deflection at the sleeper ends (Figure 7.66). Near the beginning of both tests the sleeper end deflection approaches 1.5 mm while the middle deflection is approximately one fifth of the sleeper end deflection, it is about 0.3 mm. In both tests there was an ongoing reduction of elastic deflection in the sleeper middle with loading cycles. However, the reduction in middle deflection was more severe in the sand ingress test and approached 0.1 mm with changes clearly occurring at 0.5 million cycles (first sand introduced) and at 5.25 million cycles (cribs and shoulders filled). A further observation is that while both tests led to sleepers deflecting more at their ends giving rise to a hogging loaded shape, introducing sand to the cribs and shoulder in the sand ingress test started a trend towards a more uniformly deflected shape. This can be seen in Figures 7.66 and 7.67 in the way the sand ingress deflection lines converge as they move from 5.25 million to 10 million loading cycles. It is possible that had the test continued for long enough these deflection lines would have converged and remained at the same magnitude.

7.5.3 Spring stiffness

Figures 7.68 and 7.69 show the average of four corners and area weighted spring stiffnesses respectively for the baseline and sand ingress tests.

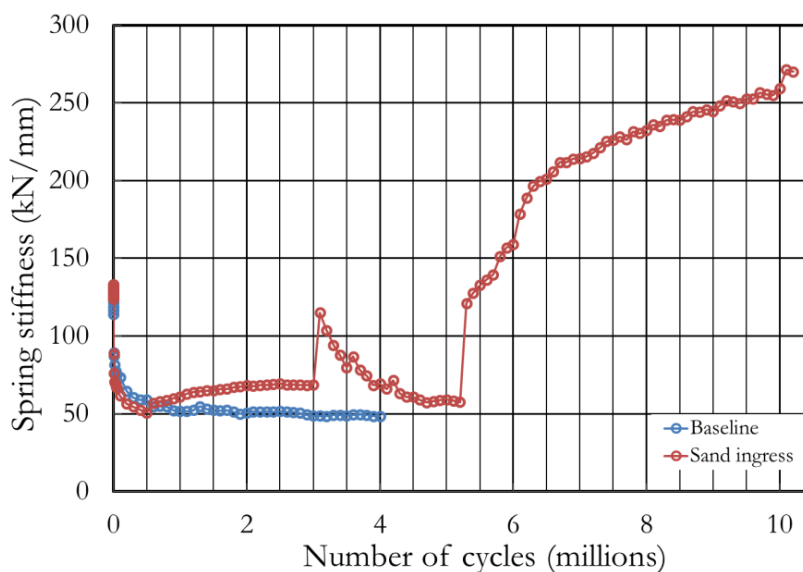


Figure 7.68: Average four corner spring stiffness of baseline and sand ingress tests

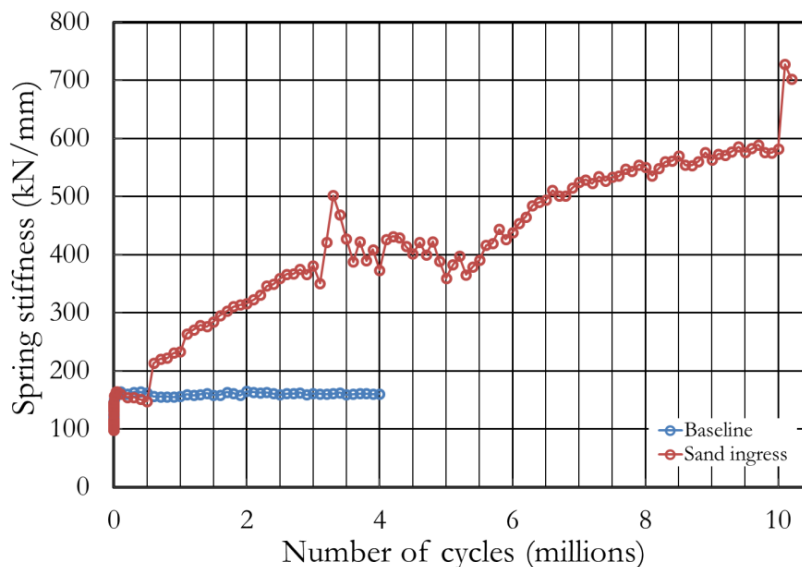


Figure 7.69: Spring stiffness averaged by area weighted method of baseline and sand ingress tests

Discussion of the results

The average four corner spring stiffness (Figure 7.68) in the baseline test reduced with the number of loading cycles throughout the full 4 million loading cycles. The same behaviour was also evident for the sand ingress test up to 0.5 million loading cycles when sand was initially introduced. Table 7.46 compares key four corner spring stiffnesses for both tests.

Table 7.46: Four corner spring stiffness and percentage increase of spring stiffness into baseline test at number of loading cycles (percentage of sand ingress introduced) in sand ingress test

Test label	Total loading cycles applied (millions)	Spring stiffness (kN/mm) at						
		Loading cycles (millions)						
		0.5	1.0	1.5	2.0	2.5	3.0	4.0
		Percentage of ballast void (%) occupied by sand at the corresponding loading cycle						
		0	15	30	45	60	80	100
Baseline	4.0	59	52	52	51	52	49	48
Sand ingress	10.25	51	61	65	68	69	69	69
Percentage increase of permanent settlement		-14.1	17.9	24.3	34.4	34.7	40.9	43.1

The introduction of 15% sand at 0.5M loading cycles increased the average four corner spring stiffness by ~18% compared with the baseline test. At each subsequent introduction of sand, further increases in the spring stiffness compared with the spring stiffness in the baseline test at the same number of loading cycles were observed (Table 7.46). A marked change in behaviour was noticed when sand was introduced to fill 100% of the ballast voids at 3 million loading cycles and the spring stiffness increased significantly (Figure 7.68). However this did not last long and over further loading cycles the spring stiffness returned to a similar magnitude as when the first sand to fill 15% of ballast voids was introduced. At 5.25 million loading cycles, sand to fill and to maintain sand in the ballast cribs and shoulders was added. At this point the spring stiffness increased markedly and continued on an increasing trend up to 10 million loading cycles. It is hypothesised that at 3 million loading cycles, the sand fill first reached the level of the sleeper soffit creating a stiffer interface with a more uniform pressure distribution. However with further loading cycles, the sand immediately beneath the sleeper became compacted or crushed and settled into the lower level voids so that the load again gradually

transferred back to the ballast/sleeper contacts. Thus the trend for reducing stiffness after 3 million loading cycles is an indication of the settlement of the sand into the ballast voids below the sleeper soffit. Filling the crib and shoulder ballast voids at 5.25 million cycles created a reservoir of sand able to fall into any gap between the sleeper and ballast, resulting in the ongoing increase in stiffness to 10 million loading cycles.

Spring stiffness averaged by the area weighted method (Figure 7.69) shows that with no sand in the ballast, the spring stiffness rapidly reached a constant value so that subsequent loading cycles did not cause any further significant change. For the sand ingress test, the area weighted spring stiffness started increasing as sand was introduced to show a first peak at 3 million loading cycles, which subsequently dropped back with a further increasing trend to a final peak after 5.25 million loading cycles. Table 7.47 compares the area weighted spring stiffnesses for both tests at key numbers of loading cycles.

Table 7.47: Area weighted spring stiffnesses and percentage increase of spring stiffness into baseline test at number of loading cycles (percentage of sand ingress introduced) in sand ingress test

Test label	Total loading cycles applied (millions)	Spring stiffness (kN/mm) at						
		Loading cycles (millions)						
		0.5	1.0	1.5	2.0	2.5	3.0	4.0
		Percentage of ballast void (%) occupied by sand at the corresponding loading cycle						
		0	15	30	45	60	80	100
Baseline	4.0	162	156	159	165	159	161	161
Sand ingress	10.25	148	233	285	316	359	381	373
Percentage increase of permanent settlement		-8.7	48.9	79.4	91.6	125.7	137.0	132.5

Table 7.47 shows that the first sand introduction caused an increase in the area weighted spring stiffness to ~49% higher than the baseline test. In the sand ingress test, further placement of sand caused a corresponding increase in the spring stiffness (Figure 7.69). At 4 million loading cycles when the ballast voids below the sleeper were expected to be 100% filled by sand, the spring stiffness of sand ingress test was ~132.5% higher than the baseline test. Further loading up to 5.25 million loading cycles decreased the spring stiffness. At 5.25 million loading cycles sand was introduced to fill the voids of the crib and shoulder ballast. Then the spring stiffness increased with the number of loading cycles, in accordance with the mechanism of behaviour described earlier. The spring stiffness sand ingress test at 10 million loading cycles of 582kN/mm is ~262.5% higher than that after 4 million loading cycles in the baseline test.

At 10 million loading cycles the magnitude of the applied load was increased to 242kN for a further 0.25 million loading cycles. This led to a large increase of spring stiffness immediately after the loading application, which then remained relatively unchanged with the further loading cycles (Figure 7.64).

7.5.4 Ballast pressure

In the baseline and sand ingress tests, the ballast pressure from plates 1 and 4 was evaluated as this showed the clearest trends for mono-block sleepers (described in Section 6.5.4). Figures 7.70 and 7.71

show the ballast pressures on plates 1 and 4 in both the baseline and sand ingress tests under the maximum and minimum loads.

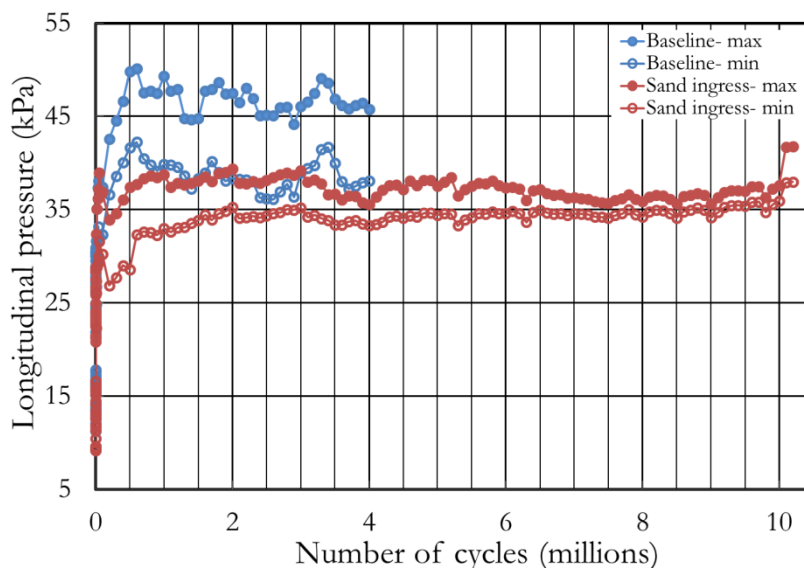


Figure 7.70: Variation of maximum and minimum longitudinal ballast pressure of plate 1 with number of loading cycles for baseline and sand ingress tests

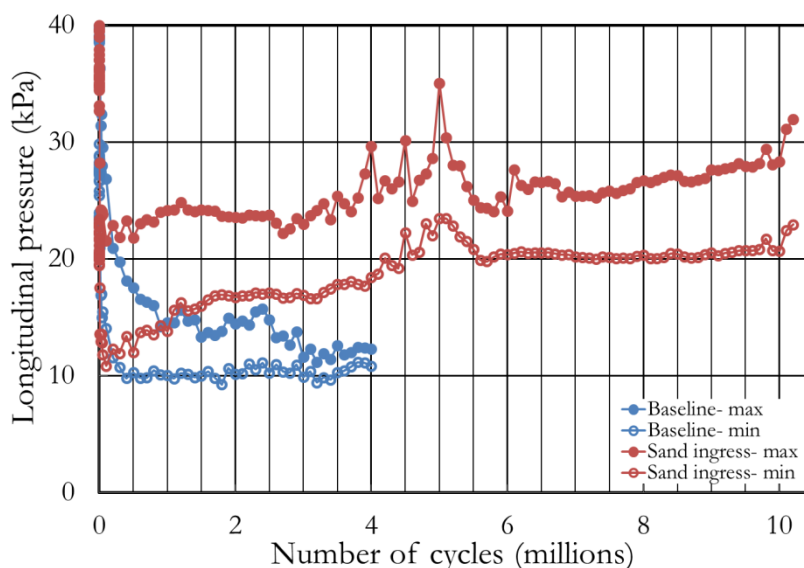


Figure 7.71: Variation of maximum and minimum longitudinal ballast pressure of plate 4 with number of loading cycles for baseline and sand ingress tests

Discussion of the results

Plate 1 for both tests (Figure 7.70) showed an increase in the ballast pressure with the number of loading cycles applied. However, there were differences in the initial magnitude of the pressures in both tests, probably caused by inherent variability between tests occurring due to the large particle sizes in relation to the plate, so that the number of ballast particles in contact with a plate can vary significantly (as in the other sleeper and ballast intervention tests: 7.2.4). The trends of pressure in the baseline test also agree well with the trends for other mono-block sleeper tests (plate 1 increase, plate 4 decrease).

In the middle of the sleeper (plate 1), the introduction of sand in the sand ingress test caused the range of ballast pressure under maximum and minimum loading to narrow (Figure 7.70). The

continued introduction of sand until the ballast shoulders and cribs were filled led to a continued narrowing in the range of pressures recorded in plate 1 until the maximum and minimum cyclic loading values were almost the same. At 4 million loading cycles in the baseline test, the pressure range on plate 1 was approximately 10kPa while in the sand ingress test the pressure range at 4 million loading cycles was about 3kPa.

At plate 4 (near the sleeper end), the ballast pressure in the baseline test (Figure 7.71) agreed with the trends of ballast pressure on plate 4 in the other mono-block sleeper tests by showing a reducing ballast pressure with number of loading cycles tending to a constant value. The same trend was followed in the sand ingress test prior to the first introduction of sand. However, after sand was introduced at 0.5 million loading cycles the ballast pressure on plate 4 gradually increased with the number of loading cycles (Figure 7.71), tending towards the values of plate 1. This implies that the introduction of sand helped to stabilise the shoulder area allowing the mobilisation of a greater confining pressure (ballast particle moving laterally rather than out of the way), hence more support to the sleeper. These pressure measurements are consistent with the more uniform sleeper deflections that occurred with increasing number of loading cycles in the sand ingress test. These findings agree with the results of the spring stiffness analysis presented earlier and also agree with the findings of previous work carried out by other researchers; Zakeri and Abbasi (2011, 2012a, 2012b) conducted field investigations for ballasted railways in sandy desert areas and concluded that the presence of sandy grains between ballast aggregates increased the stiffness of the ballast layer and led to an increase of the spring stiffness and a lower maximum pressures beneath the sleeper with the sleeper pressure tending to be more uniformly distributed with loading cycles.

7.5.5 Mobilised earth pressure ratio

To determine the mobilised earth pressure ratios (K_{min} and K_{max}) and angle of effective shearing resistance (ϕ'_{mob}), Equations 6.5 to 6.10 were used (the same method as for the sleeper and ballast intervention tests). Table 7.48 shows the maximum and minimum vertical pressures (based on the maximum and minimum vertical loads of 156.96kN and 5kN respectively and the soffit area of the sleeper (Table 6.10)) and the corresponding mobilised earth pressure ratio and the mobilised angle of effective shear resistance implied in both the baseline and sand ingress tests.

Table 7.48: Summary of the highest and the lowest of measured earth pressure among the data recorded by all plates for entire loading cycles in the baseline and sand ingress tests.

Test ID	Average vertical pressure (kPa)		Measured horizontal pressure (kPa)		Mobilised earth pressure ratios		ϕ'_{mob} implied by ($^{\circ}$)	
	Max	Min	Max	Min	K_{min}	K_{max}	K_{min}	K_{max}
Baseline	204.64	6.52	50.11	42.25	0.245	6.480	37.34	47.11
Sand ingress	204.64	6.52	39.98	35.91	0.195	5.508	42.31	43.84

Discussion of the results

In both baseline and sand ingress tests, at the maximum and minimum vertical pressures, the mobilised earth pressure ratio moved towards the active and passive condition respectively (Table 7.48). This is a similar trend as in the sleeper and ballast intervention tests and can be seen by comparing K_{max} and K_{min} in Tables 7.48 to Table 7.13. The mobilised earth pressure ratio at the minimum vertical load is between 5.5 and 6.5 which is significantly above the estimated normal

consolidation earth pressure ratio obtained using the method of Jaky (1948) (Table 7.13) and due to the ballast at minimum load being overconsolidated (Brooker and Ireland, 1965).

Based on a simplified method, the mobilised angle of effective shearing resistance in the baseline and sand ingress tests (when the whole area of ballast was covered by sand) at the maximum and minimum vertical pressures was found to be in the range of 37 to 48 degrees (Tables 7.48). This range also agrees with the results from sleeper and ballast intervention tests and fits well with the previous work described in section 7.2.5.

Table 7.48 also shows that in the sand ingress test, the ballast pressure was lower than the baseline test; perhaps, is because the sand helping to distribute the pressure to a larger area. The sand also caused the mobilised angle of effective shearing resistance to increase at the maximum vertical pressure and reduce at the minimum vertical pressure. In the sand ingress test, sand seemed to stabilise the ballast by keeping the mobilised angle of effective shearing resistance relatively constant regardless at the maximum or the minimum vertical pressure.

7.5.6 Pressure paper

In both baseline and sand ingress tests, pressure paper was located as for earlier tests (e.g. sleeper/ballast, ballast/subgrade and ballast/wall interfaces). The placement of pressure paper was described in Section 6.4.2.

Sleeper/ballast interface

Figure 7.72 shows the contacts recorded by the pressure paper located at the level of the sleeper soffit and Table 7.49 presents the numbers of contacts per sleeper. However, it was not possible to analyse the contact area in the sand ingress test due to damage to the pressure paper beneath the railseats. Pressure paper placed beneath the railseats was also covered by sand powder (thought to be due to sand grain crushing) and could not be reliably scanned. Therefore the images for the railseats were taken by a camera (Figure 7.72), this method of image capture resulted in a greyer background colouring.

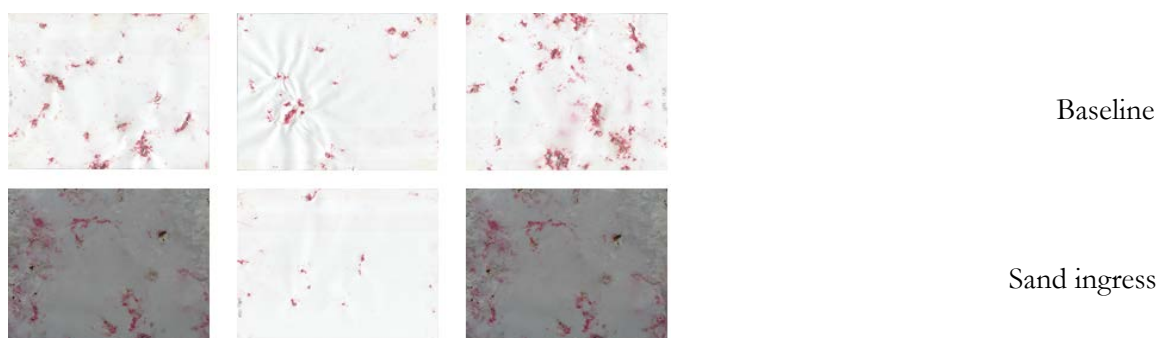


Figure 7.72: The contact areas recorded at the ballast/sleeper interface in baseline and sand ingress tests

Table 7.49: The number of particle contact at sleeper/ballast interface in baseline and sand ingress tests

Test ID	Sleeper	Number of contact on the pressure paper at			Contact per sleeper, 10-50MPa rated pressure paper
		Left railseat	Middle	Right railseat	
Baseline	PCM	23	22	34	380
Sand ingress		40	12	35	419

At the base of the ballast layer

Figures 7.73 and 7.74 show the contacts recorded on the pressure paper sheets placed at the base of ballast layer with ranges of 2.5-10MPa and 10-50MPa respectively, after each test.

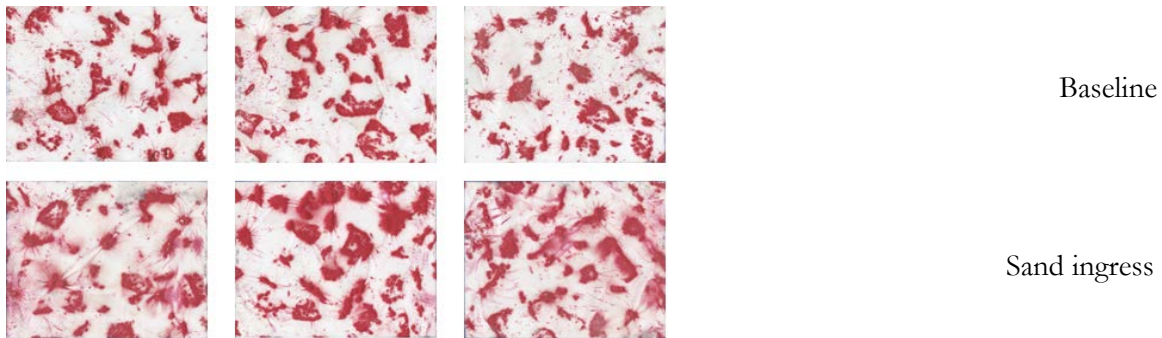


Figure 7.73: Contact areas recorded on the pressure paper rated 2.5-10MPa at the ballast/subgrade interface in baseline and sand ingress tests

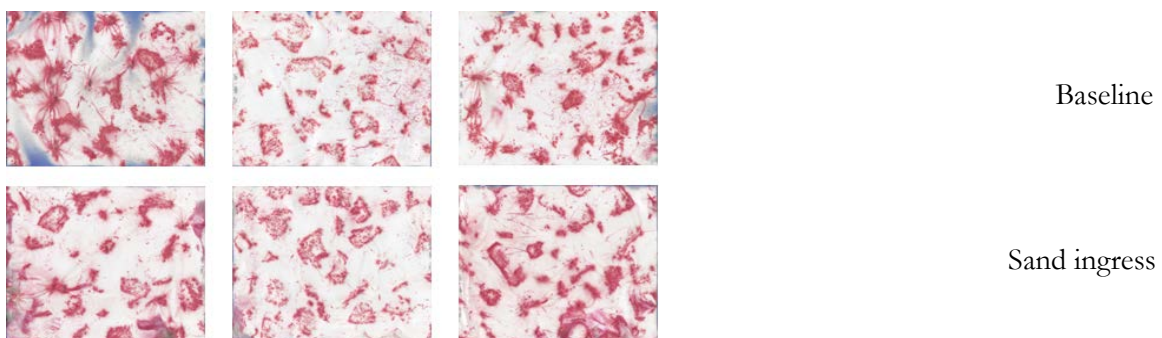


Figure 7.74: Contact areas recorded on the pressure paper rated 10-50MPa at the ballast/subgrade interface in baseline and sand ingress tests

Tables 7.50 and 7.51 present the proportional of contact area recorded using pressure papers in the ranges 2.5-10MPa and 10-50MPa respectively, at each location in the baseline and sand ingress tests.

Table 7.50: The percentage of particle contact area at ballast/subgrade interface in baseline and sand ingress tests rated by 2.5-10MPa pressure paper

Test ID	Sleeper	Percentage of contact area recorded on the pressure paper at			Percentage of contact area per sleeper, 2.5-10MPa pressure paper
		Left railseat	Middle	Right railseat	
Baseline	PCM	20.75	24.22	19.84	21.60
Sand ingress		26.52	32.90	31.41	30.28

Table 7.51: The percentage of particle contact area at ballast/subgrade interface in baseline and sand ingress tests rated by 10-50MPa pressure paper

Test ID	Sleeper	Percentage of contact area recorded on the pressure paper at			Percentage of contact area per sleeper, 10-50MPa pressure paper
		Left railseat	Middle	Right railseat	
Baseline	PCM	22.57	10.68	18.34	17.20
Sand ingress		18.73	12.60	22.04	17.79

Figures 7.73 and 7.74 and Tables 7.50 and 7.51 show that for the lower range (more sensitive) pressure paper, the area of contact was greater below the sleeper middle. However, for the higher pressure paper the reverse was true: the area of contact beneath the railseats was greater than that below the middle section of the sleeper.

The average particle contact pressure on the subgrade was also analysed based on the RI recorded on the 10-50MPa pressure paper together with the pressure paper calibration graph (Figure 6.42) (described in Section 7.2.6). A range of values is given, based on the upper and lower bounds of the pressure paper calibration curve in Figure 6.42. The analysis results and the range of load per m² subgrade area from the 10-50MPa pressure paper are presented in Tables 7.52 and 7.53 respectively.

Table 7.52: The magnitude of particle pressure at ballast/subgrade interface in baseline and sand ingress tests

Test ID	Sleeper	Magnitude of particle pressure (MPa) at the location of			Average particle pressure on the subgrade, by 10-50MPa rated paper (> 2.5MPa)
		Left railseat	Middle	Right railseat	
Base	PCM	42.85-50.00	30.00-40.00	37.77-48.57	36.87-46.19
Sand ingress		30.00-40.00	30.00-40.00	37.78-47.14	32.59-42.38

Table 7.53: The range of load per m² subgrade area in baseline and sand ingress tests

Test ID	Sleeper	Proportions area of contacts on subgrade, 10-50MPa pressure paper	Average range of particle pressure on subgrade (MPa), 10-50MPa pressure paper	Range of load per m ² subgrade area (MN)
Baseline	PCM	17.20	36.87-46.19	6.34-7.94
Sand ingress		17.79	32.59-42.38	5.80-7.54

The range of load per m² subgrade area (Tables 7.53) is then compared to the average vertical pressure on the subgrade based on an assumed 2:1 load spread with the inclusion of ballast self-weight to obtain comparison factors as was carried out in the sleeper and ballast intervention tests (Section 7.2.6). Table 7.54 presents the magnitudes of pressures determined using the 2:1 spread method assumption and the pressure paper, and the comparison factor between them.

Table 7.54: Magnitude of vertical pressure on subgrade analysed by both pressure paper and 2:1 load spread methods and its comparison factor for baseline and sand ingress tests

Test ID	Sleeper	Range of load per m ² subgrade area (MN)	Average vertical pressure (2:1 spread method with the inclusion of self-weight of ballast) (kPa)	Comparison factor
Baseline	PCM	6.34-7.94	97.78	64.8-81.2
Sand ingress		5.80-7.54	97.82	59.3-77.08

On the modified SRTF apparatus wall

Table 7.55 presents the proportion of contact area at ballast/wall interface based on the 10-50MPa pressure paper, in the baseline and the sand ingress tests. The lower range pressure paper (2.5-10MPa) was not used at this location in these tests. This was because earlier results (Section 7.2.6) showed that 2.5-10MPa pressure paper was too low range to measure the particle contact pressure at this interface.

Table 7.55: Proportions of the ballast/wall interface area over which the contact pressure is at least 2.5MPa in baseline and sand ingress tests

Test ID	Sleeper	Percentage of contact area recorded on the pressure paper at the location of		Average % contact area on the wall, by 10-50MPa rated paper (> 2.5MPa)
		Left railseat	Middle	
Baseline	PCM	1.40	1.96	1.68
Sand ingress		1.51	1.51	1.51

Tables 7.56 presents the average particle contact pressure at the ballast/wall interface which was obtained from the pressure paper using the same analysis as in sleeper and ballast intervention tests. Table 7.57 shows the range of load per m² ballast area.

Table 7.56: The magnitude of particle pressure at ballast/wall interface in baseline and sand ingress tests

Test ID	Sleeper	Magnitude of particle pressure (MPa) at the location of		Average of particle pressure on the wall, by 10-50MPa rated paper (> 2.5MPa)
		Left railseat	Middle	
Base	PCM	29.62-39.44	30.0-40.0	29.81-39.72
Sand ingress		26.92-33.33	34.44-45.71	30.68-39.52

Table 7.57: The range of load per m² ballast area in baseline and sand ingress tests

Test ID	Sleeper	Proportions area of contacts on the wall, 10-50MPa pressure paper	Average range of particle pressure on the wall (MPa), 10-50MPa pressure paper	Range of load per m ² subgrade area (MN)
Baseline	PCM	1.68	29.81-39.72	0.50-0.67
Sand ingress		1.51	30.68-39.52	0.46-0.60

Table 7.55 presents the cumulative ballast pressure measured from the pressure paper, the highest ballast pressure recorded by the pressure plates over the entire loading history applied and the comparison factor.

Table 7.58: Magnitude of ballast pressure analysed from pressure paper and measured by pressure plate and its comparison factor in baseline and sand ingress tests

Test ID	Sleeper	Range of load per m ² ballast area (MN), 10-50MPa rated pressure paper	Maximum ballast pressure measured by plates (kPa)	Comparison factor
Baseline	PCM	0.50-0.67	50.11	9.9-13.4
Sand ingress		0.46-0.60	41.77	11.0-14.4

Discussion of the results

Comparing the pressure paper results at the sleeper/ballast interface in both tests, the number of contacts in both the baseline and sand ingress tests was not significantly different (380 and 419 being within 10% of each other). There were 39 additional contacts in the sand ingress test; this increase could be a result of the inherent variability of sample preparation and/or the application of more loading cycles and a higher load for the final 0.25 million loading cycles. The application of the higher load at the end of the test may also have led to the breakage of ballast particles in contact with sleeper soffit thus new broken off particles created a small number of new contacts. The introduction of sand was not thought to have significantly altered the contact points recorded because when the sand filled the ballast voids at the sleeper/ballast interface, it levelled the contact so that the contact pressure from the sand remained below the threshold (2.5MPa) for detection by the pressure paper.

At the ballast/subgrade interface, Figure 7.73 and Table 7.50 show that for the lower rated paper at the middle section of the sleepers, the area of contact was larger than beneath the railseats. However the 10-50MPa range pressure paper indicates that for the higher pressures present (Figure 7.74 and Table 7.51), the contact areas beneath the railseats were larger than that at the middle section of the sleeper. This agrees with the results of earlier tests. At the middle section of the sleeper, the contact area in the sand ingress test (Table 7.51) was larger than in the baseline test. This suggests that the

introduction of sand acted to homogenise the contact pressure distribution. The introduction of sand slightly increased the average contact area and reduced the magnitude of particle pressure at the ballast/subgrade interface (Tables 7.51 and 7.52). The application of a higher load in the final stage of the sand ingress test seemed not to affect the pressure paper results. This may be because by this stage of the test the sand was able to distribute the load uniformly below the threshold for detection of the 10-50MPa rated paper.

In Table 7.54, the comparison factor obtained from the baseline test was in the range of 64.8 to 81.2. However, the comparison factor obtained from the sand ingress test was in a lower range (59.3 to 77.08). The lower comparison factor might indicate that the sand was able to constrain the ballast particles from rotation or changing their orientation; thus with cyclic loading, the ballast particles were always in relatively the same position or there was no significant area of contact being developed recorded on the pressure paper. Comparison factors obtained from both tests support the earlier test results that ballast particles moved due to cyclic loading.

At the sidewalls of the testing apparatus, the pressure paper showed that the contact area adjacent to the middle of the sleeper (Table 7.55) was larger than that adjacent to the railseats. This agrees with the results from sleeper and ballast intervention tests. The introduction of sand again seemed to homogenise the load distribution (Table 7.55). The average ballast particle contact pressure adjacent to the middle section of the sleeper was also higher than that adjacent to the railseat (Table 7.56), for both baseline and sand ingress tests. This agrees with the trends in data from the pressure plates that the horizontal pressure at the middle section of sleeper increased with the number of loading cycles. The average particle contact pressure for the sand ingress test was slightly higher than that in the baseline test. However, taking into account the contact area, the introduction of sand reduced the range of load per m² of ballast area (Table 7.57). Comparing the magnitude of pressure from the pressure paper with the highest pressure recorded among the pressure plates for the entire number of loading cycles applied shows that the contact area recorded on pressure paper increased by between 9.9 to 13.4 times for the baseline test and by 11.0 to 14.5 times for the sand ingress tests (this possibly occurred before the sand was introduced).

7.5.7 Particle breakage

In the baseline and sand ingress tests, ballast breakage was investigated using the same methods (i.e. visual observation, PSD and measurement of random ballast particle) as in the earlier tests (Section 7.2.7).

Visual observation

Visual observation of the ballast bed directly beneath the sleeper soffit was used to evaluate particle breakage. In the sand ingress test this meant it was necessary to excavate the ballast and sand from the cribs and shoulders. Figure 7.75a shows the condition immediately after testing was completed.

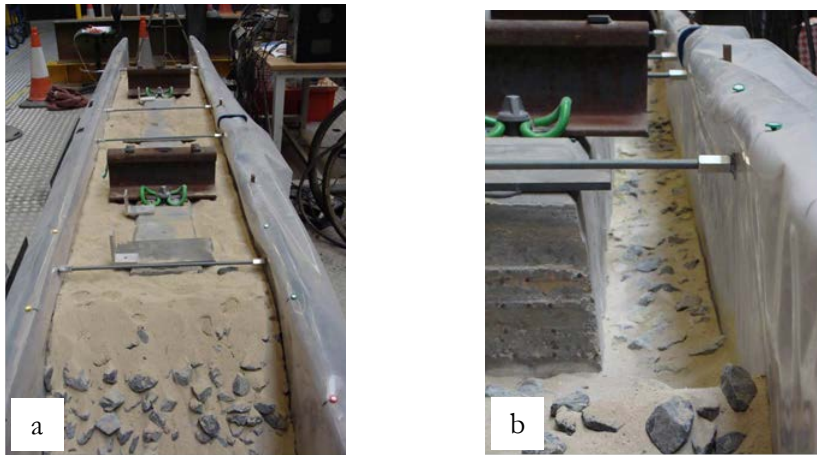


Figure 7.75: Ballast and sand in the modified SRTF apparatus, a) immediately after loading stage, b) with ballast and sand were removed

Figure 7.75b shows the cribs and shoulders carefully removed to the level of the sleeper soffit. This was intended to ensure that no sand could fall into the space under the sleeper during its subsequent removal. On careful removal of the sleeper it was seen that sand completely filled the ballast underneath it, with a clear outline of where the sleeper was sitting (Figure 7.76).



Figure 7.76: Appearance of ballast surface underneath the sleeper after sleeper removal viewed from opposite ends

There was also a noticeable difference in the appearance of the sand. Directly under the railseats (at the ends of the sleeper), the sand had patches that appeared whiter with significantly finer grain sizes, with a more flour-like appearance indicating that it had been crushed. This crushing occurred when sand reached the level necessary to make direct contact with the sleeper soffit. This flour-like material from beneath the sleeper soffit was covered the surface of the ballast and sleeper (Figure 7.77). At the centre portion of the sleeper however, there was no significant evidence of sand crushing although the sand completely filled the space under the centre of the sleeper.



Figure 7.77: Flour-like fines arising from sand crushing brought to the ballast and sleeper surface because of cyclic movement of the sleeper

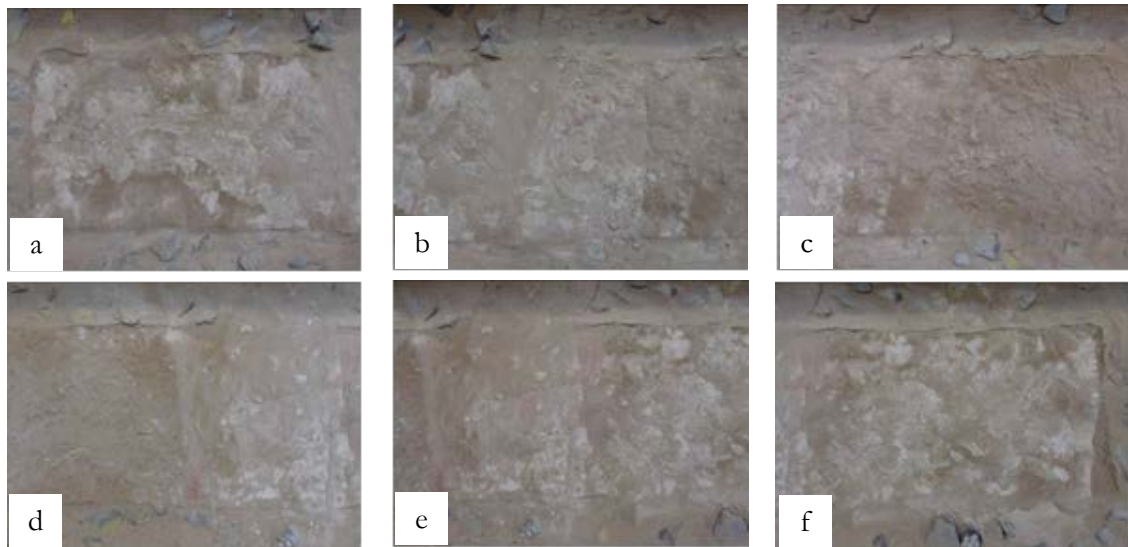


Figure 7.78: Close up of ballast and sand under the sleeper shows the ballast/sleeper interface area for right railseats (a) progressing through to left railseat (f)

Figure 7.78 shows close-up views along the sleeper footprint after sleeper removal, to highlight the differences in the surface texture between the sand under the railseat (a and f) and under the centre of the sleeper (b to e). The difference in texture was the result of extensive crushing of the sand under the railseats which was thought to have occurred because of higher pressures and ranges of sleeper movement at the ballast/sleeper interface at these locations.

Table 7.59 presents the number of ballast particle breakages found in baseline and sand ingress tests based on visual observation.

Table 7.59: The number of ballast particle breakages found in baseline and sand ingress test based on visual observation

Test ID	Ballast grading	Total load cycles applied (millions)	Number of breakage
Baseline	NR (Gabbro)	4.0	12
Sand ingress		10.25	None

Discussion of the results

The results of the visual observation evaluation for the baseline test (Table 7.59) suggest that very little ballast breakage occurred. In the sand ingress test, it was difficult to observe any ballast particle breakages with the sand present. However, through carefully brushing off the sand from the ballast surface, it was found that there was no breakage present. The breakage that was present in the baseline test was located at the edges of the sleeper soffit. This agrees with earlier findings in sleeper and ballast intervention tests. Although in the sand ingress test no breakage was observed, there was a noticeable difference in the appearance of the sand under the railseats showing an extensive crushing of sand at this location. The presence of the sand and its ability to homogenise the pressure distribution through the ballast is thought to have helped to protect the ballast particles from breakage in this test.

PSD method

Figures 7.79 and 7.80 compare the results of PSD tests on ballast before and after testing. Ballast samples for PSD tests were taken from the same locations as in the previous sleeper and ballast intervention tests. However, an additional ballast sample was taken from the shoulder area.

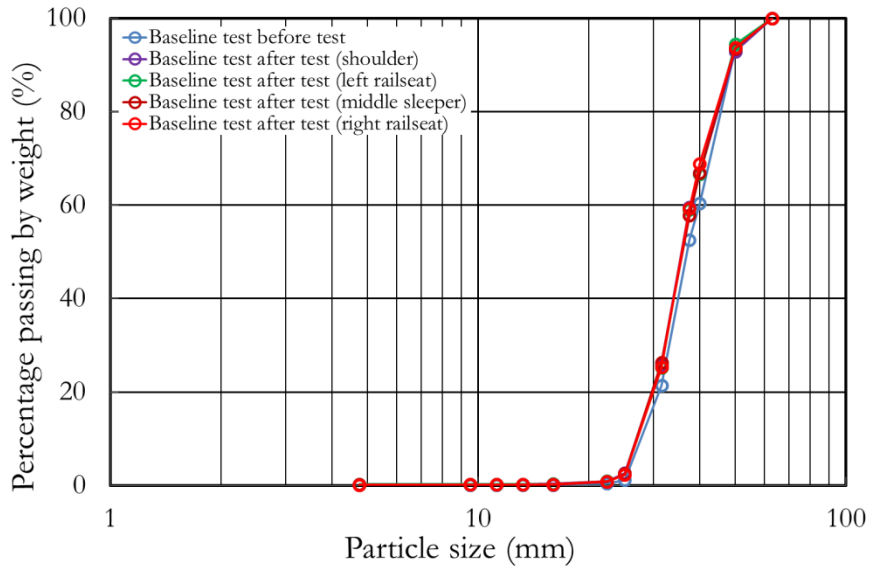


Figure 7.79: PSD graphs of ballast after testing taken from different locations compared to prior to the baseline test

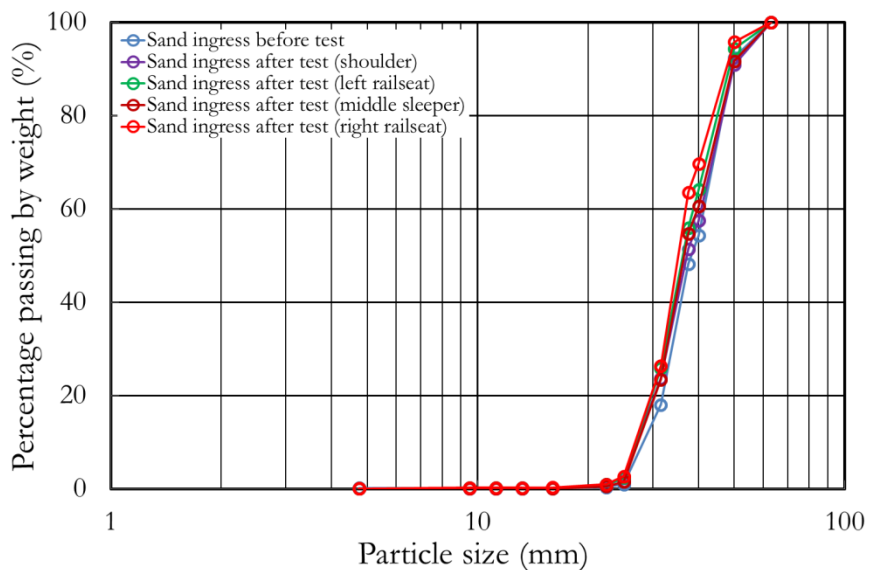


Figure 7.80: PSD graphs of ballast after testing taken from different locations compared to prior to the sand ingress test

Discussion of the results

The results of the PSD tests (Figures 7.79 and 7.80) suggest that no appreciable change of PSD occurred after loading. There were only minor variations in the after PSD to that from the initial tests in both baseline and sand ingress tests. The PSD graphs of the sand ingress test after testing show a slightly larger variation than the baseline test, perhaps due to the larger of number loading cycles, although this may have been mitigated by protection afforded by the sand and so it is not clear why there was more, albeit still very minor increases in the percentage passing on some parts of the PSD

graph. Overall the minor variations in the PSD graphs suggest that ballast breakage was barely detectable beyond the inherent variability of testing different samples.

Measurement of selected ballast particles

In the baseline and sand ingress tests, measurement of 50 randomly selected particles was also carried out as in the previous sleeper and ballast intervention tests. Figures 7.81 to 7.82 show the before and after PSDs of the 50 randomly selected particles in the baseline and sand ingress tests respectively. Table 7.60 shows the results of individual ballast particle measurement.

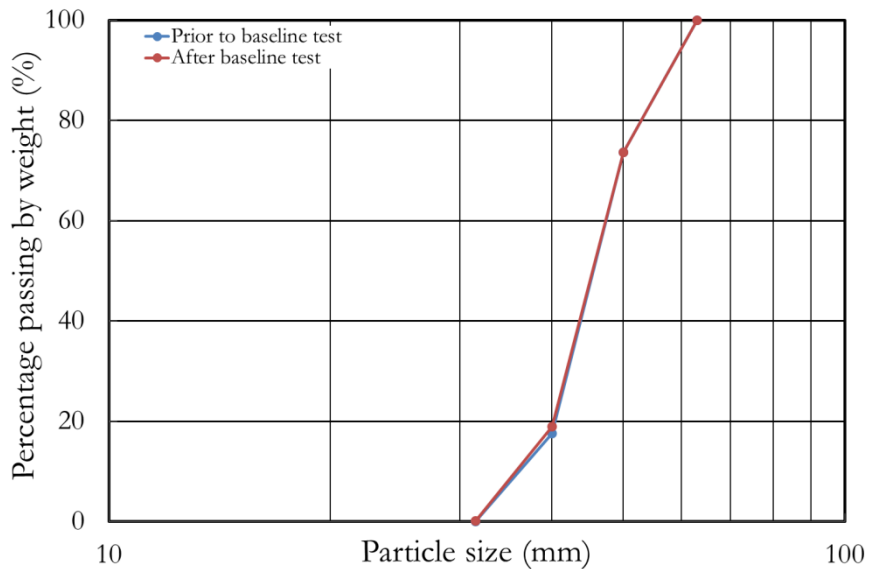


Figure 7.81: PSD graphs of randomly selected particles on variant 3 before and after test

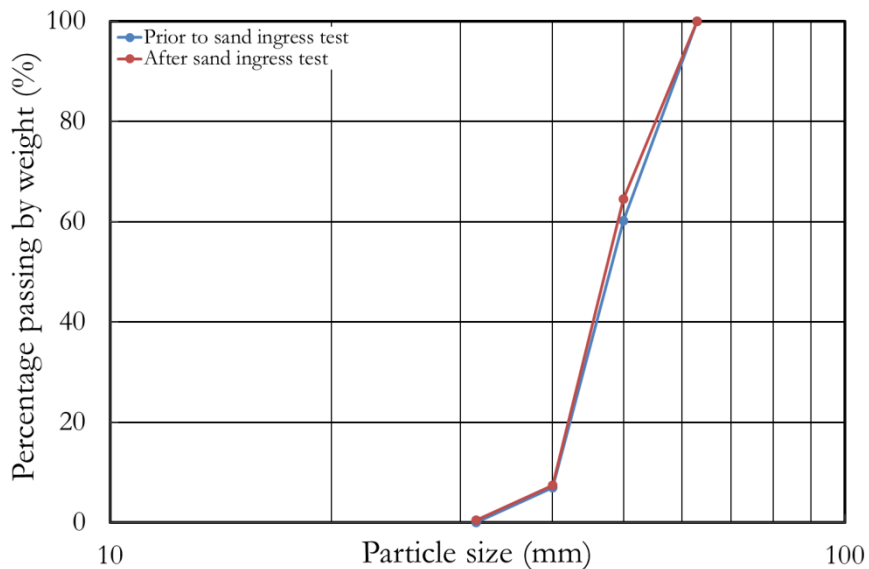


Figure 7.82: PSD graphs of randomly selected particles on variant 3 before and after test

Table 7.60: Percentage of total loss of mass of randomly picked ballast used in baseline and sand ingress tests

Test ID	Ballast grading	Total load cycles applied (millions)	Range of min to max loss of mas of individual particle (%)	The average loss of mass for 50 particles (%)
Baseline	NR (gabbro)	4.0	0.03-0.47	0.11
Sand ingress		10.25	0.06-16.87	0.46

Discussion of the results

Figures 7.81 and 7.82 show that the PSD of 50 randomly selected ballast particles for the baseline and sand ingress tests confirm that there was a minor breakage occurred in both tests. Table 7.60 shows that in the baseline test, the reduction of mass from 50 randomly selected ballast particle was in the range of 0.03 to 0.47% whilst in the sand ingress test the range was 0.06 to 16.87%. The maximum range for the sand ingress test was higher than for the baseline test and the previous sleeper and ballast intervention tests. This was because within the 50 randomly selected ballast particles, particle breakage was occurred. However, this was unobserved during visual investigation due to the breakage not being at the sleeper/ballast interface, but at ballast/ballast contacts which became apparent when it was recovered for measurement. Table 7.60 also shows that there was only a 0.11% loss of total mass in the baseline test. This is consistent with the results of both visual observation and PSD methods which indicated only minor breakage occurred. However, in the sand ingress test, the total loss of mass was almost 5 times higher than in the baseline test. This may have been a result of the increased total number of loading cycles and an increased magnitude of vertical loading over the final cycles. Raymond (1987) suggested that the use of concrete sleeper for a heavier loading needs to be considered to avoid ballast abrasion. However, the use of a concrete sleeper with higher load is still possible on higher quality ballast which has a Moh's hardness value greater than concrete (normally in scale of 5) to avoid abrasion (Raymond, 1987). Based on Table 6.20, ballast for railway tracks with a heavier load and concrete sleepers, the use of granite (Moh's hardness ranges 6 to 7) is more suitable than gabbro (Moh's hardness ranges 5 to 7).

7.6 A trial test on combined variables

On the basis of the tests so far described, the most advantageous and mutually compatible testing variables from sleeper and ballast intervention tests were identified for a combined test based on consideration of the least amount of permanent settlement. Ballast grading variant 3 performed best with the G44 sleeper, while the best sleeper performance on the current standard NR ballast grading was of the twin-block sleeper. A trial test (combination 1) was therefore carried out using a twin-block sleeper on ballast grading variant 3. Table 7.61 shows the test conditions of combination 1 and other tests used for comparison in this section.

Table 7.61: Detail of the combination of sleeper and ballast interventions carried out

Test label (for graphs)	Sleeper type	Ballast grading	Shoulder slope	Total loading cycles applied (millions)
Baseline	G44	NR	1:1	3.0
Twin-block	Twin-block			4.5
Variant 3	G44	Variant 3		5.0
Combination 1	Twin-block			

7.6.1 Permanent settlement

Figure 7.83 shows the ballast permanent settlement (averaged by area weighted method) of combination 1 compared to other tests which had a parameter included in the combination 1 test.

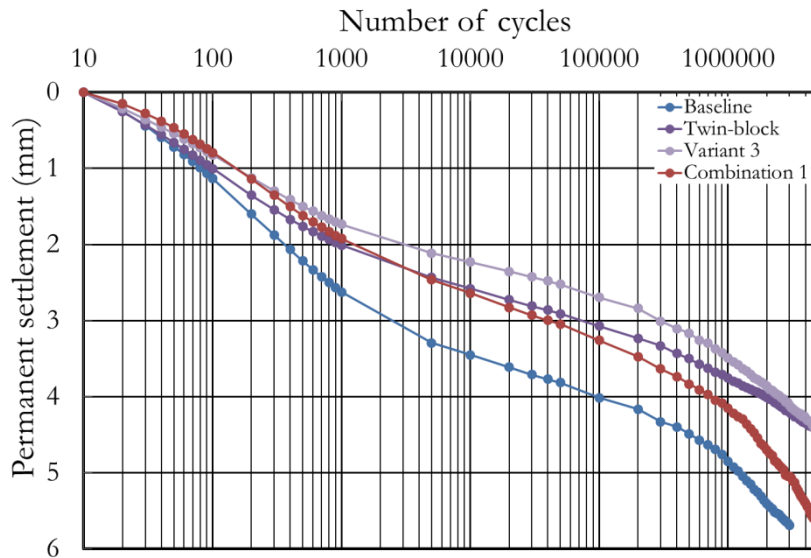


Figure 7.83: Area weighted average of permanent settlement of combination 1 and other tests which had a parameter included on the combination 1 test.

Discussion of the results

Prior to testing, combination 1 test was designed and expected to produce permanent settlement less than that of both the twin-block and variant 3 tests. However, the permanent settlement produced by combination 1 test (Figure 7.83), while less than that of baseline test, was not better than either the variant 3 or the twin-block test after 3 million loading cycles. Looking in more detail, initially the permanent settlement from combination 1 was the least among the other tests until it deteriorated at 0.3 million loading cycles. It was later hypothesised that this was perhaps due to the shape of twin-block sleeper which has smaller soffit area thus higher vertical stresses were induced at this interface than for the G44 mono-block sleepers which had larger footprint areas. It is thought that the combination of the finer grading with higher stresses may have led to increased densification during the test, hence greater overall settlement. Thus the benefit from the sleeper shape was lost because the finer grading performed worse at the higher localised stresses beneath the twin-block sleeper. In this test the higher vertical pressure induced by the twin-block sleeper might also have caused the ballast particles to spread horizontally as described by Budiono et al (2004). These results are instructive in that they demonstrate that combining optimised single parameters or particular tests does not necessarily optimise the performance of the whole track system.

7.6.2 Spring stiffness

Figure 7.84 shows the area weighted spring stiffness for combination 1 and the other related tests.

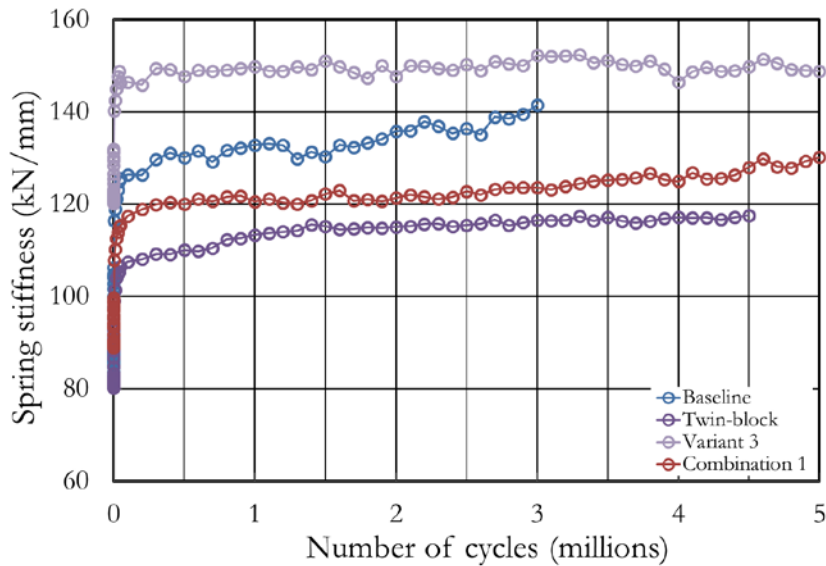


Figure 7.84: Area weighted spring stiffness for combination 1 and other related tests

Discussion of the results

Figure 7.84 shows that the average spring stiffness for combination 1 was slightly greater than for the twin-block test on the current standard NR ballast grading but not as stiff as the baseline or variant 3 tests. This comparison shows that using a finer gradation of ballast tends to increase the spring stiffness for the same sleeper type, but that the reduction in contact area of the twin-block compared to the mono-block tends to reduce the support stiffness for the same ballast gradation.

7.7 A comparison of results of permanent settlement and spring stiffness

In the field, track engineers sometimes simplify a complex method of analysis. One such simplification in relation to track maintenance or renewal is to correlate track spring stiffness with permanent settlement. The relationship between these two parameters has been investigated in different ways; Frohling (1997) proposed a ballast settlement model which had a stiffness parameter included; Hunt (2005) described qualitatively the direct influence of track stiffness on ballast settlement based on the findings of the EUROBALT project, that a low trackbed stiffness directly produced an increase of ballast settlement. Full-scale laboratory tests were carried out by Kennedy (2011) to obtain data modelling the relationship between these two parameters using the same approach as Frohling (1997).

To investigate the relationship between permanent settlement and spring stiffness of ballast, data obtained from the sleeper and ballast intervention tests using full-scale modified SRTF apparatus have been used. Figures 7.85 to 7.88 present the spring stiffness data (X-axis) and the corresponding ballast permanent settlement data (Y-axis) at 1 million and 3 million loading cycles. The ballast permanent settlement data plotted in X axis were taken from the first loading cycle and after re-zeroed at 10 loading cycles.

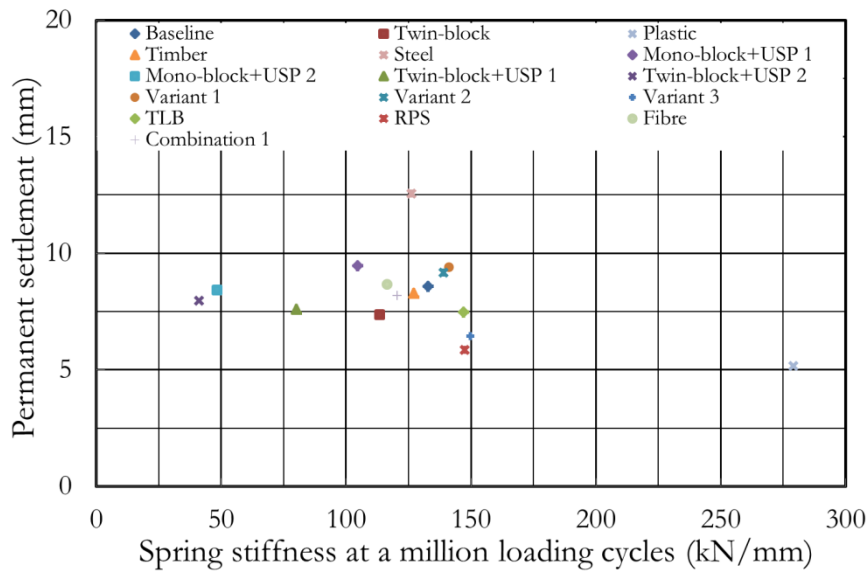


Figure 7.85: The spring stiffness and corresponding ballast permanent settlement (without zeroing) at 1 million loading cycles from sleeper and ballast intervention test

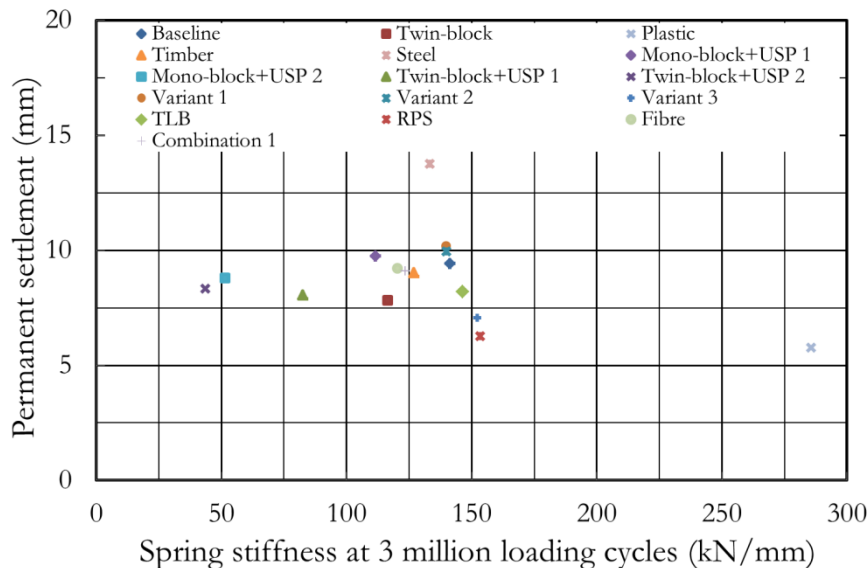


Figure 7.86: The spring stiffness and corresponding ballast permanent settlement (without zeroing) at 3 million loading cycles from sleeper and ballast intervention test

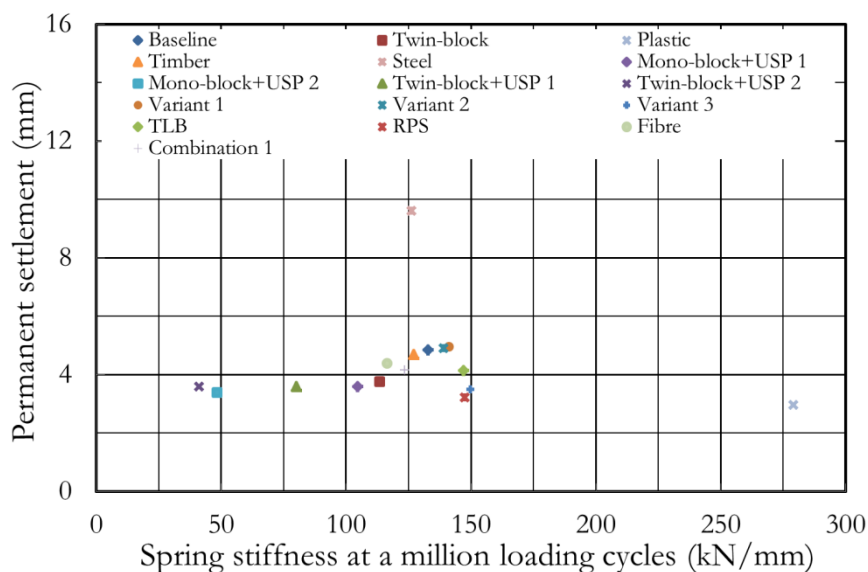


Figure 7.87: The spring stiffness and corresponding ballast permanent settlement (re-zeroed at 10 loading cycles) at 1 million loading cycles from sleeper and ballast intervention test

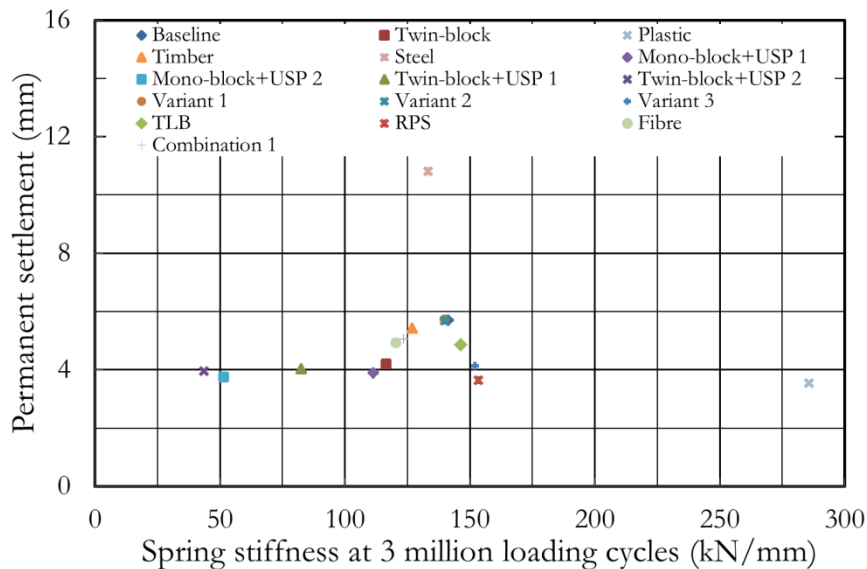


Figure 7.88: The spring stiffness and corresponding ballast permanent settlement (re-zeroed at 10 loading cycles) at 3 million loading cycles from sleeper and ballast intervention test

In general, these figures show no noticeable relationship between the permanent settlement and the spring stiffness, suggesting that there is no correlation between these two parameters.

7.8 A proposed ballast permanent settlement model

In Section 5.3, ballast settlement models were described and in this section some which have fixed and/or substitutable (can be replaced using parameter from the SRTF apparatus tests) parameters are recalled. These models are summarised in Table 7.62. The notes column shows key values used to apply these models.

Table 7.62: Detail of settlement models for comparison

Model label (for graphs)	Reference to equation	Proposed by	Notes
ORE	5.2	ORE	$(\sigma_1 - \sigma_3) = 0.1377\text{MPa}$, $n = 41.75\%$
Shenton 1	5.3	Shenton	$C = 0.2$, $\epsilon_1 = 1.1621\%$
Shenton 2	5.5		$K_s = 1.1$, $A_c = 20$, $L = 0$
Hettler	5.14	Hettler	$r = 0.00095$, $F = 98.1$, $C = 0.43$
Alva-Hurtado	5.19	Alva-Hurtado & Selig	$\epsilon_1 = 1.1621\%$
Stewart 1	5.20	Stewart & Selig	$\epsilon_1 = 1.1621\%$, $C = 0.29$
Stewart 2	5.21		$d_1 = 3.4863$, $C = 0.35$
Selig 1	5.24	Selig & Waters	$d_1 = 3.4863$, $C_b = 0.2$ triaxial
Selig 2	5.25		Box test
Selig 3	5.26		Fast track
Thom 1	5.31	Thom & Oakley	
Thom 2	5.32		$\sigma = 137.7\text{kPa}$, $k = 42\text{MN/m}$
Cedex	5.33	Cedex	
Indraratna	5.39	Indraratna	$a = 0.345$, $S_1 = 2.31$

7.8.1 Comparing the modified SRTF apparatus data to the existing settlement models

For comparison, a permanent settlement graph using linear axes is plotted in Figure 7.89, using the models presented in Table 7.62. The parameters in each model were obtained from the testing set up for G44 mono-block sleeper with the current standard NR ballast grading in the modified SRTF

apparatus. Where applicable the coefficients/powers etc. unique to each model were taken from literature specific to each model (see Notes column of Table 7.62).

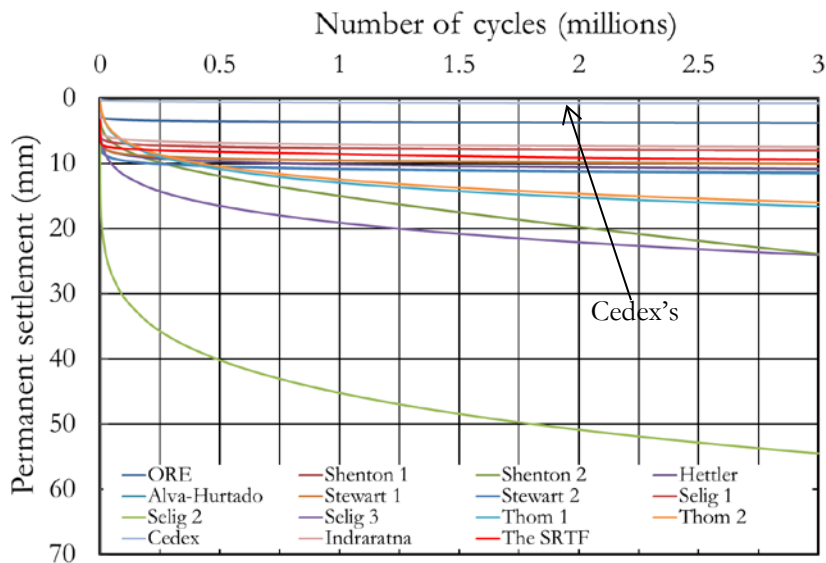


Figure 7.89: Comparison of permanent settlement graphs based on previous models compared to the modified SRTF apparatus data

The permanent settlement graph of the modified SRTF apparatus was plotted using the area weighted method from the data for the test on a G44 sleeper with the current standard NR ballast grading (red line).

Discussion of the results

Figure 7.81 shows that each settlement model produces a pattern of an initially rapid rate of accumulation of settlement that gradually reduces with number of loading cycles. A close up of Figure 7.89 is presented (Figure 7.90) which covers the initial 0.5 million loading cycles. The same legend applies to both figures.

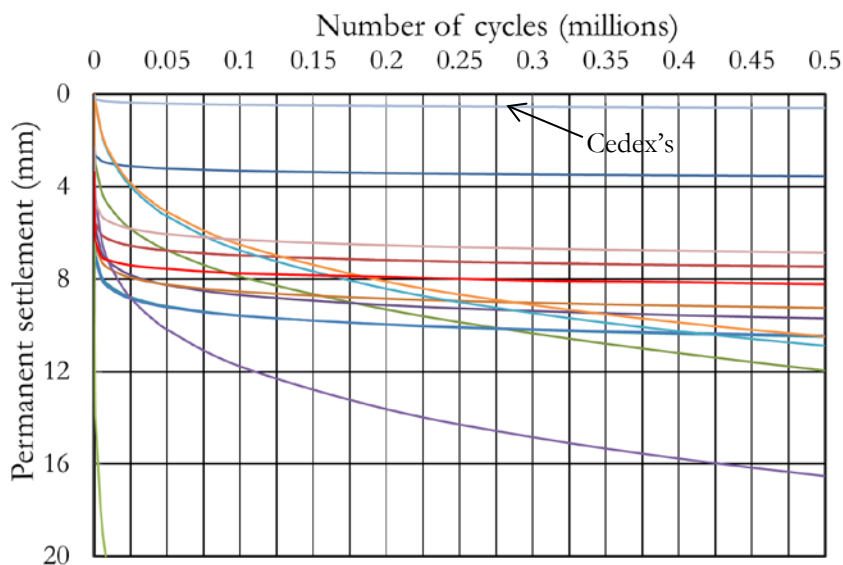


Figure 7.90: A close up view of ballast settlement graphs based on previous models and the modified SRTF data

From Figure 7.90, most of the settlement models shows that most settlement occurred within the first 25,000 loading cycles. This variation may be because they were based on experimental and/or

field data for ballast with a lower degree of compaction and/or a higher applied load. Cedex's model (light grey line) produced the least ballast settlement; this model may perhaps model ballast settlement after the ballast has been stabilised by some loading cycles or dynamic stabilisation methods.

The most ballast settlement was produced by the model of Selig 2 (the green line in Figure 7.89), which was based on ballast box tests. The higher settlement produced may be because perhaps the ballast sample used in the ballast box was in a loose condition and the sleeper dimensions used in the tests were not proportionally scaled, leading to a larger induced pressure.

In addition to these settlement models, data obtained from the modified SRTF apparatus tests with different magnitudes of load were also available. Figure 7.91 shows ballast permanent settlement graphs for two baseline tests (for sleeper and ballast interventions and sand ingress), using different magnitudes of vertical load on the current standard NR ballast grading.

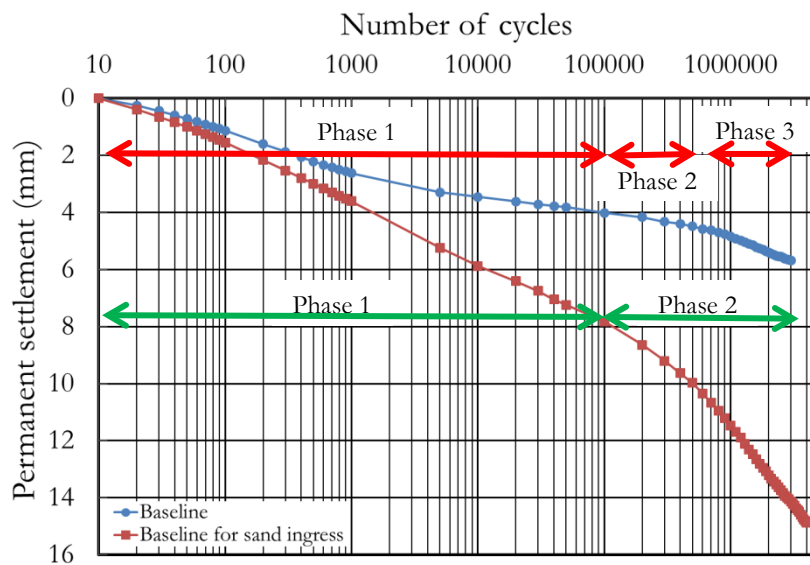


Figure 7.91: Ballast permanent settlement graphs of baseline test for sleeper and ballast interventions (20 tonnes axle load) and baseline test for sand ingress test (32 tonnes axle load)

It is shown that the magnitude of load has influenced the behaviour of ballast permanent settlement where the lighter load (20 tonnes for the baseline of sleeper and ballast intervention tests) created more phases in the development of ballast permanent settlement than the heavier one (32 tonnes for the baseline of sand ingress test) (Figure 7.91). The load for the baseline in the sand ingress test was 60% higher than the load for the baseline in the sleeper and ballast intervention tests. The findings shown in Figure 7.91 support the conclusion described by both Shenton (1984) and Raymond and Bathurst (1987) that the maximum load has a dominant effect on ballast settlement and a certain ballast support has a critical load level that if exceeded will cause a dramatic increase in ballast settlement, and loads below 50% of the maximum are not significant contributors.

7.8.2 A proposed ballast settlement model

Tests on sleeper and ballast interventions using the modified SRTF apparatus provided a large amount of data which can be used to propose a ballast settlement model.

Prior to proposing a ballast settlement model, the previous ballast settlement models presented in section 5.3 were evaluated to investigate the general form of the models and to choose the most

appropriate to be adopted using the data from the modified SRTF apparatus tests. All models give a rapid initial rate of settlement reducing as the number of loading cycles increases. The severity of settlement is perhaps due to different initial ballast compaction and/or the magnitude of vertical load. Therefore, in designing a proposed ballast settlement model in this research, these two parameters were also considered to be key factors for the severity of ballast settlement particularly in the initial loading cycles.

As a first step to proposing a ballast settlement model, curve fitting was applied to the test data which show the best fit regression curves. Curve fitting was automatically carried out for a range of selected curve types using Microsoft Excel. Two options fit the data well: logarithmic and power curves.

Figures 7.92 and 7.93 show example results of curve fitting in the two baseline tests for each sleeper and ballast intervention and sand ingress tests.

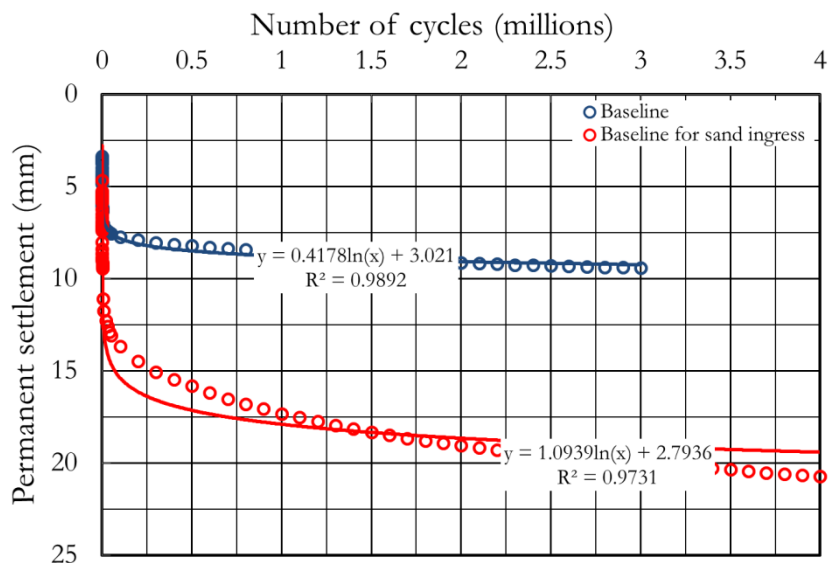


Figure 7.92: Curve fitting of two baseline data tests using logarithmic curve

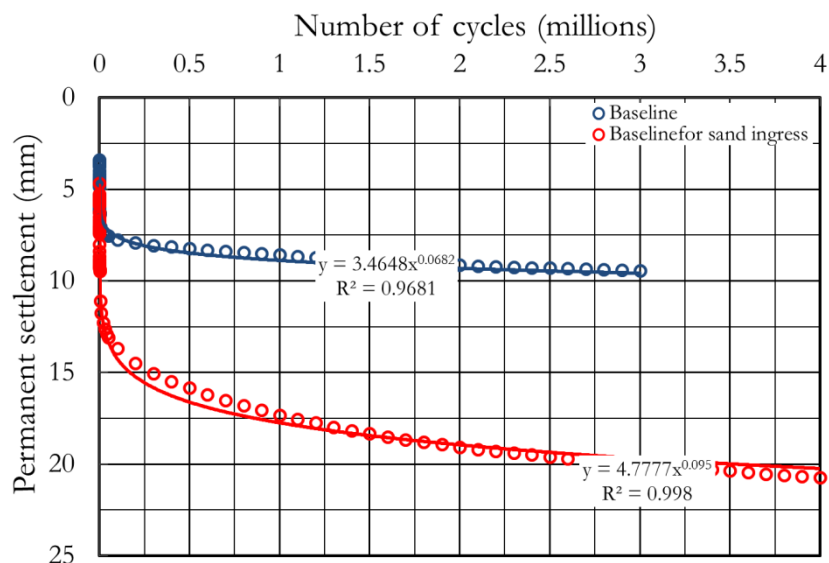


Figure 7.93: Curve fitting of two baseline data tests using power curve

It can be seen that these two types of curve fit the data well. However the R² value obtained is not consistent for each curve (Figures 7.92 and 7.93). It is also seen that each curve fitted provides an

equation with involving two constants. During curve fitting, it was also found that in each test using the same sleeper type and load magnitude (i.e. G44 sleeper) the two constants obtained by the logarithmic curve fitting were varied while the power curve fitting provided one with almost the same values each time. Therefore a power curve type equation is proposed as it matches better the general form of the settlement with number of loading cycles. The general form of the equation for this type of ballast settlement model can be written as:

$$S_{WN} = B(N)^G \quad \text{Equation 7.3}$$

where S_{WN} is the ballast permanent settlement at the N^{th} loading cycles and B and G are constants found from curve fitting.

This general form of the proposed ballast settlement models also used by Selig and Waters (1994) in modelling ballast settlement based on the data obtained from both ballast box and FAST track tests.

The next step turns to evaluating B and G. Firstly looking at G, Table 7.63 shows the evaluation of G for a range of tests using a mono-block sleeper.

Table 7.63: The exponent numbers obtained by curve fitting for each test

Test ID	Load (ton)	Exponent, (G) number obtained	Average
Baseline	10 (20 ton axle load)	0.0682	0.06565
Variant 1		0.0639	
Variant 2		0.0629	
Variant 3		0.0654	
RPS		0.0654	
TLB		0.0681	
Baseline	16 (32 ton axle load)	0.0950	0.0868
Sand ingress		0.0786	

The consistency shown in Table 7.63 gives confidence to use the parameters and results of the baseline test on G44 sleeper with 98.1kN load as a basic form of the proposed ballast settlement model. In Table 7.63, values from the data for the tests using a higher vertical load are also presented. The values of G for the higher load tests are slightly different. For implementation in the proposed ballast settlement model, the exponent numbers obtained by the lowest load (10 tons) were averaged and a correction was applied to take into account a higher vertical load.

In this case, there were only two averaged data points available. This led to some regression of curve fittings into these data were suitable for use e.g. exponential, power and liner curves. However, the first two of those curve fittings provided an overestimation of G for the higher load (although the R^2 values of these curve fittings were higher than linear curve fitting) and since the exponent numbers for vertical loads of 10 and 16 tons were in a very small range, to investigate the influence of a higher load into the exponent number, a relationship defined using a linear curve fitting (Figure 7.94) was good enough to provide a representative value.

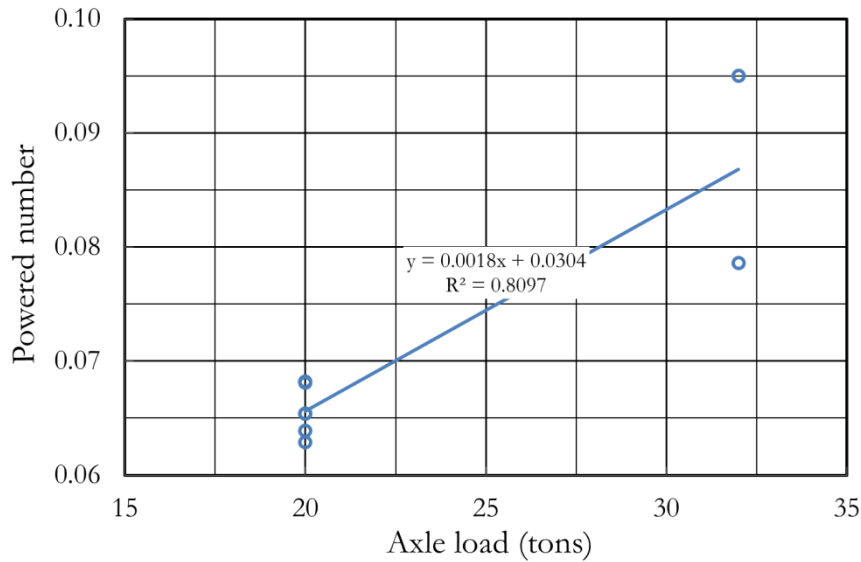


Figure 7.94: Linear curve fitting for the influence of higher load to the exponent number

Using the average exponent number obtained by the lowest axle load and combining it with the result of curve fitting to adjust for a higher axle load (A_L), G in Equation 7.3 can be substituted by:

$$G = 0.06565 + 0.0018 (A_L - 20) \quad \text{Equation 7.4}$$

The following step turns to evaluating B . B can be termed the “ballast permanent settlement factor or coefficient” in accordance with the model used by Selig and Waters (1994). B may be a combined factor representing both the initial degree of ballast compaction and the magnitude of the applied load. In the proposed ballast settlement model, this B factor is separated, so each factor represents a correction from each element taken into consideration. The correction factors included in B are:

- initial degree of ballast compaction (B_{ic}) (in terms of porosity (n)),
- pressure at sleeper soffit (V_{pf}),
- correction factor for a higher load (efficiency) (L_{ef}),
- sleeper material (M_{sf}),
- sleeper shape (S_{sf}),
- sleeper/ballast interface (S_{if}) (includes changing grading),
- shoulder slope profile (SL_f),
- ballast reinforcement (R_f)

The B factor can then be expressed as:

$$B = (B_{ic})(V_{pf})(L_{ef})(M_{sf})(S_{sf})(S_{if})(SL_f)(R_f) \quad \text{Equation 7.5}$$

B_{ic} (the initial degree of ballast compaction) can be obtained based on the relationship between the permanent settlement produced at the first loading cycles (recalled from the ballast permanent settlement graphs) and the initial porosity (n) (recalled from Tables 6.25 to 6.27) in the test using G44 sleeper with the same magnitude of load (98.1kN) and shoulder slope profile (1:1). This is shown in Table 7.64 and Figure 7.95.

For all data presented in Figure 7.95, a relationship based on linear and logarithmic curve fittings could be used. However, the R^2 value obtained by logarithmic curve fitting was higher than liner

curve fitting. It was also hypothesised that there will be a very loose condition of the ballast performed where the highest porosity was represented, meaning that the ballast porosity remained constant at the highest value. To accommodate these two key factors, therefore logarithmic curve fitting was more suitable than linear curve fitting and used for the relationship.

Table 7.64: Ballast property and the corresponding permanent settlement at the first loading cycle for each test using the same sleeper type (G44 sleeper) and load magnitude (98.1kN)

Test ID	Porosity of ballast (n) (%)	Permanent settlement at the first loading cycles by weighted area method (SW1) (mm)
Baseline	41.75	3.4863
Baseline 2	40.16	3.5000
Variant 2	38.80	3.3431
Variant 3	36.64	2.3512
TLB	37.41	2.7313
Fibre	41.37	3.4529

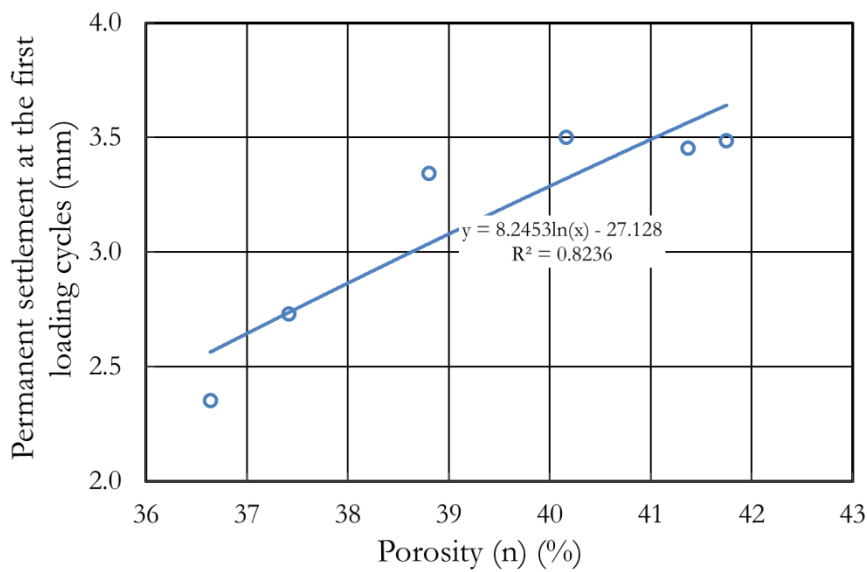


Figure 7.95: Curve fitting to determine a relationship between porosity (n) and permanent settlement at the first loading cycle

Based on the result of curve fitting (Figure 7.95), B_{ic} can be evaluated using:

$$B_{ic} = 8.2453 \ln(n) - 27.128 \quad \text{Equation 7.6}$$

The correction factor for vertical pressure at the sleeper soffit (V_{pf}) is found by normalising the vertical pressure at the sleeper soffit (V_p) for any given load by the vertical pressure at the G44 sleeper soffit due to a 10 ton vertical load (137.68kPa). This can be expressed as:

$$V_{pf} = \frac{V_p}{137.68} \quad \text{Equation 7.7}$$

At this stage, Equation 7.3 can be re-written as:

$$S_{WN} = (8.2453 \ln(n) - 27.128) \left(\frac{V_p}{137.68} \right) (L_{ef})(M_{sf})(S_{sf})(S_{if})(SL_f)(R_f)(N)^{(0.06565 + 0.0018(A_L - 20))} \quad \text{Equation 7.8}$$

To obtain the undefined remaining correction factors in Equation 7.3, curve fitting analyses were carried out using all the remaining experimental data by assuming that all the remaining parameters were 1 except where they were specifically varied in a test.

Table 7.63 presents each correction factor produced by this process.

Table 7.65: Load efficiency, sleeper material, shape, interface, shoulder slope and reinforcement factors for the proposed ballast settlement model

Test ID	Correction factor for					
	Load (L_{ef})	Sleeper material (M_{sf})	Sleeper shape (S_{sf})	Sleeper/ballast interface (S_{if})	Shoulder slope profile (SL_f)	Ballast reinforcement (R_f)
Baseline	1.0	1.0	1.0	1.0	1.0	1.0
Variant 1	1.0	1.0	1.0	1.25	1.0	1.0
Variant 2	1.0	1.0	1.0	1.25	1.0	1.0
Variant 3	1.0	1.0	1.0	1.05	1.0	1.0
RPS	1.0	1.0	1.0	1.0	0.68	1.0
TLB	1.0	1.0	1.0	1.15	1.0	1.0
Mono-block + USP 1	1.0	1.0	1.0	1.05	1.0	1.0
Mono-block + USP 1	1.0	1.0	1.0	1.10	1.0	1.0
Twin-block	1.0	1.0	0.55	1.0	1.0	1.0
Twin-block + USP 1	1.0	1.0	0.55	1.0	1.0	1.0
Twin-block + USP 2	1.0	1.0	0.55	1.0	1.0	1.0
Timber	1.0	0.95	1.0	1.0	1.0	1.0
Fibre	1.0	1.0	1.0	1.0	1.0	0.98
Baseline 2 (for sand ingress)	0.95	1.0	1.0	1.0	1.0	1.0

The proposed ballast settlement model is intended to be able to estimate the ballast permanent settlement behaviour using the initial ballast condition and the magnitude of vertical load from the first loading cycle to any number of loading cycles. Therefore each factor presented in Table 7.65 is meant to represent the entire ballast permanent behaviour from the first loading cycle. The model captures behaviour consistent observed behaviour in that:

- a. Increasing the vertical load will increase the vertical pressure at the sleeper soffit. However this increase is a direct proportional transferred to the ballast permanent settlement. A 60% increase of vertical load has actually causes an increase in the ballast permanent settlement by only $95\% \times 60\% = 57\%$.
- b. Sleeper material can reduce the severity of ballast permanent settlement. Less rigid materials can reduce pressure with the ballast and help to homogenise the pressure through the ballast. E.g. a mono-block timber sleeper has shown an ability to reduce by 5% the effect of the G44 mono-block concrete sleeper on the ballast permanent settlement.
- c. Ballast permanent settlement can be influenced by sleeper shape.
- d. If data from the first loading cycle are considered, the USP modifications at the sleeper/ballast interface appear to increase the ballast permanent settlement. However, this is not necessarily because the ballast settles more, but to the compression at the initial loading cycle of the material used at sleeper/ballast interface. Changing ballast grading and TLB also increases the ballast permanent settlement. This implies that changing ballast grading and the introduction of the TLB system with finer material requires some initial loading cycles before benefits are seen.
- e. Re-profiling the shoulder slope by 1V:2H has the ability to prevent lateral ballast spreading thus reducing ballast permanent settlement.

- f. Fibre reinforced ballast had the same effect as re-profiling the shoulder slope. However, it only reduced slightly the ballast permanent settlement; greater improvement may be observed if the fibre type and content used were optimised.

Figure 7.96 shows the comparison of ballast permanent settlement graphs for some tests obtained by the modified SRTF apparatus with the results of the proposed ballast settlement model using ballast parameters and factors presented in Tables 7.64 and 7.65.

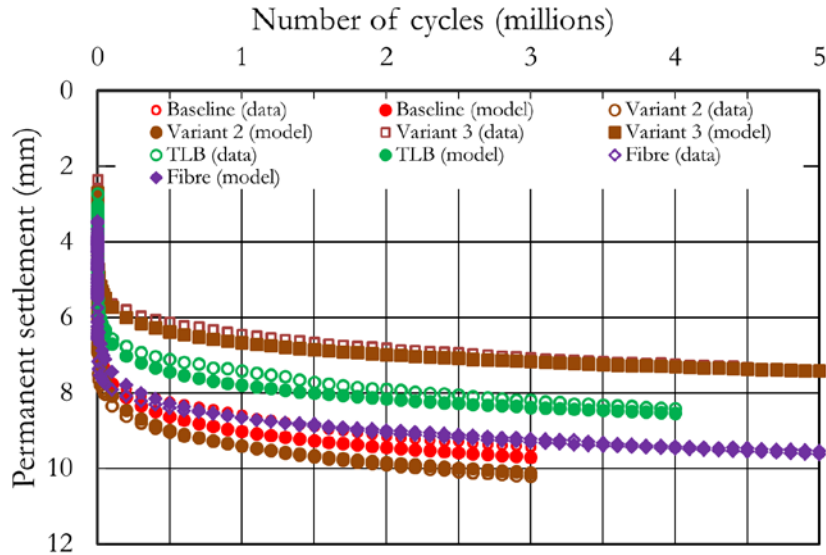


Figure 7.96: Comparison of ballast permanent settlement graphs of some tests obtained by the modified SRTF apparatus and the results of the proposed ballast settlement model

It can be seen that the factors adopted in the proposed ballast settlement model produce graphs which are very close to the data obtained by the modified SRTF apparatus tests.

In section 7.6, a trial test on combined parameters (combination 1) was described; this test was not included in determining the proposed ballast settlement model. Using the proposed ballast settlement model, the ballast permanent settlement of combination 1 test is generated and compared to the data obtained from the modified SRTF apparatus test. In this test, using the factors presented in Table 7.65, Equation 7.8 can be re-written as:

$$S_{WN} = (8.2453 \ln(n) - 27.128) \left(\frac{197.94}{137.68} \right) (1)(1)(0.55)(S_{if})(1)(1)(N)^{(0.06565)} \quad \text{Equation 7.9}$$

The average of ballast porosity (n) for this test was 38.34%, however the sleeper interface factor (S_{if}) for this test was unavailable. Therefore, to obtain this value, a linear regression process was carried out using the data of vertical pressures at the sleeper soffit of G44 (137.68kPa) and twin block (197.94kPa) concrete sleepers with the S_{if} of variant 3 test on G44 sleeper. It can then be calculated that S_{if} for twin-block concrete sleeper on variant 3 was 1.51. Using this value, Equation 7.9 can be simplified as:

$$S_{WN} = 3.5085 (N)^{(0.06565)} \quad \text{Equation 7.10}$$

Using Equation 7.10, the ballast permanent settlement graph can be generated and the result is compared with the data obtained from the modified SRTF test (Figure 7.97).

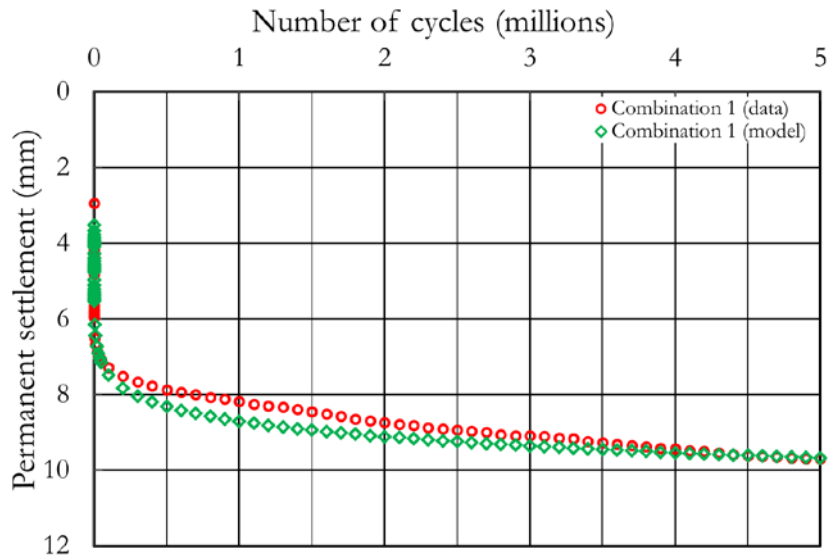


Figure 7.97: Comparison of ballast permanent settlement graphs obtained by the proposed settlement model and the modified SRTF apparatus test

It can be seen that the proposed ballast settlement model provides a satisfactory result in estimating ballast permanent settlement. However, there are some features of behaviour that the proposed relationship does not satisfactorily capture. This is mainly because the model is heavily biased by the initial number of cycles and thus some results appear contradictory – e.g. while experiments with USPs showed better performance after 10 loading cycles, the model equation contradicts this perhaps because the introduction of a compressible material leads to a large initial settlement on first loading cycle. Further work may therefore be needed to adapt the model proposed so that the correction factors indicate the performance after 10 loading cycles to indicate the performance after some initial compaction effort representative of field track laying procedures.

Chapter 8: Conclusions and further research

8.1 Conclusions

It was stated earlier in Chapter 1 that the aim of this research was to develop an improved understanding of how different sleeper and ballast interventions influence the performance of railway track, with specific focus on: 1) effect of sleeper types and type of sleeper/ballast interface and 2) effect of ballast grading, geometry, fouling by fine sand and reinforcement. This aim was achieved through specific testing objectives which were set out at the end of Chapter 1; these are highlighted below and addressed in turn:

✚ *To investigate the effect of sleeper type by testing mono-block concrete (G44), twin-block concrete, steel, plastic, and timber sleepers with the current standard NR ballast grading.*

In railway track, the sleeper has a very complex interaction system and it was demonstrated that a given type of sleeper on ballast behaves differently from other sleeper types. However, the same pattern of ballast permanent settlement was produced by each sleeper type tested, with a rapid settlement during the initial loading cycles and the rate of accumulation of permanent settlement gradually reducing with subsequent loading cycles. After being zeroed at 10 loading cycles to take out the effect of initial inconsistency in ballast/sleeper contact quality, the twin-block sleeper produced the least average permanent settlement among the sleeper types tested. The twin-block concrete sleeper also produced the lowest average spring stiffness of the sleeper types tested. However, the spring stiffness produced by twin-block concrete sleeper was the closest to the recommended sleeper support stiffness value suggested in NR's standard for new track with a designated speed of 100 mph, if no modification of the ballast/sleeper interface is planned.

Mono-block sleepers (G44 and timber) tend to bend with increasing number of loading cycles applied. This behaviour was caused by the combination of an increase in sleeper end deflection and a reduction in the deflection at the middle section of the sleeper. This led to the vertical load on the sleeper being transmitted to the ballast primarily by the middle portion of sleeper. Excess bending of a mono-block concrete sleeper may cause concrete failure and lead to instability of the track. The same effect was found with a timber sleeper, although the risk of failure with this type of sleeper is minimal as it has higher elasticity than a concrete sleeper. With increasing number of loading cycles, the use of mono-block sleepers also caused the ballast pressure to increase at the centre of the track in the longitudinal direction and reduced the confinement in the shoulder zone.

The twin-block concrete sleeper showed better performance in avoiding sleeper bending with the application of increasing loading cycles. This type of sleeper exhibited a pattern of reducing rather than increasing sleeper end deflection. This showed that the twin-block sleeper was always in contact with the ballast surface to support the vertical load on the sleeper without any risk of concrete failure. In addition, since there was a reduction in the deflection at the twin-block concrete sleeper ends with increasing number of loading cycles, the spring stiffness of the twin-block concrete sleeper ends was greater than that of the other sleeper types tested. The twin-block concrete sleeper also showed no change in the pressure in the ballast with increasing number of loading cycles. The longitudinal

pressure in the ballast was relatively evenly distributed, meaning that there was no increased pressure in the centre of the track or reduced confinement at the shoulder area.

It was found that the quality of the installation of the sleepers in the track and components of the sleeper also influenced the performance of the sleeper. In the laboratory test a poorly installed steel sleeper performed worst among the sleeper types tested. The “n” shape of the steel sleeper soffit made it difficult to ensure that the steel sleeper was fully supported by ballast, causing large deflections and potentially fatigue at the railseats. It was also found that the proper installation of rail chairs was required on the plastic sleeper to distribute vertical load to a wider area. The exclusion of rail chairs led to plastic sleeper forming a “ω” shape with the application of vertical loading cycles. This “ω” shape result was associated with a lower spring stiffness beneath the railseats and therefore would require frequent maintenance at this location.

Taking these factors into consideration, it was determined that twin-block concrete sleeper performed the best among the sleeper types tested.

✚ *To investigate the effect of ballast grading through tests where the current standard NR ballast grading was modified by adding finer particles.*

Regardless of sleeper type, the initial permanent settlement of all ballast gradings followed a similar pattern. Tests on different types of sleeper established for each grading tested that during the initial loading cycles there was a rapid settlement which led to a variation in the severity of permanent settlements. The severity of the permanent settlement depends on the degree of ballast compaction and the magnitude of vertical cyclic loading applied. Increasing the degree of ballast compaction could be achieved by the introduction of finer particles to obtain a broader grading. This ballast would have a greater coordination number and better particle interlocking, hence less permanent settlement. For comparison, the variation of the initial sleeper/ballast contact condition was minimised by re-zeroing all the gradings tested after 10 loading cycles. This led to ballast grading variant 3 producing the lowest average permanent settlement among the gradings tested. This shows that the introduction of the right sizes and proportions into the uniformly grade standard NR ballast as represented by variant 3 is an option to minimise permanent ballast settlement, thereby reducing the need for maintenance. However, the introduction of other sizes and proportion into uniformly graded ballast may lead to no improvement (variants 1 and 2).

Changing a uniform ballast grading by introducing finer particles to achieve a broader grading led to an increase in the average spring stiffness. However, changing the ballast gradation was not able to prevent the G44 sleeper used in the test from bending. This was because on mono-block sleepers, deflection at sleeper ends became larger toward the end of the test and a gap between the sleeper soffit and ballast surface was created, while at the middle section of sleeper the deflection became smaller than it had been at the beginning of the test. This confirmed that bending of the sleeper was due to the shape of the sleeper used in the tests, not the ballast grading. This also demonstrated that at the sleeper ends there was a reduction of spring stiffness after a number of loading cycles had been applied.

It was also found that the longitudinal ballast pressure increased at the centre of the track and reduced at the ballast shoulders with the application of loading cycles for each grading tested. This

showed that ballast densification occurred in the middle section of the sleeper, with reduction in ballast confinement in the ballast shoulder zones. This behaviour was also caused by the sleeper shape used in the tests and agreed with the conclusion reached regarding different sleeper types.

✚ *To investigate the effect of USPs by testing two different types of USP both employing mono-block and twin-block concrete sleepers.*

The attachment of USPs to a G44 sleeper soffit was more beneficial than the attachment of USPs to a twin-block sleeper. The use of USPs on the G44 sleeper produced a significant reduction in ballast permanent settlement compared with the baseline test. The use of USPs on the G44 sleeper also altered the behaviour of the average four corner sleeper deflection, where with increased number of loading cycles, the deflection at sleeper ends reduced instead of increased as in the other tests on mono-block sleepers. This showed that the G44 sleeper was prevented from hogging and there were always positive contacts between the sleeper soffit and ballast surface. The use of USPs also prevented a large reduction of ballast confinement at the ballast shoulders and kept the ballast confinement higher than it had been in tests without the attachment of USPs. In the middle section of the sleeper, the deflection behaviour remained unchanged although the use of USPs increased the extent of deflection due to the attachment of the additional material which was softer than the sleeper itself. In the centre of the track, there was no significant increase in longitudinal pressure in the ballast with increasing number of loading cycles. This showed that USPs were able to distribute vertical load to a larger area and decentralising the longitudinal pressure in the ballast.

The attachment of USPs to the twin-block sleeper soffit, however, did not significantly reduce the ballast permanent settlement produced. Although there was a reduction, this was less than 10%. It was also found that the use of USPs on twin-block sleeper did not change the behaviour of sleeper deflection and longitudinal pressure in the ballast.

The attachment of USPs to both G44 and twin-block sleeper soffits produced a lower spring stiffness than in tests on the same type of sleepers without USPs. This showed that USPs provide a solution to the problem of adjusting a higher spring stiffness to the required level for specific locations e.g. in transition zones.

✚ *To investigate the effect of two layered ballast (TLB) system which was constructed from two different gradings; the current standard of NR ballast grading at the base and 10/20 grading on top.*

The modification made at the interface of G44 sleeper and ballast by the introduction of TLB system produced less ballast permanent settlement and a higher spring stiffness than the baseline test. However, since TLB system test was carried out using G44 sleeper which was mono-block sleeper, an increase in longitudinal pressure in the ballast at the centre of the track and deflection at sleeper ends occurred and the hogging behaviour of the sleeper was demonstrated with the sleeper bending in the middle section.

- ✚ *To investigate the effect of re-profiling trackbed geometry by testing a shallower shoulder slope than current practice in the UK.*

The test with a shallower shoulder slope (1V:2H) produced similar results to the test using the TLB system and the tests on mono-block sleepers. However, the test with a shallower shoulder slope produced the best performance, resulting in the least ballast permanent settlement and the highest spring stiffness among all the tests carried out on sleeper and ballast interventions. This was because a shallower shoulder provides better lateral confinement and prevents ballast lateral spreading. This demonstrated that re-profiling the shoulder was the most effective option to minimise ballast permanent settlement and if the spring stiffness produced was too high, then this option could be combined with the USPs.

- ✚ *To investigate the effect of fibre reinforcement in the ballast.*

Although the test on fibre reinforced ballast was an initial trial, some positive effects were observed. Fibre reinforcement produced less ballast permanent settlement than was observed in the baseline test in which no fibre was used. Fibre reinforced ballast required the application of more number of loading cycles to reach a given level of ballast permanent settlement than in the baseline test. This shows that fibre reinforcement also provided lateral resistance similarly to re-profiling the shoulder slope to prevent lateral ballast spreading. Most of the fibre introduced occupied the space between ballast particles and this required more number of loading cycles to mobilise the ballast to be in contact or interlocked. This mechanism resulted in a slightly smaller spring stiffness than in the baseline test. However, it was found that the spring stiffness at sleeper ends was relatively constant throughout all number of loading cycles. Although the sleeper was bending, fibre reinforcement prevented the gaps between sleeper soffit and the ballast surface at sleeper ends from increasing. Fibre reinforcement also enabled the almost uniform distribution of pressure in the ballast along the sleeper length, with no significant difference developing throughout all of number loading cycles applied, implying that the loss of the confinement at sleeper ends was also prevented.

- ✚ *To investigate the effect of the presence of fine sand as a fouling material within the ballast.*

The introduction of sand to occupy at least 15% of the ballast voids reduced the overall accumulated ballast permanent settlement from that observed in the baseline test. This was probably due to the sand helping to prevent slippage, thereby reducing overall settlement. On the other hand, there was no appreciable effect on the spring stiffness at sleeper ends. It is hypothesized that, when the sand occupies less than 100% of the ballast voids, the sand plays only a minor part in the transmission of load through the ballast, as the load paths are still predominantly through ballast-to-ballast grain contacts.

Bending of the sleeper was observed in the baseline test, with the deflection at the sleeper ends increasing with the number of loading cycles applied while in the middle section the sleeper deflection decreased. However, the introduction of sand prevented the sleeper from bending, so that the deflections at sleeper ends and at the middle section of the sleeper was within a similar range.

An appreciable reduction in the deflection per cycle of the sleeper was observed when the sand filled 100% of the void space, implying a significant increase in spring stiffness. It is hypothesised that,

once the sand fills the void space under the sleeper, the sand starts acting as a load carrying component of the ballast, and that the resulting load sharing is responsible for the increase in stiffness. If no more sand is available, further loading cycles may densify the sand until it is no longer in contact with the sleeper soffit. This leads to ballast-to-ballast particle contact again being the dominant mechanism for transferring load from the sleeper to the subgrade. If sufficient sand is available to maintain 100% void filling, densification of the sand can give rise to a denser ballast/sand aggregate mix and a further increase in spring stiffness. Increasing the spring stiffness can lead to increased dynamic loads, and potentially to early component failure. Although there is no widely accepted consensus on what constitutes “too stiff”, a range of 30-100kN/mm has been suggested as minimum target values for support stiffness by NR. However, a high spring stiffness value can easily be adjusted by the introduction of USPs to fit with the requirement as long as modification into sleeper/ballast interface is permitted.

In the baseline test, it was found that at the centre of the track in the longitudinal direction, pressure in the ballast increased with the number of loading cycles applied while that at the sleeper ends reduced. This implies that there was densification of the ballast in the centre of the track and loss of ballast confinement at sleeper ends. However, the introduction of sand was able to prevent these effects and redistribute the pressure in the ballast so that it was almost equal at the sleeper ends and in the centre of the track.

✚ *To estimate the number and area of contacts at sleeper/ballast interfaces along with the particle contact area and pressures at ballast/subgrade interface using pressure paper.*

Pressure paper can be used to obtain a record of contact locations and the percentage of the total real area of contact between ballast particles and the sleeper soffit or the sub-grade, as aggregate values over a number of loading cycles. However, not all of the indicated contacts would necessarily have been active at the same time. The tests reported in this research have quantified and demonstrated the potential for different ballast/sleeper combinations to improve the number and area of contacts at the sleeper to ballast interface and to some extent to modify these parameters at the ballast to subgrade interface. The changes in contact area imply large changes in the real contact stresses. Values have been presented in the preceding sections, and the key findings can be summarised as follows:

For the sleeper to ballast interface, increases in the number and area of contacts can be achieved by:

- Finer ballast gradations, including the use of a layer of finer material beneath the sleeper
- USPs, with softer USPs producing the greatest increase
- Using lower stiffness sleeper materials such as timber or plastic

When considered in terms of mobilising larger proportions of potentially available contacts, the most effective interventions are the use of timber sleepers, a shallower ballast shoulder slope, and the use of softer USPs (USP2). However, timber sleepers are not an option anymore on a modern railway.

Perhaps most significantly it has been shown that under normal conditions the sleeper to ballast contact area is less than 1% of the sleeper footprint and the contact stresses that this implies are orders of magnitude greater than those calculated from the simplistic pressure distributions commonly used. Thus the contact behaviour cannot be understood without considering the discrete

nature of the contacts at the interface. Larger numbers of contacts and larger contact areas imply lower stresses and greater homogeneity of load transfer from the sleeper to the ballast. This is desirable as it will lead to less ballast breakage and a more uniform and predictable response to train loading along the sleeper soffit and along the track length.

At the ballast/subgrade interface the different sleeper and ballast combinations tested showed much less influence on the contact area and it was difficult to identify clear trends due to natural variation in the data. However, most notably the twin-block sleeper on NR ballast showed the smallest contact area while the concrete mono-block sleeper on the finest ballast gradation showed the highest contact area. At the ballast base to subgrade interface, the contact areas under railseats were larger than at middle section of sleeper. One of the causal factors of this was hypothesised to be that the ballast beneath railseats appears to migrate outwards so it is an artefact of the cumulative measured pressure.

Apart from the above conclusions which are related to specific objectives, this research has resulted in some other findings, from which the following conclusions can also be drawn:

It was revealed that ballast breakage, attrition and abrasion occurred to a minor degree in each test carried out in this research. If there was breakage of corners of ballast particles, this was mostly found at the sleeper edges. Comparison of PSDs showed minimal change between pre- and post-test sample. However, difficulties in obtaining exactly the same sample for before and after testing leads to some doubt over the analysis results. Visual observation and individual ballast particle measurement method showed minor breakage and abrasion to have occurred, but not to an extent that would alter significantly the PSD of the ballast. The same findings also applied to the baseline and sand ingress tests. In the sand ingress test, when the ballast voids were completely filled with sand, the sand directly under the rail seats was visibly crushed, which perhaps helped to protect the ballast particles from damage.

Since only minor breakage, attrition and abrasion were found in the ballast, the main cause of ballast permanent settlement was a combination of ballast particle arrangement and lateral ballast spreading. Ballast particle arrangement was not explicitly monitored. However in some tests the movement of ballast on the shoulder slope was investigated. The results revealed that there was always a movement of ballast particles on the shoulder slope in a lateral direction and the most effective option to prevent this from happening was the application of shallower shoulder slopes.

Based on the results of a test on combined parameters, it was shown that benefits cannot simply be summed and that optimisation of individual parts of the track structure does not necessarily lead to the optimisation of the system as a whole.

It has also been shown, unequivocally, that no relationship can be defined between spring stiffness and the permanent settlement of ballast.

Ballast permanent settlement can be estimated using a proposed relationship between initial degree of ballast compaction, the magnitude of vertical loading and some influencing factors involved for the test as well as the number of loading cycles.

8.2 Relevance for practice

In-service, the geometry of railway track experiences loss of line and level. Generally this is due to a significant settlement of the ballast during loading cycles. To restore this to an acceptable standard, maintenance is required. To minimise track maintenance costs, it is important to choose components of the track and appropriate methods for track maintenance and design which would provide longer periods of service without maintenance, or with less maintenance required.

This research has explored not only the performance of two major track components to define combinations that would provide the best performance, but also the effect of the presence of fouling material in the ballast. The key implications of this research are:

1. With the current standard NR ballast grading, there sleepers made from a softer material tend to perform better in the track than the current widely used of mono-block concrete sleeper. Performance might be also improved by the shape of the sleeper. This has been demonstrated by twin-block sleeper which performed the best among the sleeper types tested. It is also necessary to eliminate (or at least to minimise) the use of sleepers with installation issues and is therefore not stable due to not being supported well by ballast, although this may have an advantage where less ballast required.
2. The current standard NR ballast grading requires modification to provide a better performance by introducing the right sizes and proportions of finer particles, which is considered will increase the coordination contacts and ballast strength. Variant 3 grading resulted in less ballast permanent settlement. Although directly replacing the current standard NR ballast grading is a huge challenge, this can be introduced on ballast renewal as an initial step.
3. The attachment of USPs to the current widely used sleeper by NR (mono-block concrete sleeper) not only improves performance but also makes the spring stiffness uniform, helping to prevent track deterioration. The results from the tests with the inclusion of USPs give additional data based on their actual response in the track to their properties provided by the manufacture as a complete information prior to decision of USPs implementation. The implementation of USPs can be carried out easily together with sleeper replacement even if only for short lengths of problematic track (i.e. transition zones, switch and crossing).
4. The introduction of a TLB system might minimise the use of tamping machines for track maintenance which, as addressed in the literature review, not only causes particle breakage but is also effective for only a short time before requiring repetition. The TLB system has performed better than the current standard NR ballast grading and if maintenance is required, stoneblowing method is more appropriate than tamping. This is because stoneblowing uses the same particle grading as the top layer of the TLB system and causes less damage to the ballast particles.
5. It was demonstrated in this research that ballast permanent settlement is mostly due to ballast particle arrangement and ballast lateral spreading. Ballast breakage, attrition and abrasion were minimal. These lead to a confidence that the service life of ballast is potentially very long and frequent ballast replacement is unnecessary. To prevent ballast from lateral spreading, the application of fibre reinforcement has potential and its benefits have been demonstrated in this research.
6. In the current standard NR trackbed profile, there is no recommendation for the slope of the shoulder ballast. It seems NR is satisfied with the current ballast shoulder slope in most UK

mainlines which are created due to the effect of gravity when ballast for new lines or replacements are placed. The test with a shallower ballast shoulder slope resulted in not only the least ballast permanent settlement but also the ability to provide more lateral confinement, preventing ballast lateral spreading.

7. If there are potential barriers to implementing re-profiling shoulder slopes due to limited space available, another option to stop lateral ballast spreading is to confine the ballast by the installation of a low rigid wall barrier along the side of the track. The application of fibre reinforced ballast is an option for the future.
8. Without water (i.e. perhaps in desert areas), the presence of fouling materials in the track is not necessarily threatening to the service life of the track. It has been demonstrated in this research that the presence of sand in the ballast has advantages in stopping (or at least reducing the rate of) ballast permanent settlement and increasing the spring stiffness. However, variable sand ingress along the track length could lead to increased variability of spring stiffness and could cause early trackbed and track component failures. Therefore regular monitoring should be adopted to assess any stiffness variation and the use of compliant components (e.g. USPs and rail pads) should be considered to mitigate the effects of very high spring stiffness.

8.3 Recommendation for further research

Based on the results of this research presented in this thesis and a consistent protocol in sample preparation, the following future research is recommended.

Different types of sleeper have been tested in this research. However, there may be many other types available. Future tests using novel types of sleeper would provide performance data which could be used to inform a decision in a suitable type of sleepers for the track. In the tests however, it must be ensured that the sleepers have sufficient components and the installation method on the trackbed is carried out so that the actual arrangement at the field is matched as closely as possible. Having an accurate installation of the sleeper on the trackbed and sufficient components on the sleeper are important. In this research, a steel sleeper was installed manually by means raising the level of the ballast bed along the steel sleeper length. It was intended that ballast would fill the space within the sleeper soffit evenly. However, this was believed as an incorrect method and there should be another method available to better install a steel sleeper to model field installation. The exclusion of the railseat chairs on the plastic sleeper also led to an underestimate of the effective bending stiffness of that sleeper during the test. The issues with the steel sleeper installation and the omission of essential components from the plastic sleeper might have resulted in either the overestimation or underestimation the actual performance of these sleeper types. This creates doubt regarding the results and repeat tests are required.

To provide more straightforward data that can be used for the implementation on the problematic track or track renewal, tests on other performance USPs using full scale apparatus to represent field conditions are required. The results from these tests may be useful to be correlated with their mechanical properties (stiffness (C_{Stat})), which is normally determined using standard tests by the manufacturers.

Variant grading performed well for the G44 sleeper, but not for the twin-block sleeper. This leads to a requirement to explore the performance of ballast grading in more detail by designing and testing more variant gradings. It is expected that this will define variant gradings that perform well for each sleeper type.

To investigate the best performance that can possibly be achieved by a whole track system, some combination tests are required. In combination tests, one or more modifications that led to individual component improvements are combined. The expectation from combination tests is that the earlier improvement can be enhanced. However, the combination test using twin-block sleeper on variant 3 grading did not perform as was expected. This may have been because the parameters combined in the test did not support each other. Further tests are required to confirm this.

Ballast breakage, attrition and abrasion occurred only to a minor extent although continuous cyclic loading was applied up to 10 million cycles. As a result, further investigation of ballast is required to answer questions on the performance recycled ballast. Recycled ballast may perform well without any strength reduction, only minor reduction or badly with a massive loss of strength. In the case of a massive loss of strength, this could be improved by the addition of fibre reinforcement or geotextile.

The presence of a fouling material in ballast voids without water had benefits. Since it is almost impossible to keep track dry all the time, the effects of water on fouled and clean ballast should be investigated. This would provide data that can be used for comparison and to analyse the actual loss of track performance due to water penetration into the track as well as to model flooded track.

Railway track can be installed with or without a sand blanket, which normally both intercepts water coming from the top and bottom layers and also prevents subgrade attrition by the ballast. The inclusion of a sand blanket in the track is worth investigating to quantify its contribution to track performance.

Appendices

Appendix A. Ballast specification used by railway authorities worldwide

Italian Ballast Specification

The parent rock of ballast used in Italian State railways are igneous and metamorphic rock. Sedimentary rock is only an option when igneous and metamorphic rocks cannot be economically sourced. The ballast size is mainly ranged between 30 to 60 mm and expected to conform to the limits in Table 8.1 (Geological Society, 2001).

Table 8.1: Italian State railways specification for ballast (after Geological Society, 2001)

Sieve size (mm)	Percentage passing sieve (%)
80	100-98
60	100-92
30	6-0
20	1-0

Spanish Ballast Specification

Ballast specifications employed by the state railway organization (RENEF) in Spain are very comprehensive and classified into two types (Geological Society, 2001):

1. Type A consists of siliceous rock, usually igneous although sedimentary and metamorphic rocks are also included. This type of ballast is used on heavily trafficked lines carrying an average of over 4000 tonnes per day.
2. Type B consists of limestone and is used where the average traffic loading is less than 4000 tonnes per day.

Mixing of these two types of ballast is prohibited and is expected to conform to Table 8.2.

Table 8.2: Spanish railways specification for ballast (after Geological Society, 2001)

Sieve size (mm)	Percentage passing sieve (%)
80	100
63	99-97
31.5	2-1
20	1-0

French Ballast Specification

Ballast used by the Société Nationale des Chemins de Fer (SNCF) in France is subject to extensive and detailed specifications. The ballast aggregate is expected to consist of freshly worked igneous rock (Geological Society, 2001) and conform to the PSD limits presented in Table 8.3.

Table 8.3: French railways ballast PSD (after Indraratna and Salim, 2005)

Sieve size (mm)	Upper rejection limit (%)	Upper excellent composition limit (%)	Lower excellent composition limit (%)	Lower rejection limit (%)
80	100			
63	98	100		
50	80	86	100	100
40	35	40	76	80
25	0	0	5	10
14			0	0

Swedish Ballast Specification

Ballast used in Sweden must range from 32 to 63 mm and conform to the grading envelope presented in Table 8.4. This is intended to support the maximum of 22.5 tonnes axle load with the maximum speed of 200km/h in the main line and the axle load of 25 tonnes for ore transport (Tolppanen et al., 2002):

Table 8.4: Swedish ballast specification (after Tolppanen et al., 2002)

Sieve size (mm)	Percentage passing sieve (%)
80	100
63	100-90
32	4-0

Turkish Ballast Specification

Turkish State Railways take advantage of an abundant supply of limestone as source of ballast material, which is uniformly graded between 30 to 60 mm. Turkey is also considering steel slag from the Eregli iron and steel works, as a cheap alternative (Kaya, 2004). However, basalt is considered for use on a planned high-speed project. Table 8.5 presents the PSD of ballast employs in Turkey.

Table 8.5: Ballast specification in Turkey (after Kaya, 2004)

Sieve size (mm)	Percentage passing sieve (%)
60	100
50	75
40	40
30	0

Indian Ballast Specification

Table 8.6 shows the ballast sizes recommended by Indian Railways (Ministry of Science and Technology Department of Technical and Vocational Education, 2007) which ranges between 20 to 50 mm. These sizes are considered performing a better interlocking between ballast particles for a certain sleeper types and locations.

Table 8.6: Diameter railway ballast particle based on type of sleepers (after Ministry of Science and Technology Department of Technical and Vocational Education, 2007)

Type of sleeper	Average ballast particle (mm)
Timber	50
Steel	40
Points and crossings	25

Railway ballast used in India needs to conform to the grading envelope presented in Table 8.7 (East Central Railway, 2005).

Table 8.7: Ballast specification in India (after East Central Railway, 2005)

Sieve size (mm)	Percentage passing sieve (%)
65	100-95
40	60-40
20	2-0

Japanese Ballast Specification

Japanese railway authorities recommend ballast grading envelope as presented in Table 8.8.

Table 8.8: Ballast specification used in Japan

Sieve size (mm)	Percentage passing sieve (%)
63.0	100
53.0	100-80
37.5	75-35
26.5	40-0
19.0	5-0

Appendix B. Graphs of rubber mat tests using Instron machine

Table 8.9: Loading and unloading data of the test on rubber mats using the Instron machine

Pressure (kPa)	15 mm thickness		6 mm thickness		Time (minutes)
	Initial deflection (mm)	Final deflection (mm)	Initial deflection (mm)	Final deflection (mm)	
0	0	0	0	0	0
10	0.04	0.05	0.04	0.05	10
20	0.08	0.09	0.06	0.07	10
50	0.12	0.13	0.08	0.10	10
10	0.1	0.1	0.10	0.09	10
100	0.16	0.18	0.10	0.12	10
10	0.12	0.11	0.11	0.10	10
200	0.23	0.25	0.12	0.14	10
10	0.14	0.13	0.12	0.11	10
300	0.31	0.33	0.15	0.17	10
10	0.17	0.15	0.14	0.14	10
400	0.38	0.4	0.18	0.20	10
10	0.19	0.17	0.16	0.15	10
500	0.44	0.48	0.20	0.22	10
10	0.21	0.19	0.17	0.15	10

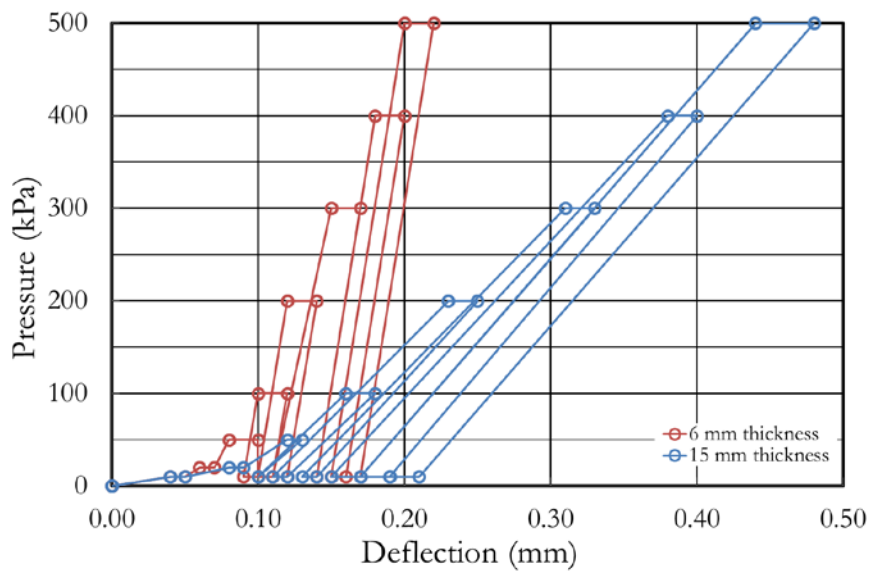


Figure 8.1: Applied pressure against deflection graphs of rubber mat tests using Instron machine

Appendix C. Graph of ballast sandwich tests on 15 mm rubber mat thickness

Table 8.10: Ballast sandwich test results on the 15 mm rubber mat thickness

Pressure (kPa)	Initial deflection corner 1 (mm)	Final deflection corner 1 (mm)	Initial deflection corner 2 (mm)	Final deflection corner 2 (mm)	Initial deflection corner 3 (mm)	Final deflection corner 3 (mm)	Initial deflection corner 4 (mm)	Final deflection corner 4 (mm)	Time (Minutes)
0.00	0.00	0.00	0.00	0.00	0.00	0.00	0.00	0.00	10
3.54	0.02	0.02	0.00	0.00	0.05	0.05	0.04	0.04	10
7.09	0.1	0.1	0.00	0.00	0.12	0.12	0.08	0.08	10
17.72	0.3	0.33	0.1	0.11	0.27	0.32	0.15	0.17	10
3.54	0.33	0.33	0.11	0.11	0.32	0.32	0.16	0.16	10
35.43	0.63	0.68	0.15	0.16	0.79	0.81	0.38	0.4	10
3.54	0.64	0.64	0.16	0.16	0.75	0.75	0.34	0.34	10
70.86	1.15	1.18	0.46	0.46	1.33	1.34	0.75	0.77	10
3.54	1.09	1.07	0.44	0.42	1.23	1.2	0.66	0.64	10
106.29	1.67	1.71	0.91	0.93	1.88	1.9	1.26	1.27	10
3.54	1.52	1.51	0.78	0.78	1.68	1.68	1.01	1.01	10
35.43	2.17	2.18	1.34	1.35	2.4	2.4	1.71	1.72	10
3.54	1.96	1.95	1.1	1.09	2.09	2.09	1.31	1.31	10
177.15	2.61	2.61	1.75	1.75	2.88	2.89	2.16	2.16	10
3.54	2.29	2.28	1.38	1.34	2.48	2.47	1.65	1.64	10

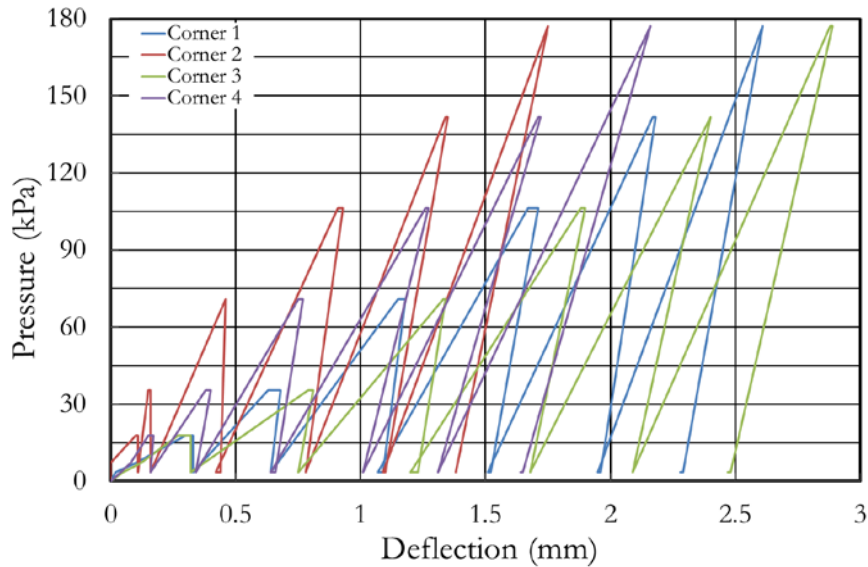


Figure 8.2: Applied pressure against deflection graphs of ballast sandwich test on 15 mm rubber mat thickness

Appendix D. Graph of ballast sandwich tests on 6 mm rubber mat thickness and without rubber mat

Table 8.11: Ballast sandwich test results on the 6 mm rubber mat thickness

Pressure (kPa)	Initial deflection corner 1 (mm)	Final deflection corner 1 (mm)	Initial deflection corner 2 (mm)	Final deflection corner 2 (mm)	Initial deflection corner 3 (mm)	Final deflection corner 3 (mm)	Initial deflection corner 4 (mm)	Final deflection corner 4 (mm)	Time (Minutes)
0.00	0.00	0.00	0.00	0.00	0.00	0.00	0.00	0.00	10
3.54	0.01	0.01	0.00	0.00	0.00	0.00	0.00	0.00	10
7.09	0.07	0.07	0.05	0.06	0.00	0.00	0.05	0.05	10
17.72	0.32	0.33	0.28	0.29	0.12	0.14	0.20	0.21	10
3.54	0.31	0.30	0.29	0.29	0.14	0.14	0.21	0.21	10
35.43	0.77	0.83	0.62	0.63	0.34	0.37	0.50	0.53	10
3.54	0.71	0.69	0.63	0.63	0.37	0.37	0.53	0.51	10
70.86	1.40	1.48	1.08	1.11	0.68	0.74	0.99	1.04	10
3.54	1.20	1.17	1.11	1.11	0.74	0.74	0.93	0.89	10
106.29	2.00	2.17	1.63	1.66	1.04	1.17	1.54	1.59	10
3.54	1.78	1.77	1.66	1.66	1.17	1.17	1.43	1.41	10
35.43	2.61	2.69	2.21	2.23	1.53	1.68	2.04	2.08	10
3.54	2.28	2.25	2.17	2.17	1.68	1.68	1.83	1.81	10
177.15	2.97	3.07	2.60	2.71	1.87	1.99	2.23	2.34	10
3.54	2.63	2.61	2.56	2.56	1.99	1.99	2.11	2.06	10

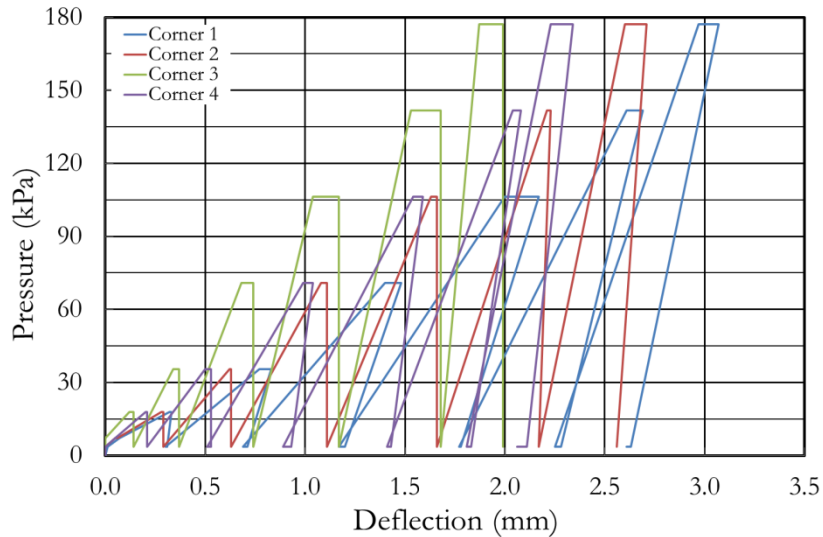


Figure 8.3: Applied pressure against deflection graphs of ballast sandwich test on 6 mm rubber mat thickness

Table 8.12: Ballast sandwich test results without rubber mat

Pressure (kPa)	Initial deflection corner 1 (mm)	Final Deflection Corner 1 (mm)	Initial Deflection Corner 2 (mm)	Final Deflection Corner 2 (mm)	Initial Deflection Corner 3 (mm)	Final Deflection Corner 3 (mm)	Initial Deflection Corner 4 (mm)	Final Deflection Corner 4 (mm)	Time (Minutes)
0.00	0.00	0.00	0.00	0.00	0.00	0.00	0.00	0.00	10
3.54	0.00	0.00	0.00	0.00	0.00	0.00	0.00	0.00	10
7.09	0.00	0.00	0.01	0.01	0.00	0.00	0.00	0.00	10
17.72	0.02	0.03	0.07	0.09	0.05	0.05	0.01	0.01	10
3.54	0.03	0.03	0.05	0.01	0.02	0.01	0.01	0.00	10
35.43	0.08	0.08	0.13	0.13	0.10	0.11	0.08	0.08	10
3.54	0.05	0.05	0.07	0.06	0.02	0.02	0.03	0.03	10
70.86	0.18	0.19	0.24	0.26	0.20	0.21	0.17	0.17	10
3.54	0.09	0.09	0.11	0.11	0.08	0.08	0.06	0.06	10
106.29	0.27	0.28	0.34	0.35	0.31	0.31	0.27	0.28	10
3.54	0.15	0.14	0.19	0.18	0.13	0.13	0.11	0.11	10
35.43	0.41	0.42	0.49	0.52	0.46	0.48	0.42	0.43	10
3.54	0.25	0.25	0.30	0.30	0.22	0.22	0.20	0.20	10
177.15	0.60	0.63	0.70	0.73	0.66	0.69	0.64	0.71	10
3.54	0.42	0.42	0.47	0.47	0.39	0.39	0.36	0.36	10

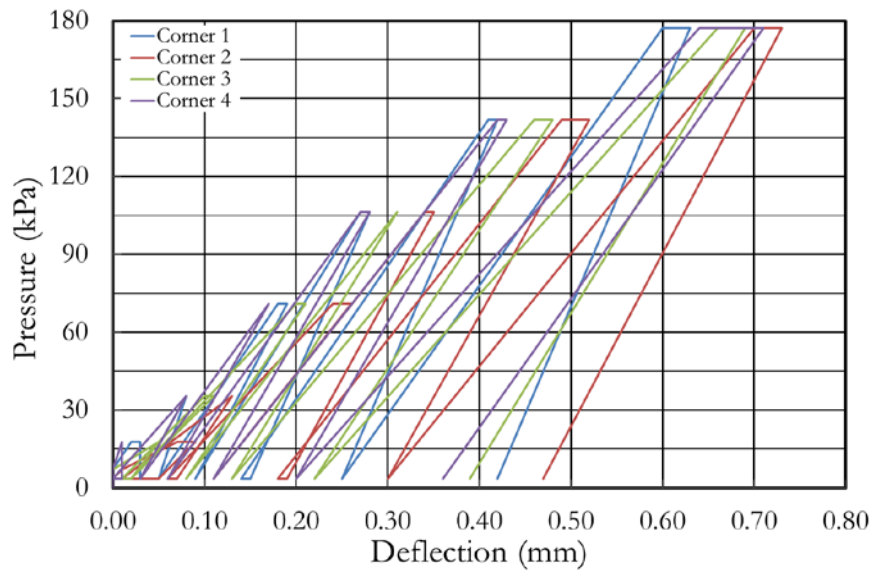


Figure 8.4: Applied pressure against deflection graphs of ballast sandwich test without rubber mat

Appendix E. Data of pressure paper calibration

Table 8.13: Calibration results of pressure paper ranged 0.5-2.5MPa for various applied loads and holding times

Pressure (MPa)	Time (minutes)												
	5	30	60	180	360	540	720	2160	5040	10080	30240	60480	121200
	Red intensity												
0.0	0.00	0.00	0.00	0.00	0.00	0.00	0.00	0.00	0.00	0.00	0.00	0.00	0.00
0.1	11.62	11.36	11.41	11.40	11.34	10.74	10.33	11.06	11.16	10.75	10.93	11.95	11.83
0.2	21.90	23.29	23.10	23.07	22.99	22.67	22.62	22.50	22.07	21.83	20.81	21.94	22.88
0.3	24.60	26.43	25.94	26.22	25.56	25.46	24.40	24.61	24.45	23.50	23.14	23.15	24.30
0.4	32.48	34.60	34.65	33.95	33.48	32.97	32.69	32.08	31.95	31.51	31.68	32.03	31.77
0.5	34.69	36.20	35.64	35.53	35.44	35.37	34.79	34.17	33.72	32.56	32.57	32.81	32.72
1.0	54.17	56.03	55.97	56.30	55.56	54.97	54.53	53.78	54.31	53.08	53.14	53.76	53.02
1.5	61.00	62.07	62.01	61.82	61.58	60.96	61.10	59.36	59.03	58.90	58.55	59.06	58.53
2.0	64.86	66.27	65.59	64.62	64.94	63.48	63.78	62.89	62.31	60.96	61.07	61.17	60.72
2.5	67.57	67.93	68.08	67.80	66.44	65.67	65.11	64.49	64.43	63.70	63.06	62.70	63.73

Table 8.14: Calibration results of pressure paper ranged 2.5-10MPa for various applied loads and holding times

Pressure (MPa)	Time (minutes)									
	5	30	60	540	1440	13260	33120	63480	125700	
	Red intensity									
0.0	0.00	0.00	0.00	0.00	0.00	0.00	0.00	0.00	0.00	
0.5	5.89	5.71	5.21	5.18	4.61	5.66	5.63	5.98	5.37	
1.0	9.16	9.03	8.49	8.19	8.25	8.95	8.49	9.27	8.29	
1.5	11.66	11.45	10.76	10.65	10.40	10.92	11.55	10.83	10.67	
2.0	15.22	15.96	14.86	14.87	14.45	15.00	14.87	15.25	14.42	
2.5	20.65	20.24	20.21	19.42	18.84	19.53	18.87	18.67	18.96	
5.0	38.19	40.23	40.78	40.98	40.03	40.59	38.36	38.50	37.70	
7.5	51.35	52.70	54.06	53.81	53.77	53.28	51.47	51.06	49.26	
10.0	59.69	61.22	61.15	61.91	61.18	61.08	59.05	57.68	56.35	

Table 8.15: Calibration results of pressure paper ranged 10-50MPa for various applied loads and holding times

Pressure (MPa)	Time (minutes)									
	5	30	60	540	1440	13260	33120	63480	125700	
	Red intensity									
0.0	0.00	0.00	0.00	0.00	0.00	0.00	0.00	0.00	0.00	
2.5	4.61	4.97	5.05	4.52	5.28	5.03	5.26	5.26	5.07	
5.0	8.15	8.60	8.22	8.34	7.65	7.90	7.96	8.35	8.10	
7.5	11.82	11.94	11.80	12.10	12.05	12.28	11.71	10.84	11.66	
10.0	17.69	18.02	17.80	17.98	17.22	17.17	16.99	17.32	16.59	
20.0	36.01	37.27	37.47	38.38	38.02	38.05	35.91	36.40	35.16	
30.0	46.63	47.60	48.01	48.98	48.33	47.87	46.85	46.27	44.49	
40.0	52.06	53.47	52.84	53.55	52.72	52.65	50.57	50.21	48.81	
50.0	57.24	57.75	57.91	58.67	57.00	56.85	55.78	55.46	53.28	

Appendix F. Graphs of PSD method for particle breakage investigation

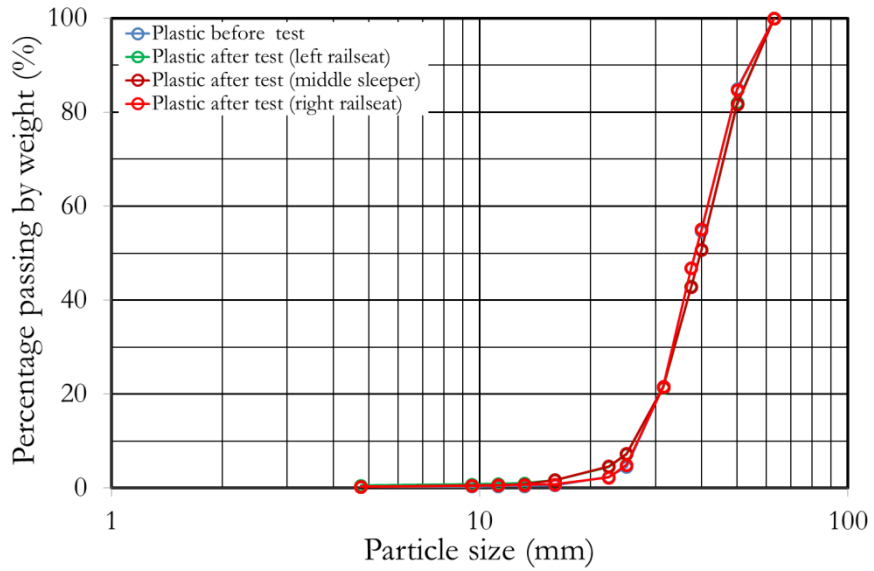


Figure 8.5: PSD graphs of ballast in different locations on plastic sleeper test, before and after testing

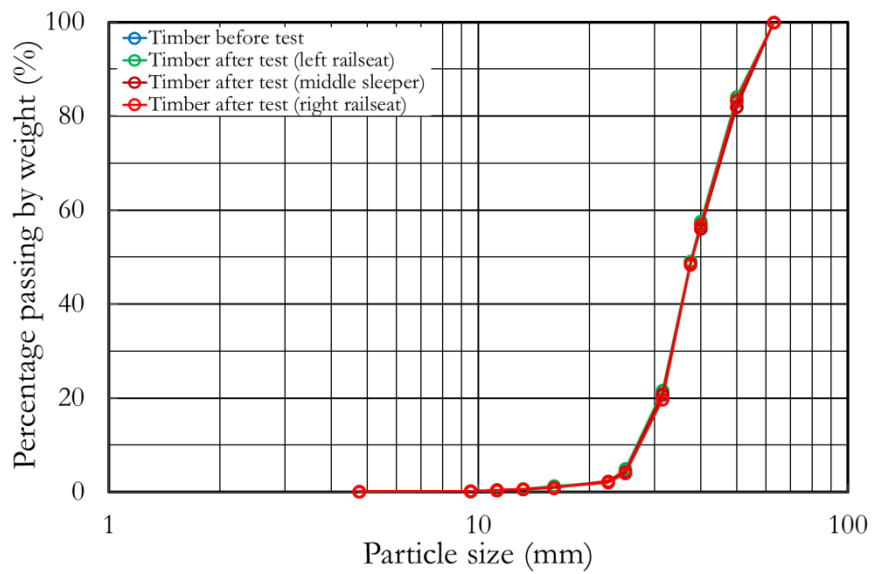


Figure 8.6: PSD graphs of ballast in different locations on timber sleeper test, before and after testing

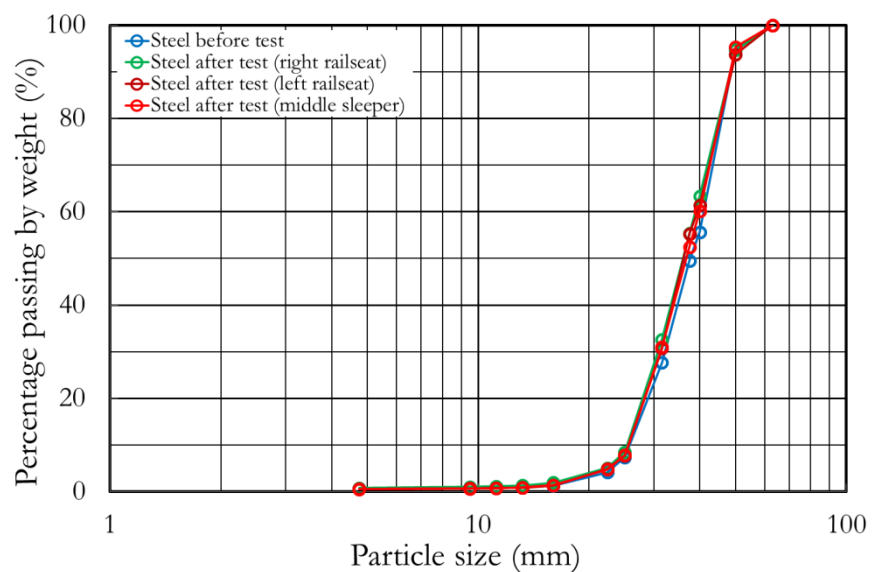


Figure 8.7: PSD graphs of ballast in different locations on steel sleeper test, before and after testing

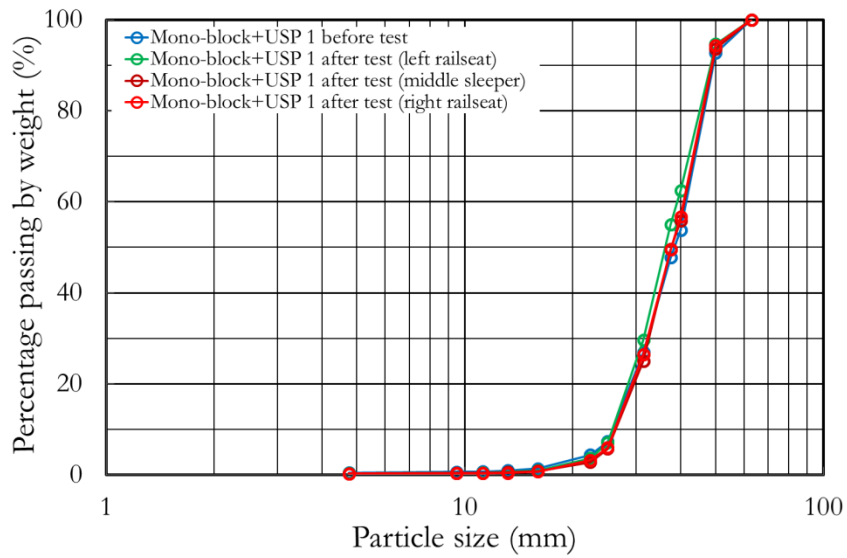


Figure 8.8: PSD graphs of ballast in different locations on mono-block sleeper with USP 1 test, before and after testing

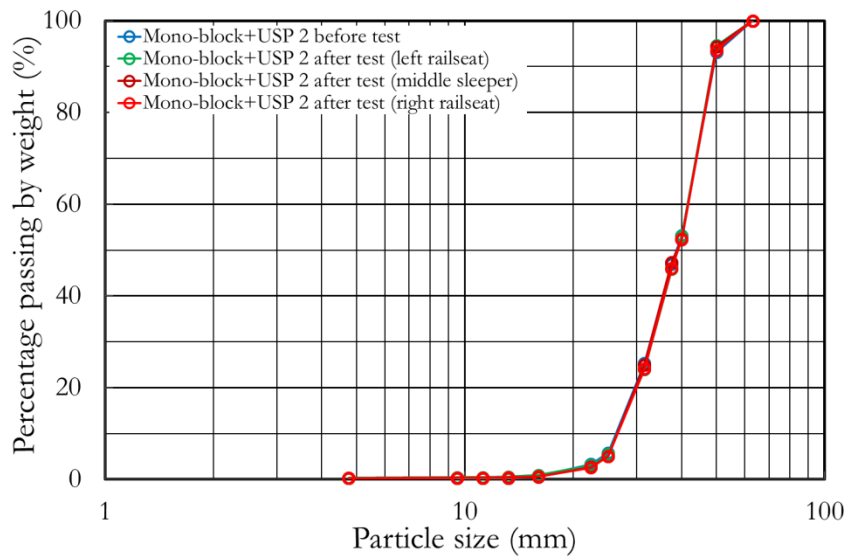


Figure 8.9: PSD graphs of ballast in different locations on mono-block sleeper with USP 2 test, before and after testing

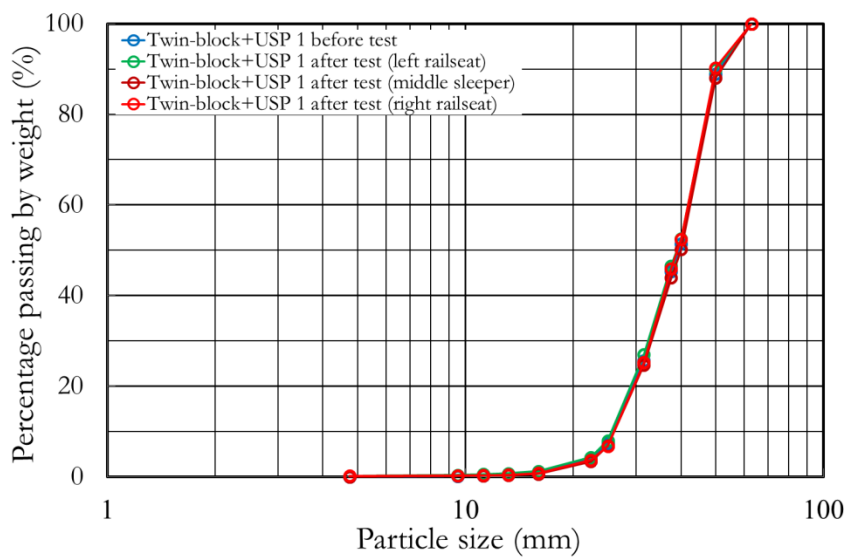


Figure 8.10: PSD graphs of ballast in different locations on twin-block sleeper with USP 1 test, before and after testing

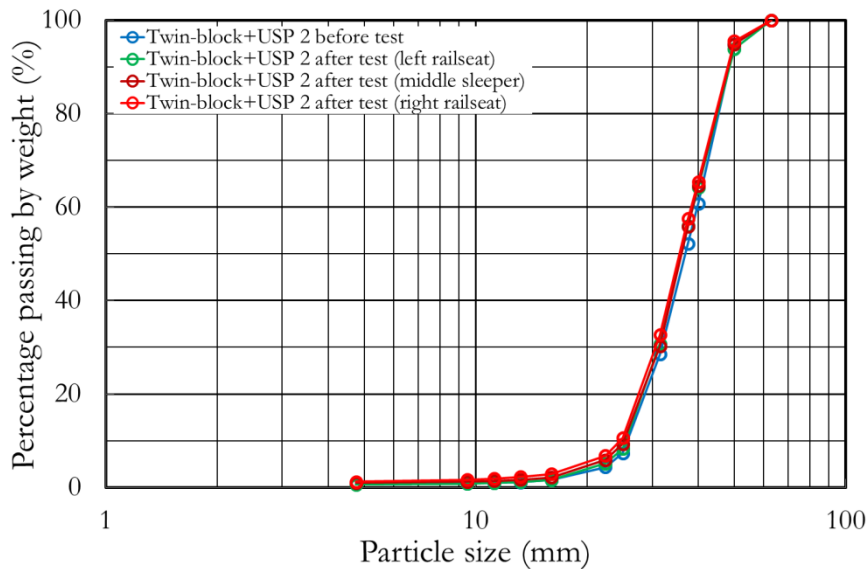


Figure 8.11: PSD graphs of ballast in different locations on twin-block sleeper with USP 2 test, before and after testing

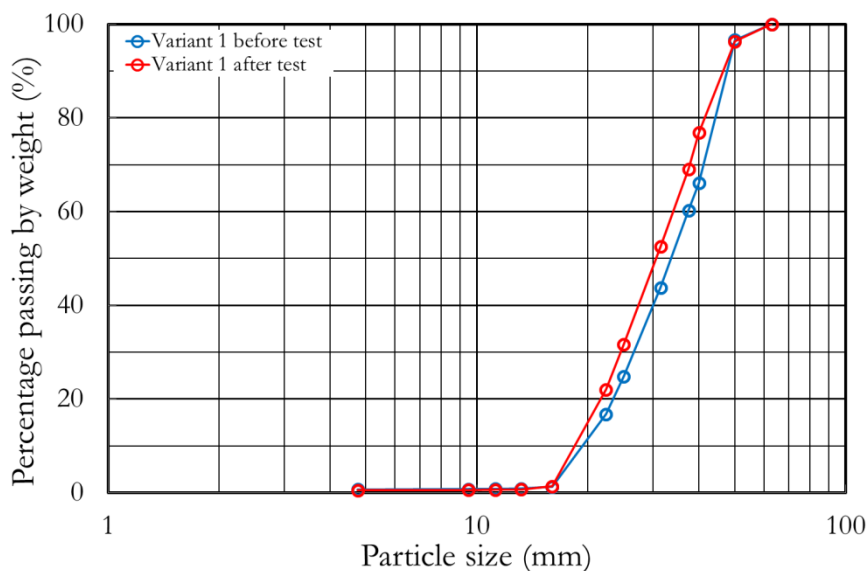


Figure 8.12: PSD graphs of ballast in different locations on variant 1 test, before and after testing

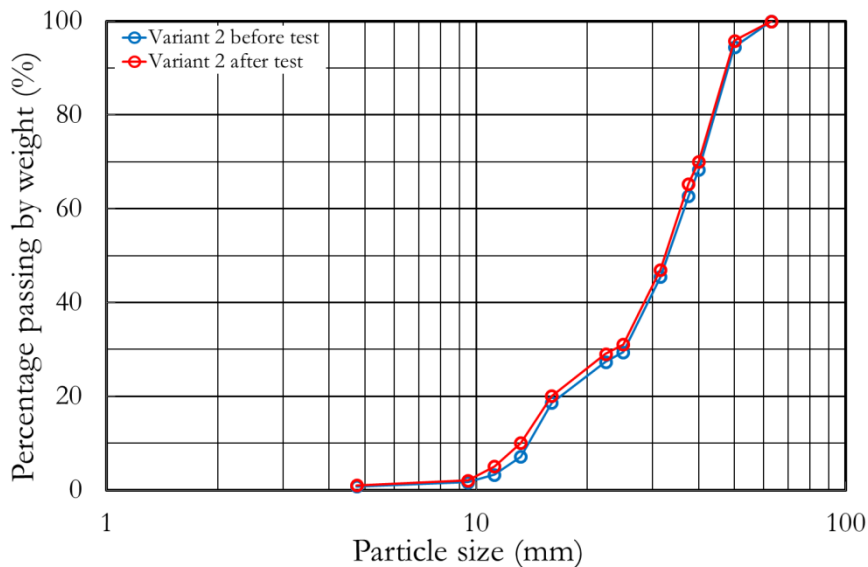


Figure 8.13: PSD graphs of ballast in different locations on variant 2 test, before and after testing

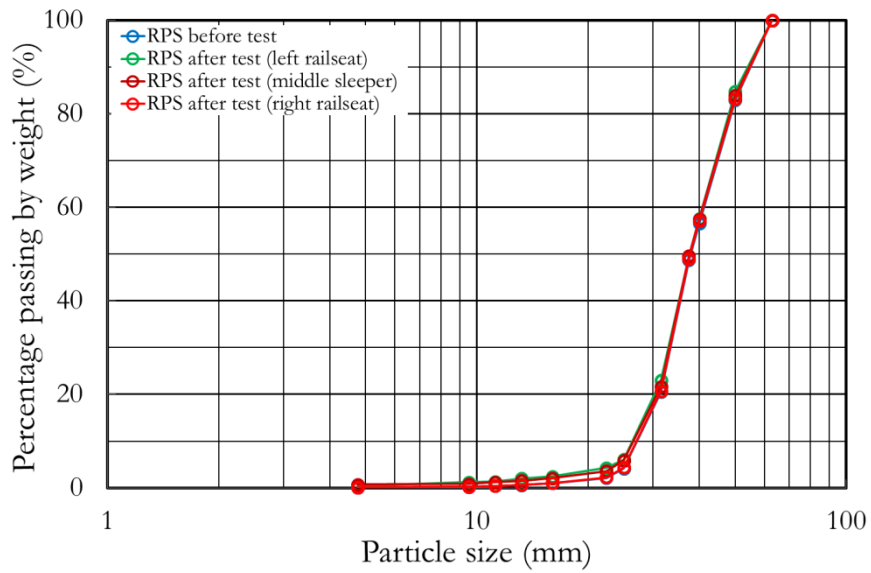


Figure 8.14: PSD graphs of ballast in different locations on RPS slope test, before and after testing

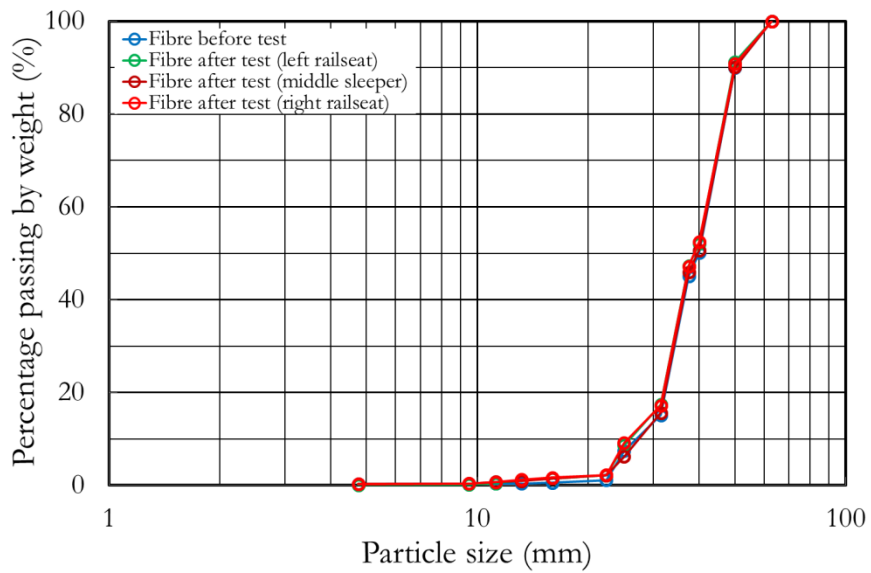


Figure 8.15: PSD graphs of ballast in different locations on fibre test, before and after testing

Appendix G. PSD graphs of 50 randomly selected ballast particles

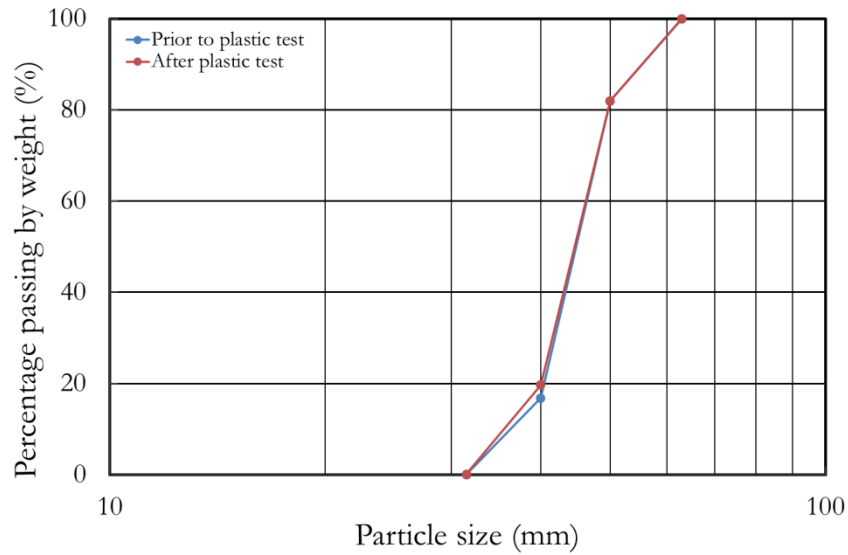


Figure 8.16: PSD graphs of randomly selected particles on plastic sleeper before and after test

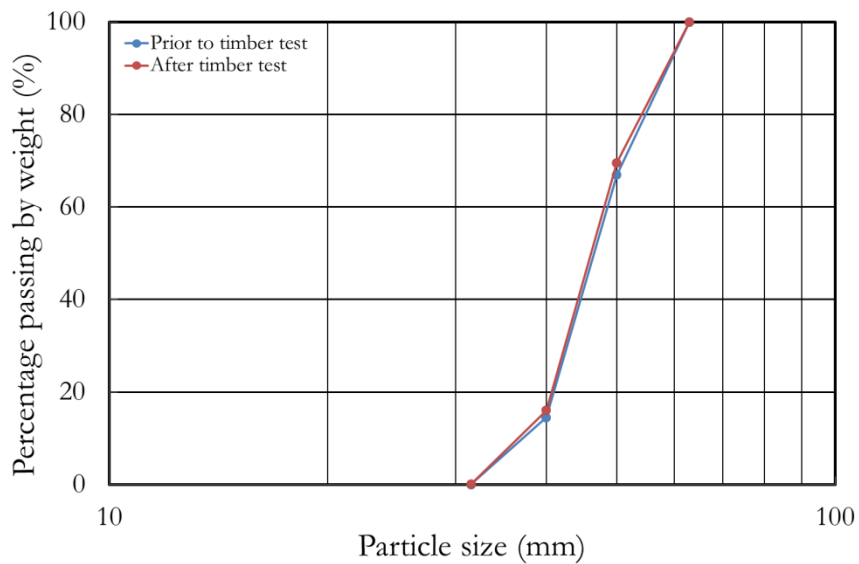


Figure 8.17: PSD graphs of randomly selected particles on timber sleeper before and after test

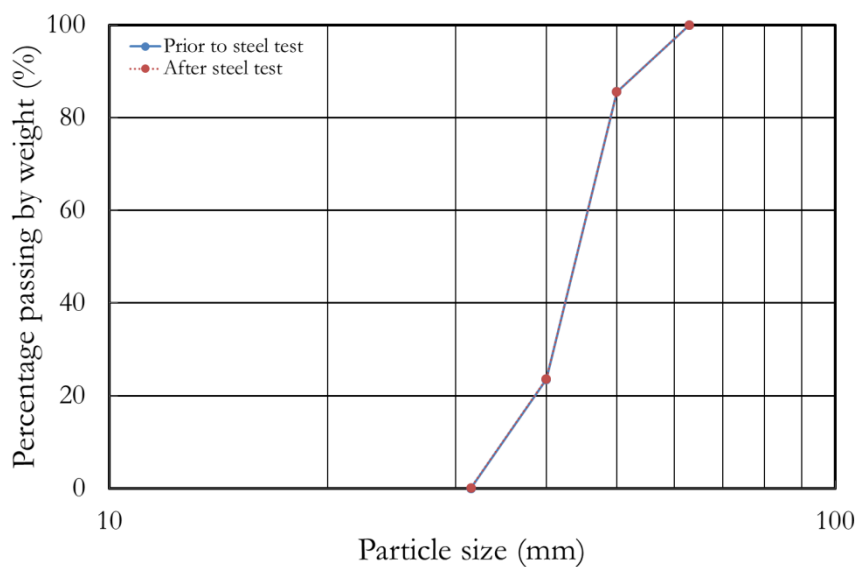


Figure 8.18: PSD graphs of randomly selected particles on steel sleeper before and after test

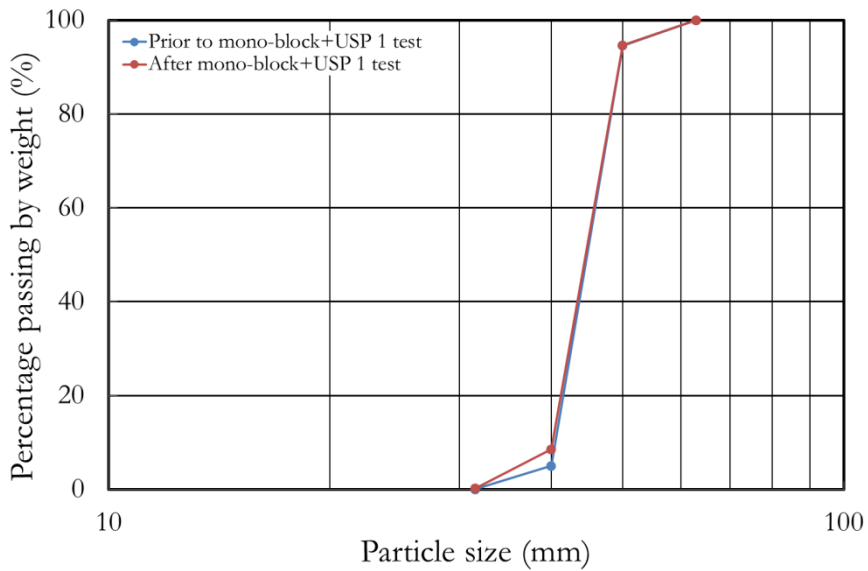


Figure 8.19: PSD graphs of randomly selected particles on mono-block + USP 1 before and after test

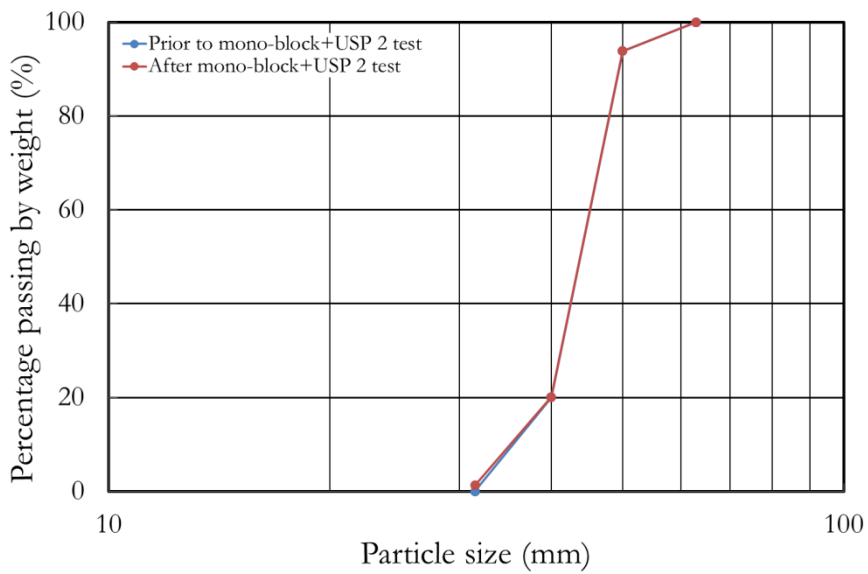


Figure 8.20: PSD graphs of randomly selected particles on mono-block + USP 2 before and after test

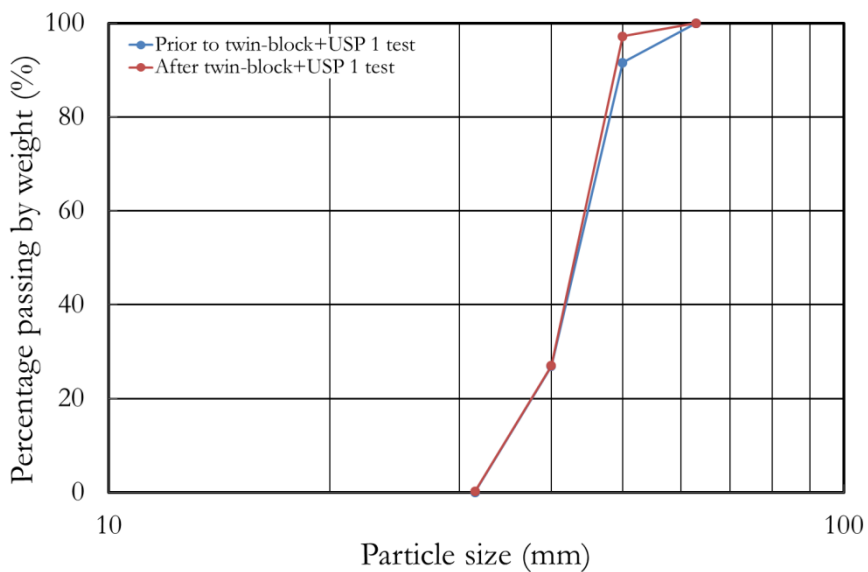


Figure 8.21: PSD graphs of randomly selected particles on twin-block + USP 1 before and after test

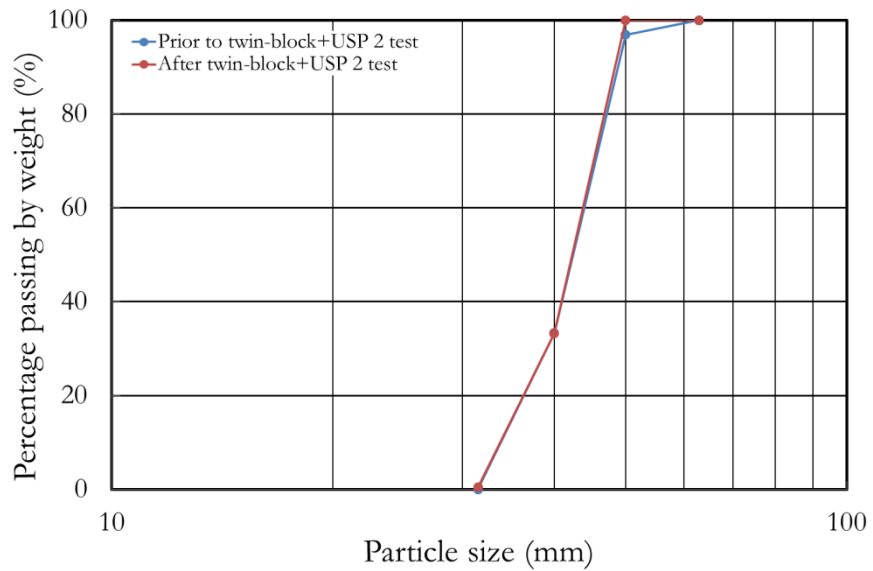


Figure 8.22: PSD graphs of randomly selected particles on twin-block + USP 2 before and after test

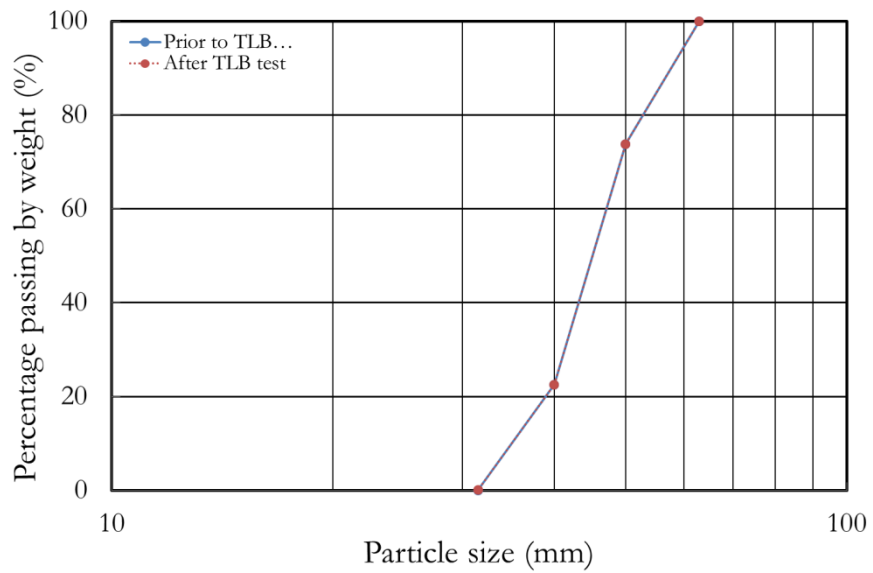


Figure 8.23: PSD graphs of randomly selected particles on TLB before and after test

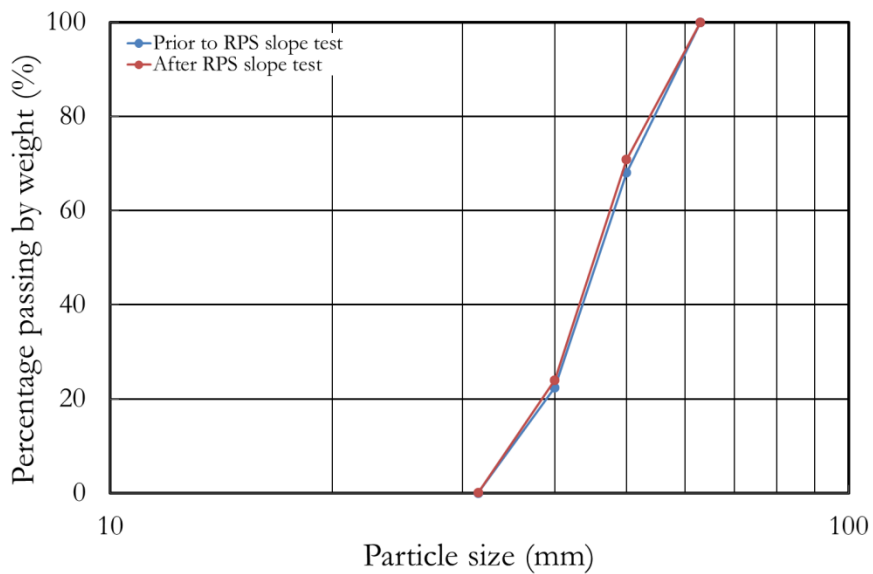


Figure 8.24: PSD graphs of randomly selected particles on RPS slope before and after test

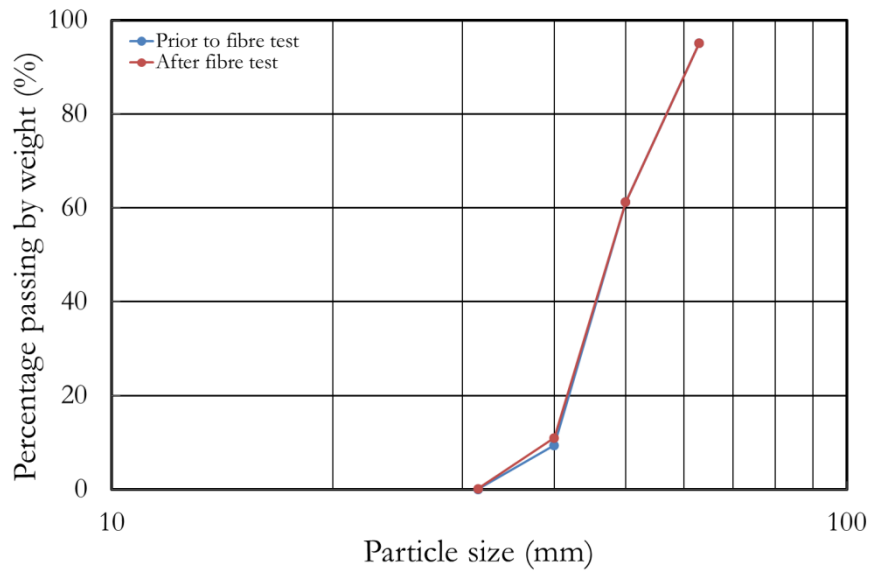


Figure 8.25: PSD graphs of randomly selected particles on RPS slope before and after test

Appendix H. Lateral movement of ballast on shoulder slope

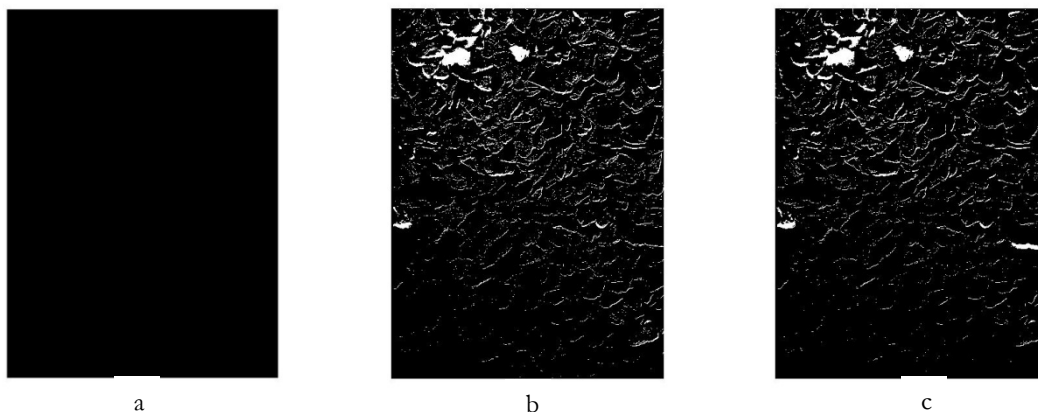


Figure 8.26: Ballast particle movements on the shoulder slope at (a) prior to testing, (b) during harvesting the data at 0.25 million loading cycles and (c) the end of mono-block sleeper with USP 1 test

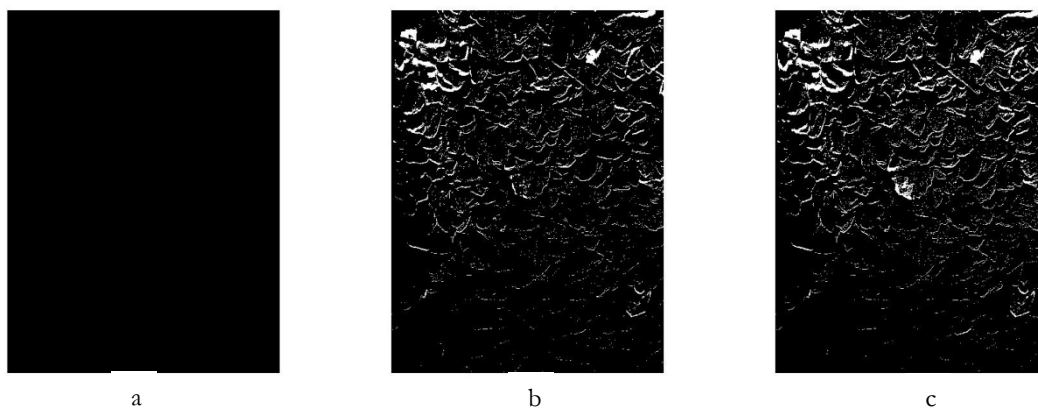


Figure 8.27: Ballast particle movements on the shoulder slope at (a) prior to testing, (b) during harvesting the data at 0.25 million loading cycles and (c) the end of mono-block sleeper with USP 2 test

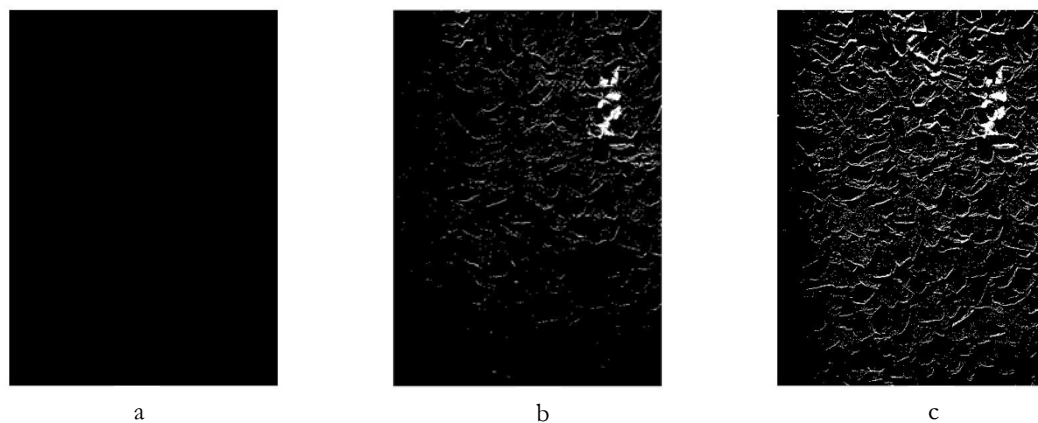


Figure 8.28: Ballast particle movements on the shoulder slope at (a) prior to testing, (b) during harvesting the data at 0.25 million loading cycles and (c) the end of twin-block sleeper with USP 1 test

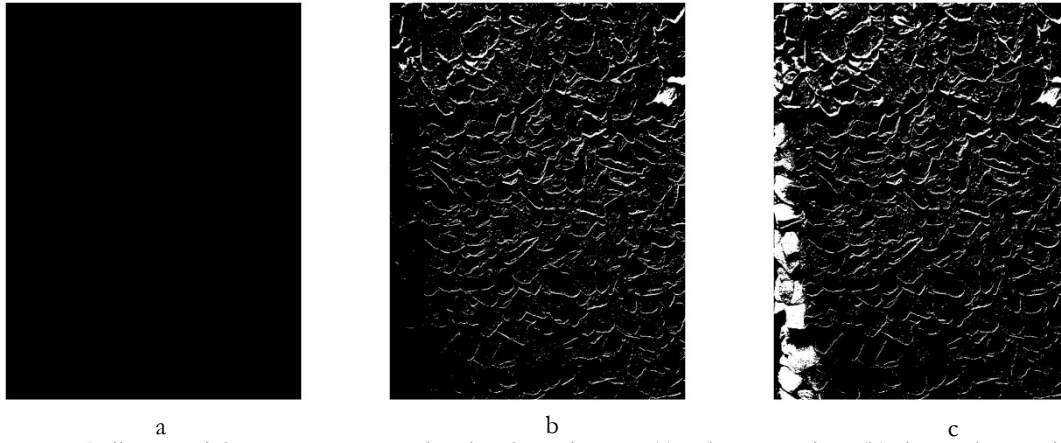


Figure 8.29: Ballast particle movements on the shoulder slope at (a) prior to testing, (b) during harvesting the data at 0.25 million loading cycles and (c) the end of twin-block sleeper with USP 2 test

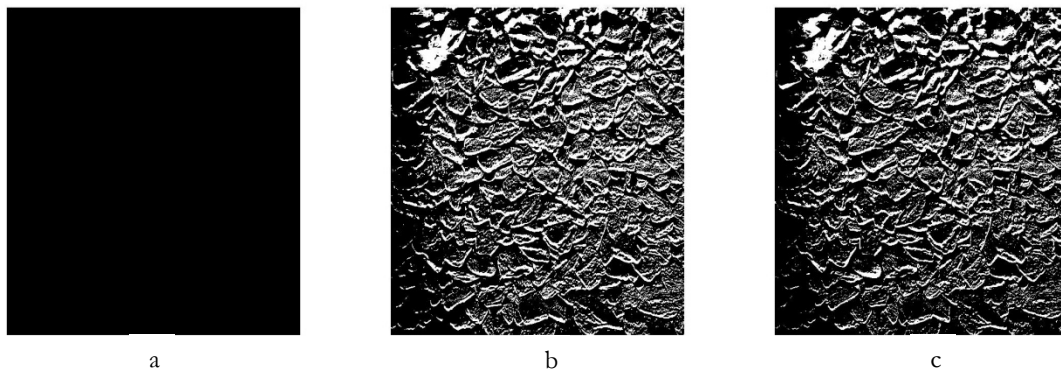


Figure 8.30: Ballast particle movements on the shoulder slope at (a) prior to testing, (b) during harvesting the data at 0.25 million loading cycles and (c) the end of steel sleeper

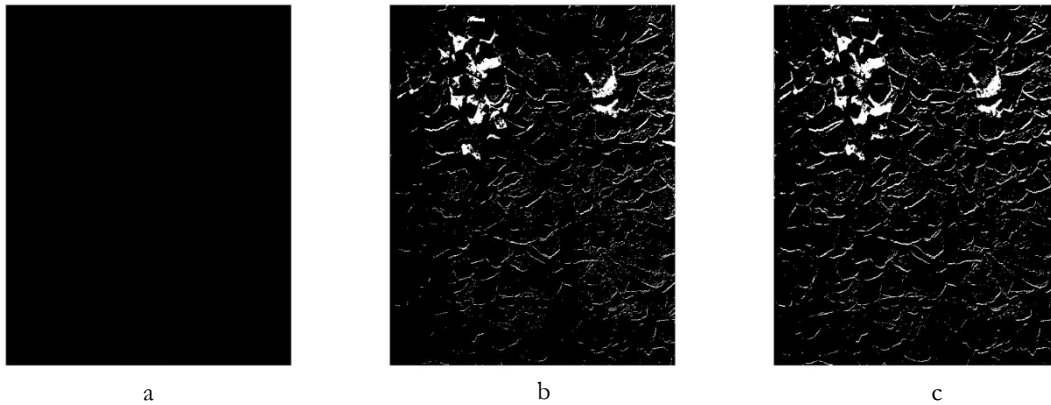


Figure 8.31: Ballast particle movements on the shoulder slope at (a) prior to testing, (b) during harvesting the data at 0.25 million loading cycles and (c) the end of plastic sleeper test

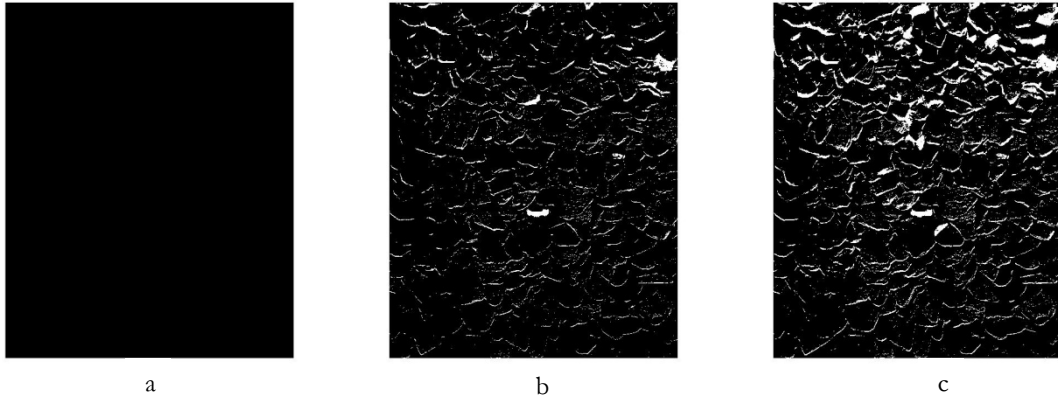


Figure 8.32: Ballast particle movements on the shoulder slope at (a) prior to testing, (b) during harvesting the data at 0.25 million loading cycles and (c) the end of timber sleeper test

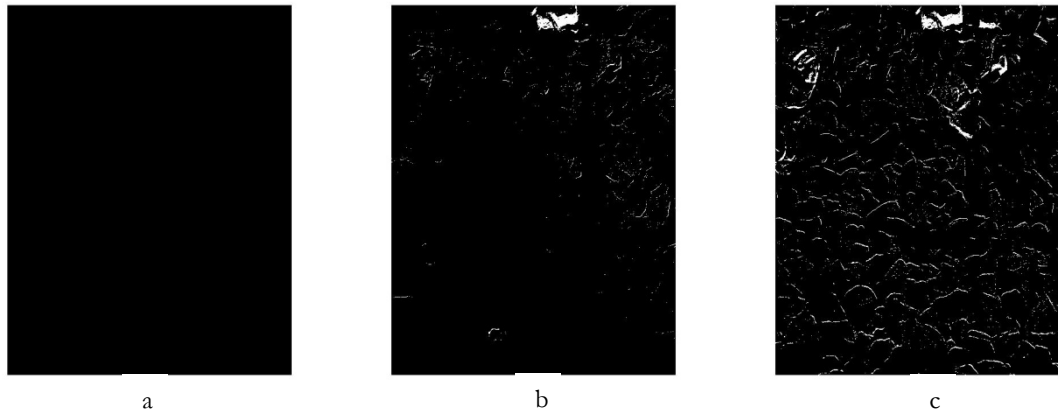


Figure 8.33: Ballast particle movements on the shoulder slope at (a) prior to testing, (b) during harvesting the data at 0.25 million loading cycles and (c) the end of TLB system test

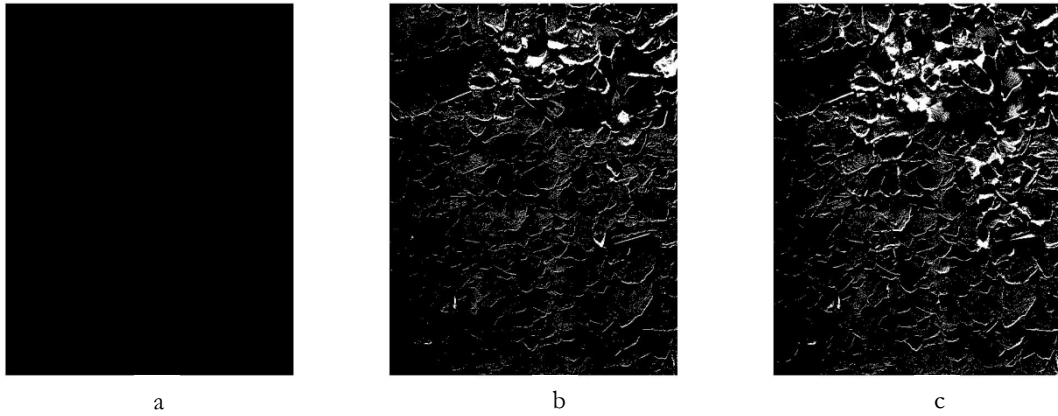


Figure 8.34: Ballast particle movements on the shoulder slope at (a) prior to testing, (b) during harvesting the data at 0.25 million loading cycles and (c) the end of fibre reinforced ballast test

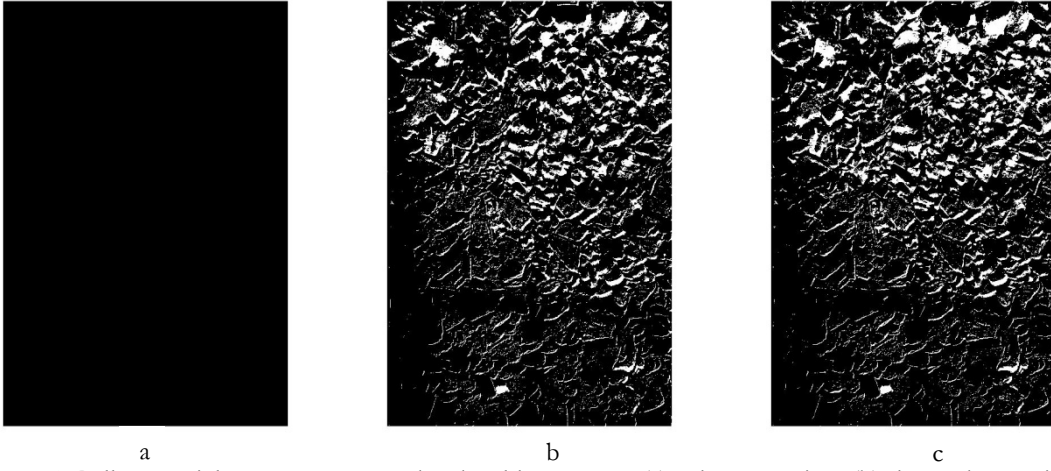


Figure 8.35: Ballast particle movements on the shoulder slope at (a) prior to testing, (b) during harvesting the data at 0.25 million loading cycles and (c) the end of combination 1 test

References

- A J P Automotive Ltd 2011. Pressure Measurement Film Prescale.
- Abadi, T. C., Le Pen, L. M., Zervos, A. & Powrie, W. 2014. Measuring the Contact Area and Pressure between the Ballast and the Sleeper. *The International Journal of Railway Technology*, Saxe-Coburg Publication, 888.
- Abadi, T. C., Le Pen, L. M., Zervos, A. & Powrie, W. 2013. Measuring the Contact Area and Pressure Between the Ballast and the Sleeper. *Railway Track Science and Engineering, International Workshop-Ballast: Issues and Challenges*. UIC Paris.
- Abadi, T. C., Le Pen, L. M., Zervos, A., Priest, J. A. & Powrie, W. "in review". Measuring the Number and Area of Ballast Particle Contacts by Pressure Paper *Transportation Engineering Journal of ASCE*, Geotechnical Special Publication.
- Aingaran, S. 2014. *Experimental Investigation of Static and Cyclic Behaviour of Scaled Railway Ballast and the Effect of Stress Reversal*. The Degree of Doctor of Philosophy, Faculty of Engineering and the Environment, Southampton University, UK.
- Ajayi, O. O. 2014. *The Effect of Fibre Reinforcements on the Mechanical Behaviour of Railway Ballast*. Doctor of Philosophy, University of Southampton.
- Ajayi, O. O., Le Pen, L. M., Zervos, A. & Powrie, W. 2014a. Effects of Random Fibre Reinforcement on the Density of Granular Materials. In: SOGA, K., KUMAR, K., BISCONTIN, G. & KUO, M. (eds.) *Geomechanics from Micro to Macro*. University of Cambridge, Cambridge, UK.: CRC Press/Balkema.
- Ajayi, O. O., Le Pen, L. M., Zervos, A. & Powrie, W. 2014b. Feasibility Study of Random Fibre Reinforced Railway Ballast. In: ARROYO, M. & GENS, A. (eds.) *23rd European Young Geotechnical Engineers Conference*. Universitat Politècnica de Catalunya, Barcelona, Spain.
- Ajp Automotive Ltd. 2014. *AJP Automomotive Ltd- Fujifilm Prescale Pressure* [Online]. Available: www.prescale.co.uk [Accessed 08/05/2014 2014].
- Allan, J. 2012. Soil Mechanics of High Speed Rail Track. *1st Civil and Environmental Engineering Student Conference*. Imperial College London.
- Alva-Hurtado, J. E. & Selig, E. T. Permanent Strain Behavior of Railroad Ballast. In: ICSMFE, P. C. O. X., ed. *10th International Conference on Soil Mechanics and Foundation Engineering*, 15-19th June 1981 Stockholm. A.A Balkema, Rotterdam.
- Anderson, W. F. & Key, A. J. 2000. Model testing of two-layer railway track ballast. *Journal of Geotechnical and Geoenvironmental Engineering*, 126, 317-323.
- Andussies, R. 2011. *RE: Pressure Measurement Film Analysing*. Type to ABADI, T.
- Arema 2012. American Railway Engineering and Maintenance-of-Way Association: Chapter 1: Roadway and Ballast. *Ballast*.
- Arema 2000. AREMA Manual for Railway Engineering. *Roadway and Ballast*. AREMA.
- Arema 2003a. Manual for Railway Engineering: Systems Management: Chapter 16. Economics of Railway Engineering and Operations.
- Arema 2003b. Practical Guide to Railway Engineering. American Railway Engineering and Maintenance-of-Way Association.
- Auer, F., Potvin, R., Godart, P. & Schmitt, L. 2013. Track Systems Supplement: Under Sleeper Pads in Track-the UIC Project. *European Railway Review*.
- Aursudkij, B. 2007. *A Laboratory Study of Railway Ballast Behaviour Under Traffic Loading and Tamping Maintenance*. Doctor of Philosophy, The University of Nottingham.
- Australian Rail Track Corporation Ltd 2007. Ballast Specification.

- Bathurst, R. J. & Raymond, G. P. 1987. Geogrid Reinforcement of Ballasted Track. *Journal Transportation Research Record*, Vol. 1153, 8-14.
- Bilow, D. N. & Randich, G. M. 2000. Slab Track for Next 100 Years. *AREMA Proceedings of the 2000 Annual Conference*. Dallas, Texas.
- Bonnett, C. F. 2005. *Practical Railway Engineering*, Imperial College Press.
- Boucher, D. L. & Selig, E. T. 1987. Application of Petrographic Analysis to Ballast Performance Evaluation. *Journal Transportation Research Record*, Vol. 1131, 15-25.
- Bowness, D., Lock, A. C., Powrie, W., Priest, J. A. & Richards, D. J. 2005. Monitoring the Dynamic Displacements of Railway Track. *Journal of Rail and Rapid Transit*, Vol. 221, 13-22.
- British Standards Institution 2000. British Standard Institution BS 500:2000: Steel Sleepers. British Standard Institution.
- British Standards Institution 2009a. British Standard Institution BS EN 13230-2:2009 Railway Applications -Track - Concrete Sleepers and Bearers: Part 2: Prestressed Mono-block Sleepers. British Standard Institution.
- British Standards Institution 2009b. British Standard Institution BS EN 13230-3:2009 Railway Applications -Track - Concrete Sleepers and Bearers: Part 3: Twin-block Reinforced Sleepers. British Standard Institution.
- British Standards Institution 2009c. British Standard Institution PD 6682-2:2009 Published Document Aggregates: Part 2: Aggregates for Bituminous Mixtures and Surface Treatments for Roads, Airfields and other Trafficked Areas-Guidance on the use of BS EN 13043. British Standard Institution.
- British Standards Institution 2004. British Standard Institution PD 6682-8:2004 Aggregates: Part 8: Aggregates for Railway Ballast-Guidance on the use of BS EN 13450. British Standard Institution.
- British Standards Institution 1990. BS 1377-2:1990. *Methods of Test for Soils for Civil Engineering Purposes Part 2: Classification Test*.
- British Standards Institution 2002. BSI Standard Publication BS EN 13450:2002 Aggregates for Railway Ballast. British Standard.
- British Standards Institution 2013. BSI Standard Publication BS EN 13450:2013 Aggregates for Railway Ballast. British Standard Institution.
- British Standards Institution 2014. Draft BS EN 16730 Railway Applications-Track-Concrete Sleepers and Bearers with Under Sleeper Pads. BSI Group Headquarters, London: British Standard Institution.
- British Standards Institution 2011. Railway Applications-Track-Rail. *Part 1: Vignole Railway Rails 46 kg/m and Above*. British Standard.
- British Standards Institution 1989. Testing Aggregates -Methods for Samplings.
- Brooker, E. W. & Ireland, H. O. 1965. Earth Pressures at Rest Related to Stress History. *Canadian Geotechnical Journal*, Vol. 2, 1-15.
- Budiono, D. S., Mcsweeney, T. & Dhanasekar, M. The Effect of Coal Dust Fouling on the Cyclic Behaviour of Railtrack Ballast. In: TRIANTAFYLLIDIS, ed. Cyclic Behaviour of Soils and Liquefaction Phenomena, 2004. Taylor and Francis Group, 627-632.
- Campbell, I. M. 1984. Railway Track in a competitive Commercial Business. *Track Technology*. London: Thomas Telford Ltd.
- Canadian National Railway 2007. Engineering Specifications for Industrial Track in U.S. CN Southern Region Technical Service Office-Engineering Department
- Canadian Pacific Rail 1984. CP Rail Specifications for Ballast. *Evaluating Processed Rock, Slag and Gravel Ballast Sources*. Canadian Pacific Rail.
- Chrismer, S. M. & Richardson, G. 1986. In-track Performance of Geotextiles at Caldwell, Texas. *Journal Transportation Research Record*, Vol. 1071.

- Chrismer, S. M. & Read, D. M. 1994. Research, Test & Development-Examining Ballast and Subgrade Conditions. *Railway Track & Structures*. Bristol: Simmons-Broadman.
- Claisse, P. & Calla, C. 2006. Rail Ballast: Conclusions from a Historical Perspective. *Proceedings of the Institution of Civil Engineers Transport* 159, 69-74.
- Claisse, P., Keedwell, M. & Calla, C. 2003. Tests on A Two-Layered Ballast System. *Proceeding of The Institution of Civil Engineers, Transport* 156, 93-101.
- Clifton, A. W., Klassen, M. J. & Watters, B. R. 1987. Production and Testing of Ballast. *Journal Transportation Research Record*, Vol. 1131, 26-34.
- Country Regional Network 2013. Engineering Standard Track. *CRN CS 240 Ballast*.
- Cuellar, V., Navarro, F., Andreu, M. A., Camara, J. L., Gonzalez, F., Rodriguez, M., Gonzalez, P., Diaz, R., Navarro, J. & Rodriguez, R. 2011. Short and Long Term Behaviour of High Speed Lines as Determined in 1:1 Scale Laboratory Tests. *9th World Congress on Railway Research*. Lille.
- Dahlberg, T. 2004. Railway Track Settlement - A Literature Review. Linkoping: Linkoping University, Sweden.
- Dahlberg, T. 2001. Some Railroad Settlement Models-A Critical Review. *Journal of Rail and Rapid Transit*, Vol. 215, 289-300.
- Dahlberg, T. 2006. Track Issues. In: IWNICKI, S. (ed.) *Handbook of Railway Vehicle Dynamic*. CRC Press Taylor & Francis Group, LLC.
- Das, B. M. 2008. *Advanced Soil Mechanics*, Taylor & Francis.
- De Bold, R. 2011. *Non-Destructive Evaluation of Railway Trackbed Ballast*. Doctor of Philosophy, University of Edinburgh.
- Demharter, K. 1982. Setzungsverhalten des Gleisrostes unter vertikaler Lasteinwirkung. *Mitteilungen des Profamtes fur Bau von Landverkehrswegen, Technische Universitat Munchen*, Part. 36.
- Department for Transport. 2013. *Passenger km Travelled from Statistical Data Set Table RAI0103 (Franchised Operators Only)* [Online]. Available: <https://www.gov.uk/government/statistical-data-sets/rai01-length-of-route-distance-travelled-age-of-stock#table-rai0103> [Accessed 06/08 2013].
- Deutsche Bahn 2004. Bahn-Norm Technische Lieferbedingunge Gleisschotter. *BN 918-061*.
- Dombrow, W., Huang, H. & Tutumluer, E. Comparison of Coal Dust Fouled Railroad Ballast Behaviour-Granite vs. Limestone. In: AL-QADI, T., ed. International Conference on The Bearing Capacity of Roads and Airfields, 2009. Taylor and Francis Group, 1349-1357.
- Doyle, N. F. 1980. Railway Track Design: A Review of Current Practice. *Occasional Paper of Bureau of Transport Economics Publication Summary*. Canberra: Bureau of Transport Economics.
- East Central Railway 2005. Specifications of Stone Ballast. *Size and Gradation*.
- Esveld, C. 2001. *Modern Railway Track*, MRT Productions.
- Fadum, R. E. Influence Values for Estimating Stresses in Elastic Foundations. Proceedings of the Second International Conference on Soil Mechanics and Foundation Engineering, 1948 Rotterdam, Netherlands.
- Fair, P. I. 2003. *The Geotechnical Behaviour of Ballast Materials for Railway Track Maintenance*. Theses of Doctor of Philosophy, University of Sheffield.
- Fair, P. I. & Anderson, W. F. 2003. Railway Track Maintenance Using The Stoneblower. *Proceeding of The Institution of Civil Engineers, Transport* 156, 155-167.
- Feldman, F. & Nissen, D. 2002. Alternative Testing Method for the Measurement of Ballast Foulling: Percentage Void Contamination. *Conference on Railway Engineering*. Wollongong: RTSA.
- Ford, R. 1995. Differential Ballast Settlement, and Consequent Undulations in Track, Caused by Vehicle-Track Interaction. In: KNOTHE, K., GRASSIE, ST.L., ELKINS, J.A. (ed.) *Interaction of Railway Vehicle with the Track and Its Substructure*. Lisse: Swets &Zeitlinger B. V.

- Frohling, R. D. 1997. *Deterioration of Railway Track due to Dynamic Vehicle Loading and Spatially Varying Track Stiffness*. Doctor of Philosophy, University of Pretoria.
- Fuji Film. 2013. *Fuji Film Prescale Pressure Measurement Film* [Online]. FujiFilm I&I Imaging & Information. Available: <http://www.fujifilm.com/products/prescale/prescalefilm/>.
- Fuller, W. B. & Thompson, S. E. 1907. The Laws of Proportioning Concrete. *Journal Transactions of the American Society of Civil Engineers*, Vol. LIX No. 2, 67-143.
- Gaskin, P. N. & Raymond, G. 1976. Contribution to Selection of Railroad Ballast. *Journal of Transportation Engineering* Vol. 102, 377-394.
- Gaskin, P. N., Raymond, G. & Powell, A. G. 1978. Response of Railroad Ballast to Vertical Vibration. *Transportation Engineering Journal*, Vol. 104, 75-87.
- Geological Society 2001. *Aggregates: Sand, Gravel and Crushed Rock Aggregates for Construction Purposes*, The Geological Society.
- Han, X. & Selig, E. T. 1997. Effects of Fouling on Ballast Settlement. *International Heavy Haul Railway Conference*. St. Louis: Spoornet.
- Hardin, B. O. 1985. Crushing of Soil Particles. *Journal of Geotechnical Engineering*, Vol. 111, 1177-1192.
- Hay, W. W. 1982. *Railroad engineering*, New York, Wiley.
- Henn, W. 1978. Auswirkung von Oberbauform und Betriebsbelastung auf die Veränderung der Gleishohenlage. *Mitteilungen des Prufamtes für Bau von Landverkehrswegen, Technischen Universität München*, Part. 30.
- Hetenyi, M. 1946. *Beams on Elastic Foundation*, Baltimore, Waverly Press.
- Hettler, A. 1984. Bleibende Setzungen des Schotteroberbaus. *ETR Eisenbahntechnische Rundschau* 33, Vol. 11, 847-853.
- Holtzendorff, K. 2001. Predicting Settlements of Ballasted Tracks due to Voided Sleepers. *World Congress Railway Research*. Germany.
- Holzlohner, U. 1978. Bleibende Setzung von Fundamenten infolge dynamischer Last. *Die Bautechnik*, No. 5, 150-158.
- Huang, H. & Tutumluer, E. 2011. Discrete Element Modelling for Fouled Railroad Ballast. *Elsevier Construction and Building Materials* 25, 3306-3312.
- Huang, H., Tutumluer, E. & Dombrow, W. 2009. Laboratory Characterization of Fouled Railroad Ballast Behavior. *Journal of the Transportation Research Board*, No. 2117, 93-101.
- Hunt, G. 2005. Review of the Effect of Track Stiffness on Track Performance, Research Project T372. Rail Safety and Standards Board (RSSB).
- Indraratna, B. & Salim, W. 2003. Deformation and Degradation Mechanics of Recycled Ballast Stabilised with Geosynthetics. *SOILS AND FOUNDATIONS Japanese Geotechnical Society*, Vol. 43, 35-46.
- Indraratna, B. & Salim, W. 2005. *Mechanics of ballasted rail tracks : a geotechnical perspective*, London, Taylor & Francis.
- Indraratna, B. & Salim, W. 2002. Modelling of Particle Breakage of Coarse Aggregates Incorporating Strength and Dilatancy. *Proceeding of The Institution of Civil Engineers, Geotechnical Engineering* 155, 243-252.
- Indraratna, B., Salim, W. & Rujikiatkamjorn, C. 2011. *Advanced rail geotechnology--ballasted track*, Leiden, The Netherlands, CRC Press/Balkema.
- Indraratna, B., Nimbalkar, S. S. & Tennakoon, N. 2010. The Behaviour of Ballasted Track Foundations: Track Drainage and Geosynthetic Reinforcement. In: ASCE (ed.) *GeoFlorida 2010 : Advance in Analysis, Modeling & Design*. Florida: ASCE.
- Indraratna, B., Ngo, N. T. & Rujikiatkamjorn, C. 2013. Deformation of Coal Fouled Ballast Stabilized with Geogrid Under Cyclic Load. *Journal of Geotechnical and Geoenvironmental Engineering*, 139, 1275-1289.

- Indraratna, B., Ngo, N. T., Rujikiatkamjorn, C. & Vinod, J. S. 2014. Behavior of Fresh and Fouled Railway Ballast Subjected to Direct Shear Testing: Discrete Element Simulation. *ASCE International Journal of Geomechanics*, Vol. 14, 34-44.
- Indraratna, B., Ionescu, D., Christie, D. & Chowdhury, D. 1997. Compression and Degradation of Railway Ballast Under One-Dimensional Loading. *Australian Geomechanics*, 48-61.
- Indraratna, B., Khabbaz, H., Salim, W. & Christie, D. 2006a. Geotechnical Properties of Ballast and The Role of Geosynthetics in Rail Track Stabilisation. *Journal of Ground Improvement*, Vol. 10, 91-102.
- Indraratna, B., Shahin, M., Rujikiatkamjorn, C. & Christie, D. 2006b. Stabilisation of Ballasted Rail Tracks and Underlying Soft Formation Soils with Geosynthetic Grids and Drains. *GeoShanghai International Conference: Geosynthetics and Ground Improvement*. Shanghai, China: ASCE Special Geotechnical Publication.
- Innotrack 2008. First Phase Report on Modelling of Poor Quality Sites. Prague.
- Insa, R., Salvador, P., Inarejos, J. & Medina, L. 2013. Analysis of the Performance of Under-Sleeper Pads in High-Speed Line Transition Zones. *Proceeding of The Institution of Civil Engineers*, Vol. 167, 63-77.
- Ionescu, D. 2004. *Evaluation of The Engineering Behaviour of Railway Ballast*. Doctor of Philosophy, University of Wollongong.
- Jaky, J. Pressure in Silos. Proceeding 2nd International Conference on Soil Mechanics and Foundation Engineering, 1948 Rotterdam, The Netherland. 103-107.
- Jeffs, T. & Marich, S. 1987. Ballast Characteristics in the Laboratory. *Conference on Railway Engineering*. Perth.
- Jing, G. Q., Zhou, Y. D., Lin, J. & Zhang, J. 2012. Ballast Flying Mechanism and Sensitivity Factors Analysis. *International Journal on Smart Sensing and Intelligent Systems*, Vol. 5, 928-938.
- Johansson, A., Nielsen, J. C. O., Bolmsvik, R. & Karlstrom, A. 2006. Under Sleeper Pads-Influence on Dynamic Train-Track Interaction. *7th International Conference on Contact Mechanics and Wear of Rail/Wheel System*. Brisbane, Australia: Elsevier.
- Kabo, E. 2006. A Numerical Study of the Lateral Ballast Resistance in Railway Tracks. *Journal of Rail and Rapid Transit*, Vol. 220, 425-432.
- Kaewunruen, S. 2011. Australian Rail Research 2012.
- Kaewunruen, S. & Remennikov, A. M. 2008. A review of loading conditions for railway track structures due to train and track vertical interaction. *Structural Control & Health Monitoring*, 15, 207-234.
- Kaya, M. 2004. *A Study on The Stress-Strain Behavior of Railroad Ballast Materials by Use of Parallel Gradation Technique*. Doctor of Philosophy, The Middle East Technical University.
- Kennedy, J. 2011. *A Full-Scaled Laboratory Investigation Into Railway Track Substructure Performance and Ballast Reinforcement*. Doctor of Philosophy, Heriot-Watt University.
- Kerr, A. D. 2003. *Fundamentals of railway track engineering*, Omaha, NE, Simmons-Boardman Books.
- Klassen, M. J., Clifton, A. W. & Watters, B. R. 1987. Track Evaluation and Ballast Performance Specifications. *Journal Transportation Research Record*, Vol. 1131, 35-44.
- Knutson, R. M. 1976. *Factors Influencing the Repeated Load Behavior of Railway Ballast*. Doctor of Philosophy, University of Illinois.
- Kuula-Vaisanen, P. & Kaivola, T.-M. 2002. Technical Requirements for Railway Ballast in Finland. 1-3.
- Kwon, H. B. & Park, C. S. An Experimental Study on the Relationship between Ballast-flying Phenomenon and Strong Wind under High-speed Train. 7th World Congress Railway Research, 2006 Montreal, Canada. 625.
- Lackenby, J., Indraratna, B., Mcdowell, G. & Christie, D. 2007. Effect of confining pressure on ballast degradation and deformation under cyclic triaxial loading. *Geotechnique*, 57, 527-536.
- Lacy, H. S. & Panne, J. 1987. Use of Geosynthetics in the Design of Railroad Tracks. *Journal Transportation Research Record*, Vol. 1131, 99-106.

- Lakusic, S., Ahac, M. & Haladin, I. 2010. Experimental Investigation of Railway Track with Under Sleeper Pad. *Slovenian Congress on Road and Traffic*. Portoroz.
- Lazaro, B. J., Gonzalez, E., Rodriguez, M., Rodriguez, M., Osma, S. & Iglesias, J. 2011. Characterization and Modeling of Flying Ballast Phenomena in High-speed Train Lines. *The 9th World Congress Railway Research*. Lille.
- Le Pen, L. M. 2008. *Track Behaviour: The Importance of The Sleeper to Ballast Interface*. Doctor of Philosophy, University of Southampton.
- Le Pen, L. M. & Powrie, W. 2011. Contribution of base, crib, and shoulder ballast to the lateral sliding resistance of railway track: a geotechnical perspective. *Journal of Rail and Rapid Transit*, Vol. 225, 113-128.
- Le Pen, L. M., Harkness, J., Zervos, A. & Powrie, W. 2014a. The Influence of Membranes on Tests of Coarsed-Grained Materials at Low Cell Pressure. *International Symposium Cambridge, Geomechanics from Micro to Macro*. Cambridge, UK.
- Le Pen, L. M., Watson, G., Powrie, W., Yeo, G., Weston, P. & Roberts, C. 2014b. The Behaviour of Railway Level Crossing: Insights Through Field Monitoring. *Elsevier Transportation Geotechnics*, Vol. 1, 201-213.
- Lees, H. M. Ballast Evaluation and Hot Mix Asphalt Performance. The 8th International Conference on Bearing Capacity of Roads, Railways and Airfield, 2009 Leiden, Netherlands. CRC Press Balkema.
- Leong, J. & Murray, M. H. 2008. Probabilistic Analysis of Train-Track Vertical Impact Forces. *Proceeding of The Institution of Civil Engineers*, Transport 161, 15-21.
- Li, D. & Selig, E. T. 1998a. Method for Railroad Track Foundation Design I: Development. *Journal of Geotechnical and Geoenvironmental Engineering*, 124, 316-322.
- Lim, W. L. 2004. *Mechanics of Railway Ballast Behaviour*. Doctor of Philosophy, The University of Nottingham.
- Manalo, A., Aravinthan, T., Karunasena, W. & Ticoalu, A. 2010. A Riview of Alternative Materials for Replacing Existing Timber Sleepers. *Journal Elsevier Composite Structures*, Vol. 92, 603-611.
- Marinos, P. & Hoek, E. 2001. Estimating the Geotechnical Properties of Heterogeneous Rock Masses such as Flysch. *Bulletin Engineering Geology Environmental*, Vol. 60, 85-92.
- Marsal, R. J. 1967. Large Scale Testing of Rockfill Materials. *ASCE Journal of The Soil Mechanics and Foundation Division*, 93, 27-43.
- Marx, L. & Mobmann, D. 2012. *DB Manual Work Procedures for Permanent Way Maintenance*, Bahn Fachverlag.
- Mathworks. 2014. *MathWorks Accelerating the Pace of Engineering and Science* [Online]. Available: www.mathworks.co.uk [Accessed 28th May 2014].
- Mauer, L. 1995. An Interactive Track-Train Dynamic Model for Calculation of Track Error Growth. In: KNOTHE, K., GRASSIE, ST.L., ELKINS, J.A. (ed.) *Interaction of Railway Vehicles with the Track and Its Substructure*. Vehicle System Dynamics Supplement 24 ed. Lisse: Swets & Zeitlinger B.V.
- Mccullough, G. J. US Railroad Efficiency : A Brief Economic Overview. Research to Enhance Rail Network Performance, 2007 Washington, D.C.: Transportation Research Board of The National Academies, 63-71.
- Mcdowell, G. R., Harireche, O., Konietzky, H., Brown, S. F. & Thom, N. H. 2006. Discrete Element Modelling of Geogrid-Reinforced Aggregates. *Proceeding of The Institution of Civil Engineers*, 35-48.
- Midland Quarry 2011. Midland Quarry Products: Meeting the Requirements of Our Customers from Enquiry through to Delivery. In: QUARRY, M. (ed.). Midland Quarry.
- Ministry of Science and Technology Department of Technical and Vocational Education 2007. Railway Engineering. *Sleepers*. Departement of Civil Engineering.
- Morgan, B. 1971. *Industrial Archaeology Civil Engineering: Railways*, London, Longman Group Limited.

- Nalsund, R. 2010. Effect of Grading on Degradation of Crushed-Rock Railway Ballast and on Permanent Axial Deformation. *Journal of the Transportation Research Board*, No. 2154, 2, 149-155.
- Network Rail 2013. Network Rail Infrastructure Limited Regulatory: Financial Statements Year Ended 31 March 2013.
- Network Rail 2009. Network Rail NR/L2/TRK/8100: Railway Ballast and Stoneblower Aggregate. King's Place, 90 York Way, London N1 9AG: Network Rail.
- Network Rail 2005. Network Rail NR/SP/TRK/9039: Business Process Document Formation Treatments. 40 Melton Street, London NW1 2EE: Network Rail.
- Network Rail 2000. Network Rail RT/CE/S/006: Railtrack Line Specification: Track Ballast and Stoneblower Aggregate. Railtrack House, Euston Square, London NW1 2EE: Railtrack Plc.
- Network Rail 2011. Network Route Utilisation Strategy (RUS) Passenger Rolling Stock Network Rail.
- Network Rail. 2010. *Value and Importance of rail Freight* [Online]. www.networkrail.co.uk. Available: www.networkrail.co.uk/9083_ValueofFreight.pdf [Accessed 23rd August 2011].
- Norfolk Southern Corporation 2011. Guidelines for Design and Construction of Privately Owned Industry Track. *Materials*. Norfolk Southern Corporation Engineering Department.
- Office for National Statistics. 2014. *Gross Domestic Product by Gross Value Added Industry of Output* [Online]. [Accessed 06/08 2014].
- Office of Transport Safety Investigation 2005. Rail Safety Investigation Report. *Steel Sleeper Introduction on NSW Class 1 Main Line Track 1996-2004*. Sydney, NSW.
- Okabe, Z. 1961. Laboratory Investigation of Railroad Ballast. *Permanent Way*, No. 13, 1-19.
- Ore 1970. Question D 71 Stresses in the Rails, the Ballast and in the Formation Resulting from Traffic Loads. Utrecht: ORE.
- Pcm Strescon Overseas Ventures Limited 2014. Growth on Strong Track. In: [HTTP://WWW.PCMSTRESCON.COM/](http://www.pcmstrescon.com/) (ed.).
- Porr Technobau Und Umwelt Ag 2014. Slab Track
- Powrie, W. 2014a. On Track : The Future for Rail Infrastructure Systems. *Proceeding of The Institution of Civil Engineers*, Civil Engineering 167, 19-27.
- Powrie, W. 2004. *Soil Mechanics : Concepts and Applications*, London, Spon Press.
- Powrie, W. 2014b. *Soil Mechanics Concepts and Applications*, CRC Press Taylor & Francis Group London.
- Powrie, W., Yang, L. A. & Clayton, C. R. I. 2007. Stress Change in the Ground Below Ballasted Railway Track During Train Passage. *Journal of Rail and Rapid Transit*, 221, 247-261.
- Priest, J. A. & Powrie, W. 2009. Determination of Dynamic Track Modulus from Measurement of Track Velocity During Train Passage. *Journal of Geotechnical and Geoenvironmental Engineering*, Vol. 135, 1732-1740.
- Priest, J. A., Le Pen, L. M., Powrie, W., Cesaretti, G. & Taglioli, R. 2013. Shah-Habshan-Ruwais Railway Project-Contract C301 (Stage 1), Sand Mitigation Measures Efficiency Track Resilience Test. Final Report.
- Profillidis, V. A. 2006. *Railway Management and Engineering*, England, Ashgate Publishing Limited.
- Quinn, A. D., Hayward, M., Baker, C. J., Schmid, F., Priest, J. A. & Powrie, W. 2010. A full-scale experimental and modelling study of ballast flight under high-speed trains. *Proceedings of the Institution of Mechanical Engineers Part F-Journal of Rail and Rapid Transit*, 224, 61-74.
- Radampola, S. S. 2006. *Evaluation and Modeling Performance of Capping Layer in Rail Track Substructure*. Doctor of Philosophy, Central Queensland University.
- Railcorp Engineering Specification Track 2009. SPC 241 Ballast. Railcorp.
- Railcorp Engineering Standard Track 2009a. ESC 200 Track System. Railcorp.
- Railcorp Engineering Standard Track 2009b. ESC 240 Ballast. Railcorp.

- Railway Group Standard 1999. Categorisation of Track. London: Safety and Standard Directorate Railtrack PLC.
- Railway Group Standard 2001. Railway Safety Approved Code of Practice GC/RC5521 Calculation of Enhanced Permissible Speeds for Tilting Trains. Railway Safety, Evergreen House, London NW1 2DX: Railway Safety.
- Raymond, G. & Bathurst, R. J. 1987. Performance of Large-Scale Model Single Tie-Ballast Systems. *Journal Transportation Research Record*, 1131, 7-14.
- Raymond, G. & Diyaljee, V. A. 1979a. Railroad Ballast Load Ranging Classification. *Journal of the Geotechnical Engineering Division*, Vol. 105, 1133-1153.
- Raymond, G. P. 1985a. Analysis of Track Support and Determination of Track Modulus. *Transportation Research Record*, Vol. 1022, 80-90.
- Raymond, G. P. 1978. Design for Railroad Ballast and Subgrade Support. *Journal of the Geotechnical Engineering Division*, Vol. 104, 45-60.
- Raymond, G. P. 1979. Railroad Ballast Prescription - State-of-the-Art. *Journal of the Geotechnical Engineering Division*, Vol. 105, 305-322.
- Raymond, G. P. 1985b. Research on Railroad Ballast Specification and Evaluation. *Journal Transportation Research Record*, Vol. 1006, 1-8.
- Raymond, G. P. 1987. Subgrade and Ballast Requirements for 125-Ton Cars. *Journal Transportation Research Record*, 1131, 64-73.
- Raymond, G. P. & Diyaljee, V. A. 1979b. Railroad Ballast Load Ranking Classification. *Journal of the Geotechnical Engineering Division*, Vol. 105, 1133-1153.
- Raymond, G. P. & Diyaljee, V. A. 1979c. Railroad Ballast Sizing and Grading. *Journal of the Geotechnical Engineering Division*, Vol. 105, 676-681.
- Remennikov, A. M. & Kaewunruen, S. 2007. A Review of Loading Conditions Railway Track Structures Due to Train and Track Vertical Interaction. *Structural Control and Health Monitoring*, Volume 15, 207-234.
- Richardson, D. N. 2005. Aggregate Gradation Optimization-Literature Search. University of Missouri-Rolla.
- Round, D. J. Sleepers. Track Technology Course, 1993. British Rail Research, 1-23.
- Rujikiatkamjorn, C., Indraratna, B., Ngo, N. T. & Coop, M. 2012. A Laboratory Study of Railway Ballast Behaviour Under Various Fouling Degree. *5th Asian Regional Conference on Geosynthetics*. Bangkok.
- Sadeghi, J. 2012. New Advances in Analysis and Design of Railway Track System. In: PERPINYA, X. (ed.) *Reliability and Safety in Railway*. InTech.
- Sadeghi, J. & Barati, P. 2010. Evaluation of Conventional Methods in Analysis and Design of Railway Track System. *International Journal of Civil Engineering*, Vol. 8, 44-56.
- Sadeghi, J. & Shoja, H. 2013. Impact of Superelevation Deficiencies on the Loading Pattern of Railway Sleepers. *Journal of Rail and Rapid Transit*, Vol. 227, 286-295.
- Sato, Y. 1995. Japanese Studies on Deterioration of Ballasted Track. In: KNOTHE, K., GRASSIE, S.T.L., ELKINS, J.A. (ed.) *Interaction of Railway Vehicles with the Track and Its Substructure*. Lisse: Swets & Zeitlinger B.V.
- Sato, Y. Optimization of Track Maintenance Work on Ballasted Track. The World Congress on Railway Research (WCRR'97), 16-19 November 1997a Florence, Italy. 405-411.
- Sato, Y. 1997b. Optimum Track Structure Considering Track Deterioration in Ballasted Track. *Sixth International Heavy Haul Railway Conference "Strategies Beyond 2000"*. Cape Town, South Africa: IHHA Press.
- Saussine, G. 2013. Ballast Flying and Projection Phenomena: Issues and Challenges. *William W. Hay Railroad Engineering Seminar*. University of Illinois.

- Sbd Crushers. 2010. *The Technical Details of Product Range by Saif Bin Darwish Crushers* [Online]. [Accessed 8 October 2013].
- Schneider, P., Bolmsvik, R. & Nielsen, J. C. O. 2011. In Situ Performance of a Ballasted Railway Track with Under Sleeper Pads. *Journal of Rail and Rapid Transit*, 299-309.
- Selig, E. T. 1985. Ballast for Heavy Duty Track. *Track Technology*. London: Thomas Telford Ltd.
- Selig, E. T. 1980. Ballast Research. *79th Annual Technical Conference*. Chicago, IL.
- Selig, E. T. & Roner, C. J. 1987. Performance of Aggregates in Railroads and Other Track Performance Issues. *Journal Transportation Research Record*, 1131, 1-6.
- Selig, E. T. & Alva-Hurtado, J. E. 1982. Predicting Effects of Repeated Wheel Loading on Track Settlement. *2nd International Heavy Haul Railway Conference*. Colorado Spring, Colorado, the U.S.A.
- Selig, E. T. & Waters, J. M. 1994. *Track Geotechnology and Substructure Management*, London & New York, T. Telford American Society of Civil Engineers, Publications Sales Dept. distributor.
- Selig, E. T. & Li, D. 1994. Track Modulus: Its Meaning and Factors Influencing It. *Transportation Research Record*, No. 1470, 47-54.
- Selig, E. T., Parsons, B. K. & Cole, B. E. 1993. Drainage of Railway Ballast. *5th International Heavy Haul Railway Conference*. Beijing, China.
- Shenton, M. J. 1984. Ballast Deformation and Track Deterioration. *Track Technology*. London: Thomas Telford Ltd.
- Shenton, M. J. Deformation of Railway Ballast under Repeated Loading Condition. *In: KERR, A. D., ed. Railroad Track Mechanics and Technology: Proceeding of a Symposium, 21st-23rd April 1978* 1978 Princeton University.
- Standards Australia 2003. Australian Standard AS 1085.14-2003 Railway Track Material Part 14: Prestressed Concrete Sleepers. Australia: Standard Australia.
- Stewart, H. E. 1985. Measurement and Prediction of Vertical Track Modulus. *Transportation Research Record*, Vol. 1022, 65-71.
- Stewart, H. E. & Selig, E. T. 1984. Correlation of Concrete Tie Track Performance in Revenue Service and at the Facility for Accelerated Service Testing. *Prediction and Evaluation of Track Settlement*. Washington, DC: U.S. Department of Transportation Federal Railroad Administration.
- Stewart, H. E. & Selig, E. T. 1982a. Predicted and Measured Resilient Response of Track. *Journal of Geotechnical Engineering Division-ASCE*, 108, 1423-1442.
- Stewart, H. E. & Selig, E. T. 1982b. Prediction of Track Settlement Under Traffic Loading. *2nd International Heavy Haul Railway Conference*. Colorado Springs, Colorado, the U.S.A.
- Stewart, H. E., Selig, E. T. & Norman-Gregory, G. M. 1985. Failure Criteria and Lateral Stresses in Track Foundation. *Transportation Research Record*, Vol. 1022, 59-64.
- Taylor, H. P. J. 1993. The Railway Sleeper: 50 Years of Pretensioned, Prestressed Concrete. *The Structural Engineer*, Volume 71.
- Thom, N. H. & Oakley, J. 2006. Predicting Differential Settlement in a Railway Trackbed. *Railway Foundations*. Birmingham, UK.
- Tiflex. 2013. *TRACKELAST Specialist Rail Solutions the High Performance Solution Provider* [Online]. Available: http://www.tiflex.co.uk/downloads/TFX-B-TRACKELAST-10092012_A4.pdf [Accessed 23/05/2013 2013].
- Timoshenko, S. Proceedings Second International Congress of Applied Mechanics: Methods of Analysis of Static and Dynamical Stresses in Rails. 1927 Zurich. 407-418
- Tolppanen, P., Stephansson, O. & Stenlid, L. 2002. 3-D Degradation Analysis of Railroad Ballast. *Bulletin Engineering Geology Environmental*, 35-42.

- Train Chartering Company Ltd. 2011. *The Environmental Benefits of Rail Travel* [Online]. Available: http://www.trainchartering.com/casestudies_environmental.html [Accessed 21/05/2012 2012].
- Transportation Research Board, N. R. C. 1996. *Estimating Marginal Social Costs of Freight Transportation*, National Academy Press.
- Turcke, D. J. & Raymond, G. P. 1979. Three-Dimensional Analysis of Rail Track Structure. *Journal Transportation Research Record*, Vol. 733, 1-6.
- Tutumluer, E., Dombrow, W. & Huang, H. 2008. Laboratory Characterization of Coal Dust Fouled Ballast Behavior. *AREMA 2008 Annual Conference & Exposition*. Salt Lake City, UT.
- Tutumluer, E., Huang, H., Hashash, Y. M. A. & Ghaboussi, J. 2009. AREMA Gradations Affecting Ballast Performance Using Discrete Element Modeling (DEM) Approach. *AREMA 2009 Annual Conference*.
- Tzanakakis, K. 2013. *The Railway Track and Its Long Term Behaviour: A Handbook for a Railway Track of High Quality*, Springer.
- Uic 2009a. UIC Code 714 R: Classification of Lines for the Purpose of Track Maintenance. UIC.
- Uic 2008a. UIC Code 719R Earthworks and Trackbed for Railway Lines.
- Uic 2008b. UIC Leaflet 713-1R: Recommendations for the use of Under Sleeper Pads-USP. In: GROUP, T. E. (ed.).
- Uic 2009b. UIC Project: Under Sleeper Pads- Semelles Sous Traverses- Schwellenbesohlungen. 4th ed. Vienna.
- Unified Facilities Criteria 2004. *Railroad Design and Rehabilitation*.
- Varandas, J. N., Holscher, P. & Silva, M. a. G. 2013. Settlement of Ballasted Track Under Traffic Loading: Application to Transition Zones. *Journal of Rail and Rapid Transit*, 1-18.
- Vishay Intertechnology Inc 2006. Interactive Data Book Strain Gage Instrumentation Vishay Micro-Measurements VSE-DB0085-0611: Stress Analysis Testing, Structural Testing, Material Testing. In: MICRO-MEASUREMENTS, V. (ed.). Raleigh, NC, U.S.A: Vishay Micro-Measurements.
- Watters, B. R., Klassen, M. J. & Clifton, A. W. 1987. Evaluation of Ballast Materials Using Petrographic Criteria. *Journal Transportation Research Record*, Vol. 1131, 45-58.
- Whitlow, R. 2001. *Basic Soil Mechanics*, Essex, Pearson Prentice Hall.
- Witt, S. 2008. *The Influence of Under Sleeper Pads on Railway Track Dynamics*. Linkoping University-Institute of Technology.
- www.foe.co.uk. 2001. *Fact Sheet Why Travelling by Rail is Better for the Environment* [Online]. Available: http://www.foe.co.uk/resource/factsheets/travelling_rail_better.pdf [Accessed 23rd August 2011].
- www.freightonrail.org.uk. 2001-2011. *The Future Of the Railway* [Online]. Available: www.freightonrail.org.uk/consultationsFutureoftheRailway.htm [Accessed 23rd August 2011].
- Zakeri, J. A. & Abbasi, R. 2012a. Field Investigation of Variation of Loading Pattern of Concrete Sleeper due to Ballast Sandy Contamination in Sandy Dessert Areas. *Journal of Mechanical Science and Technology*, 3885-3892.
- Zakeri, J. A. & Abbasi, R. 2011. Field Investigation on Distribution of Contact Pressure Between Sleeper and Saturated Ballast with Flowing Sand. *11th International Conference on Railway Engineering*. London.
- Zakeri, J. A. & Sadeghi, J. 2007. Field investigation on load distribution and deflections of railway track sleepers. *Journal of Mechanical Science and Technology*, 21, 1948-1956.
- Zakeri, J. A. & Abbasi, R. 2012b. Field Investigation on Variation of Rail Support Modulus in Ballasted Railway Tracks. *Latin American Journal of Solids and Structures*, Vol. 9, 643-656.